

*EXPLORING THE EVOLVABILITY OF
OLD YELLOW ENZYMES
FOR ORGANIC SYNTHESIS*

Nathalie Nett, M.Sc.

from Bendorf am Rhein

Philipps-Universität Marburg

Department of Chemistry

**This dissertation is submitted
for the degree of Doctor of Science
(Dr. rer. nat.)**

Marburg/Lahn 2017

Die vorliegende Dissertation entstand in der Zeit von März 2014 bis Oktober 2017 am Fachbereich Chemie der Philipps-Universität Marburg in der Arbeitsgruppe Hoebenreich und unter der Betreuung von Frau Dr. Sabrina Hoebenreich und Herrn Prof. Dr. Eric Meggers.

Vom Fachbereich Chemie der Philipps-Universität Marburg (Hochschulkennziffer: 1180) als Dissertation am 24.11.2017 angenommen.

Erstgutachter: Prof. Dr. Eric Meggers

Zweitgutachterin: Dr. Sabrina Hoebenreich

Tag der mündlichen Prüfung: 01.12.2017

Zu tun was du willst ist Freiheit

Zu mögen was du tust ist Glück

ERKLÄRUNG

Ich erkläre, dass eine Promotion noch an keiner anderen Hochschule als der Philipps-Universität Marburg, Fachbereich Chemie, versucht wurde.

Ich versichere, dass ich meine vorgelegte Dissertation „Exploring the Evolvability of Old Yellow Enzymes for Organic Synthesis“ selbst und ohne fremde Hilfe verfasst, nicht andere als die in ihr angegebenen Quellen oder Hilfsmittel benutzt, alle vollständig oder sinngemäß übernommenen Zitate als solche gekennzeichnet sowie die Dissertation in der vorliegenden oder einer ähnlichen Form noch bei keiner anderen in- oder ausländischen Hochschule anlässlich eines Promotionsgesuchs oder zu anderen Prüfungszwecken eingereicht habe.

Marburg den: 18.10.2017

Unterschrift: N. Nett

Nathalie Nett

ZUSAMMENFASSUNG

In der vorliegenden Arbeit werden Leitlinien zur Evolution flavinabhängiger Enreduktasen, eine industriell wichtige Katalysatorklasse, dargelegt. Die erarbeiteten Konzepte und Richtlinien, die allgemeingültig für diese Enzymfamilie und deren Substrate sind, könnten in zukünftigen *protein-engineering*-Projekten zu einer erheblichen Effizienzsteigerung führen.

Der erste Teil dieser Dissertation beschäftigt sich mit einer konzeptuellen Fragestellung zur Vereinfachung von *protein-engineering* Studien. Im Speziellen wurden die bereits vorhandenen Kenntnisse über einzelne Enreduktasen, der *Old Yellow Enzyme* (OYE) Familie, die von gerichteten Evolutionsstudien herrühren, herangezogen, um diese auf den gesamten Sequenzbereich der Enzymfamilie zu übertragen. Dadurch soll die Weiterentwicklung neuer effizienterer Enreduktasen verkürzt werden. Identifizierte *hotspot* Positionen, wie C26D/I69T und C26G, in der Bindetasche von YqjM aus *Bacillus subtilis*, die für eine Aktivitätserhöhung und Stereokomplementarität verantwortlich sind, wurden in sieben weitere OYE Familienmitglieder eingebaut. Die ersten Screenings dieser neu synthetisierten Varianten mit drei unterschiedlichen Substraten zeigten jeweils stereokomplementäre Paare mit hohen Wechselzahlen von bis zu 660 h⁻¹ und exzellenten Stereoselektivitäten bis zu >99%. Obwohl die systematische Vorhersage der absoluten Enantioselektivität für OYE-Varianten sich weiterhin als schwierig erweist, wurde die Methode des „*scaffold samplings*“ als schnelles Engineering-Verfahren für diese Familie bestätigt, die den Zugang zu neuen, potenten Biokatalysatoren für die organische Synthese ermöglicht.

Der Fokus des zweiten Teils der Arbeit liegt auf der Entwicklung und Charakterisierung industriell interessanter Varianten der thermostabilen Enreduktase aus *Thermus scotoductus* SA-01 (*TsER*). Diese Varianten zeigen hohe Aktivitäten und Selektivitäten in industriell interessanten Prozessparametern, wie Temperaturen bis zu 70 °C, organische Lösungsmittelzusätzen von bis zu 40% (v/v) und präparative Ansätze, mit Produktisolationen von 3.8 g. Die erreichten Wechselzahlen von bis zu 40 000 h⁻¹ sind mit denen der hetero- und homogenen Katalyse von Hydrierungen vergleichbar. Um strukturelle Einblicke in die stereoselektive Hydrierung von *TsER* zu erlangen, wurden *in silico* Studien anhand der Kristallstrukturen des Wildtyps und der Varianten C25D/I67T, C25G/I67T und C25D/I67T/A102H durchgeführt. Die umfassende Charakterisierung dieser Sammlung an thermostabilen Enreduktasen zeigt ein hohes Potential für den Einsatz in der organischen Synthese.

Im dritten Teil dieser Arbeit wird das Substratspektrum auf strukturell anspruchsvollere Substanzen erweitert, im Speziellen die Klasse der Cumarine. Im Allgemeinen besteht ein großes Interesse darin den Substratbereich von Enreduktasen auf sperrige Substrate zu erweitern, um diese hochselektiven Transhydrierungskatalysatoren in einem späten Stadium der organischen Synthese komplexer Moleküle zu verwenden. Dabei wurden chemoselektive Varianten entdeckt, die zum Einen die bekannte Hydrierung katalysieren aber zum Anderen auch eine Säure/Base Aktivität in der aktiven Tasche von *TsER* aufweisen, wodurch das Hydrolyse Produkt des Lactones entsteht.

ABSTRACT

In the presented thesis, guidelines for the evolution of flavin-dependent ene reductases, an industrially important catalyst class, are reported.

In the first part of this thesis it should be tested if mining the existing knowledge of the Old Yellow Enzyme family (OYE), obtained from directed evolution studies, may allow guided traversing through the sequence space and thereby shortcutting biocatalyst development. Identified hotspot positions of YqjM from *Bacillus subtilis*, i.e. C26D/I69T and C26G for improvement of activity and stereoselectivity, respectively, were transferred to seven OYE scaffolds. The newly created variants were tested with three compounds revealing more stereocomplementary OYE pairs with potent turnover frequencies (up to 660 h⁻¹) and excellent stereoselectivities (up to >99%). Although systematic prediction of absolute enantioselectivity still remains for OYE variants, 'scaffold sampling' was confirmed as a fast engineering method for this family allowing access to new, potent biocatalysts for organic synthesis.

In the second part of this thesis the development and characterisation of an engineered panel of ene reductases (ERs) from *Thermus scotoductus* SA-01 (*TsER*) is reported, that combines control over facial selectivity in the reduction of electron deficient carbon-carbon double bonds with thermostability (up to 70 °C), organic solvent tolerance (up to 40% (v/v)) and a broad substrate scope (23 compounds, three of them new). The panel shows excellent enantiomeric excess (*ee*) and yields during gram scale synthesis (3.8 g). Exquisite turnover frequencies (TOF) up to 40 000 h⁻¹ are achieved, which are comparable to rates in hetero- and homogeneous metal catalysed hydrogenations. Efforts to rationalize the stereocomplementarity are reported, using the obtained crystal structure of *TsER* C25D/I67T and *in silico* docking studies. Our holistic characterisation, together with the preparative scale reactions, shows that these engineered ERs are truly practical catalysts for preparative organic synthesis.

In the third section the aforementioned panel of *TsER* variants was screened for bulkier substrate classes and further mutation sites were identified over semi-rational design for the successful biotransformation of coumarin-like structures. Thereby chemoselective variants with either hydrogenation or evidence for acid/base catalysis in the active site of *TsER* have been discovered. In general there is a great interest in using these highly selective *trans*-hydrogenation catalysts in the late stage synthesis of complex organic molecules.

DANKE...

... an Prof. Dr. Eric Meggers für die Übernahme des Erstgutachtens und die langjährige gemeinsame Zusammenarbeit schon während meiner Bachelor- und Master-Arbeit. Ihre uneingeschränkte Unterstützung, nicht nur bei fachlichen Fragen, schätze ich sehr.

... an Dr. Sabrina Hoebenreich für die Betreuung während der letzten drei Jahre und die Möglichkeit an einem Projekt arbeiten zu dürfen, das meine Begeisterung für die Forschung weiter verstärkt hat, sowie die Übernahme des Zweitgutachtens.

... für die finanzielle Unterstützung während meiner Promotion an: das LOEWE Schwerpunktprojekt des Landes Hessen SynChemBio, dem Deutschen Akademischen Austausch Dienst (DAAD) und der Marburg University Research Academy (MARA).

... my collaboration partner Dr. Diederick J. Opperman for providing the plasmid of the thermophilic TsER, the crystallization of the protein variants and the always professional support. Big thanks to Prof. Adrian Mulholland and Dr. Kara Ranaghan for showing me the world of computational enzymology and an awesome time in Bristol. My special thanks go to my host family Watteau, who gave me a home in Bristol.

...an alle Serviceabteilungen des Fachbereichs Chemie der Philipps-Universität Marburg, im Speziellen der Masseabteilung mit Dr. Uwe Linne für das immer offene Ohr und im Besonderen die Hilfe bei der Durchführung der H/DX Experimente.

... an alle ehemaligen und aktuellen Mitglieder des Arbeitskreises Hoebenreich für die freundliche und produktive Stimmung im Labor. Es war an keinem Tag langweilig oder einsam. Im Besonderen möchte ich dir, Sabine, danken. Ohne dich wäre mir der Alltag im Labor nicht so leicht gefallen, vielen Dank für dein nettes Lächeln am Morgen und die fachliche Unterstützung bei allen aufkommenden Fragen.

... an alle jetzigen und ehemaligen Mitglieder der Arbeitsgruppe Meggers und Vázquez. Ich hatte eine tolle Zeit mit euch.

It also has been a great pleasure to work with the international group member. It was really exciting to learn more about Chinese and Japanese culture.

... an alle meine Bachelor-, Vertiefer- und Master-Studenten: Monika Ballmann, Gerrit Ernst Benary, Max Biermeier, Natalie Brüll, Saskia Döhring, Matthäus

Drabek, Sabine Düwel, Johannes Karges, Viola Krein, Bastian Langer, Jessica Pilgram, Alexandra A. Richter, Moritz Ruf. Ihr habt einen wichtigen Beitrag zum Gelingen dieser Arbeit geleistet.

... an alle Korrekturleser: Sabine Düwel, Olalla Vázquez, Elisabeth Martin, Kara Ranaghan, Richard Lonsdale, Asher Goodenough und Martin Bruch.

...an alle meine Freunde, im Besonderen in Marburg für die Unterstützung und das tolle Leben in Marburg.

... an meine Familie, die mich immer wieder auf den Boden der Tatsachen zurück holt und mir zeigt, was wirklich wichtig im Leben ist. Besonders möchte ich dir, Martin, danken, dass du immer für mich da warst und bist und mich in Allem unterstützt!

PUBLICATIONS

Parts of this work have been published in peer-reviewed scientific journals or have been presented at conferences and summer schools:

Peer-reviewed Articles

N. Nett, S. Duewel, A. A. Richter, S. Hoebenreich, *Revealing Additional Stereocomplementary Pairs of Old Yellow Enzymes by Rational Transfer of Engineered Residues*, *ChemBioChem* **2017**, 18, 685-691.

N. Nett, S. Duewel, L. Schmermund, G. E. Benary, K. E. Ranaghan, D. J. Opperman, A. Mulholland, S. Hoebenreich, *A Robust and Stereocomplementary Panel of Ene-Reductase Variants for Gram-Scale Asymmetric Hydrogenation*, **submitted 2017**.

N. Nett, M. Ruf, D. J. Opperman, S. Hoebenreich, *Evidences for Consecutive Coumarin Reduction and Lactone Hydrolysis within the Active Site of TsER Variants*, **submitted 2017**.

Contributions at Conferences and Summer Schools

Poster Presentations

N. Nett, S. Hoebenreich, at *Summer School "Biotransformations"* **2014**, Bad Herrenalb, Germany

Exploring the Evolvability Potential of Ene-Reductases

N. Nett, S. Duewel, S. Hoebenreich, at *Summer School "Energy Dreams: from Proteomics to Materials and Catalytic Applications"* **2015**, Marburg, Germany

Expanding the Substrate Scope of Ene-Reductases *DrER* and *RmER* by Protein Engineering

N. Nett, S. Duewel, S. Hoebenreich, at *BioTrans***2015**, Vienna, Austria

Expanding the Substrate Scope of Ene-Reductases *DrER* and *RmER* by Protein Engineering

S. Duewel, N. Nett, S. Hoebenreich, at *BioTrans***2015**, Vienna, Austria

Why is the Ene-Reductase *TsER* Ca²⁺ dependent?

N. Nett, S. Duetzel, A. A. Richter, S. Hoebenreich, at *Bristol University* **2017**, United Kingdom

Shortcutting Enzyme Engineering of Old Yellow Enzymes via Hotspot Position Transfer

N. Nett, S. Duetzel, A. A. Richter, S. Hoebenreich, at *BioTrans2017*, Budapest, Hungary

Shortcutting Enzyme Engineering of Old Yellow Enzymes via Hotspot Position Transfer

N. Nett, S. Duetzel, L. Schmermund, G. E. Benary, K. Ranaghan, A. Mulholland, D. J. Opperman, S. Hoebenreich, at *BioTrans2017*, Budapest, Hungary

A Stereocomplementary, Thermostable and Solvent Resistant Ene-Reductase Panel for Synthesis

Oral Presentation

N. Nett, at *Biotransformations* **2014**, Bad Herrenalb, Germany

Exploring the Evolvability Potential of Ene-Reductases

Additional Contributions to Projects Outside of the Thesis Scope

Peer-reviewed Articles and Book Chapters

C. Ritter, N. Nett, C. G. Acevedo-Rocha, R. Lonsdale, K. Kräling, F. Dempwolff, S. Hoebenreich, P. L. Graumann, M. T. Reetz, E. Meggers, *Bioorthogonal Enzymatic Activation of Caged Compounds*, *Angew. Chem. Int. Ed.* **2015**, 54 (45), 13440–13443 (**Hot Paper**).

C. Ritter, N. Nett, C. G. Acevedo-Rocha, R. Lonsdale, K. Kräling, F. Dempwolff, S. Hoebenreich, P. L. Graumann, M. T. Reetz, E. Meggers, *Bioorthogonale enzymatische Aktivierung maskierter Verbindungen*, *Angew. Chem.* **2015**, 127 (45), 13640–13644 (**Hot Paper**).

S. Hoebenreich, M. Spink, N. Nett, *Laboratory-Scale Hydroxylation of Steroids by P450_{BM3} Variants*, *Methods in Molecular Biology: Microbial Steroids*, Springer **2017**, 239-257.

C. G. Acevedo-Rocha, C. Gamblec, R. Lonsdale, A. Lia, N. Nett, S. Hoebenreich, J. B. Lingnaua, C. Wirtz, C. Fares, H. Hinrichs, A. Deege, A. J. Mulholland, Y. Nove, D. Leysc, A. W. Munroc, M. T. Reetz, *Targeted Regio- and Diastereoselective Steroid Hydroxylation Using P450-BM3: Readdressing the Numbers Problem in Directed Evolution* **2017**, under revision.

Contributions at Summer School

Poster Presentation

N. Nett, C. Ritter, C. G. Acevedo-Rocha, R. Lonsdale, K. Kräling, F. Dempwolff, S. Hoebenreich, P. L. Graumann, M. T. Reetz, E. Meggers, at *Summer School "Selectivity as a Key for Sustainable Chemistry"*, **2016** Tongji University in Shanghai, China

Bioorthogonal Enzymatic Activation of Caged Compounds

Selected Oral Presentation

N. Nett at *Summer School "Selectivity as a Key for Sustainable Chemistry"*, **2016** Tongji University in Shanghai, China

Bioorthogonal Enzymatic Activation of Caged Compounds

TABLE OF CONTENTS

1 INTRODUCTION.....	1
1.1 ASYMMETRIC CARBON-CARBON DOUBLE BOND REDUCTION IN ORGANIC SYNTHESIS.....	1
1.2 BIOCATALYSIS IN ORGANIC SYNTHESIS	5
1.3 PROTEIN ENGINEERING	6
1.4 THE OLD YELLOW ENZYME FAMILY.....	11
1.4.1 <i>Reaction Mechanism of the OYE Family</i>	14
1.4.2 <i>Bioreductions with Ene Reductases</i>	17
1.5 CHALLENGES IN THE FIELD OF BIOREDUCTIONS WITH OYES	20
2 OBJECTIVE OF THE THESIS.....	22
3 RESULTS AND DISCUSSION.....	27
3.1 SCAFFOLD SAMPLING STRATEGY FOR THE OYE FAMILY	27
3.1.1 <i>Review of the Recent Literature</i>	27
3.1.2 <i>Target Positions for Presented Transferability Study</i>	29
3.2 DEHYDROGENATION REACTIONS BY OLD YELLOW ENZYMES.....	46
3.3 CHARACTERIZATION OF A ROBUST AND STEREOCOMPLEMENTARY PANEL OF TsER VARIANTS	51
3.3.1 <i>Substrate Scope and Selectivity of TsER Variants</i>	52
3.3.2 <i>Reaction Conditions for Industrial Applications</i>	62
3.3.3 <i>Preparative Scale Reactions</i>	69
3.4 STRUCTURAL INSIGHTS	74
3.4.1 <i>Structural Dynamic Study by H/DX Measurement</i>	74
3.4.2 <i>X-Ray Structures</i>	80
3.5 PREDICTION OF SUBSTRATE BINDING AND AFFINITY BY COMPUTATIONAL METHODS	81
3.5.1 <i>Prediction of Substrate-Catalyst Interactions by In-Silico Docking Studies</i>	81
3.5.2 <i>Prediction of Substrate Affinity by Molecular Dynamics Simulations and WaterSwap Calculations</i>	87
3.6 GOING TO BULKIER SUBSTRATE CLASSES.....	101
3.6.1 <i>Synthesis of Bulkier Substrates</i>	106
3.6.2 <i>Screening with TsER Panel of Chapter 3.3</i>	108
3.6.3 <i>Generation and Screening of Libraries</i>	124
4 CONCLUSION	136
4.1 DEVELOPMENT OF THE ‘SCAFFOLD SAMPLING’ STRATEGY FOR ENE REDUCTASES.....	136

4.2 FULL CHARACTERISATION OF A HIGHLY ACTIVE, ROBUST AND STEREOCOMPLEMENTARY T _{SER} VARIANT PANEL	138
4.3 PREDICTION OF SUBSTRATE BINDING AND AFFINITY BY <i>IN-SILICO</i> STUDIES.....	139
4.4 SUCCESSFUL BIOTRANSFORMATIONS OF INDOLE AND COUMARIN DERIVATIVES BY T _{SER} VARIANTS.....	141
5 OUTLOOK	143
5.1 BROADENING THE 'SCAFFOLD SAMPLING' METHOD OF ENE REDUCTASES.....	143
5.2 INVESTIGATIONS IN DIVERSE CHEMICAL REACTIONS OF OYES	143
5.3 FURTHER MECHANISTICALLY EXAMINATIONS BY <i>IN-SILICO</i> STUDIES	145
6 MATERIAL AND METHODS.....	146
6.1 SYNTHESSES OF COMPOUNDS.....	146
6.1.1 Foreword to Compound Synthesis and Analytical Methods.....	146
6.1.2 Synthesis of 2-Butenoic acid.....	148
6.1.3 Synthesis of Methyl (E/Z)-2-bromo-3-phenylacrylate.....	148
6.1.4 Synthesis of Methyl (E/Z)-2-chloropent-2-enoate.....	149
6.1.5 Synthesis of Ethyl-2-benzylideneacetoacetate.....	151
6.1.6 Synthesis of Methyl-2-(hydroxymethyl)acrylate.....	152
6.1.7 Synthesis of Methyl 3-hydroxy-2-methylenebutanoate.....	152
6.1.8 Synthesis of (E)-(1-Nitroprop-1-en-2-yl)benzene.....	153
6.1.9 Synthesis of (R,E)-1-Methyl-4-(1-nitroprop-1-en-2-yl)cyclohex-1-ene.....	154
6.1.10 Synthesis of (2-Nitroethene-1,1-diyl)dibenzene.....	155
6.1.11 Synthesis of 3-Acetyl-7-hydroxy-2H-chromen-2-one.....	156
6.1.12 Synthesis of 3-Carboxycoumarinethylester.....	157
6.1.13 Synthesis of Meldrum's acid.....	158
6.1.14 Synthesis of 3-Oxo-3H-benzo[f]chromene-2-carboxylic acid.....	158
6.1.15 Synthesis of 1-Methyl-3H-benzo[f]chromen-3-one.....	159
6.2 MICROORGANISMS, VECTORS, PRIMERS	161
6.3 MEDIA, BUFFERS AND ADDITIVES.....	163
6.3.1 Nutrition Media.....	163
6.3.2 Media Additives.....	163
6.3.3 Buffers and Solutions.....	164
6.4 GENERAL METHODS.....	165
6.4.1 Isolation of Plasmid DNA from <i>E.coli</i>	165
6.4.2 Agarose Gel Electrophoresis.....	166
6.4.3 Preparation of Electrocompetent <i>E. coli</i>	166

6.4.4 Transformation of Electrocompetent <i>E.coli</i>	167
6.5 OLD YELLOW ENZYME PROTOCOLS.....	168
6.5.1 <i>Ene</i> Reductases Mutagenesis	168
6.5.2 Heterologous Expression of <i>Ene</i> Reductases.....	170
6.5.3 Purification of His-tagged <i>Ene</i> Reductases	171
6.5.4 Purification over Size Exclusion Chromatography.....	172
6.5.5 Purification of Thermostable TsER.....	172
6.5.6 SDS-Page Analysis	173
6.5.7 Protein Identification via Mass Analysis	174
6.5.8 Determination of Active Enzyme Concentration by UV-Vis Spectroscopy.....	177
6.5.9 Circular Dichroism Spectroscopy	178
6.5.10 Spectrophotometric Measurements of FMN-Oxidation with Molecular Oxygen	178
6.6 THERMOSTABLE GLUCOSE DEHYDROGENASE PROTOCOLS	179
6.6.1 Heterologous Expression and Purification	179
6.6.2 Activity Test	179
6.7 LYOPHILISATION OF ENZYMES.....	180
6.8 PROTEIN CRYSTALLIZATION AND X-RAY STRUCTURE DETERMINATION.....	180
6.8.1 X-Ray Structure of TsER C25D/I67T	180
6.8.2 X-Ray Structure of TsER C25D/I67T/A102H.....	181
6.9 BIOTRANSFORMATIONS	183
6.9.1 Reactions with Cell Lysate in 96-Deep Well Plates.....	183
6.9.2 Reaction with Purified Enzyme	184
6.9.3 Residual Activity of TsER C25D/I67T and C25G/I67T.....	184
6.9.4 Upscale Reactions to Determine Enantiomeric Excess	185
6.9.5 Upscale for Polarization Measurement	185
6.9.6 Upscale of 13a with TsER C25D/I67T	186
6.9.7 Preparative Scale Bioreductions.....	187
6.9.8 Reduction of 22a in Sequential Bi-Phasic Batch Reactions	190
6.9.9 Analytic Methods for Screening	192
6.10 COMPUTATIONAL METHODS AND DETAILS	196
7 REFERENCES	200
8 APPENDICES	217
8.1 LIST OF ABBREVIATIONS AND ACRONYMS.....	217
8.2 NMR SPECTRA OF UPSCALE REACTION WITH 3-CCE	220
8.3 DNA AND PROTEIN SEQUENCES	222

8.3.1 <i>Vector Maps</i>	222
8.3.2 <i>OYE Genes</i>	224
8.3.3 <i>Protein Sequences</i>	224
8.4 GC CHROMATOGRAMS	226
8.5 DOCKING	230

1 INTRODUCTION

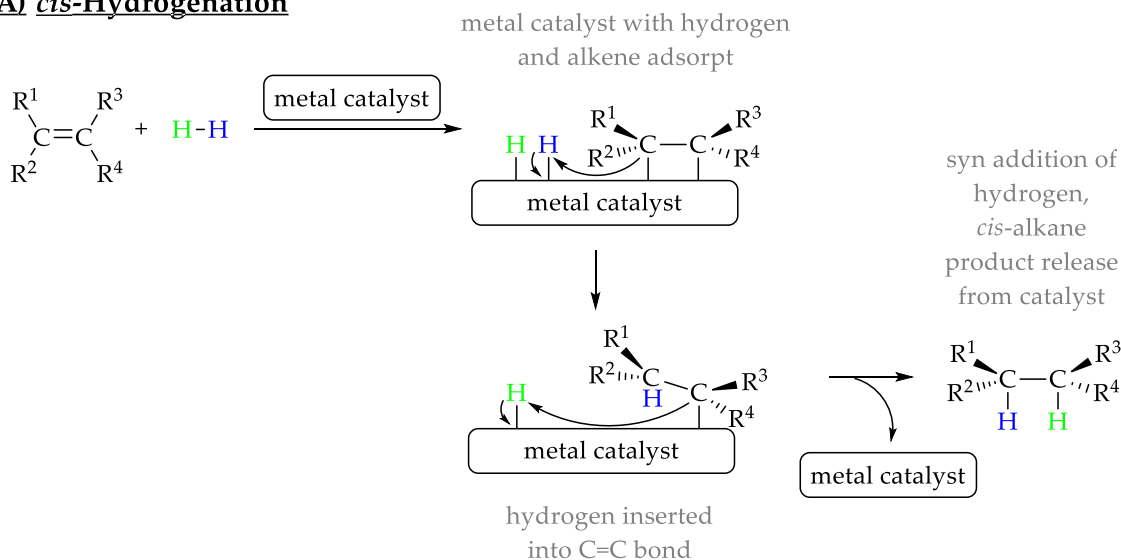
1.1 Asymmetric Carbon-Carbon Double Bond Reduction in Organic Synthesis

One field in organic chemistry is the homogeneous or heterogeneous asymmetric catalysis of sp^2 -carbon centres into sp^3 based on transition metal catalysts to generate chiral compounds with high enantiomeric excess (*ee*).^[1] Notably, the importance of asymmetric hydrogenation was finally recognized in 2001 by the Nobel Prize in Chemistry awarded to WILLIAM S. KNOWLES, RYOJI NOYORI and KARL B. SHARPLESS.^[2-4] The asymmetric catalytic reduction of carbon-carbon double bonds can occur in two different fashions: via *cis*-hydrogenation and *trans*-hydrogenation (Scheme 1). In both cases, two chiral centres are formed at the same time, opening a broadly appreciated approach to produce chiral compounds.^[5]

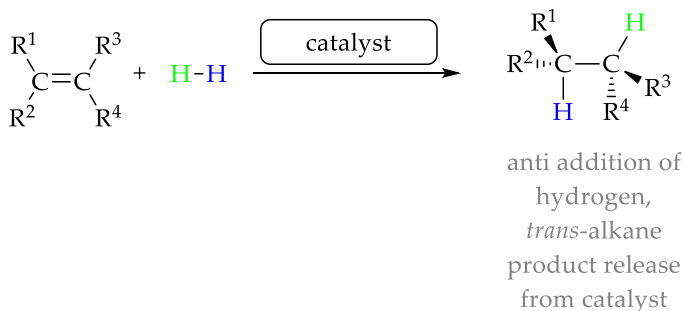
For the *cis*-hydrogenation there are widely used homogeneous and heterogeneous transition-metal catalyst systems.^[6] The reaction takes place at the surface of the metal, where the hydrogen atoms attach. The relatively strong H-H sigma bond is broken and replaced with two weak metal H-bonds. The pi bond of the alkene interacts with the metal catalyst weakening the bond. A hydrogen atom is transferred from the catalyst surface to one carbon of the double bond. Due to the coordination of the second hydrogen and the alkene to the metal catalyst, the second hydrogen atom is transferred from the same face forming the *cis*-alkane (Scheme 1A).^[7-9]

The *trans*-hydrogenation of alkenes is challenging with transition metal catalysis, caused by attaching the hydrogens and the alkene to the same site of the metal. For this type of reactions further alternatives must be found.^[10,11]

A) *cis*-Hydrogenation



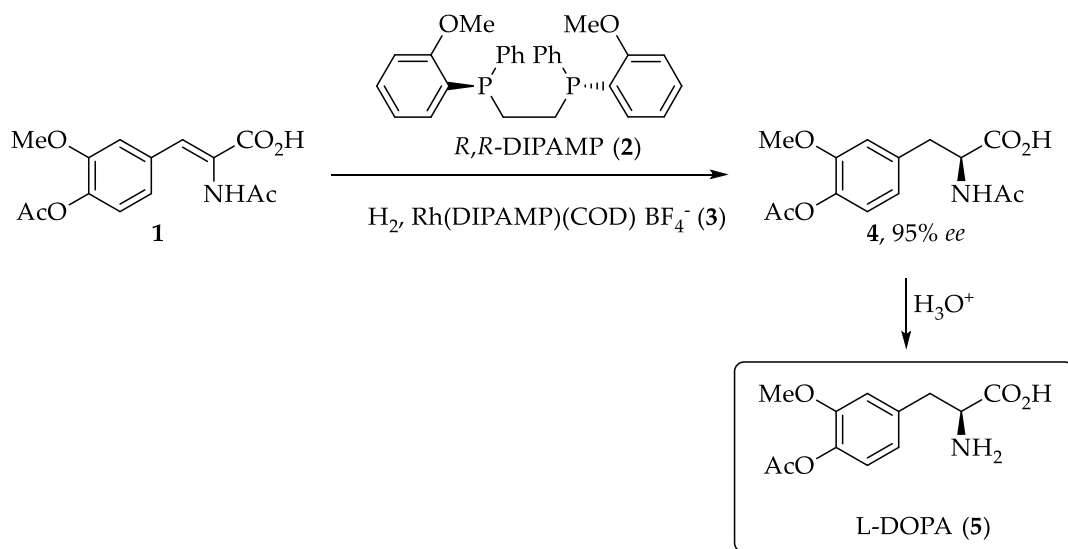
B) *trans*-Hydrogenation



Scheme 1. Two different additions of hydrogen to a carbon-carbon double bond. A) Both hydrogen atoms add to the same face of the alkene (syn- or *cis*-addition) triggered by a metal catalyst. B) Hydrogens add to the opposite faces (anti- or *trans*-addition).

The need for optical active compounds is an elementary basis in different industrial fields like the production of fine chemicals, pharmaceuticals and agrochemical intermediates.^[12] The synthesis of chirally pure molecules is of immense importance to organic synthesis, especially for the pharmaceutical industry. A frequent requirement for regulatory approval of drugs is to understand the *in vivo* activity of both enantiomers, because one enantiomer may exhibit enhanced therapeutic properties over the other, so that the provision of a single

enantiomer is often essential.^[13] Indeed, the percentage of chiral drugs, which were approved by the US Food and Drug Administration (FDA), has increased significantly from 58% in 1992 to 80% in 2006, whereby 75% are single enantiomers.^[14] The earliest commercial application of asymmetric hydrogenation was for L-DOPA (**5**) developed by KNOWLES in the 1970s (Scheme 2).



Scheme 2. Final two steps of the asymmetric synthesis of L-DOPA (**5**) developed by KNOWLES.^[1] DIPAMP **2** is a chelating diphosphine, where each phosphorus centre bears three different substituents, anisyl, phenyl and an ethylene group. COD = 1,5-cyclooctadiene.

The range of other applications for asymmetric hydrogenation was somewhat limited by the diversity of ligands accessible in the early years, but to date there are more than 1000 ligand systems available. More recently launched drugs, such as an intermediate for the potent atrial natriuretic factor potentiator Candoxatril (**7**)^[15], the HIV protease inhibitor Tipranavir (**8**)^[16], and the anticonvulsant Pregabalin (**9**)^[17] are reported to use the [(*R,R*)-Me-DuPhos Rh (COD)]BF₄ complex (**6**) for the asymmetric hydrogenation in the synthesis route (Figure 1). The name of the ligand DuPhos is derived from the chemical company DUPONT that developed this type of ligand and the compound class of phospholanes (Phos) it belongs to.^[16]

It can be noted that in the short term, chiral drugs will become the rule and that the new chemical entities (NCEs) which make it to the market will all be opti-

cally pure if a stereochemical centre is present. Thus chiral chemistry must become a state of the art method in organic chemistry.^[18]

As mentioned above, based on homogeneous catalysis the design of transition-metal catalysts for *cis*-hydrogenation has reached an impressive level, whereas the asymmetric *trans*-hydrogenation is still at an early stage of development.^[19] Despite the kinetic inertness of the transition metals, a certain cytotoxicity of the complexes cannot be excluded, which might be a disadvantage for usage in pharmaceutical syntheses.^[20]

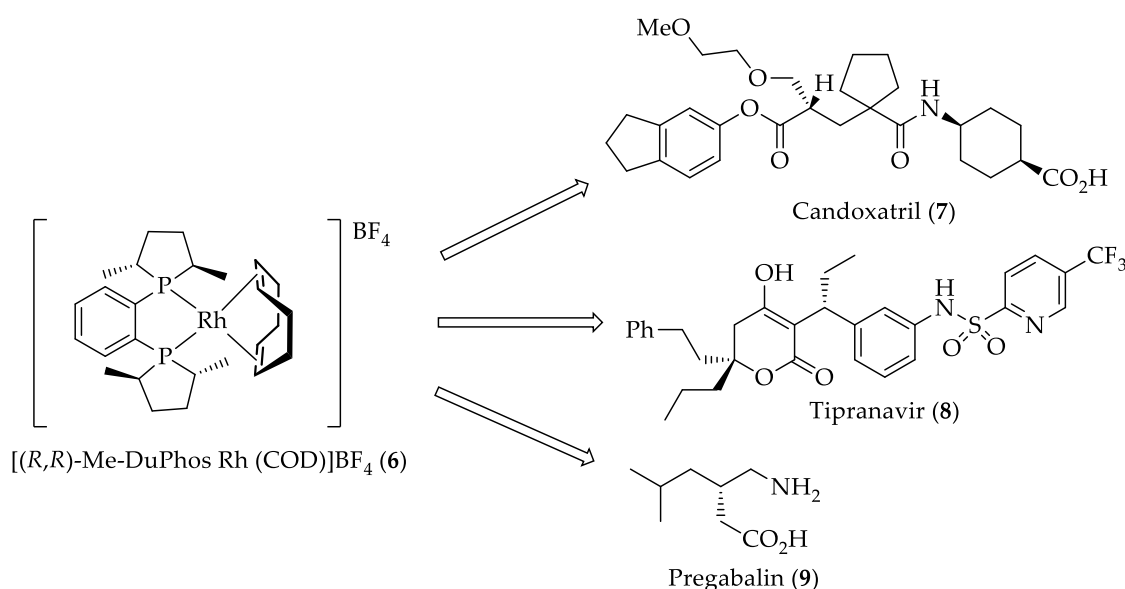


Figure 1. Pharmaceutical applications of Rh-Me-DuPhos **6** which is used in the synthesis of a key intermediate for the potent atrial natriuretic factor potentiator Candoxatril (**7**), the HIV protease inhibitor Tipranavir (**8**), and the anticonvulsant Pregabalin (**9**).^[16]

A better understanding of diseases at the molecular level will lead to structurally more complex and more diverse small-molecule pharmaceuticals and therefore need new synthetic tools.^[21] Due to their inherent chirality enzymes represent attractive alternatives to 'traditional' chemical catalysts.^[22] The method of choice for the derivatization of natural product leads will also be enzyme derivatization.^[21]

Therefore the field of biocatalysis is a rapidly growing area of research. The use of enzymes for the transformation of non-natural compounds, i.e. in organic synthesis, is one part in the field of biocatalysis.^[23] To use catalysts provided by

nature would be a great alternative due to their safety, environmentally friendly and stereoselective way of synthesis.

1.2 Biocatalysis in Organic Synthesis

The enormous catalytic potential of enzymes for asymmetric synthesis was discovered mainly during the 1980s.^[24] Enzymes are the proteins responsible for the catalysis of life. They are grouped into families and superfamilies defined by sharing a common ancestor, which can be identified by similarities in sequences and structures.^[25]

Most chemical catalysts catalyse a wide range of reactions. They are usually not very selective. In contrast enzymes are highly selective, catalysing specific reactions only. This specificity is due to the shapes of the enzyme molecules and their function in nature.^[26] With the help of biocatalysis process chemists and medicinal researchers will have an ever growing field of options for replacing expensive or toxic chemical reagents with more chemo- and stereoselective biocatalysts to conduct the synthesis routes in a more efficient and economically feasible way.

In the beginning, crude commercial enzymes extracted from microorganisms were applied in the food, detergent and tanning industries and it was more focused on examining activity and less on selectivity for the catalyst.^[27] In the 1990s chemists started to screen whole microbial organisms in the search for novel activities, but enzyme isolation was still a complex task. With the help of molecular biology, by means of genomics, proteomics and metabolomics, the sequence-based search for similar catalysts and the easy production via cloning and overexpression into a reliable host paved the methodology for efficient biocatalysis by chemists.^[28]

With the work of PERUTZ and KENDREW in the 1950s, X-ray diffraction of protein crystals began to provide structural information at atomic resolution.^[29,30] Today

the increasing number of available protein crystal structures is essential to understand the catalytic mechanism and to design new properties.^[31] To bring enzymes into industrial processes they must have specific properties like inheriting a desired substrate scope, stereoselectivity, catalytic efficiency, as well as robustness to organic solvents, high substrate loading, pH extremes and higher temperatures.^[32]

As a result of these considerable developments, nowadays various chemical reactions like asymmetric amination of ketones (transaminases), carbon-carbon bond formations (aldolases, oxynitrilases), oxidations (amine/alcohol oxidase, P450 monooxygenases, BAYER-VILLIGER monooxygenases) and reductions (ene reductases, amino acid dehydrogenases) as well as hydrolysis (nitrilases, nitrile hydratases, epoxide hydrolases) are performed enzymatically on an industrial scale.^[28,33,34]

The conversion of non-natural substances by enzymes is a break through, especially for pharmaceutically relevant targets and bulk chemicals.^[35] Due to the increasing demand of environmentally friendly processes, more often biocatalysis became an alternative for the production of low-cost bulk chemicals. The ability to develop the next generation of biocatalysts and adapt them to the process was enabled through protein engineering and design technologies in the last twenty years.^[36]

1.3 Protein Engineering

A desired conversion of a non-natural substrate or the improvement of existing biocatalysts in a laboratory or industrial process is often limited by the low performance of naturally existing commercially available biocatalysts. The process of altering the structure of an existing protein to improve its properties is described by protein engineering.^[37]

A protein engineering study involves three steps: choosing the protein changes (engineering strategies, such as rational design or randomization), making those changes (mutagenesis) and evaluating the protein variants for improved properties (screening or selection, see Figure 2).^[37]

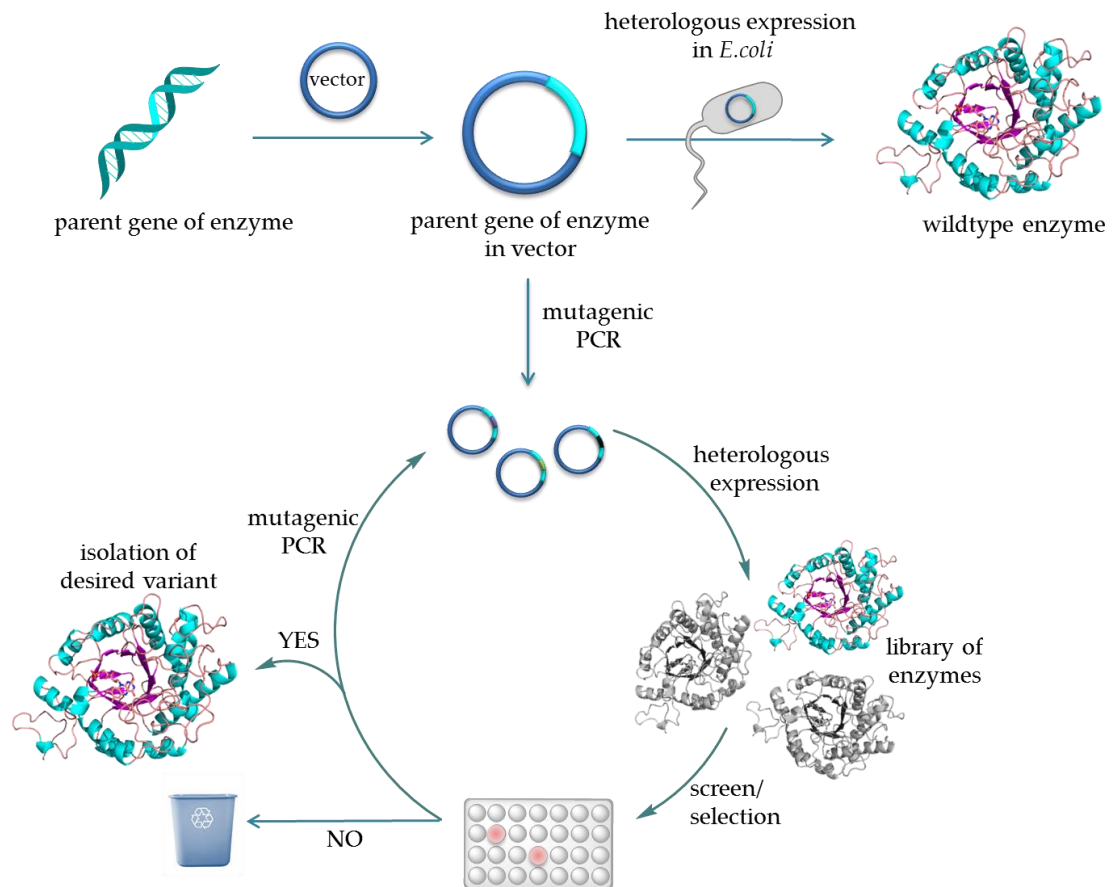


Figure 2. Workflow of a protein engineering study. First choosing the target enzyme and protein changes, second making these changes by mutagenesis and third evaluating the enzyme variants for improved properties through screening or selection.

First of all, the choice of the best location for amino acid substitution must be taken and depends on the preferred improvements. The X-ray structure of the enzyme can clarify the decision. For example to increase the thermostability of an enzyme, specific stabilizing interactions such as disulfide bonds or salt bridges can be introduced or highly flexible regions removed from the target protein.^[37] Other common goals are to increase the stereoselectivity or catalytic activity of enzymes. In this case substitutions closer to the active site give larger improvements in enantioselectivity or diastereoselectivity than substitutions

further away from the catalytic centre.^[38] In contrast, substitutions that increase the catalytic activity are scattered widely throughout the protein.^[37]

Once the location of the changes is set, the method for introducing single substitutions or, more likely, multiple substitutions must be chosen. For single substitutions, researchers can use site-saturation mutagenesis^[39] or error-prone PCR (epPCR).^[40] Site-saturation mutagenesis will substitute all nineteen possible amino acids at the chosen position, but epPCR randomly substitutes only an average of six of the possible amino acids over the selected DNA region.^[41]

Making multiple amino acid substitutions introduces extra choices. It is possible to make these substitutions stepwise, which will miss any cooperative interactions. Making them simultaneously creates an exponentially larger library wherein most of the variants are inactive, but cooperative effects can be observed at the cost of much more screening.^[42-44] Cooperativity is most likely between nearby amino acids, so the combinatorial active-site saturation test (CASTing) is a convenient method. It chooses two amino acids nearby in a linear sequence, so only one mutagenic primer is needed.^[45]

Another approach to handle simultaneous mutations is to reduce library size by eliminating duplicate codons. With the often used degenerated codon NNK (where N represents A, T, C or G, and K represents G or T) 32 possible codons are yielded to encode 20 amino acids, so 12 of the codons are duplicates. Whereby the NDT codon (where D represents G, A or T) yields 12 codons that encodes 12 different amino acids.^[46]

The third approach to deal with the large number of variants created by simultaneous mutations is a statistical approach called ProSAR, for protein structure-activity relationship.^[47] Even if the performance of a particular variant is poor, statistical comparison to other variants that contain the same substitution will reveal whether that substitution is beneficial or not.^[37]

The limitation in protein engineering is still the unknown structure-function relationship, which is often hard to predict. Therefore the engineering strategies have evolved from the first phase of rational design to the second phase with combinatorial design or 'directed evolution', and most recently to the third phase, data-driven design of biocatalysts.^[48] In Figure 3 an overview of these different protein engineering strategies is illustrated.

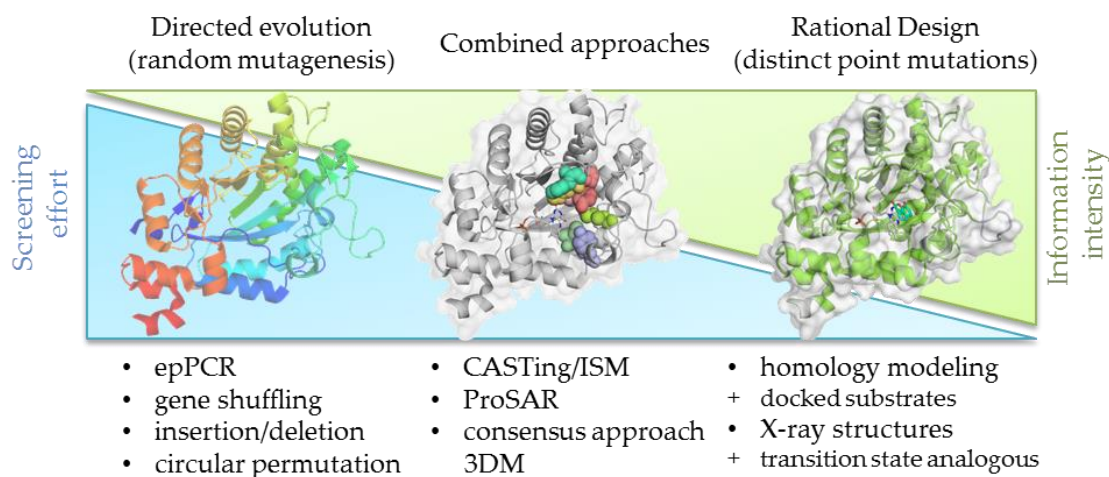


Figure 3. Overview of approaches for protein engineering methods. The evolutionary methods, like error prone PCR (epPCR) involve an enormous screening effort, whereupon little is known about the system. The combined approaches, like combinatorial active-site saturation testing (CASTing) and iterative saturation mutagenesis (ISM) provide a mean of screening effort and information intensity. Whereas for rational methods, like *in silico* studies with homology models and distinct point mutations a big amount of data must be known.^[49]

One approach is rational design, where structural and mechanistic information as well as molecular modelling is used to calculate a new enzyme structure with the desired properties. In order to achieve a process in which less laboratory screening is necessary and more robust information about the biocatalytic systems is available, the advances in computational technology plays a crucial role.^[50–53]

To be able to generate large libraries of enzyme variants and test them by high throughput screening (HTS) the directed evolution strategy was evolved.^[54–56] In directed evolution mutant libraries are created either by random changes, using methods such as gene shuffling or epPCR, or by semi-rational methods like site-saturation mutagenesis, and further screened for the desired property. The var-

iants showing promising results are subjected to further rounds of evolution (Figure 2).^[57] This strategy is, therefore, accompanied by a massive screening effort.

Iterative saturation mutagenesis (ISM) is a more efficient method for directed evolution of functional enzymes. By performing iterative cycles of saturation mutagenesis at rationally chosen sites in an enzyme, such as two or three amino acid positions important for catalytic properties, it reduces the necessary molecular biological work and the screening effort remarkably.^[57,58]

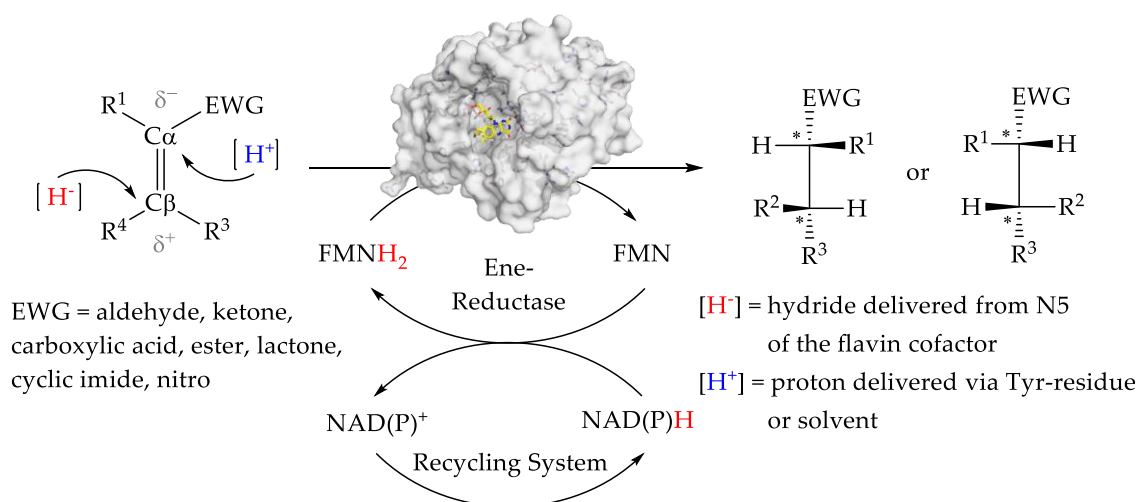
Another approach, the structure-guided consensus technique combines sequence-based and structural data and employs a set of phylogenetically diverse but functionally proven proteins. This data-driven protein design method utilizes structural information to limit the number of variants created.^[59]

The question arises: what strategy is the best? It would be the strategy that allows one to reach the goal with the least effort. This criterion makes it unlikely that a purely rational design or purely random mutagenesis approach will be the best. The available information from related protein structures, families and mutants is combined and further used for targeted randomisation of certain regions of the protein (Figure 3).^[49] The exponential growth in the field of enzyme engineering by more and more evolution based techniques and semi-rational design, based on the growing knowledge about genome sequences, number of X-ray structures and biochemical data, will require less screening effort.^[60]

Comparison will also establish principles of protein engineering and increase the understanding of how enzymes work. This understanding will make rational design more reliable and further speed up the path to expand the synthesis toolbox by biocatalysts.^[37]

1.4 The Old Yellow Enzyme Family

The Old Yellow Enzyme (OYE, EC 1.6.99.1) family is a large group of flavin-dependent redox biocatalysts with major applications in the industrial reduction of activated alkenes.^[61] These enzymes use flavin mononucleotide (FMN), a nicotinamide based hydride source (NAD(P)H), and the surrounding solvent for proton delivery to catalyse the *trans*-specific reduction of carbon-carbon double bonds of α,β -unsaturated carbonyl, nitro and cyano substrates to produce a variety of industrially useful compounds (Scheme 3).^[62]



Scheme 3. Asymmetric bioreduction of activated alkenes using flavin-dependent ene reductases. The FMNH₂ is non-covalently bound to the enzyme shown as yellow structure. EWG = electron withdrawing group.

As aforementioned this *trans*-hydrogenation is quite challenging in chemistry. Hence, the family has attracted quite some attention as tool in organic synthesis over the last years.^[23,24] Historically, OYE from *Saccharomyces pastorianus* (OYE1)^[63,64] was the first flavoprotein identified for its reductive activity on electron poor alkenes. Until today a wide variety of homologues has been discovered. These enzymes have been most commonly identified in bacteria^[65-70], plants^[71-83], and yeast, although a few have been found in other organisms.^[84-93]

The OYEs are divided in two groups, classic and thermophilic-like, which differ by their distinct sequence and structural characteristics.^[61,65,94] The overall physiological role of these enzymes is unknown, but OYEs from *Bacillus subtilis*^[95] and *Shewanella oneidensis*^[66] have been implicated in the oxidative stress response. OYEs from plants such as *Oryzae sativa* L^[96] and *Solanum lycopersicum*^[74] are known to be involved in the biosynthesis of the plant hormone jasmonic acid. An analysis of multiple sequence alignments of 19 OYEs shows that the overall sequence homology across group member is quite low, in total between 23-34% (Figure 4). But the amino acid sequence alignments show high conservation in selected regions of the protein, such as residues involved in catalysis, FMN and substrate binding.^[65]

		group 1											group 2							
		OPRI	OPR3	NemA	PETNR	XenB	Gox	NCR	OYE2.6	KYE1	OYE3	OYE1	OYE2	XenA	Rm ER	TOYE	Dr ER	Ts ER	YqjM	GkOYE
group 1	OPRI		56	42	42	42	39	38	34	36	40	39	39	26	24	29	27	25	26	27
	OPR3	56		41	40	42	41	37	31	34	36	37	37	25	25	27	28	27	24	28
	NemA	42	41		69	45	40	38	35	37	38	36	37	27	30	31	32	30	30	29
	PETNR	42	40	69		48	42	42	38	39	40	38	39	26	30	31	34	30	33	29
	XenB	42	42	45	48		46	48	35	35	39	38	38	30	31	32	34	31	31	32
	Gox	39	41	40	42	46		70	34	34	36	34	35	27	29	32	33	31	32	33
	NCR	38	37	38	42	48	70		30	32	35	32	32	29	29	30	31	30	30	30
	OYE2.6	34	31	35	38	35	34	30		41	41	41	41	25	25	27	25	24	26	25
	KYE1	36	34	37	39	35	34	32	41		68	72	72	24	26	25	26	24	24	25
	OYE3	40	36	38	40	39	36	35	41	68		80	82	23	26	26	26	23	23	26
	OYE1	39	37	36	38	38	34	32	41	72	80		92	23	26	24	27	24	25	25
	OYE2	39	37	37	39	38	35	32	41	72	82	92		24	26	26	27	24	26	26
	group 2	XenA	26	25	27	26	30	27	29	25	24	23	23	24		43	39	42	47	41
Rm ER		24	25	30	30	31	29	29	25	26	26	26	26	43		40	49	49	41	44
TOYE		29	27	31	31	32	32	30	27	25	26	24	26	39	40		46	50	53	53
Dr ER		27	28	32	34	34	33	31	25	26	26	27	27	42	49	46		52	48	50
Ts ER		25	27	30	30	31	31	30	24	24	23	24	24	47	49	50	52		50	55
YqjM		26	24	30	33	31	32	30	26	24	23	25	26	41	41	53	48	50		67
GkOYE		27	28	29	29	32	33	30	25	25	26	25	26	44	44	53	50	55	67	

pairwise sequence identity (%)

0	10	20	30	40	60	80	100
---	----	----	----	----	----	----	-----

Figure 4. The pairwise sequence identity analysis of 19 full length proteins shows 39-67%, 30-92% and 23-34% identity within group 1, within group 2 or across group member, respectively. Percent sequence identity matrix was created by Clustal 2.1 using EMBLs Clustal Omega web tool for sequence analysis with standard settings.^[97]

Whereas the structural alignment of members from both subgroups adopt a similar single domain (α,β)₈-barrel (TIM barrel) fold of the monomer homologue (Figure 5). OYE family enzymes are known to exist as monomers (PETNR^[98], RmER^[99]), active dimers (e.g. OYE1^[100]), tetramers (dimer of a dimer; YqjM^[94], TOYE^[65], TsER^[101]) and most recently multiple oligomeric states of thermostable homologues including octamers^[65,101] and dodecamers^[65]. The most

significant differences between the OYE structures are the positions and amino acid compositions of surface loops.

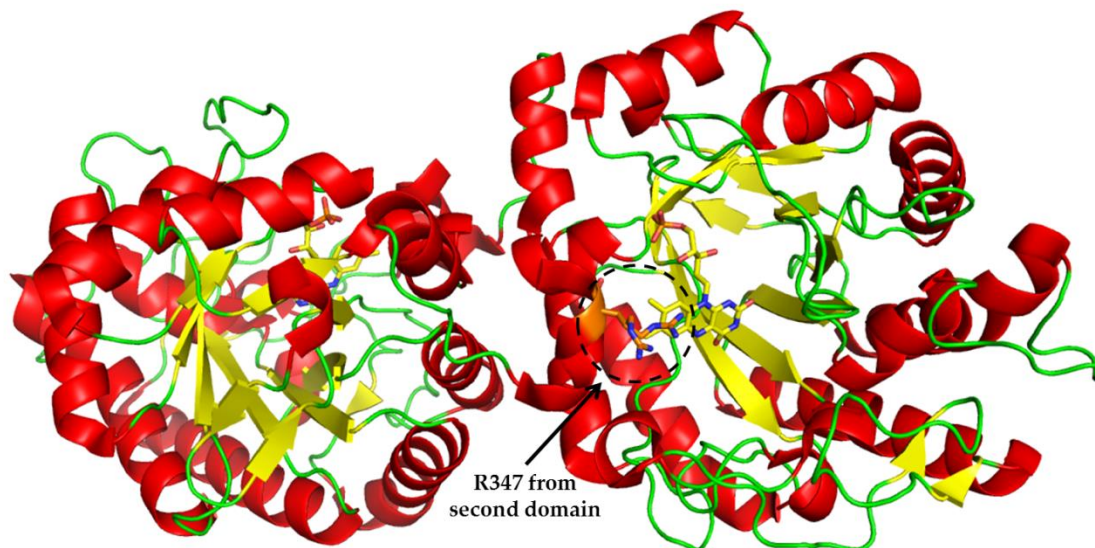


Figure 5. X-ray structure of TsER from *Thermus scotoductus* SA-01 (pdb 3HGJ^[101]) presented as active dimer. All OYE homologue monomers adopt a similar single domain (α,β)-barrel (TIM barrel). The active dimer of TsER is formed by interaction of R347 from one domain to the second (presented as orange sticks). α -Helices are red, β -sheets yellow and loops green. The non-covalently bound cofactor FMN is illustrated as yellow sticks.

The active site architecture is remarkably similar, despite the low sequence homology of OYEs (Figure 6). The binding site displays highly conserved residues, like the H181 and H/N184 (PETNR numbering) as anchor points for the carbonyl (EWG) coordination and the tyrosine in position 186 as potential proton donor for the asymmetric hydrogenation. Residue T26 in group 1 and the highly conserved cysteine at this position in group 2, interacts with the FMN isoalloxazine ring O4 atom and is known to influence the flavin redox potential by stabilizing the negative charge of the reduced flavin.^[101–103] In group 1, W102 is a highly conserved residue, whereas in group 2 the same spatial position is occupied by small amino acids, like alanine and glycine. This exchange may improve the binding of more bulky substrates within the active site and contributes to the overall increased active site volume in this subgroup.

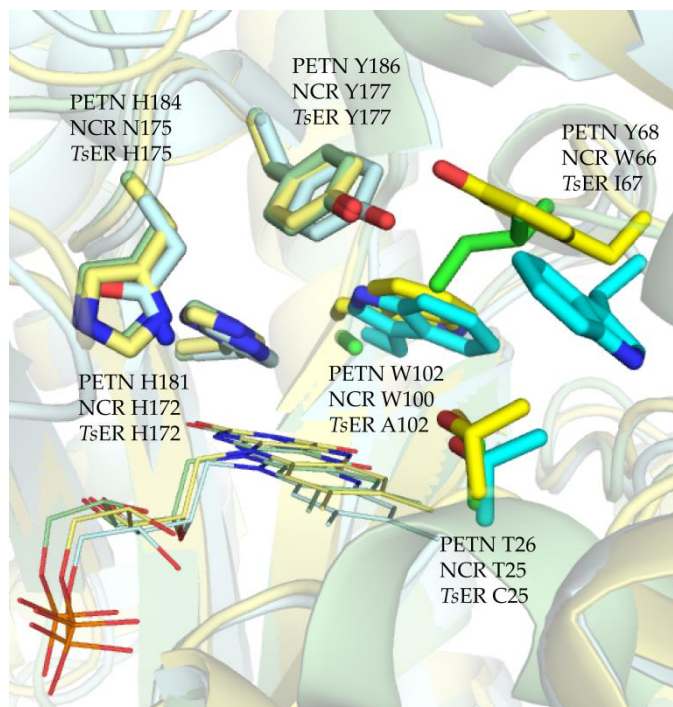


Figure 6. Active site of the structural alignment of PETNR from *Enterobacter cloacae* PB2 (group1, yellow, pdb 3P81), NCR from *Zymomonas mobilis* (group1, cyan, pdb 4A3U) and TsER from *Thermus scotoductus* SA-01 (group2, green, pdb 3HGJ) with PyMOL v0.99. The highly conserved residues of both groups are shown in sticks, the non-covalently bound FMN as lines.

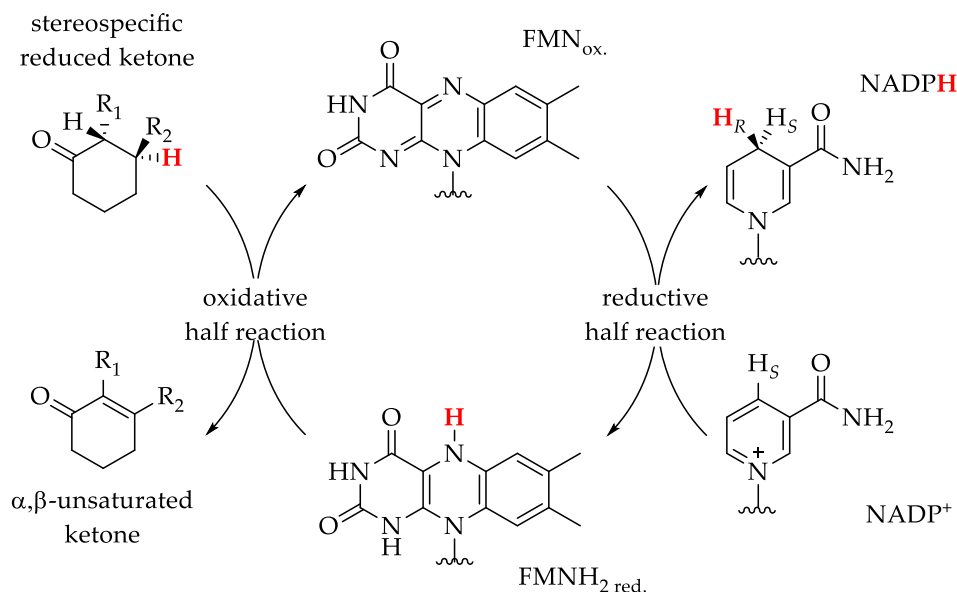
The reaction mechanism of *trans*-specific hydrogenation is described in the following chapter.

1.4.1 Reaction Mechanism of the OYE Family

OYEs are biocatalysts for asymmetric hydrogenation of electron-poor alkenes with high *trans*-selectivity. The reaction mechanism occurs via a bi-bi ping-pong mechanism, where the reductive and oxidative substrate binds in the same active site.^[102]

In the first part, the reductive half reaction takes place, which proceeds in three kinetically distinct steps.^[104] Initially the reductive reagent NAD(P)H binds in the oxidized enzyme where the hydride transfer occurs to the cofactor FMN (Scheme 4). Based on a crystal structure of OYE1 in complex with NADP⁺ it is well appreciated, that the amide oxygen of the nicotinamide ring undergoes a hydrogen bond formation with the highly conserved H191/N194 residues,

the bioreduction of alkenes bears a strong resemblance to a Michael-type 1,4-addition of a hydride to a conjugated carbon-carbon double bond.



Scheme 5. The catalytic mechanism of the asymmetric reduction of alkenes catalysed by ene reductases from the OYE family. The hydride is stereoselectively transferred onto C_β from the N5 of the reduced FMN.

With some substrates it was observed, that the stereoperference and enantiopurity of the products are influenced by the choice of reaction conditions, namely oxygen level and the buffer conditions.^[61,109]

Important to appreciate is the diversity of flavoenzyme chemistry caused by the tricyclic isoalloxazine ring system of flavins.^[110] Although the redox potential for two-electron reduction of flavin lies at -200 mV, it can be modulated by the enzyme environment to span a range from -400 mV to $+60$ mV, thus conferring diverse reactivity to the enzyme.^[111,112]

One additional reaction can occur with molecular oxygen to affect C=C-epoxidation, C-H-hydroxylation and R-SO₃H-, R-NO₂-, alcohol-, amine-, thio-ether- and Baeyer-Villiger-oxidations.^[110] It is also known, that flavoenzymes are involved in redox-neutral processes, such as C=C-isomerization, magnetoreception and light-responsiveness.^[113–115]

In flavin-dependent ene reductases, like OYEs, in addition to hydride transfer from/to nicotinamide, the FMN cofactor can also function as an acid/base catalyst in redox neutral isomerization reactions, or it may directly transfer a hydride between two substrate molecules in a disproportionation reaction, bypassing the otherwise essential nicotinamide cofactor.^[110]

All of the diverse chemical reactions, that are possible with ene reductases from the OYE family make these extremely versatile catalysts an interesting component for organic synthesis.

1.4.2 Bioreductions with Ene Reductases

The OYE family has been shown to be able to reduce an extensive diversity of α,β -unsaturated alkene compounds (see Figure 7).

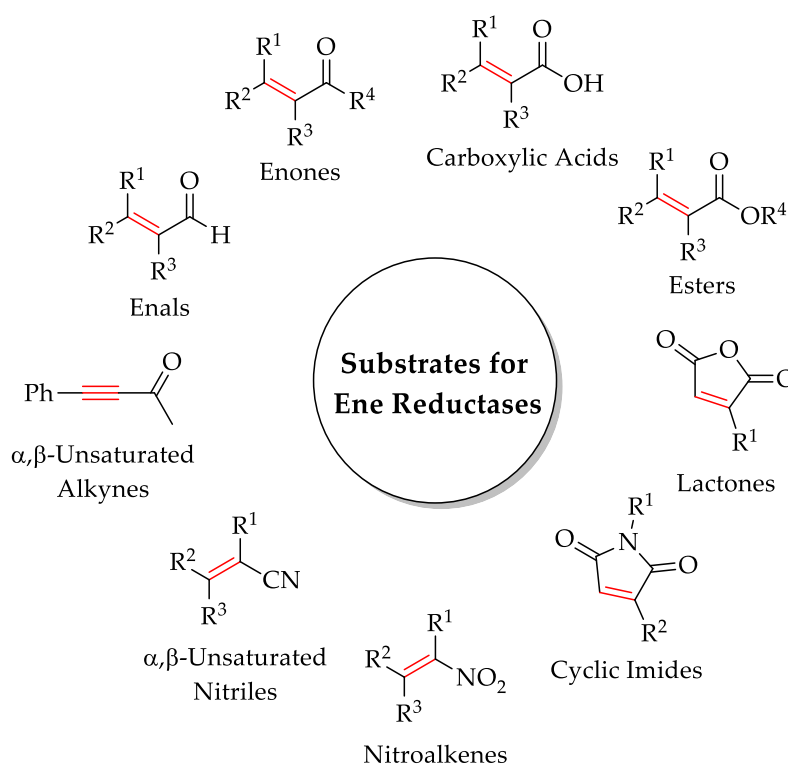
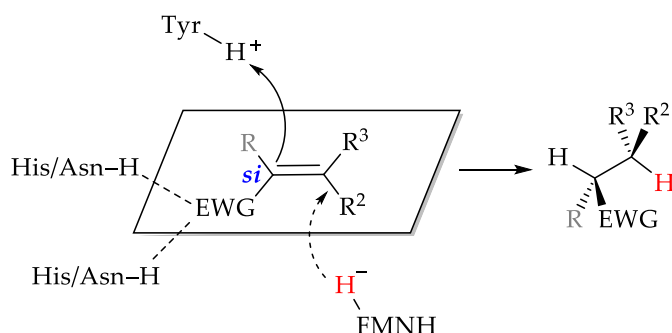


Figure 7. List of substrate classes, which have been shown to be convertible by ene reductase hydrogenation.

They typically contain electron-withdrawing groups, like aldehydes, acyclic and cyclic ketones, carboxylic acids, esters, cyano or nitro functionalities, which build a Michael acceptor system.

As mentioned before, the electron withdrawing group (EWG) enables an interaction with the highly conserved H/H or H/N in the binding pocket of OYEs to position the substrate for hydride transfer. The final stereochemical outcome depends on which stereoheterotopic faces of the alkene are available for hydride and proton addition, according to the orientation of the substrate in the active site.^[116] Until now, two possibilities have been described: the so-called 'normal' or 'flipped' binding pose (Figure 8).^[117]

A) 'normal' binding pose



B) 'flipped' binding pose

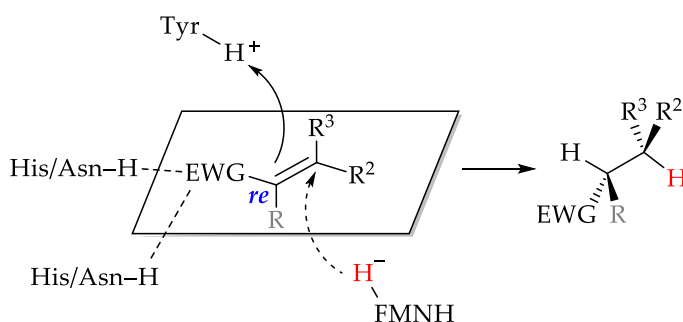


Figure 8. Mechanism of OYE-mediated reduction of carbon-carbon double bonds, according to two possible substrate-binding modes. The priority rules employed to assign stereochemical descriptors are following ones: for double bonds EWG > R, R³ > R²; for stereoheterotopic faces EWG > =CR²R³ > R.^[116]

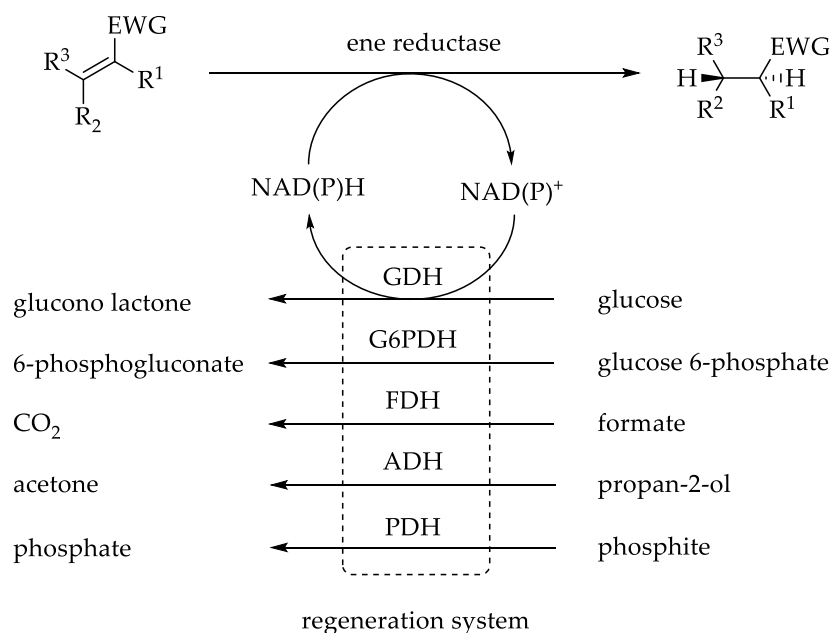
In the normal binding pose the compound is bound in such a way that the proton is delivered to the C_α-*si* face, whereas in the flipped binding pose it will be delivered to the C_α-*re* face.^[117] Most substrates are not tightly bound in the active

site, which gives the possibility of both binding orientations, explaining the sometimes low enantiomeric excess (*ee*) of the product by ene reductase hydrogenation.^[118,119]

One difficulty in using biocatalytic versus synthetic hydrogenation of activated alkenes is the necessity of an external expensive reducing agent, like NAD(P)H. The vast majority of biotransformations using ERs have been performed using whole cells, most prominently being baker's yeast^[120–123] and bacteria.^[124–126] With this strategy cofactor recycling issues are avoided, because the reducing agents get produced and recycled by the cells. The usefulness of this technique however, is limited due to the frequent poor product yields often caused by side reactions such as carbonyl group reduction, ester hydrolysis, acyloin reactions and acetyl cleavage caused by other enzymes present in the cell.^[61]

This disadvantage can be overcome by the use of purified enzymes, but requires again the presence of either large quantities of cofactor or, more efficiently, a suitable recycling system. This so-called coupled enzyme approach, where an additional enzyme is present in the reaction medium together with an inexpensive sacrificial cosubstrate like glucose, is broadly used (Scheme 6). The choice of the regeneration system should take into account that the resulting coproduct does not have negative consequences on the catalytic efficiency, like inhibition effects. Moreover the chosen regenerating enzyme should not inherit a catalytic activity towards the used target substrate and product, such as carbonyl reduction.

The common enzyme systems used for regeneration are glucose dehydrogenase/glucose, glucose 6-phosphate dehydrogenase/glucose 6-phosphate, formate dehydrogenase/formate, alcohol dehydrogenase/propan-2-ol and phosphite dehydrogenase/phosphite.^[23]



Scheme 6. Cofactor Regeneration Systems in ene reductase catalysed hydrogenation reactions. GDH = glucose dehydrogenase, G6PDH = glucose 6-phosphate dehydrogenase, FDH = formate dehydrogenase, ADH = alcohol dehydrogenase and PDH = phosphite dehydrogenase.^[23]

1.5 Challenges in the Field of Bioreductions with OYEs

Although the OYE from *Saccharomyces carlsbergensis* was isolated in 1933^[127], the use of ERs as biocatalysts in stereoselective carbon-carbon double bond reduction still needs further development, especially for substrate scope and stereo-complementarity. A major challenge in the field of carbon-carbon reduction employing OYE homologues is the current lack of global understanding of what governs selectivity and activity.

So far the substrate scope for ene reductases is most often shown with small five and six membered ring compounds.^[23,61] But a better understanding of diseases on molecular level will lead to structurally more complex and more diverse small-molecule pharmaceuticals.^[21] If OYEs would accept such structurally demanding compounds, they could be used at a late stage in the synthesis.

The big challenge in *trans*-hydrogenation with ERs is the access of both enantiomers, since stereocomplementary pairs of OYE wild types (wt) for control of

facial selectivity are extremely rare and substrate specific among the OYE family.^[73,84,128,129] To get stereocomplementary products, a flipped binding mode has to be enabled, for high enantiomeric excess even selectivity favoured over the normal binding mode. This, especially for bulkier substrates, could be difficult because of steric hindrance in the active site (see Figure 8).

2 OBJECTIVE OF THE THESIS

This thesis focuses on the engineering of ene reductases from the Old Yellow Enzyme (OYE) family. These new ene reductases will have superior substrate scope, stereocomplementarity and handling properties to establish them as industrially relevant catalysts in organic synthesis. The work presented here is divided into four main parts:

Part One: *Scaffold Sampling Strategy for the OYE Family*

Analysing the existing knowledge about the OYE family from labor intensive directed evolution studies, will allow the identification of beneficial mutations to achieve desired properties, such as expanded substrate scope or stereocomplementarity. The transferability of these engineered residues to other members of the OYE family to rationally design new catalysts is investigated here.

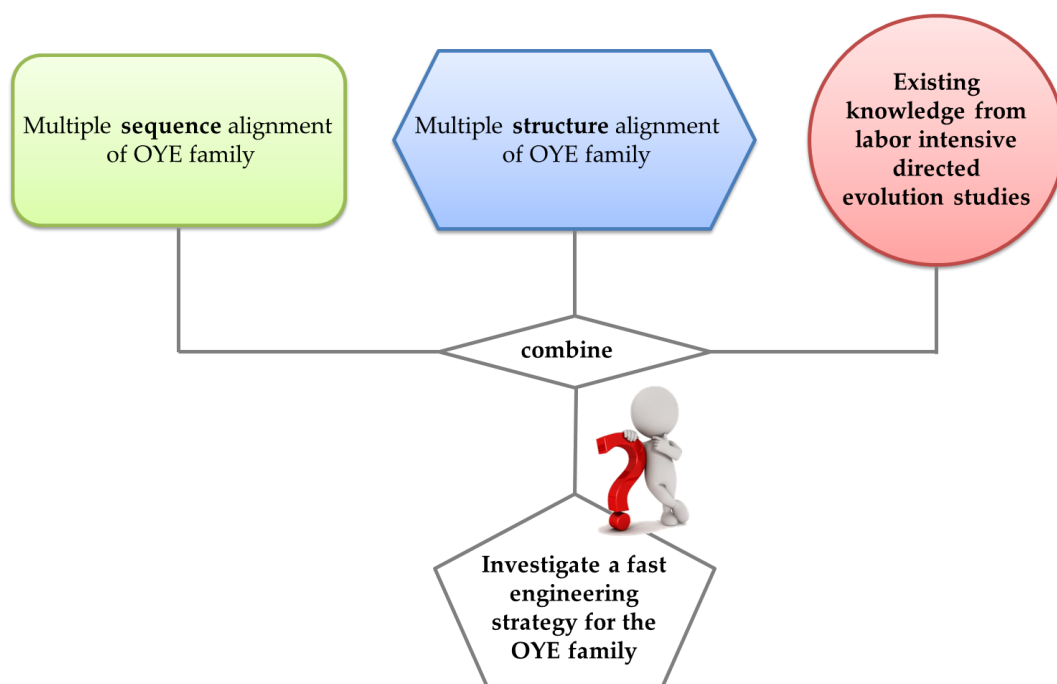


Figure 9. Working hypothesis for engineering the OYE family via the scaffold sampling strategy.

This so-called scaffold sampling strategy should reduce the search space involved in the directed evolution process, providing a shortcut to the discovery of new potent ene reductase variants, which should give access to both stereoisomers of selected substrates.

Identified hot spot residues of YqjM from *Bacillus subtilis* for the model compound 3-methylcyclohex-2-en-1-one, i.e. C26D/I69T and C26G for activity and selectivity, respectively, will be transferred to seven OYE scaffolds. One of these scaffolds is a thermostable ER, which might be, due to its robustness, more interesting for applications in organic synthesis. This tested strategy would provide a fast engineering method for this enzyme family allowing access to new, potent biocatalysts for organic synthesis.

Part Two: *Characterization of a Robust and Stereocomplementary Panel of Ene Reductases from Thermus Scotoductus SA-01 (TsER)*

The second section will cover the full characterization of a robust ene reductase variant panel from *Thermus scotoductus* SA-01 (*TsER*). Here, it will be demonstrated that *TsER* variant pairs can form a small panel of engineered ene reductases that combine a broad substrate scope, tolerance to organic solvents and high temperature with convenient catalyst handling and control over facial selectivity (Figure 10). This combination of properties allows improved handling at gram-scale and conversion of poorly water-soluble compounds. The control over facial selectivity will be examined for a broad substrate scope.

In collaboration with D.J. OPPERMAN (University of the Free State, Bloemfontein), crystal structures of *TsER* variants will be obtained to provide structural insights into the factors controlling stereoselectivity and achieving activity towards non-substrates for the *TsER* wild type.

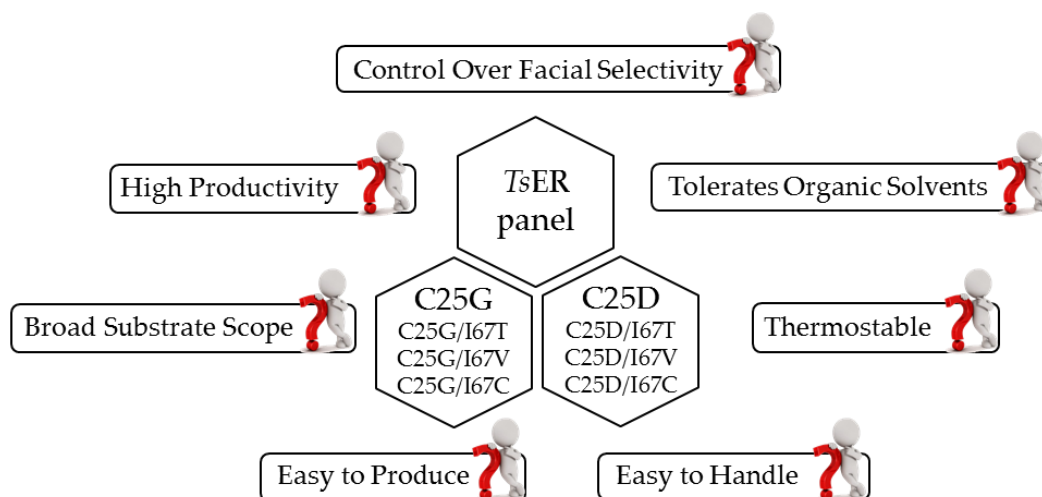


Figure 10. Characterization of ene reductase variants from *Thermus scotoductus* SA-01 (*TsER*) derived from part one. Investigation of properties and advantages of these variants for applications in organic synthesis.

Part Three: Prediction of Substrate Binding and Affinity towards *TsER* variants by Computational Methods

As mentioned in the introduction a major challenge in the field of carbon-carbon reduction employing OYE homologues is the current lack of global understanding of what governs selectivity and activity. To set up general rules the experimental studies will be examined with the help of fundamental computational methods.

Theoretical studies, such as those employing docking, molecular dynamics simulations and hybrid quantum mechanics/molecular mechanics (QM/MM) simulations, can provide important insights into mechanistic details that may not be possible via experimental means. Relatively few theoretical studies have been performed on the OYE family.^[130–132]

Performing *in silico* studies with the obtained *TsER* variant panel will gain a better understanding of the factors governing substrate acceptance and facial selectivity. More importantly, the docking data will be analysed to see whether the predicted stereochemistry matches the experimental observations.

Additionally, molecular dynamics simulations combined with methods for predicting binding free energies will clarify substrate affinity, which will allow a computational pre-screening for new substrate libraries.

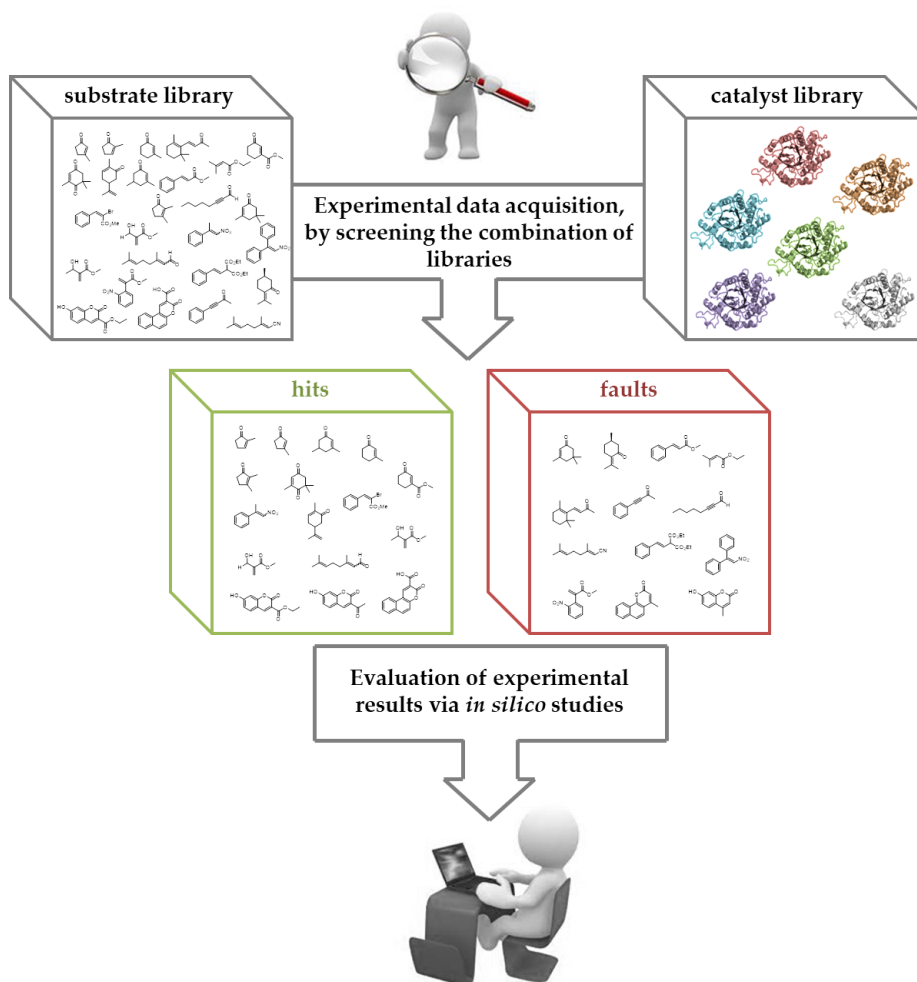


Figure 11. Workflow for using computational methods to gain more information about the experimental results.

Part Four: *Development of a Set of Compounds as Molecular Probes for Active Site Geometry*

In the fourth section, the substrate scope of TsER will be expanded to bulkier substrate classes such as indole and coumarin derivatives. The different coumarin scaffolds, shown in Figure 12, should help to obtain insights into the binding pocket of TsER for the identification of potential new engineering residues. Due

to the fluorescent properties of the used coumarin derivatives, an easy and fast fluorescence screening will be established.

To achieve this, all coumarin scaffolds have first to be synthesised and secondly, another round of mutagenesis must be performed to create a set of active site libraries. In general, there is a great interest in broadening the substrate scope of ene reductases to bulkier substrates to use these highly selective *trans*-hydrogenation catalysts in the late stage synthesis of complex organic molecules. So far the substrate scope is most often shown with small five and six membered ring compounds.

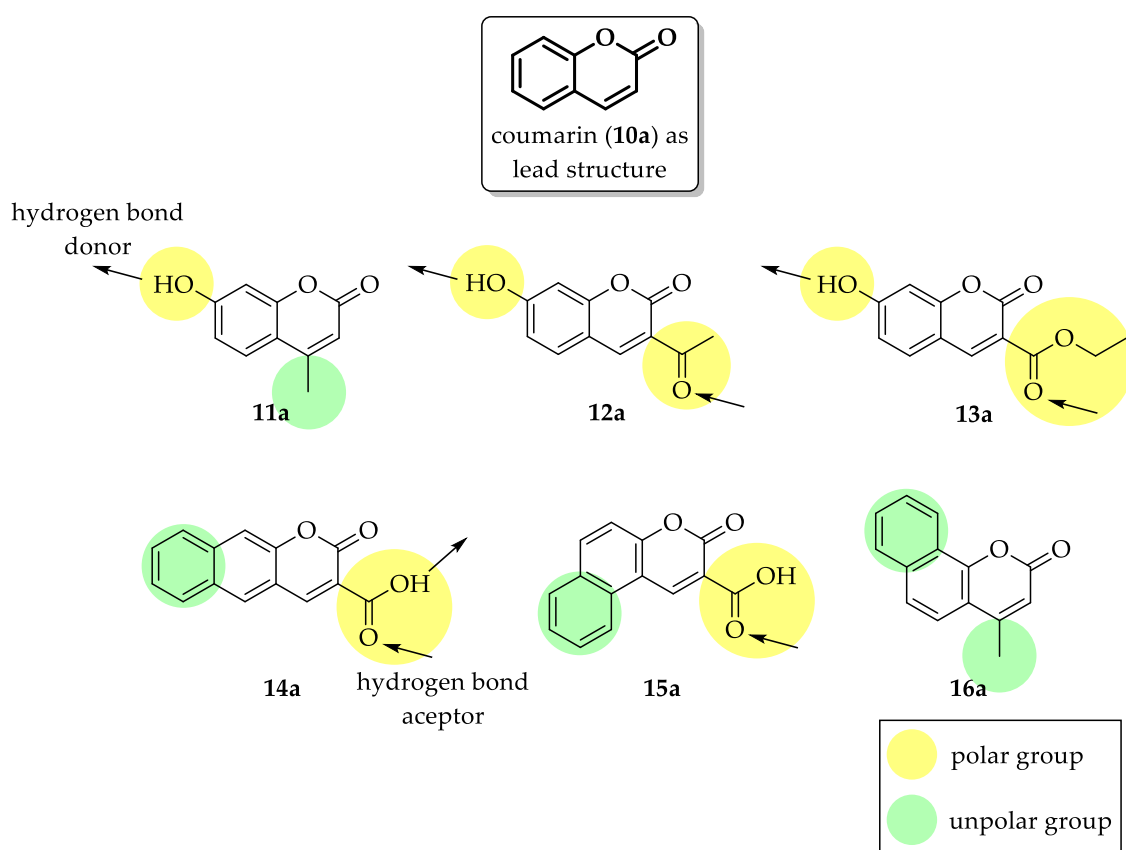


Figure 12. Different structural scaffolds based on coumarin (10a) to obtain insights into the active site of *TsER* for finding potential new engineering sides to convert more bulky substrates with ene reductases from the OYE family. Arrows are indicating possible, further introduced sites for hydrogen bonding.

3 RESULTS AND DISCUSSION

3.1 Scaffold Sampling Strategy for the OYE Family

3.1.1 Review of the Recent Literature

Implementing enzyme catalysis as a diverse compilation of tools into our chemical synthesis toolbox is a busy research area and a prerequisite for the 21st century of sustainable synthesis. The need to improve and adapt Nature's given catalysts is high and protein engineering, as well as directed evolution, is inevitable as we currently lack sufficient knowledge to design *any* functional enzyme from first principles.^[133–135] Engineering principles cycle iteratively through stages of '*design-build-test-learn*' to optimize a system for a defined application. The more data and engineering strategies are available, the better the outcome. Every year numerous directed evolution studies are published, either increasing the data an enzyme engineer can use as knowledge base or adding refined and new strategies to the protein engineer's repertoire.

Considering that natural evolution "repeats itself", as does experimental evolution in the laboratory,^[136] obtaining the existing knowledge from labor intensive directed evolution studies and transferring it to homologous protein scaffolds, may allow guided traversing through the sequence space and shortcutting biocatalyst development.

Indeed, two recent studies have provided first evidence that this shortcut to enzyme engineering is possible in two distinct enzyme families.^[137,138] Scaffold sampling through transferring non-natural mutations is a result of two merged concepts: The transfer of non-natural occurring mutations from one to another

homologous protein structure^[139,140] and the transfer of natural mutations obtained by the consensus approach to several scaffolds.^[59]

The consensus method is a related engineering strategy, where multiple sequence alignments of wild types are used to identify Nature's solutions for an addressed enzyme trait.^[141] This "check nature first, than evolve"^[142] strategy includes rational assignment of function to key sequence motives as well as using the obtained diversity as a small amino acid alphabet for smart library creation.^[143-145]

In fact, transfer of naturally occurring residues or mutations to another closely-related enzyme is widely used to improve properties.^[136] But it is also known that most improved variants from directed evolution do not occur naturally.^[146] In addition, and contrary to the consensus approach and its derivatives, directed evolution also reveals beneficial mutations in positions of high sequence conservation.^[141,142] As a point of fact, many empirical discovered hotspot residues are conserved in sequence and structure, even among sequences that share little overall sequence identity. Once being responsible to ensure the natural function, such conserved sites are no longer subjected to do so and are free to adapt to the new non-natural environments.

One of these families with high conservation in the active site is the ene-reductase family of OYEs. The active site architecture and sequence is rather conserved despite a low overall sequence identity. Minor differences in volume have been shown to cause the reported diversity in substrate scope and stereoselectivity. The natural function is under debate, but the family can use flavin and NADPH to catalyse the trans-specific reduction of α,β -unsaturated carbonyl, nitro and cyano compounds (see chapter 1.4). Therefore it has attracted quite some attention for synthesis in recent years and a fast engineering strategy for this family would further benefit this area.

The OYE family consists of two subclasses and protein engineering and directed evolution studies are available for both.^[67,91,147–152] They revealed several hotspot residues, and as expected, most of the newly identified amino acids at these positions do not occur naturally in other homologues of the family. Engineering of YqjM from *Bacillus subtilis* identified the combination of C26D/I69T for an increased specific activity towards the model compound 3-methyl cyclohexenone (**17a**) and seven additional compounds, while preserving excellent enantioselectivity.^[67] In addition, the highly conserved residue C26 turned out to be a stereocontrolling switch, yielding the other enantiomer when changed to C26G.

Building on this basis of BOUGIOUKOU *et al.*, the presented thesis hypothesized that the DT and G mutation, discovered in one OYE, would induce the same function when transferred to homologous OYE scaffolds. Of special interest is the transfer of excellent activity to the thermostable family member TsER from *Thermus scotoductus* SA-01. To test if the newly emerged shortcut strategy is generally applicable in OYE, three additional members from subclass 1 and three from subclass 2 were chosen, which have already been used in cascade reactions^[153–157] and large scale synthesis^[128].

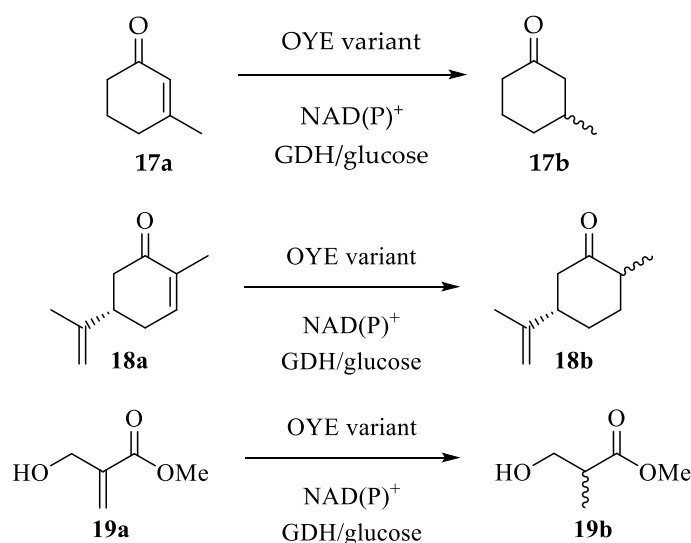
3.1.2 Target Positions for Presented Transferability Study

In the presented thesis the strategy was examined with the potential industrially interesting ene reductases from the Old Yellow Enzyme family. OYEs use flavin and a nicotinamide based hydride source to catalyse the *trans*-specific hydrogenation of α,β -unsaturated carbonyl, nitro and cyano compounds.

Because only medium and low throughput screens based on gas or high-pressure liquid chromatography are suitable for most OYE transformations, effective strategies for engineering of family members by avoiding screening-

intensive protein engineering or directed evolution studies are needed. The big challenge therefore is the access of both enantiomers, since stereocomplementary pairs of OYE wild types (wt) for control of facial selectivity are extremely rare, and substrate specific among the OYE family.^[73,84,128,129] To get stereocomplementary products from the same enzyme, both binding modes, the normal and flipped poses have to be enabled. For high enantiomeric excess, selectivity favoured over one binding mode must be given. This, especially for bigger substrates, could be challenging because of steric hindrance in the active site.

Evaluating the existing OYE protein engineering literature reveals that OYEs have been mostly evolved towards three common compounds (Scheme 7).



Scheme 7. Most common transformation in directed evolution and protein engineering studies of OYE for control of facial selectivity of the hydride attack. The goal is to find complementary catalyst pairs allowing access to both enantiomers with excellent stereoselectivities.

The first discovered OYE variant from PADHI *et al.*, able to switch facial selectivity, was W116I in OYE1 from *Saccharomyces pastorianus* for the reduction of (*S*)-carvone ((*S*)-2-methyl-5-(prop-1-en-2-yl) cyclohex-2-en-1-one, **18a**) to (*2S,5S*)-**18b**.^[91] The wild type enzyme and the W116F variant produce (*2R,5S*)-**18b**, as well as all other reported OYE wild types. Interestingly, W116X variants were identified by an activity based screening for the reduction of 3-methylcyclohex-2-en-1-one (**17a**), but no flip in stereoselectivity was observed.^[91]

The second stereocomplementary pair reported by BOUGIOUKOU *et al.* was the C26G and C26D/I69T variants of YqjM from *Bacillus subtilis*, allowing access to both enantiomers for the reduction of 3-methylcyclohex-2-en-1-one (**17b**).^[67] Also, YqjM variants with mutations in A104 were found to contribute to higher (*R*)-selectivity, which are analogous to W116 of OYE1 in hotspot position III (Figure 13).

When the precursor methyl-2-(hydroxymethyl)-acrylate (**19a**) of the industrial important 'Roche ester' **19b** was introduced as an OYE substrate, all tested wild types produced (*R*)-**19b**.^[158] Access to (*S*)-**19b** was achieved upon discovery of OYE2.6 from *Pichia stipites* by WALTON *et al.*^[159] The same study also showed that single site saturation mutagenesis of OYE1 at hotspot position W116 likewise produced stereocomplementary variant pairs for **19b**. In a follow up directed evolution study, additional complementary pairs with improved conversion levels were discovered for the OYE2.6 scaffold.^[160] Lately, a rational design study identified variants C26N/I69A and I69A/H167A of YqjM to induce the same stereochemical flip.^[152] In addition to the aforementioned studies, a few single-residue saturation mutagenesis^[161–165], rational design^[151,166] or directed evolution studies^[167,168] exist, which allow extraction of beneficial mutations.

Taken all together, several hotspot positions have been identified through immense literature research and especially positions I, II and III (Figure 13) were found to control facial selectivity, activity and substrate scope in OYE1, OYE2.6, PETNR, KYE and YqjM.^[67,91,160,162,165]

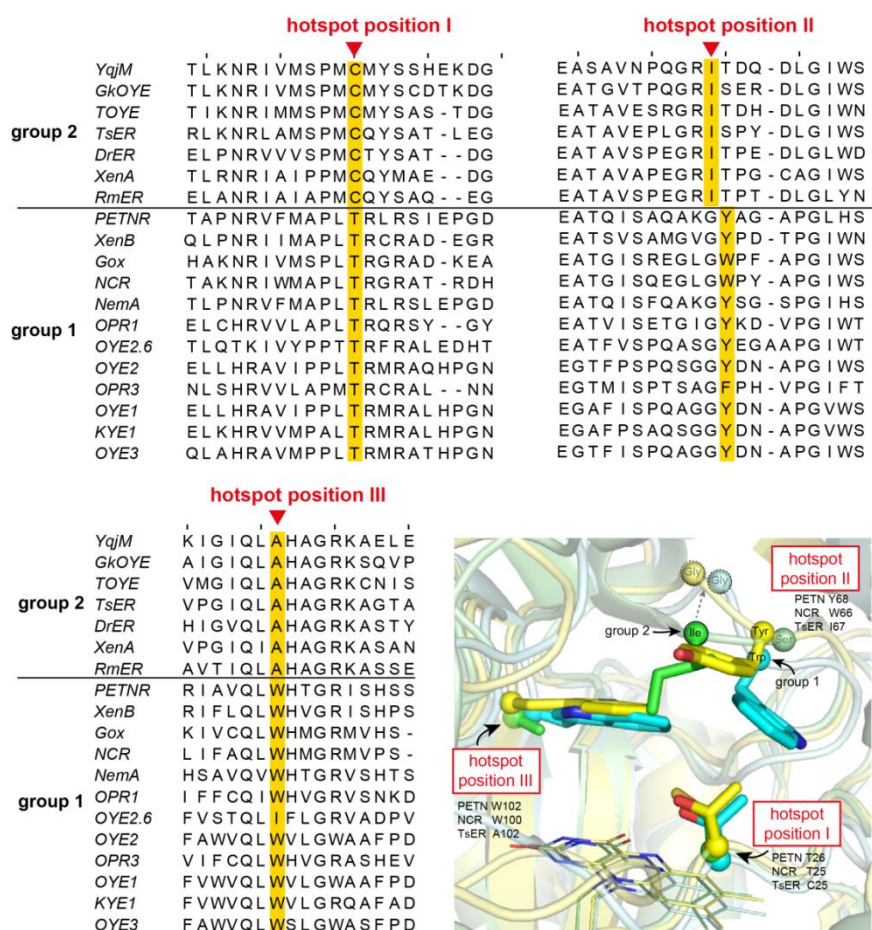


Figure 13: Sequence alignment showing position and residues of hotspots in primary and tertiary structure of wild type OYEs, which have a low sequence homology across group member (23-34%) and which consist of two subgroups, possessing distinct conserved residues at targeted hotspot positions.^[61,169] Sequence alignment was created with Clustal Omega and sequences are sorted by pairwise identity. Structures of *TsER* (3HGJ, green)^[101], *PETNR* (3P81, yellow)^[161] and *NCR* (4A3U, cyan)^[170] have been aligned using PyMOL 1.5.x. Residues at hotspot positions are shown as sticks, FMN as lines. The C_{α} atoms of residues are shown as spheres. The side chains of hotspot position II fill the same space, but residues have different positions in primary structure.

Probing of all combinatorial possibilities arising from empirically identified hotspot positions including their amino acid combinations, the screening substrates and available OYE scaffolds, would be too resource intensive. Therefore this presented study was restricted to seven scaffolds, three groups of variants and three substrates (17a-19a). The scaffolds from group 1 are *NCR* from *Zymomonas mobilis*, *XenB* and *NemA* from *Pseudomonas putida* ATCC 17453 and from group 2 *XenA* from *Pseudomonas putida* ATCC 17453, *TsER* from *Thermus scotoductus* SA-01, *RmER* from *Ralstonia metallidurans* and *DrER* from *Deinococcus radiodurans*. The created variants for all of these scaffolds contain the afore-

mentioned stereoselective switch residues for group 2 member, which are glycine and aspartate in hotspot positions I and threonine in hotspot position II (see Figure 13). Also the isoleucine residue in hotspot position III, which is responsible for a stereoselective switch in group 1 was introduced in scaffolds from both groups, namely NCR and *TsER*.

Wild type scaffolds were partially selected based on their proven potential as bio-catalyst in cascade reactions^[153–156,171], large scale synthesis^[128,172,173], use of NAD(P)H mimics^[174] or stability.^[101,175] With this setup, the OYE family was tested for specific response when applying the scaffold sampling strategy. The focus is on accessing new stereocomplementary variants with preparative useful turnover numbers and if the new OYE biocatalysts are superior relative to their starting scaffolds and to the original engineered wild types.

3.1.2.1 Creation of the OYE Variants by Rational Design

The overall high GC content (63-70%) of the seven OYE genes used in this thesis and the local occurrence of stable secondary DNA structures at hotspot positions have made mutagenesis of used OYE scaffolds more challenging than expected compared to previous mutagenesis experience of *YqjM* (46% GC content). Quik Change and megaprimer based mutagenesis protocols, betaine and/or DMSO as additives, new primer design, as well as hot-start methods were tried. Megaprimer, hot-start and additives were an absolute requirement for successful mutagenesis in *ncr*, *tser*, *rmer* and *drer* genes. The genes of *xenA* and *xenB* were more challenging and after several rounds of PCR optimisation, mutagenesis of these genes was not further pursued. The *nemA* gene was most resistant to the mutagenesis trials and only C26D was obtained. In combination with an extremely low expression level in *E. coli*, it disqualifies NemaA as an enzyme with biocatalytic potential.

The introduction of the mutations in hotspot positions I-II for all OYE scaffolds were achieved in collaboration with SABINE DUEWEL^[176] and ALEXANDRA A. RICHTER.^[177] After introducing aspartate/glycine at hotspot position I and threonine at hotspot position II into *TsER*, *RmER*, *DrER*, NCR and *XenB*, a first heterologous expression test with wt and all 14 variants was performed. To avoid a later falsification of biotransformation data due to contaminations with *E. colis'* own OYE, a $\Delta nemA$ knockout strain for enzyme production was used.^[178] The tested expression conditions and subsequent activity test showed the necessity to reduce the expression temperature to 22 °C after induction with only 10 μ M IPTG. The OD₆₀₀ normalized SDS-PAGE analysis (Figure 14) reveals that the tested variants were produced.

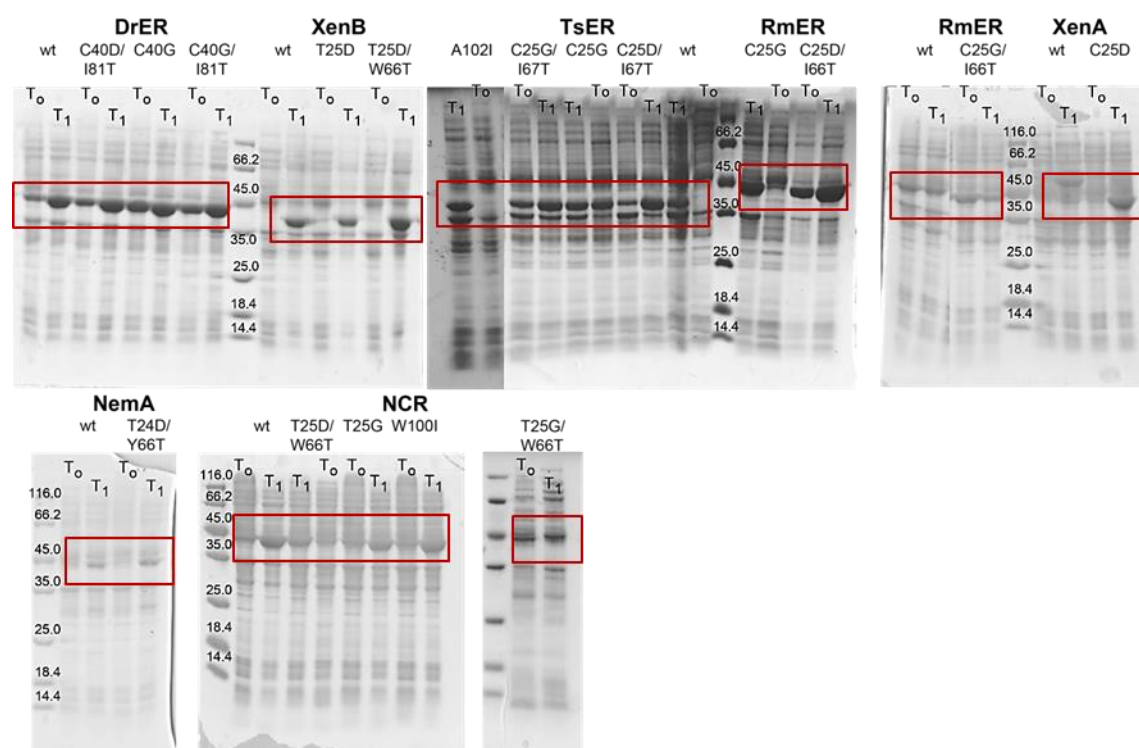


Figure 14. SDS PAGE analysis of heterologously expressed ene reductases. All samples were normalized to an OD₆₀₀ of 1, resulting in equal cell mass per lane. Samples before (T₀) and after (T₁) induction are shown, pET based plasmid show a significant leaky expression. Red squares indicate the recombinant expressed OYE as confirmed by mass analysis. *XenA* wt appears almost 10 kDa to high (exp. mass 41 kDa), but ORF of both plasmids encoding wt and *XenA* C25D variant are identical and correct.

Variant *XenB* T25D/Y66T did not yield any protein after affinity purification, confirming recent reports^[157], *XenB* studies were not further pursued. Mutagen-

esis and expression problems can sometimes be solved by changing the plasmid backbone to smaller or newest generation plasmids. This might be especially promising for XenA, XenB (pGaston) and NCR (pET28).

Overall, site directed mutagenesis yielded 14 heterologous expressed variants from group 1 and 2 members, which were further identified by purification and characterized with a thermal stability test, as well as examined for turnover and stereoselectivity.

DrER and *RmER* carried an *N*-terminal His-Tag whereby they were purified by immobilized metal ion affinity chromatography (IMAC) while monitoring the purification process with UV spectroscopy and SDS-Page analysis. Yields of about 6-9 mL with 30-50 μ M per 300 mL expression culture (25-40 mg/L) could be obtained for all variants.

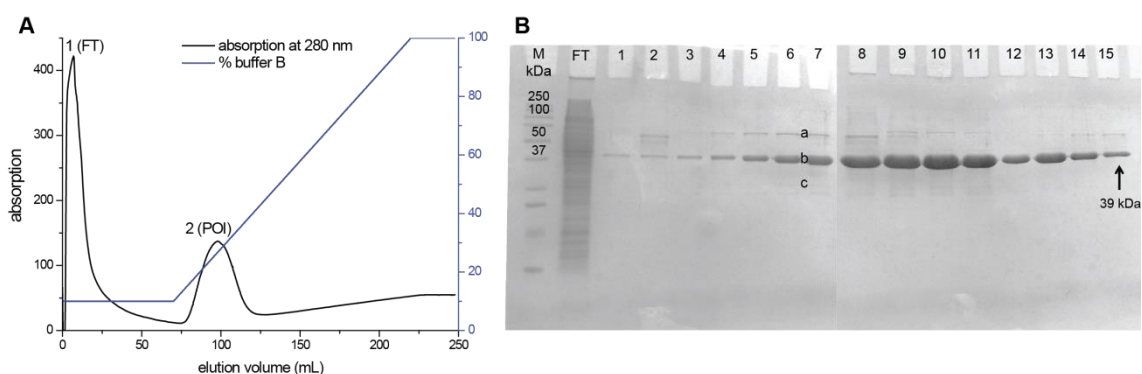


Figure 15. A) Representative absorption spectrum of protein elution profile at 280 nm during immobilized metal ion affinity chromatography (IMAC) of *DrER* C40G with buffer B: 100 mM potassium phosphate, 0.5 M NaCl, 0.5 M imidazole, pH 7.4. FT: flow through, POI: protein of interest. B) SDS-PAGE of the elution profile after purification of *DrER* C40G by FPLC. M: molecular marker, FT: flow through, 1-15: elution fractions, bands a-c were characterized via trypsin digestion and mass analysis as: a: *E. coli* chaperone DnaK, b: *DrER*, c: 50s ribosomal protein L1 from *E. coli*.

TsER is a thermostable enzyme discovered by the studies of BERNARD *et al.*^[179]. By increasing the reaction temperature, also the specific activity for ketoisophorone (**22a**) rises. Furthermore, it was shown that *TsER* retains 50% activity after 25 h at 70 °C. Since the here used *TsER* construct is untagged but thermostable, it was heat-purified (90 min, 70 °C). With this method all non-thermophilic proteins in solution denatured and can be separated by centrifugation. Yields of

about 10-15 mL with 100-120 μ M per 300 mL expression medium (110-130 mg/L) were obtained for all *TsER* variants.

To determine the active enzyme concentration absorption spectra of the purified ene reductases were recorded. Here, the fully oxidized FMN cofactor showed characteristic absorption maxima at 369 nm and 455 nm (Figure 16) and was used to determine the active enzyme concentration.

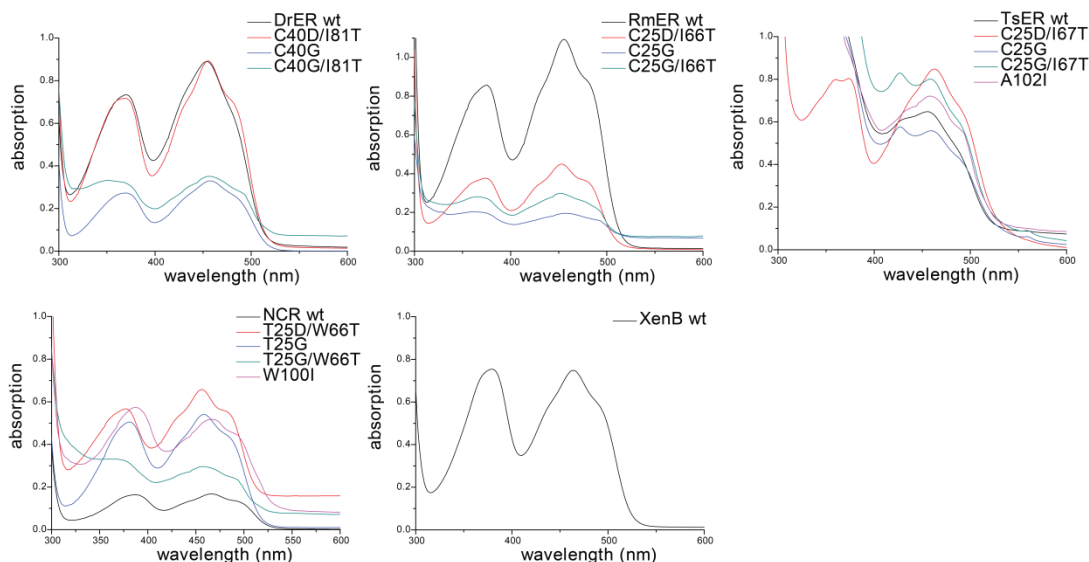


Figure 16. Absorption spectra of purified OYE wt and variants used to determine active enzyme concentration. Some variants show a slightly shifted maximum. The peak maximum, located around 455 nm, was always used for concentration determination.

The SDS PAGE analysis of 10 μ M enzyme solutions for every purified OYE shows on one hand the excellent purity but on the other hand, that the supplied amounts of enzyme are not identical as expected. It can be explained by the presence of apo-protein in the purified enzyme solution, which is mainly owned by an incomplete reconstitution with excess of FMN. This demonstrates the advantage of determining the active enzyme concentration for activity assays over the bound FMN absorption maximum instead of the BRADFORD^[180] method, where just the whole protein concentration as sum of holo and apo-protein would be determined.

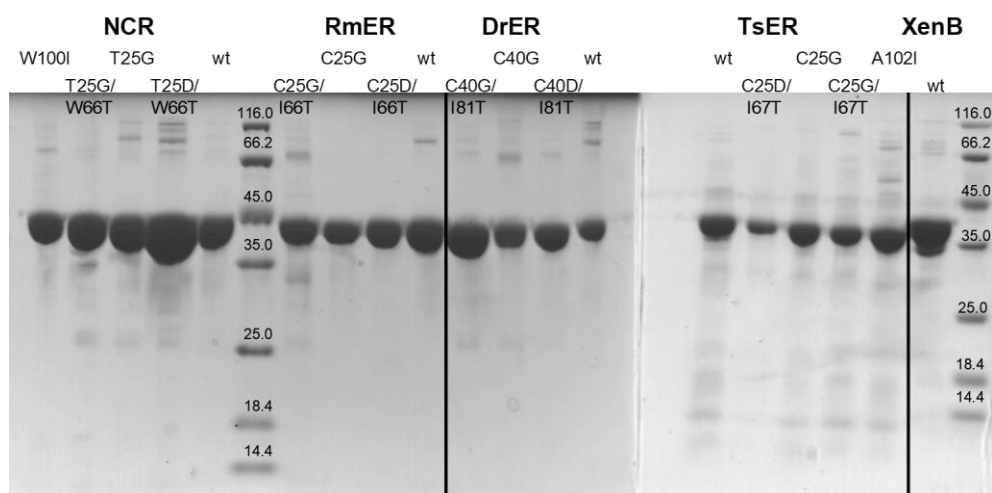


Figure 17. SDS PAGE of all purified variants. A 12% self-casted SDS-PAGE (coomassie brilliant blue staining) loaded with approx. 2 μ l purified OYEs of a 10 μ M solution determined via UV/Vis spectrum. *TsER* showing the expected size of around 37.9 kDa, *NCR* of around 41.6 kDa, *XenB* of around 38.8 kDa, *RmER* of around 40.1 kDa and *DrER* of around 41.7 kDa.

To determine the influence of introduced mutations, the thermal stability was measured by CD spectroscopy.^[176] As can be seen in Figure 18, the introduced mutations decreased the thermal stability for *DrER* and *RmER* by 10 °C and 4 °C, respectively. *RmER* wt is 7 °C less temperature stable than *DrER* wt. Overall, *RmER* wt and variants turned out to be the least active OYEs, possibly due to dimer-dimer instabilities.^[99]

For *TsER* no melting curve was observed up to 94 °C, indicating high thermal stability of the enzyme against unfolding. Instead, precipitation of *TsER* wt and variant was observed at the end of the measurement. This result is not surprising, because *OPPERMAN et al.* showed that *TsER* wt is still active above 80 °C.^[175]

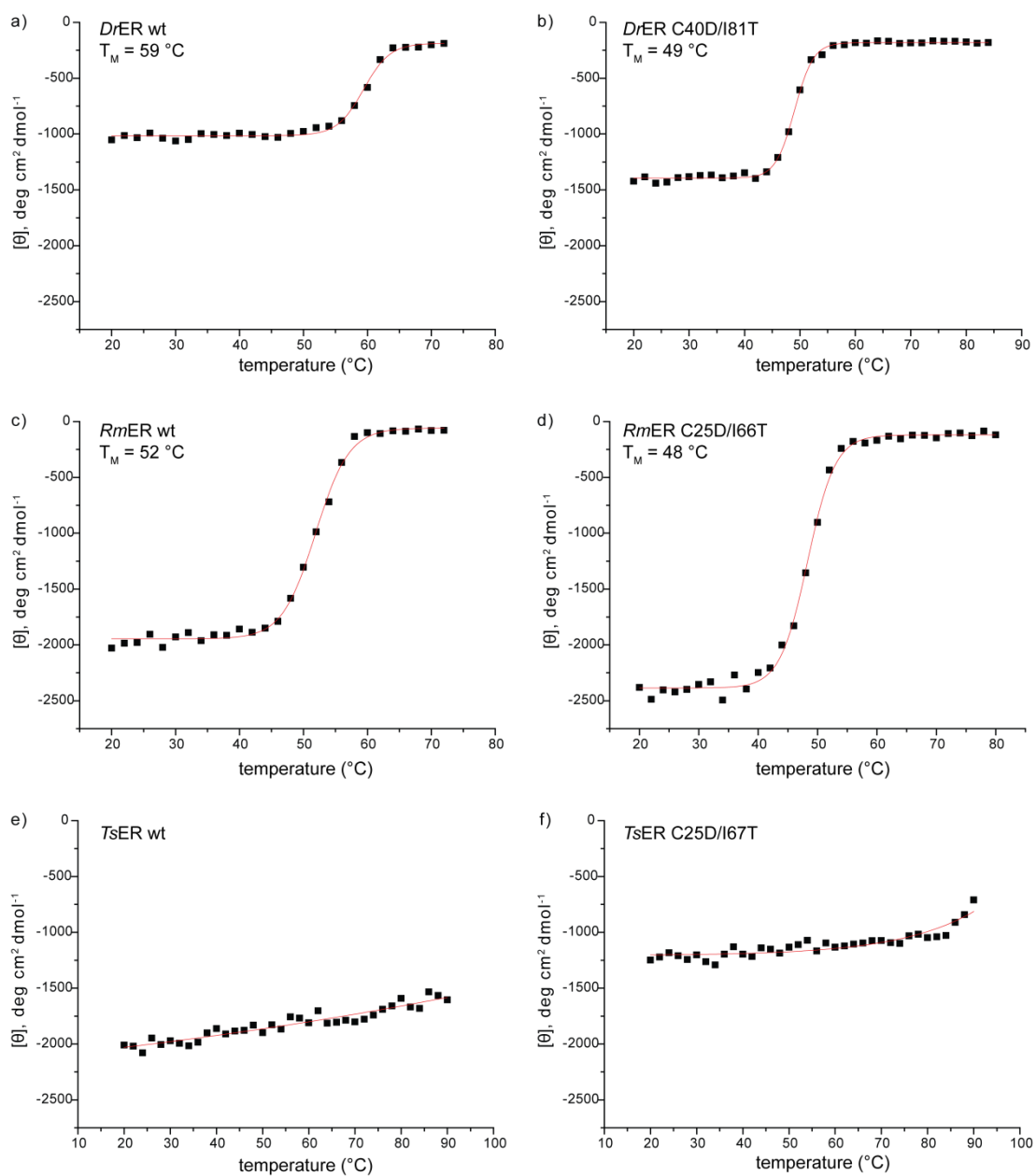


Figure 18. Melting curves of group 2 OYE wt and variants, measured by CD spectroscopy. The molar ellipticity θ was measured at 220 nm as an average of three accumulation steps. The received data was fitted by ORIGIN 8 with a BOLTZMANN sigmoidal fit. T_M = melting temperature.

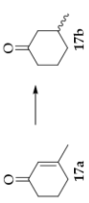


3.1.2.2 Substrate Scope and Facial Selectivity of First Variants

All five purified wild types and 14 variants were obtained as active enzymes, making it possible to convert 10 mM of **18a** containing an electronic activated carbon-carbon double bond with turnover numbers (TON) between 60 and 1000 (Table 1). With the used catalyst loading of 10 μM (0.1 mol%) and the chosen

reaction conditions a maximal TON of 1000 is possible. Reduction of **18a** achieved turnover frequencies (TOF) between 40 and 667 molecules per hour, showing that most of these new variants are faster than literature reported variants (TOF, 18 – 300 h⁻¹).^[65,91,162,181] With the standardized, non-optimized conditions, the TOF numbers are already close to the best reported TOF for (*S*)-carvone (**18a**) (~1000 h⁻¹) by LacER.^[172] As expected, the wild types of group 2, *TsER*, *RmER*, *DrER* and *XenA*, had a rather low activity ($\leq 1\%$) for **17a**.^[65,67,99,173,182–185] NCR wt, *TsER* C25D/I67T, C25G/I67T and *DrER* C40D/I81T reach the best TOF of 82 - 190 h⁻¹ for reduction of **17a** (Table 1). The electronic deactivation of the beta position reduced TOF almost ten-fold. A more significant effect on TOF was observed, when the hydrogen bond acceptor potential of the anchoring group is altered by switching from ketones to esters, as in the case of **19a**, where only six (Table 1) of the 19 tested enzymes showed detectable formation of **19b**. A reasonably active enzyme catalyst should have at least a TON of 10 - 100 and a conversion of >90% for industrial applications.^[186] *TsER* wt and *TsER* C25D/I67T achieved this with 94 and 98% conversion after 24 h, albeit with a moderate TOF of 39 and 41 h⁻¹, respectively.

Transfer of engineered residues into group 1 OYE scaffold NCR did increase conversion of **19a**, since NCR W100I improved from no detectable to 46% production of **19b**. A similar trend was observed for OYE1 W116X variants, but not for OYE2.6 variants, even when mutating at the same three hotspot positions discussed here.^[160,187] In group 2, conversion of **19a** was significantly reduced for engineered variants of *YqjM*, where substrate engineering circumvented the problem.^[152]

Table 1. Assays were performed aerobically, in 200 μ l containing 10 μ M OYE, 10 mM substrate, a NADP⁺, glucose, GDH based cofactor recycling system for 5 h (**17a**), 1.5 h (**18a**) or 24 h (**19a**) in 100 mM potassium phosphate buffer (KPi), pH = 7.4. All reactions were done in triplicates. (a) mean from triplicates, standard deviation \pm 5%; (b) 5 h; (c) 1.5 h; (d) 24 h; n.c. no conversion under assay conditions, n.a. not applicable, n.d. not determined.

							conv. ^(a) (%GC)	TON	TOF ^(c) (h ⁻¹)	de ^(a) (%GC)	conv. ^(a) (%GC)	TON	TOF ^(d) (h ⁻¹)	ee ^(a) (%GC)
	conv. ^(a) (%GC)	TON	TOF ^(b) (h ⁻¹)	ee ^(a) (%GC)	conv. ^(a) (%GC)	TON								
NCR wt	47	465	93	>99S	84	840	560	96 (2R,5S)	n.c.	n.a.	n.a.	n.a.	n.a.	
XenB wt	10	100	20	>99S	68	680	453	96 (2R,5S)	n.c.	n.a.	n.a.	n.a.	n.a.	
RmER wt	n.c.	n.a.	n.a.	n.a.	93	930	620	95 (2R,5S)	n.c.	n.a.	n.a.	n.a.	n.a.	
DtER wt	1	10	2	93S	99	990	660	92 (2R,5S)	2	20	1	97S		
TsER wt	1	10	2	76S	100	1000	667	91 (2R,5S)	94	940	39	76S		
NCR T25G	9	93	19	99S	43	430	287	96 (2R,5S)	n.c.	n.a.	n.a.	n.a.	n.a.	
RmER C25G	n.c.	n.a.	n.a.	91S	16	160	107	92 (2R,5S)	n.c.	n.a.	n.a.	n.a.	n.a.	
DtER C40G	n.c.	n.a.	n.a.	n.a.	28	280	187	91 (2R,5S)	n.c.	n.a.	n.a.	n.a.	n.a.	
TsER C25G	7	70	14	99S	97	970	647	78 (2R,5S)	n.c.	n.a.	n.a.	n.a.	n.a.	
NCR T25G/W66T	1	14	3	65S	6	60	40	99 (2R,5S)	n.c.	n.a.	n.a.	n.a.	n.a.	
RmER C25G/I66T	2	20	4	84S	19	190	127	38 (2S,5S)	n.c.	n.a.	n.a.	n.a.	n.a.	
DtER C40G/I81T	5	50	10	65S	85	850	567	68 (2S,5S)	n.c.	n.a.	n.a.	n.a.	n.a.	
TsER C25G/I67T	41	410	82	74S	99	990	660	92 (2S,5S)	11	110	5	79S		
NCR T25D/W66T	3	34	7	67R	69	690	460	96 (2R,5S)	n.c.	n.a.	n.a.	n.a.	n.a.	
RmER C25D/I66T	7	70	14	93R	96	960	640	93 (2R,5S)	n.c.	n.a.	n.a.	n.a.	n.a.	
DtER C40D/I81T	73	730	146	96R	99	990	660	93 (2R,5S)	6	60	3	9R		
TsER C25D/I67T	95	950	190	98R	100	1000	667	91 (2R,5S)	98	980	41	97R		
NCR W100I	1	6	1	n.d.	31	310	207	99 (2R,5S)	46	460	19	>99R		
TsER A102I	<1	4	1	n.d.	81	810	540	96 (2R,5S)	n.c.	n.a.	n.a.	n.a.	n.a.	

More trends are apparent; C26G homologues showed either unaltered or decreased conversion, irrespective of the substrate. Literature also reports the same trend for YqjM and XenA, especially when substrates without C α activation are used,^[67,173] and saturation mutagenesis studies of OYE2.6^[187] or PETNR^[162] did not yield a homolog glycine variant when selected by conversion. Since it has become apparent that double/triple variants with mutations in hotspot position II generally favour higher conversion levels,^[67,160,188] a threonine at the respective position was introduced in all C26G homologues and indeed conversion of **17a** and **18a** for glycine/threonine variants increased compared to the single C26G variants.

Interestingly the C26D/I69T pair did generally increase conversion and TOF in group 2 members (Table 1). The introduction into group 1 member NCR and XenB however resulted in a loss of conversion from 47 to 3% or in enzyme insolubility, respectively. A similar phenomenon was observed when hotspot position II in OYE2.6 (Y78) was converted to smaller residues and abolished carvone conversion.^[160] Vice versa, incorporation of W116I homologues into group 2 member *TsER* was not able to induce increased conversion levels. Mixed reports are apparent in the literature demonstrating that the influence of hotspot III on conversion might be weaker than other hotspots and highly substrate dependent. No activity for **17a** was observed with PETNR W102I, but other amino acids at this hotspot position and other substrates showed increased conversion.^[162,189] Incorporation of W116I into circularly permuted OYE1 variants lowered conversion of **18a**,^[164,190] a saturation mutagenesis library at W116 showed no hits for **17a**^[147] and biocatalytic characterisation of all 20 variants showed that W116I is not the best engineered residue for this position.^[159,191] Nevertheless, the NCR data supports the importance of hotspot position III itself. Additionally, data mining also reveals an importance for fine-tuning reactivity, either alone^[159,162,187,191] or in context with variations at other hotspot positions.^[67,160,181]

Results for reduction of **17a** and **18a** reflect that evolution of the active site towards improved turnover of **17a** was performed in a group 2 member. Therefore, it was surprising that variant *TsER* C25D/I67T converts the structurally different **19a** equally well as the wt, and the aspartate/threonine variant of *DrER* showed marginally (from 2 to 6%) increased conversions. Overall *RmER* wt and variants turned out to be the least active OYE, possibly due to dimer-dimer instabilities.^[99]

It appears that group 1 wild types, with their bulky residues in hotspot position II and III prefer a binding mode of **17a** that leads to (*S*)-**17b** (see Figure 19).^[73,109,192–194] Reports of facial selectivity for group 2 members are rare. *XenA* wt favours (*S*)-**17b** (>99%)^[157] like all other OYE wild types and only *YqjM* wt produces (*R*)-**17b** with 76% *ee*.^[67] It is expected that *TsER* wt and *DrER* wt will likewise produce the (*R*)-enantiomer with their structurally almost identical active sites.^[175]

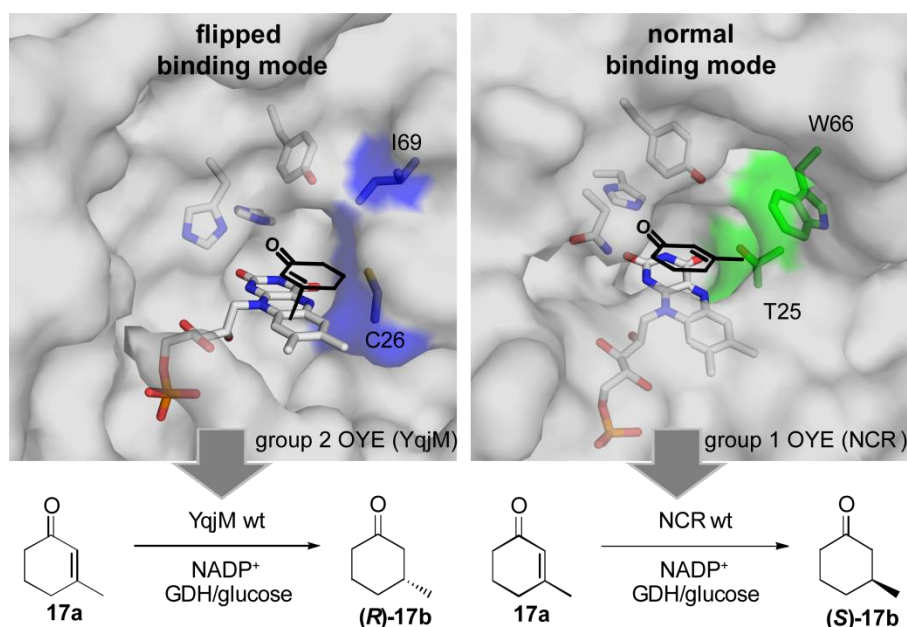


Figure 19. Scheme depicting normal and flipped binding modes of **17a** in OYE scaffolds from group 1 and group 2. A 180° flip along the C=O axis presents the other face of the carbon-carbon double bond to the hydride and leads to the inverted isomer

To access accurate stereoselectivities for entries with such low conversions ($\leq 2\%$, Table 1), their reactions were performed in large scale (10 mL). Surprisingly, group 2 member *DrER* wt and *TsER* wt produced (*S*)-**17b** with

93% and 76% *ee*, respectively, and YqjM wt reproducibly (*R*)-**17b** with 78% *ee* (Figure 20). It would be interesting to understand what determines the *re*-face orientation of **17a** in YqjM wt compared to *DrER* and *TsER*.

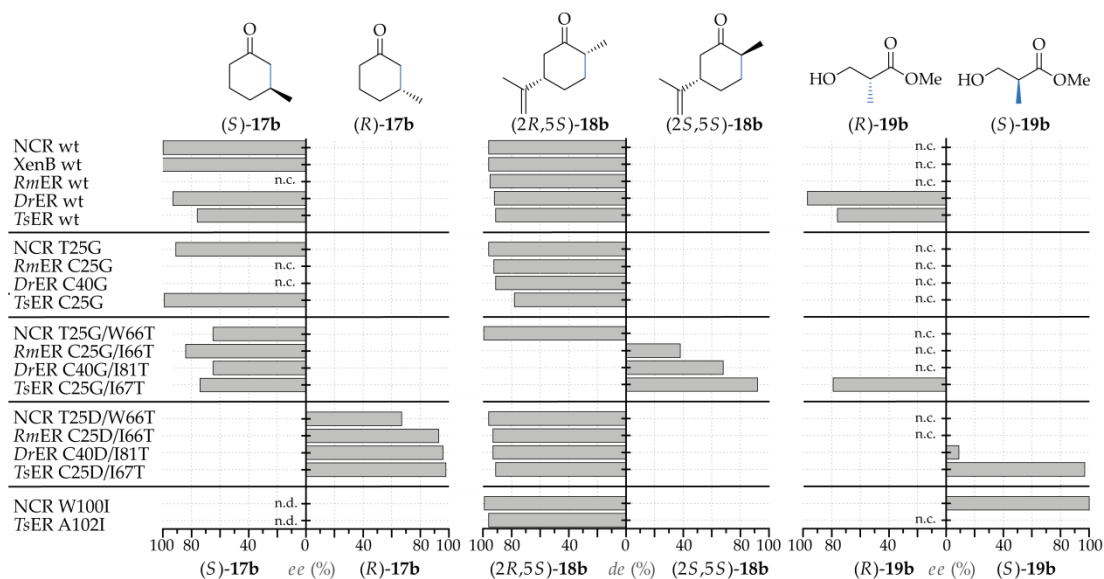


Figure 20. Overview of stereoselectivity of purified OYE variants producing **17b**, **18b** and **19b**. The selectivity on the left is the prevailing selectivity accessible with wt OYEs. A selectivity switch for all three substrates is observed with the created variants in hotspot positions I+II. Assays were performed aerobically, in 200 μ l containing 10 μ M OYE, 10 mM substrate, a NADP⁺, glucose, GDH based cofactor recycling system for 5 h (**17a**), 1.5 h (**18a**) or 24 h (**19a**) in 100 mM KP_i, pH = 7.4. Enantiomeric excess was determined by GC. n.c. no conversion, n.d. not determined.

All currently known OYE wild types reduced **18a** with a facial selectivity yielding exclusively (*2R,5S*)-**18b**.^[148,172] The data from this study confirms this trend for *TsER*, *DrER*, *RmER* and *XenB*, and additionally shows that NCR wt is no exception.^[195] Furthermore, the data showed 76% or 97% *ee* for (*R*)-**19b** by *TsER* and *DrER* wt, respectively, and confirms the trend that all current known OYE wt scaffolds exclusively yield the (*R*)-enantiomer of **19b**,^[158] where the only known exception is OYE2.6 wt.^[159] It could be shown that the control of facial selectivity previously observed for the YqjM variant pair C26G and C26D/I69T is transferable to NCR, *RmER*, *DrER* and *TsER* for the reduction of **17a**. Glycine variants in hotspot position I give access to (*S*)-**17b** and the aspartate/threonine combination in hotspot position I+II allows access to (*R*)-**17b**, irrespective of the scaffold or the selectivity of the wild type.

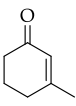
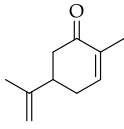
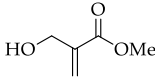
It appears that for the substrate/residue pair **17a** and aspartate/threonine in hotspot position I+II the flipped orientation is predominant and the glycine based variants showed the same facial selectivity as the majority of wt. Notably, *TsER* C25G, *DrER* C40D/I81T and *TsER* C25D/I67T showed increased stereoselectivity compared to *YqjM* variants. Achieved selectivities are excellent, up to 98% yield of (*R*)-**17b**, which is one of the best results obtained so far with OYEs. Only engineering of group 2 achieved good TON, TOF and enantioselectivity values for (*R*)-**17b** production.^[195] Since the literature reported engineered group 1 members all favour (*S*)-**17b**.^[91,162,181], the NCR T25D/W66T variant from this study is the first (*R*)-**17b** selective group 1 example, but with rather low activity. An exception might be *XenA* C25G, where a report by YANTO *et al.*^[173] indicates >99% (*R*)-**17b** with a TOF of 53 h⁻¹, but stands in sharp contrast to the systematic appearance of (*S*)-**17b** preference of hotspot I glycine variants reported here.

Further, the same pattern of stereocomplementarity for the glycine/threonine and aspartate/threonine variants was observed for the reduction of **18a**, allowing access to (2*S*,5*S*)-**19b** or (2*R*,5*S*)-**19b** with excellent diastereoselectivity of up to 92 or 96% *de*, respectively.^[195] This is the first report of group 2 members producing (2*S*,5*S*)-**19b** and besides OYE1 W116X variants from group 1,^[163] the only other set of variants so far for this reaction.^[148] All other new variants led to (2*R*,5*S*)-**19b**, even the hotspot position III homologues NCR W100I and *TsER* A102I.^[195]

Lastly, reduction of **19a** confirms the generality of the stereocomplementary pair, since *TsER* C25G/I67T and C25D/I67T gave 79% (*R*)-**19b** or 97% (*S*)-**19b** *ee*. The combination of **19a** and glycine based variants showed the same facial selectivity as the wt and the aspartate/threonine combination flipped it. This represents the second variant of group 2 that is able to access (*S*)-**19b**.^[195] RÜTHLEIN *et al.* discovered *YqjM* variants C26N/I69A and H167A/I69A for production of (*S*)-**19b**,^[152] albeit with TOFs of 10.3 and ~0.3 h⁻¹, respectively, compared to 41 h⁻¹ (*TsER* C26D/I67T) and 19 h⁻¹ (NCR W100I). A combinatorial library of *TsER*

(chapter 3.6.3.1) contained some of the *in silico* designed variants of RÜTHLEIN *et al.*,^[152] but they showed no conversion of **19a** under the here used reaction conditions (Table 2).

Table 2. Variants of TsER and NCR having the same mutations as published by RÜTHLEIN *et al.*^[152] and POMPEU *et al.*^[163], but were identified as hits in combinatorial mutant libraries in other projects^[177] (chapter 3.6.3.1). Even though these variants were not selected for the first project in the presented thesis, the occurrence further supports the high value of residues identified in hotspot positions by directed evolution and their transferability to family member.

						
		17a	18a	19a		
		conv. (%GC)	% <i>ee</i>	conv. (%GC)	% <i>de</i>	conv. (%GC)
TsER	C25N/H175A ^(a)	0.0	n.d.	1	>99 (2 <i>R</i> ,5 <i>S</i>)	0.0
	C25N ^(a)	0.7	n.d.	82	95 (2 <i>R</i> ,5 <i>S</i>)	0.0
	C25G/A102I	0.2	n.d.	34	90 (2 <i>R</i> ,5 <i>S</i>)	0.0
	C25D/A102I	4.0	53 (<i>R</i>)	82	95 (2 <i>R</i> ,5 <i>S</i>)	0.0
NCR	W100V ^(b)	0.6	n.d.	77	95 (2 <i>R</i> ,5 <i>S</i>)	0.0
	W66Y	11.0	99 (<i>S</i>)	78	96 (2 <i>R</i> ,5 <i>S</i>)	0.0
	T25N	44.0	98 (<i>S</i>)	79	96 (2 <i>R</i> ,5 <i>S</i>)	0.0

(a) homologue to YqjM variants engineered for (*S*)-selective reduction of **19a** by RÜTHLEIN *et al.*^[152], using rational design. (b) homologue to OYE1 W116V variant, engineered for (2*S*,5*S*)-selective reduction of **18a** by POMPEU *et al.*^[163]. Although W116I and W116V of OYE1 flip stereoselectivity, NCR W100I and W100V do not for the reduction of **18a**. n.d. not determined.

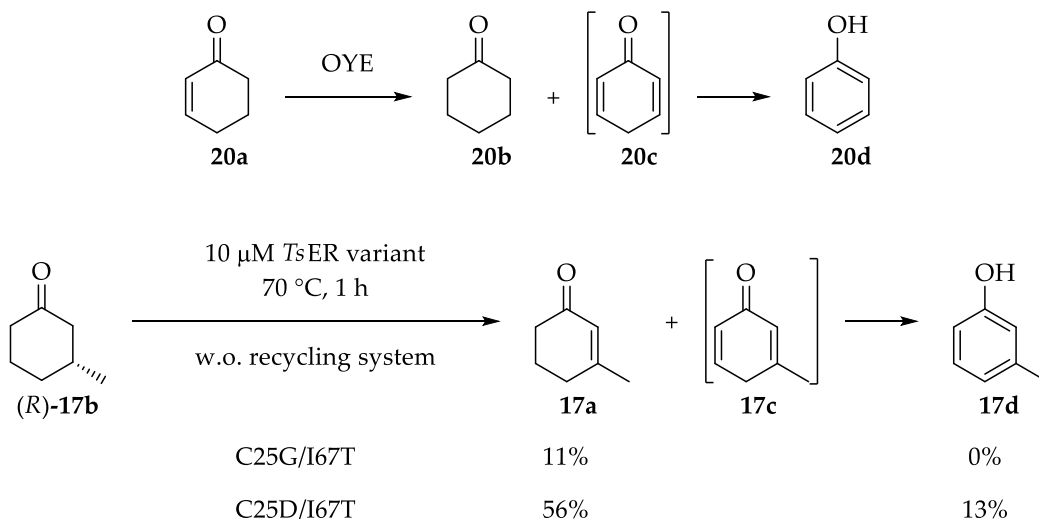
For variants with incorporated isoleucine at hotspot position III, no flip in facial selectivity could be found for the reduction of **18a**, which is contrary to the original report,^[91] but consistent with cpOYE1 and OYE2.6 engineering results.^[181,190] Nevertheless, NCR W100I showed >99% (*S*)-**19b** selectivity, presumably representing a flipped facial selectivity compared to the wt.^[158] This supports follow up studies by STEWART and co-workers, where it was shown that hotspot position III in group 1 indeed controls stereoselectivity, but highly depends on amino acid substitution in this position and tested substrate.^[159,160,191] ALEXANDRA RICHTER could identify a homologue of one of the most promising OYE W116X variants from the STEWART study^[148], the NCR W100V, in a combinatorial library.^[177] Interestingly, this NCR W100V variant was not able to switch facial selectivity for reduction of **17a** or **18a** (Table 2).

Compared to the C25/I67 variants generated by the scaffold sampling method, the NCR variants obtained through site-directed saturation mutagenesis^[177] show low conversion for **17a** and **18a** and no conversion for **19a**.

Recently two groups simultaneously applied the here presented 'scaffold sampling' strategy, as a fast protein engineering strategy accessing significantly improved biocatalysts with virtually no screening and creation of low numbers of variants. The strategy assumes that catalytically important residues obtained earlier by protein engineering, either rational or random, will induce the same improvements of traits when transferred to their hotspot positions in other family member. DUNN *et al.*^[137] transferred XNA polymerase activity to three polymerase scaffolds, overcoming the limitation of the originally evolved one. GOBER *et al.*^[138] quickly identified new olefin cyclopropanation biocatalysts that allow access to all four stereoisomers by transferring engineered residues into twelve P450 scaffolds. The overall success rate to obtain an improved biocatalyst by this protein engineering strategy appears high, as demonstrated by the results of both studies and the here presented thesis.

3.2 Dehydrogenation Reactions by Old Yellow Enzymes

VAZ *et al.*^[196] published 1995 a study about dismutation reaction by Old Yellow Enzymes, exclusively for cyclic enones. The cyclic enone **20a** was first used as hydride source for the FMN, instead of the nicotinamide cofactor, and was oxidized to **20c** followed by tautomerisation to the phenol **20d**. A second enone serves as substrate and was reduced at the olefinic bond to the corresponding alkane **20b** (Scheme 8).^[196-199] Two following studies showed the potential of ene reductases as desaturases for cyclic ketones^[198,200] and tetralones^[197].



Scheme 8. Dismutation reaction with 2-cyclohexenone (**20a**) investigated by VAZ *et al.*^[196] and a reversed reaction in absence of a recycling system, promoted by higher temperatures. Production of 13% phenol **17d** indicates that TsER C25D/I67T is only marginally inhibited in contrast to most ene reductase wild types.

Under the standard screening conditions, in the here presented thesis, with purified enzyme and GDH/NADP⁺ recycling system, the TsER wild type produces 6% 3-methylphenol (**17d**) in 24 h at 30 °C. In contrast, none of the variants from the TsER panel produced **17d**, not even at elevated temperatures. It is known that the dehydrogenation of cyclohexenone is strongly endothermic (+109 kJmol⁻¹)^[201], which can explain why higher temperatures are necessary for this reaction.

Nevertheless, C25D/I67T in particular did not completely lose the ability to catalyse the desaturation reaction. In the absence of a recycling system, at 70 °C and starting from (*R*)-**17b**, 13% of **17d** and 56% **17a** are formed (Scheme 8). A similar report of *GkOYE*^[200] exists, where 3-methylcyclohexan-1-one (**17b**) was dehydrogenated on the less hindered side leading to 16% 5-methylcyclohex-2-en-1-one with 23% *ee* at 70 °C without NADPH for 24 h. However, no *m*-cresol (**17d**), as by-product was observed under their screening conditions.^[200] In contrast, C25G/I67T only forms 11% of **17a** and no *m*-cresol (**17d**). For the oxidative transformation no nicotinamide cofactor was required, proposing that the catalytic cycle was closed via aerobic re-oxidation of FMNH₂, which is also supported by absorption measurements shown in Figure 21.^[202] It is known that phenol-

ic compounds are inhibitors to OYEs due to the formation of a charge transfer complex with the FMN, this can perhaps explain the moderate yield for **17a** in the C25D/I67T reaction.^[64]

Dehydrogenation reactions of ketones are traditionally synthesised in a chemical way often with toxic phenylselenium derivatives^[203–205] or strong oxidants such as SeO₂, 2,3-dichloro-5,6-dicyano-1,4-benzoquinone (DDQ) or oxoacids of iodine^[206–208]. The enzymatic transformation would lead to an environmentally-friendly biocatalytic option for the preparation of α,β -unsaturated ketones.

Secondly, flavin dependent ene reductases are also NAD(P)H oxidases. Reduced FMN is able to oxidase molecular oxygen forming hydrogen peroxide, which may react with activated alkenes in a non-enzymatic WEITZ–SCHEFFER epoxidation,^[209] or oxidatively damage the enzyme.^[160,210] The most significant consequence is that reducing equivalents are consumed but the desired product is not formed, commonly known as cofactor decoupling. Therefore, the question arises whether the increased productivity of the variants is caused partially by the loss of NAD(P)H oxidase activity, but it was found by SASKIA DÖHRING, that all variants from the *TsER* panel still react with molecular oxygen (Figure 21). Under the aerobic screening conditions, and in the absence of a substrate, wild type and C25D/I67T react similarly fast, whereas C25G/I67T is twice as fast as the wild-type and C25G/I67V is 2.8 times slower.

Although performing OYE reductions under anaerobic conditions was suggested to minimize side reactions,^[210] by mass analysis it could be found that at least *TsER* wt and C25D/I67T are not oxidized at any position in the enzyme by hydrogen peroxide and neither epoxides nor the hydrolysis products thereof were observed. Additionally, an excess of reducing equivalents, supplied by cheap glucose, ensures sufficient reduction when working aerobically.

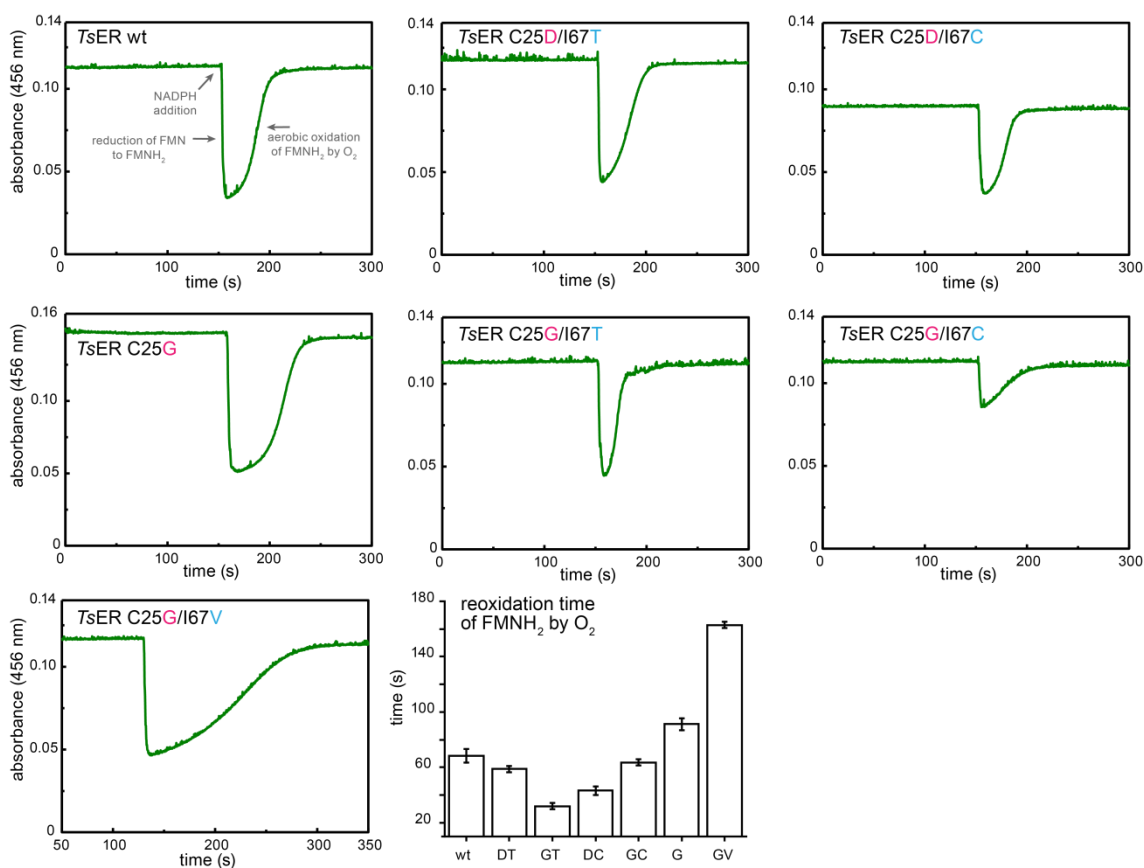
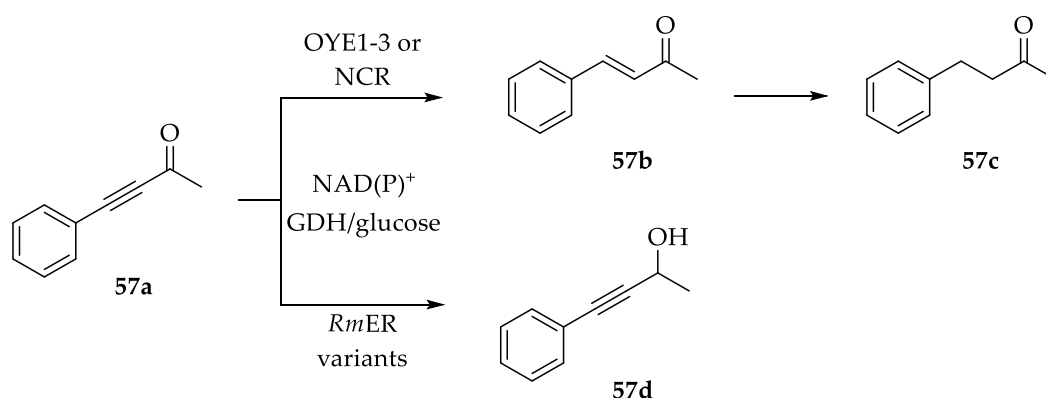


Figure 21. Time needed to re-oxidize 10 μM *TsER* variants under aerobic screening conditions. Upon NADPH addition, the cofactor is reduced to FMNH₂ and rapidly re-oxidized by dissolved oxygen to FMN, which can be followed at 456 nm. Reaction were performed in 100 mM KP_i, pH 7.4, with 10 mM CoCl₂ and 100 μM final concentration of NADPH in a stirring cuvette (1000 rpm) with a JASCO V-650 spectrophotometer equipped with a PAC-743 Peltier temperature control unit.

As mentioned above, flavin dependent ene reductases also have an oxidase function, but until now this has only been observed for the oxidation of molecular oxygen. Activity screenings of purified *RmER* wt, C25D/A102I and A59V/I66T with 4-phenylbut-3-yn-2-one (**57a**) under standard reaction conditions result in conversion to the corresponding alcohol **57d**, for the wt 1%, C25D/A102I in 29% and A59V/I66T in 17%. This turnover could be confirmed over fragmented GC-MS measurements. The activity towards reduction of 4-phenyl-3-but-3-yn-2-one (**57a**) to the enone **57b** was first reported by MÜLLER *et al.* with the OYE1-3 and NCR as whole cell catalysts (Scheme 9).^[89] They did not observe a reduction reaction to the corresponding alcohol **57d**, also only minimal by *E. coli* (less than 2.4%).^[89]



Scheme 9. Possible reactions of **57a** with OYEs. The OYE 1 to 3 and NCR wt enzymes reduce the double bond in whole cell assays^[89], whereas *RmER* variants from this study produce the alcohol **57d**.

From the Rigid Body Docking (RBD) studies of chapter 3.5.1, the highest ranked poses in the *TsER* wild type and C25D/I67T variant structures are shown in Figure 22. It can be seen that the H175 serves as an anchor point for the carbonyl function and coordinates the benzene residue over a pi-pi stacking interaction.

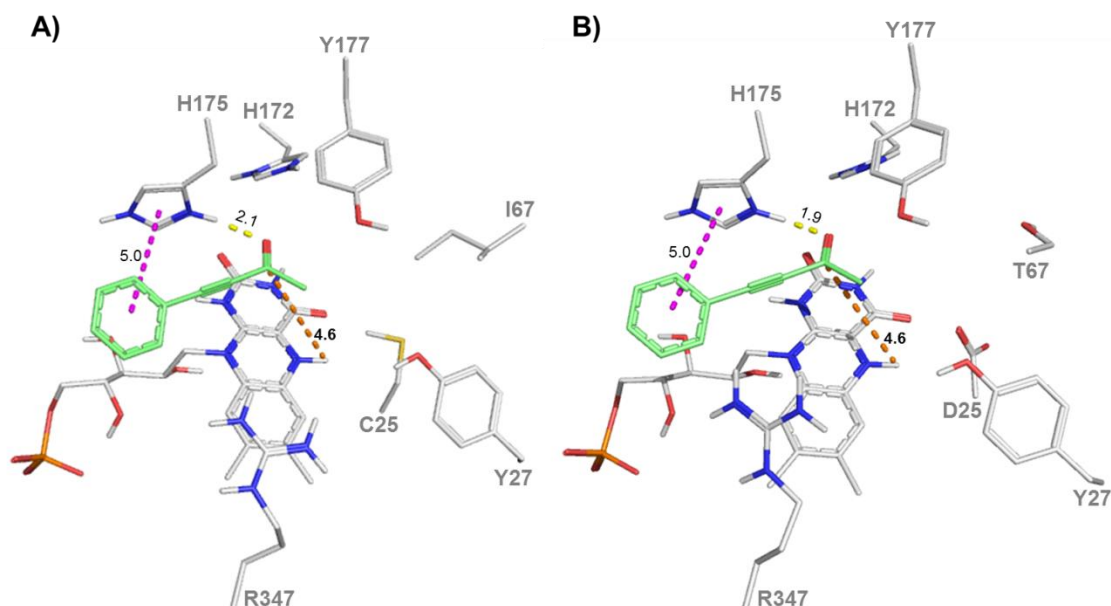


Figure 22. Rigid body docking (RBD) poses of **57a** in A) *TsER* wt with reduced FMNH₂ and protonated H172/H175 and B) in *TsER* C25D/I67T with reduced FMNH₂ and protonated H172/H175. H-bonds are illustrated as yellow dashes, pi-pi stacking as purple dashes and the hydride attack distance as orange dashes.

Due to this positioning in the active site of *TsER*, the distance from the carbonyl carbon to the N5H of FMNH₂ is 4.6 Å with an ideal Bürgi-Dunitz^[211] angle of

107.9° in C25D/I67T and 105.2° in the wild type structure, which might lead to a successful carbonyl reduction.

In order to confirm the production of **57d** by OYEs, upscale reactions must be performed to isolate the exact product and fully characterize it by NMR spectroscopy and mass spectrometry. This reaction would need further investigation, but is a first hint that Old Yellow Enzymes also have a ketoreductase function.

3.3 Characterization of a Robust and Stereocomplementary Panel of *TsER* variants

As mentioned in chapter 3.1 the thermostable ene reductase of *Thermus scotoductus* SA-01 (*TsER*, also named *TsOYE* or CrS)^[195] and its variants can be interesting for industrial applications based on their properties. For industrial synthesis boosted solvent resistance, change of pH and temperature optima and enhanced and even reversed enantioselectivity are important features concerning the catalyst.^[32] This chapter will show that the obtained variant pairs of *TsER* combine a broad substrate scope, tolerance to organic solvents and high temperature with convenient catalyst handling. This combination of properties allows easy use at gram-scale and conversion of poorly water-soluble compounds. Control over facial selectivity was achieved for 10 out of 24 substrates, described in detail in chapter 3.3.1. Crystal structures of the *TsER* C25D/I67T and C25D/I67T/A102H variants, docking and molecular dynamics studies are used to provide possible insights into the factors controlling stereoselectivity on molecular level.

3.3.1 Substrate Scope and Selectivity of *TsER* Variants

A wide range of substrate classes has been studied for ene reductases, which vary in the nature of the activating group as well as in the alkene substituents.^[61,62,71] The motivation in this study was the creation of a convenient set of ene reductases, spanning all aspects from substrate scope, over high stereoselectivity and control over facial selectivity to tolerance of organic solvents and stability at higher temperatures. Purified enzymes are rarely used in the production of fine chemicals, due to the costs of producing the enzyme with sufficient purity to eliminate competing side reactions caused by other enzymes. For *TsER* usage, simple protocols were examined for production, handling and storage of the catalyst. All variants reported in this study are easily separated from the host proteins by heat treatment for 90 min at 70 °C. It was also examined that shock-frozen catalyst solutions maintain their activity when stored at -80 °C for over a year; only repetitive thawing and freezing had negative effects. This was observed with a reaction of a *TsER* C25D/I67T enzyme stock, which was stored for more than two years with repetitive thawing and freezing. The substrate **22a** leads to a conversion of just 20% after 24h. Using a freshly produced enzyme stock could reach full conversion within 5 h. To overcome this limitation, freeze-dried powders were produced, which offer advantages upon storage and handling.^[212,213]

Encouraged by the stereocomplementarity of variants *TsER* C25D/I67T and C25G,^[195] first the active site shape was fine-tuned by modifying residue I67, incorporating either valine (V), threonine (T) or cysteine (C), and residue A102 to histidine (H), tyrosine (Y) or isoleucine (I) into variants C25D or C25G. The mutation to tryptophan (W) at position A102 led to no productive heterologous expression in *E.coli*. This panel of thirteen engineered *TsER* variants and the wild type was tested against a total of 38 activated alkenes (Table 3), mainly cyclohexenones and cyclopentenones, α,β -unsaturated linear alkenones and

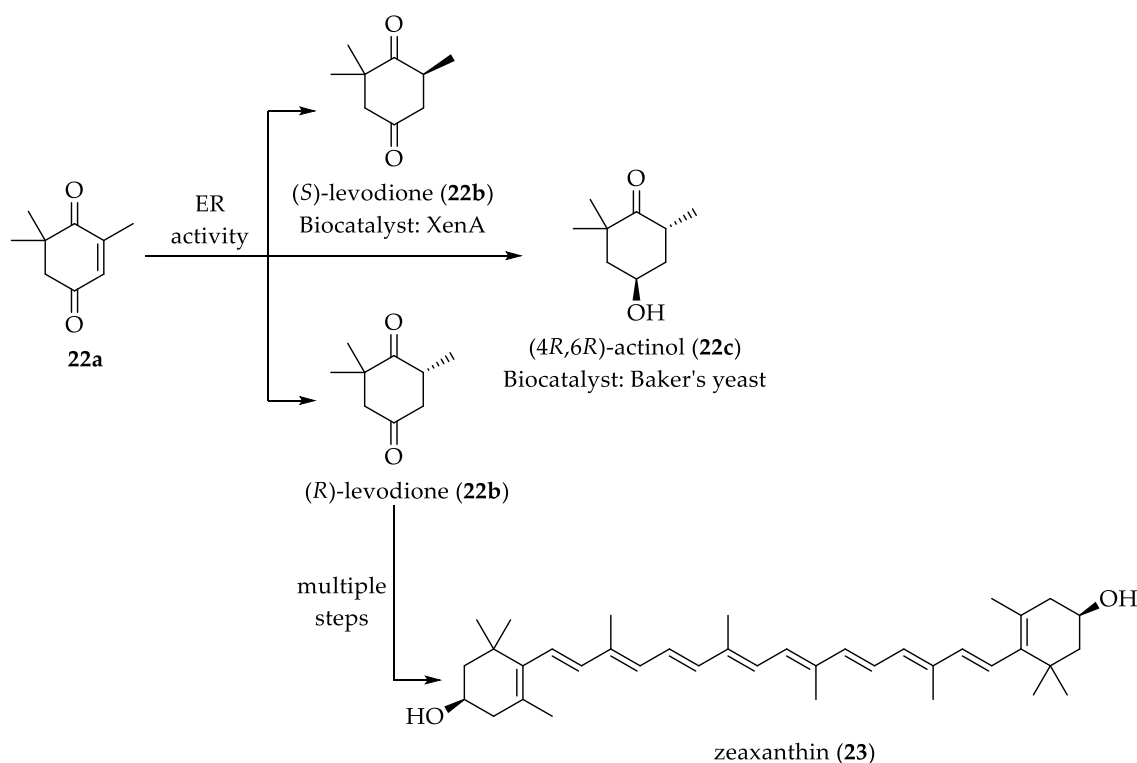
alkenals, acrylesters and nitroalkenes. Cyclic and acyclic ketones are important industrial compounds due to their use as either synthons or solvents in many processes such as polymerizations and pharmaceutical synthesis.^[214] A maleimide, citronellylnitrile, two alkynals and an alkynone were tested as well.

A total of 23 compounds were reduced at the carbon-carbon double bond, introducing new stereocenters with high stereoselectivity (Table 3). For all substances, the control reaction, without enzyme was negative. The stereocomplementary variants give access to both stereoisomers in 10 cases (**17-19a**, **24-25a**, **28-29a**, **35a**, **37a**, **41a**) with stereoselectivities ranging from 17 to >99% *ee*. This represents a novel example of broad stereocomplementarity for a single set of ene reductase variants.

In eight additional cases (**18a**, **22a**, **30-33a**, **38a**, **40a**) high chiral purity (88 to >99% *ee*) for one stereoisomer is obtained, however this panel is accessing the same stereoisomer as known ene reductases. In addition, mainly excellent productivities were achieved under screening conditions, indicating that the *TsER* variants consist of valuable biocatalysts.

(*R*)-Levodione (**22b**) is for example an important industrial synthon as it is used in the production of actinaol, a precursor for the synthesis of carotenoids such as zeaxanthin (Scheme 10).^[215] The reduction of ketoisophorone (**22a**) with OYE is well studied, also the here used *TsER* panel is able to perform the rapid reaction in good conversions and *ee*. Preparative scale reactions are shown in chapter 3.3.3. The presence of two 'activating' keto groups enables the substrate to bind in the active site in more than one conformation (see Figure 36, *in silico* docking results). However, as both conformations lead to the production of (*R*)-levodione (**22b**), the sometimes low *ee* reported in different studies is due to significant water-mediated product racemization.^[216] This was also investigated for the *TsER* panel and is described in chapter 3.3.2.2. The high *ee* values ob-

tained here are due to the short reaction time of 2.5 h, whereby the time spent in the presence of water from **22b** is minimized.



Scheme 10. Literature known reduction of ketoisophorone (**22a**) by whole cells and isolated enzymes to a precursor for zeaxanthin synthesis, ER = ene reductase.^[65,73,74,109,173,217,218]

Terpenoids and their reduced products, such as citral (**38a**) and carvone (**18a**, **30a**) are a large group of naturally occurring cyclic and acyclic compounds which are used industrially as fragrance and flavour substances.^[219] For that reason this compound class was also tested with the *TsER* panel. Interesting is the observation for 3-substituted cyclopentenones, where **34a** has really low conversion, whereas the production of the larger methyl ester residue **35b** is quantitative. This trend was also examined in former studies by BOUGIOUKOU *et al.*^[67] Bioreduction of 3-substituted cyclohex-2-enones (**17a**, **24a**) by wild type enzymes generally produced lower yields than with 2-substituted cyclohex-2-enones (**18a**, **29-30a**) although the products were often enantiopure.^[109,162,218,220] For the here shown *TsER* panel the poor conversion was overcome by introducing mutations in C25 and I67 position and the enantiopurity was kept.

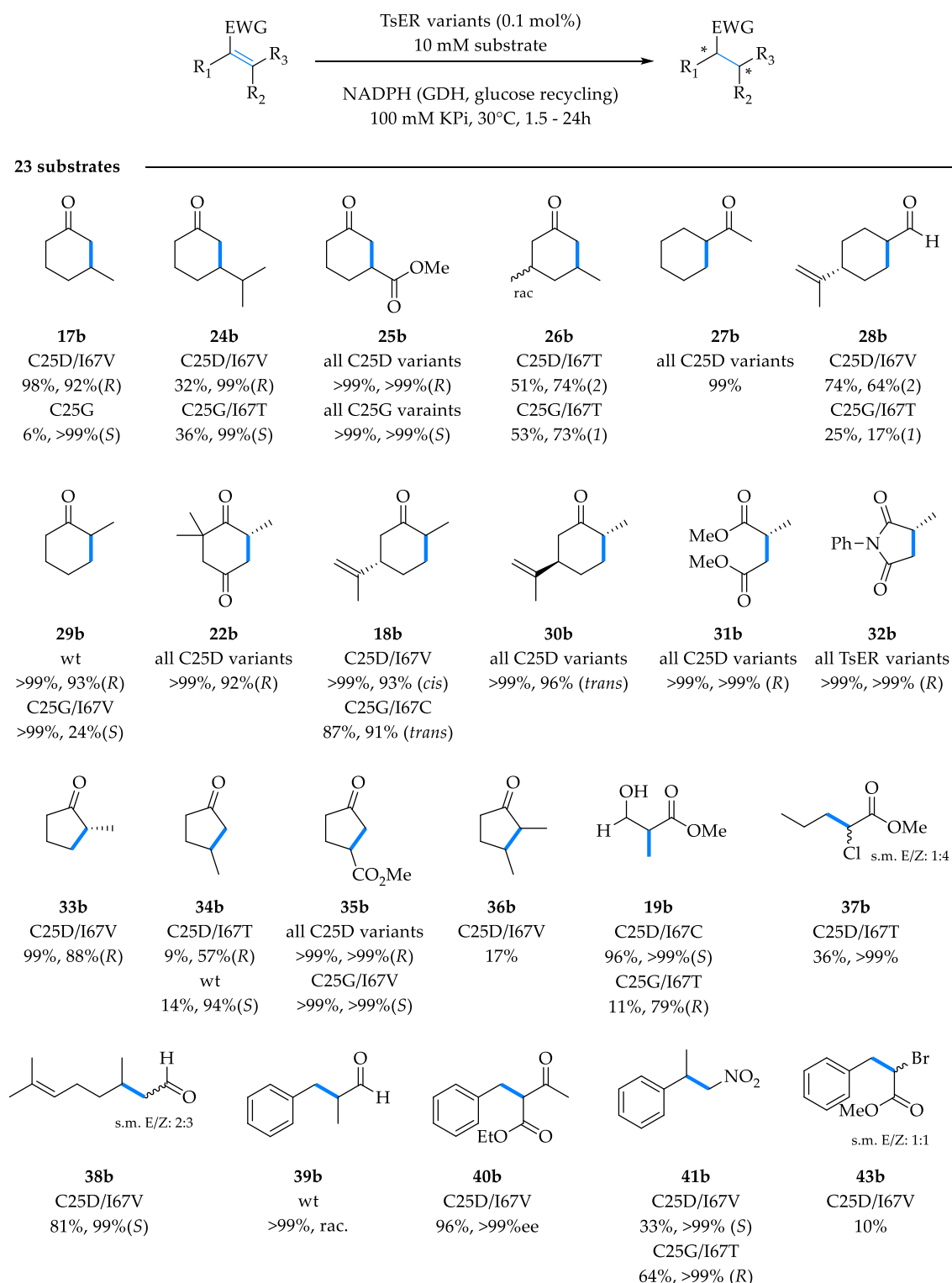


Figure 23. Substrate scope and stereoselectivities obtained using the TsER variant panel. Shown are the best results for activity and stereoselectivity, a detailed overview of all enzymes is given in Table 3. Control reactions without ER showed no background reduction of C=C or C=O bonds. The stereochemical outcome of **33a** reduction using wt TsER (previously reported to be (S))^[73,99,221] was unambiguously corrected to be (R) by optical rotation. The numbers in brackets behind **28b** indicate the major diastereomer based on retention times. rac, racemic; .s.m., starting material.

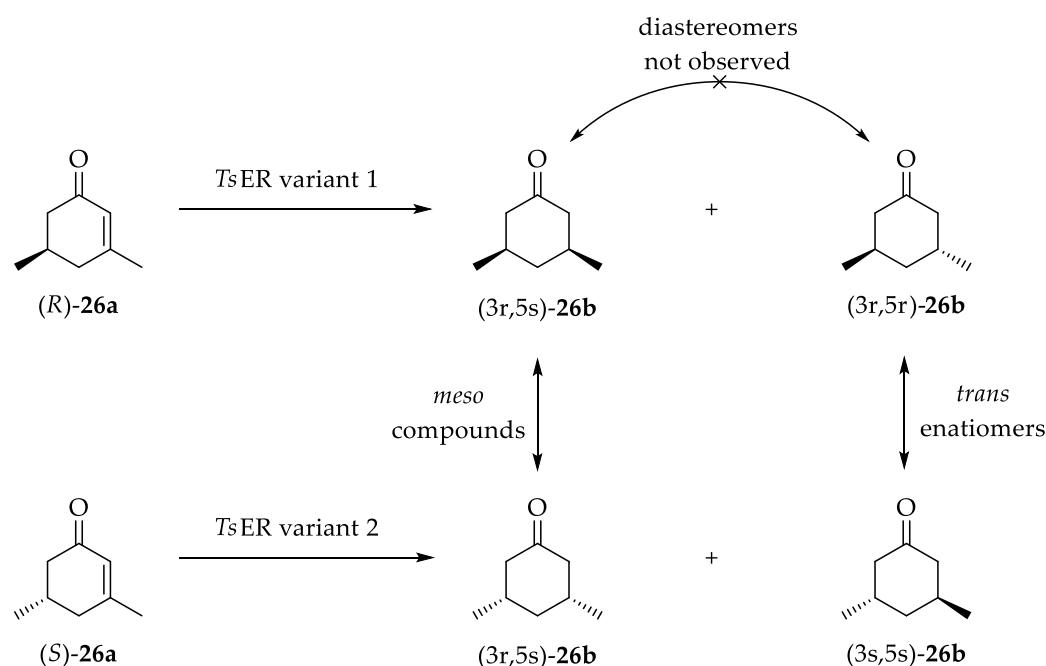
Table 3. Substrate Scope and stereoselectivities of the TsER variant panel with 24 substrates. All reactions were done in triplicates; standard deviation for conversion is $\pm 5\%$. The reaction was stopped after 24 h unless otherwise specified. With the wild type comparable conversion were obtained, as were previously reported,^[22] but the differences in reaction conditions lead to a 40% increase in citral reduction. Use of 10% v/v organic solvents suppressed background racemisation of stereocenters, especially for **33b**. The numbers in brackets behind **28b** indicate the major diastereomer; and for **26b** the consumed starting enantiomer assignment of absolute stereochemistry was not done.

Product	wt conv% ee/%	C25D/167C conv% ee/%	C25D/167T conv% ee/%	C25D/167V conv% ee/%	C25D/167T/ A102H conv% ee/%	C25D/167C/ A102Y conv% ee/%	C25G conv% ee/%	C25G/167C conv% ee/%	C25G/167T conv% ee/%	C25G/167V conv% ee/%	C25G/167T/ A102H conv% ee/%	C25G/167T/ A102Y conv% ee/%	C25G/167C/ A102I conv% ee/%	C25G/167C/ A102H conv% ee/%
17b^a	1	63 94R	95 93R	98 92R	18 99R	38 >99R	6 >99S	6 57S	49 74S	97 62S	2 n.d.	6 n.d.	3 n.d.	2 n.d.
24b^a	n.c.	22 99R	29 99R	32 99R	n.c.	n.c.	1 n.d.	6 99S	36 99S	34 99S	n.c.	22	n.c.	2
25b^a	>99 >99R	>99 >99R	>99 >99R	>99 >99R	>99 >99R	>99 >99R	>99 >99S	>99 >99S	>99 88S	>99 >99S	>99 >99S	>99 >99S	>99 >99S	>99 >99S
26b	1 rac	46 99 ee 49(2) ^y	51 >99 ee 47(2) ^y	33 >99 ee 7(2) ^y	18 >99 ee 19(2) ^y	1 n.d.	10 >99 ee 10(1) ^y	4 n.d. 2(1) ^y	53 >99 ee 46(1) ^y	21 >99 ee 10(1) ^y	n.c.	2 n.d.	n.c.	23 >99 ee 8(2) ^y
27b^a	99	99	99	99	>99	n.c.	85	99	99	99	40	>99	28	>99
28b^{a,b}	88 83(2)	68 49(2)	84 27(2)	74 64(2)	82 32(2)	6 99(2)	38 57(2)	8 24(1)	25 17(1)	6 17(1)	n.c.		n.c.	43 37(2)
29b^a	>99 93R	>99 13S	>99 5R	>99 5R	>99 rac	>99 rac	>99 72R	>99 18S	>99 14S	>99 24S	>99 11S	>99 24S	>99 11R	>99 rac
22b^a	>99 90R	>99 92R	>99 92R	>99 92R	>99 59R	>99 46R	72 86R	25 91R	88 88R	71 86R	>99 59R	97 47R	82 54R	>99 51R
18b^d	>99 91 (2R,5S) cis	>99 92 (2R,5S) cis	>99 92 (2R,5S) cis	>99 93 (2R,5S) cis	96 99 (2R,5R) cis	98 99 (2R,5R) cis	86 89 (2R,5S) cis	87 91 (2S,5S) trans	87 88 (2S,5S) trans	90 86 (2S,5S) trans	(2S,5S) trans	(2S,5S) trans	68 77 (2S,5S) trans	97 66 (2S,5S) trans
30b^d	>99 96 (2R,5R) trans	>99 96 (2R,5R) trans	>99 96 (2R,5R) trans	>99 96 (2R,5R) trans	95 96 (2R,5R) trans	96 96 (2R,5R) trans	97 98 (2R,5R) trans	86 95 (2R,5R) trans	98 98 (2R,5R) trans	58 99 (2R,5R) trans	84 87 (2R,5R) trans	74 79 (2R,5R) trans	68 77 (2R,5R) trans	99 75 (2R,5R) trans
31b^a	>99 >99R	>99 >99R	>99 >99R	>99 ^d >99R	>99 >99R	52 >99R	38 >99R	25 >99R	97 96R	34 54R	84 63R	90 96R	39 >99R	93 81R

32b*		97 >99R	99 >99R	>99 >99R	99 >99R	>99 >99R	>99 >99R	>99 >99R	>99 >99R	>99 >99R	>99 >99R	>99 >99R	>99 >99R	>99 >99R	>99 >99R	>99 >99R	93 >99R
33b*		99 79R 96R ^e	99 66R 71R ^e	91 57R 88R ^e	99 69R 88R ^e	99 82R	>99 >99R	99 84R 82R ^e	99 81R 80R ^e	96 85R 84R ^e	n.c.	n.c.	>99 82 85R 74R	95 71R	>99 72R		
34b		14 94S	8 47R	9 57R	10 37R	2 n.d.	>99 >99R	n.c.	n.c.	n.c.	n.c.	n.c.	n.c.	n.c.	n.c.	n.c.	n.c.
35b*		>99 >99R	>99 >99R	>99 >99R	>99 >99R	>99 >99R	>99 >99R	>99 96S	>99 90S	>99 99S	>99 99S	>99 96S	>99 96S	>99 98S	>99 97S	>99 97S	
36b		2 n.d.	7 n.d.	2 n.d.	17 n.d.	33 n.d.	9 n.d.	<1 n.d.	2 n.d.	1 n.d.	n.c.	n.c.	1 n.d.	1 n.d.	2 n.d.	2 n.d.	
19b*		94 76R	96 >99S	98 97S	83 >99S	>99 64R	21 89R	2 n.d.	11 79R	n.c.	n.c.	n.c.	n.c.	n.c.	n.c.	8 n.d.	
37b		94 46S	35 26R	51 5R	27 47R	64 n.d.	n.d.	7 51R	37 92R	36 >99R	19 n.d.	36 n.d.	36 n.d.	12 n.d.	13 n.d.		
38b		60 99S	52 99S	70 99S	81 99S	34 85S	51 83S	31 87S	49 94S	14 88S	49 >99S	40 >99S	40 >99S	3 n.d.	2 n.d.		
39b		92 rac	85 rac	47 rac	57 rac	26 rac	39 rac	97 rac	94 rac	98 rac	98 rac	99 rac	99 rac	99 rac	99 rac	99 rac	
40b*		40 91 ^e	58 88 ^e	43 88 ^e	60 96 ^e	>99 >99 ^{ee}	>99 >99 ^{ee}	38 39 ^e	48 90 ^e	37 37 ^e	>99 >99 ^{ee}	>99 >99 ^{ee}	>99 >99 ^{ee}	>99 >99 ^{ee}	>99 >99 ^{ee}	>99 >99 ^{ee}	
41b		13 >99S	27 >99S	28 >99S	33 >99S	10 >99S	12 >99S	62 >99R	64 >99R	63 >99R	96 >99R	98 >99R	98 >99R	98 >99R	86 >99R		
42b		n.c.	n.c.	n.c.	n.c.	n.c.	40	n.c.	n.c.	n.c.	n.c.	n.c.	n.c.	n.c.	n.c.	n.c.	
43b		4 n.d.	1 n.d.	4 n.d.	10 n.d.	1 n.d.	n.d.	1 n.d.	3 n.d.	7 n.d.	6 n.d.	13 n.d.	3 n.d.	3 n.d.	11 n.d.		

a = 5 h, b = 2 h, c = 2.5 h, d = 90 min; e = 10% (v/v) *tert*-butyl methyl ether (MTBE); f = kinetic resolution of **26a** see below; * confirmed by mass analysis; † *ee* determined via upscale and polarisation measurement, also YqjM C26D/168V showed (R)-**33b**; rac. = racemic, s.m. = starting material; n.c. = no conversion, n.d. = not determined.

Substrate **26a** was used as a racemic starting material, from which all C25D variants consumed mostly the enantiomer with a retention time of 12.25 min, whereas all C25G variants consumed mostly the enantiomer at 11.10 min. All conversions end up with the same product in the achiral and chiral GC measurement determined by retention time, which argue for the formation of the *meso* compound (Scheme 11). It shows that with the *TsER* panel the access to both stereo-selectivities at position C5 from **26a** is possible; otherwise the formation of diastereomers had to be detected in the achiral measurement. The enantiopure reference compounds of **26b** are not commercially available; thereby it was not possible to determine the exact produced product.



Scheme 11. Kinetic resolution of **26a** with the shown *TsER* variant panel. To start from a racemic mixture can end-up in diastereomers, *trans* enantiomers and *meso* compounds. In the achiral and chiral GC measurements from the biotransformation of **26a** with *TsER* variants just one product could be observed. This would argue for the formation of the *meso* compounds.

Succinimides are cyclic imides that have pharmaceutical applications such as in the production of anticonvulsant drugs, like ethosuzimide^[222] and phensuximide^[223]. In addition, *N*-aryl succinimides, like **32b** have potential use as fungicides, such as *N*-(3,5-dichlorophenyl) succinimide.^[224] Seventeen ene reductases are able to convert **32a** in high yields and near optical purity to (*R*)-**32b**, also the *TsER* panel described here can be added to this OYE

list.^[65,73,85,99,109,220,221] The high activity rates towards five-membered cyclic imides can be explained by the presence of two activating carbonyl groups next to the carbon-carbon double bond.

Originally, these *TsER* variants were evolved for cyclohexenone derivatives; therefore it is particularly interesting that structures such as **19a** and **37-38a** as well as derivatives of cinnamic acid (**39-40a**) are also accepted with excellent conversions. Aldehydes such as citral (**38a**) and cinnamaldehyde (**39a**) are used in the production of perfumes.^[225] The asymmetric bioreduction of nitroalkenes like **41a** or **42a** is an attractive method for chiral nitroalkane formation. Compounds that contain nitro groups are versatile intermediates for the synthesis of natural products and other complex organic molecules, because the nitro group can be transformed efficiently into a variety of diverse functionalities.^[226,227] Nitroalkanes are often used as industrial synthons, because they can be converted into corresponding amines, aldehydes, carboxylic acids, oximes, hydroxylamines or denitrated compounds.^[227] In the study here both stereoisomers of **41b** could be obtained in excellent *ee* values (>99% *S* and >99% *R*), with the easy to use *TsER* panel. Previously only PETNR of group 1 showed high selectivity for production of (*S*)-**41b**.^[167]

The performed screening contained several new substances for ene reductases, of which four were transformed (**26a**, **36a**, **40a** and **42a**). Especially **40b** is formed with high conversion and as a single enantiomer. Small structural modifications (**50a**, **51a**) abolish reduction.

To fine-tune the activity and stereoselectivity of these double variants a third residue was targeted. As mentioned above, A102 forms a side pocket together with C25 and I67. In the directed evolution study of YqjM from *Bacillus subtilis*, variants with mutations in positions C26 and A104 contribute to higher activity towards β -substituted cyclohexenones.^[67] Especially the introduction of polar and bulky residues, like histidine and tyrosine were obtained. Based on this, the

TsER variant panel was enlarged by introducing either H, Y or I at position A102. Also tryptophan was introduced at this position, but did not lead to the successful production in *E.coli*. These triple variants were then tested against the aforementioned 38 compounds (Table 3). Increased activity for some previously poorly accepted compounds was observed. Compared to the double variants^[228] the production of **36b** increased from 17% for C25D/I67V to 33% with C25D/I67T/A102H. Conversion of **41a** was enhanced from 64% with C25G/I67T to 98% with C25G/I67T/A102Y and C25G/I67C/A102I without loss of enantiopurity (>99% *R*). The nitro limonene derivative **42a**, which is not converted by any double variant, is now reduced by C25G/I67T/A102Y up to 40%.

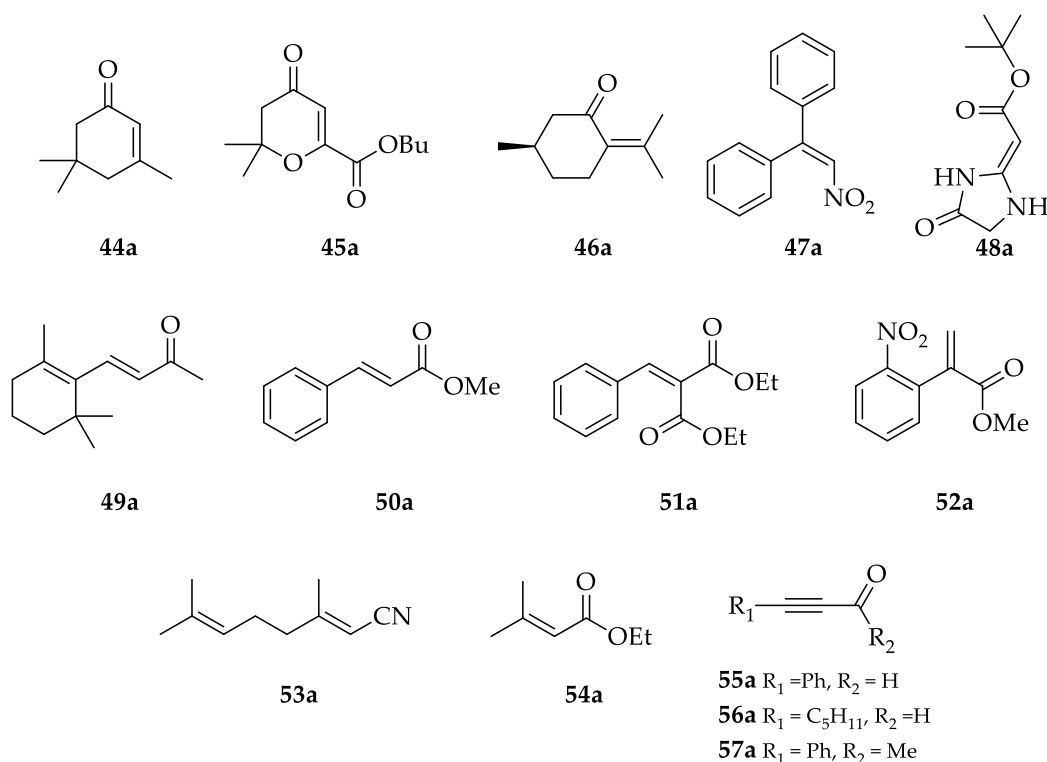
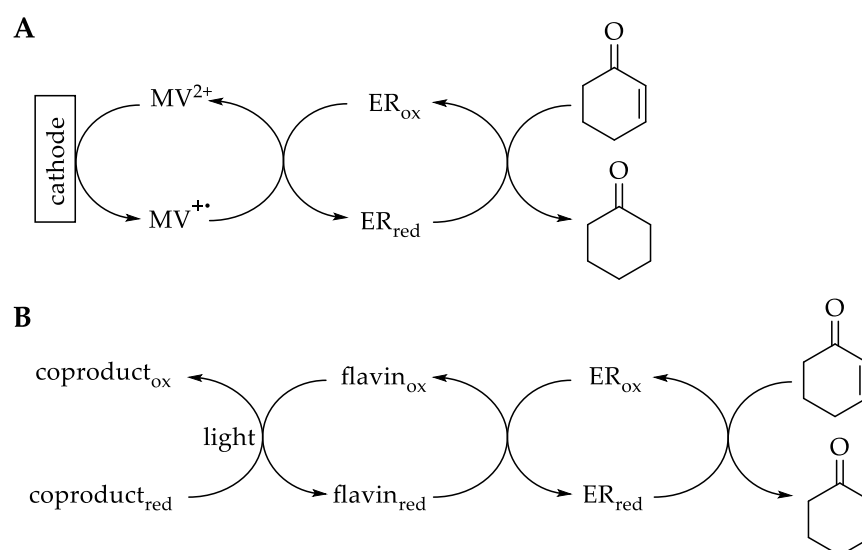


Figure 24. Non-substrates for *TsER* variant panel under screening conditions.

Overall, 14 compounds were not reduced under the used screening conditions (Figure 24). These molecules vary too much in structure and electronic properties to derive an explanation, only poor water solubility as possible cause was excluded by working in biphasic system. Therefore, investigations by docking and molecular dynamic studies were performed to better understand steric and electronic influence on the panel's substrate scope (see chapter 3.5).

It could be shown that a diverse range of industrially relevant compounds can be biocatalytically converted over an alkene reduction, which highlights the potential of the *TsER* panel belonging to the biological asymmetric synthesis manufacture. By using the purified thermostable enzyme, by-product formation can be avoided, but a disadvantage is the requirement for a cofactor-recycling system.

At the moment a research field is growing, which tries to solve the expensive cofactor problematic by electro- and photochemical methods. For example the use of a mediator that can transfer electrons directly to the enzyme would offer a nicotinamide-free alternative to the classical recycling system.



Scheme 12. A) Electrochemical reduction of cyclohex-2-enone by ene reductases (ER) using methyl viologen (MV) as mediator.^[229] B) Photoenzymatic reduction of cyclohex-2-enone with ER.^[78,230]

Such mediators, most prominently *N,N'*-dimethyl-4,4'-bipyridinium dichloride were already investigated in 1981 with the enoate reductase from *Clostridia* sp.^[231] The mediator is first electrochemically reduced at the cathode, and the resulting radical cation species can subsequently reduce flavin in the ene reductase (Scheme 12A). To date, related mediator-based systems have been investigated but practical applicability has not been demonstrated.^[179,229,232]

Another way to regenerate the enzyme is photochemically using an external flavin, like riboflavin, flavin mononucleotide or flavin adenine dinucleotide, while EDTA, formate or phosphite serve as sacrificial electron donors (Scheme 12B).^[78,230] Also some investigations were performed in synthetic nicotinamide cofactors as replacement for NAD(P)H for biotransformations with the *TsER* wild type by PAUL *et al.*^[233] On the basis that the here shown *TsER* variants have great activity to a large range of substrates, compared to the wild type, it would be worth investigating whether the presented methods solve the cofactor problem with these biocatalysts.

3.3.2 Reaction Conditions for Industrial Applications

3.3.2.1 Solvent Effects

The effect of organic solvents as a process parameter on the bioreduction should be tested, if a catalyst is to consider for use in an industrial approach. Low water-solubility of most ene reductase substrates, in combination with substrate/product inhibition, presents a considerable challenge, often resulting in low substrate loadings and significant amounts of waste water.^[22] Addition of organic co-solvents and use of biphasic reaction systems therefore offer significant advantages, often increasing the biocatalyst performance in synthetic chemistry.^[234,235] It is important to keep in mind that the reaction system used here consists of two enzymes, the ene reductase and a glucose dehydrogenase that belongs to the recycling system, which supplies the consumed hydride from a sacrificial agent. The following results are therefore specific to the reaction system.

It could be determined that water-miscible solvents lead to diminished activities when 10% (v/v) is exceeded (Figure 25). The most destructive effect on activity shows the panel of *TsER* variants with small polar solvents like C1 to C3

alcohols, dimethyl sulfoxide or acetonitrile, common co-solvents for organic molecules in biotransformation. Other ene reductases have likewise shown a similar intolerance against such co-solvents,^[81,84,220] but no clear trend is apparent.^[65,236–240] In contrast, the combination of *TsER* variant and the glucose dehydrogenase (GDH-60 from *EVOCATAL*) tolerates up to 20% (v/v) of various water-immiscible solvents without any loss in activity for the production of **40b**. Importantly, already a small volumetric amount of organic solvent (5-10% (v/v)) increased **40b** productivity up to 2-fold, enabling full conversion of the substrate. Encouraged by this result, the non-active substrates **49a** and **52a** were tested in the presence of 10% *tert*-butyl methyl ether (MTBE). No conversion was observed, excluding the possibility that they are not converted due to their low solubility.

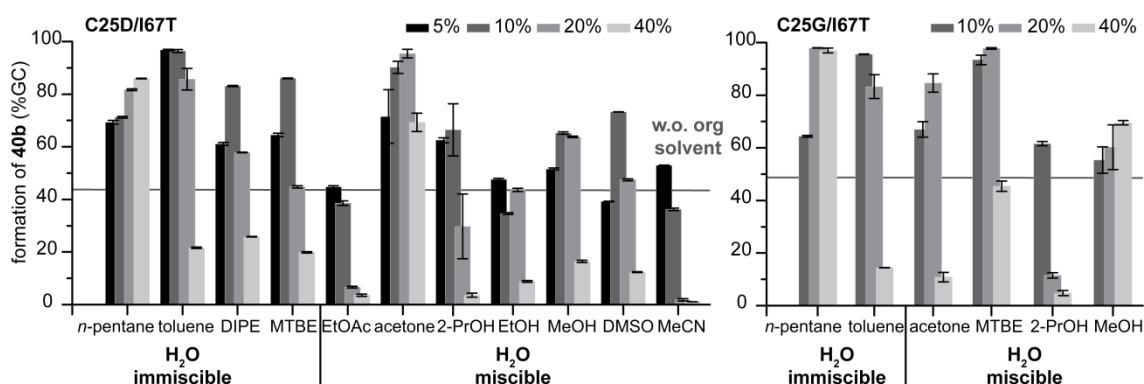


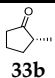
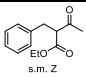
Figure 25. Effect of organic solvents to the biocatalyst. Addition of organic solvents increased formation of **40b**. Full conversion was reached with toluene, *n*-pentane and MTBE with either of the variants. Using 20% (v/v) organic solvent has a positive effect in most cases, and *n*-pentane is even tolerated up to 40% (v/v). Grey line indicates the conversion rate without (w.o.) organic solvent (C25D/I67T 43%, C25G/I67T 48%). MTBE, methyl *tert*-butyl ether; MeOH, methanol, 2-PrOH, 2-propanol; DIPE, diisopropylether; EtOAc, ethyl acetate; EtOH, ethanol; DMSO, dimethyl sulfoxide; MeCN, acetonitrile.

Addition of *n*-pentane, MTBE, diisopropyl ether (DIPE) or toluene proved to be particularly effective. The low water miscibility of *n*-pentane (39 mg·l⁻¹)^[241] even allowed reactions with 40% (v/v) and the recovery of a clean product by simple phase separation. The findings that immiscible solvents are more compatible and enhanced conversion levels confirm observations made for other OYE wild types.^[81,220,242] Immiscible solvents provide a substrate and product sink for the

organic compound, keeping concentrations of reactants in the aqueous phase low.^[243–246] This is beneficial for enzyme catalysis, because such a reaction setup often circumvents inhibition due to high product concentrations in the aqueous phase.

It was noted that the enantiopurity of **33b** increased up to 30% upon addition of an organic phase. Interestingly, the effect was only observed for the wild type and *TsER* C25D based variants (Table 4). The beneficial effect of a biphasic system on enantiopurity was previously described for compounds prone to racemization, like **33b** and **22b**.^[65]

Table 4. Solvent effect on conversion and *ee* of **33a** and **40a**. For **40b** the *ee* values were always >99%. All reactions were done in triplicates; standard deviation for conversion is $\pm 5\%$. The reactions were stopped after 24 h.

	wt	C25D/I67C	C25D/I67T	C25D/I67V	C25G	C25G/I67C	C25G/I67T	C25G/I67V
 33b	conv% <i>ee</i> /%	conv% <i>ee</i> /%	conv% <i>ee</i> /%	conv% <i>ee</i> /%	conv% <i>ee</i> /%	conv% <i>ee</i> /%	conv% <i>ee</i> /%	conv% <i>ee</i> /%
without solvent	99 79R	99 66R	91 57R	99 69R	90 87R	>99 84R	99 81R	96 85R
with 10%(v/v) MTBE	99 96R	99 71R	91 88R	99 88R	90 88R	>99 82R	99 80R	96 84R
 40b	conv%	conv%	conv%	conv%	conv%	conv%	conv%	conv%
without solvent	40	58	43	60	38	45	48	37
with 10%(v/v) MTBE	91	88	88	96	39	42	90	37

In addition, pH variation,^[191] choice of nicotinamide recycling system, as well as the enzyme concentration or the presence of oxygen^[210] are also described to have a small but notable effect on the enantiopurity of ene reductase reactions. While all these observations might be explained by the solvent effect on stereoselectivity and the formation of different solute-solvent clusters at various reaction conditions,^[247] it was surprising to see such a significant difference between the two variant groups.

3.3.2.2 Temperature Effects

Enzymes with high thermal stability are of particular interest to biotechnology and basic research.^[248] Increased stability and life-times enables more flexibility in process design, use in new reactions and exploration of basic research questions without the limitation of a narrow temperature window.

Before investigating the thermal stability of the whole reaction system, the individual thermal stability of both enzymes, glucose dehydrogenase and ene reductase in the reaction system, used during this thesis, was assessed. The recycling system based on GDH-60 from EVOCATAL was found to be active up to 50 °C (Table 5). The engineered GDH from *Bacillus subtilis* (*BsGDH* E170K/Q252L)^[59] showed still 60% specific activity at 70 °C under the reaction conditions which were used in this thesis. Thus, the investigation of temperature differences was performed with the *BsGDH*.

Table 5. Spectrophotometric determination of temperature dependency of used glucose dehydrogenases. The engineered *BsGDH* shows highest activity at temperatures between 40-60 °C. Activity is reduced by 50% at 30 and 70 °C, whereas the GDH-060 from EVOCATAL shows no activity at 60 and 70 °C. Therefore, *BsGDH* was used analysing the temperature dependency of the bioreduction. The temperature range of the spectrophotometer is 0-70 °C.

	Temperature	30 °C	40 °C	50 °C	60 °C	70 °C
<i>BsGDH</i>	activity [U/mL]	32.80	57.78	61.70	58.94	38.31
	relative activity	0.53	0.93	1.00	0.95	0.62
GDH-60 (EVOCATAL)	activity [U/mL]	23.05	41.42	46.78	0.00	0.00
	relative activity	0.49	0.88	1.00	0.00	0.00

The thermal stability of variant C25G/I67T and C25D/I67T was assessed by incubating the purified enzymes in buffer at temperatures between 4 and 70 °C for 14.5 h prior to a reaction at 30 °C (Figure 26A). Both *TsER* enzymes retain full activity up to an incubation temperature of 60 °C. At 70 °C incubation, C25D/I67T lost 3% and C25G/I67T 14% of its initial activity. This thermal stability is comparable to that of the wild type.^[179] Notable is the 1.06-fold activity enhancement for C25G/I67T after incubation at 30 °C compared to no pre-

incubation, while the activation effect might be masked for C25D/I67T, since full conversion was reached.

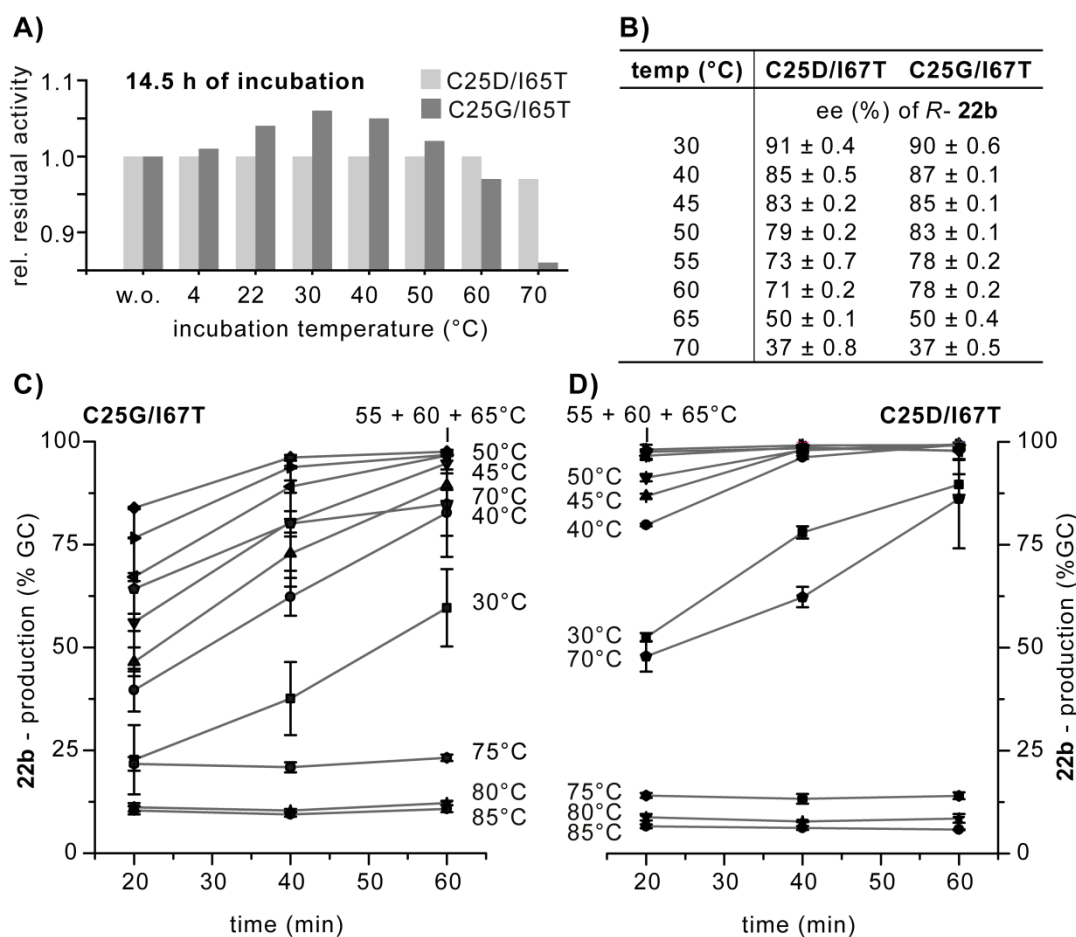


Figure 26. Thermostability assessment of the ene reductase reaction system. A) Residual activity at screening conditions of *TsER* C25G/I67T and C25D/I67T after 14.5 h incubation at different temperatures. Temperature-time dependent formation of **22b** with the reaction system containing a *TsER* variant and the engineered *BsGDH*^[59] at temperatures between 30 and 85 °C. C) C25G/I67T, D) C25D/I67T, B) Enantioselectivity of **22b** in the presence of *TsER* decreases rapidly with higher temperatures, while in absence of an ene reductase and recycling system, the enantioselectivity is stable up to 60 °C but at 65 °C and above, **22b** racemizes and an *ee* of 8% is observed.

After ensuring thermal stability of both enzymes, the reaction system was tested for levodione (**22b**) production at reaction temperatures between 30 °C and 85 °C. Formation of **22b** completes in 150 min under screening conditions. Increasing the temperature accelerated the reaction, now reaching full conversion in less than 20 min (C25D/I67T) or 40 min (C25G/I67T) at 55 °C (Figure 26C, D). Productivity is not affected up to 65 °C, whereas both variants start losing activity at 70 °C and above. In general, working above 75 °C reduced the lifetime of

the reaction system below 20 min. Not only the enzymes, but also the nicotinamide cofactor (NADPH/NADP⁺) is labile at higher temperatures. The half-life of dissolved NADPH at 70 °C and above is less than 10 min.^[249,250] Therefore, it is impossible to distinguish between cofactor or enzyme degradation as source for lost activity at high temperatures. This might be a general challenge for processes with oxidoreductases at higher reaction temperatures and long reaction times. The enzyme can be engineered to be more stable,^[51,251,252] but the stability of the cofactor cannot be altered unless another molecule is used. Consequently, as long as thermolabile nicotinamide cofactors are used, increased reaction temperatures may negatively impact yields for reaction times longer than a few hours, despite the increased reaction rate and enhances solubility of organic molecules at higher temperatures.

It is known that (*R*)-levodione (**22b**) racemizes in buffered aqueous solution approximately 3% *ee* per hour at ambient temperatures.^[218,253] It was expected, that the effect would be more dominant at increased temperatures and could be found that incubation of (*R*)-**22b** in aqueous buffer without ene reductase at 65 °C and above for one hour results in a loss of enantiopurity yielding an *ee* of 8%. The reaction system used here produces (*R*)-**22b** with an *ee* of 92% at 30 °C. When increasing the temperature, the enantiopurity drops by 50% (Figure 26B). At 70 °C, 37% *ee* is still observed, indicating that the reduction is faster than the racemization. Thus, an increased reaction temperature seems only beneficial for non-racemizable or achiral compounds.

3.3.2.3 Divalent Metal Impacts and pH Effects

The glucose based recycling system is irreversible due to the hydrolytic cleavage of gluconolactone to gluconic acid, benefitting NADPH production but also leading to acidification of the reaction. Therefore investigations for the effect of pH on the reaction system were performed and it was found to work well in the

range between pH 6-8 (Figure 27A and C). The C25D/I67T variant is less affected by a change in pH and still shows production of **22b** without loss of efficiency at pH 9.

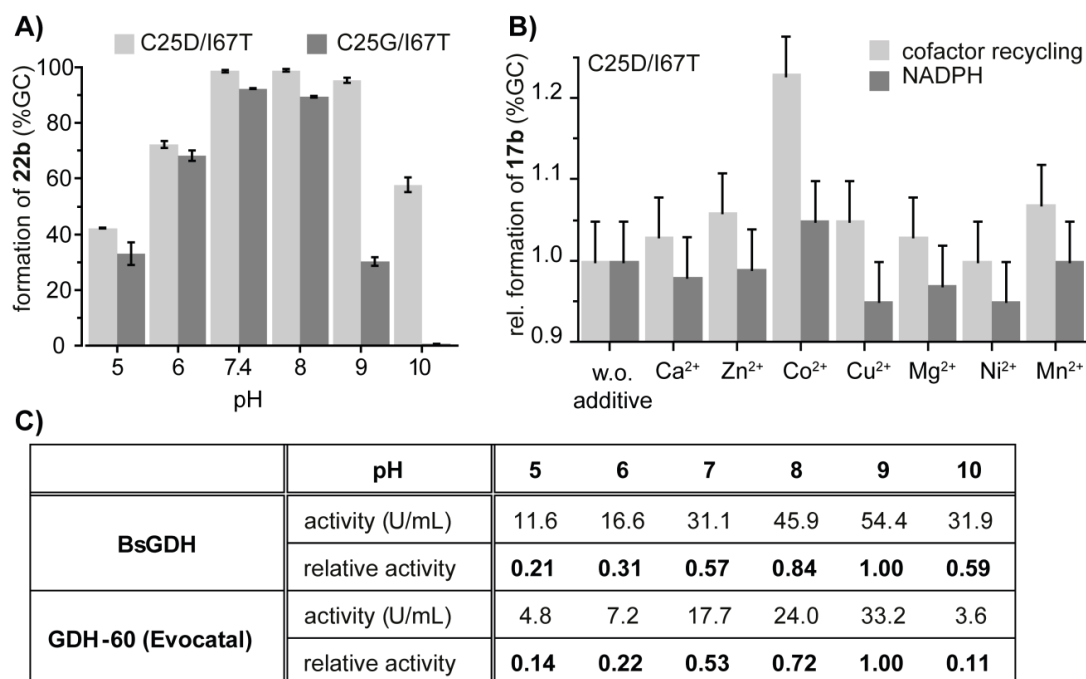


Figure 27. Effect of pH and divalent metal salts on productivity. A) Effect of pH on **22b**-production with the reaction system consisting of C25D/I67T or C25G/I67T and GDH-60. B) Divalent metal chloride salts marginally affect productivity of **17b** with stoichiometric amounts of NADPH (light grey). When the recycling system is used instead (GDH-60/glucose), higher productivities are achieved and the addition of Co²⁺ becomes slightly beneficial. C) pH dependency of the two used recycling systems, consisting glucose dehydrogenase, glucose and NADP⁺.

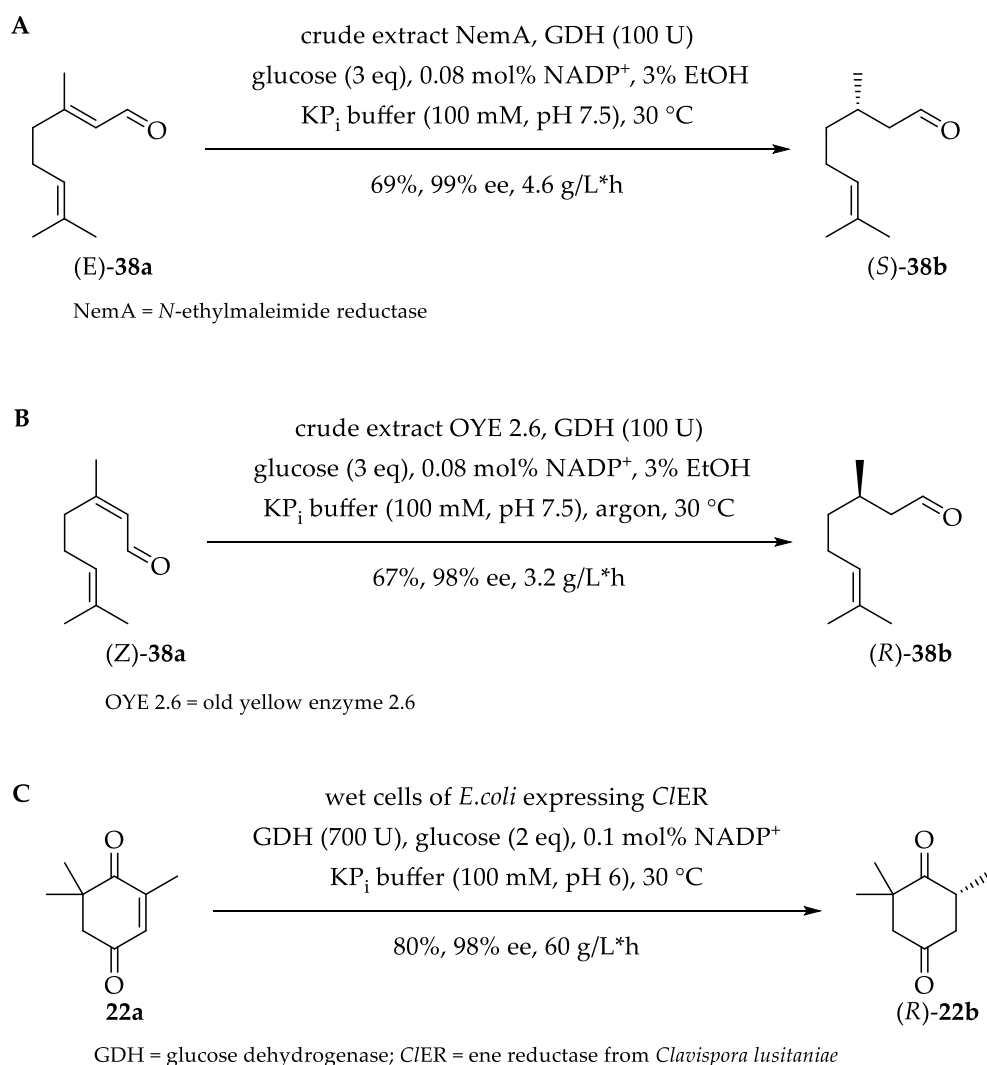
Remarkably, 40-60% formation of **22b** was still observed at a pH of 5 and 10, especially considering that NADPH/NADP⁺ rapidly degrade at pH values below 7.^[254] The buffer capacity is 100 mM, ten-times higher than the amount of possible acid equivalents under screening conditions. On this scale, acidification of the reaction mixture was never observed. When aiming for higher substrate loadings (>100 mM), gluconic acid equivalents exceed the buffer capacity and process engineering is needed to compensate for the pH drop.

In view of the fact that enzymes and classical catalysis are more and more combined in one-pot reactions,^[255,256] the effect of divalent metal salts on the *TsER* variant panel and on the reaction system was tested. Water soluble chloride salts of divalent metals (Figure 27B) had no significant effect on productivity of

17b. The metal salts had a minimal positive effect when the GDH-60 based recycling system was used, where the minimal improvement of Co^{2+} became significant and an overall improvement of 0.2 fold was observed.

3.3.3 Preparative Scale Reactions

Due to the highly selective hydrogenation of especially α,β -unsaturated alkenes the Old Yellow Enzyme family is a quite interesting target for biotransformations in industrial production. Nowadays the large-scale production of (*R*)-levodione (**22b**) from ketoisophorone (**22a**) is the most prominent biocatalytic reduction catalysed by Baker's yeast^[217] and other ene reductases^[257], which was also mentioned in chapter 3.3.1. Examples of currently used synthetically relevant OYE bioreductions are presented in Scheme 13. These three examples of multigram scale products with industrial relevance are obtained by different ene reductases in whole cell synthesis. Whole cell synthesis has advantages, as well as disadvantages, over isolated enzymes for industrial applications. First of all whole cells allow the production of compounds through multi-step reactions and with cofactor regeneration. But for a pharmaceutical application it is disfavoured to use genetically modified organisms (GMOs) in the process.^[258,259] To broaden the substrate scope and stereoselectivity of ene reductases most often the enzymes are modified by protein engineering methods and heterologously expressed in *E.coli*. To avoid these genetically modified organisms, it would be important to use purified enzymes.



Scheme 13. Synthetically relevant examples of bioreductions realized with ene reductases for industrial relevant alkenes obtained in high enantiopurity in up to multigram scale.

In the presented thesis so far, the reduction of electron-deficient alkenes was demonstrated only at the screening scale (10 mM, Table 3). Therefore bioreductions at a preparative scale between 2.5 and 25.6 mmol (equivalent to 275 mg and 3.84 g) with selected variants for compounds **17a**, **22a**, **18a** and **40b** at 30 °C were performed (Table 6). Up-scaling successfully reproduced conversion and selectivity values of the screening scale (Table 3). Substrate loadings could even be increased to 125 mM (19 g/L), demonstrating that the reaction system is easily scaled to gram quantities producing excellent yields up to 93%. Also the amount of glucose could be decreased from a ten-fold excess to 1.75 molar equivalents, possible through the reactor design, minimizing the available gas volume in the reactor thereby reducing the oxygen concentration which avoids

side reactions of uncoupling processes. In addition, use of a bi-phasic reaction system has helped to increase overall substrate concentration at constant reaction volumes, thus increasing the space-time-yield. Furthermore, it simplified the down-stream processing, and reduced the amount of waste water. Substitution of the standard extraction solvent ethyl acetate by diethyl ether increased yields from 72 to 91% for **17b**, and 78 to 93% for **18b**. Overall, the examples in Table 6 demonstrate the synthetic potential of the TsER variant panel for the synthesis of chiral and achiral compounds.

Table 6. Preparative scale bioreduction at 30 °C using TsER variants and BsGDH. Part of this work was performed by LUCA SCHMERMUND during his master thesis.

Product	TsER Variant	Scale mmol	catalyst loading	substrate loading	Time ^a (h)	Conv. %GC	% ee or % de	Yield %	TON	TOF ^c h ⁻¹
17b ^(d)	C25G/I67T	2.5	0.02 mol% 10 μM	50 mM 5.5 g/L	8.0	78	51S	72 ^(g)	3900	1986
17b ^(d)	C25D/I67T	2.5	0.02 mol% 10 μM	50 mM 5.5 g/L	9.0	99	>99R	91 ^(g)	4970	3911
22b ^(e)	C25D/I67T	2.5	0.008 mol% 10 μM	125 mM 19.0 g/L	1.5	91	98R	65	11375	7583 ^(b)
18b	C25G/I67T	6.9	0.005 mol% 3.4 μM	69 mM 10.4 g/L	4.5	>99	88 ^(f) <i>trans</i>	90	20294	5958
18b	C25D/I67T	6.9	0.005 mol% 3.4 μM	69 mM 10.4 g/L	6.8	>99	96 ^(d) <i>cis</i>	78	20294	4928
18b ^(d)	C25D/I67T	25.6	0.01 mol% 5 μM	51 mM 7.7 g/L	7.0	>99	96 ^(f) <i>cis</i>	93 ^(g)	10189	40634
40b ^(e)	C25D/I67T	1.0	0.02 mol% 10 μM	50 mM 10.9 g/L	2.0	81	>99	76	4050	2025 ^(b)

(a) Time until completion of reaction. (b) Determined after completion of reaction. (c) Determined after 30 min. Time dependent product formation is shown in Figure 28. (d) Addition of 10% (v/v) *n*-pentane. (e) Addition of 10% (v/v) DIPE. (f) Starting material contains 2% of enantiomer **30b** (*R*)-Carvone. (g) Extraction with diethyl ether increased yield.

In addition, the results in Table 6 reflect the electronic deactivation effect of alkyl substituents at C_β-position. These substrates require twice the catalyst loading and longer reaction times, as shown for **17b**-production. In contrast, substrates like **22a**, **18a** and **40b** complete approximately 10 times faster, as judged by obtained turnover frequencies (TOF).

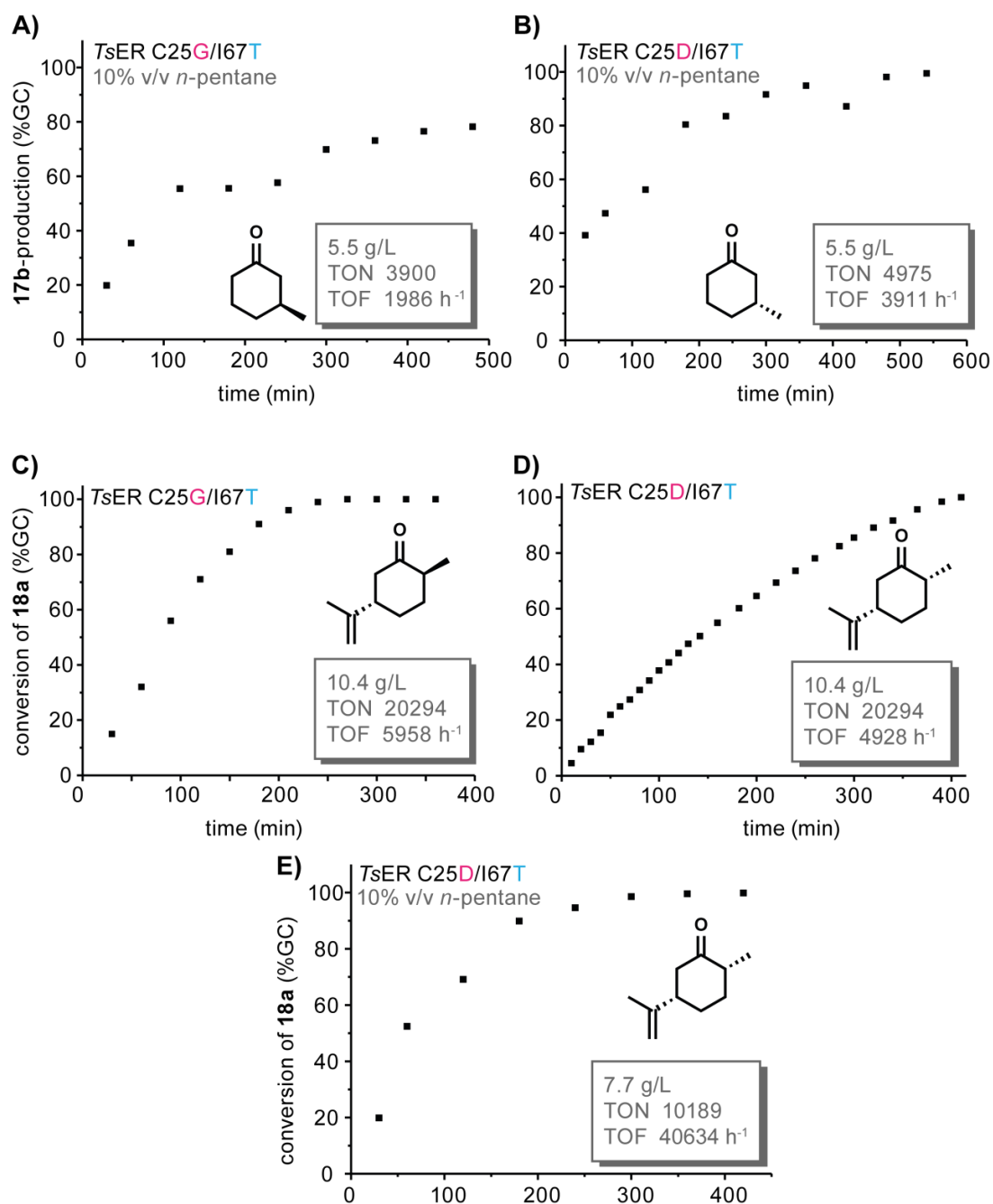


Figure 28. Preparative scale bioreduction with *TsER* C25G/I67T and C25D/I67T. Doubling the enzyme concentration was required to achieve (A) 78% or (B) >99% production of **17b** in reasonable times of 8 or 9 h, respectively. Total conversion of **18a** was achieved after (C) 4.5 h and (D) 6.8 h. (E) Variant C25D/I67T was able to convert 3.85 g of **18a** in 7 h.

Long term stability and enzyme reusability are additional requirements of a convenient catalyst system, and therefore experiments in which the substrate in its organic solvent (here DIPE) is repeatedly replaced after each transformation were performed, leaving the enzyme and recycling system in the aqueous phase. Figure 29 shows three consecutive batches in sum producing 2.5 mmol **22b**. More than 50% conversion was still observed in the third batch, despite no

visible precipitation to indicate denaturation of the enzymes. A pH determination also excluded a drop in pH as potential cause. Only one other case of repetitive batch experiments has been reported for an ene reductase, where four cycles without loss of activity were observed in a continuous electrochemical reduction on chip, producing 0.07 mmol cyclohexanone with an turnover number (TON) of 2500 and a turnover frequency (TOF) of 7 min^{-1} ,^[229] whereas in the study presented here a TON of 12 500 and a TOF of 25 min^{-1} could be achieved.

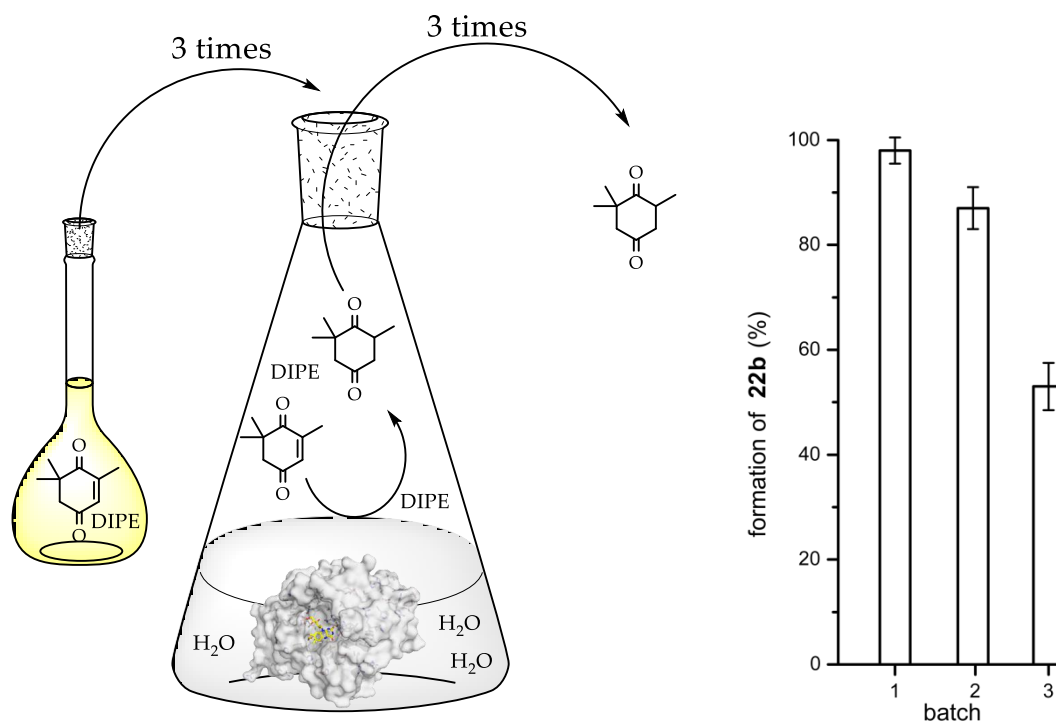


Figure 29. Effect of reusability of the biocatalyst in a sequential batch reaction. Three consecutive batches with ketoisophorone (**22a**) in 10% DIPE were performed. After each batch, phases were separated and a new amount of **22a** in 10% DIPE was added. DIPE, diisopropylether.

In general, the up-scale reactions complete in less than 9 h, whereas other preparative scale bioreductions with ene reductases are reported to run for 20-96 h^[84,260,261] or at 10 to 40 times higher catalyst loadings.^[255] The catalytic systems show TOF rates of 0.13 to 2 s^{-1} , which are comparable to hydrogenation rates by transition metal catalysis.^[262] The panel of variants shown and the conditions developed here expand the possibility of employing ene reductases in preparative-scale reactions.

3.4 Structural Insights

3.4.1 Structural Dynamic Study by H/DX Measurement

To study higher-order structures (HOS) of enzymes and their dynamics the hydrogen/deuterium exchange (H/DX) method provides a powerful established mass spectrometric process. Recent innovations in this technique by automation of the procedure coupled with advanced liquid chromatography (LC) and mass spectrometry (MS) as well as the development of informatics techniques reveal its great potential for academic research and industrial applications.^[263] Classical analytical tools like circular dichroism (CD), differential scanning calorimetry (DSC), isothermal titration calorimetry (ITC), or analytical ultracentrifugation, are capable of illustrating a global conformational change, but are not suitable for the investigation of dynamic conformational changes in proteins. H/DX MS on the other hand provides a great resolution at the peptide level in order to determine local changes of HOS. Combined with X-ray crystallography and nuclear magnetic resonance spectroscopy (NMR), it provides given structures with further information regarding flexibility and dynamics in solution.^[264]

The setup of the automated H/DX experiment is shown in Figure 30. The first step is the so-called on-exchange phase, where the sample is incubated in D₂O buffer. Afterwards, the deuterium exchange gets quenched by adding a cold acidic solution. To obtain analysable peptide fragments the protein gets unspecific digested by the protease pepsin. In the last step the gained fragments are separated by chromatographic methods coupled with mass analysis.^[265]

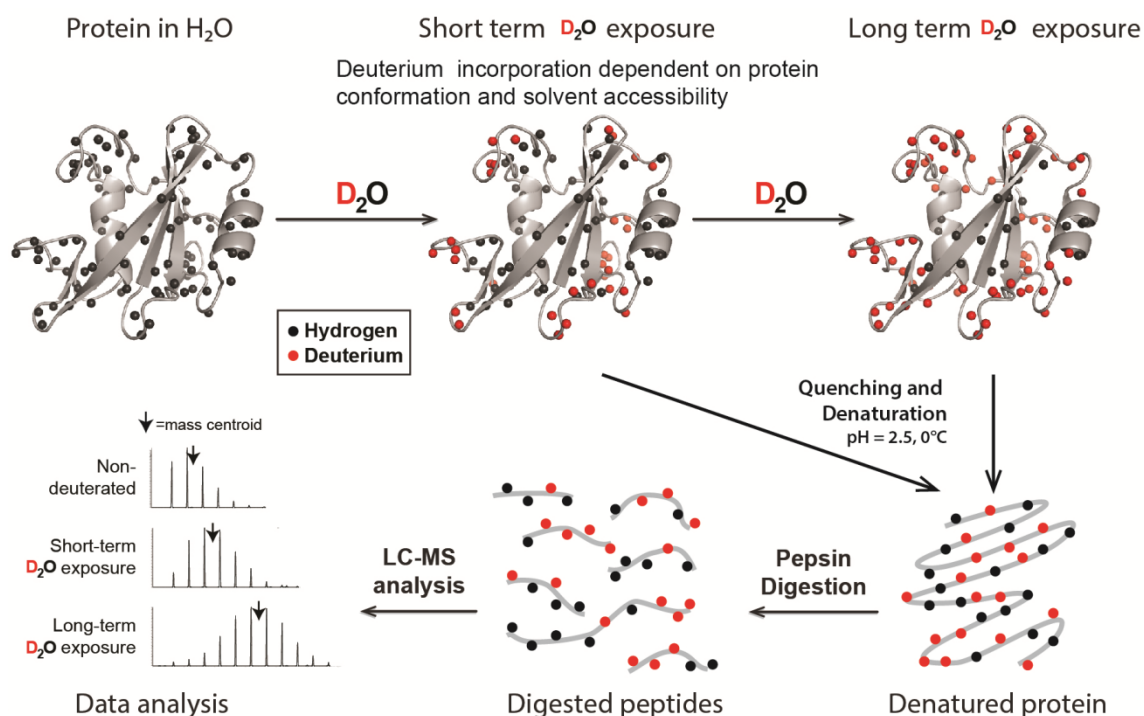


Figure 30. Workflow of an automated H/DX MS experiment. In the first step a protein of interest gets exposed to deuterated solvent for a period of time, followed by quenching in a low pH buffer where exchange rates are dramatically decreased, followed by fragmentation of the protein and mass analysis.^[266]

In the presented thesis a successful H/DX study for the OYE family member *DrER* from *Deinococcus radiodurans* R1 is reported. The attempt to examine such a structural dynamic study with *TsER* proved to be not feasible with the available setup. Due to the thermostability and robustness of this enzyme, it was not possible to rapidly denature the protein by quenching and digest it to obtain small enough peptide fragments for the analysis. All possible parameter changes, which were undertaken, such as higher temperatures of the digest, did not lead to an analysable dataset. Consequently, the H/DX study was performed with the related, but not thermostable ene reductase *DrER*, to gain more structural information about this family member, since to date no crystal structure is available.

The enzyme was analysed in three different states, one apo-state, that means just the holo-protein without any additive, the second state with calcium chloride added and the third state with the addition of calcium chloride and NADP⁺. The addition of a divalent metal ion was used, because it is known that

OYEs from group 2 benefit from the presence of calcium or magnesium during catalysis.^[99] But neither the location of the divalent metal binding site nor the role this ion plays is known.

Labelling of the protein samples occurred at four different time intervals, which were chosen to be $t_0 = 0$ min, $t_1 = 0.5$ min, $t_2 = 1$ min and $t_3 = 5$ min. During this time the amide hydrogens of the protein backbone were able to exchange with the deuterated solvent. Depending on its solvent accessibility and hydrogen bonding, the deuterium uptake of a local peptide fragment differs from the native control fragment. To interrupt the exchange reaction, the medium becomes quenched with a cold acidic buffer and is injected into the H/DX manager at 0 °C. The quenching does not just stop the exchange, but also leads to a denaturation of protein, which facilitates the following proteolysis by pepsin. To ensure that the pepsin is not injected into the LC-MS system, it is immobilized to a stationary phase and packed into a column.^[267] These quantities of peptide fragments, which are a result of the unspecific digestion of pepsin, are of random size and therefore have to be identified by the PLGS Software of WATERS. Digestion of the unlabelled protein constructs gives the initial peptide map, which in combination of the digestion of labelled proteins results in a creation of a so-called heat map, representing the local uptake of deuterium (Figure 31).

For the analysis of *DrER* a total coverage of 96.8% by 259 peptides was calculated and led to a redundancy of 6.75. In the context of the heat map, remarkably high uptake of deuterium can be observed at the C- and N-terminus of the enzyme, indicated by the red fields, but changes in uptake over time are marginal just as the differences to between each state. In addition, this is highlighted by the heat map, where all of the measured states are compared to each other, showing no significant differential uptake.

Through b-factors, which can be obtained from the software DYNAMX 3.0, the two dimensional heat map can be plotted on a user-chosen crystal structure to

get a three dimensional picture with dynamic features. No crystal structure of *DrER* wt is available so far, but with the online bioinformatic tool SWISS-MODEL a homology model was created (Figure 32). The results show that the b-factors of H/DX calculation fit quite well to the homology structure. For example loops, which are dangling mainly at the outer face of the enzyme, have a higher uptake over time than conserved regions, like most α -helices and β -sheets. Quite low fractional uptake is present between *N*- and *C*-terminus with exception to a few fragments.

An interesting strong fractional uptake over time takes place at the position 29-32 (amino acids: ELPN), whereas broad and more moderate to low uptake over time can be observed for positions 87-94, 128-138, 157-161, 247-257, 273-301, 304-308, 314-326 (marked with black arrows in Figure 32).

DAUGHERTY *et al.* showed via a synthetic circular permutation library of the OYE1 from *Saccharomyces pastorianus*, that structural rearrangements of some flexible loops and domains play an important role in the catalytic function of OYE enzymes.^[168] During the strategy of circular permutation (CP), the original *N*- and *C*-termini of the protein are covalently linked by a peptide linker and new termini are introduced elsewhere in the protein structure through breakage of a peptide bond.^[268] The selected flexible regions for CP are comparable with the results from H/DX plotted b-factors to the homology model of *DrER*. They chose three different sites as locations for new termini. One is the exterior helical subdomain (OYE1 residues 125-160), which is also highly flexible in *DrER* at positions 285-301. The second sector includes loop and helix in regions from 250-265 at OYE1, which is comparable to residues 317-325 in *DrER*. The third part represents a short loop, residues 375-380 in OYE1 that is also present with a big exchange in *DrER* (residues 87-94).^[168]

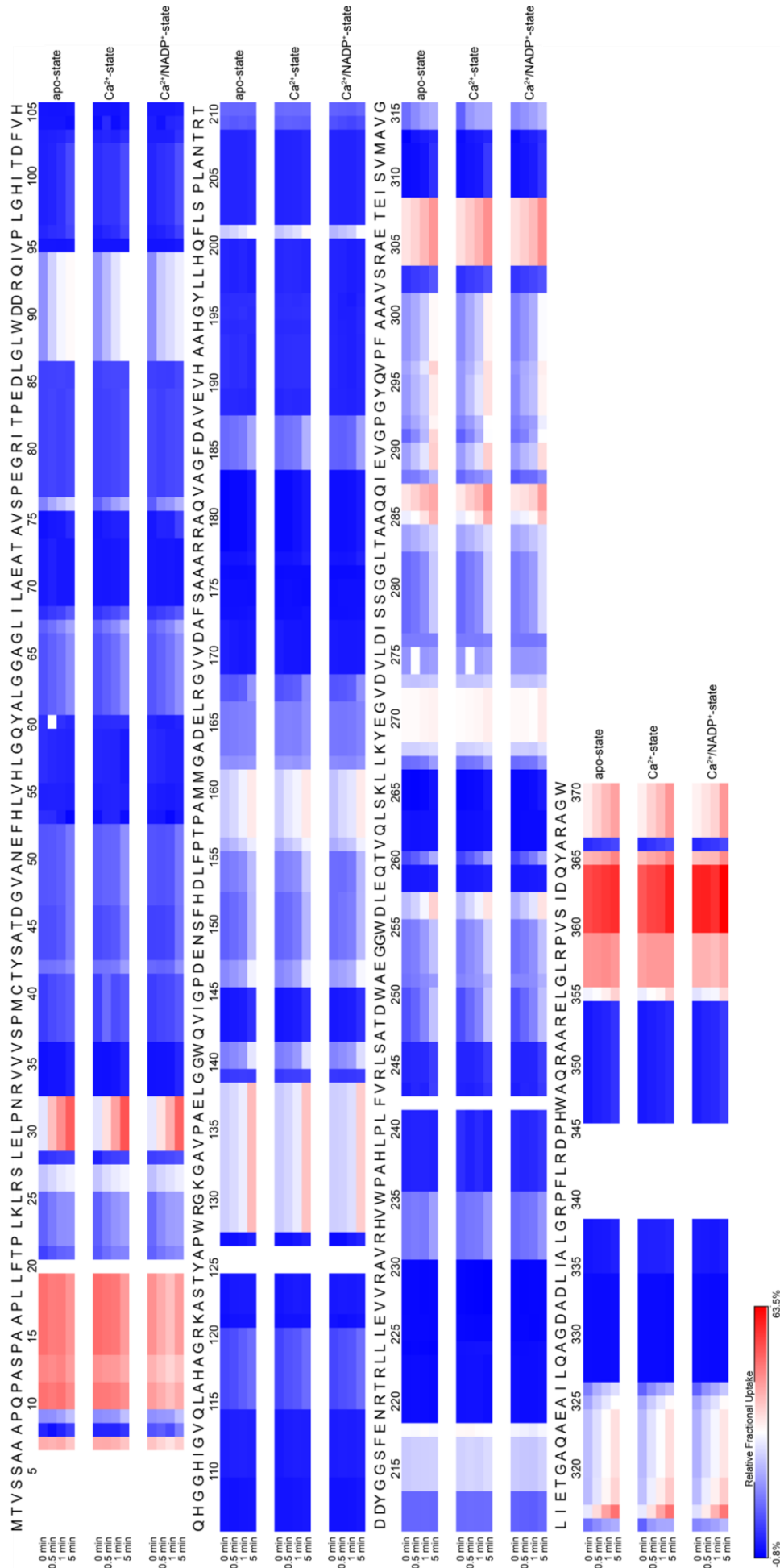


Figure 31. Heat map generated with the Software DYNAMX 3.0 for the sequence of DrER wild type. The coloring indicates the relative fractional uptake, which is scaled to a data range of -0.77 to 63.54% within the given amino acid sequence for its three states Apo, Ca²⁺ and Ca²⁺/NADP⁺ in respect to the different time intervals of 0 min, 0.5 min, 1 min and 5 min. Deuterium exchange ranges from poor (blue) to strong (red) uptake

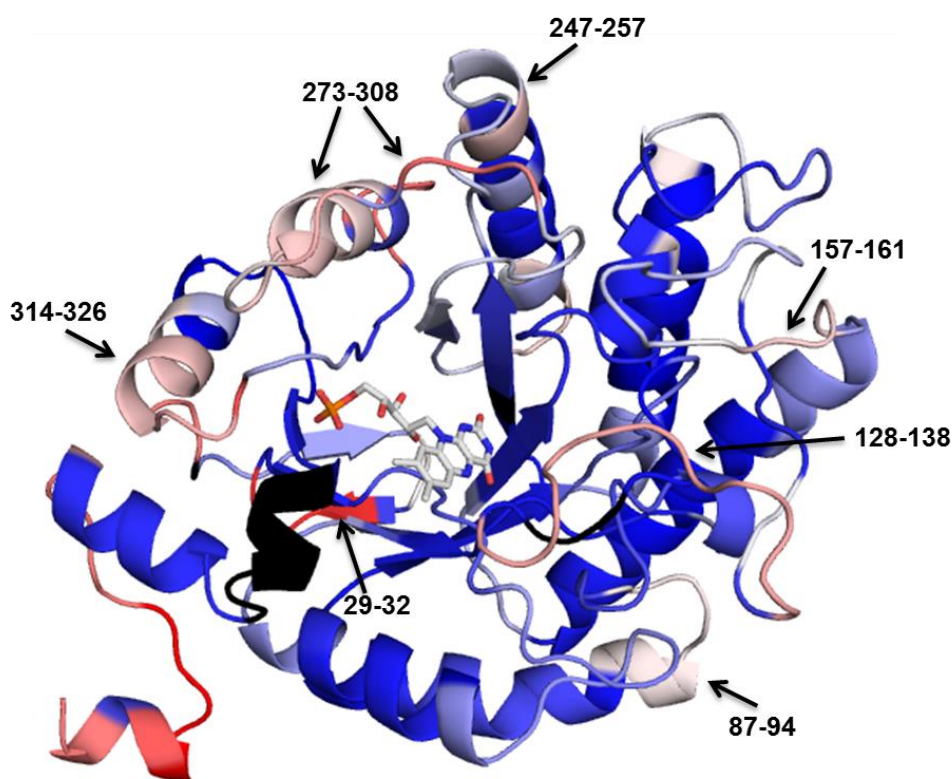


Figure 32. Homology model of *DrER* wt, based on pdb 1Z44^[94], representing fractional uptake of the peptide amino-backbone after 5 min within the $\text{Ca}^{2+}/\text{NADP}^+$ state, ranging from no/low (dark to light blue) to moderate/high (white to red, marked with black arrows and peptide numbers). Black color fragments indicate mapping gaps, for which no peptides were available. Cofactor FMN is shown in grey sticks.

In addition, H/DX analysis was performed to find a potential divalent metal binding site in *DrER*. To identify the calcium binding site, it is expected that at this specific position in the peptide, less uptake will take place when Ca^{2+} is bound in the Ca^{2+} and $\text{Ca}^{2+}/\text{NADP}^+$ states compared to the apo state.

However the heat map did not show any difference in uptake in the different states. Even though it has not been possible to identify the divalent metal binding site, the H/DX results give good insights into the structure and dynamics of *DrER* in solution.

3.4.2 X-Ray Structures

In collaboration with D. J. OPPERMAN (University of Free State, Bloemfontein) it was possible to obtain a crystal structure of the most promising stereo-complementary variant *TsER* C25D/I67T compared to the *TsER* wild type. The biological dimer was generated from chain A and its crystallographic 2-fold rotational symmetry operator (Figure 33).

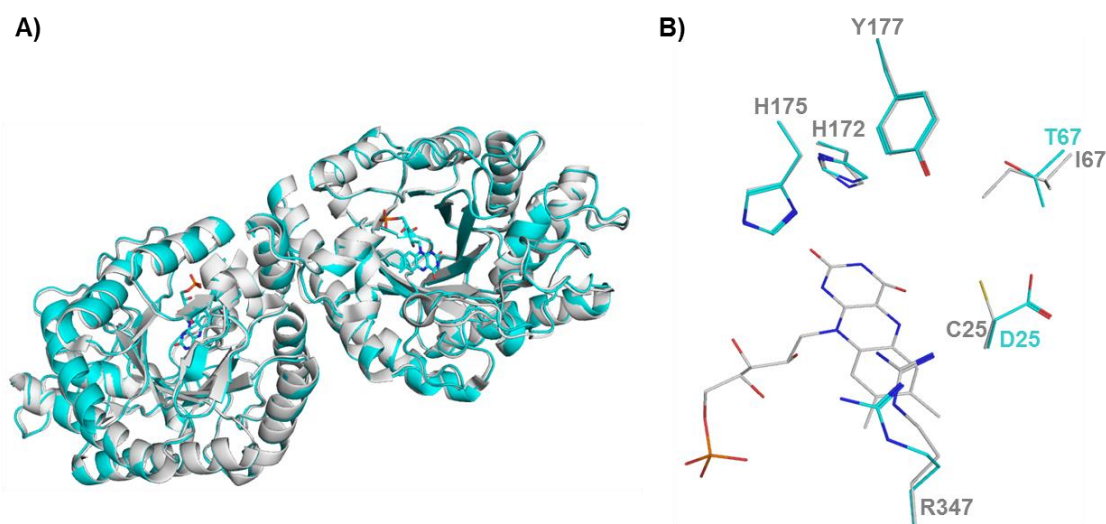


Figure 33. A) Structural alignment of the active dimer of *TsER* wild type (grey, pdb 3HGJ^[101]) and *TsER* C25D/I67T (cyan, pdb 5NUX) created with PyMOL 1.5.x. B) Zoom shows the active site, with both mutated residues and the anchor points, H172 and H175, for the substrate binding.

No significant differences could be observed in the main chain conformation in the active site as compared with the *TsER* wt (pdb 3HGJ)^[101] structure. The side chain of D25 adopts a conformation that is rotated away from the FMN with the threonine replacement of isoleucine at position 67 marginally increasing the volume of the active site, but with the introduction of a polar group.

Numerous attempts at co-crystallization of the *TsER* C25D/I67T with different substrates to evaluate binding orientations were unsuccessful. When crystallized without the addition of any substrates or inhibitors, *TsER* C25D/I67T exhibited unresolved density within the active site, which could not be attributed to any of the components of the crystallization solution. This explains the slightly different orientation of R347, because in the wt structure the inhibitor *p*-

hydroxybenzaldehyde is bound, which pulls the guanidinium group into the active site.

It was also possible to get a crystal structure of the triple variant *TsER* C25D/I67T/A102H (Figure 34). This variant plays a crucial role in chapter 3.6.2. Just as for *TsER* C25D/I67T, numerous attempts at co-crystallization different substrates were again unsuccessful.

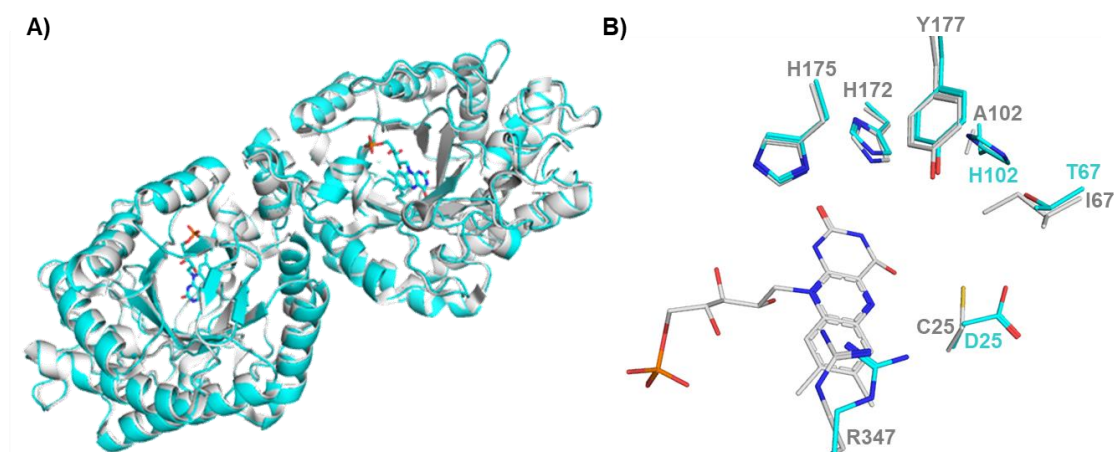


Figure 34. A) Structural alignment of the active dimer of *TsER* wild type (grey, pdb 3HGJ^[101]) and *TsER* C25D/I67T/A102H (cyan, pdb 5OGT) created with PyMOL 1.5.x. B) Zoom shows the active site, with mutated residues and the anchor points, H172 and H175, for the substrate binding.

Computational chemistry was investigated to obtain an insight into the binding poses in the wt, *TsER* C25G/I67T, *TsER* C25D/I67T and *TsER* C25D/I67T/A102H.

3.5 Prediction of Substrate Binding and Affinity by Computational Methods

3.5.1 Prediction of Substrate-Catalyst Interactions by *In-Silico* Docking Studies

To gain a broader understanding of the factors governing substrate acceptance and facial selectivity, the substrate-catalyst interactions were studied for all 23 substrates and 15 non-substrates from chapter 3.3.1 by rigid body docking (RBD)^[269] using GLIDE from SCHRÖDINGER for *TsER* wt, C25G/I67T and

C25D/I67T. The enzymes were prepared with a reduced FMN co-factor^[270] and the potential substrate anchors (H172 and H175) as fully protonated.^[132] The conjugate acid (protonated form) of the imidazole side chain in histidine has a pK_a of approximately 6.0.^[271] This means that, at physiologically relevant pH values, the side chain can be protonated or neutral and is highly dependent on the specific environment of each residue.^[271]

The docking was performed on the *TsER* wt structure with *p*-hydroxybenzaldehyde (HBA) as inhibitor (pdb 3HGJ^[101]). As a control experiment, HBA was first re-docked in the oxidized wt structure. Figure 35 shows the structural alignment of the original and re-docked active site, which looks quite similar, despite the different oxidation states of the cofactor.

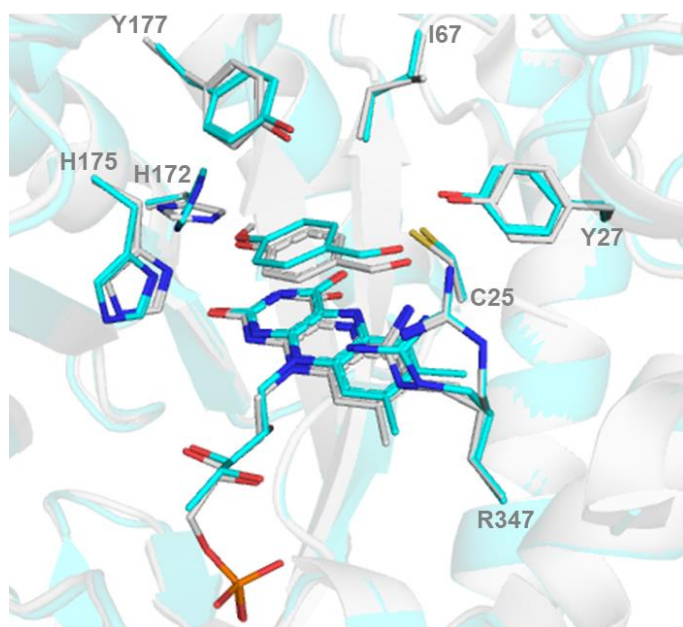


Figure 35. Structural alignment of the active dimer of *TsER* wild type in complex with HBA (grey, pdb 3HGJ^[101]) and the re-docked result of HBA in the *TsER* wild type with oxidized FMN (cyan) created with PyMOL 1.5.x.

In general, poses showing the ligand inside of the active site were found for all substrates and non-substrates. Poses were considered potentially productive when the hydride transfer angle ranges from 80-120°^[272] and the distance between the hydride of N5 and C_{β} is in the range of 3.00 to 4.85 Å. Docking results predicted almost all substrates in potentially productive poses in all three vari-

ants, reflecting the experimental observations. However, no productive poses were obtained for **40a**, **Z-39a** or **Z-31a** in neither the wt or C25D/I67T structures. It was observed that the productive poses contain a hydrogen bond between the carbonyl group and H175, but not to H172. This is unexpected, since mutagenesis studies predict that H172 is essential and exchange abolishes reduction. In contrast, H175 tolerates side chain variations, which can also be seen in chapter 3.6.3.1.^[152,167] A new binding pose was found, especially for **25a** and **35a**, where the carbonyl oxygen from the ring forms a hydrogen bond to the R347 residue of the other chain, whereas the methoxy group forms a hydrogen bond to H175. Similarly, non-substrates were predicted with non-productive poses. In those cases (**44-46a**, **E-47a**, **48a**, **E-53a** and **57a**) where a hydride attack angle and distance would define the pose as potentially productive, bad contacts between atoms of cut-off ratios $< 0.89 \text{ \AA}$ are observed, excluding them as productive poses. The only false positives are **54a** for wt and **55a** for C25G/I67T. In general, poses for non-substrates appear productive by visual inspection, but the hydride transfer angle is either too small (ranges between 13° and 79.9°) or too big (ranges between 120.5° and 175°) and the distance of the flavin N5 hydride and the unsaturated bond is too large (ranges between 4.86 \AA and 9.51 \AA), preventing reduction.

More importantly, the rigid docking data was analysed to see whether the predicted stereochemistry matches the experimental observations. For the wt with **25a** and **Z-37a** and for C25D/I67T with **Z-31a** and **39a**, only incorrectly predicted selectivities were found. In addition, inconclusive results were obtained for **27a** and **18a** with C25D/I67T and wt, respectively. In these cases, equally likely productive poses are obtained, predicting either one or the other stereoisomer. Correct facial selectivity was therefore predictable in 50 and 44% cases for the wt and C25D/I67T, respectively. Correct facial selectivity for C25G/I67T was predicted in 24% of all cases, 6 ligands did not confirm experimental results and 7 were inconclusive. The detailed evaluation for every pose is given in the ap-

pendix (Table 27 Table 29). Nevertheless, the prediction of 70-74% of molecules in accordance with the experimentally observed turnovers and 24-50% with the correct facial selectivity is within the performance expected of current RBD methods.^[269,273]

The predicted poses for ketoisophorone **22a** and isophorone **44a** are interesting. The highest ranked pose for substrate **22a**, shows the methyl group to be in an alpha position for the hydride transfer, whereas in **44a**, a non-substrate, it is in the beta position. This provides a possible explanation for the experimental reactivity of these substrates (Figure 36). This result was further investigated by molecular dynamics simulations and the estimation of the binding free energy using the WaterSwap method (see chapter 3.5.2.5).

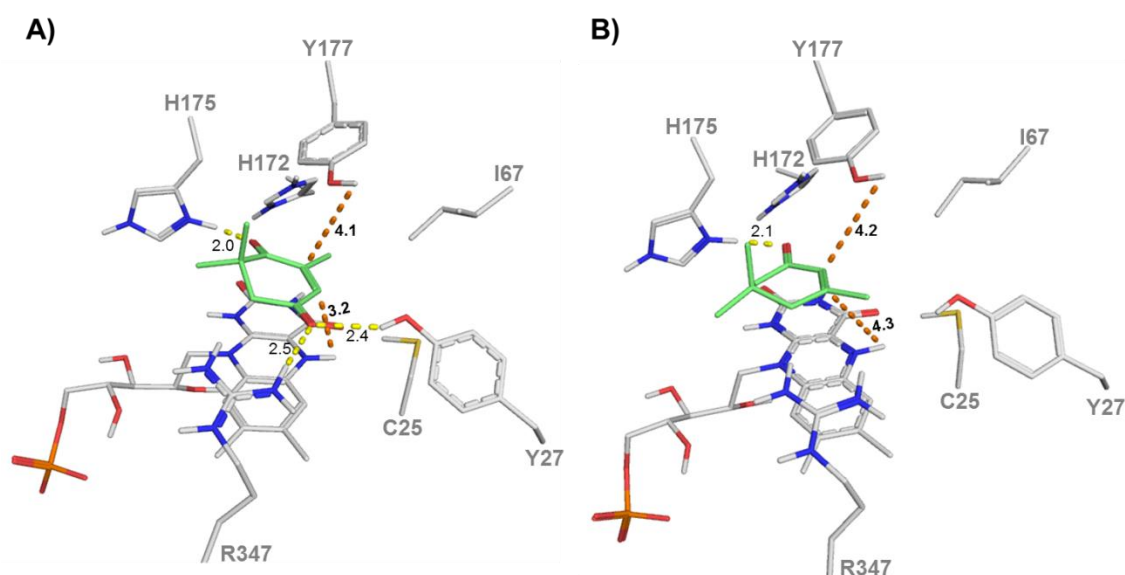


Figure 36. A) RBD of **22a** in TsER wt B) and **44a** in TsER wt. Highest ranked pose for **22a** is located as "flipped" orientation with the methyl group in alpha position, whereas the orientation of the methyl group in **44a** is positioned in beta position. Interactions between the substrate and surrounded residues are shown by dashed lines (yellow = H-bonds, orange = distance of N5H to C3 and of Y177 to C2).

RBD of the model compound **17a** in the wt yielded two poses that might result in hydride transfer. The flipped binding mode,^[98] resulting in the experimentally observed (*S*)-selectivity, has a hydride attack angle of 68.4° and a distance of 4.04 Å for the hydride transfer between C3 and the hydride at N5. The hydride attack angle is just slightly off from ideal values, which might explain the al-

most negligible activity of the wt. The second pose shows a new binding mode, resulting in (*R*)-selectivity, anchoring the substrate via H-bonds to R347 with an angle of 85.3° and a distance of 3.86 \AA for hydride attack. In C25D/I67T, two poses are observed with contradicting results. A normal binding mode with a hydride attack angle of 81.4° and distance of 4.83 \AA which might result in the experimentally observed (*R*)-selectivity, but bad contacts between Y177 and C6 are observed. The second pose shows no hydrogen bonding of the ligand to the receptor, with a hydride attack angle of 108.3° and distance of 3.68 \AA , resulting in (*S*)-selectivity. This variant shows experimentally a 93% (*R*)-selectivity, so the second pose is not in agreement with the experimental outcome.

In C25G/I67T the normal and flipped binding modes for **17a** are also observed. In the normal orientation, a hydrogen bond to H175 is formed and the distance for hydride transfer is 3.29 \AA with an angle of 107.9° , but bad contacts to Y177 and Y27. This orientation would lead to (*R*)-**17b**. Whereas in the flipped orientation of **17a**, the hydrogen bond to H175 also exists, without any bad contacts and a hydrogen attack angle of 102.1° and transfer distance of 3.46 \AA , leading to the experimentally observed (*S*)-**17b**.

Because the results of RBD for **17a** with all three variants are inconclusive, the docking was repeated using the more complex and time-consuming, induced-fit docking (IFD) method.^[274] This method allows flexibility of the residues surrounding the binding pocket, enabling more realistic substrate binding positions. Figure 37 shows an overlay of the best RBD and IFD pose for the wt (A), C25D/I67T (B) and C25G/I67T (C) variants with **17a**.

The difference between the poses for **17a** in the wt are more noticeable than in the variants, which can be explained by the movement of residues I67 and Y27, opening a pocket for the 3-methyl-group to slip into. The pose obtained by IFD shows a better H-bond angle (160.56° from donor) and distances for the carbonyl interaction with H175 (1.85 \AA compared to RBD 2.05 \AA). Also, H172 changes

position significantly, which has previously been observed after the soaking of a cyclopentenone substrate in OYE1 variant W116I.^[159] Positioning of the substrate in productive poses improved and multiple poses with hydride attack angles between 90-95° and distances between 3.21 to 3.78 Å are obtained. Interestingly, poses for (*R*)-selectivity could also be obtained, which fits to the experimental result of 76% *ee* indicating that (*R*)-selective conformations exist.

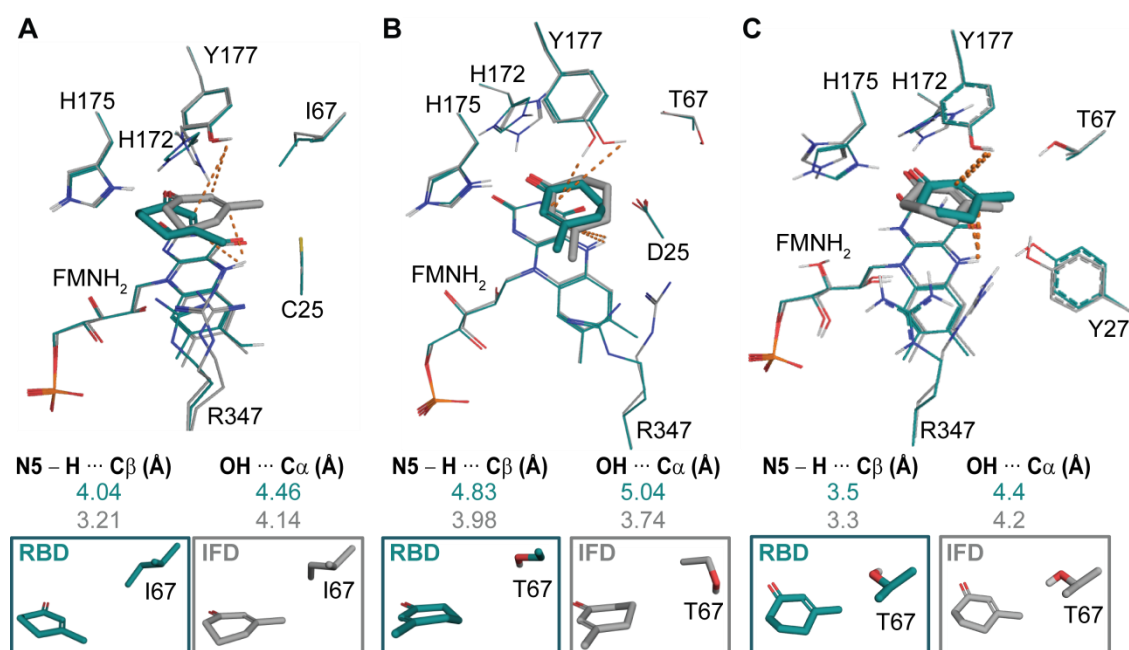


Figure 37. A) Overlay of RBD (cyan, pose 5) and IFD (grey, pose 4) of **17a** in the reduced *TsER* wt structure. **17a** is located in the flipped orientation, which would result in *S*-**17b**. The grey box shows zooms of residue I67 to highlight the side-chain flip. B) Overlay of RBD (cyan, pose 2) and IFD (grey, pose 4) of **17a** in the reduced *TsER* C25D/I67T structure. **17a** is located in the normal orientation, which would result in *R*-**17b**. The boxes highlight the side-chain flip of T67. C) Overlay of RBD (cyan, pose 3) and IFD (grey, pose 1) of **17a** in the reduced *TsER* C25G/I67T structure. **17a** is located in the flipped orientation, which would result in *S*-**17b**. The boxes highlight the side-chain flip of T67.

C25D/I67T also shows a side chain flip of T67 (zoom in Figure 37 (B)) and small rearrangements in the positions of Y27, H172 and Y177. Notably, Y177 changes position in the IFD structure, adopting a position in the correct orientation to the double bond for proton transfer, as shown in the work of LONSDALE *et al.*^[132] Hydride attack angles and distances are likewise improved for the C25D/I67T mutant (hydride attack angle = 93.8° and distance = 3.98 Å), predicting the experimentally observed (*R*)-selectivity (93% *ee*). Just as for the wt, a good

(*S*)-selective pose with a hydride attack angle of 90.5° and distance of 3.68 \AA is observed, which has a lower score than the (*R*)-selective poses.

In the induced-fit docking of C25G/I67T with **17a**, all found poses are in the flipped orientation which will give rise to (*S*)-**17b**. This result is in quite good agreement with the experimental value of 76% (*S*)-selectivity. Notably, rearrangements of H172 and H175 are seen, by which hydrogen bonds of both residues to the carbonyl can occur.

The docking results show **17a** in C25G with the flipped pose and C25D with the normal pose and therefore give an explanation for the facial selectivity of these two variants. Overall, docking revealed that the larger hydrophobic pocket opened through C25G and I69T exchange allows sufficient space and stabilizing van-der Waals interactions to host smaller substituents like methyl, ethyl or methoxy groups, allowing flipped binding poses similar to the one of **17a** in the wt to occur. When C25D is present, a polar pocket is formed, disfavoured such interactions. Substrates are forced to flip into normal binding poses, thereby presenting the other face of the carbon-carbon bond to the hydride. Nevertheless, a bit more space is generated in the C25D/I67T variant, which allows the normal poses to approach closer to the hydride in an optimal angle (Figure 37B).

3.5.2 Prediction of Substrate Affinity by Molecular Dynamics Simulations and WaterSwap Calculations

3.5.2.1 Molecular Dynamics Simulations

Crystal structures are only static models of highly flexible enzymes. Computational studies that simulate this flexibility (e.g. molecular dynamics simulations) can identify different conformations of the active site that are more relevant for substrate binding and conversion.^[275] Thus, the simulations provide structural

understanding of the molecular interactions between the *TsER* proteins and substrates, enabling analysis of the effects of mutation on protein dynamics and substrate binding.

The results of the experimental studies should be examined with the help of fundamental techniques in theoretical chemistry. Theoretical studies, such as those employing molecular dynamics (MDs) simulations, can provide important insights into mechanistic details that may not be possible via experimental means. Relatively few theoretical studies have been performed on the OYE family.^[130-132] An explanation for the different reactivities of *TsER* wt and the double variants C25D/I67T and C25G/I67T towards especially **17a** is expected from the MD simulations.

3.5.2.2 Molecular Dynamics Simulations with *TsER* Wildtype

The IFD pose of the flipped 3-methylcyclohex-2-en-1-one (**17a**, MCH) in the *TsER* wt structure based on pdb 3HGJ with FMNH₂ described in chapter 3.5.1 was used as basis for simulations (see Figure 37A). PROPKA^[276] was used to predict the protonation state of titratable residues in the protein at working pH 7.4. This method predicted both histidine residues in positions 172 and 175 to be neutral, which was considered in the MD simulations.

During the early stages of MD simulations some small restraints were applied to all C α atoms, see chapter 6.10 for details. Analysis of the trajectories showed that the hydrogen bonds between the substrate and H172 and H175 were broken after 2 ns. The distance between the carbonyl oxygen and H172 stayed in range of 2-4 Å between 5-20 ns before moving to much larger distances (Figure 38E). The substrate remained above the flavin in the flipped orientation, which is illustrated by the dominant cluster from the 100 ns MD simulations (see Figure 38A).

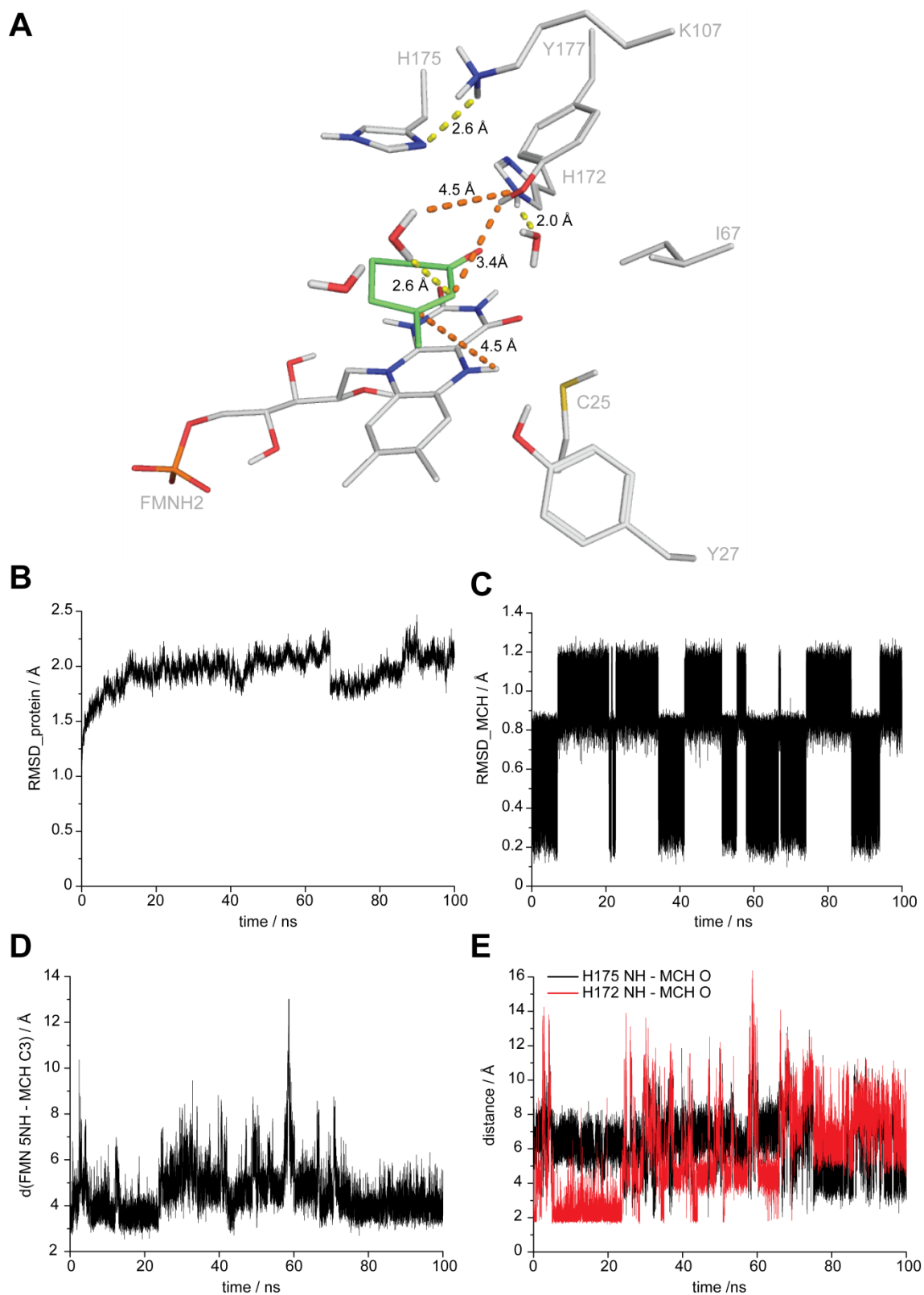


Figure 38. MD simulations of *TsER* wildtype with reduced FMNH₂ and 3-methyl cyclohexenone (**17a**). A) Active site of *TsER* wt in the dominant cluster from MD simulations with **17a** (green lines) in complex. Water molecules within 4 Å are shown in stick form. B) Root mean square deviation (RMSD) of all protein over 100 ns. C) RMSD of **17a** in *TsER* wt over 100 ns. D) The distance between N5H of FMNH₂ and C3 of **17a** over the course of 100 ns MD simulations. E) The distance between NH of H175 (black) and NH of H172 (red) to O of **17a** over the course of 100 ns MD simulations.

The high fluctuation of **17a** can be seen in the root-mean-square deviation (RMSD) of atomic positions (Figure 38C). The distance between the substrate C3 with the flavin N5 hydride was monitored over the course of the simulations, giving an average value of 4.55 Å (Figure 38D) for this distance.

LONSDALE *et al.* discussed the role of Y169 as proton donor in OYE YqjM.^[132] They observed that the proton of Y169 points away from the substrate during the majority of the simulation, even though they suggest that Y169 is more likely to protonate the substrate directly, rather than via a bridging water molecule.^[132] In *TsER* the corresponding residue is Y177. In the clustered pose the OH group of Y177 points towards the C2 atom of **17a**, with a distance of 3.4 Å, indicating that protonation would be possible. Additionally, the OH group of Y177 interacts with nearby water molecules which could lead to protonation over a water network, in agreement with the study of YqjM.^[132]

Experimentally, *TsER* wt is found to reduce **17a** with just a 1% yield; however, these simulations indicate that reactive conformations are accessible. Structures from these MD simulations were used to initiate binding energy calculations using the WaterSwap method, (described in chapter 3.5.2.5), to predict absolute binding free energies of **17a** to *TsER* wt.

As mentioned in chapter 3.5.1, why the conversion of ketoisophorone **22a** by most OYEs is possible but not isophorone **44a** is still unresolved. The RBD studies gave an initial explanation by indicating different binding poses for both compounds (Figure 36). In the pose for **22a**, the methyl group is in α -position for hydrogenation, whereas for **44a** it is in β -position. These docking poses were taken as a starting point for MD simulations.

Figure 39 shows the dominant cluster from 70 ns MD simulations with **22a** (KIP). The enzyme substrate complex stayed stable over the whole simulation, with the methyl group in α -position for hydrogenation. According to the analysis of the distances between C2 of **22a** and the N5 hydride of FMN as well as

between the carbonyl oxygens of **22a** and H172/H175, the substrates stayed in the active side for at least 60 ns.

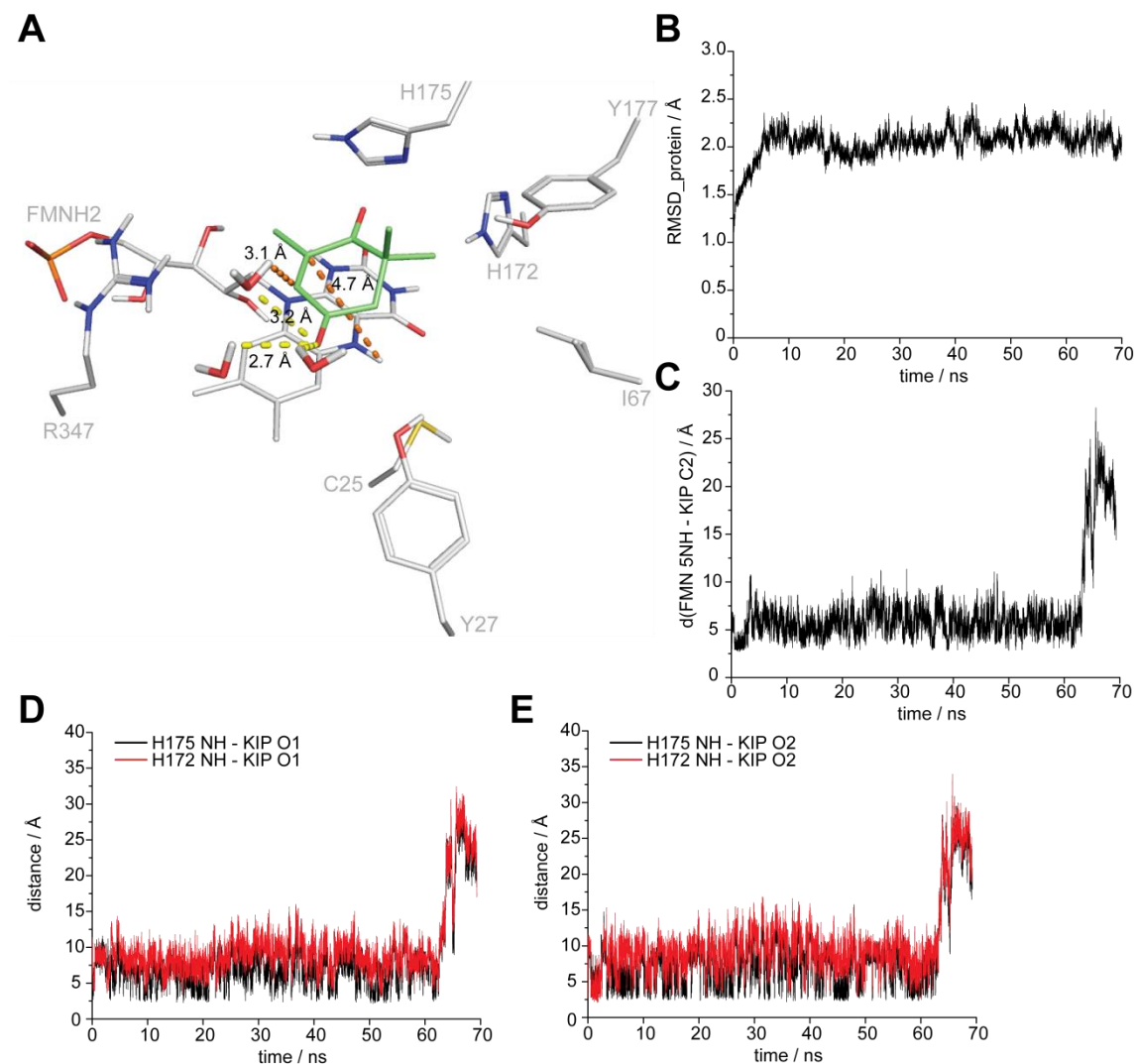


Figure 39. MD simulations of *TsER* wildtype with reduced FMNH₂ and ketoisophorone (KIP, **22a**). A) Active site of *TsER* wt in the dominant cluster from MD simulations with **22a** (green lines) in complex. Water molecules within 4 Å are shown in stick form. B) Root mean square deviation (RMSD) of protein over 70 ns. C) The distance between N5H of FMNH₂ and C3 of **22a** over the course of 70 ns MD simulations. D) The distance between NH of H175 (black) and NH of H172 (red) to O1 of **22a** over the course of 70 ns MD simulations. E) The distance between NH of H175 (black) and NH of H172 (red) to O2 of **22a** over the course of 70 ns MD simulations.

In the starting conformation from docking, **22a** is orientated in the flipped mode, whereas in the dominant cluster from MD simulations it is orientated in the normal pose. Experimentally *TsER* wt produces 90% (*R*)-**22b**, which means that the hydride must attack C2 from the bottom (distance 4.7 Å) and C3 gets protonated from the top in the normal binding pose. In Figure 39A, it can be

seen that Y177 is too far from the substrate to interact directly and the protonation can only occur via a nearby water molecule.

Figure 40 shows the dominant cluster from 70 ns MD simulations with **44a** (IPN). The distance between the substrate C3 with the flavin N5 hydride was monitored over the course of the simulations and is most often between 4-6 Å. The initial docking pose showed **44a** in the flipped orientation with C3 in β -position for hydride transfer, whereas in the dominant cluster from MD simulations it is oriented in the normal pose and not stacking above FMN. The positioning of **44a** makes it impossible for hydride transfer with a distance of 6.5 Å and a hydride attack angle of 51.7°.

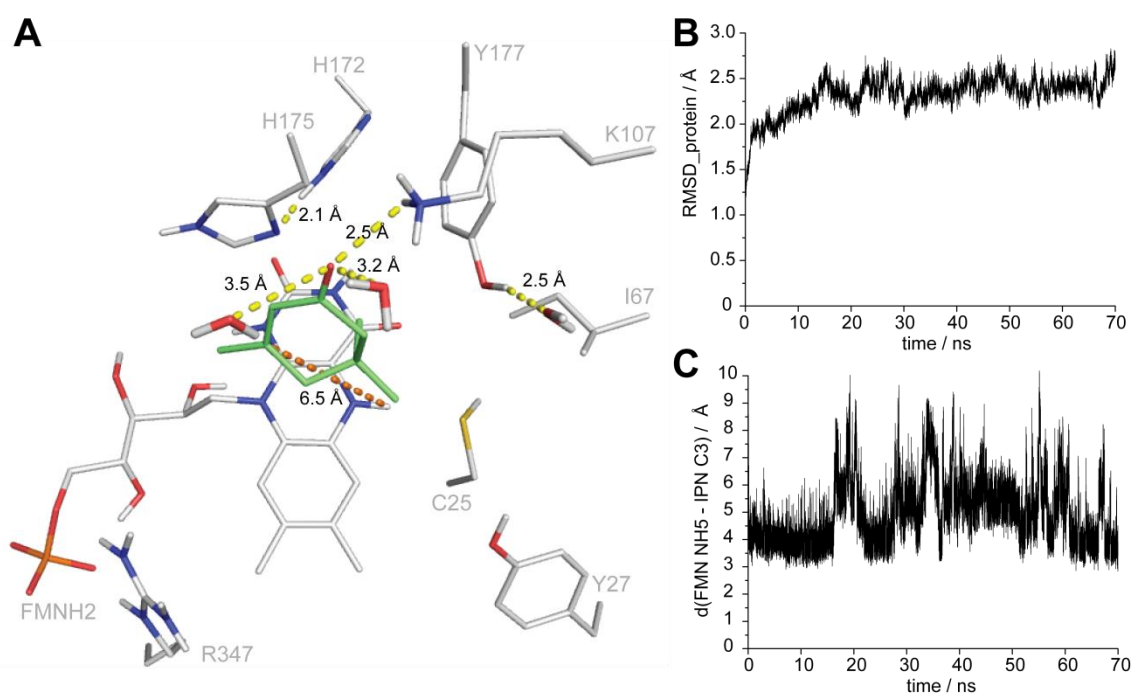


Figure 40. MD simulations of *TsER* wildtype with reduced FMNH₂ and isophorone (**44a**). A) Active site of *TsER* wt in the dominant cluster from MD simulations with **44a** (green lines) in complex. Water molecules within 4 Å are shown in stick form. B) Root mean square deviation (RMSD) of protein over 70 ns. C) The distance between N5H of FMNH₂ and C3 of **44a** over the course of 70 ns MD simulations.

Comparison of the dominant structures from simulations of both **22a** and **44a** gives an explanation of the experimental results. **22a** is consistently in a reactive conformation, allowing quantitative conversion by *TsER* wt, whereas **44a** cannot adopt a reactive conformation and is not converted at all.

3.5.2.3 Molecular Dynamics Simulations with TsER C25G/I67T

The IFD of 3-methylcyclohex-2-en-1-one (**17a**, MCH) in the prepared TsER C25G/I67T structure based on the wildtype crystal structure (pdb 3HGJ) with FMNH₂ was used as basis for simulations.

Figure 41 shows the dominant cluster from 70 ns MD simulations with **17a**. The RMSD of the whole protein over 70 ns MD simulations is shown in Figure 41B. The average value for the RMSD is 3 Å, indicating that there is quite a significant difference in atomic positions to the crystal structure. According to the analysis of the distances between C3 of **17a** and the N5 hydride of FMN (Figure 41D) as well as between the carbonyl oxygens of **17a** and H172/H175 (Figure 41E) the substrate leaves the active site after 20 ns.

The structure of the binding site from the dominant cluster of the simulations with TsER C25G/I67T and **17a** confirmed that the substrate leaves the active site (Figure 41A). That a substrate is able to leave the active site of TsER is quite important for the catalytic reaction, because otherwise it would not be possible to follow the bi-bi ping pong mechanism with NADPH. In contrast to an inhibitor, a converted substrate should not have an enormous binding affinity, otherwise the reaction will stop. FITZPATRICK *et al.* experimentally observed weak binding affinities of substrate cyclohexenone to YqjM.^[277]

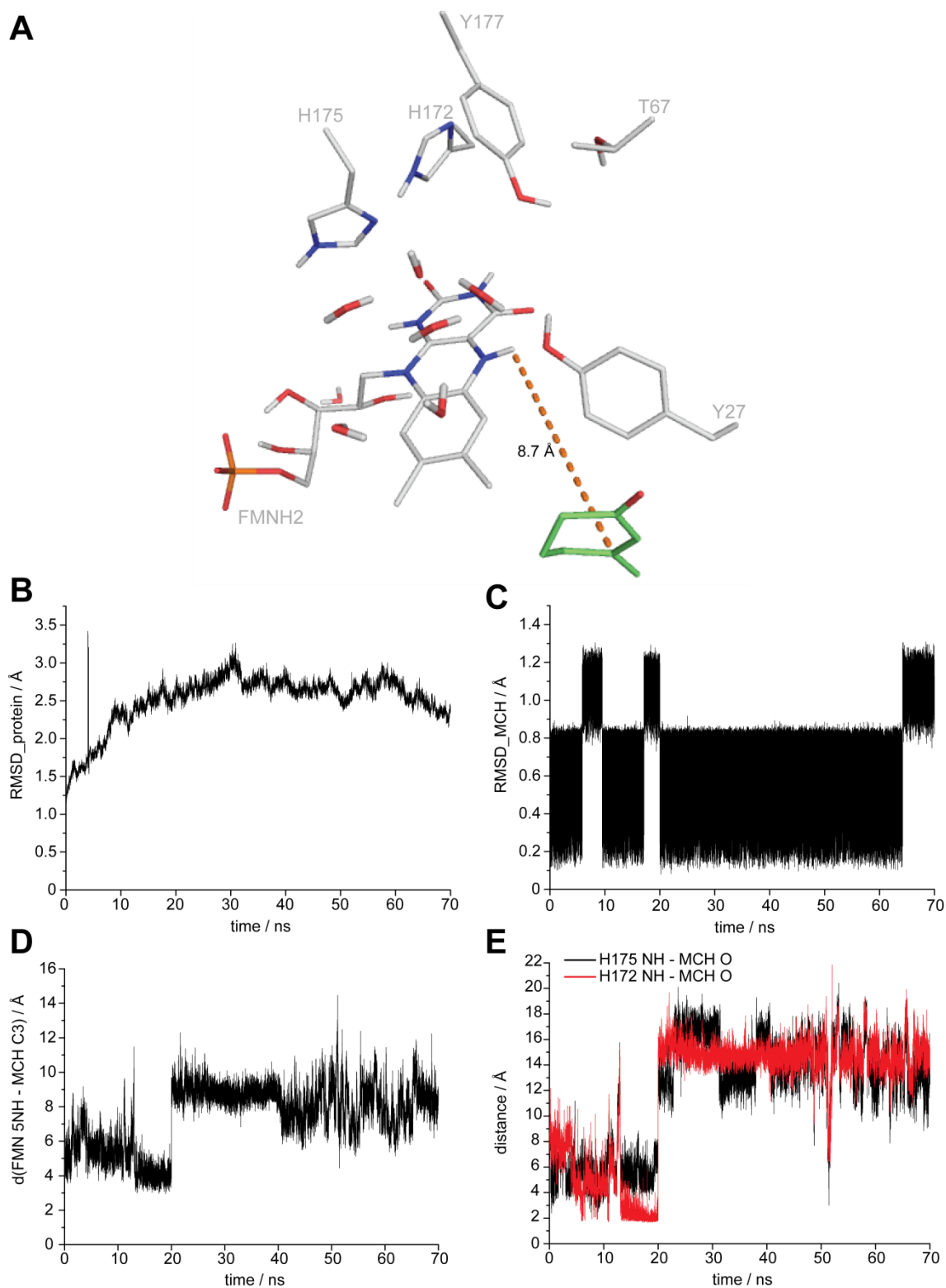


Figure 41. MD simulations of *TsER* C25G/I67T with reduced FMNH₂ and 3-methyl cyclohexenone (**17a**). A) Active site of *TsER* C25G/I67T in the dominant cluster from MD simulations with **17a** (green lines) in complex. Water molecules within 4 Å of FMN are shown in stick form. B) Root mean square deviation (RMSD) of protein over 70 ns. C) RMSD of **17a** in *TsER* C25G/I67T over 70 ns. D) The distance between N5H of FMNH₂ and C3 of **17a** over the course of 70 ns MD simulations. E) The distance between NH of H175 (black) and NH of H171 (red) to O of **17a** over the course of 70 ns MD simulations.

3.5.2.4 Molecular Dynamics Simulations with TsER C25D/I67T

The IFD pose of 3-methylcyclohex-2-en-1-one (**17a**) in the prepared TsER C25D/I67T structure based on the wildtype crystal structure (pdb 3HGJ) with FMNH₂ was used as basis for simulations. The variant model based on the wildtype structure was used due to the higher resolution compared to the crystal structure of C25D/I67T (pdb 5NUX).

The first round of MD simulations was performed with the same parameters as described for the wildtype and C25G/I67T variant with neutral H172 and H175. In these simulations the protein-substrate complex was not stable and the substrate **17a** left the active site within the first nanosecond of simulation. Figure 42C illustrates the dominate cluster from the 100 ns MD simulations.

For this reason, alternative protonation states of H172 and H175 were tested, as in the study of LONSDALE *et al.* for YqjM.^[132] The MD simulations were repeated with protonated H172 and H175. The dominant cluster from the 100 ns MD simulations is shown in Figure 42D, which illustrates a stable complex of FMN with **17a**, but shows a flip of the cofactor-substrate complex out of the binding pocket. Further inspection of the non-covalently bound cofactor FMN reveals that the hydrogen bond between the phosphate moiety and R319 is broken, allowing this flip to occur.

Hence, the MD simulations were repeated a third time with harmonic restraints of 20 kcal/mol · Å² from FMN to the backbone of R319 (Figure 42 grey, Figure 43). The first 10 ns of simulations showed a stable substrate-enzyme complex with the flavin correctly positioned in the binding site. After 10 ns, substrate **17a** moved from its position above the flavin. For this reason the simulations were stopped after 30 ns.

Figure 42A shows the structural alignment of the enzyme backbone over the three different MD simulations, which did not indicate any extreme changes, like unfolding in the dimeric structure. Whereas Figure 42B clearly illustrates

the different binding modes of the flavin in the active site of *TsER* C25D/I67T depending on the protonation states of H172/H175.

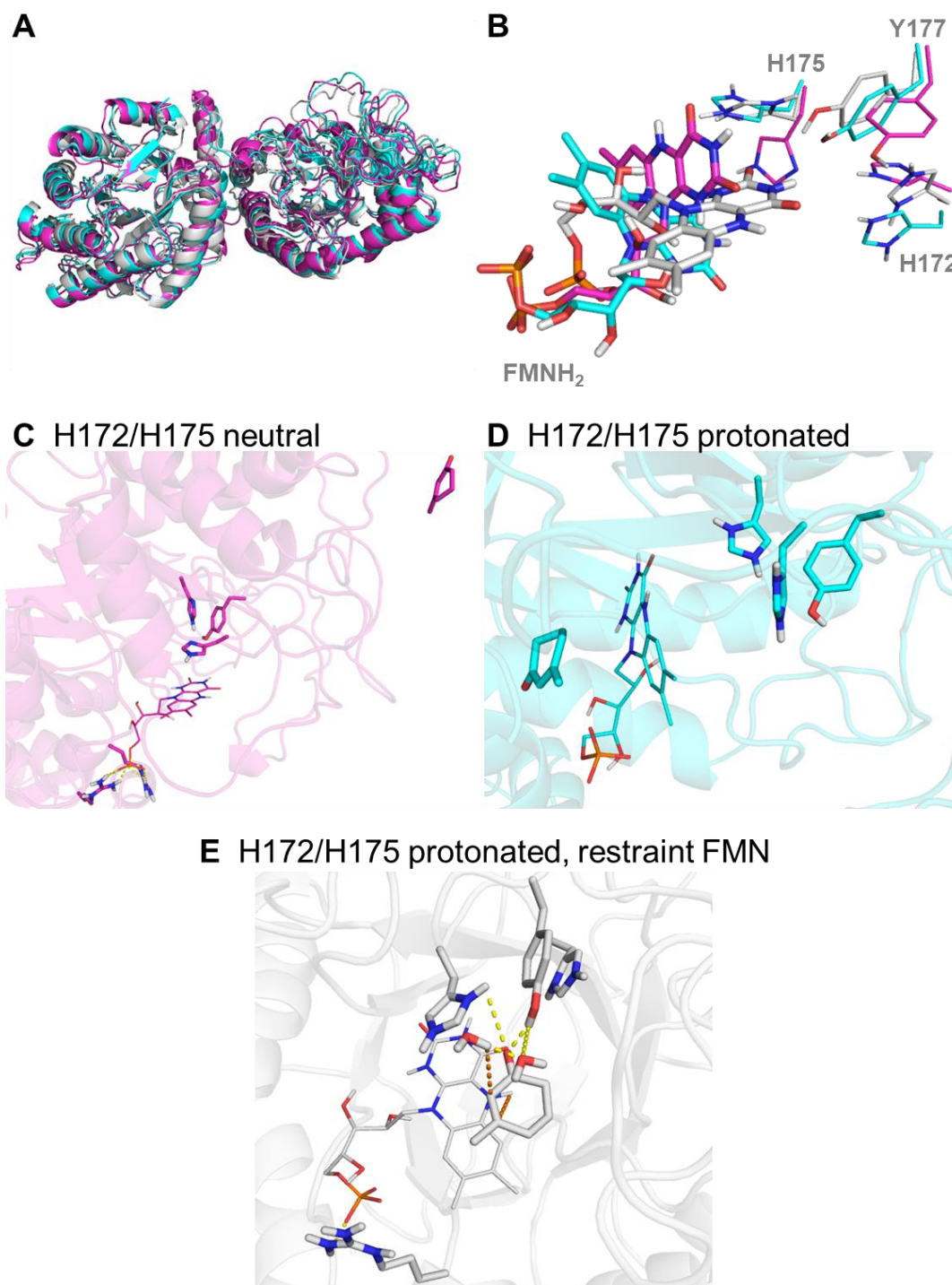


Figure 42. Comparison of MD simulations of three different *TsER* C25D/I67T structures with reduced FMNH₂ and 3-methyl cyclohexenone (**17a**). A) Structural alignment of MD simulations of *TsER* C25D/I67T with neutral H172/H175 (purple), with H172/H175 protonated (cyan) and with H172/H175 protonated and distance restraint of FMN to backbone (grey). B) Illustration of FMN and H172/H175/Y177 in alignment. C) Active site with **17a** and neutral H172/H175, D) with **17a** and protonated H172/H175, E) with **17a** and protonated H172/H175 and backbone restraints to FMN.

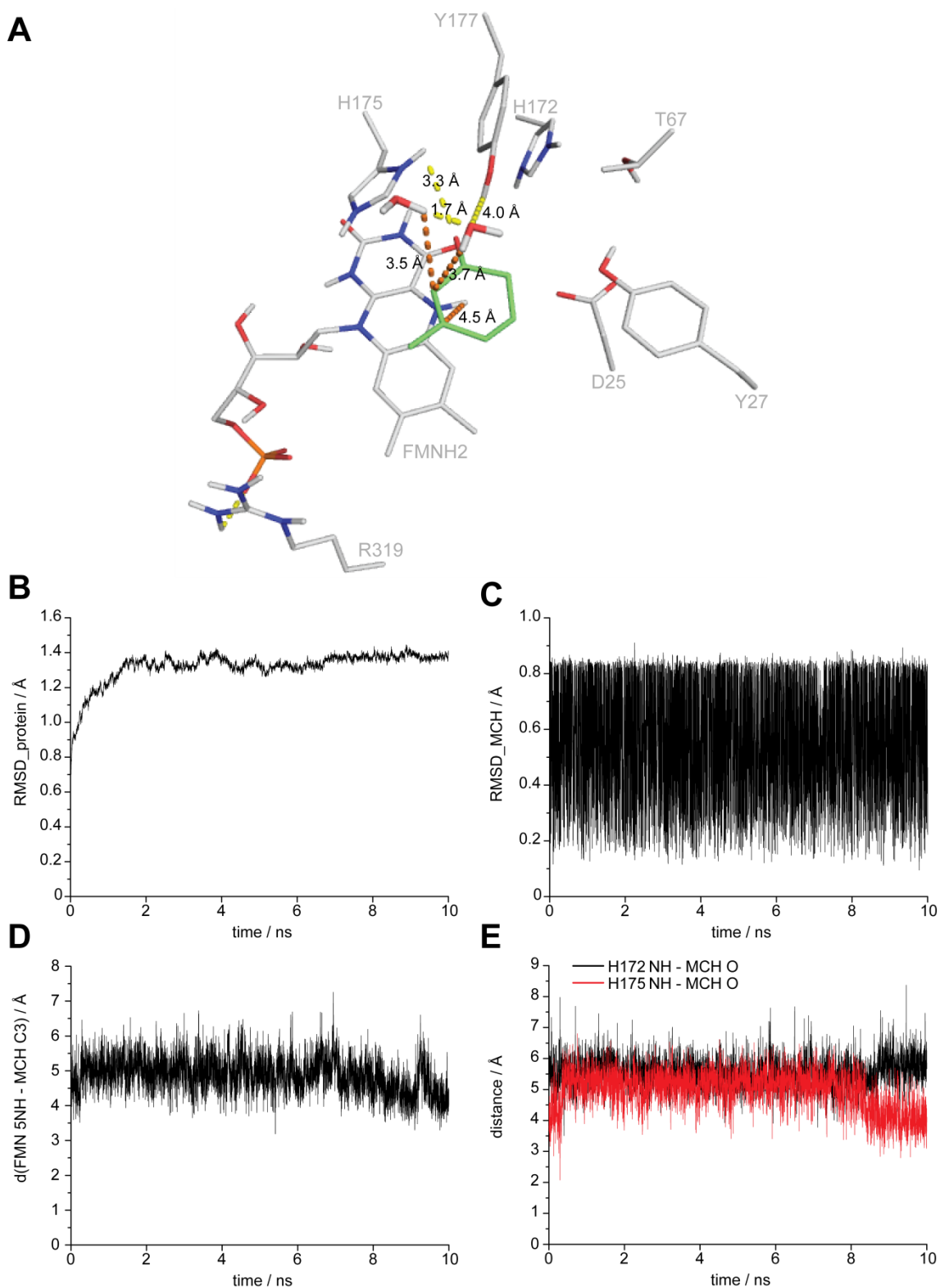


Figure 43. MD simulations of *TsER* C25D/I67T with reduced FMNH₂, restraints of FMN to backbone, protonated H172/H175 and 3-methyl cyclohexenone (**17a**). A) Active site of *TsER* C25D/I67T after 10 ns MD simulations with **17a** (green lines) in complex. Water molecules within 4 Å are shown in stick form. B) Root mean square deviation (RMSD) of protein over 10 ns. C) RMSD of **17a** in *TsER* C25D/I67T over 10 ns. D) The distance between N5H of FMNH₂ and C3 of **17a** over the course of 10 ns MD simulations. E) The distance between NH of H175 (black) and NH of H171 (red) to O of **17a** over the course of 10 ns MD simulations.

Due to this observation constant pH MD simulations^[278] for C25D/I67T with **17a** in complex were performed. With this method pK_a values for the titratable side chains of residues D25, H172, H175 and Y177 were calculated, to gain more insight into their different protonation states at the working pH of 7.4.

Table 7. Predicted pK_a values for titratable residues D25, H172, H175 and Y177 from constant pH MD simulations at pH 7.4.

residue	Offset ^(a)	predicted pK _a	Fraction protonated ^(b)	Transitions ^(c)
D25	2.479	9.879	0.997	1
H172	-4.108	3.292	0.000	1
H175	-2.754	4.646	0.002	23
Y177	4.848	12.248	1.000	2

a) is the difference between the predicted pK_a and the system pH, b) is the fraction of time the residue spends protonated, c) gives the number of accepted protonation state transitions over 100 fs.

The results of populations of every state for every titratable residue show that D25 is deprotonated for 0.33% of the time and only syn-protonated (>99% of the time) on each oxygen. The H172 residue is deprotonated for 0.0078% of the time, syn-protonated for 0.24% and anti-protonated for 99.7% on each nitrogen. Residue H175 is deprotonated for 0.17% of the time, syn-protonated for 74% and anti-protonated for 25.7% on each nitrogen. Y177 stayed always protonated during the simulations.

These results indicated the different protonation states of at least three residues, which are important for the catalytic activity. To achieve stable molecular dynamics structures for *TsER* C25D/I67T all of these protonation states have to be considered. This would be a highly computational intensive calculation which needs further investigation.

3.5.2.5 Calculations of Binding Free Energies with WaterSwap and MM-PBSA

The WaterSwap method works by constructing a reaction coordinate that swaps the ligand bound to the protein with an equivalent volume of water molecules. The affect is to move the substrate from being bound to the protein, to

being free in solution, while simultaneously transferring an equivalent volume of water from being free in solution to being bound to the protein.^[279] The advantage of WaterSwap is that it allows calculation of absolute binding free energies.^[280] This simplifies investigation of the effect of protein mutation on binding compared to relative binding free energy methods, as differences in absolute binding free energies capture changes in binding mode of the ligand upon protein mutation.^[280]

The input files for a WaterSwap calculation are the AMBER format coordinate and topology files from MD simulations that represent the solvated protein-ligand complex.^[279] WaterSwap^[279] absolute binding free energy calculations of the ligand 3-methyl cyclohex-2-en-1-one (**17a**) bound to TsER wt followed the MD simulations, using the structure after 100 ns from the dynamics simulations.

MM-PBSA is another post-processing end-state method to calculate free energies of molecules in solution from MD simulations.^[281] This end-state free energy method reduces computational cost by eliminating the need for simulating intermediate states. Modelling the solvent implicitly further reduces the computational cost by eliminating the noise caused by explicit solvent molecules.^[282]

To experimentally determine binding free energies of substrates to OYEs is a challenging task. Most often steady state kinetics under anaerobic conditions with purified enzyme are performed.^[95,283] Using WaterSwap as *in-silico* pre-screening for substrate libraries in OYEs would be a great breakthrough.

The WaterSwap calculation for the dominant cluster of TsER wt with **17a** (Figure 38) resulted in a calculated binding free energy of 12 ± 2.266 kcal/mol. Unfortunately, there is no comparable value from an experiment, therefore the second *in-silico* binding free energy method MM-PBSA was used. With this method it was not possible to get any analysable data. Table 8 shows that all

other performed calculations with the variants C25D/I67T and C25G/I67T and also with the substrates **22a** and **44a** failed.

Table 8. Performed calculations of binding free energies with WaterSwap and MM-PBSA.

enzyme	substrate	WaterSwap	MM-PBSA
wildtype	17a	12 kcal/mol	<i>non analysable</i>
C25D/I67T	17a	<i>non analysable</i>	<i>non analysable</i>
C25G/I67T	17a	<i>non analysable</i>	<i>non analysable</i>
wildtype	22a	<i>non analysable</i>	<i>non analysable</i>
C25D/I67T	22a	<i>non analysable</i>	<i>non analysable</i>
C25G/I67T	22a	<i>non analysable</i>	<i>non analysable</i>
wildtype	44a	<i>non analysable</i>	<i>non analysable</i>
C25D/I67T	44a	<i>non analysable</i>	<i>non analysable</i>
C25G/I67T	44a	<i>non analysable</i>	<i>non analysable</i>

A reason for this might be the unstable MD simulations with the variants and all tested substrates and also the presence of a non-covalently bound cofactor. These calculation methods are not yet optimized for such complex systems and need further investigations.

3.6 Going to Bulkier Substrate Classes

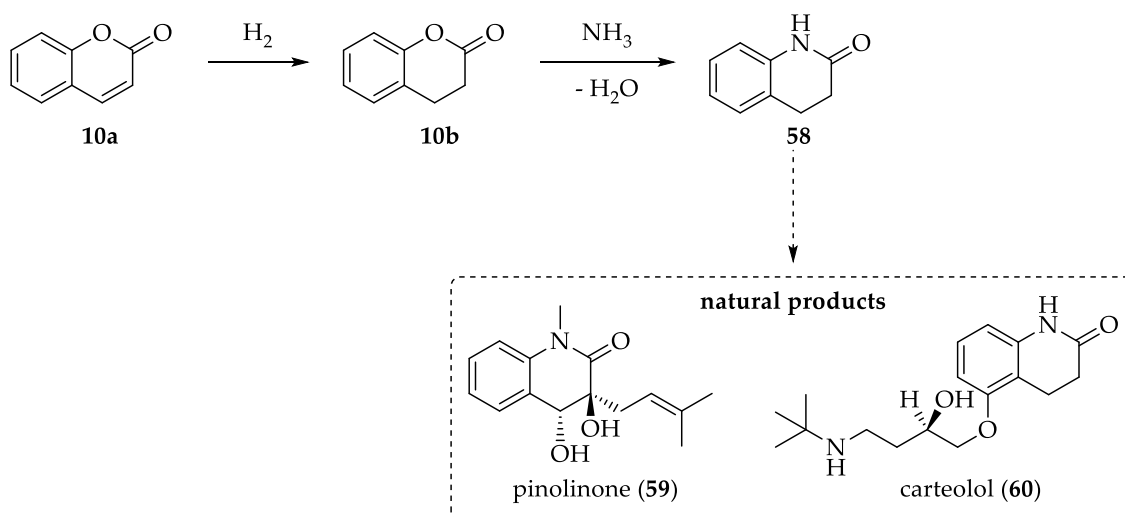
So far the substrate scope of ene reductases is most often shown with small five and six membered ring compounds as described in the introduction chapter 1.4.2. In general there is a great interest in broaden the substrate scope of ERs to bulky substrates to use these highly selective *trans*-hydrogenation catalysts in the late stage synthesis of complex organic molecules.

One structural complex substance class, the steroids, was already investigated for binding properties of OYEs and it was found that many steroids are inhibitors and some could even be reduced by OYEs.^[98,100] Progesterone for example is an inhibitor, whereas 1,4-androstadiene-3,17-dione and prednisone are substrates for PETNR.^[98] Another interesting class would be coumarin derivatives; due to their fluorescent properties a fast screening method for OYE variants might be established.

Coumarin is a fragrance used in soaps, lotions and perfumes but it is also used in laser dyes and it is a building block for several pharmaceuticals. In nature coumarins are produced by plants, like sweet-clover, sweet grass and meadow-sweet, to protect them from natural enemies, because in high amounts it operates as appetite suppressant.^[284] In the past coumarin was also used as food additive, for example as a vanilla substitute, but since 1954 it is forbidden, because of the suspicion of being hepatotoxic in animal models.^[284] 4-Hydroxycoumarin, for example, is an inhibitor for vitamin K epoxide reductase, whereas it can be used as rodenticide.

Moreover the dihydrocoumarins are valuable as fine chemicals and chemical intermediates, for example they can be converted to the corresponding quinolone analogues **58** which are valuable for their use as building blocks for the synthesis of pharmaceutical compounds (Scheme 14).^[285] To generate the dihydrocoumarin (**10b**) out of coumarin (**10a**) the selective reduction of unsaturated carbon-carbon double bond must proceed in the presence of an aromatic ring.

This hydrogenation is described in the literature for example over palladium-based catalysts, like Pd/C^[286], the bimetallic PdAu^[287] or also traditional reducing agents, like sodium borohydride^[288] and Raney nickel^[289]. The important class of quinolones can also be synthesised via a sequential Heck reduction-cyclization (HRC) reaction by using a palladium catalyst.^[290]



Scheme 14. Both coumarin **10a** and dihydrocoumarin **10b** are valuable as fine chemicals and chemical intermediates. ITO and OOSHIDA^[291] described the conversion of lactones to their corresponding lactams, which are represented in natural products and drugs.

However, more an environmentally friendly process would be a biocatalytic synthesis route, especially for the production of biologically active compounds that require low metal contamination (at least less than 4 ppm).^[290]

GRIESE *et al.*^[292] studied the microbial degradation pathway of coumarin to quinolone by *Pseudomonas putida* 86. They characterized the FMN-containing xenobiotic reductase A (XenA), which catalyses the reduction of 8-hydroxycoumarin and coumarin to 8-hydroxy-3,4-dihydrocoumarin and 3,4-dihydrocoumarin. The oxidized crystal structures of XenA in complex with both coumarins show different modes of binding in the active site. While coumarin is ideally positioned for hydride transfer from N5 of FMN to C4 of coumarin (Figure 44, blue), 8-hydroxycoumarin forms a non-productive complex with the oxidized XenA (Figure 44, green), which did not match the experimental results, because both substances can be transformed by XenA.

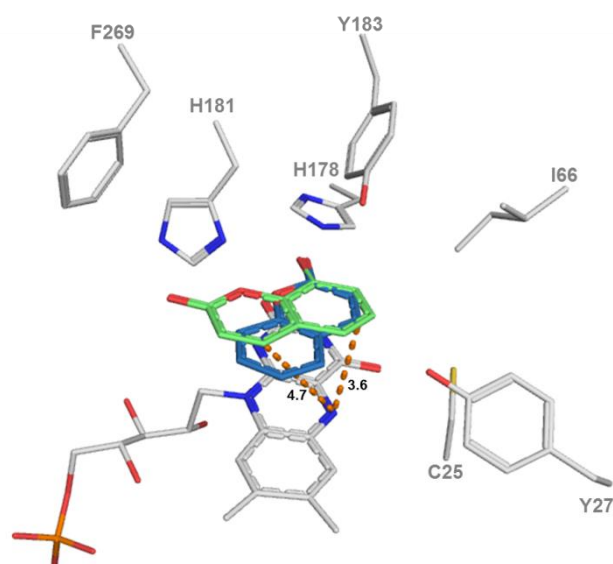


Figure 44. Active site of XenA in complex with 8-hydroxycoumarin (green, pdb 2H8Z)^[292] and coumarin (blue, pdb 2H90).^[292] Distance of the C3 atom of 8-hydroxycoumarin to the N5 of the oxidized FMN is 4.7 Å, whereas for C3 of coumarin and the N5 of FMN is 3.6 Å.

Recently WERTHER *et al.* showed a remarkably difference in 8-hydroxycoumarin binding, depending on the oxidation-state of FMN in XenA.^[293]

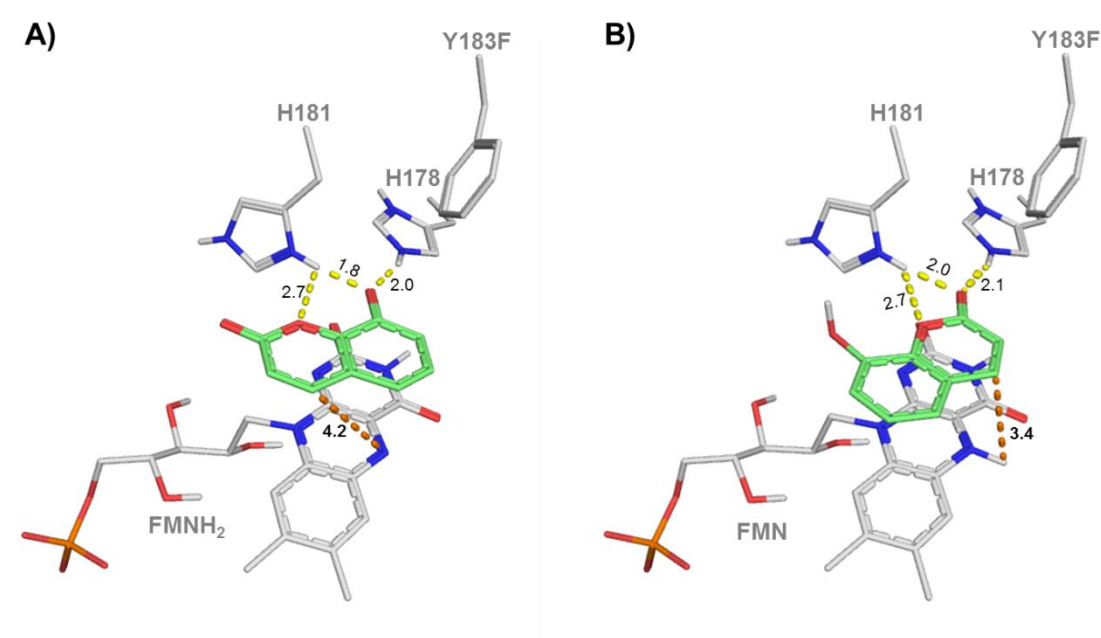


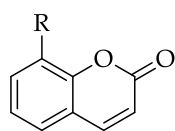
Figure 45. Oxidation-state-dependent substrate-binding to the active site of XenA. A) Active site view of the deprotonated phenolate-state of 8-hydroxycoumarin (green lines) in complex with oxidized Y183F-XenA (pdb 4UTJ).^[293] B) Active site view of the Michaelis complex between reduced Y183F-XenA and 8-hydroxycoumarin (green lines) (pdb 4UTM).^[293] The orange dashed lines illustrate the distance between C4 of coumarin and N5 or N5H of FMN. Yellow dashes illustrate hydrogen bonds.

In the crystal structure with the reduced and active FMNH₂, the positioning of 8-hydroxycoumarin would lead to a successful hydride transfer (Figure 45B), whereas in the oxidized enzyme, due to a proton release of hydroxycoumarin to the buffer the phenolate binds in a flipped pose, with hydrogen bonding to H178 and H181 (Figure 45A).

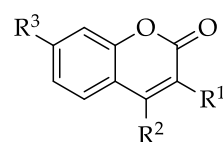
Furthermore Turrini *et al.* point out that chiral lactones are important for applications in antibiotics, plant hormones, fragrances and flavor compounds.^[294] They found a novel biocatalytic route for the synthesis of optical active, most often five-membered ring γ -lactones, by asymmetric bioreduction with a set of isolated and purified ene reductases from the OYE family, more precisely: OYE1, OYE2, OYE3, NCR, YqjM, OPR1, OPR3, XenA, NerA. Coumarins with the structure shown in Figure 46 are non-substrates for their screening system caused by instability and decomposition in the used Tris-HCl buffer at pH 7.5.

The combination of the aforementioned studies from Griese *et al.* and Turrini *et al.* plus the pharmacogenomics of coumarins were the motivation to study this compound class as potential new substrates for the potential industrially interesting TsER panel. Additionally, by enlarging the ring system of coumarin at different positions, as seen in Figure 46, insights into the binding site of TsER should be obtained to find potential new variants for the conversion of bulky substrates with an easy and fast pre-screening fluorescence assay.

By the additional introduction of functional groups, such as the polar 7-hydroxy and 3-acyl group or the non-polar 4-methyl group, different interactions with the enzyme can occur. The polar groups can undergo hydrogen bonding to polar amino acids in the active site and orient the substrate in a different way, whereas the methyl group and also the additional phenyl ring can undergo hydrophobic interactions.

substrates from *Turrini* study

61 R = H
62 R = Me

non-substrates from *Turrini* study

63 R¹ = COCH₂Br, R² = R³ = H
64 R¹ = Cl, R² = R³ = H
65 R¹ = Cl, R² = Me, R³ = OH
66 R¹ = NO₂, R² = Cl, R³ = H
67 R¹ = CN, R² = R³ = H
68 R¹ = CN, R² = Me, R³ = H

planned coumarin scaffolds in the presented thesis

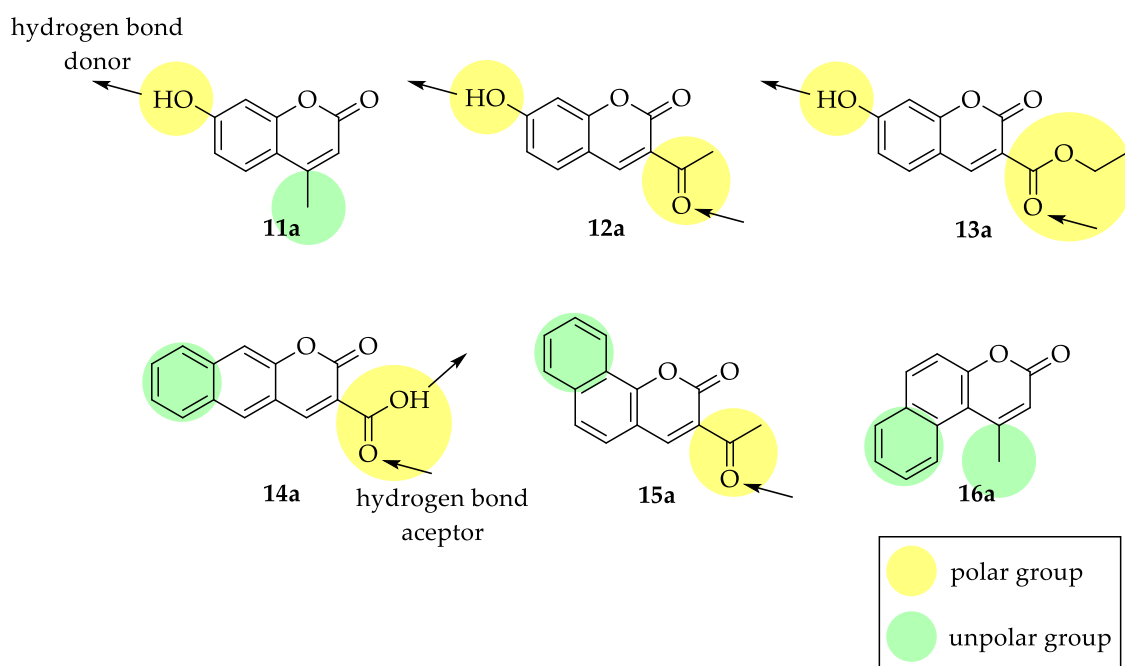
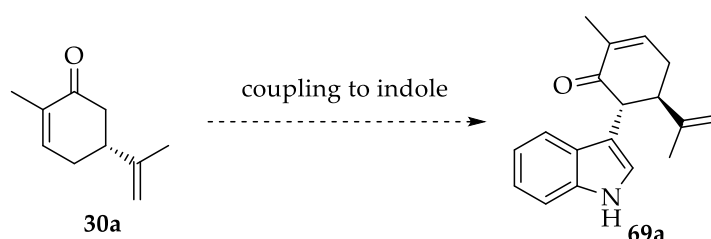


Figure 46. Different planned structural scaffolds based on coumarins from the work of Turrini *et al.*^[294] to obtain insights into the active site of TsER for finding potential new engineering sides to convert more bulky substrates with ene reductases from the OYE family. Arrows are indicating hydrogen bond possibilities. Introduced polar groups are marked light orange and nonpolar groups light green.

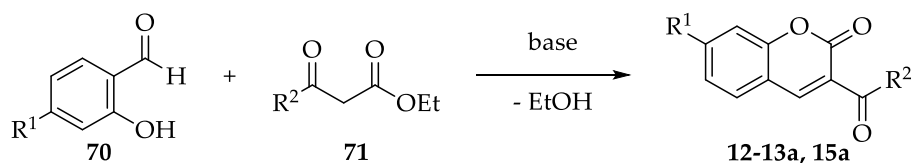
3.6.1 Synthesis of Bulkier Substrates

For the PhD project of SABINE DUEWEL in the working group of SABRINA HOEBENREICH hapaindole structures were synthesized as screening substrates for the halogenase WelO15 from *Westiella intricata* HT-29-1. Therefore, (*R*)-carvone (**30a**) was coupled to indole according to an instruction of BARAN *et al.*,^[295] to obtain substance **69a**, which can also serve as a substrate for ene reductases. This was tested with the *TsER* variant panel and wild type of chapter 3.3. The results are listed in Table 9.



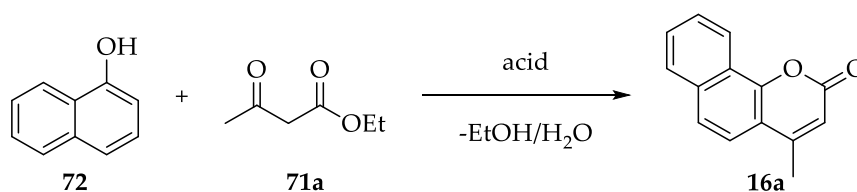
Scheme 15. Synthesis route for **69a** from PhD project of SABINE DUEWEL, based on the protocol of BARAN *et al.*^[295]

Another bulky substrate class, as described in detail above, represents coumarin derivatives. Parts of this work were carried out by GERRIT E. BENARY^[296] and MORITZ RUF^[297] during their bachelor theses. The coumarins presented in this work are synthesized over two different reactions. One mechanism is the KNOEVENAGEL-condensation, followed by a lactonization (Scheme 16). The condensation occurs between a carbonyl compound, most often an aldehyde, and activated methylene to afford an α,β -unsaturated compound. The initial formed enol intermediate reacts with the aldehyde, and the resulting aldol undergoes subsequent base-induced elimination. Michael addition leading to the formation of the coumarin skeleton occurs, followed by re-aromatization.^[298–300]



Scheme 16. KNOEVENAGEL-condensation of aldehydes **70** and activated methylene **71** to form coumarins **12-13a** and **15a**.

The second used synthesis route occurs via a PECHMANN-condensation, where the starting materials are phenols and β -keto esters, and due to an acid the transesterification as well as keto-enol tautomerisation is catalysed to form the lactone ring (Scheme 17).^[301]



Scheme 17. PECHMANN-condensation of phenol **72** and β -keto ester **71a** to form coumarin **16a**.

With these two methods it was possible to synthesize four different structural coumarins shown in Figure 47. 7-Hydroxy-4-methylcoumarin (**11a**) is commercial available. For the integrity of the different structural scaffolds, the expanded linear coumarin **14a** would have been an important substance. But in spite of several synthesis instructions it was not possible to isolate the desired compound **14a**.^[302-305] Most often the starting materials were recovered.

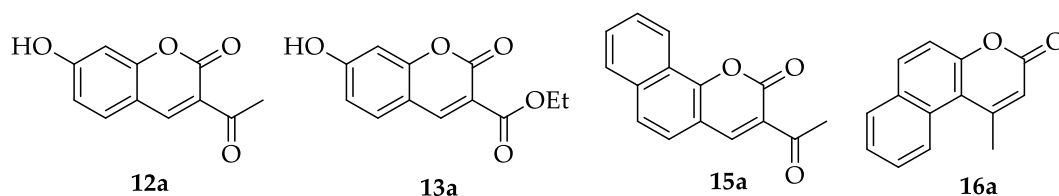
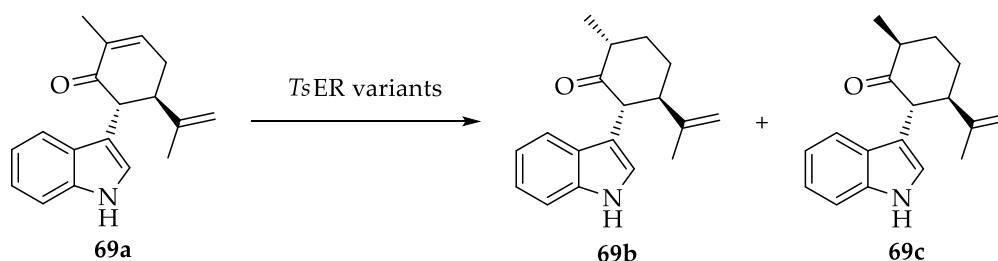


Figure 47. Coumarin derivatives. **12-13a** and **15a** were synthesized via a KNOEVENAGEL-condensation and **16a** via a PECHMANN-condensation.

3.6.2 Screening with *TsER* Panel of Chapter 3.3

First of all, the aforementioned indole **69a** and coumarins **11-13a** and **15-16a** were screened with the panel of *TsER* variants from chapter 3.3 to get an indication of whether the former introduced mutations lead to conversion. The reactions were done with purified enzyme according to chapter 6.9.2.

For indole **69a** the highest conversion of 48% could be observed with *TsER* C25D/I67C/A102Y. All variants with an aspartate in position 25 and a threonine in position 67 showed comparable conversion rates, whereas the variants with a glycine in position 25 lose in mean 12-fold of activity compared to the best variant C25D/I67C/A102Y. Due to solubility problems of indole **69a** in the reaction buffer, the conversion rates could perhaps be increased by using a biphasic system. Nevertheless, this is the first example of modified indole-type substrates for the successful biotransformation with ene reductases from the OYE family. Due to the stereoselective reduction of the carbon-carbon double bond two possible diastereoisomers **69b** and **69c** can be formed (Scheme 18). Experimentally only one peak in the HPLC chromatograms was obtained, but the absolute configuration of the product could not be assigned based on the low amount of compound.



Scheme 18. Possible produced diastereoisomers from **69a** through the reduction with *TsER* variants.

To gain more information about the possible substrate binding in the active site of *TsER* C25D/I67T and C25D/I67T/A102H and the stereochemical outcome, induced-fit docking studies were performed in the available X-ray structures (Figure 48). Both poses show a productive binding with the (*R*)-carvone moiety

oriented above the FMNH₂ and a hydride transfer distance from FMN_{N5H} to C3 of 3.4 Å. The indole moiety points out of the binding cavity illustrated in the surface depiction in Figure 48 and is coordinated by pi-pi stacking to H175. In comparison to C25D/I67T, the indole is vertically flipped in the triple variant, which leads to a pi-pi stacking interaction with the pyrrole ring. The docking results show that it might be possible, in further studies, to enlarge the indole moiety to sizes which are still fitting through the existing cavity.

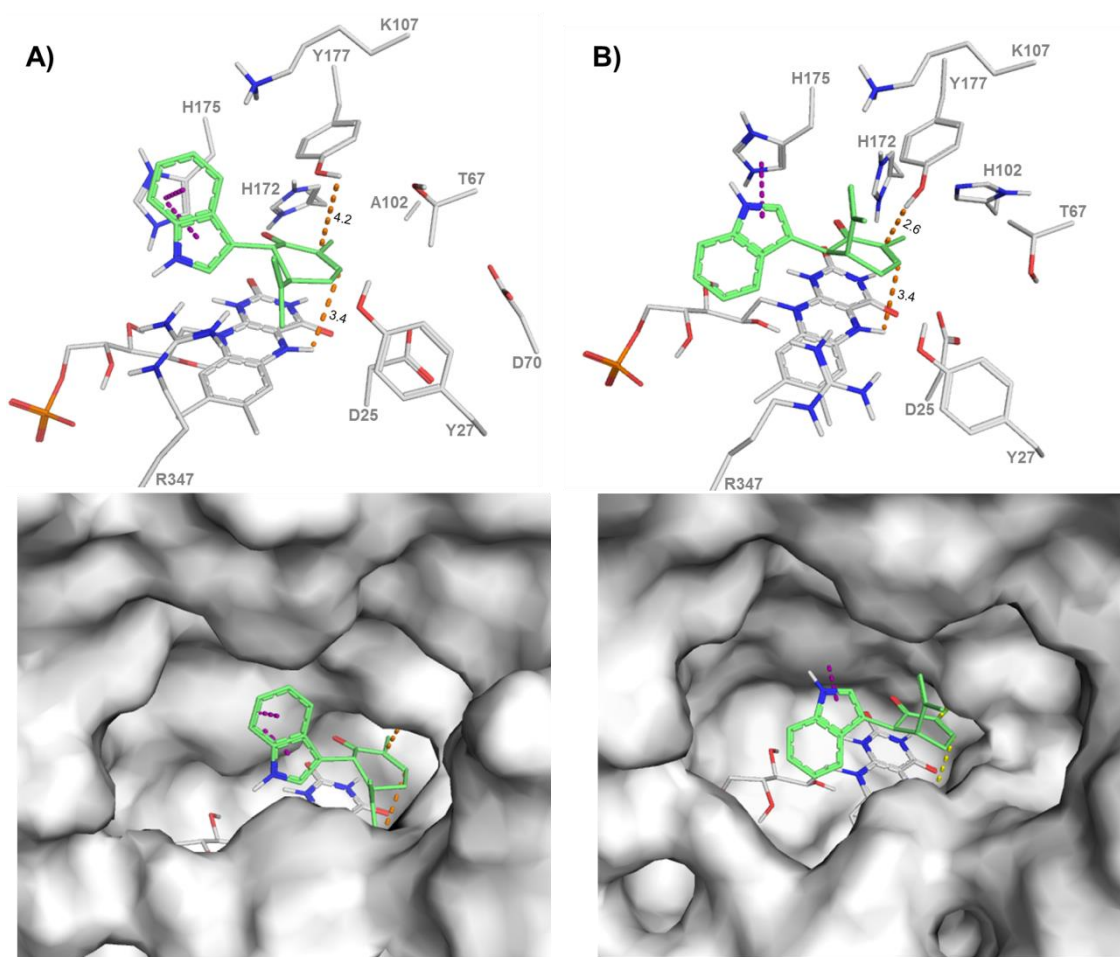
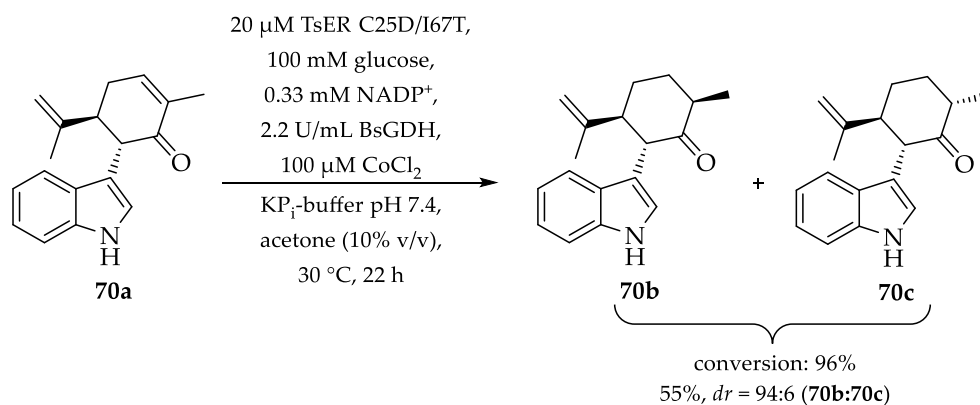


Figure 48. Induced-fit docking results of **69a** (green) A) in the active form of C25D/I67T with FMNH₂ based on pdb 5NUX and B) in the active form of C25D/I67T/A102H with FMNH₂ based in pdb 5OGT. Specific residues in the active site are presented as lines (grey), pi-pi stacking interaction are presented as purple dashes, important distances for hydrogenation as orange dashes.

The predicted stereochemistry from the obtained docking poses, would lead in both cases to **69b**, where the methyl- and the propenyl-moiety are *trans* to each other. This *in-silico* result would also confirm the obtained diastereoselectivity

for the reduction of (*R*)-carvone (**30a**) with all *TsER* variants, which always lead to *trans*-**30b** as major diastereomer (Table 9).


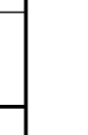
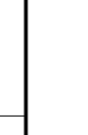
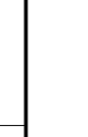
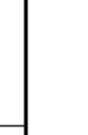
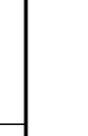
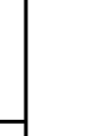
In further studies by LUCA SCHMERMUND^[306], the coupled (*S*)-carvone indole **70a** was also tested with the *TsER* C25D/I67T variant. He was able to determine the absolute configuration of the products **70b** and **70c** by NMR spectroscopy. The major product in this biocatalytic reduction is the *cis*-isomer **70b**, which is also the obtained diastereomer in the production of **18b** by C25D/I67T (Table 3).



Scheme 19. Biocatalytic reduction of **70a** by *TsER* C25D/I67T from the work of LUCA SCHMERMUND.^[306]

The study with **70a** and the IFD results corroborate the presumed stereochemical outcome of **69a** with the *TsER* variants. For experimental confirmation, up-scale reactions with **69a** and C25D/I67T should be performed, to gain enough product for NMR studies.

Table 9. Substrate scope of *TsER* variant panel from chapter 3.3 with indole **69a** and coumarin derivatives **11a-16a**. All reactions were done with purified enzyme in triplicates; standard deviation for conversion is $\pm 5\%$. The reaction was stopped after 24 h. The given conversion rates are determined by HPLC. For **15b** the three values are newly observed peaks at retention times 1.40 min, 1.59 min and 2.13 min. By LC-MS the peak at 1.40 min was identified as the expected dihydrocoumarin **15b**, the other two peaks could not be assigned to any optional by-product. * forms only **13c**.

Product	wt conv%	C25D/I67C conv/%	C25D/I67T conv%	C25D/I67V conv%	C25D/I67T/A102H conv%	C25D/I67C/A102Y conv%	C25G conv%	C25G/I67C conv/%	C25G/I67T conv/%	C25G/I67V conv%	C25G/I67T/A102H conv%	C25G/I67T/A102Y conv%	C25G/I67C/A102I conv%	C25G/I67C/A102H conv%
 69b	38	18	39	23	26	48	10	4	17	10	26	17	11	16
 11b	n.c.	n.c.	n.c.	n.c.	n.c.	n.c.	n.c.	n.c.	n.c.	n.c.	n.c.	n.c.	n.c.	n.c.
 12b	n.c.	40	88	4	72	76	79		68	71	75	78	76	56
 13a → 13b	n.c.	9	n.c.*	22	75	68	n.c.*	3	2	n.c.*	77	70	71	70
 13a → 13c	n.c.	74	36	19	n.c.	n.c.	n.c.	11	92	54	n.c.	n.c.	n.c.	n.c.
 15b	n.c.	39/11/6	0/24/52	n.c.	70/11/2	8/1/0	n.c.	7/0/0	79/7/3	44/0/0	38/0/0	63/3/0	29/0/0	37/0/0
 16b	n.c.	4	n.c.	n.c.	13	63	n.c.	15	9	n.c.	19	11	17	10

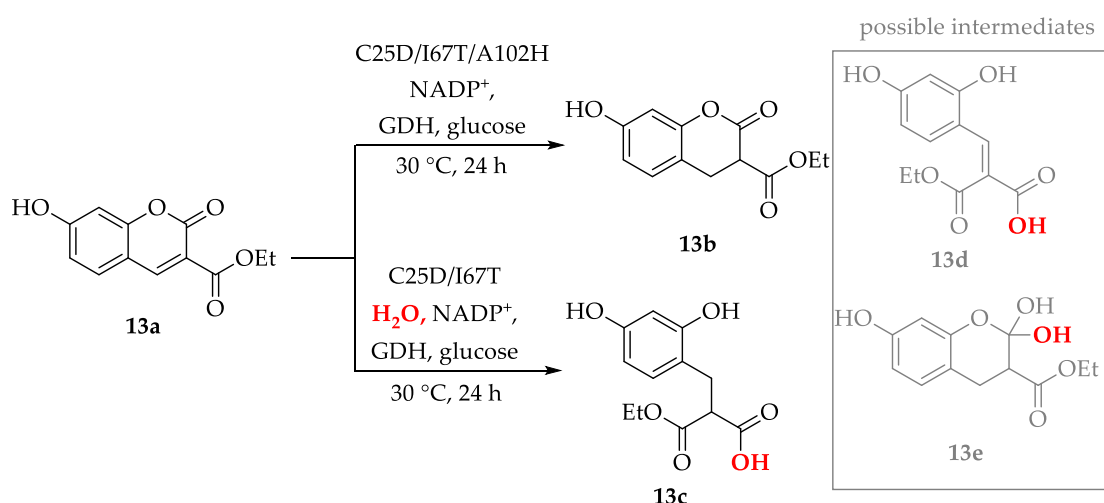
The coumarin substrates **12-13a** and **15-16a** are newly discovered for ene reductase hydrogenation. The substrate loading in the biocatalytic assay had to be reduced, due to solubility problems of the coumarin derivatives. They are barely soluble in water and most organic solvents, such as ethanol, methanol and ethers which are often used for biological assays. For that reason the stock solutions were prepared in dimethylformamide (DMF). The first tests showed that solubility of the substrates was an issue due to precipitation at 10 mM, limiting the working concentration to just 1 mM. In future work this might be avoided by working in bi-phasic systems with DMF as the organic phase.

Normally, the reduction of the double bond in the lactone moiety is expected to generate the dihydrocoumarin. However, the biotransformation of 7-hydroxy-3-carboxy-coumarin ethyl ester (**13a**) yielded two different products depending on the used variant, which were identified as either the expected dihydrocoumarin (**13b**) or the hydrolysis product 3-(2,4-dihydroxyphenyl)-2-ethoxypropanoic acid (**13c**).

HÄSER *et al.* described a bioprocess for the production of natural dihydrocoumarin from coumarin by *Saccharomyces cerevisiae*.^[307] In whole cell biosynthesis the dihydrocoumarin is further degraded to melilotic acid by hydrolases. As a consequence, they had to follow up with a distillation of the primary isolated product melilotic acid in the presence of natural citric acid to obtain the pure dihydrocoumarin.^[307] Therefore it was important for the reduction of the lactones to work with purified *TsER* variants to exclude the lactone hydrolysis by other enzymes presented in whole cells. It was previously shown by NMR studies, that the OYE XenA only reduces coumarin but is not responsible for the subsequent hydrolysis.^[292]

In the work of TURRINI *et al.*, it is mentioned that some of their tested coumarins are unstable and decomposed in Tris-HCl buffer with a pH of 7.5.^[294] This was not observed for the screening system in potassium phosphate buffer used here.

In this thesis all reactions were performed in the same potassium phosphate buffer system at pH 7.4, including the recycling system consisting of glucose, BsGDH and NADP⁺ at 30 °C for 24 h. The buffer capacity is 100 mM, ten-times higher than the amount of possible acid equivalents under screening conditions, and ensures a constant pH, even when considering uncoupling. In the used scale acidification of the reaction mixture was never observed. Both the negative control with 7-hydroxy-3-carboxy-coumarin ethyl ester (**13a**) in reaction buffer without enzyme, and the biotransformation with *TsER* wt result in the isolation of the intact starting material **13a**. This is an indication that the lactone hydrolysis not occur in the used buffer system. However, the biocatalytic reaction of **13a** with C25D/I67T and all other double variants produced a transformation product with an m/z about 254 and a retention time of 1.73 min (determined over reverse phase HPLC). By large scale reaction, enough product could be isolated to perform HSQC-NMR experiments to identify the exact product. It could clearly be identified as **13c**. The biotransformation with the triple variants resulted in a major product with a retention time at 1.33 min and a m/z of 236, which corresponds to **13b** (determined by reverse-phase LC-MS).



Scheme 20. Biotransformations of **13a** with *TsER* variants C25D/I67T and C25D/I67T/A102H lead to two different products. **13d** and **13e** are possible intermediates, if the hydrolysis occurs before reduction or after reduction.

The results presented in this thesis show that hydrolysis might occur in the active site of *TsER*, otherwise it is difficult to explain why after transformation in

the same buffer system for the C25D/I67T variant the acid **13c** was isolated, whereas the C25D/I67T/A102H variant only produces the dihydrocoumarin **13b** (Scheme 20).

To gain more information about the binding of **13a** in both variants, a crystal structure of the C25D/I67T/A102H variant was obtained in collaboration with D.J. OPPERMAN (pdb 5OGT, details are shown in chapter 3.4.2). Unfortunately, soaking and co-crystallization experiments with substrate **13a** failed. Therefore, to acquire more information about the possible binding and mechanism of lactone hydrolysis in the different active sites, molecular docking studies were performed. The most likely models were chosen based on experimental data.

In the obtained crystal structures the cofactor FMN is oxidized, whereby no hydride transfer to the substrate is possible. Accordingly, the structures were prepared to mimic the active enzyme with the reduced FMNH₂ by the use of ANTECHAMBER. The level of theory used during receptor preparation (PROPKA)^[308,309] predicts both imidazole's of H172 and H175 as neutral in both oxidation states. At pH 7.4 the imidazole ring is approximately protonated to 10% when free in solution. Moreover, the protonation state of the two active site histidines is actually unexplored experimentally. The work of LONSDALE *et al.*^[132] showed that the two active site histidines had to be protonated and harmonic constrains were needed, otherwise the substrate protein complex was not maintained during MD calculations. Whereas others have not reported on similar observations or on the protonation state chosen in their calculations,^[130,152,310,311] in the here presented *in-silico* studies productive docking poses without the expected hydrogen bonds to one or both histidines were observed.^[67,228] Therefore, the decision was made to protonate both residues for the IFD experiments as in the former *in silico* studies shown in chapter 3.5.1.

The first question to address is whether reduction of the carbon-carbon double bond occurs before or after lactone hydrolysis. IFD of **13a** in the reduced forms of C25D/I67T, C25G/I67T, C25D/I67T/A102H and the wild type results in pro-

ductive poses for all variants. Three anchoring modes of the two carbonyl groups were observed: a) both point towards H172/H175 forming H-bonds with one or both of them; b) both form H-bonds with R347, and Y27 has a polar contact to the lactones alcohol oxygen; or c) one forms a H-bond with H175 and the other with R347 (Figure 49A, B). Most of these binding modes still show reasonable angles and distances for hydride and proton transfer upon reduction. Therefore, further experiments need to be performed to identify the experimentally relevant orientation.

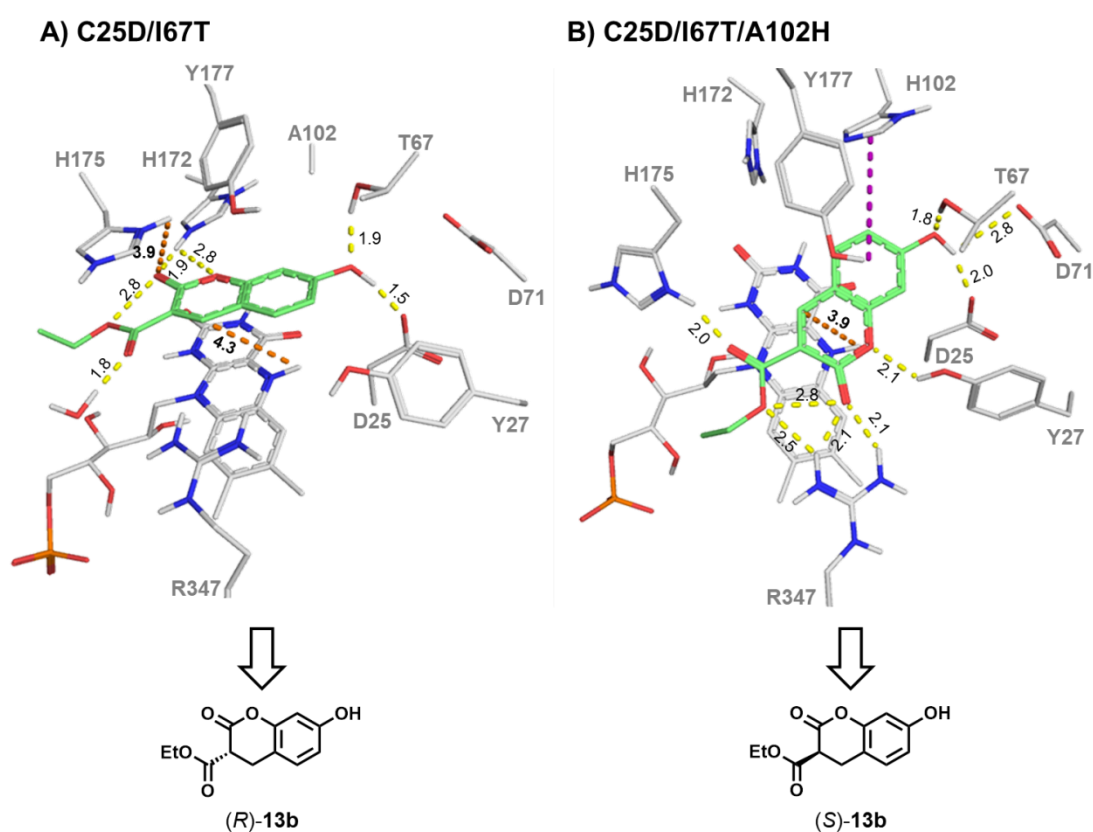


Figure 49. A) IFD of reduced TsER C25D/I67T structure with protonated H172/H175 and **13a** (green lines). Closest and most acidic proton to C=O is δNH^+ from H175, shown in orange dashes B) IFD of reduced TsER C25D/I67T/A102H structure with protonated H172/H175 and **13a** (green lines). The essential amino acids (grey) and FMNH₂ (grey) are shown as lines, pi-pi stacking between H102 and phenol ring of **13a** is marked as purple dashes. Hydrogen bonds are shown as yellow dashes and the distance between N5H of FMNH₂ and C4 as orange dashes.

In addition, H-bonds of the 7-hydroxy group from **13a** with D25 and T67 are often observed. In the less polar C25G/I67T variant, residue D71 takes over this function, still orienting **13a** in productive poses for hydride transfer (3.2 Å, 108.1°, see Figure 50A). The IFD docking for TsER wild type results in no pro-

ductive poses, caused by the missing interaction partners D25 and T67 or inaccessible D71 (see Figure 50B and Table 54). All of these results correlate well with the experimental results (Table 9)

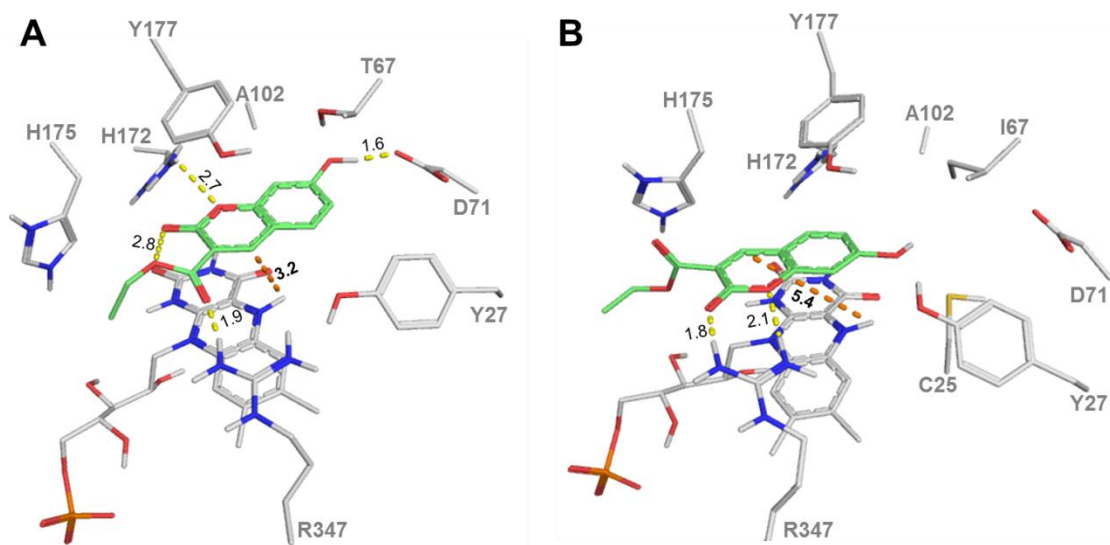


Figure 50. A) Second highest ranked pose of IFD of reduced *TsER* C25G/I67T structure with protonated H172/H175 and **13a**. B) Highest ranked pose of IFD of reduced *TsER* wt structure with protonated H172/H175 and **13a**. The essential amino acids (grey), FMNH₂ (grey) and **13a** (green) are shown as lines, hydrogen bonds are shown as yellow dashes and the distance between N5H of FMN and C4 of **13a** as orange dashes.

The situation is different with the opened coumarin intermediate **13d**, which would exist if the hydrolysis occurs before reduction. A small cavity formed by H172, A102 and T67 hosts the dihydroxybenzene group, allowing the carboxylate of **13d** to form a salt bridge with R347 in all docking poses of variant C25D/I67T (Figure 51A). This orientation perfectly positions the ester carbonyl group to form a hydrogen bond with Y27 and sometimes H175. This interaction bends the double bond away from an optimal orientation for orbital overlap, very likely preventing reduction. Poses of **13d** in C25D/I67T/A102H resulted in many non-productive binding modes (Figure 51B). The smaller cavity, due to A102H, has eliminated most poses with the salt bridge, nevertheless the dihydroxybenzene group is more often observed pointing towards D25 than towards the solvent. Currently, it is proposed that substrate orientation and subsequently stereoselectivity, can be altered by creating new substrate anchors.^[152] H102 would have this potential, but in none of the IFD poses H-bonds to

A102H have been observed, hence this residue is not a new substrate anchor for **13a-e**.

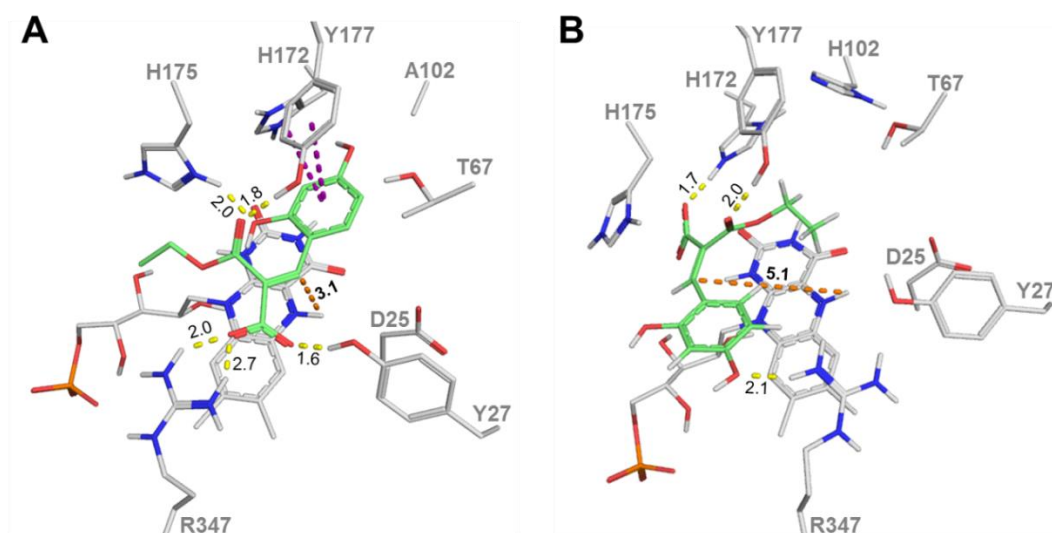


Figure 51. A) IFD of reduced *TsER* C25D/I67T structure with protonated H172/H175 and **13c**. Pi-pi stacking between H172 or Y177 and phenol of **13d** is marked with purple dashes. B) IFD of reduced *TsER* C25D/I67T/A102H structure with protonated H172/H175 and **13c**. The essential amino acids (grey), FMN_{H2} (grey) and **13d** (green) are shown in lines. Hydrogen bonds are shown in yellow dashes and the distance between N5H of FMN and C4 of **13c** is shown in orange dashes.

Overall, docking of **13a** in reduced C25D/I67T and C25D/I67T/A102H receptors (Figure 50) yielded productive poses for hydride transfer, whereas none were found with **13d** (Figure 51). In addition, formation of **13d** was not observed in the performed assays, strongly suggesting that reduction occurs first, followed by lactone hydrolysis.

In this case, two scenarios exist: 1.) hydrolysis occurs directly after reduction, before **13b** leaves the active site (route 2, Figure 52), or 2.) **13b** dissociates and binds again to either the reduced or oxidized form in a new binding mode that enables hydrolysis (route 1 and 3, Figure 52). IFD was performed with *R*- and *S*-**13b**, *R/S*-**13e** and reduced/oxidized C25D/I67T and C25D/I67T/A102H to mimic the relevant states of the reaction (Figure 52).

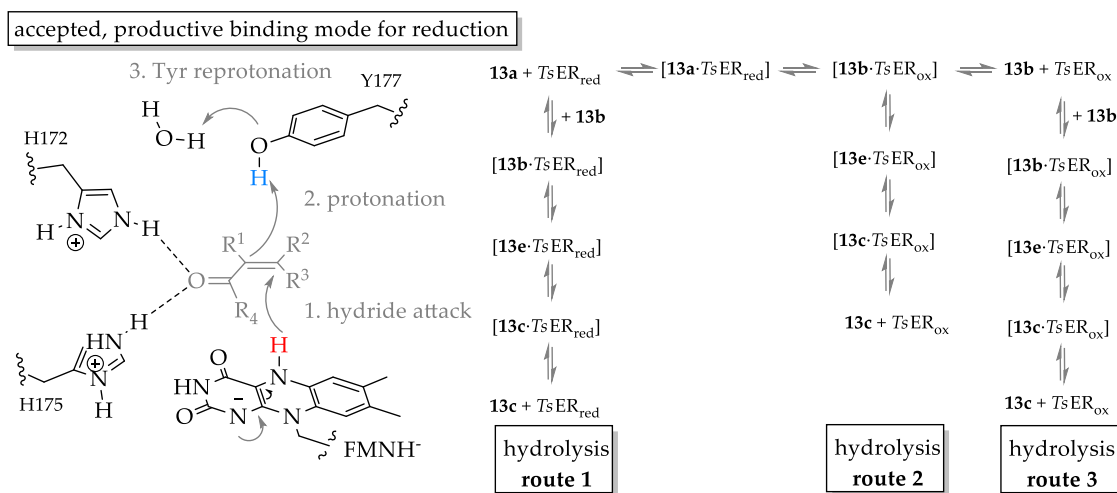


Figure 52. Accepted mechanism of the asymmetric reduction of α,β -unsaturated alkenes with ene-reductases. The educt is anchored via hydrogen bonds above the reduced flavin. After hydride transfer, the enolate is most likely protonated from a tyrosine.^[102,107,118,132,174,312,313] Afterwards, Y177 will be re-protonated from a water molecule, creating nucleophilic water in close proximity to the reduced lactone ring, an ideal situation for hydrolysis directly after reduction.

It is known that γ - and δ -lactones react readily in mildly acidic media due to their basicity.^[314] This can be partially explained in terms of their acid dissociation constants: the higher the acidity, the lower the concentration of the highly reactive protonated ester and hence the lower the catalytic effect of hydronium ions.^[314] In C25D/I67T a hydrogen bond between H175 and the carbonyl oxygen of the lactone is formed (Figure 53A-C), whereby the carbonyl group came in close proximity to the protonated delta nitrogen of H175, which might result in protonation of the carbonyl group from **13b**. Due to the protonation of the carbonyl group from **13b** an acid-catalysed hydrolysis of the δ -lactone might occur and explain the experimental observation. This is presumably due to an A_{AC}2 mechanism, where the attack of a water molecule on the protonated carbonyl is base-catalysed by an additional water (Scheme 21A).^[314] The A_{AC}2-mechanism is the most usual acid-catalysed hydrolysis pathway. It takes place in two steps, the protonation of the carbonyl group followed by an addition of water to get the tetrahedral intermediate (**13e**), which in turn decomposes.

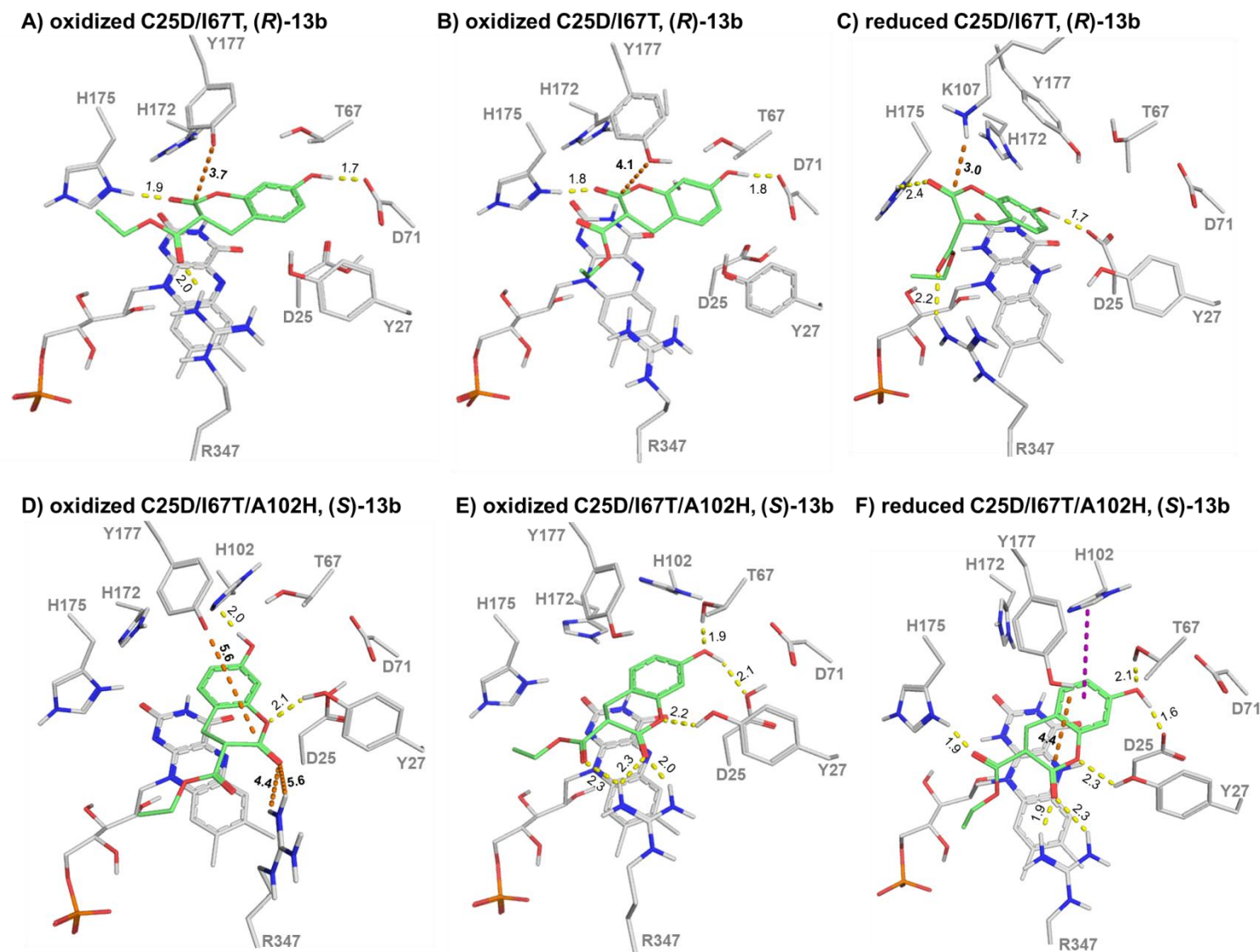


Figure 53. IFD of the potential produced isomer of (R)-13b in TsER C25D/I67T and (S)-13b in TsER C25D/I67T/A102H, A) oxidized FMN, charged Y177 and protonated H172/H175 of C25D/I67T, B) oxidized FMN, protonated Y177 and H172/H175 of C25D/I67T, C) reduced FMNH₂, protonated H172/H175 of C25D/I67T, D) oxidized FMN, charged Y177 and protonated H175 of C25D/I67T/A102H, E) oxidized FMN, protonated Y177 and H175 of C25D/I67T/A102H, F) reduced FMNH₂, protonated H172/H175 of C25D/I67T/A102H.

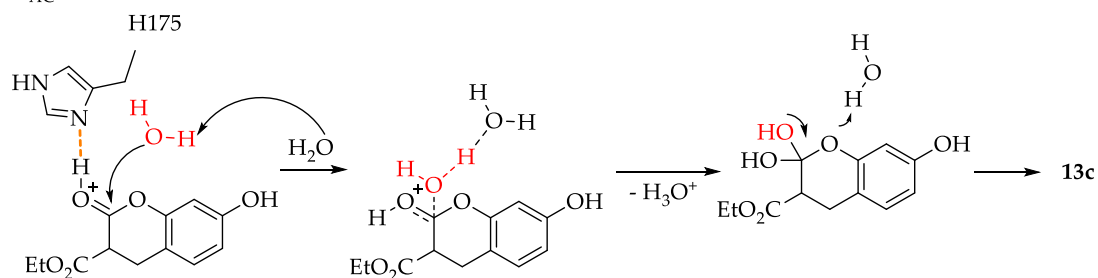
The essential amino acids (grey), FMN (grey) and 13b (green) are shown as lines, pi-pi stacking marked as purple dashes, hydrogen bonds are shown as yellow dashes, distance of closest and most acidic proton to C=O of 13b is shown in orange dashes

In OYEs, Y177 plays a crucial role in the hydrogenation reaction by delivering the proton (Figure 52).^[61,102,107,108,118,132] If the double bond reduction occurs before the lactone hydrolysis, the charged Y177 might be acting as a base and could get re-protonated by a coordinating water molecule (Scheme 21B).^[314] It is known from QM/MM studies with YqjM, that a water molecule can be activated by Y177 for the hydrogenation step, but it is more likely that Y177 protonates the substrate directly.^[132] Therefore, dihydrocoumarin **13b** was docked into the oxidized TsER variants (Figure 53A,B). In accordance with the work from LONSDALE *et al.*^[132], the oxidized receptor was prepared with and without protonated Y177. In contrast to the reduced structure, the PROPKA program predicted D25 in the oxidized structure as protonated.

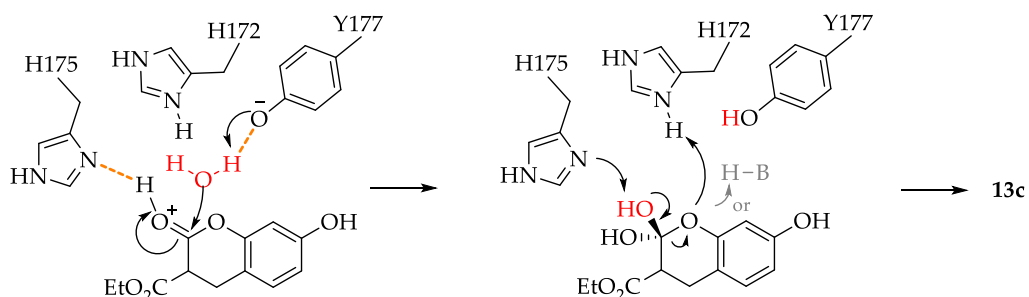
Recently, WERTHER *et al.* showed via X-ray crystallography a remarkable difference in hydroxycoumarin binding, depending on whether the FMN cofactor in XenA is oxidized or reduced (Figure 45).^[293] A binding difference, according to the oxidation state of FMN, was also observed in the *in silico* studies shown here (compare Table 37 and Table 39).

Poses of **13b** in oxidized C25D/I67T are slightly different to the reduced complex with **13a**. The epsilon nitrogen of H172 is at a distance of 4.4 Å to the carbonyl oxygen of the lactone, whereas the protonated delta nitrogen of H175 forms a hydrogen bond to this carbonyl. The charged Y177 is close enough (4.3 Å) to deprotonate a water molecule. In contrast to the pose in C25D/I67T/A102H, where the Y27 forms a hydrogen bond to the lactone oxygen, that the coumarin is flipped in the binding site and the closest polar residue to the carbonyl is R347 with 4.4 Å and 5.6 Å. Through polarization of the carbonyl by R347 a nucleophilic attack of a water molecule can occur. Subsequently hydrolysis of the lactone occurs by protonation of the former lactone oxygen by Y27 (Scheme 21C).

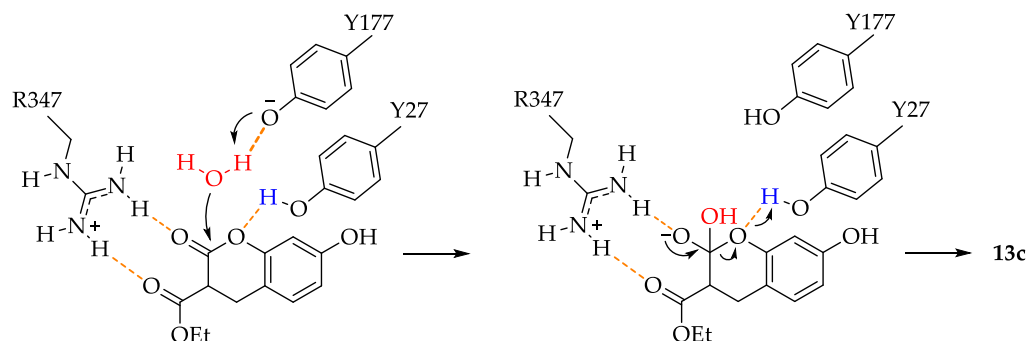
A) A_{AC2} mechanism with water from the bulk solvent as base



B) A_{AC2} mechanism with Y177 as base in the 1. step and H172 in the 2. step



C) Hydrolysis mediated by residues R347, Y177 and Y27



Scheme 21. Postulated hydrolysis mechanisms of **13b** in the binding site of *TsER*.

There is existing evidence for acid-base chemistry in the active site of ene reductases. Known in the literature is the redox-neutral acid-base function of the cofactor FMNH₂ in OYEs, which catalyses carbon-carbon double bond isomerization reactions.^[110] In the proposed acid-base mechanism presented here, the cofactor FMN is not directly involved. The acid-base catalysts are presented by the side chains of Y177, H175, H172, Y27 or R347.

For the acidic hydrolysis following the A_{AC2} mechanism, the next step mechanistically would be the formation of the diol intermediate **13e**. The IFD for (*R*)-**13e** in C25D/I67T showed a binding pose quite similar to the former protonation state, where H175 interacts via hydrogen bonding with one OH-group

and Y177 with the second. The interaction of Y177 with the second OH-group confirms the proposed mechanism in Scheme 21B. However, it should also be mentioned that in the majority of poses for C25D/I67T, the lactone oxygen is oriented in the direction of Y27 (Table 49). In comparison, all poses for (*S*)-**13e** in C25D/I67T/A102H are oriented as shown in Figure 54B, with a highly distinct hydrogen bonding network. The distance between Y177 and one OH-group of the diol is quite far with 4.2 Å. This distance might not lead to a re-protonation of Y177, such as that postulated in Scheme 21C.

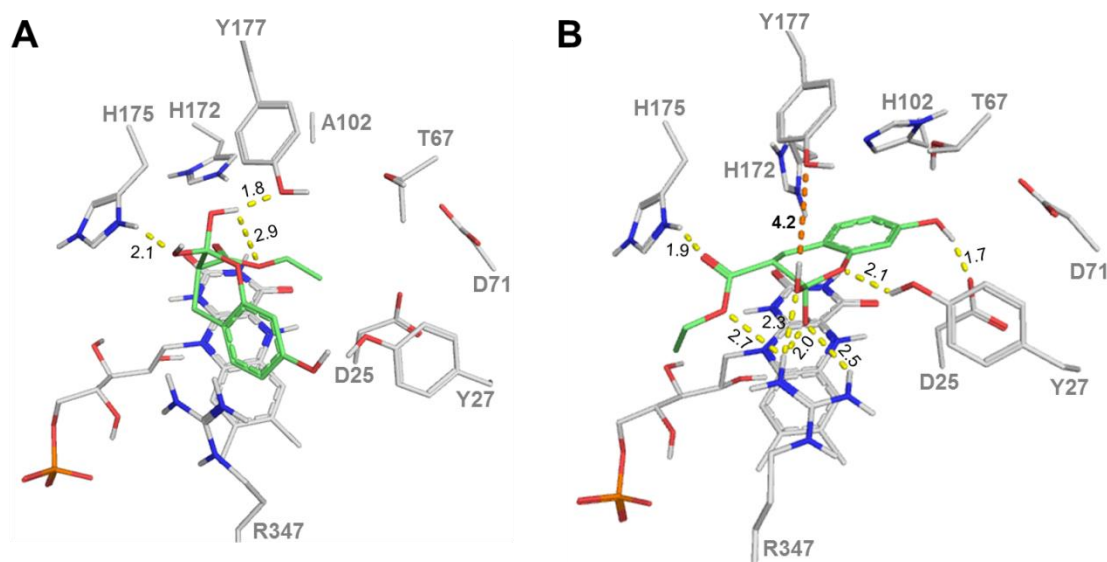


Figure 54 A) IFD pose of reduced TsER C25D/I67T structure with protonated H172/H175 and intermediate **13e**. B) IFD pose of reduced TsER C25D/I67T/A102H structure with protonated H172/H175 and intermediate **13e**. The essential amino acids (grey), FMNH₂ (grey) and **13e** (green) are shown as lines, hydrogen bonds are shown as yellow dashes.

In conclusion, due the combination of X-ray crystallography and *in silico* studies, possible lactone hydrolysis mechanisms by the *TsER* variant C25D/I67T could be hypothesized. The observed docked poses with the lactone oxygen pointing in the direction of H172 promote a possible protonation of the carbonyl oxygen by H175 and a further hydrolysis via an A_{ac}2 mechanism.

To explore the exact catalytic mechanism of lactone hydrolysis, molecular dynamics (MD) simulations along with combined quantum mechanics/molecular mechanics (QM/MM) studies should be applied. With these methods, details such as those concerning stable binding of the substrate to the active site, the

order of the reaction steps, and the nature of transition states to hydride and proton transfer as well as the role of water in the catalytic reaction and lactone hydrolysis can be addressed.

With the *TsER* variant panel of chapter 3.3, for almost every coumarin derivative in Table 9 a biotransformation product was obtained. The exceptional case is 7-hydroxy-4-methylcoumarin (**11a**) whereby no variant showed any conversion. This might be due to the deactivating methyl group at the double bond. In the RBD of **11a** in C25D/I67T and C25G/I67T no productive pose within sufficient distance of the FMN hydride to the C4 could be found (Table 28, Table 29). Even more surprisingly were the successful conversion rates with the even bulkier **16a**. Rigid body docking analysis of both substrates in the C25D/I67T/A102H structure show a preferred pose for **16a** for hydride transfer with an N5H to C4 distance of 3.5 Å and 4.1 Å for proton delivery of Y177-OH to C3.

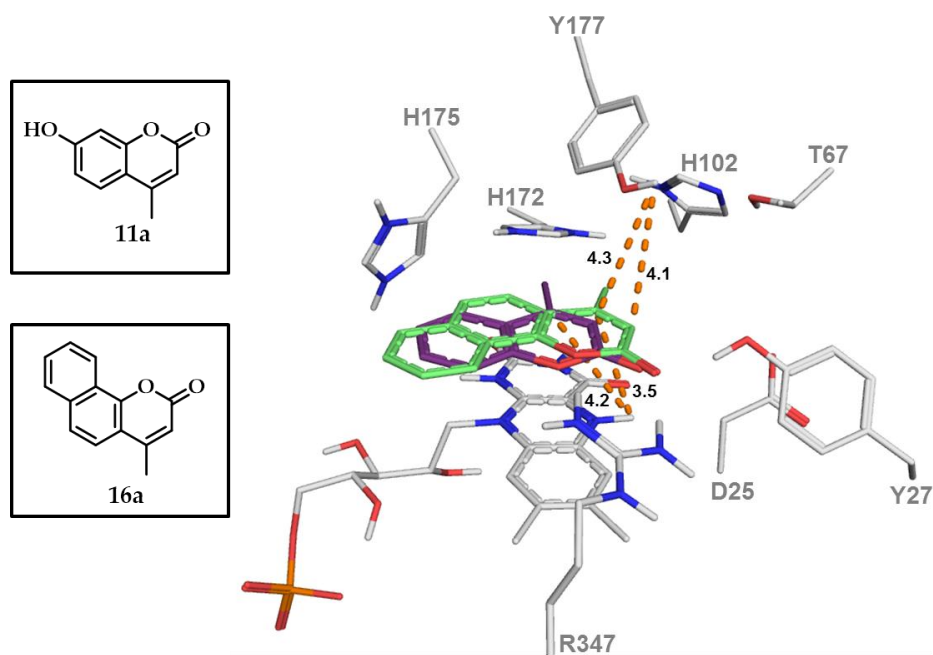


Figure 55. RBD results of **11a** (purple lines) and **16a** (green lines) in C25D/I67T/A102H structure with FMNH₂ and protonated H172/H175. Important residues are shown in grey lines, distance from FMN N5H to C4 and from Y177OH to C3 shown as orange dashes.

Active variants were also found for the bulky coumarin **15a**, with up to 79% conversion to the dihydrocoumarin identified by LC-MS (retention time of 1.40 min, m/z of 241). **15a** reduction yielded two different products with different variants. C25D/I67T yielded two products with retention times of 1.59 min and 2.13 min (Table 9). This observation is comparable to the results with **13a**. To date it was not possible to clearly identify these two products. Attempts to upscale the reaction failed mainly due to solubility problems. In analogy to the retention times of the clearly identified hydrolysis product of **13a**, the main product produced with C25D/I67T and **15a** might also be the dicarboxylic acid. This is just an assumption and has to be investigated further in a follow up project.

For the first time *TsER* variants were identified, which reduce coumarin-like structures as **13a**, **15a** and **16a**. For clearly identifying the produced side products upscale reactions must be performed to analyze them via NMR spectroscopy. The reaction should be performed in a bi-phasic system with DMF to avoid solubility problems.

3.6.3 Generation and Screening of Libraries

Inspired by the work of RÜTHLEIN *et al.*^[152] the residue H175 from *TsER* was considered as potential new mutation site. They redesigned the binding pocket of YqjM to alter the binding mode of Roche ester precursor **19a** consequently reversing the stereopreference, by mutating the mechanistically essential amino acid H167 to alanine. Figure 56 shows *in silico* docking studies of the Roche ester precursor **19a** in YqjM and one planned variant. It can be seen that due to the alanine mutation in position 167 more space in this area of the binding pocket is generated. The additional incorporation of hydrogen donating amino

acids like asparagine or histidine in position 26 is postulated to induce a substrate flip.

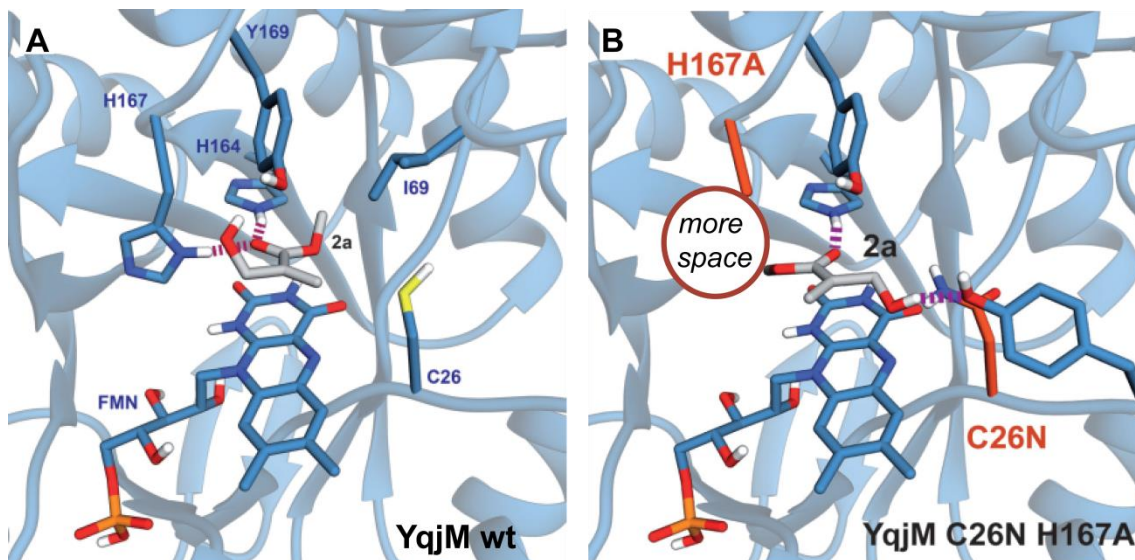


Figure 56. A) Structure of YqjM wt active site. The essential amino acids, FMN, and the positions for the mutagenesis study are shown explicitly. The binding mode of the Roche ester precursor **19a** resulting from *in silico* docking is shown in grey. B) The Roche ester precursor **19a** docked into the active site of YqjM C26N/H167A. The mutation in position 167 to alanine offers more space. Hydrogen bonds are drawn in dashed lines.^[152]







Based on this work it was thought that gaining space in position 175 of TsER enables binding and therefore leads to transformation of the bulkier coumarin-like substrates. For this reason a library with the mutation sites C25 and H175 of TsER was planned.

3.6.3.1 Library C25NNK/H175NNK

Protein engineering and evolution applications frequently use protein libraries that include defined amino acid mixtures at certain positions of interest.^[57] A widely used approach for introducing diversity is the use of degenerate codons incorporated during oligonucleotide synthesis that include mixtures of nucleotides at each position.^[315] This approach should also be applied for the positions C25 and H175 in TsER, by introducing the complete set of standard amino acids, which is encoded using NNK, where N = A, T, C or G and K = G or T.

The introduction of the reduced codon NNK for position H175 was successful via a megaprimer PCR method, whereas at position C25 just with two Quik-Change PCRs a relatively sufficient degeneration of NNK was achieved. The quality of the library was checked by performing sequence analysis of pooled plasmids prior to transformation into the expression strain. This concept is called “Quick Quality Control” (QQC).^[316,317] The degeneracy of saturation mutagenesis at position C25 and H175 can be seen in Table 10. Conspicuously the four bases are not equally represented as they ideally should be for A/T/C/G degeneracy with the used codon NNK. Due to the possible imbalance at the synthesis level of the primers a small deviation of 5-10% can occur.^[67] Additionally, the pooled primers have different annealing efficiencies, what has to be taken in account.^[39]

Table 10. Degeneracy of *TsER* saturation mutagenesis libraries at position C25 and H175 on wild type templates. The percentage of each base was calculated from the sequencing data of the pooled plasmids for each library. The following color code is used: green: C, black: G, red: T, blue: A.

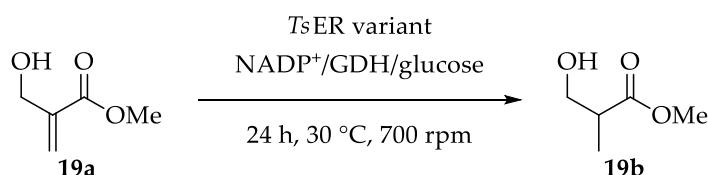
Library	first base	second base	third base	Library	first base	second base	third base
wild type	T	G	C		C	A	T
C25_NNK	T	G	T	H175_NNK	G	G	G
							

The NNK codon allows all twenty amino acids (32 codons), which results for two simultaneous sites in 1024 different codons. To get coverage of 95% over the sequence space 3066 colonies should be picked and screened. As starting point 910 colonies were picked in 96 deep-well plates, which correspond to a 28% coverage.

First of all, this generated library was screened with the Roche ester precursor **19a** to compare the results with those of RÜTHLEIN *et al.*^[152] Out of the 910 screened colonies 30 different hit variants were found, which result in a hit rate of 3.3% (Table 11). This value is quite good for that library size and the introduced degeneracy (compare Table 10). The hit rate depends on the library size

and numbers of screened colonies, but the number here is comparable with literature values for directed evolution studies.^[46,318]

Table 11. Hit variants of *TsER* library C25NNK/H175NNK found by substrate screening with methyl 2-hydroxymethyl acrylate **19a**. Conversion rates were determined by GC.



<i>TsER</i> variant	conversion (%)	<i>TsER</i> variant	conversion (%)
C25D	10	C25N/H175S	4
C25D/H175V	1	C25R/H175K	1
C25H	20	C25S	6
C25H/H175A	1	C25S/H175A	2
C25H/H175K	5	C25S/H175F	2
C25H/H175S	2	C25V	31
C25H/H175T	2	C25V/H175G	10
C25H/H175Y	2	C25V/H175Q	46
C25I	36	H175A	4
C25I/H175W	19	H175G	2
C25L	47	H175K	1
C25L/H175A	5	H175L	3
C25L/H175E	1	H175S	8
C25N	21	H175T	3
C25N/H175A	1	H175V	2

The identified hits are both single and double variants in the positions C25 and H175. The conversion rates are comparable with those of the RÜTHLEIN study, where also the single variants in position C26 of YqjM show higher conversion rates than the double variants. In comparison, YqjM C26H produced **19b** in 56%^[152] while *TsER* C25H showed 20% conversion. However it should be mentioned that the YqjM results were achieved in a biotransformation with purified enzyme. That means the concentration conditions could be controlled, whereas in the *TsER* lysate screening this was not possible. In assays with purified enzymes conversion rates can be increased in controlled conditions as could be shown for *TsER* wt. In the lysate screening only 12% of **19b** was produced, whereas in the controlled assay with purified enzyme 94% of **19b** was formed (see Table 9).

As aforementioned this library was first of all generated to screen with the bulkier coumarin substrates. 7-Hydroxy-3-carboxycoumarin ethyl ester (**13a**) is due to the aromatic system and the 7-hydroxy group fluorescent, for which reason a fluorescence screening method could be adapted from known protocols.^[317,319] Changing the analysis method from chromatography to fluorometric highly reduces labor costs and expenses for the screening, since time-consuming steps such as extraction, filtration and chromatographic separation are replaced by simply transferring the reaction mix into a black flat-bottom 96-well microtiter plate (MTP) and measuring either spectra or single-point results. The best conditions for **13a** in the fluorescence assay were determined in a former study^[319], which result in an excitation wavelength of 400 nm, an emission wavelength of 440 nm and a cut-off at 420 nm.

Former screening of **13a** with purified *TsER* wt showed no activity, whereas the C25D/I67T variant produced 36% of the reduced and hydrolyzed **13c** (see Table 9). That implies, for the fluorescence assay, samples which showed less fluorescence than the *TsER* wt were identified as active hits and send to sequencing for identifying the incorporated mutations (Figure 57). With this simple and fast pre-screening method 16 hit variants out of 910 screening samples could be identified for **13a** as substrate. This relates to a hit rate of 1.8%. In 12 out of the 16 variants always one of the introduced residues is a hydrogen donating group, like serine, threonine, asparagine, glutamine, tyrosine and lysine, which can serve as the anchor point for the carbonyl group of 7-hydroxy-3-carboxycoumarin ethyl ester (**13a**).

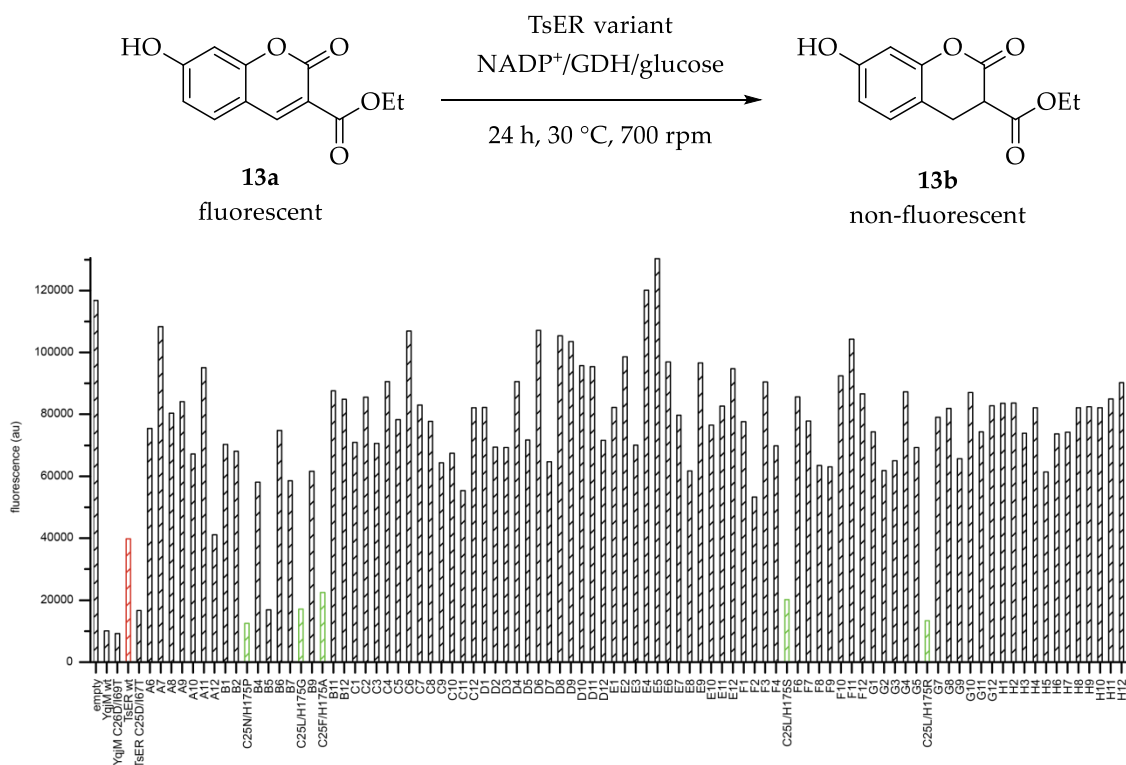


Figure 57. Fluorescence read out of one exemplary screening plate of the *TsER* C25NNK/H175NNK library with **13a**. *TsER* wild type as negative control colored red and *TsER* hit variants are colored green. On each plate five controls were presented: reaction buffer (A1), YqjM wild type (A2), YqjM C26D/I69T (A3), *TsER* wild type (A4) and *TsER* C25D/I67T (A5).

To determine the exact conversion rates of **13a** with the new found variants, lysate reactions with subsequent HPLC screening were performed. The results are shown in Table 12.

Table 12. Hit variants of *TsER* C25NNK/H175NNK library found by fluorometric substrate screening with **13a**. Conversion rates are determined by HPLC.

<i>TsER</i> variant	conversion (%)	<i>TsER</i> variant	conversion (%)
C25D/H175R	15	C25L/H175S	9
C25F/H175A	14	C25L/H175T	13
C25G	8	C25N/H175K	13
C25H/H175stop	15	C25N/H175P	7
C25I/H175L	12	C25N/H175Q	10
C25L/H175G	12	C25R/H175V	14
C25L/H175P	15	C25S/H175A	6
C25L/H175R	11	C25Y/H175W	13

With this generated library it could be shown that H175 is not essential for the catalytic activity of *TsER*, although it is most often described that the triad of

H172, H175 and Y177 participate directly in the catalytic process.^[91,94,175] Nevertheless activity towards **13a** compared to variants in hotspot positions I, II and III (see chapter 3.6.2) drops significantly.

Due to this observation, a combination of variants from chapter 3.6.2 and the position H175 was planned to gain a positive additional effect in activity towards coumarins. By having a closer look at the active site of *TsER* wild type in complex with *p*-hydroxybenzaldehyde, the alanine residue in position 58 lies in close proximity to the bound inhibitor. In the first ISM study of YqjM by BOUGIOUKOU *et al.* this residue was also chosen to improve the activity towards 3-methylcyclohex-2-en-1-one (**17a**). It was supposed that A60 from YqjM presumably pointing to the alpha carbon atom of **17a**.^[67] Double variants in position C26/A60 of YqjM showed conversion rates of up to 60% for **17a**. For that reason the newly generated library includes also this site.

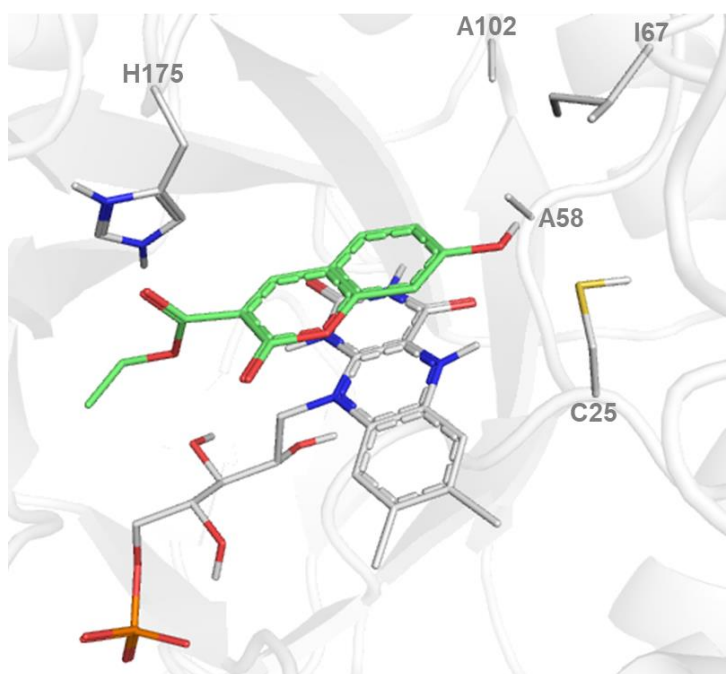


Figure 58. Active site of *TsER* wild type in complex with **13a** (green lines, pdb 3HGJ). Five residues selected for mutation in a second library are shown as grey lines.

3.6.3.2 Library C25/A58/I67/A102/H175

To generate the library with five mutation sites, a mix of six triple variants in position C25/I67/A102 were chosen as template and over a megaprimer PCR the positions A58 and H175 were degenerated with NNK. The six different templates are shown in Table 13.

Table 13. Six templates for the generation of libraries in five positions C25, A58, I67, A102 and H175. These templates are described in chapter 3.3.

template	position in active site		
	C25	I67	A102
1	G	C	I
2	G	T	Y
3	G	C	H
4	G	T	H
5	D	T	H
6	D	C	Y

The quality of the generated six new libraries was checked by performing sequence analyses of pooled plasmids for each library prior to transformation into the expression host (chapter 6.5.1.4). The percentage of incorporated base per position is given in Table 14. The degeneration for position A58 demonstrated poor quality. The four bases A/T/G/C should be equally represented at the first and second template base, as described in chapter 3.6.3.1. In the case of position A58 the template bases are GCC, for the first base an additional C was successfully incorporated, which can only lead to proline or the wild type alanine, instead of all 20 essential amino acids. The attempt to build in a higher degeneracy by changing PCR conditions and additives failed for that specific position. A reason might be the high GC content of 65.9% at this specific position in the *TsER* gene.

For position H175, with the wild type codon CAT, the degeneration looks quite moderate. Reasons for the unequal degeneration of every base are given in chapter 3.6.3.1.

Table 14. Degeneracy of *Ts*ER saturation mutagenesis libraries at position A58 and H175 for six different templates. The percentage of each base was calculated from the sequencing data of the pooled plasmids for each library. The following color code is used: green: C, black: G, red: T, blue: A.

Library	first base	second base	third base	Library	first base	second base	third base
wild type	G	C	C		C	A	T
C25G/I67C/A102I A58_NNK	C	C	G	H175_NNK	G	G	G
C25G/I67T/A102Y A58_NNK	C	C	G	H175_NNK	G	G	G
C25G/I67C/A102H A58_NNK	C	C	G	H175_NNK	G	G	G
C25G/I67T/A102H A58_NNK	C	C	T	H175_NNK	G	G	G
C25D/I67T/A102H A58_NNK	C	C	G	H175_NNK	G	A	G
C25D/I67C/A102Y A58_NNK	G	C	C	H175_NNK	C	A	T

For every new generated library 91 colonies were picked. This results in two degenerated positions, like in the library of C25NNK/H175NNK, with again 1024 possible codons to get a 95% coverage. The 91 colonies cover around 8% of possibilities per library. Due to the poor degeneration of both positions, these first plates should give an indication as to whether it is worth screening more clones from the generated libraries.

To reduce the screening effort a pooling strategy was applied. First of all the six library plates were heterologously expressed separately at 22 °C for 16 h. Afterwards three clones were pooled together, which reduces the number of screening plates from six to just two. The first pool contains clones from plate 1-3 and the second pool clones from plate 4-6. A possible pitfall of this approach

is the low signal to noise ratio of the detected parameter due to the high background; this relates to high amounts of cells without activity, thereby counterfeiting the desired enzyme property.^[67] The two plates were screened with **11a**, **13a**, **15-16a** and analyzed by HPLC. For **11a** and **15a** no hits could be detected, whereas for **13a** and **16a**, several wells with up to full conversion were observed (Figure 59).

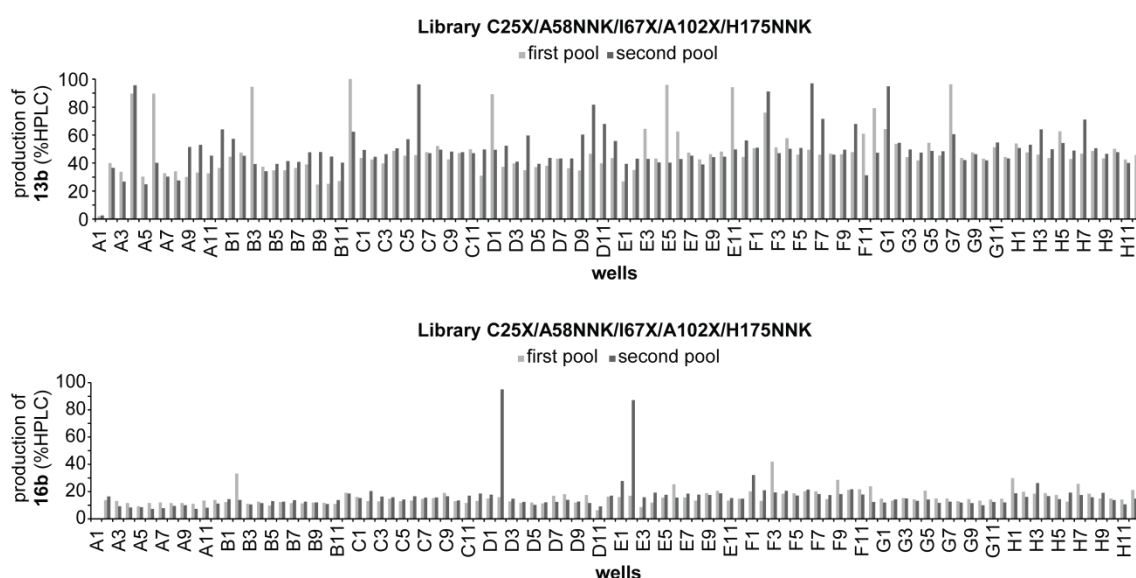


Figure 59. Evaluation of pooling experiment for library C25X/A58NNK/I67X/A102X/H175NNK with the screening substrates **13a** and **16a**. The light grey bars represent the first pool (plate 1-3) and the dark grey bars the second pool (plate 4-6).

To identify the right variant for production of **13b**, the pooled clones from the hit wells need to be screened separately in a second round. In the first pool wells A6, B3, B12, E5, E11 and G7 from plates 1-3 and in the second pool A4, C6, F2, F6 and G1 from plates 4-6 were screened again towards **13a** activity. Results are shown in Figure 60. The well A4 contains the control variant C25D/I67T, which previously showed activity towards **13a** which explains the observed activity in all plates.

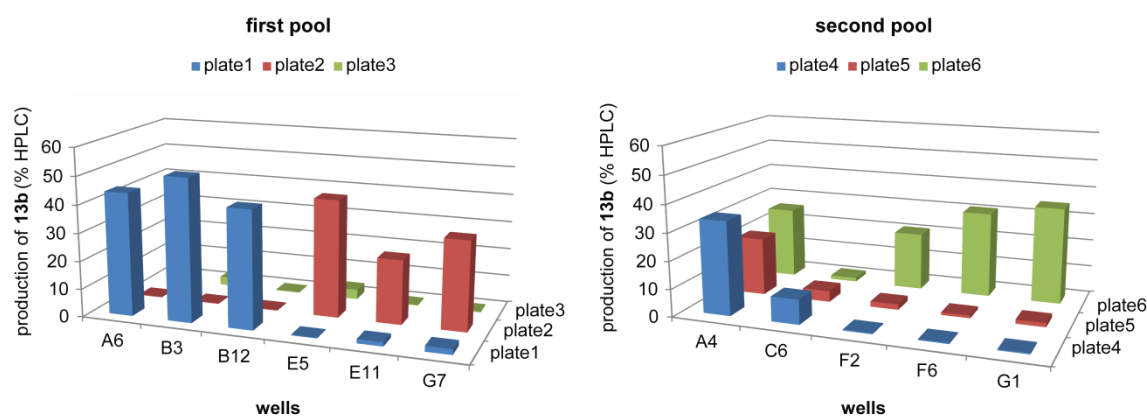


Figure 60. Conversion rates of hit wells from further pooling experiment in separated assays with substrate **13a**.

As a result of the second screening, clones A6, B3 and B12 out of plate 1, E5 out of plate 2, F2, F6 and G1 out of plate 6 were sent for sequencing to identify the active variants.

As can be seen in Figure 59 for **16a** just in the second pool two clones D2 and E2 showed a high activity. Also clone F1 with a moderate activity of 20% was chosen for a second screening. The results of the second screening are illustrated in Figure 61 and show only that the clones D2 from plate 5 and 6 are active towards **16a**. Considering, the identification by sequencing of these two variants.

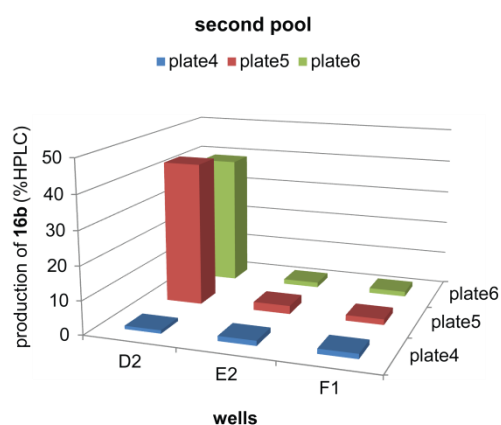


Figure 61. Conversion rates of hit wells from further pooling experiment in separated assays with substrate **16a**.

The sequence identification of the nine selected hits is given in Table 15. Unfortunately no quadruple or quintuple variant was determined, which reflects the quite poor degeneration of positions A58 and H175 observed in the quick quality control (see Table 14).

Table 15. Sequencing results of identified hits from screening with library C25X/A58NNK/I67X/A102X/H175NNK. The first number in the sample column stands for the plate and the letter and number for the well.

sample	amino acid position				
	C25	A58	I67	A102	H175
wt					
1_A6	G	A	C	I	H
1_B3	G	A	C	I	H
1_B12	G	A	C	I	H
2_E5	G	A	T	Y	H
8_F2	G	A	T	H	H
8_F6	G	A	T	H	H
8_G1	G	A	T	H	H
6_D2		sequencing failed			
8_D2		sequencing failed			

Based on this result it was deemed unnecessary to screen more clones of these libraries. In future work it would be potentially advantageous to identify a new PCR strategy to incorporate sufficient degeneration at GC rich sequences. One method might be the recently invented QickLib procedure.^[320] The reaction is very similar to a QuikChange protocol, but with asymmetric primer pairs, which leads to exponential amplification rather than a simple replication. It starts with a full plasmid PCR amplification using a long partially degenerate primer and a short non-degenerate primer sharing complementary 5' ends. After the PCR, a Gibson reaction circularizes the library of linear plasmids. Furthermore, the original matrix is eliminated by restriction with DpnI.^[320]

4 CONCLUSION

4.1 Development of the ‘Scaffold Sampling’ Strategy for Ene Reductases

The relatively broad specificity of OYE family members and the possible expansion of reactivity and control over facial selectivity through combined engineering and screening methods, presents a real opportunity to develop a new set of ene reductases with high synthetic value for industrial biocatalysis for the reduction of carbon-carbon double bonds. The hope is that such efforts will generate new and established processes by satisfying the demand for new catalysts while simultaneously reducing the environmental impact of industrial chemicals’ manufacture.

First, in the thesis presented here a protein engineering strategy was developed to rapidly access improved OYE variants with minimal screening effort. This strategy is termed ‘scaffold sampling’ and together with DUNN *et al.*^[137] and GOBER *et al.*^[138] has proven its usefulness for protein engineering. It has been shown that scaffold sampling by transfer of engineered residues into wild types is an extremely valuable protein engineering strategy with high success rates, allowing quick access to improved biocatalysts. It is related to approaches which use naturally occurring sequence diversity, but these engineering techniques have a lower success rate with non-natural substrates.

To summarise the first section of this thesis, two sets of hotspot positions, obtained previously via directed evolution^[67], were successfully transferred to seven different OYE scaffolds from group 1 and group 2. The activity enhancing C25D/I67T combination transferred its traits only within group 2 and was

found to be unfavourable for group 1 scaffolds (Figure 62). The transfer of selectivity controlling hotspot positions was successful irrespective of the subclass. This demonstrates that hotspot positions and not the OYE scaffolds determine if the normal or flipped binding mode for **17-19a** is preferred, therefore leading to the same stereoselectivity irrespective of the scaffold. To rationalise the sometimes poor activity or selectivity it should be mentioned that an engineering process is always designed for one specific property. That means no universal enzyme/catalyst exists, because otherwise it will lose the selectivity.

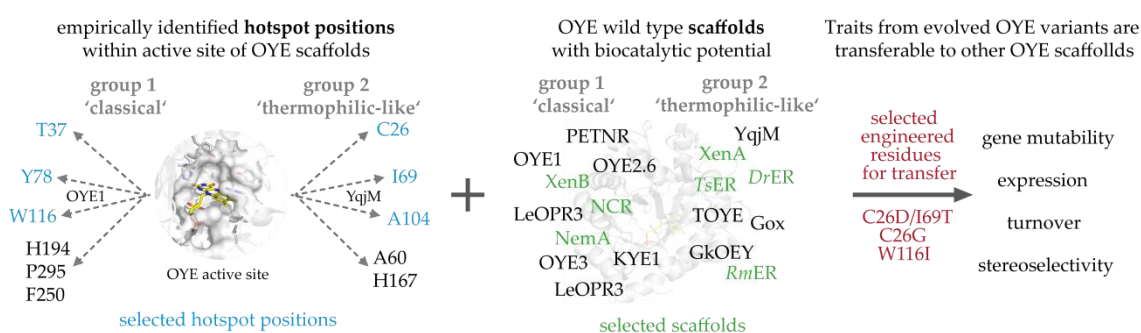


Figure 62. Conceptual overview of protein engineering strategy applied in this thesis. Choosing engineered residues (red) identified in directed evolution and protein engineering studies in hotspot positions (blue) and transferring them to OYE scaffolds (green).^[195]

Applied to ene reductases from the OYE family, the newly created variants were tested with three compounds **17a-19a** revealing more stereocomplementary OYE pairs with potent turnover frequencies (up to 660 h⁻¹) and excellent stereoselectivities (up to >99%) (Figure 63). It remains to be seen if the other recently identified stereocontrolling hotspots^[147] and engineered residues^[160,181] will be equally transferable among the OYE scaffolds, but the presented results allude towards it.

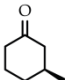
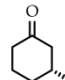
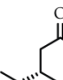

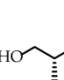


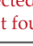
	 (S)-17b	 (R)-17b	 (2R,5S)-18b	 (2S,5S)-18b	 (R)-19b	 (S)-19b
ene-reductase old yellow enzyme						
Group 1	+ NCR T25G	 NCR T25D/W66T	+ NCR T25G NCR W100I	? expected but not found	no conversion	+ NCR W100I
Group 2	+ TsER C25G DrER C40G	+ TsER C25D/I67T DrER C40D/I81T	+ TsER C25G TsER C25D/I67T	 TsER C25G/I67T	+ TsER C25G/I67T	+ TsER C25D/I67T

Figure 63. Shortcuts in enzyme engineering: Transfer of engineered residues in seven ene reductase wild type scaffolds revealed additional stereocomplementary pairs, respectively C25D and C25G (*TsER* numbering) and provided a fast engineering method for OYEs.

Protein engineers can start to use knowledge obtained previously by protein engineering and directed evolution studies systematically, thereby avoiding wasting of resources when creating new and improved biocatalysts.

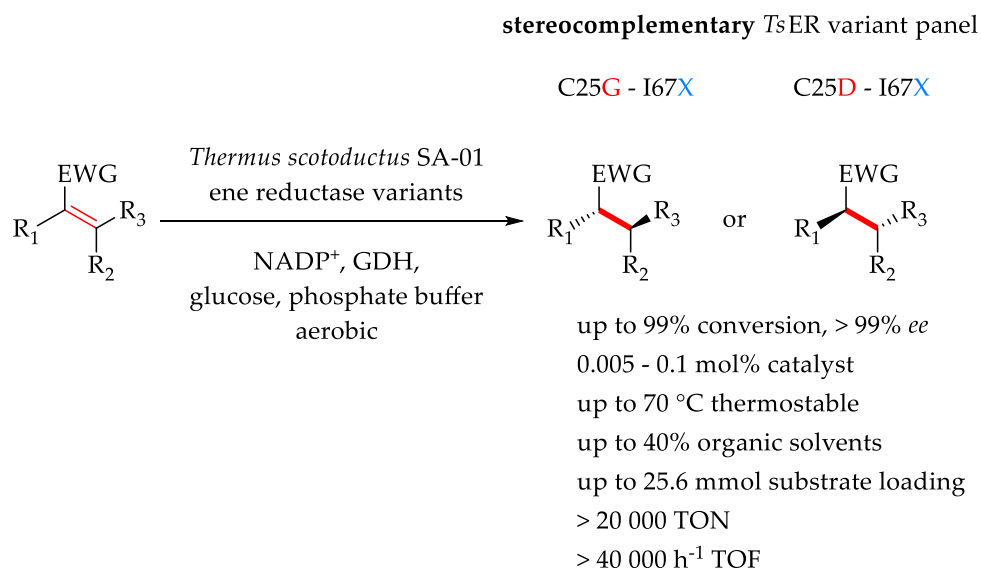
Importantly, all *TsER* variants in this study maintained their thermostability, creating a set of thermostable, solvent tolerant, active and stereoselective biocatalysts of high potency for organic synthesis.

4.2 Full Characterisation of a Highly Active, Robust and Stereocomplementary *TsER* Variant Panel

In the second section of this thesis the created panel of *TsER* variants for *trans*-specific hydrogenation was characterised to access its potential in organic synthesis. These variants incorporate mutations in positions C25, I67 and A102. The broad stereocomplementarity of the panel, especially of double variants in position C25G/I67X and C25D/I67X, is unprecedented and the variants mainly show excellent enantioselectivities. Out of the 38 screened substances, 24 were converted and 10 showed a stereoselective switch depending on the used variant. The control over facial selectivity for such an amount of different substrates with the same catalyst system is quite impressive, because excellent stereoselectivities for both isomers are only accessible for a handful of substrates.^[73,128,129] For one substrate **26a** a kinetic resolution was obtained, which needs further investigation to characterize the obtained product.

The reaction system, consisting of two engineered enzymes *BsGDH* and *TsER*,^[59,195] is convenient to prepare and handle and shows TOF of up to 40 000 h⁻¹, which are comparable to hydrogenation rates by heterogeneous and homogeneous transition metal catalysis.^[262,321] The observed tolerance of organic solvents allows working at high substrate concentrations and simplifies product recovery. Although working at higher temperatures is possible, it bears the risk of product racemization and increases the lability of the nicotinamide cofactors.

Moreover the successful biotransformations at preparative scale (3.8 g) estimate the *TsER* variant panel as an interesting catalyst class for industrial applications.



Scheme 22. Robust panel of ene reductase variants from *TsER* with a summary of the best catalytic values obtained in this thesis.

In summary, by coupling high enzyme activity, robustness and stereocomplementarity, the *TsER* panel provides a solid base to further exploit ene reductases as a tool in preparative organic synthesis, especially for cascade and chemo-enzymatic one-pot reactions.^[256,322,323]

4.3 Prediction of Substrate Binding and Affinity by *In-Silico* Studies

As part of this thesis, prediction of substrate binding and affinity towards the *TsER* variant panel was investigated by *in-silico* studies. The RBD results of compounds **17-19a**, **22a** and **24-43a** highlight the challenge to reliably predict experimentally observed facial selectivity for ene reductases. While only subtle differences in size and polarity were found to govern the preferred substrate, binding poses and consistently distinguish between substrates and non-substrates in all 38 cases, and the predicting power for the facial selectivity was found to be moderate. Conversely, non-substrates were less correctly predicted

with non-productive poses. Whereas the wt docking correctly identified 67% of non-substrates, the two variants predicted just 37% of molecules as non-substrates. Often, bad contacts between atoms with a cut-off ratio less than 0.89 Å are observed in those cases where a hydride attack angle and distance would define the pose as potentially productive. Caution is needed when interpreting docking results, since most non-substrate poses appear productive by visual inspection, but the hydride transfer angle is incorrect or the distance for hydride attack too large, preventing reduction.

Flexibility is an intrinsic feature of proteins playing an essential role in protein-ligand binding, even a different orientation of a single side chain in the active site will significantly influence the docking results, and indeed, flexible docking with IFD yielded better angles and distances for hydride transfer to **17a**, nevertheless, IFD is currently too demanding for *in silico* compound library screening.

The molecular dynamics simulations of the *TsER* variants have proven to be challenging. Just with the model substrate **17a** and the *TsER* wt structure stable MD simulations could be obtained, whereas with the variants C25D/I67T and C25G/I67T **17a** left the active site within several ns. Constant pH MD simulations for C25D/I67T indicated different protonation states of H172, H175 and D25, which are important for the catalytic activity. To achieve stable molecular dynamics structures for C25D/I67T all of these protonation states have to be considered. This would be a highly computational intensive calculation which needs further investigation.

An answer to the question why the conversion of ketoisophorone (**22a**) by most OYEs is possible, whereas isophorone (**44a**) is not reacted could be found. Comparison of the dominant structures from MD simulations of both **22a** and **44a** gives an explanation of the experimental results. **22a** is consistently in a reactive conformation, allowing quantitative conversion by *TsER* wt, whereas **44a** cannot adopt a reactive conformation and is not converted at all.

4.4 Successful Biotransformations of Indole and Coumarin Derivatives by *TsER* variants

In the third section the substrate scope of the engineered *TsER* variant panel was enlarged to bulkier substrates, especially one indole derivative and a set of coumarin-like structures. The successful biotransformation with ene reductases from the OYE family was firstly shown for these compounds. Especially the triple variants in positions C25, I67 and A102 showed moderate activity rates towards **12a-16a**. Further investigations in targeting new mutation sides, like A58 and H175 in the binding site of *TsER* proved to be challenging. Position A58 could not be degenerated and also variants of position H175 did not shown higher conversion rates towards **13a**, than the previously tested triple variants. Nevertheless the mutation of H175 still leads to active variants, which disproves the necessity of this residue for the catalytic activity of OYEs.

It seems that remodeling of the active site with more polar residues, leads to optimal interactions for the functionalized coumarin **13a**. In most of the docking poses the 7-hydroxygroup interacts with D25 and I67 through hydrogen bonding. In the A102H variant a further interaction over pi-pi stacking with the phenol group is presented. In the less polar C25G/I67T variant, the residue D71 inherit the hydrogen bond of the hydroxyl group, whereby **13a** is still oriented in a productive position for hydride transfer (3.2 Å, 108.1°).

Due to *in silico* studies evidences for acid-base catalysis within the active site of ene reductases was found. The presumed mechanisms for the lactone hydrolysis of **13a** by *TsER* C25D/I67T can perhaps be proven by real-time NMR studies in comparison with the biocatalytic reaction of C25D/I67T/A102H. To explore the exact catalytic mechanism of lactone hydrolysis, molecular dynamics (MD) simulations along with combined quantum mechanics and molecular mechanics (QM/MM) studies should be applied.^[324,325]

The reported results pave the way for future applications of ene reductases, especially the variants of the thermostable family member *TsER*, in industrially relevant organic synthesis.

5 OUTLOOK

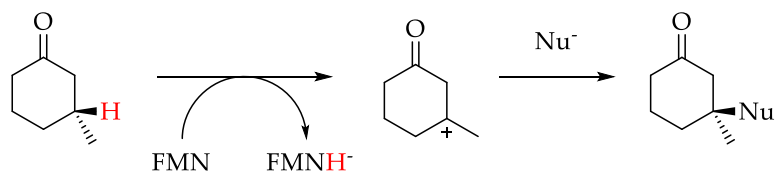
5.1 Broadening the 'Scaffold Sampling' Method of Ene Reductases

As part of this thesis the 'scaffold sampling' method for the OYE family was successfully developed, to generate stereocomplementary catalyst pairs for the *trans*-specific hydrogenation of α,β -unsaturated compounds. Within following studies the scaffold scope should be extended to confirm the tolerance of the method. Especially OYE family members of group1, which are proven to tolerate mutagenesis in the selected gene positions, should be examined. The HOEBENREICH group recently gained access to the plasmids of OYE2 and OYE3 from *Saccharomyces cerevisiae*^[90,326], as well as Gox from *Gluconobacter oxydans*.^[327] OYE2 and OYE3 are 91 and 81% identical to the well-studied OYE1 from *Saccharomyces cerevisiae* which showed control over facial selectivity by mutating hotspot position III (residue W116).^[91,105,147,160] The Gox enzyme has been rarely used in synthesis so far.^[327,328] In the presented thesis data for group 2 combinations of hotspot positions I+II+II were created, but a dataset for hotspot position I in context with the other two positions for group 1 members is currently missing.^[195] This incompleteness can be resolved by a study with OYE2, OYE3 and Gox.

5.2 Investigations in Diverse Chemical Reactions of OYEs

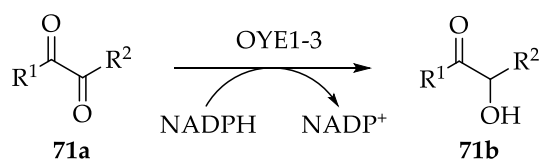
The additional observed dehydrogenation reaction by the ER panel can perhaps be used for further reactions. As mentioned in chapter 3.2, in the absence of the

cofactor NADPH the provided substrate gets oxidized to the α,β -unsaturated ketone or further to the aromatic system by OYEs. In theory it might be possible to react the carbo-cation intermediate with a provided nucleophile (Scheme 23). This would generate a totally new product scope for OYEs.



Scheme 23. Possible follow up reaction of the dehydrogenation by OYEs to incorporate nucleophiles in a stereoselective fashion.

Recently VAN BERGEN *et al.* discovered the reduction of vicinal diketones (VDKs) by OYE1-3 from *Saccharomyces cerevisiae* (Figure 64).^[329] VDKs are by-products of amino acid synthesis and glycolysis in cells.^[330,331] This causes problems in the fermentation industry, since the production of diacetyl negatively affects the properties of beverages, such as beer, by contributing an undesirable butter-scotch-like aroma and flavour.^[332] It would be interesting, if group 2 members of the OYE family also have ketoreductase activity, as assumed in chapter 3.2, Scheme 9.



possible 1,2-diketone substrates for OYE panel in *Hoebenreich* group

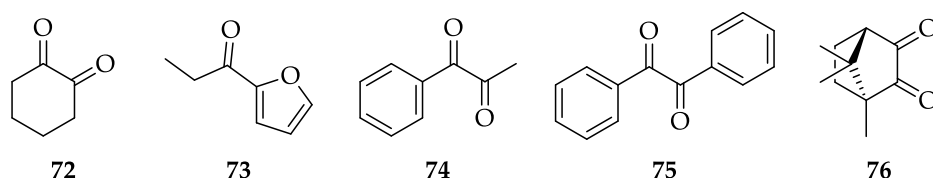


Figure 64. OYEs from *Saccharomyces cerevisiae* as enzymes capable of catalysing vicinal diketone reduction reported by VAN BERGEN *et al.*^[329] and a list of possible 1,2-diketone substrate for screening the OYE panel existing in the HOEBENREICH group.

5.3 Further Mechanistic Examinations by *In-Silico* Studies

Within the scope of this thesis, predictions of substrate binding and affinity, especially for the model compound 3-methyl cyclohexenone (**17a**), by molecular docking and MD simulations were examined. To obtain stable MD simulations further investigation is required, stable MD simulations of the substrates in OYE, would allow the use of the WaterSwap method for predicting binding free energies of substrates. This would be the first implementation of this method for a biocatalytic process. Using WaterSwap as an *in-silico* pre-screening for substrate libraries in OYEs would be a substantial breakthrough, since the experimental determination of binding free energies is a very complex task.^[95,283]

Chapter 3.6.2 described the possible acid-base catalysed hydrolysis of 7-hydroxy-3-carboxycoumarinethylester (**13a**), which needs further investigation. Hybrid quantum mechanics/molecular mechanics (QM/MM) umbrella sampling MD calculations might be used to investigate the mechanism of hydrolysis, in a similar manner to that shown for carbapenem hydrolysis in class A β -lactamases.^[333]

With these methods, details such as those concerning stable binding of the substrate to the active site, the order of the reaction steps, and the nature of transition states to hydride and proton transfer, as well as the role of water in the catalytic reaction and lactone hydrolysis, can be addressed.

6 MATERIAL AND METHODS

6.1 Syntheses of Compounds

6.1.1 Foreword to Compound Synthesis and Analytical Methods

General Annotations for Reagents and Working Methods

If not especially announced all reactions were done under atmospheric conditions. If reactions were done under inert gas, the SCHLENK-technique or septum and syringes were used. The denoted yields refer to products which were dried in high vacuum atmosphere. The chemicals that were bought from ACROS, ALFA AESAR, FLUKA, SIGMA ALDRICH and FLUROCHEM were used without further purification

Annotations for Analytic Methods

Column Chromatography

The purification of raw products with column chromatography was done at room temperature and with a continued nitrogen flow. As stationary phase silica gel 60 (grading 0.04 - 0.063 mm) from MERCK was used. The eluents are given in the current experimental procedure.

Thin Layer Chromatography (TLC)

The TLCs were done on TLC silica gel F₂₅₄ plates from MERCK. The detection was done with a UV-lamp ($\lambda = 254 \text{ nm}$ or 365 nm) or with a Permanganate-dip.

Nuclear Magnetic Resonance Spectroscopy

All NMR spectra were measured at a BRUKER ADVANCE 300 system (^1H -NMR resonance: 300 MHz, ^{13}C -NMR resonance: 75 MHz). The 2D spectra were measured at a (^1H -NMR resonance: 500 MHz, ^{13}C -NMR resonance: 126 MHz). The analysis of spectra was done with MESTRENOVA. The spectra were calibrated on the solvent proton signal. The chemical shifts of the solvents were used as an internal standard.^[334]

DMSO- d_6 : ^1H : $\delta = 2.50$ ppm, ^{13}C : $\delta = 39.52$ ppm

CDCl_3 : ^1H : $\delta = 7.26$ ppm, ^{13}C : $\delta = 77.16$ ppm

The multiplicities from the spectra are denoted as followed: s = singlet, m = multiplet, d = duplet, dd = double duplet, dt = doublet of a triplet, t = triplet, q = quartet. Protons, which might not be identified, were only stated with the shift and the coupling constant. The given coupling constants were calculated by the program MESTRENOVA.

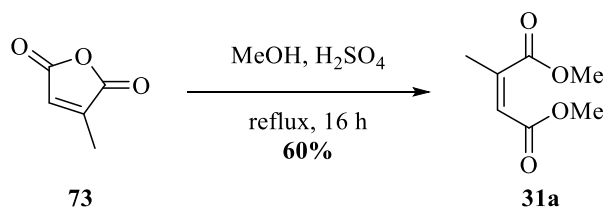
Mass Spectrometry

The mass analytic of compounds and enzymes were performed by member of the service department of the PHILIPPS-UNIVERSITÄT MARBURG. The masses are given in units of m/z. HR-ESI and HR-APCI mass spectra were acquired with a LTQ-FT Ultra mass spectrometer (THERMO FISCHER SCIENTIFIC). The resolution was set to 100.000. HR-EI mass spectra were acquired with an AccuTOF GCv 4G (JEOL) Time of Flight (TOF) mass spectrometer. An internal or external standard was used for drift time correction.

Photometer

The measurements of absorption and fluorescence spectra were done with a *Plate-Reader-Spectra Max M5* from MOLECULAR DEVICES LTD equipped with the program SOFTMAX PRO 5.2. The evaluation of the spectra was done with the program ORIGIN8.

6.1.2 Synthesis of 2-Butenoic acid

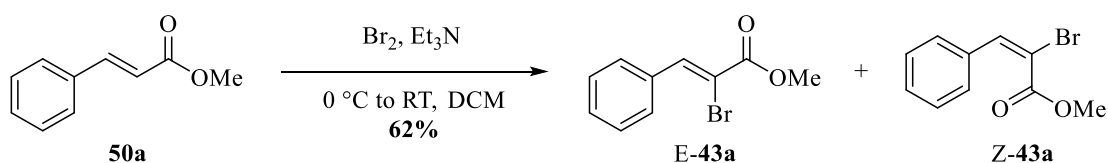


Reflux a solution of citraconic anhydride (**73**, 1 mL, 8.92 mmol, 1.00 eq) in MeOH (10 mL, 0.312 mol, 35 eq) and H₂SO₄ (0.125 mL, 1.27 mmol, 0.14 eq) under nitrogen for 16 h. After evaporation of the MeOH under vacuum, the leftover was diluted in water and extracted two times with EtOAc, washed with brine; the organic phase was dried over Na₂SO₄ and evaporated under vacuum. The pure *Z*-**31a** could be obtained in 70% yield (988 mg, 6.24 mmol).^[335]

¹H-NMR: (300 MHz, CDCl₃); δ = 5.86 (q, ⁴J = 1.6 Hz, 1H, CH), 3.83 (s, 3H, OCH₃), 3.73 (s, 3H, OCH₃), 2.06 (d, ²J = 1.6 Hz, 3H, CH₃) ppm.

¹³C-NMR: (300 MHz, CDCl₃); δ = 169.5, 165.5, 145.8, 120.8, 52.5, 52.0, 20.6 ppm.

6.1.3 Synthesis of Methyl (E/Z)-2-bromo-3-phenylacrylate



Methyl cinnamate (**50a**, 2.67 g, 18.3 mmol, 1.00 eq) was solved in 30 mL DCM at 0 °C. Br₂ (0.930 mL, 18.3 mmol, 2.93 g, 1.00 eq) was added until the solution turned slightly red. After stirring for 3 h at 0 °C, Et₃N (10.8 mL, 107 mmol, 5.85 eq) was added and a color change from red to brown occurred. The solution was stirred overnight at room temperature. The solution was quenched with 45 mL saturated NH₄Cl solution, extracted with DCM and the combined organic layers were dried over MgSO₄ and evaporated under pressure. After

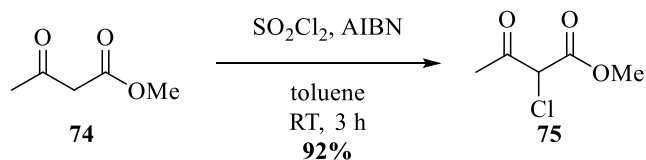
silica column chromatography (*n*-hexane : toluene 1:1) and *Kugelrohr* distillation at 3 mbar and 90 °C the product could be isolated as racemic mixture in a yield of 62% (2.73 g, 11.3 mmol, E/Z 1:1).

¹H-NMR: (300 MHz, CDCl₃); δ = 8.21 (s, 1H, CH), 7.84 (m, 2H, C_{Ar}-H), 7.42-7.30 (m, 8H, C_{Ar}-H), 3.89 (s, 3H, CH₃), 3.74 (s, 3H, CH₃) ppm.

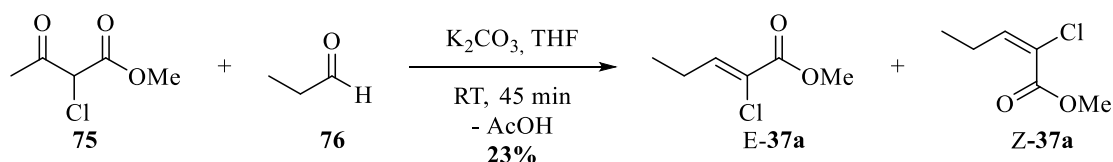
¹³C-NMR: (300 MHz, CDCl₃); δ = 164.9 (E), 163.9 (Z), 141.2 (Z), 140.1 (E), 134.8 (E), 133.8 (Z), 130.4 (Z), 130.3 (Z), 129.1 (E), 128.5 (E), 128.5 (Z), 128.2 (E), 112.6 (Z), 111.1 (E), 53.6 (Z), 53.0 (E) ppm.

HR-MS (ESI+) [C₁₀H₉BrO₂ + Na⁺] m/z = cal.: 262.9678 found: 262.9679.

6.1.4 Synthesis of Methyl (E/Z)-2-chloropent-2-enoate



In the first step sulfuryl chloride (900 g, 55.0 mmol, 5.39 mL, 1.10 eq) and catalytic amounts of AIBN were added to a solution of methyl acetoacetate (**74**, 6.00 g, 50.0 mmol, 5.66 mL, 1.00 eq) in toluene and stirred for 3 h at rt. The solution was evaporated in vacuum and purified by column chromatography (EtOAc : *n*-hexane 2:3). Methyl 2-chloro-3-oxobutanoate (**75**) was received as colorless oil in a yield of 92 % (6.95 g, 46.1 mmol).



Next, K_2CO_3 (5.51 g, 39.8 mmol, 1.50 eq) was added to a solution of propanal (76, 1.85 g, 31.9 mmol, 2.28 mL, 1.20 eq) with methyl 2-chloro-3-oxobutanoate (75, 4.00 g, 26.6 mmol, 3.24 mL, 1.00 eq) in dry THF. After 45 minutes the suspension turned orange. The mixture was quenched with 40 mL H_2O , extracted three times with 60 mL EtOAc and washed with 40 mL saturated $NaHCO_3$ solution. The organic phase was dried over $MgSO_4$ and evaporated in vacuum. The crude product was purified by column chromatography (*n*-hexane : EtOAc 32:1). The product was obtained as racemic mixture in a yield of 23 % (0.924 g, 6.22 mmol, E/Z 1:4).

Analytic methyl 2-chloro-3-oxobutanoate (75):

1H -NMR: (300 MHz, $CDCl_3$); δ = 4.76 (s, 1H, CH), 3.91 (s, 1H, OH), 3.83 (s, 3H, CH_3), 2.48 (s, 1H, OH), 2.37 (s, 3H, CH_3) ppm.

HR-MS (ESI+) [$C_5H_7ClO_3 + Na^+$] m/z = cal.: 172.9976 found: 172.9974.

Analytic second step (final product 37a):

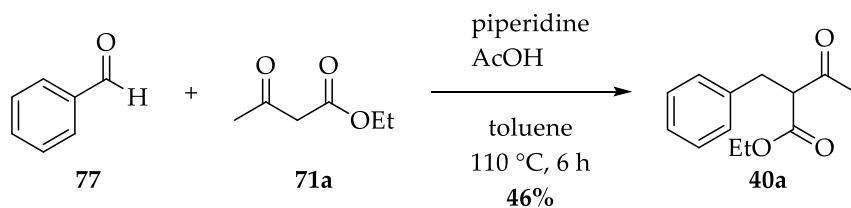
TLC: R_f (E) = 0.57 (*n*-hexane : EtOAc 32:1).

R_f (Z) = 0.49 (*n*-hexane : EtOAc 32:1).

1H -NMR: (300 MHz, $CDCl_3$); δ = 7.06 (t, 1H, 3J = 7.3 Hz, CH), 6.44 (t, 1H, 3J = 7.8 Hz, CH), 2.61-2.50 (m, 2H, CH_2), 2.36 (p, 2H, 3J = 7.5 Hz, CH_2), 1.12-1.02 (m, 6H, 2x CH_3) ppm.

^{13}C -NMR: (75 MHz, $CDCl_3$); δ = 163.1, 143.9, 123.7, 53.2, 52.9, 22.8, 12.0 ppm.

6.1.5 Synthesis of Ethyl-2-benzylideneacetoacetate



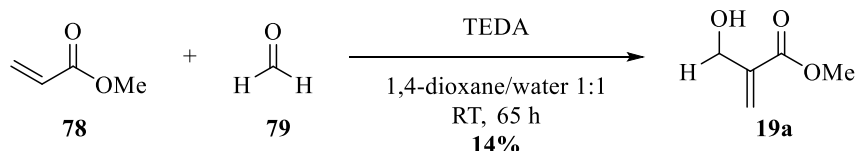
Ethyl acetoacetate (**71a**, 704 μL , 5.50 mmol, 1.1 eq) was stirred in 3 mL toluene and acetic acid (190 μL , 3.30 mmol, 0.6 eq). Piperidine (50.0 μL , 550 μmol , 0.11 eq) and benzaldehyde (**77**, 1.30 mL, 5.00 mmol, 1.0 eq) was added and the reaction mixture was stirred at 110 °C for 6 h followed by TLC control (DCM : MeOH 100:1). Upon completion, the reaction was quenched by adding 10 mL NaOH solution (0.2 M). The aqueous phase was acidified with 1M HCl to pH 4 and extracted with EtOAc, washed with brine and the combined organic phases dried over MgSO_4 . The crude product was purified via column chromatography (*n*-pentane : EtOAc 10:1) and **40a** could be obtained in 46% yield (500 mg, 2.20 mmol) as yellow oil.

$^1\text{H-NMR}$: (300 MHz, CDCl_3); δ = 7.57 (s, 1H, CHO), 7.47-7.38 (m, 5H, CAr-H), 4.33 (q, ^3J = 7.0 Hz, 2H, CH_2), 2.42 (s, 3H, CH_3), 1.27 (t, ^3J = 7.0 Hz, 3H, CH_3) ppm.

$^{13}\text{C-NMR}$: (75 MHz, CDCl_3); δ = 194.7, 167.9, 141.4, 134.8, 133.2, 130.8, 129.8, 129.7, 129.0, 61.9, 26.7, 14.0 ppm.

HR-MS (APCI+) [$\text{C}_{13}\text{H}_{14}\text{O}_3 + \text{H}^+$] m/z =cal.: 218.0943, found: 219.1017.

6.1.6 Synthesis of Methyl-2-(hydroxymethyl)acrylate

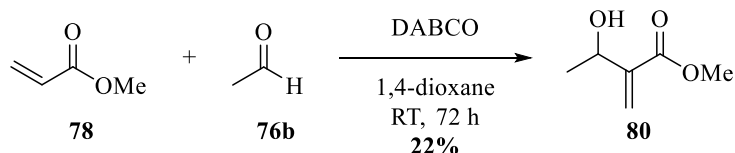


A suspension of paraformaldehyde (**79**, 1.03 g, 34.4 mmol, 1.00 eq), methyl acrylate (**78**, 9.36 mL, 103 mmol, 3.00 eq) and triethylenediamine (3.86 g, 34.4 mmol, 1.00 eq) in 1,4-dioxane/water (1:1, 344 mL) was stirred for 65 h at room temperature. The colorless solution was extracted with methyl *tert*-butyl ether (7 times 150 mL), washed with brine and the combined organic phases were dried over MgSO₄. The raw product was purified by column chromatography (*n*-pentane : EtOAc 3:1), and methyl 2-hydroxymethyl acrylate (**19a**, 547 mg, 4.71 mmol, 14%) was isolated as colorless liquid.

¹H-NMR: (300 MHz, DMSO-d₆); δ = 6.12 (pq, 1H, ²J = 3.5 Hz, ⁴J = 1.7 Hz, H1_{cis}), 5.84 (pq, 1H, ²J = 3.8 Hz, ⁴J = 1.9 Hz, H1_{trans}), 5.08 (t, 1H, ³J = 5.5 Hz, OH), 4.12 (dt, 2H, ³J = 5.5 Hz, ⁴J = 1.8 Hz, CH), 3.68 (s, 3H, CH₃) ppm.

¹³C-NMR: (75.5 MHz, DMSO-d₆); δ = 165.9, 140.7, 123.4, 59.5, 51.5 ppm.

6.1.7 Synthesis of Methyl 3-hydroxy-2-methylenebutanoate



A suspension of acetaldehyde (**76b**, 1.00 g, 17.2 mmol, 1.0 eq), methyl acrylate (**78**, 7.00 g, 81.3 mmol, 5.0 eq) and DABCO (2.54 g, 22.6 mmol, 1.3 eq) in 1,4-dioxane/water (1:1, 344 mL) was stirred for 72 h at room temperature. The solution was quenched with water and extracted with dichloromethane (3 x 150 mL), washed with brine and the combined organic phases were dried

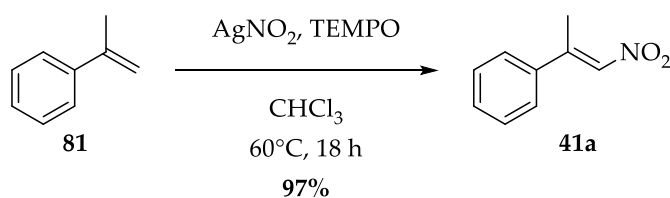
over MgSO_4 . The raw product was purified by column chromatography (*n*-hexane : ethyl acetate 3:1) and 22% methyl 3-hydroxy-2-methylenebutanoate (485 mg, 3.78 mmol) was isolated as colorless liquid.

$^1\text{H-NMR}$: (300.1 MHz, CDCl_3); δ = 6.20 (s, 1H, H1*cis*), 5.81 (m, 1H, H1*trans*), 4.61 (q, 1H, ^3J = 5.5 Hz, CH), 3.74 (s, 3H, OCH_3), 1.36 (d, 3H, ^3J = 5.5 Hz, CH₃) ppm.

$^{13}\text{C-NMR}$: (75.5 MHz, CDCl_3); δ = 124.3, 67.4, 60.6, 52.1, 22.3, 14.4 ppm.

HR-MS (ESI+) [$\text{C}_6\text{H}_{10}\text{O}_3 + \text{Na}^+$] m/z = cal.: 153.0522; found: 153.0521.

6.1.8 Synthesis of (*E*)-(1-Nitroprop-1-en-2-yl)benzene

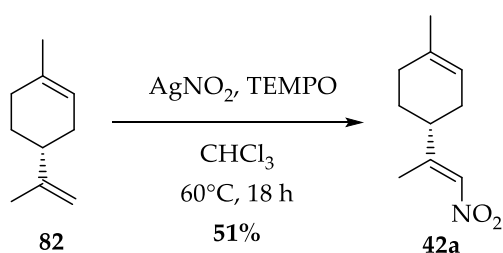


AgNO_2 (1.75 g, 11.4 mmol, 3.0 eq) and TEMPO (240 mg, 1.52 mmol, 0.4 eq) were suspended in 2 mL absolute chloroform with 100 mg activated molecular sieves (4 Å), α -methylstyrol (**81**, 0.5 mL, 3.08 mmol, 1.00 eq) was added and stirred over night at 60°C . The reaction mixture was cooled to room temperature and filtered over celite with EtOAc as eluent and concentrated *in vacuo*. The crude product was purified with a silica column chromatography (*n*-pentane : EtOAc 5:95). The product *E*-**41a** was isolated in 97% yield (600 mg, 3.67 mmol).^[336]

$^1\text{H-NMR}$: (300 MHz, CDCl_3); δ = 2.63 (d, 3H, ^4J = 1.6 Hz, CH₃), 7.28-7.31 (q, 1H, ^4J = 1.4 Hz, CH-NO₂), 7.41-7.45 (m, 5H, C_{Ar}-H) ppm.

$^{13}\text{C-NMR}$: (75 MHz, CDCl_3); δ = 18.9, 127.1, 129.4, 130.7, 136.7, 138.7, 150.1 ppm.

HR-MS (ESI+) [$\text{C}_9\text{H}_9\text{NO}_2 + \text{Na}^+$] m/z = cal.: 186.0526; found 186.0525.

6.1.9 Synthesis of (*R,E*)-1-Methyl-4-(1-nitroprop-1-en-2-yl)cyclohex-1-ene

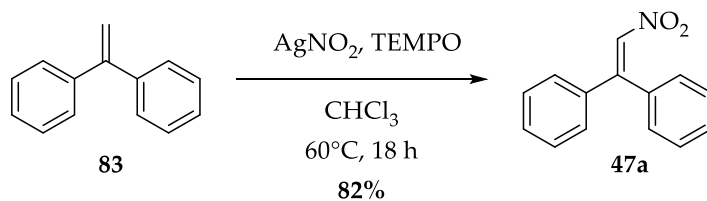
AgNO_2 (1.42 g, 9.24 mmol, 3.0 eq) and TEMPO (192 mg, 1.23 mmol, 0.4 eq) were suspended in 2 mL absolute chloroform with 100 mg activated molecular sieves (4 Å), *R*-(+)-limonene (**82**, 0.5 mL, 3.08 mmol, 1.00 eq) was added and stirred over night at 60°C . The reaction mixture was cooled to room temperature and filtered over celite with EtOAc as eluent and concentrated *in vacuo*. The crude product was purified with a gradient silica column chromatography (*n*-hexane : EtOAc 15:1 to 10:1 to 5:1). The product **42a** was isolated in 51% yield (283 mg, 1.56 mmol, E/Z 3:1).^[336]

$^1\text{H-NMR}$: (300 MHz, CDCl_3); δ = 6.96 - 6.97 (m, 1H, CH), 5.39 - 5.40 (m, 1H, CH), 2.23 (s, 3H, CH_3), 1.78 - 2.22 (m, 7H, $\text{C}_{4,6,7}\text{H}_2$; C_5H), 1.66 (s, 3H, CH_3) ppm.

$^{13}\text{C-NMR}$: (75 MHz, CDCl_3); δ = 156.8, 135.0, 134.1, 119.1, 42.0, 29.8, 26.8, 23.3, 16.9 ppm.

HR-MS (ESI+) [$\text{C}_{10}\text{H}_{15}\text{NO}_2 + \text{Na}^+$] m/z = cal.: 204.0996; found 204.0995.

6.1.10 Synthesis of (2-Nitroethene-1,1-diyl)dibenzene



AgNO₂ (1.00 g, 6.49 mmol, 3.0 eq) and TEMPO (130 mg, 830 μmol, 0.4 eq) were suspended in 2 mL absolute chloroform with 100 mg activated molecular sieves (4 Å) and ethane-1,1-diyl)dibenzene (**83**, 0.4 mL, 2.22 mmol, 1.00 eq) was added and stirred over night at 60 °C. The reaction mixture was cooled to room temperature and filtered over celite with EtOAc as eluent and concentrated *in vacuo*. The crude product was purified with a silica column chromatography (*n*-pentane : EtOAc 20:1). The product **47a** was isolated in 82% yield (410 mg, 1.82 mmol).^[336]

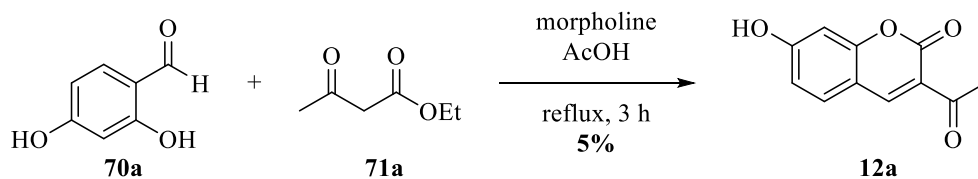
TLC: R_f = 0.4 (*n*-pentane : EtOAc 20:1).

¹H-NMR: (300 MHz, DMSO-d₆); δ = 7.95 (s, 1H, CH), 7.52-7.42 (m, 6H, C_{Ar}-H), 7.36-7.33 (m, 2H, C_{Ar}-H), 7.23-7.20 (m, 2H, C_{Ar}-H) ppm.

¹³C-NMR: (75 MHz, DMSO-d₆); δ = 148.3, 135.6, 130.7, 128.9, 128.8, 128.6, 128.5, 128.3 ppm.

HR-MS (ESI+) [C₁₄H₁₁NO₂ + Na⁺] m/z = cal.: 248.0685; found: 248.0682.

6.1.11 Synthesis of 3-Acetyl-7-hydroxy-2H-chromen-2-one



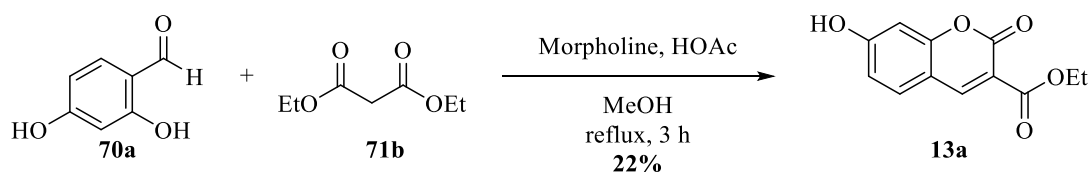
2,4-Dihydroxybenzaldehyde (**70a**, 7.99 g, 57.9 mmol, 1.0 eq) was solved in 43 mL methanol and ethyl acetoacetate (**71a**, 5.72 mL, 57.9 mmol, 1.0 eq) was added. The solution was refluxed and while refluxing morpholine (440 μ L, 5.20 mmol, 0.095 eq) and acetic acid (160 μ L, 2.89 mmol, 0.053 eq) were added. After 3 h reflux, the reaction mixture was cooled down to room temperature and stored over night at 4 °C, which causes a yellowish precipitant. The suspension was filtered and the solid recrystallized out of methanol. The pure product **12a** could be isolated in 5% yield (609 mg, 2.98 mmol).

¹H-NMR: (300 MHz, DMSO- d_6); δ = 11.10 (s, 1H, OH), 8.59 (s, 1H, CH), 7.79 (d, 1H, 3J = 8.6 Hz, CAr-H), 6.85 (dd, 1H, 3J = 8.6 Hz, CAr-H), 6.75 (d, 1H, 4J = 2.2 Hz, CAr-H), 2.54 (s, 3H, CH₃) ppm.

¹³C-NMR: (75 MHz, DMSO- d_6); δ = 194.6, 164.2, 157.2, 174.8, 135.6, 119.2, 114.2, 110.7, 101.7, 48.5, 29.9 ppm.

HR-MS (ESI+) [C₁₁H₈O₄ + Na⁺] m/z = cal.: 227.0315; found: 227.0314.

6.1.12 Synthesis of 3-Carboxycoumarinethylester



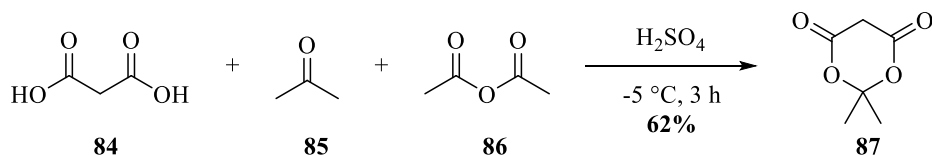
2,4-Dihydroxybenzaldehyde (**70a**, 2.99 g, 21.6 mmol, 1.1 eq) was dissolved in dry methanol, and diethylmalonate (**71b**, 3.15 g, 19.7 mmol, 1.0 eq) was added and heated to boiling. As catalyst mixture morpholine (163 μ L, 1.87 mmol, 0.09 eq) and acetic acid (52 μ L, 0.90 mmol, 0.05 eq) in 1 ml dry methanol was added to the reaction. After 3 h, the reaction mixture was cooled to room temperature and the yellow solid was filtered and washed with methanol. Purification by crystallization from methanol yielded the product **13a** as a colorless solid (1.03 g, 22%).

$^1\text{H-NMR}$: (300 MHz, DMSO- d_6); δ = 8.67 (s, 1H, CAr-H), 7.75 (d, 3J = 8.6 Hz, 1H, CAr-H), 6.84 (dd, $^3,^4J$ = 8.6, 2.3 Hz, 1H, CAr-H), 6.72 (d, 4J = 2.2 Hz, 1H, CAr-H), 4.26 (q, 3J = 7.1 Hz, 2H, CH_2), 1.29 (t, 3J = 7.1 Hz, 3H, CH_3) ppm.

$^{13}\text{C-NMR}$: (75 MHz, DMSO- d_6); δ = 164.0, 162.9, 157.1, 156.4, 132.1, 114.0, 112.1, 110.4, 101.8, 60.8, 48.6, 14.1 ppm.

HR-MS (APCI+) [$\text{C}_{12}\text{H}_{10}\text{O}_5 + \text{Na}^+$] m/z = cal.: 257.0420; found: 257.0420.

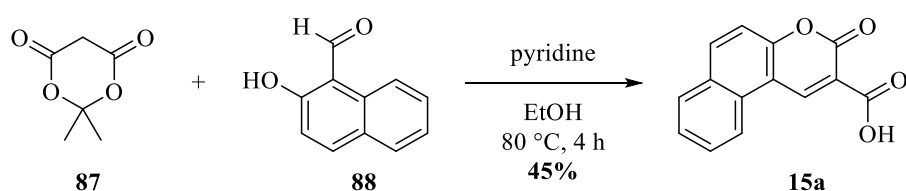
6.1.13 Synthesis of Meldrum's acid



Malonic acid (**84**, 3.46 g, 30.0 mmol, 1.0 eq) was dissolved in acetone (**85**, 2.70 mL, 36.7 mmol, 1.10 eq), acetic anhydride (**86**, 3.95 mL, 43.0 mmol, 1.25 eq) and catalytic amount of sulfuric acid was added. The clear reaction mixture was stirred at -5 °C for 3 h before the reaction was quenched with water. The solvent was removed *in vacuo* and the residue recrystallized out of ethanol. The suspension was filtered and the pure meldrum's acid **87** was obtained as white needles in 62% yield (2.67 g, 18.5 mmol).

¹H-NMR: (300 MHz; acetone-d₆); δ = 3.87 (s, 2H, CH₂), 1.77 (s, 6H, 2CH₃) ppm.

6.1.14 Synthesis of 3-Oxo-3H-benzo[f]chromene-2-carboxylic acid



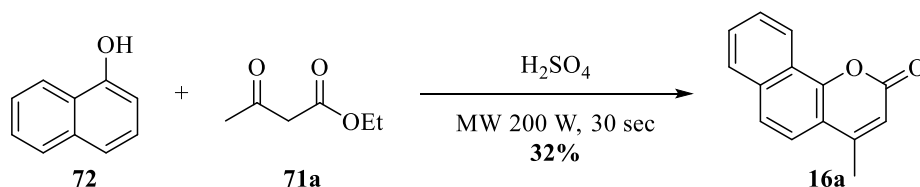
Meldrum's acid (**87**, 210 mg, 1.46 mmol, 1.0 eq), 2-hydroxy-1-naphthaldehyde (**88**, 350 mg, 2.00 mmol, 1.4 eq) and a catalytic amount of pyridine was dissolved in 2.75 mL ethanol and stirred for 4 h at 80 °C. The color was changing and a yellow solid precipitated. The suspension was filtered and the solid dried *in vacuo*. The pure product **15a** was obtained in 45% yield (160 mg, 660 μmol) as yellow solid.

¹H-NMR: (300 MHz; CDCl₃); δ = 12.33 (s, 1H, CO₂H), 9.72 (s, 1H, C=CHC), 8.43 (d, ³J = 9.0 Hz, 1H, CArH), 8.24 (d, ³J = 8.1 Hz, 1H, CArH), 8.00 (d, 1H, ³J = 8.1 Hz, CArH), 7.84 (s, 1H, CArH), 7.70 (s, 1H, CArH), 7.58 (d, ³J = 9.2 Hz, 1H, CArH) ppm.

¹³C-NMR: (75 MHz, CDCl₃); δ = 164.2, 156.8, 155.0, 143.6, 135.8, 129.8, 129.0, 128.9, 128.9, 126.4, 122.3, 117.3, 116.4, 112.0 ppm.

HR-MS (APCI+) (C₁₄H₈O₄ +H⁺) m/z = cal.: 240.0423, found: 241.0449.

6.1.15 Synthesis of 1-Methyl-3H-benzo[f]chromen-3-one



1-Naphthol (**72**, 144 mg, 1.00 mmol, 1.0 eq.) was mixed in a beaker with ethyl acetoacetate (**71a**, 126 mL, 1.00 mmol, 1.0 eq.) and dissolved over sonication. 2 mL sulfuric acid was added, the color changed to dark red. After that the shoot-beaker was put in the microwave for 30 seconds at 200 watt, the color changed to dark brown. The reaction mixture was poured in 50 mL ice water and was centrifuged at 4 °C, for 10 min, at 4000 rpm. A brownish solid was isolated and dried in vacuum. The brownish solid was solved in 50 mL brine and 50 mL DCM and the aqueous layer was extracted three times with DCM. The combined organic layers were dried over MgSO₄. After the solvent was removed *in vacuo* 32% (67.0 mg, 320 μ mol) of the desired product **16a** was obtained as yellow solid.

¹H-NMR: (300 MHz; DMSO-d₆); δ = 8.43-8.34 (m, 1H, CArH), 8.10-8.02 (m, 1H, CArH), 7.85 (dd, 2H, ⁴J = 22.1, ³J = 8.8 Hz, CArH), 7.78-7.68 (m, 2H, CArH), 6.52 (s, 1H, C=CH-C), 2.55 (s, 3H, CH₃) ppm.

¹³C-NMR: (75 MHz, DMSO-d₆); δ = 134.4, 128.6, 127.9, 127.4, 123.9, 121.6, 121.3, 115.1, 113.8, 18.6 ppm.

HR-MS (EI+) [C₁₃H₁₀O₂ + H⁺] m/z = cal.: 210.0681, found: 210.068.

6.2 Microorganisms, Vectors, Primers

Table 16. List of microorganisms used in this study.

strain	source	antibiotic resistance
Dh5 α	in house	TET
BL21 Gold (DE3)	NOVAGEN	TET
BL21 (DE3) Δ nemA	Group MIHOVILOVIC, Vienna	-
GB05-dir	in house	-

Table 17. List of vectors and plasmids used in this study.

vector	source	antibiotic resistance
pET28a(+)	Group ESSEN, Marburg	KAN
pET22	in house	AMP

Table 18. List of primers and their properties. Mutated bases are colored in red. Underlined bases are the targeted mutations.

name	sequence 5' \rightarrow 3'	salt-adjusted T _m (°C) ^(a)	GC (%) ^(a)
T7minus1	AATACGACTCACTATAGGG	48.0	42.1
T7T	CTAGTTATTGCTCAGCGG	50.0	50.0
T ₃ ER_C25D_F	GTCCCCATG <u>GAC</u> CAGTACTCC	61.2	63.6
T ₃ ER_C25G_F	GTCCCCATG <u>GGT</u> CAGTACTCC	61.2	63.6
T ₃ ER_C25W_F	GTCCCCATG <u>TGG</u> CAGTACTCC	61.8	63.6
T ₃ ER_C25N_F	GTCCCCATG <u>AAC</u> CAGTACTCCGC	63.3	62.5
T ₃ ER_I67T_R ^(b)	CATAAGGGCT <u>GGT</u> ACGACCCAAAG	59.5	54.2
T ₃ ER_I67V_R ^(b)	CATAAGGGCT <u>CAC</u> ACGACCCAAAG	60.5	54.2
T ₃ ER_I67C_R ^(b)	CATAAGGGCT <u>GCA</u> ACGACCCAAAG	60.5	54.2
T ₃ ER_A102H_R	CGGCGTG <u>ATG</u> CAGCTGGATCC	63.3	66.7
T ₃ ER_A102W_R	CGGCGTG <u>CCA</u> CAGCTGGATC	63.9	70.0
T ₃ ER_A102Y_R	CCGGCGTG <u>ATA</u> CAGCTGGATCC	62.1	63.6
T ₃ ER_A102I_R	CCGGCGTG <u>AAT</u> CAGCTGGATCC	62.6	63.6
T ₃ ER_HI75A_R	GGAAAGGAGGT <u>AAC</u> TGCTGCCATGTG	63.1	55.6
T ₃ ER_C25MNN_R	GCGGAGTACT <u>MNN</u> CATGGGTGAC	60.3	58.7
T ₃ ER_C25NNK_F	GTCACCCATG <u>NNK</u> CAGTACTCCGC	60.3	58.7
T ₃ ER_C25NDT_QC_F	CCCATG <u>NDT</u> CAGTACTCCGCCACCTTG	64.1	58.6
T ₃ ER_C25AHN_QC_R	GAGTACTG <u>AHN</u> CATGGGGGACATGGCCAG	64.9	58.0
T ₃ ER_A59RTC_F	GAGGCCACCC <u>RTC</u> GTTGAACCTTTGG	63.0	58.0
T ₃ ER_A59GAY_R	CCAAAGGTTCAAC <u>GAY</u> GGTGGCCTC	63.0	58.0
T ₃ ER_A59WGC_F	GAGGCCACCC <u>WGC</u> GTTGAACCTTTGG	64.3	60.0
T ₃ ER_A59GCW_R	CCAAAGGTTCAAC <u>GCW</u> GGTGGCCTC	64.3	60.0
T ₃ ER_A58NNK_F	CTGGTAGAG <u>NNK</u> ACCGCGTGG	62.6	65.9
T ₃ ER_A58MNN_R	CCACGGCGGT <u>MNN</u> CTTACCAG	62.6	65.9
T ₃ ER_HI75RNC_F	CACATGGCA <u>RNC</u> GGTTACCTCCTTTCC	63.1	55.6

<i>Ts</i> ER_HI75GNY_R	GGAAAGGAGGTAACCGNYTGCCATGTG	63.1	55.6
<i>Ts</i> ER_HI75MNN_R	GGAAAGGAGGTAGCCMNNGGCCATGTG	65.5	61.1
<i>Ts</i> ER_HI75NNK_F	CACATGGCCNNKGGCTACCTCCTTCC	65.5	61.1
<i>Rm</i> ER_C25D_F	GCCGATGGATCAGTACTCGGC	63.0	60.0
<i>Rm</i> ER_C25G_F	CGCCGATGGGCCAGTACTCG	63.9	65.2
<i>Rm</i> ER_C25W_F	CGCCGATGTGGCAGTACTCGG	63.6	62.5
<i>Rm</i> ER_I66T_F	GAAGGCCGCACCACGCCGACC	68.2	76.2
<i>Rm</i> ER_I66C_F	GAAGGCCGCAGCACGCCGACC	68.4	76.2
<i>Rm</i> ER_I66V_F	GAAGGCCGCGTGACGCCGACC	68.0	76.2
<i>Rm</i> ER_A59V_R	CAGGCGAAACCACGGTGGCTTCG	65.0	65.2
<i>Rm</i> ER_A59C_R	CAGGCGAAACGCAGGTGGCTTCG	65.2	65.2
<i>Rm</i> ER_A59I_R	CTTCAGGCGAAACGATGGTGGCTTCG	63.7	57.7
<i>Rm</i> ER_A59W_R	CAGGCGAAACCCAAGTGGCTTCG	64.8	65.2
<i>Rm</i> ER_I66T_R	GGTCGGCGTGTGCGGCCCTTC	68.2	76.2
<i>Rm</i> ER_I66C_R	GGTCGGCGTGACGCCCTTC	68.4	76.2
<i>Rm</i> ER_I66V_R	GGTCGGCGTGTGCGGCCCTTC	68.0	76.2
<i>Rm</i> ER_A102W_R	GGCCAGCATGCCAAAGCTGGATGGTC	66.2	61.5
<i>Rm</i> ER_A102Y_R	CGGCCAGCATGATAAAGCTGGATGGTC	63.3	55.6
<i>Rm</i> ER_A102I_R	CGGCCAGCATGAATAAAGCTGGATGGTC	63.3	55.6
<i>Rm</i> ER_A102H_R	GGCCAGCATGATGAAGCTGGATGGTC	63.6	57.7
<i>Ds</i> ER_C40D_F	CTCGCCCATGGACACCTACTCGG	63.3	65.2
<i>Ds</i> ER_C40G_F	CTCGCCCATGGGTACCTACTCGG	63.0	65.2
<i>Ds</i> ER_C40W_F	CTCGCCCATGTGGACCTACTCGG	63.3	65.2
<i>Ds</i> ER_I81V_F	GGGCCGCGTTACCCCCGAGGAC	68.9	77.3
<i>Ds</i> ER_I81C_F	GGGCCGCGTGTACCCCCGAGGAC	68.6	77.3
<i>Ds</i> ER_I81T_R ^(b)	CAGGGGTGGTGCACCCCTC	63.4	73.7
<i>Ds</i> ER_I81V_R ^(b)	CAGGGGTGACGCGACCCCTC	63.3	65.2
<i>Ds</i> ER_I81C_R ^(b)	CAGGGGTGACGCGACCCCTC	63.3	65.2
<i>Ds</i> ER_A116W_R	CCGGCGTGCAGAGCTGCACC	63.3	65.2
<i>Ds</i> ER_A116H_R	CCGGCGTGTGAGAGCTGCACC	63.3	65.2
<i>Ds</i> ER_A116Y_R	CCGGCGTGTGAGAGCTGCACC	63.3	65.2
<i>Ds</i> ER_A116I_R	CCGGCGTGTGAGAGCTGCACC	63.3	65.2
XenA_C25D_R	GTACTGATCCATGGGCGGAATGG	59.8	56.5
XenA_T67_F	GGCGCATCACCCCTGGTTG	62.0	68.4
XenB_T25D_R	GGCAGCGATCGAGTGGGGCCATGATG	67.1	65.4
XenB_Y66T_F ^(b)	ATGGGGGTGGCACCCGGATACC	66.3	64.6
NCR_T25D_R	CACGGTCCAGAGGCCCATCCA	66.1	68.2
NCR_T25G_R	CACGTCCAGAGGCCCATCCA	66.1	68.2
NCR_W66_F	GGAAGGTTTGGGCACACCTTATGCTCCG	66.3	60.7
NCR_W66T_F	GAAGGTTTGGGCACCCCTTATGCTCCG	65.0	55.6
NCR_W66I_F	GAAGGTTTGGGCACACCTTATGCTCCG	63.3	55.6
NCR_W100I_F	GCGGTCCTTATCTTTGCCAGCTAATTCATATG	60.6	43.8
NCR_W100I_R	GCACCATACGTCCCATATGAATAGCTG	59.1	46.4
NemA_T24D_R ^(b)	CAGGCGATCGAGGGGTGCCATG	64.5	68.2
NemA_Y66T_F	CAGGCAAGGGCACCTCTGGCTCG	68.0	70.8

(a) <http://eu.idtdna.com/analyzer/applications/oligoanalyzer/>, Standard Settings: Oligo conc. 0.25 μ M, Na⁺ conc. 50 mM. The used annealing temperature for the PCR reaction was calculated according to $T_a = (\text{highest } T_M \text{ of the primer pair}) - 3 \text{ } ^\circ\text{C}$.

(b) Primer without silent-mutations leads to extremely stable secondary structures and no PCR amplification.

6.3 Media, Buffers and Additives

6.3.1 Nutrition Media

All media were sterilized via steam autoclaving.

LB-Media: 10 g tryptone, 5 g yeast extract and 10 g NaCl in 1 L H₂O.

TB-Media: 12 g tryptone, 24 g yeast extract and 4 mL glycerol in 900 mL H₂O.

10 x TB phosphate: 23.1 g KH₂PO₄ and 156.9 g K₂HPO₄ x 3H₂O in 1 L H₂O.

ZYP-5052 media^[337]: 46.4 mL ZY-Stock, 100 µL MgCl₂ (1M), 1 mL 50 x 5052, 2.5 mL 20 x P.

ZY-Stock: 1 g N-Z amine AS, 500 mg yeast extract, 100 mL H₂O.

50 x 5052: 25 g glycerol, 2.5 g glucose, 10 g α-lactose monohydrate, 73 mL H₂O.

20 x P: 14.2 g Na₂HPO₄, 13.6 g KH₂PO₄, 6.6 g (NH₄)₂SO₄, 90 mL H₂O.

6.3.2 Media Additives

Table 19. List of media additives with used concentrations and origins.

media additive	stock solution	working solution	solvent	origin
Kanamycin (KAN)	50 mg/ml	50 µg/ml	H ₂ O	APPLICHEM
Ampicillin (AMP)	100 mg/ml	100 µg/ml	H ₂ O	APPLICHEM
IPTG	100 mM	10 µM	H ₂ O	APPLICHEM
Tetracyclin (TET)	10 mg/ml	10 µg/ml	EtOH	APPLICHEM

6.3.3 Buffers and Solutions

<i>1M KPi buffer:</i>	160 g $K_2HPO_4 \cdot 3H_2O$ and 40.6 g KH_2PO_4 in 1 L H_2O (pH 7.4, adjusted with 3 M HCl and sterile filtrated), storage at 4 °C.
<i>20 mM MOPS:</i>	4.19 g MOPS and 5.84 g NaCl in 1 L H_2O (pH 7.4 adjusted with NaOH and sterile filtrated), storage at 4 °C.
<i>50 mM MOPS:</i>	5.23 g MOPS, 0.28 g $CaCl_2$ in 1 L H_2O (pH 7.4 adjusted with 5 M KOH and sterile filtered), storage at 4 °C.
<i>Lysis buffer:</i>	100 mM KP_i , pH 7.4 with 1 mg/mL lysozyme.
<i>Dialysis solution:</i>	5 mM EDTA in 100 mM KP_i (pH 7.4).
<i>Buffer A (FPLC):</i>	100 mM KP_i buffer (pH 7.4, adjusted with 3 M HCl and sterile filtration), storage at 4 °C.
<i>Buffer B (FPLC):</i>	100 mM KP_i buffer (pH 7.4), 0.5 M imidazole, 0.5 M NaCl in 1 L H_2O , sterile filtration, and storage at 4 °C.
<i>TAE buffer:</i>	40 mM tris acetate, 1 mM EDTA, pH 8.
<i>10 x SDS-Buffer</i>	10 g SDS, 144 g glycine, 30 g Tris in 1 L H_2O , pH adjusted to 8.3 with HCl.
<i>SDS-PAGE stain</i>	0.25 (w/v) Coomassie Blue R250, 5% (v/v) acetic acid, 50% (v/v) ethanol filled up with H_2O .
<i>4 x SDS-PAGE loading buffer</i>	250 mM Tris-HCl (pH = 6.8), 8% (w/v) SDS, 0.2% (w/v) bromophenol blue, 40% (v/v) glycerol, 20% (v/v) β -mercaptoethanol.

6.4 General Methods

6.4.1 Isolation of Plasmid DNA from *E.coli*

For the plasmid preparation the GenElute HP plasmid miniprep kit from SIGMA-ALDRICH was used. The cells were resuspended by mixing them in 200 μ L re-suspension solution. Afterwards 200 μ L of lysis buffer was added and the mixture was inverted 8 times. The suspension was cleared by leaving it to stay for 5 min and 350 μ L of neutralization and binding buffer was added. The mix was inverted 6 times and centrifuged in an EPPENDORF 5418 centrifuge at 14 000 rpm for 10 min. If the solution was not cleared, the mixture was centrifuged again at 14 000 rpm for 10 min. The column was equilibrated by adding 500 μ L of column preparation solution and centrifugation in an EPPENDORF mini spin plus centrifuge at 14 000 rpm for 1 min. Thereafter the cleared lysate was transferred to the column and centrifuged in an EPPENDORF 5418 centrifuge at 14 000 rpm for 1 min. The flow-through liquid was discarded. The plasmid DNA was washed to remove contaminants by adding wash solution 1 and centrifuging it in an EPPENDORF 5418 centrifuge at 14 000 rpm for 1 min. The flow-through liquid was discarded and the same procedure was done with wash solution 2. After that the DNA sample was centrifuged again in an EPPENDORF 5418 centrifuge at 14 000 rpm for 1 min and left at room temperature for 2 min to remove the excess of ethanol. After the washing and drying the plasmid DNA was eluted by adding 30 μ L of water and centrifugation at 12 000 rpm for 1 min. The purification is checked by measuring concentration and absorption coefficients. A_{260/280} should be about 1.8, A_{260/230} should be about 2.0-2.2. If the values are differing, it may indicate the presence of proteins or phenols, respectively.

6.4.2 Agarose Gel Electrophoresis

Agarose gel electrophoresis is a method to separate DNA fragments depending on their base pair length. DNA reacts as a negative charged particle because of its phosphate backbone. When an electronic field is applied to agarose gel the DNA fragments migrate through it with different speed depending on their base pair length. The migration of the sample through agarose is also a speed defining parameter as well as the applied voltage. Smaller DNA fragments tend to migrate faster than taller ones. A marker with fragments of known base pair length is used to identify the length of the sample. To make the DNA fragments visible, a fluorescent dye is used either together with the DNA sample or in the agarose gel.

For the setup, 1% agarose in TAE buffer has to be prepared and heated up in a microwave until all agarose is solved. After it is cooled to 60 °C, 3 µl/100 ml of midori green dye can be added that interacts with the DNA. Pour the solution into the mould, without generating bubbles. After casting, chill the gel for 15 to 30 min to complete gelation. The DNA samples have to be mixed with 6 x DNA sample buffer (NEB) which consists of glycerol and bromophenol. This will increase the density of the sample so it falls into the well of the gel and provides a visible marker to monitor the progress of electrophoresis. A voltage is applied until the running front is at the end of the gel. The DNA bands can then be monitored with UV-light.

6.4.3 Preparation of Electrocompetent *E. coli*

Electrocompetent *E. coli* were prepared as described early by INOUE *et al.*^[338] Briefly, 5 mL LB preculture *E. coli* BL21 (DE3) Δ nemA without antibiotic were inoculated from a glycerol stock and incubated overnight at 37 °C, 200 rpm (HT INFORS shaker). In the next morning, a 2 L baffled flask with 300 mL LB-Media was inoculated with 3 mL preculture. The flask was incubated in the shaker with 200 rpm, 37 °C. At the point the OD₆₀₀ reached 0.4-0.6, the flask was cooled on ice for 30 min. Then the

cell suspension was transferred into precooled 50 mL reaction tubes and centrifuged at 4000 rpm, 4 °C for 8 min. The supernatant was discarded and the pellets washed and resuspended in several steps, using 45, 25, 2 and 0.5 mL chilled 10% glycerol. After every resuspension step, the cells were pelleted at 4 °C and 4000 rpm for 8 min. Finally, all cells were pooled together, centrifuged and resuspended in 1.7 mL 10% glycerol. The cells were aliquoted in 50 µL, shock frozen in liquid nitrogen and kept frozen at -80 °C until further usage.

6.4.4 Transformation of Electrocompetent *E.coli*

During a transformation, exogenous DNA is taken up through the cell membrane and incorporated in the competent cell. Since *E. coli* does not have natural competence it has to be made competent for DNA uptake. The transformation proceeds through an electromagnetic pulse. Before the pulse, the positive and negative charged particles are allocated counterbalanced. During the pulse an electromagnetic field is established and an electric potential is been induced across the cell membrane which is able to increase the cell permeability and as a consequence the cells are able to take up the exogenous DNA.

The transformation was carried out by adding 1 µL (3 µL) of digested and dialyzed DNA to 25 µL (50 µL) of competent cells on ice. The mixture was transferred to an electroporation cuvette with 2 mm gap and the BIO-RAD micropulser with the settings EC2 was used with typical durations for the electro transformation of 5.8-6.0 ms. Immediately 1 mL of LB-medium was added and the mixture was incubated in an EPPENDORF Thermomixer comfort at 37 °C and 700 rpm for 60 min. Then the cells were centrifuged and resuspended in 100 µl LB-medium. The suspension was plated on LB-Agar-antibiotic plates and the plates were incubated over night at 37 °C. The plates were then kept at 4 °C.

6.5 Old Yellow Enzyme Protocols

6.5.1 Ene Reductases Mutagenesis

6.5.1.1 Megaprimer PCR

The PCR reactions contained 2.5 μL of 10x KOD hot start polymerase buffer, 2.5 μL of dNTPs (stock 2 mM each), 1 μL Mg_2SO_4 (stock 25 mM), 2.5 μL of the appropriate forward and reverse primers (stock 2.5 μM each), the appropriate template (25 ng), 2.5 μL DMSO (stock 100%) and 0.5 μL KOD Hot Start polymerase (stock 1 U/ μL , NOVAGEN) in millipore water in a final volume of 25 μL .

The megaprimer PCR was done as one-pot reaction: First, hot start at 95 °C (3 min), then formation of mega-primer with ten cycles of 95 °C (30 s), T_a in Table 18, (1 min) and 72 °C (30 s and 11.4 min for small and large megaprimer respectively), followed by twenty-five cycles of 95 °C (30 s) and 68 °C (12.5 min) to generate the whole plasmid. PCR reactions finished with 10 min at 72 °C and storage at 4 °C.

6.5.1.2 Quik-Change PCR

In a Quik-Change polymerase chain reaction, according to its specification a polymerase amplifies a circular plasmid with a pair of complementary primers, which are completely overlapping to each other. XIA *et al.* found out, that the use of only partially overlapping primers is advantageous over total complementary primers, which are prone to form quite stable primer dimers that make the annealing difficult. The use of partially overlapping primers should generate linear DNA molecules with short homologous ends, which requires homologous recombination to generate the plasmid with the desired mutations after transformation into *E. coli*.^[339]

For the C25 position this method was used, because it was not successful to degenerate this position with megaprimer PCR.

The PCR reactions contained 5 μL of 10x KOD hot start polymerase buffer, 5 μL of dNTPs (stock 2 mM each), 3 μL Mg_2SO_4 (stock 25 mM), 1.5 μL of the appropriate forward and reverse primers (stock 10 μM each), the appropriate template (10 ng) and 1 μL KOD Hot Start polymerase (stock 1 U/ μL , NOVAGEN) in millipore water in a final volume of 50 μL . The Quik-Change PCR was done with following temperature protocol: First, hot start at 95 $^\circ\text{C}$ (3 min), followed by twenty-five cycles of 95 $^\circ\text{C}$ (25 s), T_a in Table 18 (30 s) and 72 $^\circ\text{C}$ (90 s). PCR reactions finished with 10 min at 72 $^\circ\text{C}$ and storage at 4 $^\circ\text{C}$.

6.5.1.3 *DpnI* Digestion and Desalting

To break down the circular methylated template plasmid, the whole PCR product was digested with 1 μL *DpnI* (20 U/ μL , NEB) at 37 $^\circ\text{C}$ for at least 2 h. Digested samples were dialyzed against millipore water on a nitrocellulose membrane filter from MERCK MILLIPORE with a pore size of 0.05 μm for 30 min and 1 μL was used to transform with electrocompetent *E. coli* BL21 (DE3) $\Delta nemA$. The transformation mixture was incubated with 1 mL LB medium at 37 $^\circ\text{C}$, 800 rpm (EPPENDORF Thermocycler) for 1 h and spread on LB-agar plates containing the appropriate antibiotic (50 $\mu\text{g}/\text{mL}$ kanamycin, 100 $\mu\text{g}/\text{mL}$ ampicillin). For rational mutagenesis one colony from plate was transferred to 5 mL LB medium with the appropriate antibiotic and grown overnight at 37 $^\circ\text{C}$, 200 rpm. For library mutagenesis all colonies from plate were dissolved in 1 mL water, harvested by centrifugation (1 min, 14 000 rpm) and used for plasmid preparation. The corresponding plasmid was extracted with the GenElute HP Plasmid Miniprep Kit (SIGMA ALDRICH) and sequenced by GATC to confirm generation of mutants.

6.5.1.4 Quick Quality Control of Libraries

Quick Quality Control (QQC) of combinatorial libraries is a cautionary step that sequences the pooled library plasmids to avoid futile screening of non-existing diversity. Transformants were streaked out onto petri dishes containing LB^{AMP} agar, followed by overnight incubation at 37 °C. The cell “carpet” was harvested with 1 mL water, and the pooled plasmids were extracted in a single vial using a GenElute HP Plasmid Miniprep Kit (SIGMA ALDRICH). The plasmid mix was sent for sequencing displayed generated diversities. If the results were not sufficient, optimization steps of PCR program parameters (e.g. annealing temperature, additives) were performed to improve the library quality.

6.5.2 Heterologous Expression of Ene Reductases

Gene constructs pET21b(+)-*yqjM*^[95], pET28a(+)-*ncr*^[170], pET28b(+)-*rmer*^[99], pET28b(+)-*drrer*^[99], pET22-*tser*^[175], pET22-*nemA*^[183], pGas-*xenA*^[183], pGas-*xenB*^[183] were transformed into electrocompetent *E. coli* (DE3) BL21 Δ *nemA*^[178]. Electrocompetent cells were prepared with a modified Inoue method^[338] as described under 6.4.3 Expression of *yqjM*, was performed as previously described^[95]. Expression of *drrer*, *rmer* and *tser* was performed using 300 mL terrific broth (TB) medium with appropriate antibiotic in a 2 L baffled flask inoculate with overnight culture (3 mL) and incubated at 37 °C, 220 rpm in a HT INFORS Shaker (MULTITRON, tray with 25 mm shaking diameters) until an OD₆₀₀ of 0.6-0.8 was reached. Enzyme production was induced with 10 μ M IPTG and temperature lowered to 22 °C. After 18-22 h cells were harvested (5000 rpm, 4 °C, 15 min) and resuspended in 5 mL 100 mM KP_i buffer, pH 7.4. Cultures for heterologous expression of *nemA* and *ncr* were grown in TB medium and were induced with 10 μ M IPTG at an OD₆₀₀ of 0.6-0.8. The temperature of the Nema culture was reduced to 30 °C while for NCR production, a temperature of 25 °C worked better. Cells used for heterologous expression of *xenA* and *xenB* were grown in LB medium and in-

duced with 0.2% rhamnose as described^[183] XenA was produced at 25 °C and XenB at 30 °C. Cells were harvested after 18-22 h by centrifugation (5000 rpm, 4 °C, 15 min) and resuspended in 5 mL 100 mM KPi buffer, pH 7.4.

6.5.3 Purification of His-tagged Ene Reductases

DrER, *RmER*, XenB and NCR were purified as histidine-tagged enzymes by IMAC giving the proteins with satisfactory purity. Cell lysis and purification was performed analogue for all above mentioned ene reductases. Cells were disrupted by sonication on ice (5x30 s, 30 s intervals, 5x10 cycles, 40% power, BANDELIN Sonoplus HD 2070 with a SGH 213G booster horn and a titanium flat tip (TT13)) and the supernatants were recovered by centrifugation (30 min, 10 000 rpm, 4 °C) in a THERMO SCIENTIFIC Sorvall RC 6 Plus centrifuge equipped with a F21S or F10S rotator.

For purification by FPLC, an *ÄKTAFPLC purifier system* (GE HEALTHCARE LIFE SCIENCES) was used. All elution profiles were plotted by *UNICORNTM* software. The column, packed with Ni-NTA agarose beads (QIAGEN), had a volume of 6 mL and was equilibrated with 90% buffer A (100 mM KPi, pH 7.4) and 10% buffer B (500 mM imidazole, 500 mM NaCl, 100 mM KPi, pH 7.4). All steps were performed in a cold room at 4 °C. The filtered lysate (filter 0.45 µM) was loaded on the column with a 10 mL loop using 90% buffer A and 10% buffer B. A flow rate of 1 mL/min was used for the whole purification process. The loop was emptied with 25 mL of 90% buffer A and 10% buffer B. If sample size exceeded 10 mL, the process was repeated. The column was washed with 12 column volumes (CV), 90% buffer A and 10% buffer B. Next, a gradient (from 10% to 60% buffer B in 12 CV) was set and protein of interest eluted around 30% buffer B. The column was washed with 5 CV, 100% buffer B. The column was stripped, cleaned in place and reloaded with nickel after every third run. The purity of proteins was checked by SDS-PAGE. The eluted fractions were concentrated at 4 °C by centrifugation using 10 kDa concentrators (MERCK MILLIPORE) and the buffer was exchanged to 100 mM KPi, pH 7.4. The concentrated

protein solution was incubated with a spatula tip of FMN for 90 min at 4 °C, except for NCR variants. Removal of salts and excessive FMN was achieved by size exclusion chromatography with 5 mL desalting columns (GE HEALTHCARE). Yields of about 1-1.5 mL of 30-50 μ M could be obtained for all variants.

6.5.4 Purification over Size Exclusion Chromatography

The *HiTrap* column (GE HEALTHCARE, CV: 5 mL) was washed with H₂O (millipore) for 10 min and then equilibrated with 100 mM KP_i buffer for 20 min and a flow rate of 100 mL/h. For *DrER* and *RmER* mutants, the buffer was stored on ice to generate enough cooling. A peristaltic pump system with a flow rate of 60 mL/h was used. For every step, the column was charged with a sample volume of 1 mL. Two separated yellow bands were observed and the elution fractions were collected. After every step, the column was again washed and equilibrated with H₂O (millipore) and 100 mM KP_i buffer. After size exclusion chromatography (SEC), BRADFORD test was repeated and product fractions were combined and concentrated. Elution fractions with pure FMN were discarded. Subsequently, absorption spectra were also measured to give an active protein concentration, since the bound FMN has a characteristic absorption maximum at 455 nm. The *DU 800 UV/Vis Spectrophotometer* (BECKMANN-COULTER) was blanked with 100 mM KP_i buffer. If necessary, the samples were diluted (1:1 or 1:10) to prevent absorption higher than one. The purified proteins were divided into aliquots, frozen with liquid nitrogen and stored at -80 °C.

6.5.5 Purification of Thermostable *TsER*

Since *TsER* is untagged but thermostable, it was purified by heat. Lysate was obtained as described above and incubated in a 50 mL plastic tube at 70 °C for 90 min in a drying oven. The clear lysate turns milky. Afterwards the suspension was stored at

room temperature for 10 min to cool down. The supernatant was obtained via centrifugation at 14 000 rpm, 4 °C, 60 min and incubated with FMN for 90 min at 4 °C. SEC was used to remove excess of salts, FMN and small molecules using 5 mL desalting columns (GE HEALTHCARE) and 100 mM KPi buffer (pH 7.4). The purity of the proteins was checked by SDS PAGE (Figure 17). Dialysis is important, since spectrophotoscopic analysis of the heat-treated catalyst revealed a new band at 428 nm, which disappears after dialysis. Using a non-dialyzed enzyme batch, sometimes coloration of the reaction media occurred, which intensified upon longer air exposure. It is assumed, that a copurification of a not further specified organic molecule takes place

6.5.6 SDS-Page Analysis

The SDS-PAGE (sodium dodecylsulfate polyacrylamide gel electrophoresis) is a size separation process for proteins in an electrical field. During the sample preparation the protein solution is combined with SDS and β -mercaptoethanol, to split the disulfide bridges and by heating the sample up to 95 °C the tertiary and secondary structures are denatured. The intrinsic charge of the protein gets thereby overlaid from the anionic detergent SDS and the molecule linearized, so that proteins are separated only depending on their charge.^[340]

12 μ L protein solution is mixed with 4 μ L 4x sample buffer (100 mM Tris/HCl, pH 6.8, 110 mM SDS, 2 mM β -mercaptoethanol, 40% (w/v) glycerol, 1% (w/v) bromophenol blue) and denatured at 95 °C for 5 min. The mixture is centrifuged for 10 min, 14 000 rpm and 10 μ L are loaded on a gel (see Table 20). The separation takes places applying 120 V. As standard the protein marker PAGE RULER 26630 by THERMO SCIENTIFIC was used. The protein bands were stained by SDS-stain solution (50% (v/v) ethanol, 10% (v/v) acetic acid and 250 mg/L coomassie brilliant blue G-250). Excessive stain was removed by washing and boiling the SDS PAGE three times for 5 min in water.

Table 20. Compositions for resolving gels for denaturing SDS-PAGE.

separation gel 12%	stacking gel 5%
6.7 mL acrylamide/bis-acrylamide solution (30%)	1.4 mL acrylamide/bis-acrylamide solution (30%)
4.0 mL 4x separation gel buffer (1.5 M Tris, pH 8.8; 0.4% (w/v) SDS)	2.0 mL 4x separation gel buffer (0.5 M Tris, pH 6.8; 0.4% (w/v) SDS)
4.6 mL millipore H ₂ O	5.3 mL millipore H ₂ O
30 μ L 10% APS (w/v)	80 μ L 10% APS (w/v)
20 μ L TEMED	8 μ L TEMED

6.5.7 Protein Identification via Mass Analysis

6.5.7.1 Tryptic Digestion

Because of the low expression levels of certain wild types and variants, assignment of SDS-PAGE gel bands were done using protein identification by mass analysis. Bands were cut from SDS gel, destained and digested "in-gel" by adding sequencing grade modified Trypsin (PROMEGA) and incubated at 37 °C overnight.

The mass spectrometric analysis of samples was performed using an OrbitrapVelos Pro mass spectrometer (THERMO SCIENTIFIC). An Ultimate nanoRSLC-HPLC system (DIONEX), equipped with a custom 20 cm x 75 μ m C18 RP column filled with 1.7 μ m beads was connected online to the mass spectrometer through a PROXEON nanospray source. 1-15 μ L of the tryptic digest (depending on sample concentration) were injected onto a C18 pre-concentration column. Automated trapping and desalting of the sample was performed at a flowrate of 6 μ L/min using water/0.05% formic acid as solvent.

Separation of the tryptic peptides was achieved with the following gradient of water/0.05% formic acid (solvent A) and 80% acetonitrile/0.045% formic acid (solvent B) at a flow rate of 300 nL/min: holding 4% B for five minutes, followed by a linear gradient to 45% B within 30 min and linear increase to 95% solvent B in additional 5 min. The column was connected to a stainless steel nanoemitter (PROXEON, Denmark)) and the eluent was sprayed directly towards the heated capillary of the mass spectrometer using a potential of 2300 V. A survey scan with a resolution of 60 000

within the Orbitrap mass analyser was combined with at least three data-dependent MS/MS scans with dynamic exclusion for 30 s either using CID with the linear ion-trap or using HCD combined with Orbitrap detection at a resolution of 7500.

Data analysis was performed using Proteome Discoverer (THERMOSCIENTIFIC) with SEQUEST and MASCOT (version 2.2; MATRIX SCIENCE) search engines using either SwissProt or NCBI databases.

6.5.7.2 Denaturation Mass Analysis

To analyse if there is a self-oxidation of the cysteine 25 in the *TsER* wild type comparing to *TsER* C25D/I67T a determination of intact protein mass over a denaturation method was used. 50 μ L of a 10 μ M enzyme solution in 100 mM KP_i buffer, pH 7.4 was desalted online using a Waters ACQUITY H-Class HPLC-system equipped with a monolithic 50/1 ProSwift RP-4H column (THERMOSCIENTIFIC). Desalted proteins were eluted into the ESI source of a Synapt G2Si mass spectrometer (WATERS) by the following gradient of buffer A (water/0.05% formic acid) and buffer B (acetonitrile/0.045% formic acid) at a column temperature of 40 °C and a flow rate of 0.1 mL/min: Isocratic elution with 5% A for two minutes, followed by a linear gradient to 95% B within 8 minutes and holding 95% B for additional 4 minutes.

Positive ions within the mass range of 500-5000 m/z were detected. Glu-Fibrinopeptide B was measured every 45 seconds for automatic mass drift correction. Averaged spectra were deconvoluted after baseline subtraction and eventually smoothing using MASSLYNX instrument software with MAXENT1 extension.

The exact mass of *TsER* wild type and C25D/I67T determined via EXPASY is 37.982 kDa, if the wild type cysteine 25 will be oxidized the mass should be 37.997 kDa. But the results are 37.852 kDa for the wt and 37.850 kDa for C25D/I67T. It fits perfect to the predicted mass of EXPASY without the *N*-terminal methionine, which is literature known for ESI.^[341]

6.5.7.3 HDX Measurements

The Hydrogen/Deuterium exchange mass spectrometric analysis of the samples were performed by the department of mass spectrometry using a commercial H/DX-automation setup (SYNAPT G2-Si, Waters) including a two-arm robotic autosampler (LEAP TECHNOLOGIES), an ACQUITY UPLC M-Class system (WATERS) and HDX manager (WATERS). The samples were transferred by PD-10 into a low salt buffer (10 mM Tris pH 7.8, 100 mM NaCl, 1 mM β -mercaptoethanol), centrifuged for 10 min at 16100 g and 4 °C prior to irradiation with 656 nm (P_r state) or 735 nm (P_{fr} state) for 4 min in darkness, afterwards wrapped in aluminum foil and cooled to 1 °C. For each LC-MS run, 7.5 μ L of the protein solution (70 μ M) were pipetted in a fresh vial of the exchange plate at 25 °C and diluted with 61.8 μ L of either H₂O-buffer (t_0 -runs) or D₂O-buffer (exchange runs). After incubation for 15 s, 30 s, 60 s and 300 s 55 μ L of this solution were transferred to a fresh quench vial containing 55 μ L of quenching solution (400 mM H₃PO₄/KH₂PO₄ pH 2.2), which was pre-dispensed and pre-cooled to 1 °C for 10 minutes before starting the first run. After quenching, 95 μ L of the resulting solution was immediately injected into the pepsin column (HDX manager, WATERS).

Digestion was done online using an Enzymate BEH pepsin column (WATERS) at 20 °C with water/ 0.1 % formic acid at a flow rate of 100 μ L/min. Subsequently, peptic peptides were trapped at 0.5 °C using a C18 trap column. Separation of peptides was achieved at 0.5 °C utilizing a 1 x 100 mm ACQUITY UPLC BEH C18 1.7 μ m column (WATERS) at a flow rate of 30 μ L/min with the following gradient of solvents A (water 0.1 % formic acid) and B (acetonitrile, 0.1 % formic acid): Linear increase from 5 % B to 35 % B within 7 minutes, followed by a ramp to 85 % B within 1 minute and holding 85 % B for additional 2 minutes. Finally, the column was washed at 95 % for 1 minute and re-equilibrated to 5 % B for 5 minutes. During separation of peptides using the chromatographic column, the pepsin column was washed by injecting 3 times 80 μ L of 4 % acetonitrile and 0.5 M guanidinium chloride.

Enhanced high definition MS (HDMSe) mode was used for t0 peptide detection, which is a workflow provided by WATERS for data independent acquisition, including ion mobility separation (IMS) of precursor ions within the gas phase and alternating lower and higher energies applied to the transfer cell (higher energies lead to fragmentation of IMS separated precursor ions, lower energies result in non-fragmented peptide molecular ion spectra), and H/D-MS (also including IMS, but with only lower energies applied to the transfer cell preventing fragmentation) for measuring exchanged peptides. Lock mass spectra were measured every 45 seconds using Glu-fibrinopeptide B as standard ($M^{2+} = 785.8427$ m/z). Blank runs were performed between each sample to avoid peptide carryover from previous runs.

t0 peptide identification was performed using ProteinLynx Global SERVER 3.0.1 (WATERS) with custom-created databases and the setting “no enzyme”. Final assignment of deuterium incorporation was done with DYNAMX 3.0 (WATERS). The minimum peak intensity was set to 20^3 counts and a peptide length between five and twenty was chosen. Moreover, tolerances of 0.5 min for the retention time and 25 ppm for m/z values were applied for the peptide assignment, generating an overall sequence coverage of 83% with a 3.2 redundancy.

6.5.8 Determination of Active Enzyme Concentration by UV-Vis Spectroscopy

Active enzyme concentration was determined by LAMBERT-BEER using a BECKMAN COULTER DU 800 spectrophotometer at FMN absorption maximum around 455 nm. The extinction coefficient of YqjM was used for calculation ($11\ 600\ M^{-1}cm^{-1}$).^[95]

6.5.9 Circular Dichroism Spectroscopy

For detection, a quartz cell with $d = 0.1$ cm in a JASCO J810 spectropolarimeter was used, equipped with a JASCO CDF 4265 peltier element and a HAAKE WKL26 water bath (THERMO). The protein was measured in 100 mM potassium phosphate, pH 7.4, with a protein concentration of 10 μ M. The melting curve was determined in 2 °C steps with three accumulation steps at 220 nm.

6.5.10 Spectrophotometric Measurements of FMN-Oxidation with Molecular Oxygen

It was determined, whether several mutations in *TsER* alter the rate of reduction and subsequent reoxidation of FMN. The purified enzymes *TsER* wild type, C25D/I67C, C25D/I67T, C25D/I67V, C25G, C25G/I67C, C25G/I67T and C25G/I67V were used in a fully-oxidized form and by addition of a 10-fold excess of NADPH in air-saturated KP_i buffer, changes in the flavin reduction status were detected spectroscopically with a *V-650 spectrophotometer* (JASCO) at a wavelength of 456 nm against time. Air-saturation of the buffer was enabled by stirring at 1000 rpm during measurements. Reaction were performed in triplicates in 100 mM KP_i , pH 7.4, with 10 mM $CoCl_2$ and 100 μ M final concentration of NADPH in a stirring cuvette (1000 rpm) with a JASCO V-650 spectrophotometer equipped with a PAC-743 Peltier temperature control unit. The spectrophotometer was blanked with buffer right before the measurement. After addition of the enzyme, it was waited for 100-150 seconds to obtain equilibration of absorption before NADPH was added. The spectrophotometer was set to 456 nm, with a range of 0.2 sec, a bandwidth of 2.0 nm and a temperature of 30 °C.

6.6 Thermostable Glucose Dehydrogenase Protocols

6.6.1 Heterologous Expression and Purification

Gene construct pACYC-*gdh* (*Bacillus subtilis* 168 glucose dehydrogenase variant E170K/Q252L)^[59] was transformed into electrocompetent *E.coli* BL21 DE3 Gold. Expression was performed using 350 mL TB medium containing 35 mg/mL chloramphenicol in a 2 L baffled flask and inoculate with 3.5 mL overnight culture. The expression cultures were incubated at 37 °C with 200 rpm in a HT INFORS Shaker (MULTITRON, tray with 25 mm shaking diameters) until the OD₆₀₀ reached 0.4-0.6. IPTG was added to a final concentration of 1 mM and the temperature was reduced to 30 °C. The cultures were incubated overnight, harvested (5000 rpm, 4 °C, 15 min) and resuspended in 5 mL KP_i buffer (100 mM, pH 7.4). Cells were lysed by sonication on ice (5x30 s, 30 s intervals, 5x10 cycles, 40% power, BANDELIN Sonoplus HD 2070 with a SGH 213G booster horn and a titanium flat tip (TT13)) and the supernatant was recovered by centrifugation (16 000 rpm, 4 °C, 45 min) in a THERMO SCIENTIFIC Sorvall RC 6 Plus centrifuge equipped with a F21S or F10S rotator. The cleared lysate was purified by incubation at 60 °C for 1 h. After centrifugation (16 000 rpm, 4 °C, 45 min) the supernatant was lyophilised and stored at -20 °C.

6.6.2 Activity Test

The activity of glucose dehydrogenase was determined by following NADPH formation according to NOLTMANN *et al.*^[342]. A reaction mix, containing of 50 mM glucose, 0.5 mM NADP⁺ in 100 mM KP_i buffer (pH 5-10), was prepared and incubated at desired temperatures (30-70 °C) for at least 15 min. Cuvettes were pre-warmed in a JASCO V-650 spectrophotometer equipped with a PAC-743 Peltier temperature control unit. 10 µL of dissolved glucose dehydrogenase (1.23 mg/mL in KP_i buffer) was added to the mix, the cuvette was inverted twice and measured immediately. The

absorption at 340 nm was recorded for 60 s, while only the slope of the first 15 s was taken to calculate activity with the following equation.

$$Activity \left[\frac{Units}{mL} \right] = \frac{\left(\frac{\Delta A_{340 \text{ nm}}}{min} \right) \cdot V_{com}}{\epsilon_{NADPH,340 \text{ nm}} * V_{GDH \text{ solution}}}$$

$\Delta A_{340 \text{ nm}}/min$ = slope of the first 15 s, V_{com} = complete reaction volume (1 mL),

$\epsilon_{NADPH,340 \text{ nm}} = 6.22 \text{ mL} \cdot \text{mol}^{-1} \cdot \text{cm}^{-1}$, V_{GDH} = added volume of glucose dehydrogenase sample

6.7 Lyophilisation of Enzymes

TsER C25G, C25G/I67T and C25D/I67T as well as *BsGDH* were lyophilized with a CHRIST lyophilisator after heat-purification. The yellow powder was stored at -20 °C until further use. Before use, active concentration was determined via absorption at 455 nm.

6.8 Protein Crystallization and X-Ray Structure Determination

6.8.1 X-Ray Structure of *TsER* C25D/I67T

Heat purified *TsER* C25D/I67T was concentrated through ultrafiltration (30 kDa NMWL, AMICON) with additional FMN added to ensure full occupancy. The protein was further purified using size exclusion chromatography (Sephacryl S100HR, GE HEALTHCARE) and eluted in 10 mM MOPS buffer (pH 7.4) containing 20 mM NaCl. Crystals of *TsER* C25D/I67T were grown using sitting-drop vapour-diffusion in 1 μ L drops consisting of equal volumes of 8 mg mL⁻¹ *TsER* C25D/I67T and crystallization solution (15% v/v 2-propanol, 0.1 M sodium citrate tribasic dihydrate pH 5.0, 10% w/v polyethylene glycol 10,000) at 289 K. Crystals were soaked in reservoir solution

containing 30% glycerol prior to cryocooling. X-ray diffraction data (Table 21) were collected at Diamond (UK) on beamline i03. Data was processed using MOSFLM^[343] and POINTLESS^[344], with intensities scaled and merged using SCALA^[344]. Molecular replacement was performed using PHASER^[345] with *TsER* wt (pdb 3HF3) as search model. Refinement was performed through iterative cycles of manual model building in COOT^[346] and restrained refinement using REFMAC^[347]. Structure was validated using programs within the CCP4 SUITE^[348].

Table 21. Data Collection and Refinement Statistics.

Data Collection and Processing	
Beamline	i03, Diamond UK
Wavelength (Å)	0.9763
Resolution (Å)	94.31-2.3 (2.42-2.3)
Space group	P 1 2 1
Unit cell parameters	a=99.68Å b=101.20Å c=104.26Å α=90° β=115.24° γ=90°
Unique reflections	83126 (12074)
Completeness (%)	99.8 (99.7)
Mn(I)/sd(I)	8.1 (2.0)
Multiplicity	3.0 (3.0)
R _{merge}	0.093 (0.736)
Refinement	
R _{work} /R _{free} ^a	0.182/0.223
Molecules in ASU	4
Average B-factor, all atoms (Å ²)	47.68
r.m.s.d. Bond lengths (Å)	0.011
r.m.s.d. Bond angles (°)	1.558
Ramachandran distribution (%) ^b	96.6/3.1/0.3

Values for the highest resolution shell given in parenthesis

^aR_{free} calculated from 5% reflections omitted from structure refinement

^bFavoured/Allowed/Outlier

6.8.2 X-Ray Structure of *TsER* C25D/I67T/A102H

The *TsER* triple mutant C25D/I67T/A102H was heat purified and concentrated through ultrafiltration (30 kDa NMWL, AMICON). Additional FMN was added to ensure full occupancy followed by size exclusion chromatography [Sephacryl S100HR (GE HEALTHCARE)] and eluted in 10 mM MOPS buffer (pH 7.4) containing 20 mM

NaCl. Crystals of *TsER C25D/I67T/A102H* were grown using sitting-drop vapour-diffusion in 1 μ L drops consisting of equal volumes of 8 mg/mL protein containing 15% DMF with 0.01 M **13a** and crystallization solution (0.1M MES monohydrate pH 6.5, 12% w/v PEG 20 000) at 289 K. Crystals were soaked in reservoir solution containing 30% glycerol and 20% DMF with 0.02 M **13a** prior to cryocooling. X-ray diffraction data (Table 22) was collected at Diamond (UK) beamline i04-1. Data was processed using MOSFLM^[343], with intensities scaled and merged using AIMLESS^[349]. Molecular replacement was performed using PHASER^[345] with *TsER C25D/I67T* (PDB 5NUX) as search model. Refinement was performed through iterative cycles of manual model building in COOT^[346] and restrained refinement using REFMAC^[347]. The final structure was validated using programs within the CCP4 SUITE^[348] and deposited in the PDB under accession number 5OGT.

Table 22. Data Collection and Refinement Statistics.

Data Collection and Processing	
Beamline	i04-1, Diamond UK
Wavelength (Å)	0.9282
Resolution (Å)	69.65-2.30 (2.34-2.30)
Space group	P 1 2 1
Unit cell parameters	a=100.27Å b=103.24Å c=102.72Å $\alpha=90^\circ$ $\beta=113.28^\circ$ $\gamma=90^\circ$
Unique reflections	85031 (4490)
Completeness (%)	99.5 (99.3)
Mn(I)/sd(I)	4.3 (2.0)
Multiplicity	2.9 (2.8)
R_{merge}	0.172 (0.627)
Refinement	
$R_{\text{work}}/R_{\text{free}}^a$	0.206/0.244
Molecules in ASU	4
Average B-factor, all atoms (Å ²)	22
r.m.s.d. Bond lengths (Å)	0.010
r.m.s.d. Bond angles (°)	1.421
Ramachandran distribution (%) ^b	97.3/0.2

Values for the highest resolution shell given in parenthesis

^a R_{free} calculated from 5% reflections omitted from structure refinement

^bFavoured/Allowed/Outlier

6.9 Biotransformations

6.9.1 Reactions with Cell Lysate in 96-Deep Well Plates

Variants were picked from glycerol stocks or agar plates to inoculate 2.2 mL 96-deep well plates (VWR) containing 900 μ L LB medium with the appropriate antibiotic per well. Plates covered with gas permeable membranes (BRAND) were cultured overnight at 37 °C with shaking (220 rpm, HT INFORS). Glycerol (20% v/v) stock solutions, in sterile 96-well microtiter plates (NUNC), were prepared at this stage and stored at -80 °C. 100 μ L overnight cultures were used to inoculate new 96 deep-well plates containing 700 μ L TB medium supplemented with the appropriate antibiotic and 10 μ M IPTG. After 2 h of growing at 37 °C, the temperature was reduced to 22 °C and the cultures grew for another 18 h. After harvesting the cells, they were lysed by incubation of the resuspended cells in 225 μ L lysis buffer (1 mg/mL lysozyme in 100 mM KP_i , pH 7.4) for 1 h at 37 °C, 220 rpm. To start the reaction 225 μ L reaction mixture with final concentrations in 450 μ L total reaction volume of 100 mM glucose, 2.2 U/mL GDH-60 (EVOCATAL) 1 mM NADP⁺, 10 mM substrate (1 M in EtOH) was added. The reaction was stopped after a specified time by extraction with 400 μ L ethyl acetate.

Variation with Pooling Strategy

For the pooling strategy to minimize the screening effort of several plates the harvested cells were resuspended in 100 μ L KP_i buffer per well and pooled together in one plate. This means, combining the cell suspension of three plates in one. After centrifugation at 4000 rpm, 4 °C and 10 min the supernatant was discarded and the pooled cells lysed and screened like described above.

6.9.1.1 Fluorescence Measurements for 3-CCE Screening

100 μ L reaction solution per well was transferred to a black plate without former extraction. Fluorescence measurements were performed in black 96-well flat bottom plates on a MOLECULAR DEVICES SpectraMax M5 using SOFTMAX Pro V5.2 software and analysed using ORIGIN8. The setting used for the detection of **13a** were $\lambda_{\text{ex}} = 400$ nm, $\lambda_{\text{em}} = 440$ nm with a cut-off filter at 420 nm.

6.9.2 Reaction with Purified Enzyme

All reactants were mixed aerobically in 1.5 mL reaction tubes resulting in the following final concentrations in 100 mM KPi buffer (pH 7.4): 100 mM glucose, 10 μ M enzyme, 0.1 mM CaCl_2 , 0.25 mM NADP^+ , 2.2 U/mL GDH-60 (EVOCATAL), 10 mM substrate (1 M in EtOH). The reactions were performed at least in triplicates in a total reaction volume of 200 μ L at 30 $^\circ\text{C}$ with gently shaking in a Thermomixer (EPPENDORF) set to 700 rpm for 5 h. To stop the reaction, the aqueous solution was extracted with 200 μ L ethyl acetate. Total turnover numbers (TON) were calculated by dividing (mmol of substrate \times conversion) by (mmol of enzyme) and the turnover frequencies equals TON per reaction time in hour.

6.9.3 Residual Activity of *TsER* C25D/I67T and C25G/I67T

Residual activity assays were performed by incubating the purified *TsER* variants at different temperatures. The purified enzyme solutions were defrosted on ice, diluted with KPi buffer to 11 μ M and incubated overnight (14.5 h) at different temperatures. After equilibrating all samples to room temperature (22 $^\circ\text{C}$) in 15 min, reaction was started by adding 100 mM glucose, 0.1 mM CoCl_2 , 0.25 mM NADP^+ , 2.2 U/mL *BsGDH* and 2 μ L **22a** (1 M, EtOH). The reaction was performed 2.5 h at 30 $^\circ\text{C}$. After

extraction with ethyl acetate, organic layers were analysed by GC. Residual activity of control without incubation was set to 100%.

6.9.4 Upscale Reactions to Determine Enantiomeric Excess

Precise *ee* determination at low conversions (< 5%) requires a larger reaction scale and higher catalyst loadings. Therefore, all reactants were mixed in a 100 mL Erlenmeyer flask resulting the following final concentrations: 100 mM glucose, 50 μ M enzyme, 0.1 mM CaCl₂, 0.25 mM NADP⁺, 2.2 U/mL GDH-60 (EVOCATAL), 50 mM substrate (1 M in EtOH). The parafilm sealed flask contained a reaction volume of 10 mL and was incubated at 30 °C with gently shaking 100 rpm (HT INFORS) for 16 h. To stop the reaction, the aqueous solution was extracted with 3 mL ethyl acetate and concentrated to ca. 200 μ L via evaporation for chiral GC measurement.

6.9.5 Upscale for Polarization Measurement

To characterize the enantiomer formed by reduction of 2-methylcyclopentenone (**33a**) an upscale reaction was performed to isolate the product **33b** for optical rotation measurement. All reactants were mixed in a 50 mL Erlenmeyer flask resulting the following final concentrations: 40 mM glucose, 20 μ M TsER C25G/I67C, 0.1 μ M NADP⁺, 1 U/mL GDH-60 (EVOCATAL), 20 μ L pure substrate in 7.53 mL 100 mM KP_i buffer, pH 7.4. The parafilm sealed flask contains a reaction volume of 10 mL and was incubated at 30 °C with gently shaking 100 rpm (HT INFORS) for 16 h. To stop the reaction, the aqueous solution was extracted with 20 mL ethyl acetate, washed with brine. The organic phase was dried over MgSO₄ and the ethyl acetate was evaporated under pressure. The optical rotation was measured with a 20 mg/mL solution in chloroform in a 50 mm cuvette at a polarimeter P800-T, KRÜSS with $\lambda = 589$ nm at

25 °C and result in $[\alpha]_D^{25}$ -81°. In comparison with literature values it is 2(*R*)-methylcyclopentanone (**33b**).^[80]

6.9.6 Upscale of **13a** with *TsER* C25D/I67T

13a (500 µL, 50 µmol, 1 mM in DMF), purified *TsER* C25D/I67T (10 µM), glucose (100 mM), NADP⁺ (0.25 mM), glucose dehydrogenase (2 U/mL) and cobalt chloride (0.1 mM) in a total volume of 50 mL potassium phosphate buffer were mixed in a 300 mL Erlenmeyer flask and covered with parafilm and incubated in a HT INFORS Shaker at 30 °C, 150 rpm for 16 h. The solution was extracted with ethyl acetate (2 x 50 mL), the combined organic layers were washed with brine, dried over MgSO₄ and the solvent was removed under reduced pressure. The product was analysed by HPLC, NMR and mass. The product was obtained in 79% yield (10 mg, 39.3 µmol). The structure was determined by 2D NMR (Figure 67).

¹H-NMR (500 MHz; dms_o-*d*₆): δ = 9.29 (s, 1H, OH), 9.03 (s, 1H, OH), 6.73 (d, ³J = 8.2 Hz, 1H, ArH), 6.25 (d, ⁴J = 2.4 Hz, 1H, ArH), 6.08 (dd, ³J = 8.1, ⁴J = 2.4 Hz, 1H, ArH), 4.02 (q, ³J = 7.1 Hz, 2H, CH₂), 3.63 – 3.58 (m, 1H, CH), 2.85 (ddd, ²J = 34.6 ²J = 13.6, ³J = 8.8 Hz, 2H, CH₂), 2.73 (s, 1H, OH), 1.12 – 1.06 (m, 3H, CH₃).

¹³C-NMR (500 MHz; dms_o-*d*₆): δ = 170.2, 169.2, 157.0, 156.0, 130.9, 114.4, 105.8, 102.3, 60.5, 51.4, 29.2, 13.9.

HR-MS(APCI⁺) (C₁₂H₁₁O₆ + Na⁺) m/z = found: 227.0686, cal: 277.0790.

6.9.7 Preparative Scale Bioreductions

In the following detailed descriptions of preparative scale bioreductions with *TsER* C25G/I67T and C25D/I67T from chapter 3.3.3 can be found.

3-Methylcyclohexan-1-one (17b): All reactants were mixed in a 100 mL Schott bottle resulting in the following final concentrations in 100 mM KPi buffer (pH 7.4): 991 mg glucose monohydrate (5.0 mmol, 1.75 eq), 9.81 mg NADP^+ disodium salt (0.25 mM), 0.55 mg *BsGDH* (2.2 U/mL), 0.02 mol% *TsER* variant (10 μM), 284 μL 3-methylcyclohex-2-en-1-one (**17a**, 2.5 mmol, 1.0 eq) and 10% v/v *n*-pentane. The reaction was performed in a total volume of 50 mL at 30 °C with gently shaking in a HT INFORS Shaker set to 150 rpm over a time period of 480 min to 540 min. At different time points (see Figure 28) a 20 μL sample for reaction control was taken from the *n*-pentane phase and diluted with 200 μL *n*-pentane for analysing via GC (HP-5). After completion the whole reaction was extracted three times with 20 mL DEE. The combined organic phases were washed with brine, dried over MgSO_4 and the solvent was evaporated under vacuum. Compound (*R*)-**17b** was obtained in 91% (255 mg, 2.27 mmol) yield with 99% *ee*. Compound (*S*)-**17b** was obtained with 78% (202 mg, 1.81 mmol) yield in 57% *ee*.

$^1\text{H-NMR}$ (500 MHz, CDCl_3), δ = 2.40-2.29 (m, 2H), 2.28-2.17 (m, 1H), 2.08-2.01 (m, 1H), 2.00-1.96 (m, 1H), 1.94-1.80 (m, 2H), 1.73-1.58 (m, 1H), 1.39-1.26 (m, 1H), 1.01 (d, 3H, 3J = 6.2 Hz, CH_3) ppm.

$^{13}\text{C-NMR}$ (125 MHz, CDCl_3), δ = 212.0, 50.1, 41.3, 34.3, 33.5, 25.4, 22.2 ppm.

HR-MS (EI^+) ($\text{C}_7\text{H}_{12}\text{O}_1$) m/z = found: 112.08836, cal.: 112.08881.

2-Methyl-5-(prop-1-en-2-yl)cyclohexan-1-one (18b): All reactants were mixed in a 300 mL Erlenmeyer flask resulting the following final concentrations in 100 mM KPi buffer (pH 7.4): 1.64 g glucose monohydrate (8.28 mmol, 1.2 eq), 16 mg NADP⁺ disodium salt (2 mM), 1 mg GDH-60 (EVOCATAL, 2.2 U/mL), 0.005 mol% *TsER* variant (3.4 μM), 1.04 mL carvone (**18a**, 6.9 mmol, 1.0 eq). The reaction was performed in total reaction volume of 100 mL at 30 °C with gently shaking in a HT INFORS Shaker set to 110 rpm over a time period of 350 min to 410 min. At different time points (see Figure 28) a 100 μL sample for reaction control was taken and extracted with 200 μL EtOAc for analysing via GC (HP-5). After completion the whole reaction was extracted two times with 100 mL EtOAc. The combined organic phases were washed with brine, dried over MgSO₄ and the solvent was evaporated under vacuum. Compound (2*S*,5*S*)-**18b** was obtained in 90% (939 mg, 6.2 mmol) yield with 88% *de*. Compound (2*R*,5*S*)-**18b** was obtained with 78% (825 mg, 5.4 mmol) yield in 96% *de*.

2-Methyl-5-(prop-1-en-2-yl)cyclohexan-1-one (18b) with 25 mmol: All reactants were mixed in a 500 mL Schott bottle resulting the following final concentrations in 100 mM KPi buffer (pH 7.4): 9.91 g glucose (50.0 mmol, 1.9 eq), 98 mg NADP⁺ disodium salt (0.25 mM), 5.5 mg BsGDH (2.2 U/mL), 0.0098 mol% *TsER* variant (5 μM), 4.0 mL **18a** (25.6 mmol, 1.0 eq) and 10% v/v *n*-pentane. The reaction was performed in a total volume of 500 mL at 30 °C with gently shaking in a HT INFORS Shaker set to 150 rpm over a time period of 420 min. At different time points (see Figure 28) a 20 μL sample for reaction control was taken from the *n*-pentane phase and diluted with 200 μL *n*-pentane for analysing via GC (HP-5). After completion the whole reaction was extracted three times with 100 mL DEE. The combined organic phases were washed with brine, dried over MgSO₄ and the solvent was evaporated under vacuum. Compound (2*R*5*S*)-**18b** was obtained in 93% (3.63 g, 23.8 mmol) yield with 96% *de*.

¹H-NMR (500 MHz, CDCl₃), δ = 4.83 (s, 1H, H₁₁), 4.69 (s, 1H, H₁₁), 2.62-2.52 (m, 2H), 2.43-2.37 (m, 2H), 1.90-1.82 (m, 3H, 1/2 H₃, H₄), 1.73 (s, 3H, H₁₀), 1.65-1.56 (m, 1H, 1/2 H₃), 1.05 (d, 3H, ³J = 6.9 Hz, H₇) ppm.

¹³C-NMR (125 MHz, CDCl₃), δ = 214.0 (CO), 147.0 (C₉), 111.5 (C₁₁), 44.6 (C₆), 44.1 (C₅), 44.0 (C₂), 30.7 (C₃), 26.4 (C₄), 21.5 (C₁₀), 15.6 (CH₃) ppm.

HR-MS (EI⁺) (C₁₀H₁₆O₁) m/z = found: 152.12014, cal.: 152.12011.

Ethyl 2-benzyl-3-oxobutanoate (40b): All reactants were mixed in a 100 mL Erlenmeyer flask resulting in the following final concentrations in 100 mM KP_i buffer (pH 7.4): 2 g glucose (10 mmol, 10 eq), 6.4 mg NADP⁺ disodium salt (0.41 mM), 6.4 mg GDH-60 (EVOCATAL, 222 U/mg), 122 mg lyophilized TsER C25D/I67T (10 μ M), 218 mg ethyl (Z)-2-benzylidene-3-oxobutanoate (**40a**, 1.0 mmol, 1.0 eq) in 2 mL diisopropylether (DIPE, 10% v/v). The reaction was performed in total reaction volume of 20 mL at 30 °C with gently shaking in a HT INFORS Shaker set to 110 rpm over a time period of 2 h. 200 μ L sample for reaction control was taken and extracted with 200 μ L EtOAc for analysing via GC (HP-5). After completion (81% conversion) the whole reaction was extracted two times with 20 mL EtOAc. The combined organic phases were washed with brine, dried over MgSO₄ and the solvent was evaporated under vacuum. The product **40b** was cleaned via column chromatography (*n*-pentane : EtOAc 10:1) and could be isolated in clean form in 76% yield (167.4 mg, 0.76 mmol).

¹H-NMR (300 MHz; CDCl₃): δ = 7.39 (s, 1H, H_{arom.}), 7.28 (s, 1H, H_{arom.}), 7.23-7.10 (m, 3H, H_{arom.}), 4.15 (q, J = 7.2 Hz, 2H, CH₂), 3.77 (t, J = 7.6 Hz, 1H, CH), 3.16 (d, J = 7.6 Hz, 2H, CH₂), 2.19 (s, 3 H, COCH₃), 1.20 (t, J = 7.1 Hz, 3H, CH₃) ppm.

HR-MS (ESI⁺) (C₁₃H₁₆O₃ + Na⁺) m/z = found: 243.0991, cal.: 243.0992.

(R)-Levodione (22b): All reactants were mixed in a 100 mL Erlenmeyer flask resulting in the following final concentrations in 100 mM KPi buffer (pH 7.4): 2 g glucose monohydrate (10 mmol, 10 eq), 6.4 mg NADP^+ disodium salt (0.41 mM), 6.4 mg *BsGDH*, 4.2 mL *TsER C25D/I67T* (final concentration 10 μM , stock concentration 48 μM), 370 μL ketoisophorone (**22a**, 2.5 mmol, 1.0 eq) in 2 mL diisopropylether (DIPE, 10% v/v). The reaction was performed in total reaction volume of 20 mL at 30 °C with gently shaking in a HT INFORS Shaker set to 150 rpm over a time period of 1.5 h. 100 μL sample for reaction control was taken and extracted with 100 μL EtOAc for analysing via GC (HP-5). After completion (91% conversion) the whole reaction was extracted two times with 20 mL EtOAc. The combined organic phases were washed with brine, dried over MgSO_4 and the solvent was evaporated under vacuum. The product **22b** could be isolated in clean form in 65% yield (250 mg, 1.62 mmol).

$^1\text{H-NMR}$ (300 MHz; CDCl_3): δ = 3.00 (m, 1H), 2.80-2.76 (m, 1H), 2.75-2.70 (m, 1H), 2.51 (d, ^2J = 15.2 Hz, 1H), 2.33 (dd, ^2J = 17.7, ^4J = 13.2 Hz, 1H), 1.21 (s, 3H, CH_3), 1.15 (d, ^3J = 6.6 Hz, 3H, CH_3), 1.12 (s, 3H, CH_3) ppm.

6.9.8 Reduction of **22a** in Sequential Bi-Phasic Batch Reactions

All reactants were mixed in a 100 mL Erlenmeyer flask resulting in 100 mM KPi buffer (pH 7.4): 2 g glucose monohydrate (10 mmol, 10 eq), 6.4 mg NADP^+ disodium salt (0.41 mM), 6.4 mg *GDH-60* (EVOCATAL, 222 U/mg), 122 mg lyophilized *TsER C25D/I67T* (10 μM), 148 μL **22a** (1.0 mmol, 1.0 eq, 50 mM) in 2 mL DIPE (10% v/v). The reaction was performed in total reaction volume of 20 mL at 30 °C with gently shaking in a HT INFORS Shaker set to 110 rpm over a time period of 2.5 h (reaction control showed 98% product formation). The two phases were separated and to the aqueous phase 1 mmol **22a** (148 μL) in 2 mL DIPE was added again. After 3 h at 30 °C and 110 rpm 90% product formation was obtained. The phases were again sep-

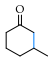
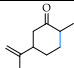
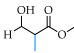
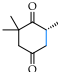
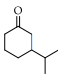
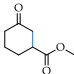
arated, 1 mmol **22a** in 2 mL DIPE was added to the aqueous phase and incubated at 30 °C, 110 rpm for 3 h. Reaction control showed 50% product formation. In total 2.5 mmol **22b** (370 μ L) could be converted over three steps (TTN = 12 500).

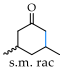
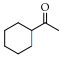
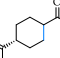
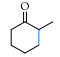
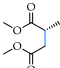
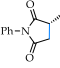
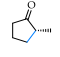
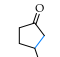
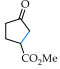
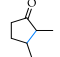
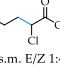
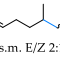
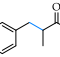
6.9.9 Analytic Methods for Screening


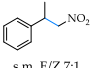
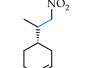
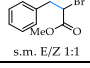
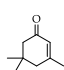
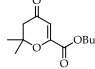
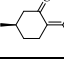
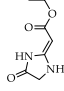
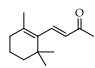
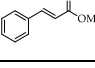
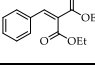
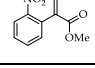
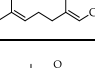
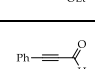
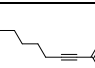
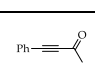

6.9.9.1 GC Measurements

GC analyses were performed by using Agilent GC7820A system with FID-detector (Heater 300 °C, H₂-Flow 30 mL/min, Air-Flow 400 mL/min, Makeup Flow 25 mL/min; Date Rate/ Min Peak width 50 Hz/0.004 min) with either a HP-5 column (30 m x 0.25 mm x 0.25 μm), a chiral BGB-178 column (30 m x 0.25 mm x 0.25 μm), a CP-Chirasil DEX CB (25 m x 0.32 mm x 0.25 μm) or a Lipodex-G column as specified in Table 23. The enantiomeric excess (*ee*) was determined by GC analysis. HR-ESI and HR-APCI mass spectra were acquired with a LTQ-FT Ultra mass spectrometer (Thermo Fischer Scientific). The resolution was set to 100.000.

Table 23. Used GC programs to analyse reaction after extraction with ethyl acetate. Product peaks in achiral column were identified using authentic standard or GC/MS, *determined with reference substance.

Substance	Program	Retention time educt	Retention time product	Lit.
17b 	40:1, flow rate 8.33 mL /min, 80 °C, 2 °C/min to 86 °C (HP5)	1.92	1.23	
	20:1, flow rate 3.32 mL/min, 50 °C hold 10 min, 1.2 °C/min to 96 °C, 18 °C/min to 220 °C hold 3 min (BGB-178)	43.51	29.12 (R)* 30.18 (S)*	[67]
18b/30b 	70:1, flow rate 8.33 mL /min, 92 °C, 4 min (HP5)	3.72	2.87 trans 3.00 cis	
19b 	40:1, flow rate 8.33 mL /min, 60 °C, 2°C/min to 65 °C, 1 min (HP5)	3.11	2.42	
	5:1, 60 °C hold 5 min, 5 °C/min to 65 °C hold 30 min, 20 °C/min to 150 °C hold 5 min (BGB-178)	-	12.05 (S) 13.04 (R)	[152]
22b 	70:1, flow rate 8.33 mL /min, 87 °C, 3 min (HP5)	2.59	2.95	
	20:1, 80 °C, 1.2 °C/min to 95 °C, 20 °C/min to 220 °C hold 2 min (BGB-178)	10.85	11.93 (R)* 12.52 (S)	[73]
24b 	40:1, flow rate 3.36 mL/min, 60 °C, 2 °C/min to 65 °C hold 2.5 min (HP-5)	4.32	3.00	
	20:1, flow rate 3.32 mL /min, 80 °C 0.5 °C/min to 90 °C, 20 °C/min to 200 °C (Lipodex-G)	-	6.35 (R) 6.46 (S)	[67]
25b 	Splitless, flow rate 8.33 mL /min, 80 °C, 4 °C/min to 108 °C (HP5)	9.37	4.60	
	20:1, 80 °C, 1.2 °C/min to 170 °C, 20 °C/min to 220 °C hold 5 min (BGB-178)	20.96	18.54 (R) 18.96 (S)	[67]

26b	 s.m. rac	40:1, flow rate 8.33 mL /min, 80°C, 2 °C/min to 86 °C (HP5)	2.34	1.42	
		70:1, flow rate 3.07 mL/min, 70 °C hold 12 min, 10 °C/min to 200 °C hold 1 min (Lipodex-G)	11.10 (1) 12.25 (2)	4.00	
27b		40:1, flow rate 7.56 mL/min, 80 °C hold 3.5 min (HP-5)	2.38	1.57	
28b		40:1, flow rate 7.56 mL/min, 80 °C hold 10 min (HP-5)	6.49	4.08 4.19	
29b		40:1, flow rate 6.5 mL /min, 80 °C, 1 °C/min to 84 °C (HP-5)	1.42	1.15	
		25:1, flow rate 2.2 mL/min, 90 °C hold 2 min, 1 °C/min to 96 °C, 20 °C/min to 180 °C hold 4 min (Hydrodex-β-Tbac)	9.22	6.37 (R) 6.63 (S)	[73]
31b		30:1, flow rate 6.5 mL/min, 80°C hold 2min, 20°C/min to 92 °C, 30°C/min to 220 °C (HP-5)	2.39	2.08	
		25:1, flow rate 2.86 mL/min, 95 °C hold 15 min, 15 °C/min to 130 °C hold 3 min, 20 °C/min to 200 °C (Hydrodex-β-Tbac)	9.10	5.21 (S) 5.59 (R)	[198]
32b		30:1, flow rate 6.5 mL/min, 110 °C hold 2 min, 30 °C/min to 210 °C (HP-5)	4.16	4.43	
		<i>n</i> -hexane/2-propanol 90:10 at 0.8 mL/min (Chiralcel OD-H, HPLC)	-	25.68 (R)	[198]
33b		70:1, flow rate 8.33 mL /min 62 °C, 2 min (HP5)	1.67	1.20	
		50°C hold 10 min; 1.2 °C/min to 96 °C; 18 °C/min to 220 °C hold 3 min (BGB-178)	23.27	14.88 (R)* 16.81 (S)	
34b		70:1, flow rate 8.33 mL /min, 62 °C, 3 min (HP5)	2.33	1.24	
		70:1, flow rate 2.81 mL/min, 50 °C hold 10 min, 1.2 °C/min to 159 °C, 18 °C/min to 220 °C hold 3 min (BGB)	20.31	6.75 (R) 6.93 (S)	[67]
35b		70:1, flow rate 6.5 mL/min, 80 °C, 4 °C/min to 96 °C (HP-5)	4.27	2.80	
		70:1, flow rate 3.07 mL/min, 60 °C, 1.2 °C/min to 160 °C, 18 °C/min to 220 °C (Hydrodex-b-TBDAC)	86.06	64.61(S) 65.75(R)	[67]
36b		40:1, flow rate 8.33 mL /min, 80 °C, 3 min (HP5)	1.88	0.99	
37b		50:1, flow rate 8.33 mL /min, 40 °C hold 2 min, 20°C/min to 180 °C hold 1 min (HP5)	3.79 4.10	3.61	
		40:1, flow rate 8.33 mL /min, 97 °C, 5 min	3.02 3.54	1.92	
38b		20:1, 40 °C hold 2 min, 4 °C/min to 120 °C, hold 1 min, 20 °C/min to 180 °C, hold 3 min (Hydrodex-b-TBDAC)	-	19.88 (S)* 20.08 (R)*	
		20:1, flow rate 2 mL/min, 100 °C hold 2 min, 20 °C/min to 220 °C hold 5 min (HP-5)	4.92	4.02	
39b					

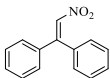
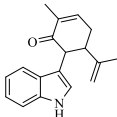
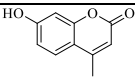
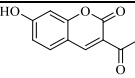
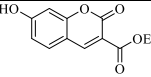
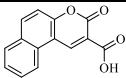
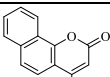
		100:1, flow rate 3 mL/min, 90 °C hold 30 min, 20 °C/min to 180 °C hold 1 min (Chirasil-DEX CB)	-	10.89 (S) 11.19 (R)	[149]
40b	 s.m. Z	20:1, flow rate 8.33 mL /min, 100 °C in 10°C/min to 160 °C (HP5)	5.22	4.26	
		20:1, flow rate 3.32 mL /min 140 °C hold 8 min, 50 °C/min to 200 °C (Lipodex-G)	7.02 (E) 7.75 (Z)	4.31	
41b	 s.m. E/Z 7:1	40:1, flow rate 8.33 mL /min, 110 °C, 2 °C/min to 120 °C (HP5)	3.36 (E) 4.41 (Z)	2.76	
		20:1, flow rate 3.32 mL /min 80 °C hold 8 min, 1 °C/min to 130 °C, 50 °C/min to 180 °C hold 2 min (Lipodex-G)	32.79 (E) 34.80 (Z)	29.12 (R) 29.50 (S)	[73]
42b	 s.m. E/Z 3:1	40:1, flow rate 8.33 mL /min, 110 °C, 3 °C/min to 134 °C (HP5)	3.97 5.85	4.36	
43b	 s.m. E/Z 1:1	20:1, flow rate 8.33 mL /min, 100 °C, 10 °C/min to 155 °C (HP5)	3.79 4.74	3.38	
44a		70:1, flow rate 8.33 mL /min, 83 °C, 3 min (HP5)	2.64	1.72*	
45a		30:1, flow rate 6.5 mL/min, 80 °C hold 2 min, 20 °C/min to 92 °C, 30 °C/min to 220 °C	5.50	-	
46a		70:1, flow rate 8.33 mL /min 80 °C, 3 °C/min to 100 °C (HP5)	4.47	-	
48a		40:1, flow rate 6.5 mL/min, 140 °C, 5 °C/min to 200 °C (HP-5)	4.26	-	
49a		70:1, flow rate 8.33 mL /min, 125 °C, 4 min (HP5)	3.52	2.72	
50a		20:1, flow rate 8.33 mL /min, 100 °C hold 0.5 min, 5 °C/min to 120 °C (HP5)	2.28 3.49	-	
51a		20:1, flow rate 8.33 mL /min, 180 °C hold 2 min (HP5)	1.51	-	
52a		70:1, flow rate 8.33 mL /min, 125 °C, 2 °C/min to 135 °C, 1 min (HP5)	5.00	-	
53a		40:1, flow rate 8.33 mL /min, 97 °C, 4 min (HP5)	2.75 3.29	-	
54a		70:1, flow rate 8.33 mL /min, 75 °C, 2.5 min (HP5)	1.35	-	
55a		70:1, flow rate 8.33 mL /min, 90 °C, 4 °C/min to 106 °C hold 1 min (HP5)	2.80	-	
56a		70:1, flow rate 8.33 mL /min, 80 °C, 2 °C/min to 90 °C, 1 min (HP5)	2.09	-	
57a		40:1, flow rate 8.33 mL /min, 90 °C, 4 °C/min to 122 °C (HP5)	3.94	-	

6.9.9.2 HPLC Measurements

HPLC analyses were performed on a SHIMAZU Prominence-i LC-2030C system equipped with a quaternary pump, autosampler, column oven and variable wavelength detector (254 nm) and analysed using LABSOLUTION Software.

All separations were performed at 25 °C, on a reversed-phase C18 column (AGILENT Eclipse XD8-C18, d = 4.6 mm, l = 150 mm, particle size 5 µm) in MeCN/water with 0.1% TFA with 10 µL injection volume. Method conditions and retention times are shown in Table 24.

Table 24. Used HPLC programs to analyse reaction after extraction with ethyl acetate. Product peaks in achiral column were identified using authentic standard or LC/MS, *determined with reference substance, (a) reduced product, (b) reduced and opened lactone product.

Substance	Program	Retention time educt	Retention time product	Lit.
 47a	50:50 MeCN/H ₂ O + 0.1%TFA for 15 min with 1 mL/min	7.25 min	-	
 69a	65:35 MeCN/H ₂ O for 9 min with 1 mL/min	6.71 min	7.47 min	
 11a	30:70 MeCN/H ₂ O + 0.1%TFA for 5.5 min with 1 mL/min	4.31 min	-	
 12a	50:50 MeCN/H ₂ O + 0.1%TFA for 5 min with 1 mL/min	2.25 min	1.40 min	
 13a	50:50 MeCN/H ₂ O + 0.1%TFA for 5 min with 1 mL/min	2.37 min	1.33 min (13b) 1.73 min (13c)	
 15a	50:50 MeCN/H ₂ O + 0.1%TFA for 5 min with 1 mL/min	3.33 min	1.40 min	
 16a	70:30 MeCN/H ₂ O + 0.1%TFA for 8 min with 1 mL/min	3.14 min	1.40 min	

6.10 Computational Methods and Details

Protein Model. The crystal structure of TsER in complex with p-hydroxybenzaldehyde (pdb 3HGJ)^[101] was used as the basis for the study. The C25D/I67T and C25G/I67T variants were generated on the basis of 3HGJ with the PyMOL Mutagenesis Wizard. The protein was prepared for docking using the Protein Preparation Wizard in the Maestro program, version 11.0, Schrödinger, LLC: New York, 2016-4. The 3HGJ crystal structure is a homodimer, where part of the B-chain, especially an arginine residue, interacts with the active site of the A-chain and vice versa. For all calculations the dimer structure was retained. Protonation states for titratable amino acids were assigned based on the most favorable interactions with neighboring residues and the PROPKA program. The His172 and His175 residues, which are believed to be important in the positioning of the substrate in the active site, were protonated at both the epsilon and delta nitrogen atoms, for the docking studies. All water molecules and co-crystallized ligands were removed, with the exception of the oxidized FMN cofactors. The oxidized FMN cofactor was converted to the reduced FMNH₂ using ANTECHAMBER.

Ligand Preparation. Substrates **11-57** were built in Maestro and prepared for docking using the LigPrep program, version 4.0, Schrödinger, LLC: New York, 2016.

Docking. Substrates **11-57** were docked into the active site of TsER wt, C25D/I67T and C25G/I67T using the rigid body docking (RBD) protocol with Standard Precision (SP) settings within the Schrödinger suite. Additionally, substrates **17a** was docked in the active site of TsER wt, C25D/I67T and C25G/I67T using the Induced fit docking (IFD) protocol within the Schrödinger suite.

Details of setup for Rigid Body Docking.

Glide SP uses a series of hierarchical filters, of the conformational, orientational and positional space, to search for possible locations of the ligand in the active site of a receptor. In this search, an initial rough positioning and scoring phase that dramati-

cally narrows the search space is followed by torsional flexible energy optimization on an OPLS3 nonbonded potential energy grid for a few hundred surviving candidate poses. Finally a small number of poses are minimized within the field of the receptor with full ligand flexibility via a Monte Carlo sampling of pose conformation.

Definitions of Interactions in Maestro:

Hydrogen bonds: The maximum donor-acceptor distance is 2.8 Å the minimum donor angle is 120.0°, and the minimum acceptor angle is 90.0°. These values are consistent with the default values that are used in Maestro.

Salt bridge: Salt bridges are defined by oppositely-charged atoms that are within 5 Å and are not directly hydrogen-bonded.

Pi-pi stacking: A pi-pi interaction is defined as an interaction between two aromatic rings in which either (a) the angle between the ring planes is less than 30° and the distance between the ring centroids is less than 4.4 Å (face-to-face), or (b) the angle between the ring planes is between 60° and 120° and the distance between the ring centroids is less than 5.5 Å (edge-to-face).

Pi-cation interaction: The maximum distance between the cation center and the ring center is 6.6 Å and the angle between the ring plane and the line between the cation center and the ring center does not deviate from the perpendicular by more than 30°.

Contacts: They are distance based with cutoff ratios of 0.89 for *bad* and 0.75 for *ugly* and exclude the H-bonds.

Details of setup for Induced Fit Docking Calculations.

The Induced Fit protocol begins by docking the ligand using Glide with Standard Precision (SP) settings using the OPLS3 force field. In order to generate a diverse ensemble of ligand poses, the procedure uses reduced van der Waals radii and an increased Coulomb-vdW cutoff, and can temporarily remove highly flexible side chains during the docking. For each pose, a Prime structure prediction is then used to accommodate the ligand by reorienting nearby side chains. The centroid of the RBD pose was used as the center of the search space. The box size for the receptor was automatically determined based on the size of the ligand. No constraints were ap-

plied to the docking poses. The ligand was permitted to sample ring conformations within a 2.5 kcal/mol window of the minimized geometry determined at the LigPrep setup stage. The maximum number of poses allowed during the initial RBD stage was set to 20, and van der Waals scaling of the receptor and ligand was set to 0.5. During the Prime refinement stage, the conformations of the side chain residues within 5.0 Å of the ligand poses were optimized. During the rigid redocking phase, the substrate was redocked into the receptor structures that were within 30 kcal/mol of the lowest energy structure with SP settings. A total of 19 ligand:receptor conformations were generated for **17a:wt** (Table 30), **17a:C25G/I67T** (Table 31) and 16 for **17a:C25D/I67T** (Table 32) The quoted IFD scores are a linear combination of the Glide GScore and $0.05 \times$ the Prime energy of the minimized protein conformation.

Molecular Dynamics Simulations. Molecular dynamics (MD) simulations were carried out in AMBER16^[350] using the ff99SB force field.^[351] Parameters for the ligand **17a** were assigned from the generalized AMBER force field (GAFF)^[352] using Antechamber to assign partial atomic charges. The protonation states of titratable residues were estimated using PROPKA^[276], and the enzymes were solvated in an cubic box of TIP3P water molecules^[353] with a buffer of at least 12 Å surrounding the protein. The charge of each model was neutralized by the addition of sodium ions.

The setup of the model consisted of the following: (i) minimization of the positions of the hydrogen atoms (all heavy atoms fixed); (ii) minimization of the solvent (with all protein heavy atoms fixed); (iii) energy minimization of the entire system with positional restraints of $5 \text{ kcal/mol} \cdot \text{Å}^2$ applied to all C_α atoms; (iv) canonical ensemble (NVT) thermalisation to 300 K over 20 ps with positional restraints of $5 \text{ kcal/mol} \cdot \text{Å}^2$ on C_α atoms; (v) 140 ps of NPT equilibration with decreasing restraints on the C_α atoms; (vii) 100 ns production simulation. MD simulations were carried out on GPUs using the PMEMD code^[354] of AMBER16.^[350]

Average linkage hierarchical clustering (after alignment of structures based on positions of active site residues) was carried out using the CPPTRAJ utility of

AMBERTOOLS16^[350] to identify representative structures of the ternary complex over the course of the simulations.

WaterSwap calculations. WaterSwap^[279] calculations were performed using the WSRC module in Sire^[355], with calculations using the same force field parameters and solvent model as the dynamics simulations. WaterSwap calculation for TsER wt used starting structures taken from the 100 ns MD trajectories. Absolute binding free energies were calculated using replica-exchange thermodynamic integration^[356] over 16 λ windows (0.005, 0.071, 0.137, 0.203, 0.269, 0.335, 0.401, 0.467, 0.533, 0.599, 0.665, 0.731, 0.797, 0.863, 0.929, 0.995) over the WaterSwap reaction coordinate. Thirty million Monte Carlo moves were performed for each window, with the free energy gradient averaged over the last 20 million steps. Simulations used the “Set A” soft-core parameters^[279], with a 15 Å coulomb and Lennard Jones non-bonded cut-off, the shifted-force cut-off^[357] used to account for long-range electrostatics, and a reflection sphere used to constrain sampling to within a 15 Å radius of the ligand.

Constant pH Molecular Dynamics.^[278] Hydrogens were added to the structure (pdb 3HGJ) using the LEaP module and force field ff10 of AMBER.^[350] The structure was then minimized to relax bad contacts by using GB model in AMBER with a salt concentration of 0.1 M and a total number of 1000 minimization cycles. A restraint with a force constant of $k=10 \text{ kcal/mol}\cdot\text{Å}^2$ was applied to the atoms of the protein backbone. The model was heated slowly from 10K to 300 K, keeping the restraints on the backbone atoms.

Simulations starting from the TsER C25D/I67T structure were performed at pH 7.4 with residues D25, H172, H175 and Y177 allowed to change protonation state. There were 10 ns between Monte Carlo steps. Monte Carlo sampling was used to select protonation states based on calculated energy differences between the possible protonation states.^[278] The program *cphstats* in AMBER was used to evaluate the data.

7 REFERENCES

- [1] W. S. Knowles, *Asymmetric hydrogenation*, *Acc. Chem. Res.* **1983**, *16*, 106–112.
- [2] W. S. Knowles, *Asymmetric Hydrogenations (Nobel Lecture)*, *Angew. Chem. Int. Ed.* **2002**, *41*, 1998–2007.
- [3] R. Noyori, *Asymmetric Catalysis: Science and Opportunities (Nobel Lecture)*, *Angew. Chem. Int. Ed.* **2002**, *41*, 2008–2022.
- [4] K. B. Sharpless, *Searching for New Reactivity (Nobel Lecture)*, *Angew. Chem. Int. Ed.* **2002**, *41*, 2024–2032.
- [5] Y. Yanto, Dissertation, *Evaluation of novel enoate reductases as potential biocatalyst for enantiomerically pure compound synthesis*, Georgia Institute of Technology, **2011**.
- [6] J. G. de Vries, Ed, *Stereoselective Synthesis 1: Hydrogenation of Carbon-Carbon Double Bonds*; Thieme, Stuttgart, **2011**.
- [7] D. H. Woodmansee, A. Pfaltz, *Asymmetric hydrogenation of alkenes lacking coordinating groups*, *Chem. Commun. (Camb)* **2011**, *47*, 7912–7916.
- [8] D. G. Blackmond, A. Lightfoot, A. Pfaltz, T. Rosner, P. Schnider, N. Zimmermann, *Enantioselective hydrogenation of olefins with phosphinooxazoline-iridium catalysts*, *Chirality* **2000**, *12*, 442–449.
- [9] X. Cui, K. Burgess, *Catalytic homogeneous asymmetric hydrogenations of largely unfunctionalized alkenes*, *Chem. Rev.* **2005**, *105*, 3272–3296.
- [10] J. W. Yang, M. Hechavarría Fonseca, N. Vignola, B. List, *Metal-free, organocatalytic asymmetric transfer hydrogenation of α,β -unsaturated aldehydes*, *Angew. Chem. Int. Ed.* **2004**, *44*, 108–110.
- [11] A. Scholtissek, D. Tischler, A. Westphal, W. van Berkel, C. Paul, *Old Yellow Enzyme-Catalysed Asymmetric Hydrogenation*, *Catalysts* **2017**, *7*, 130.
- [12] M. Breuer, K. Ditrach, T. Habicher, B. Hauer, M. Kessler, R. Stürmer, T. Zelinski, *Industrial methods for the production of optically active intermediates*, *Angew. Chem. Int. Ed. Engl.* **2004**, *43*, 788–824.
- [13] W. H. de Camp, *The FDA perspective on the development of stereoisomers*, *Chirality* **1989**, *1*, 2–6.
- [14] N. B. Johnson, I. C. Lennon, P. H. Moran, J. A. Ramsden, *Industrial-scale synthesis and applications of asymmetric hydrogenation catalysts*, *Acc. Chem. Res.* **2007**, *40*, 1291–1299.
- [15] M. J. Burk, F. Bienewald, S. Challenger, A. Derrick, J. A. Ramsden, *Me-DuPHOS-Rh-Catalyzed Asymmetric Synthesis of the Pivotal Glutarate Intermediate for Candoxatril*, *J. Org. Chem.* **1999**, *64*, 3290–3298.
- [16] I. C. Lennon, C. J. Pilkington, *The Application of Asymmetric Hydrogenation for the Manufacture of Pharmaceutical Intermediates: The Need for Catalyst Diversity*, *Synthesis* **2003**, *11*, 1639–1642.
- [17] M. J. Burk, P. D. de Koning, T. M. Grote, M. S. Hoekstra, G. Hoge, R. A. Jennings, W. S. Kissel, T. V. Le, I. C. Lennon, T. A. Mulhern, J. A. Ramsden, R. A. Wade, *An enantioselective synthesis of (S)-(+)-3-aminomethyl-5-methylhexanoic acid via asymmetric hydrogenation*, *J. Org. Chem.* **2003**, *68*, 5731–5734.
- [18] T. Nogrady, D. F. Weaver, *Medicinal chemistry: A molecular and biochemical approach*; Oxford University Press, New York, N.Y., **2005**.
- [19] J. W. Yang, M. Hechavarría Fonseca, N. Vignola, B. List, *Metal-Free, Organocatalytic Asymmetric Transfer Hydrogenation of α,β -Unsaturated Aldehydes*, *Angew. Chem. Int. Ed.* **2005**, *117*, 110–112.
- [20] T. Breiding, J. Henker, C. Fu, Y. Xiang, S. Glöckner, P. Hofmann, K. Harms, E. Meggers, *Synthesis and Functionalization of Hexacoordinate (Arenediolato)bis(polypyridyl)silicon(IV) Complexes*, *Eur. J. Inorg. Chem.* **2014**, *2014*, 2924–2933.
- [21] H.-P. Meyer, O. Ghisalba, J. E. Leresche, *Biotransformations and the Pharma Industry in Handbook of Green Chemistry*, Wiley-VCH Verlag GmbH & Co. KGaA, **2010**.
- [22] F. Hollmann, I. W. C. E. Arends, D. Holtmann, *Enzymatic reductions for the chemist*, *Green Chem.* **2011**, *13*, 2285.

- [23] K. Faber, W.-D. Fessner, N. Turner, *Science of synthesis: Biocatalysis in organic synthesis 2*; Georg Thieme Verlag KG, Stuttgart, **2015**.
- [24] K. Faber, *Biotransformations in Organic Chemistry*; Springer Berlin Heidelberg, Berlin, Heidelberg, **2000**.
- [25] S. Martínez Cuesta, S. A. Rahman, N. Furnham, J. M. Thornton, *The Classification and Evolution of Enzyme Function*, *Biophys. J.* **2015**, *109*, 1082–1086.
- [26] H. Lodish, *Molecular cell biology: Section 3.3, Functional Design of Proteins.*; Freeman, New York, NY, **2002**.
- [27] D. R. Headon, G. Walsh, *The Industrial Production Of Enzymes*, *Biotechnol. Adv.* **1994**, *12*, 635–646.
- [28] K. Faber, W.-D. Fessner, N. Turner, *Science of synthesis: Biocatalysis in organic synthesis 1-3*; Georg Thieme, Stuttgart, **2015**.
- [29] M. F. Perutz, M. G. Rossmann, A. F. Cullis, H. Muirhead, G. Will, A. C. T. North, *Structure of Hæmoglobin*, *Nature* **1960**, *185*, 416–422.
- [30] J. C. Kendrew, G. Bodo, H. M. Dintzis, R. G. Parrish, H. Wyckoff, D. C. Phillips, *A Three-Dimensional Model of the Myoglobin Molecule Obtained by X-Ray Analysis*, *Nature* **1958**, *181*, 662–666.
- [31] G. Steinkellner, C. C. Gruber, T. Pavkov-Keller, A. Binter, K. Steiner, C. Winkler, A. Lyskowski, O. Schwamberger, M. Oberer, H. Schwab, K. Faber, P. Macheroux, K. Gruber, *Identification of promiscuous ene-reductase activity by mining structural databases using active site constellations*, *Nat Comms* **2014**, *5*, 4150.
- [32] C. M. Clouthier, J. N. Pelletier, *Expanding the organic toolbox: a guide to integrating biocatalysis in synthesis*, *Chem. Soc. Rev.* **2012**, *41*, 1585–1605.
- [33] S. Wenda, S. Illner, A. Mell, U. Kragl, *Industrial biotechnology—the future of green chemistry?*, *Green Chem.* **2011**, *13*, 3007.
- [34] J.-M. Choi, S.-S. Han, H.-S. Kim, *Industrial applications of enzyme biocatalysis: Current status and future aspects*, *Biotechnol. Adv.* **2015**, *33*, 1443–1454.
- [35] M. T. Reetz, *Biocatalysis in organic chemistry and biotechnology: past, present, and future*, *J. Am. Chem. Soc.* **2013**, *135*, 12480–12496.
- [36] U. T. Bornscheuer, G. W. Huisman, R. J. Kazlauskas, S. Lutz, J. C. Moore, K. Robins, *Engineering the third wave of biocatalysis*, *Nature* **2012**, *485*, 185–194.
- [37] R. J. Kazlauskas, U. T. Bornscheuer, *Finding better protein engineering strategies*, *Nat. Chem. Biol.* **2009**, *5*, 526–529.
- [38] K. L. Morley, R. J. Kazlauskas, *Improving enzyme properties: when are closer mutations better?*, *Trends Biotechnol.* **2005**, *23*, 231–237.
- [39] A. Airaksinen, T. Hovi, *Modified base compositions at degenerate positions of a mutagenic oligonucleotide enhance randomness in site-saturation mutagenesis*, *Nucleic Acids Res.* **1998**, *26*, 576–581.
- [40] M. T. Reetz, A. Zonta, K. Schimossek, K.-E. Jaeger, K. Liebeton, *Creation of Enantioselective Biocatalysts for Organic Chemistry by In Vitro Evolution*, *Angew. Chem. Int. Ed. Engl.* **1997**, *36*, 2830–2832.
- [41] C. Neylon, *Chemical and biochemical strategies for the randomization of protein encoding DNA sequences: library construction methods for directed evolution*, *Nucleic Acids Res.* **2004**, *32*, 1448–1459.
- [42] J. D. Bloom, S. T. Labthavikul, C. R. Otey, F. H. Arnold, *Protein stability promotes evolvability*, *Proc. Natl. Acad. Sci. USA* **2006**, *103*, 5869–5874.
- [43] D. M. Weinreich, N. F. Delaney, M. A. Depristo, D. L. Hartl, *Darwinian evolution can follow only very few mutational paths to fitter proteins*, *Science* **2006**, *312*, 111–114.
- [44] M. T. Reetz, J. Sanchis, *Constructing and analyzing the fitness landscape of an experimental evolutionary process*, *ChemBioChem* **2008**, *9*, 2260–2267.
- [45] M. T. Reetz, J. D. Carballeira, A. Vogel, *Iterative saturation mutagenesis on the basis of B factors as a strategy for increasing protein thermostability*, *Angew. Chem. Int. Ed.* **2006**, *45*, 7745–7751.
- [46] M. T. Reetz, D. Kahakeaw, R. Lohmer, *Addressing the Numbers Problem in Directed Evolution*, *ChemBioChem* **2008**, *9*, 1797–1804.

- [47] R. J. Fox, S. C. Davis, E. C. Mundorff, L. M. Newman, V. Gavrilovic, S. K. Ma, L. M. Chung, C. Ching, S. Tam, S. Muley, J. Grate, J. Gruber, J. C. Whitman, R. A. Sheldon, G. W. Huisman, *Improving catalytic function by ProSAR-driven enzyme evolution*, *Nat. Biotechnol.* **2007**, *25*, 338–344.
- [48] A. S. Bommarius, J. K. Blum, M. J. Abrahamson, *Status of protein engineering for biocatalysts: how to design an industrially useful biocatalyst*, *Curr. Opin. Chem. Biol.* **2011**, *15*, 194–200.
- [49] G. A. Behrens, A. Hummel, S. K. Padhi, S. Schätzle, U. T. Bornscheuer, *Discovery and Protein Engineering of Biocatalysts for Organic Synthesis*, *Adv. Synth. Catal.* **2011**, *353*, 2191–2215.
- [50] U. T. Bornscheuer, M. Pohl, *Improved biocatalysts by directed evolution and rational protein design*, *Curr. Opin. Chem. Biol.* **2001**, *5*, 137–143.
- [51] H. Yang, L. Liu, J. Li, J. Chen, G. Du, *Rational Design to Improve Protein Thermostability: Recent Advances and Prospects*, *ChemBioEng Rev.* **2015**, *2*, 87–94.
- [52] A. Seifert, S. Vomund, K. Grohmann, S. Kriening, V. B. Urlacher, S. Laschat, J. Pleiss, *Rational design of a minimal and highly enriched CYP102A1 mutant library with improved regio-, stereo- and chemoselectivity*, *ChemBioChem* **2009**, *10*, 853–861.
- [53] D. F. A. R. Dourado, S. Pohle, A. T. P. Carvalho, D. S. Dheeman, J. M. Caswell, T. Skvortsov, I. Miskelly, R. T. Brown, D. J. Quinn, C. C. R. Allen, L. Kulakov, M. Huang, T. S. Moody, *Rational Design of a (S)-Selective-Transaminase for Asymmetric Synthesis of (1S)-1-(1,1'-biphenyl-2-yl)ethanamine*, *ACS Catal.* **2016**, *6*, 7749–7759.
- [54] M. T. Reetz, K.-E. Jaeger, *Biocatalysis-From Discovery to Application: Superior Biocatalysts by Directed Evolution*; Springer, **1999**.
- [55] F. H. Arnold, A. A. Volkov, *Directed evolution of biocatalysts*, *Curr. Opin. Chem. Biol.* **1999**, 54–59.
- [56] U. T. Bornscheuer, *Directed Evolution of Enzymes*, *Angew. Chem. Int. Ed.* **1998**, 3105–3108.
- [57] C. Acevedo-Rocha, S. Hoebenreich, M. Reetz, *Iterative Saturation Mutagenesis: A Powerful Approach to Engineer Proteins by Systematically Simulating Darwinian Evolution in Directed Evolution Library Creation*, *Methods in Molecular Biology*; (Eds. E. M. Gillam, J. N. Copp, D. Ackerley), Springer New York, **2014**, 103–128.
- [58] M. T. Reetz, J. D. Carballeira, *Iterative saturation mutagenesis (ISM) for rapid directed evolution of functional enzymes*, *Nat. Protoc.* **2007**, *2*, 891–903.
- [59] E. Vázquez-Figueroa, J. Chaparro-Riggers, A. S. Bommarius, *Development of a thermostable glucose dehydrogenase by a structure-guided consensus concept*, *ChemBioChem* **2007**, *8*, 2295–2301.
- [60] K. Steiner, H. Schwab, *Recent advances in rational approaches for enzyme engineering*, *Comput Struct Biotechnol J* **2012**, *2*, e201209010.
- [61] H. S. Toogood, J. M. Gardiner, N. S. Scrutton, *Biocatalytic Reductions and Chemical Versatility of the Old Yellow Enzyme Family of Flavoprotein Oxidoreductases*, *ChemCatChem* **2010**, *2*, 892–914.
- [62] R. E. Williams, N. C. Bruce, 'New uses for an Old Enzyme'—the Old Yellow Enzyme family of flavoenzymes, *Microbiology* **2002**, *148*, 1607–1614.
- [63] K. Saito, D. J. Thiele, M. Davio, O. Lockridge, V. Massey, *The cloning and expression of a gene encoding Old Yellow Enzyme from *Saccharomyces carlsbergensis**, *J. Biol. Chem.* **1991**, *266*, 20720–20724.
- [64] A. S. Abramovitz, V. Massey, *Purification of Intact Old Yellow Enzyme Using Affinity Matrix for the Sole Chromatographic Step*, *J. Biol. Chem.* **1976**, *251*, 5321–5326.
- [65] B. V. Adalbjörnsson, H. S. Toogood, A. Fryszkowska, C. R. Pudney, T. A. Jowitt, D. Leys, N. S. Scrutton, *Biocatalysis with Thermostable Enzymes: Structure and Properties of a Thermophilic 'ene'-Reductase related to Old Yellow Enzyme*, *ChemBioChem* **2010**, *11*, 197–207.
- [66] A. Brigé, D. van den Hemel, W. Carpentier, L. de Smet, J. J. van Beeumen, *Comparative characterization and expression analysis of the four Old Yellow Enzyme homologues from *Shewanella oneidensis* indicate differences in physiological function*, *Biochem. J.* **2006**, *394*, 335–344.
- [67] D. J. Bougioukou, S. Kille, A. Taglieber, M. T. Reetz, *Directed Evolution of an Enantioselective Enoate-Reductase: Testing the Utility of Iterative Saturation Mutagenesis*, *Adv. Synth. Catal.* **2009**, *351*, 3287–3305.
- [68] D. S. Blehert, B. G. Fox, G. H. Chambliss, *Cloning and sequence analysis of two *Pseudomonas* flavoprotein xenobiotic reductases*, *J. Bacteriol.* **1999**, *181*, 6254–6263.

- [69] T. Barna, H. L. Messiha, C. Petosa, N. C. Bruce, N. S. Scrutton, P. C. E. Moody, *Crystal structure of bacterial morphinone reductase and properties of the C191A mutant enzyme*, *J. Biol. Chem.* **2002**, *277*, 30976–30983.
- [70] M. Bühler, H. Giesel, W. Tischer, H. Simon, *Occurrence and the possible physiological role of 2-enoate reductases*, *FEBS Letters* **1980**, *109*, 244–246.
- [71] R. Stuermer, B. Hauer, M. Hall, K. Faber, *Asymmetric bioreduction of activated C=C bonds using enoate reductases from the old yellow enzyme family*, *Curr. Opin. Chem. Biol.* **2007**, *11*, 203–213.
- [72] T. Hirata, K. Shimoda, T. Gondai, *Asymmetric Hydrogenation of the C-C Double Bond of Enones with the Reductases from *Nicotiana tabacum**, *Chem. Lett.* **2000**, 850–851.
- [73] M. Hall, C. Stueckler, H. Ehammer, E. Pointner, G. Oberdorfer, K. Gruber, B. Hauer, R. Stuermer, W. Kroutil, P. Macheroux, K. Faber, *Asymmetric Bioreduction of C=C Bonds using Enoate Reductases OPR1, OPR3 and YqjM: Enzyme-Based Stereocontrol*, *Adv. Synth. Catal.* **2008**, *350*, 411–418.
- [74] M. Hall, C. Stueckler, W. Kroutil, P. Macheroux, K. Faber, *Asymmetric bioreduction of activated alkenes using cloned 12-oxophytodienoate reductase isoenzymes OPR-1 and OPR-3 from *Lycopersicon esculentum* (tomato): a striking change of stereoselectivity*, *Angew. Chem. Int. Ed.* **2007**, *46*, 3934–3937.
- [75] T. Hirata, A. Matsushima, Y. Sato, T. Iwasaki, H. Nomura, T. Watanabe, S. Toyoda, S. Izumi, *Stereo-specific hydrogenation of the CC double bond of enones by *Escherichia coli* overexpressing an enone reductase of *Nicotiana tabacum**, *J. Mol. Catal. B: Enzym.* **2009**, *59*, 158–162.
- [76] A. Matsushima, Y. Sato, M. Otsuka, T. Watanabe, H. Yamamoto, T. Hirata, *An enone reductase from *Nicotiana tabacum**, *Bioorg. Chem.* **2008**, *36*, 23–28.
- [77] C. K. Winkler, C. Stueckler, N. J. Mueller, D. Pressnitz, K. Faber, *Asymmetric Synthesis of O-Protected Acyloins Using Enoate Reductases: Stereochemical Control through Protecting Group Modification*, *Eur. J. Org. Chem.* **2010**, *2010*, 6354–6358.
- [78] A. Taglieber, F. Schulz, F. Hollmann, M. Rusek, M. T. Reetz, *Light-driven biocatalytic oxidation and reduction reactions: scope and limitations*, *ChemBioChem* **2008**, *9*, 565–572.
- [79] E. Burda, M. Kraußer, G. Fischer, W. Hummel, F. Müller-Uri, W. Kreis, H. Gröger, *Recombinant $\Delta^{4,5}$ -Steroid 5 β -Reductases as Biocatalysts for the Reduction of Activated C=C-Double Bonds in Monocyclic and Acyclic Molecules*, *Adv. Synth. Catal.* **2009**, *351*, 2787–2790.
- [80] K. Shimoda, N. Kubota, H. Hamada, *Asymmetric reduction of α,β -unsaturated carbonyl compounds with reductases from *Nicotiana tabacum**, *Tetrahedron: Asymmetry* **2004**, *15*, 2443–2446.
- [81] C. Stueckler, N. J. Mueller, C. K. Winkler, S. M. Glueck, K. Gruber, G. Steinkellner, K. Faber, *Bioreduction of alpha-methylcinnamaldehyde derivatives: chemo-enzymatic asymmetric synthesis of Lilial and Helional*, *Dalton Trans.* **2010**, *39*, 8472–8476.
- [82] F. Schaller, E. W. Weiler, *Molecular Cloning and Characterization of 12-Oxophytodienoate Reductase, an Enzyme of the Octadecanoid Signaling Pathway from *Arabidopsis thaliana**, *J. Biol. Chem.* **1997**, *272*, 28066–28072.
- [83] K. Shimoda, N. Kubota, H. Hamada, M. Kaji, T. Hirata, *Asymmetric reduction of enones with *Synechococcus* sp. PCC 7942*, *Tetrahedron: Asymmetry* **2004**, *15*, 1677–1679.
- [84] D. J. Bougioukou, A. Z. Walton, J. D. Stewart, *Towards preparative-scale, biocatalytic alkene reductions*, *Chem. Commun.* **2010**, *46*, 8558–8560.
- [85] M. Hall, C. Stueckler, B. Hauer, R. Stuermer, T. Friedrich, M. Breuer, W. Kroutil, K. Faber, *Asymmetric Bioreduction of Activated C=C Bonds Using *Zymomonas mobilis* NCR Enoate Reductase and Old Yellow Enzymes OYE 1–3 from Yeasts*, *Eur. J. Org. Chem.* **2008**, *2008*, 1511–1516.
- [86] J. F. Chaparro-Riggers, T. A. Rogers, E. Vazquez-Figueroa, K. M. Polizzi, A. S. Bommarius, *Comparison of Three Enoate Reductases and their Potential Use for Biotransformations*, *Adv. Synth. Catal.* **2007**, *349*, 1521–1531.
- [87] J. Z. Cheng, C. M. Coyle, D. G. Panaccione, S. E. O'Connor, *A role for Old Yellow Enzyme in ergot alkaloid biosynthesis*, *J. Am. Chem. Soc.* **2010**, *132*, 1776–1777.
- [88] M. Kataoka, A. Kotaka, R. Thiwthong, M. Wada, S. Nakamori, S. Shimizu, *Cloning and overexpression of the old yellow enzyme gene of *Candida macedoniensis*, and its application to the production of a chiral compound*, *J. Biotechnol.* **2004**, *114*, 1–9.

- [89] A. Müller, R. Stürmer, B. Hauer, B. Rosche, *Stereospecific Alkyne Reduction*, *Angew. Chem. Int. Ed.* **2007**, *46*, 3316–3318.
- [90] Y. S. Niino, S. Chakraborty, B. J. Brown, V. Massey, *A New Old Yellow Enzyme of Saccharomyces cerevisiae*, *J. Biol. Chem.* **1995**, *270*, 1983–1991.
- [91] S. K. Padhi, D. J. Bougioukou, J. D. Stewart, *Site-saturation mutagenesis of tryptophan 116 of Saccharomyces pastorianus old yellow enzyme uncovers stereocomplementary variants*, *J. Am. Chem. Soc.* **2009**, *131*, 3271–3280.
- [92] D. J. Bougioukou, J. D. Stewart, *Opposite stereochemical courses for enzyme-mediated alkene reductions of an enantiomeric substrate pair*, *J. Am. Chem. Soc.* **2008**, *130*, 7655–7658.
- [93] B. Kosjek, F. J. Fleitz, P. G. Dormer, J. T. Kuethe, P. N. Devine, *Asymmetric bioreduction of α,β -unsaturated nitriles and ketones*, *Tetrahedron: Asymmetry* **2008**, *19*, 1403–1406.
- [94] K. Kitzing, T. B. Fitzpatrick, C. Wilken, J. Sawa, G. P. Bourenkov, P. Macheroux, T. Clausen, *The 1.3 Å crystal structure of the flavoprotein YqjM reveals a novel class of Old Yellow Enzymes*, *J. Biol. Chem.* **2005**, *280*, 27904–27913.
- [95] T. B. Fitzpatrick, N. Amrhein, P. Macheroux, *Characterization of YqjM, an Old Yellow Enzyme homolog from Bacillus subtilis involved in the oxidative stress response*, *J. Biol. Chem.* **2003**, *278*, 19891–19897.
- [96] H. Sobajima, M. Takeda, M. Sugimori, N. Kobashi, K. Kiribuchi, E.-M. Cho, C. Akimoto, T. Yamaguchi, E. Minami, N. Shibuya, F. Schaller, E. W. Weiler, T. Yoshihara, H. Nishida, H. Nojiri, T. Omori, M. Nishiyama, H. Yamane, *Cloning and characterization of a jasmonic acid-responsive gene encoding 12-oxophytodienoic acid reductase in suspension-cultured rice cells*, *Planta* **2003**, *216*, 692–698.
- [97] W. Li, A. Cowley, M. Uludag, T. Gur, H. McWilliam, S. Squizzato, Y. M. Park, N. Buso, R. Lopez, *The EMBL-EBI bioinformatics web and programmatic tools framework*, *Nucleic Acids Res.* **2015**, *43*, W580–W584.
- [98] T. M. Barna, H. Khan, N. C. Bruce, I. Barsukov, N. S. Scrutton, P. C. Moody, *Crystal structure of pentaerythritol tetranitrate reductase: “flipped” binding geometries for steroid substrates in different redox states of the enzyme*, *J. Mol. Biol.* **2001**, *310*, 433–447.
- [99] S. Litthauer, S. Gargiulo, E. van Heerden, F. Hollmann, D. J. Opperman, *Heterologous expression and characterization of the ene-reductases from Deinococcus radiodurans and Ralstonia metallidurans*, *J. Mol. Catal. B: Enzym.* **2014**, *99*, 89–95.
- [100] K. M. Fox, P. Karplus, *Old yellow enzyme at 2 Å resolution: overall structure, ligand binding, and comparison with related flavoproteins*, *Structure* **1994**, *2*, 1089–1105.
- [101] D. J. Opperman, B. T. Sewell, D. Litthauer, M. N. Isupov, J. A. Littlechild, E. van Heerden, *Crystal structure of a thermostable old yellow enzyme from Thermus scotoductus SA-01*, *Biochem. Biophys. Res. Commun.* **2010**, *393*, 426–431.
- [102] P. A. Karplus, K. M. Fox, V. Massey, *Flavoprotein structure and mechanism. 8. Structure-function relations for old yellow enzyme*, *The FASEB Journal* **1995**, *9*, 1518–1526.
- [103] D. Xu, R. M. Kohli, V. Massey, *The role of threonine 37 in flavin reactivity of the old yellow enzyme*, *Proc. Natl. Acad. Sci. USA* **1999**, *96*, 3556–3561.
- [104] C. R. Pudney, S. Hay, N. S. Scrutton, *Bipartite recognition and conformational sampling mechanisms for hydride transfer from nicotinamide coenzyme to FMN in pentaerythritol tetranitrate reductase*, *FEBS J.* **2009**, *276*, 4780–4789.
- [105] B. J. Brown, J.-W. Hyun, S. Duvvuri, P. A. Karplus, V. Massey, *The role of glutamine 114 in old yellow enzyme*, *J. Biol. Chem.* **2002**, *277*, 2138–2145.
- [106] V. Massey, L. M. Schopfer, *Reactivity of old yellow enzyme with alpha-NADPH and other pyridine nucleotide derivatives*, *J. Biol. Chem.* **1986**, *261*, 1215–1222.
- [107] J. Basran, R. J. Harris, M. J. Sutcliffe, N. S. Scrutton, *H-tunneling in the Multiple H-transfers of the Catalytic Cycle of Morphinone Reductase and in the Reductive Half-reaction of the Homologous Pentaerythritol Tetranitrate Reductase*, *J. Biol. Chem.* **2003**, *278*, 43973–43982.
- [108] T. Knaus, C. E. Paul, C. W. Levy, S. de Vries, F. G. Mutti, F. Hollmann, N. S. Scrutton, *Better than Nature: Nicotinamide Biomimetics That Outperform Natural Coenzymes*, *J. Am. Chem. Soc.* **2016**, *138*, 1033–1039.

- [109] N. J. Mueller, C. Stueckler, B. Hauer, N. Baudendistel, H. Housden, N. C. Bruce, K. Faber, *The Substrate Spectra of Pentaerythritol Tetranitrate Reductase, Morphinone Reductase, N -Ethylmaleimide Reductase and Estrogen-Binding Protein in the Asymmetric Bioreduction of Activated Alkenes*, *Adv. Synth. Catal.* **2010**, 352, 387–394.
- [110] K. Durchschein, M. Hall, K. Faber, *Unusual reactions mediated by FMN-dependent ene- and nitro-reductases*, *Green Chem.* **2013**, 15, 1764.
- [111] M. W. Fraaije, W. J. van Berkel, J. A. Benen, J. Visser, A. Mattevi, *A novel oxidoreductase family sharing a conserved FAD-binding domain*, *Trends Biochem. Sci.* **1998**, 23, 206–207.
- [112] M. W. Fraaije, R. H. H. van den Heuvel, W. J. H. van Berkel, A. Mattevi, *Covalent Flavinylation Is Essential for Efficient Redox Catalysis in Vanillyl-alcohol Oxidase*, *J. Biol. Chem.* **1999**, 274, 35514–35520.
- [113] S. O. Mansoorabadi, C. J. Thibodeaux, H.-W. Liu, *The diverse roles of flavin coenzymes — nature’s most versatile thespians*, *J. Org. Chem.* **2007**, 72, 6329–6342.
- [114] C. Lin, D. E. Robertson, M. Ahmad, A. A. Raibekas, M. S. Jorns, P. L. Dutton, A. R. Cashmore, *Association of Flavin Adenine Dinucleotide with the Arabidopsis Blue Light Receptor CRY1*, *Science* **1995**, 269, 968–970.
- [115] P. Müller, M. Ahmad, *Light-activated cryptochrome reacts with molecular oxygen to form a flavin-superoxide radical pair consistent with magnetoreception*, *J. Biol. Chem.* **2011**, 286, 21033–21040.
- [116] E. Brenna, G. Fronza, C. Fuganti, F. Parmeggiani, *Investigation of the stereochemical course of ene reductase-catalysed reactions by deuterium labelling*, *Isotopes Environ. Health Stud.* **2015**, 51, 1–9.
- [117] E. Brenna, F. G. Gatti, A. Manfredi, D. Monti, F. Parmeggiani, *Steric Effects on the Stereochemistry of Old Yellow Enzyme-Mediated Reductions of Unsaturated Diesters: Flipping of the Substrate within the Enzyme Active Site Induced by Structural Modifications*, *Adv. Synth. Catal.* **2012**, 354, 2859–2864.
- [118] R. M. Kohli, *The Oxidative Half-reaction of Old Yellow Enzyme. The Role Of Tyrosine 196*, *J. Biol. Chem.* **1998**, 273, 32763–32770.
- [119] H. Theorell, K. Yagi, G. D. Ludwig, F. Egami, *Effect of Flavin Monosulphate on Old Yellow Enzyme*, *Nature* **1957**, 180, 922–923.
- [120] S. Servi, *Baker’s Yeast as a Reagent in Organic Synthesis*, *Synthesis* **1990**, 1990, 1–25.
- [121] R. Csuk, B. I. Glaenger, *Baker’s yeast mediated transformations in organic chemistry*, *Chem. Rev.* **1991**, 91, 49–97.
- [122] G. Fogliato, G. Fronza, C. Fuganti, S. Lanati, R. Rallo, R. Rigoni, S. Servi, *Baker’s yeast reduction of arylidenecycloalkanones*, *Tetrahedron* **1995**, 51, 10231–10240.
- [123] P. Gramatica, P. Manitto, D. Monti, G. Speranza, *Stereoselective total synthesis of natural phytol double bond reductions by baker’s yeast*, *Tetrahedron* **1987**, 43, 4481–4486.
- [124] A. Müller, B. Hauer, B. Rosche, *Enzymatic reduction of the α,β -unsaturated carbon bond in citral*, *J. Mol. Catal. B: Enzym.* **2006**, 38, 126–130.
- [125] B. Rambeck, H. Simon, *Stereospecific Hydrogenation of \oplus - or (S)-2-Ethyl-4-phenylallenecarboxylic Acid to cis- or trans-2-Ethyl-4-phenyl-3-butenecarboxylic Acid by Means of Clostridium kluyveri*, *Angew. Chem. Int. Ed. Engl.* **1974**, 13, 609.
- [126] H. Günther, H. Simon, *Artificial Electron Carriers for Preparative Biocatalytic Redox Reactions Forming Reversibly Carbon Hydrogen Bonds with Enzymes Present in Strict or Facultative Anaerobes*, *Biocatal. Bio-transform.* **2009**, 12, 1–26.
- [127] O. Warburg, W. Christian, *Yellow enzymes*, *Biochem. Ztschr.* **1933**, 266, 377–411.
- [128] T. Reiß, W. Hummel, S. P. Hanlon, H. Iding, H. Gröger, *The Organic-Synthetic Potential of Recombinant Ene Reductases: Substrate-Scope Evaluation and Process Optimization*, *ChemCatChem* **2015**, 7, 1302–1311.
- [129] C. Stueckler, M. Hall, H. Ehammer, E. Pointner, W. Kroutil, P. Macheroux, K. Faber, *Stereocomplementary bioreduction of alpha,beta-unsaturated dicarboxylic acids and dimethyl esters using enoate reductases: enzyme- and substrate-based stereocontrol*, *Org. Lett.* **2007**, 9, 5409–5411.
- [130] G. M. Chateaneuf, R. E. Brown, B. J. Brown, *Computational studies of electron-transfer processes in old yellow enzyme*, *Int. J. Quantum Chem.* **2001**, 85, 685–692.

- [131] J. Pang, S. Hay, N. S. Scrutton, M. J. Sutcliffe, *Deep tunneling dominates the biologically important hydride transfer reaction from NADH to FMN in morphinone reductase*, *J. Am. Chem. Soc.* **2008**, *130*, 7092–7097.
- [132] R. Lonsdale, M. T. Reetz, *Reduction of α,β -Unsaturated Ketones by Old Yellow Enzymes: Mechanistic Insights from Quantum Mechanics/Molecular Mechanics Calculations*, *J. Am. Chem. Soc.* **2015**, *137*, 14733–14742.
- [133] M. Goldsmith, D. S. Tawfik, *Directed enzyme evolution: beyond the low-hanging fruit*, *Curr. Opin. Struct. Biol.* **2012**, *22*, 406–412.
- [134] M. P. Frushicheva, M. J. L. Mills, P. Schopf, M. K. Singh, R. B. Prasad, A. Warshel, *Computer aided enzyme design and catalytic concepts*, *Curr. Opin. Chem. Biol.* **2014**, *21*, 56–62.
- [135] K. Swiderek, I. Tunon, V. Moliner, J. Bertran, *Computational strategies for the design of new enzymatic functions*, *Arch. Biochem. Biophys.* **2015**, *582*, 68–79.
- [136] A. Martin, V. Orgogozo, *The Loci of repeated evolution: a catalog of genetic hotspots of phenotypic variation*, *Evolution* **2013**, *67*, 1235–1250.
- [137] M. R. Dunn, C. Otto, K. E. Fenton, J. C. Chaput, *Improving Polymerase Activity with Unnatural Substrates by Sampling Mutations in Homologous Protein Architectures*, *ACS Chem. Biol.* **2016**, *11*, 1210–1219.
- [138] J. G. Gober, A. E. Rydeen, E. J. Gibson-O'Grady, J. B. Leuthaeuser, J. S. Fetrow, E. M. Brustad, *Mutating a Highly Conserved Residue in Diverse Cytochrome P450s Facilitates Diastereoselective Olefin Cyclopropanation*, *ChemBioChem* **2016**, *17*, 394–397.
- [139] H. Flores, A. D. Ellington, *A modified consensus approach to mutagenesis inverts the cofactor specificity of *Bacillus stearothermophilus* lactate dehydrogenase*, *Protein Eng. Des. Sel.* **2005**, *18*, 369–377.
- [140] J. Murciano-Calles, D. K. Romney, S. Brinkmann-Chen, A. R. Buller, F. H. Arnold, *A Panel of TrpB Biocatalysts Derived from Tryptophan Synthase through the Transfer of Mutations that Mimic Allosteric Activation*, *Angew. Chem. Int. Ed.* **2016**, *55*, 11577–11581.
- [141] B. T. Porebski, A. M. Buckle, *Consensus protein design*, *Protein Eng. Des. Sel.* **2016**, *29*, 245–251.
- [142] A. S. Bommarius, *Protein engineering: Check nature first, then evolve*, *Nat. Chem. Biol.* **2010**, *6*, 793–794.
- [143] M. Höhne, S. Schätzle, H. Jochens, K. Robins, U. T. Bornscheuer, *Rational assignment of key motifs for function guides in silico enzyme identification*, *Nat. Chem. Biol.* **2010**, *6*, 807–813.
- [144] H. Jochens, U. T. Bornscheuer, *Natural diversity to guide focused directed evolution*, *ChemBioChem* **2010**, *11*, 1861–1866.
- [145] G. Oberdorfer, G. Steinkellner, C. Stueckler, K. Faber, K. Gruber, *Stereopreferences of Old Yellow Enzymes: Structure Correlations and Sequence Patterns in Enoate Reductases*, *ChemCatChem* **2011**, *3*, 1562–1566.
- [146] E. G. Hibbert, T. Senussi, S. J. Costelloe, W. Lei, M. E. B. Smith, J. M. Ward, H. C. Hailes, P. A. Dalby, *Directed evolution of transketolase activity on non-phosphorylated substrates*, *J. Biotechnol.* **2007**, *131*, 425–432.
- [147] L. T. Quertinmont, S. Lutz, *Cell-free protein engineering of Old Yellow Enzyme 1 from *Saccharomyces pastorianus**, *Tetrahedron* **2016**, *72*, 7282–7287.
- [148] E. D. Amato, J. D. Stewart, *Applications of protein engineering to members of the old yellow enzyme family*, *Biotechnol. Adv.* **2015**, *33*, 624–631.
- [149] M. K. Peers, H. S. Toogood, D. J. Heyes, D. Mansell, B. J. Coe, N. S. Scrutton, *Light-driven biocatalytic reduction of α,β -unsaturated compounds by ene reductases employing transition metal complexes as photosensitizers*, *Catal. Sci. Technol.* **2016**, *6*, 169–177.
- [150] S. Kille, M. T. Reetz, *Protein Engineering: Development of Novel Enzymes for the Improved Reduction of C=C Double Bonds in Synthetic Methods for Biologically Active Molecules. Exploring the Potential of Bioreductions*; (Ed. E. Brenna), Wiley-VCH Verlag GmbH & Co. KGaA, Weinheim, Germany, **2013**, 113–138.
- [151] C. K. Winkler, D. Clay, S. Davies, P. O'Neill, P. McDaid, S. Debarge, J. Steflik, M. Karmilowicz, J. W. Wong, K. Faber, *Chemoenzymatic asymmetric synthesis of pregabalin precursors via asymmetric bioreduction of β -cyanoacrylate esters using ene-reductases*, *J. Org. Chem.* **2013**, *78*, 1525–1533.

- [152] E. Rütthlein, T. Classen, L. Dobnikar, M. Schölzel, J. Pietruszka, *Finding the Selectivity Switch - A Rational Approach towards Stereocomplementary Variants of the Ene Reductase YqjM*, *Adv. Synth. Catal.* **2015**, 357, 1775–1786.
- [153] S. Reich, B. M. Nestl, B. Hauer, *Loop Grafted Old Yellow Enzymes in the Biocatalytic Cascade Reduction of Allylic Alcohols*, *ChemBioChem* **2016**, 17, 561–565.
- [154] E. Brenna, F. G. Gatti, D. Monti, F. Parmeggiani, A. Sacchetti, J. Valoti, *Substrate-engineering approach to the stereoselective chemo-multienzymatic cascade synthesis of Nicotiana tabacum lactone*, *J. Mol. Catal. B: Enzym.* **2015**, 114, 77–85.
- [155] T. Knaus, F. G. Mutti, L. D. Humphreys, N. J. Turner, N. S. Scrutton, *Systematic methodology for the development of biocatalytic hydrogen-borrowing cascades: application to the synthesis of chiral α -substituted carboxylic acids from α -substituted α,β -unsaturated aldehydes*, *Org. Biomol. Chem.* **2014**, 13, 223–233.
- [156] R. Agudo, M. T. Reetz, *Designer cells for stereocomplementary de novo enzymatic cascade reactions based on laboratory evolution*, *Chem. Commun.* **2013**, 49, 10914–10916.
- [157] L. Skalden, C. Peters, L. Ratz, U. T. Bornscheuer, *Synthesis of (1R,3R)-1-amino-3-methylcyclohexane by an enzyme cascade reaction*, *Tetrahedron* **2016**, 72, 7207–7211.
- [158] C. Stueckler, C. K. Winkler, M. Bonnekessel, K. Faber, *Asymmetric Synthesis of @-3-Hydroxy-2-methylpropanoate ('Roche Ester') and Derivatives via Biocatalytic C-C-Bond Reduction*, *Adv. Synth. Catal.* **2010**, 352, 2663–2666.
- [159] A. Z. Walton, W. C. Conerly, Y. Pompeu, B. Sullivan, J. D. Stewart, *Biocatalytic Reductions of Baylis–Hillman Adducts*, *ACS Catal.* **2011**, 1, 989–993.
- [160] A. Z. Walton, B. Sullivan, A. C. Patterson-Orazem, J. D. Stewart, *Residues Controlling Facial Selectivity in an Alkene Reductase and Semirational Alterations to Create Stereocomplementary Variants*, *ACS Catal.* **2014**, 4, 2307–2318.
- [161] H. S. Toogood, A. Fryszkowska, M. Hulley, M. Sakuma, D. Mansell, G. M. Stephens, J. M. Gardiner, N. S. Scrutton, *A site-saturated mutagenesis study of pentaerythritol tetranitrate reductase reveals that residues 181 and 184 influence ligand binding, stereochemistry and reactivity*, *ChemBioChem* **2011**, 12, 738–749.
- [162] M. E. Hulley, H. S. Toogood, A. Fryszkowska, D. Mansell, G. M. Stephens, J. M. Gardiner, N. S. Scrutton, *Focused directed evolution of pentaerythritol tetranitrate reductase by using automated anaerobic kinetic screening of site-saturated libraries*, *ChemBioChem* **2010**, 11, 2433–2447.
- [163] Y. A. Pompeu, B. Sullivan, J. D. Stewart, *X-ray Crystallography Reveals How Subtle Changes Control the Orientation of Substrate Binding in an Alkene Reductase*, *ACS Catal.* **2013**, 3, 2376–2390.
- [164] L. T. Quertinmont, R. Orru, S. Lutz, *RApid Parallel Protein EvaluatoR (RAPPER), from gene to enzyme function in one day*, *Chem. Commun.* **2015**, 51, 122–124.
- [165] J. T. Park, L. M. Gómez Ramos, A. S. Bommarius, *Engineering towards Nitroreductase Functionality in Ene-Reductase Scaffolds*, *ChemBioChem* **2015**, 16, 811–818.
- [166] S. Horita, M. Kataoka, N. Kitamura, T. Nakagawa, T. Miyakawa, J. Ohtsuka, K. Nagata, S. Shimizu, M. Tanokura, *An engineered old yellow enzyme that enables efficient synthesis of (4R,6R)-Actinol in a one-pot reduction system*, *ChemBioChem* **2015**, 16, 440–445.
- [167] A. Fryszkowska, H. Toogood, M. Sakuma, G. M. Stephens, J. M. Gardiner, N. S. Scrutton, *Active site modifications in pentaerythritol tetranitrate reductase can lead to improved product enantiopurity, decreased by-product formation and altered stereochemical outcome in reactions with α,β -unsaturated nitroolefins*, *Catal. Sci. Technol.* **2011**, 1, 948–957.
- [168] A. B. Daugherty, S. Govindarajan, S. Lutz, *Improved biocatalysts from a synthetic circular permutation library of the flavin-dependent oxidoreductase old yellow enzyme*, *J. Am. Chem. Soc.* **2013**, 135, 14425–14432.
- [169] E. Brenna, Ed, *Synthetic Methods for Biologically Active Molecules: Exploring the Potential of Bioreductions*; Wiley-VCH Verlag GmbH & Co. KGaA, Weinheim, Germany, **2013**.
- [170] S. Reich, H. W. Hoeffken, B. Rosche, B. M. Nestl, B. Hauer, *Crystal Structure Determination and Mutagenesis Analysis of the Ene Reductase NCR*, *ChemBioChem* **2012**, 13, 2400–2407.
- [171] C. Zhang, D. K. Schneiderman, T. Cai, Y.-S. Tai, K. Fox, K. Zhang, *Optically Active β -Methyl- δ -Valerolactone*, *ACS Sustainable Chem. Eng.* **2016**, 4, 4396–4402.

- [172] X. Chen, X. Gao, Q. Wu, D. Zhu, *Synthesis of optically active dihydrocarveol via a stepwise or one-pot enzymatic reduction of $\text{C}=\text{C}$ and (S)-carvone*, *Tetrahedron: Asymmetry* **2012**, *23*, 734–738.
- [173] Y. Yanto, H.-H. Yu, M. Hall, A. S. Bommarius, *Characterization of xenobiotic reductase A (XenA): study of active site residues, substrate spectrum and stability*, *Chem. Commun.* **2010**, *46*, 8809–8811.
- [174] A. Geddes, C. E. Paul, S. Hay, F. Hollmann, N. S. Scrutton, *Donor-Acceptor Distance Sampling Enhances the Performance of “Better than Nature” Nicotinamide Coenzyme Biomimetics*, *J. Am. Chem. Soc.* **2016**, *138*, 11089–11092.
- [175] D. J. Opperman, L. A. Piater, E. van Heerden, *A novel chromate reductase from Thermus scotoductus SA-01 related to old yellow enzyme*, *J. Bacteriol.* **2008**, *190*, 3076–3082.
- [176] Sabine Düwel, Master Thesis, *Exploring the Evolvability of Ene-Reductases TsER, DrER and RmER towards Activity*, Philipps-Universität Marburg, **2015**.
- [177] Alexandra A. Richter, Master Thesis, *Directed Evolution of the Ene-Reductase NCR*, Philipps-Universität Marburg, **2016**.
- [178] N. Oberleitner, C. Peters, J. Muschiol, M. Kadow, S. Saß, T. Bayer, P. Schaaf, N. Iqbal, F. Rudroff, M. D. Mihovilovic, U. T. Bornscheuer, *An Enzymatic Toolbox for Cascade Reactions: A Showcase for an In Vivo Redox Sequence in Asymmetric Synthesis*, *ChemCatChem* **2013**, *5*, 3524–3528.
- [179] J. Bernard, E. van Heerden, I. W. C. E. Arends, D. J. Opperman, F. Hollmann, *Chemoenzymatic Reduction of Conjugated C=C Double Bonds*, *ChemCatChem* **2012**, *4*, 196–199.
- [180] M. M. Bradford, *A rapid and sensitive method for the quantitation of microgram quantities of protein utilizing the principle of protein-dye binding*, *Anal. Biochem.* **1976**, *72*, 248–254.
- [181] A. Patterson-Orazem, B. Sullivan, J. D. Stewart, *Pichia stipitis OYE 2.6 variants with improved catalytic efficiencies from site-saturation mutagenesis libraries*, *Bioorg. Med. Chem.* **2014**, *22*, 5628–5632.
- [182] X.-Q. Pei, M.-Y. Xu, Z.-L. Wu, *Two “classical” Old Yellow Enzymes from Chryseobacterium sp. CA49*, *J. Mol. Catal. B: Enzym.* **2015**, *123*, 91–99.
- [183] C. Peters, R. Kölzsch, M. Kadow, L. Skalden, F. Rudroff, M. D. Mihovilovic, U. T. Bornscheuer, *Identification, Characterization, and Application of Three Enoate Reductases from Pseudomonas putida in In Vitro Enzyme Cascade Reactions*, *ChemCatChem* **2014**, *6*, 1021–1027.
- [184] X. Gao, J. Ren, Q. Wu, D. Zhu, *Biochemical characterization and substrate profiling of a new NADH-dependent enoate reductase from Lactobacillus casei*, *Enzyme Microb. Technol.* **2012**, *51*, 26–34.
- [185] A. Riedel, M. Mehnert, C. E. Paul, A. H. Westphal, W. J. H. van Berkel, D. Tischler, *Functional characterization and stability improvement of a ‘thermophilic-like’ ene-reductase from Rhodococcus opacus 1CP*, *Front. Microbiol.* **2015**, *6*, 1–14.
- [186] P. Tufvesson, J. Lima-Ramos, N. A. Haque, K. V. Gernaey, J. M. Woodley, *Advances in the Process Development of Biocatalytic Processes*, *Org. Process Res. Dev.* **2013**, *17*, 1233–1238.
- [187] Y. A. Pompeu, B. Sullivan, A. Z. Walton, J. D. Stewart, *Structural and Catalytic Characterization of Pichia stipitis OYE 2.6, a Useful Biocatalyst for Asymmetric Alkene Reductions*, *Adv. Synth. Catal.* **2012**, *354*, 1949–1960.
- [188] S. Kille, Dissertation, *Flavoproteins in Directed Evolution, Iterative CASTing to evolve YqiM and P450_{BMB}*, Ruhr Universität Bochum, **2010**.
- [189] H. Khan, T. Barna, R. J. Harris, N. C. Bruce, I. Barsukov, A. W. Munro, P. C. E. Moody, N. S. Scrutton, *Atomic resolution structures and solution behavior of enzyme-substrate complexes of Enterobacter cloacae PB2 pentaerythritol tetranitrate reductase. Multiple conformational states and implications for the mechanism of nitroaromatic explosive degradation*, *J. Biol. Chem.* **2004**, *279*, 30563–30572.
- [190] A. B. Daugherty, J. R. Horton, X. Cheng, S. Lutz, *Structural And Functional Consequences Of Circular Permutation On The Active Site Of Old Yellow Enzyme*, *ACS Catal.* **2015**, *5*, 892–899.
- [191] E. Brenna, M. Crotti, F. G. Gatti, D. Monti, F. Parmeggiani, R. W. Powell, S. Santangelo, J. D. Stewart, *Opposite Enantioselectivity in the Bioreduction of (Z)- β -Aryl- β -cyanoacrylates Mediated by the Tryptophan 116 Mutants of Old Yellow Enzyme 1*, *Adv. Synth. Catal.* **2015**, *357*, 1849–1860.
- [192] A. Müller, B. Hauer, B. Rosche, *Asymmetric alkene reduction by yeast old yellow enzymes and by a novel Zymomonas mobilis reductase*, *Biotechnol. Bioeng.* **2007**, *98*, 22–29.

- [193] M. A. Swiderska, J. D. Stewart, *Asymmetric bioreductions of β -nitro acrylates as a route to chiral β^2 -amino acids*, *Org. Lett.* **2006**, *8*, 6131–6133.
- [194] D. Monti, M. C. Forchin, M. Crotti, F. Parmeggiani, F. G. Gatti, E. Brenna, S. Riva, *Cascade Coupling of Ene-Reductases and ω -Transaminases for the Stereoselective Synthesis of Diastereomerically Enriched Amines*, *ChemCatChem* **2015**, *7*, 3106–3109.
- [195] N. Nett, S. Duewel, A. A. Richter, S. Hoebenreich, *Revealing Additional Stereocomplementary Pairs of Old Yellow Enzymes by Rational Transfer of Engineered Residues*, *ChemBioChem* **2017**, *18*, 685–691.
- [196] A. D. Vaz, S. Chakraborty, V. Massey, *Old yellow enzyme: Aromatization of cyclic enones and the mechanism of a novel dismutation reaction*, *Biochemistry* **1995**, *34*, 4246–4256.
- [197] P. P. Kelly, D. Lipscomb, D. J. Quinn, K. Lemon, J. Caswell, J. Spratt, B. Kosjek, M. Truppo, T. S. Moody, *Ene Reductase Enzymes for the Aromatisation of Tetralones and Cyclohexenones to Naphthols and Phenols*, *Adv. Synth. Catal.* **2016**, *358*, 731–736.
- [198] C. K. Winkler, D. Clay, M. Entner, M. Plank, K. Faber, *NAD(P)H-independent asymmetric C=C bond reduction catalyzed by ene reductases by using artificial co-substrates as the hydrogen donor*, *Chem. Eur. J.* **2014**, *20*, 1403–1409.
- [199] C. Stueckler, T. C. Reiter, N. Baudendistel, K. Faber, *Nicotinamide-independent asymmetric bioreduction of CC-bonds via disproportionation of enones catalyzed by enoate reductases*, *Tetrahedron* **2010**, *66*, 663–667.
- [200] M. Schittmayer, A. Glieder, M. K. Uhl, A. Winkler, S. Zach, J. H. Schrittwieser, W. Kroutil, P. Macheroux, K. Gruber, S. Kambourakis, J. D. Rozzell, M. Winkler, *Old Yellow Enzyme-Catalyzed Dehydrogenation of Saturated Ketones*, *Adv. Synth. Catal.* **2011**, *353*, 268–274.
- [201] D. W. Rogers, Y. Zhao, M. Traetteberg, M. Hulce, J. Liebman, *Enthalpies of hydrogenation and formation of enones. Resonance energies of 2-cyclopentenone and 2-cyclohexenone*, *J. Chem. Thermodyn.* **1998**, *30*, 1393–1400.
- [202] Q. H. Gibson, J. W. Hastings, *The oxidation of reduced flavin mononucleotide by molecular oxygen*, *Biochem. J.* **1962**, *83*, 368–377.
- [203] H. J. Reich, J. M. Renga, I. L. Reich, *Organoselenium chemistry. Conversion of ketones to enones by selenoxide syn elimination*, *J. Am. Chem. Soc.* **1975**, *97*, 5434–5447.
- [204] K. B. Sharpless, R. F. Lauer, A. Y. Teranishi, *Electrophilic and nucleophilic organoselenium reagents. New routes to α,β -unsaturated carbonyl compounds*, *J. Am. Chem. Soc.* **1973**, *95*, 6137–6139.
- [205] T. Mukaiyama, J. Matsuo, H. Kitagawa, *A New and One-Pot Synthesis of α,β -Unsaturated Ketones by Dehydrogenation of Various Ketones with *N*-tert -Butyl Phenylsulfonimidoyl Chloride*, *Chem. Lett.* **2000**, *29*, 1250–1251.
- [206] J. N. Marx, J. H. Cox, L. R. Norman, *2-Carbomethoxycyclopent-2-enone*, *J. Org. Chem.* **1972**, *37*, 4489–4491.
- [207] D. Walker, J. D. Hiebert, *2,3-Dichloro-5,6-dicyanobenzoquinone and Its Reactions*, *Chem. Rev.* **1967**, *67*, 153–195.
- [208] K. C. Nicolaou, Y.-L. Zhong, P. S. Baran, *A New Method for the One-Step Synthesis of α,β -Unsaturated Carbonyl Systems from Saturated Alcohols and Carbonyl Compounds*, *J. Am. Chem. Soc.* **2000**, *122*, 7596–7597.
- [209] C. K. Winkler, D. Clay, E. van Heerden, K. Faber, *Overcoming co-product inhibition in the nicotinamide independent asymmetric bioreduction of activated C=C-bonds using flavin-dependent ene-reductases*, *Biotechnol. Bioeng.* **2013**, *110*, 3085–3092.
- [210] A. Fryszkowska, H. S. Toogood, D. Mansell, G. Stephens, J. M. Gardiner, N. S. Scrutton, *A surprising observation that oxygen can affect the product enantiopurity of an enzyme-catalysed reaction*, *FEBS J.* **2012**, *279*, 4160–4171.
- [211] H. B. Bürgi, J. D. Dunitz, J. M. Lehn, G. Wipff, *Stereochemistry of reaction paths at carbonyl centres*, *Tetrahedron* **1974**, *30*, 1563–1572.
- [212] M. T. Ru, J. S. Dordick, J. A. Reimer, D. S. Clark, *Optimizing the salt-induced activation of enzymes in organic solvents: Effects of lyophilization time and water content*, *Biotechnol. Bioeng.* **1999**, *63*, 233–241.
- [213] I. Roy, M. N. Gupta, *Freeze-drying of proteins: some emerging concerns*, *Biotechnol. Appl. Biochem.* **2004**, *39*, 165–177.

- [214] R. E. Kirk, D. F. Othmer, *Kirk-Othmer Encyclopedia of Chemical Technology*; John Wiley & Sons, Inc, Hoboken, NJ, USA, **2005**.
- [215] M. Wada, A. Yoshizumi, Y. Noda, M. Kataoka, S. Shimizu, H. Takagi, S. Nakamori, *Production of a Doubly Chiral Compound, (4R,6R)-4-Hydroxy-2,2,6-Trimethylcyclohexanone, by Two-Step Enzymatic Asymmetric Reduction*, *Appl. Environ. Microbiol.* **2003**, *69*, 933–937.
- [216] H. S. Toogood, D. Mansell, J. M. Gardiner, N. S. Scrutton, *7.11 Reduction: Enantioselective Bioreduction of C–C Double Bonds in Comprehensive Chirality*, Elsevier, **2012**, 216–255.
- [217] H. G. W. Leuenberger, W. Boguth, E. Widmer, R. Zell, *Synthese von optisch aktiven, natürlichen Carotinoiden und strukturell verwandten Naturprodukten. I. Synthese der chiralen Schlüsselverbindung (4R, 6R)-4-Hydroxy-2,2,6-trimethylcyclohexanon*, *Helv. Chim. Acta* **1976**, *59*, 1832–1849.
- [218] A. Fryszkowska, H. S. Toogood, M. Sakuma, J. M. Gardiner, G. Stephens, N. S. Scrutton, *Asymmetric Reduction of Activated Alkenes by Pentaerythritol Tetranitrate Reductase: Specificity and Control of Stereochemical Outcome by Reaction Optimisation*, *Adv. Synth. Catal.* **2009**, *351*, 2976–2990.
- [219] W. Frank Shipe, *Ullmann's Food and Feed, 3 Volume Set*; Wiley, **2017**.
- [220] Y. Yanto, C. K. Winkler, S. Lohr, M. Hall, K. Faber, A. S. Bommarius, *Asymmetric bioreduction of alkenes using ene-reductases YersER and KYE1 and effects of organic solvents*, *Org. Lett.* **2011**, *13*, 2540–2543.
- [221] C. E. Paul, S. Gargiulo, D. J. Opperman, I. Lavandera, V. Gotor-Fernández, V. Gotor, A. Taglieber, I. W. C. E. Arends, F. Hollmann, *Mimicking nature: synthetic nicotinamide cofactors for C=C bioreduction using enoate reductases*, *Org. Lett.* **2013**, *15*, 180–183.
- [222] T. A. Glauser, A. Cnaan, S. Shinnar, D. G. Hirtz, D. Dlugos, D. Masur, P. O. Clark, E. V. Capparelli, P. C. Adamson, *Ethosuximide, valproic acid, and lamotrigine in childhood absence epilepsy*, *N. Engl. J. Med.* **2010**, *362*, 790–799.
- [223] S. J. Wallace, *Use of ethosuximide and valproate in the treatment of epilepsy*, *Neurol. Clin.* **1986**, *4*, 601–616.
- [224] J. A. Seijas, M. P. Vázquez-Tato, M. M. Martínez, G. Núñez-Corredoira, *Direct Synthesis of Imides from Dicarboxylic Acids using Microwaves*, *J. Chem. Res. (S)* **1999**, *0*, 420–421.
- [225] W. A. Poucher, *Perfumes, Cosmetics and Soaps: Volume I The Raw Materials of Perfumery*; Springer Netherlands, **2012**.
- [226] E. Brenna, M. Crotti, F. G. Gatti, D. Monti, F. Parmeggiani, S. Santangelo, *Asymmetric Bioreduction of β -Acylaminonitroalkenes: Easy Access to Chiral Building Blocks with Two Vicinal Nitrogen-Containing Functional Groups*, *ChemCatChem* **2017**, *9*, 2480–2487.
- [227] N. Ono, H. Feuer, *The Nitro Group in Organic Synthesis*; John Wiley & Sons, Inc, New York, USA, **2001**.
- [228] N. Nett, S. Duewel, L. Schmermund, G. E. Benary, K. E. Ranaghan, D. J. Opperman, A. J. Mulholland, S. Hoebenreich, *A Robust and Stereocomplementary Panel of Ene-Reductase Variants for Gram-Scale Asymmetric Hydrogenation* **2017**, submitted.
- [229] K. Fisher, S. Mohr, D. Mansell, N. J. Goddard, P. R. Fielden, N. S. Scrutton, *Electro-enzymatic oxygen-mediated substrate reduction using pentaerythritol tetranitrate reductase and a parallel, segmented fluid flow system*, *Catal. Sci. Technol.* **2013**, *3*, 1505–1511.
- [230] M. M. Grau, J. C. van der Toorn, L. G. Otten, P. Macheroux, A. Taglieber, F. E. Zilly, I. W. C. E. Arends, F. Hollmann, *Photoenzymatic Reduction of C=C Double Bonds*, *Adv. Synth. Catal.* **2009**, *351*, 3279–3286.
- [231] H. Simon, H. Günther, J. Bader, W. Tischer, *Electro-Enzymatic and Electro-Microbial Stereospecific Reductions*, *Angew. Chem. Int. Ed. Engl.* **1981**, *20*, 861–863.
- [232] H. S. Toogood, T. Knaus, N. S. Scrutton, *Alternative Hydride Sources for Ene-Reductases: Current Trends*, *ChemCatChem* **2014**, *6*, 951–954.
- [233] C. E. Paul, F. Hollmann, *A survey of synthetic nicotinamide cofactors in enzymatic processes*, *Appl. Microbiol. Biotechnol.* **2016**, *100*, 4773–4778.
- [234] A. M. Klibanov, *Improving enzymes by using them in organic solvents*, *Nature* **2001**, *409*, 241–246.
- [235] P. A. Fitzpatrick, A. M. Klibanov, *How can the solvent affect enzyme enantioselectivity?*, *J. Am. Chem. Soc.* **1991**, *113*, 3166–3171.

- [236] C. K. Savile, V. Mitchell, X. Zhang, G. W. Huisman, *Enone reductases*; Google Patents, **2016**.
- [237] H. S. Toogood, A. Fryszkowska, V. Hare, K. Fisher, A. Roujeinikova, D. Leys, J. M. Gardiner, G. M. Stephens, N. S. Scrutton, *Structure-Based Insight into the Asymmetric Bioreduction of the C=C Double Bond of α,β -Unsaturated Nitroalkenes by Pentaerythritol Tetranitrate Reductase*, *Adv. Synth. Catal.* **2008**, 350, 2789–2803.
- [238] M. Biermann, H. Größ, W. Hummel, H. Gröger, *Guerbet Alcohols: From Processes under Harsh Conditions to Synthesis at Room Temperature under Ambient Pressure*, *ChemCatChem* **2016**, 8, 895–899.
- [239] M.-Y. Xu, X.-Q. Pei, Z.-L. Wu, *Identification and characterization of a novel “thermophilic-like” Old Yellow Enzyme from the genome of Chryseobacterium sp. CA49*, *J. Mol. Catal. B: Enzym.* **2014**, 108, 64–71.
- [240] N. Tsuji, K. Honda, M. Wada, K. Okano, H. Ohtake, *Isolation and characterization of a thermotolerant ene reductase from Geobacillus sp. 30 and its heterologous expression in Rhodococcus opacus*, *Appl. Microbiol. Biotechnol.* **2014**, 98, 1–11.
- [241] K. Lee, J. Neff, Eds, *Produced Water: Environmental Risks and Advances in Mitigation Technologies, Measurement of Oil in Produced Water*; Springer Science+Business Media LLC, New York, NY, **2011**.
- [242] M. Bechtold, E. Brenna, C. Femmer, F. G. Gatti, S. Panke, F. Parmeggiani, A. Sacchetti, *Biotechnological Development of a Practical Synthesis of Ethyl (S)-2-Ethoxy-3-(p-methoxyphenyl)propanoate (EEHP): Over 100-Fold Productivity Increase from Yeast Whole Cells to Recombinant Isolated Enzymes*, *Org. Process Res. Dev.* **2012**, 16, 269–276.
- [243] G. Carrea, *Biocatalysis in water-organic solvent two-phase systems*, *Trends Biotechnol.* **1984**, 2, 102–106.
- [244] C. Laane, S. Boeren, K. Vos, C. Veeger, *Rules for optimization of biocatalysis in organic solvents*, *Biotechnol. Bioeng.* **1987**, 30, 81–87.
- [245] M. Eckstein, T. Daußmann, U. Kragl, *Recent Developments in NAD(P)H Regeneration for Enzymatic Reductions in One- and Two-Phase Systems*, *Biocatal. Biotransform.* **2009**, 22, 89–96.
- [246] G. Carrea, S. Riva, *Properties and Synthetic Applications of Enzymes in Organic Solvents*, *Angew. Chem. Int. Ed.* **2000**, 39, 2226–2254.
- [247] G. Cainelli, P. Galletti, D. Giacomini, *Solvent effects on stereoselectivity: more than just an environment*, *Chem. Soc. Rev.* **2009**, 38, 990–1001.
- [248] M. Lotti, F. Secundo, *Editorial: protein stabilization - crossroad for protein-based processes and products*, *Biotechnol. J.* **2015**, 10, 341–342.
- [249] L. Kulishova, K. Dimoula, M. Jordan, A. Wirtz, D. Hofmann, B. Santiago-Schübel, J. Fitter, M. Pohl, A. C. Spiess, *Factors influencing the operational stability of NADPH-dependent alcohol dehydrogenase and an NADH-dependent variant thereof in gas/solid reactors*, *J. Mol. Catal. B: Enzym.* **2010**, 67, 271–283.
- [250] L. Kulishova, *Dissertation, Analysis of factors influencing enzyme activity and stability in the solid state*, Heinrich-Heine-Universität Düsseldorf, **2010**.
- [251] A. S. Bommarius, M. F. Paye, *Stabilizing biocatalysts*, *Chem. Soc. Rev.* **2013**, 42, 6534–6565.
- [252] D. Suplatov, V. Voevodin, V. Svedas, *Robust enzyme design: bioinformatic tools for improved protein stability*, *Biotechnol. J.* **2015**, 10, 344–355.
- [253] Y. Fu, K. Castiglione, D. Weuster-Botz, *Comparative characterization of novel ene-reductases from cyanobacteria*, *Biotechnol. Bioeng.* **2013**, 110, 1293–1301.
- [254] J. T. Wu, L. H. Wu, J. A. Knight, *Stability of NADPH*, *Clin. Chem.* **1986**, 32, 314–319.
- [255] Y. Wang, M. J. Bartlett, C. A. Denard, J. F. Hartwig, H. Zhao, *Combining Rh-Catalyzed Diazocoupling and Enzymatic Reduction To Efficiently Synthesize Enantioenriched 2-Substituted Succinate Derivatives*, *ACS Catal.* **2017**, 7, 2548–2552.
- [256] H. Gröger, W. Hummel, *Combining the ‘two worlds’ of chemocatalysis and biocatalysis towards multi-step one-pot processes in aqueous media*, *Curr. Opin. Chem. Biol.* **2014**, 19, 171–179.
- [257] Y. Ni, H.-L. Yu, G.-Q. Lin, J.-H. Xu, *An ene reductase from Clavospora lusitaniae for asymmetric reduction of activated alkenes*, *Enzyme Microb. Technol.* **2014**, 56, 40–45.
- [258] R. Fischer, S. Schillberg, S. Hellwig, R. M. Twyman, J. Drossard, *GMP issues for recombinant plant-derived pharmaceutical proteins*, *Biotechnol. Adv.* **2012**, 30, 434–439.
- [259] G. Moschini, *Pharmaceutical And Industrial Traits In Genetically Modified Crops: Coexistence With Conventional Agriculture*, *Amer. J. Agr. Econ.* **2006**, 88, 1184–1192.

- [260] D. Mangan, I. Miskelly, T. S. Moody, *A Three-Enzyme System Involving an Ene-Reductase for Generating Valuable Chiral Building Blocks*, *Adv. Synth. Catal.* **2012**, *354*, 2185–2190.
- [261] B. Dominguez, U. Schell, S. Bisagni, T. Kalthoff, *Reduction of Activated Carbon-Carbon Double Bonds using Highly Active and Enantioselective Double Bond Reductases*, *Johnson Matthey Technol. Rev.* **2016**, *60*, 243–249.
- [262] M. Boudart, *Turnover Rates in Heterogeneous Catalysis*, *Chem. Rev.* **1995**, *95*, 661–666.
- [263] D. Houde, S. A. Berkowitz, J. R. Engen, *The utility of hydrogen/deuterium exchange mass spectrometry in biopharmaceutical comparability studies*, *J. Pharm. Sci.* **2011**, *100*, 2071–2086.
- [264] R. Lindner, U. Heintz, A. Winkler, *Applications of hydrogen deuterium exchange (HDX) for the characterization of conformational dynamics in light-activated photoreceptors*, *Front. Mol. Biosci.* **2015**, *2*, 33.
- [265] M. J. Chalmers, S. A. Busby, B. D. Pascal, G. M. West, P. R. Griffin, *Differential hydrogen/deuterium exchange mass spectrometry analysis of protein-ligand interactions*, *Expert Rev. Proteomics* **2011**, *8*, 43–59.
- [266] O. Vadas, M. L. Jenkins, G. L. Dornan, J. E. Burke, *Using Hydrogen-Deuterium Exchange Mass Spectrometry to Examine Protein-Membrane Interactions*, *Meth. Enzymol.* **2017**, *583*, 143–172.
- [267] S. A. Busby, M. J. Chalmers, P. R. Griffin, *Improving digestion efficiency under H/D exchange conditions with activated pepsinogen coupled columns*, *Int. J. Mass Spectrom.* **2007**, *259*, 130–139.
- [268] Y. Yu, S. Lutz, *Circular permutation: a different way to engineer enzyme structure and function*, *Trends Biotechnol.* **2011**, *29*, 18–25.
- [269] R. A. Friesner, J. L. Banks, R. B. Murphy, T. A. Halgren, J. J. Klicic, D. T. Mainz, M. P. Repasky, E. H. Knoll, M. Shelley, J. K. Perry, D. E. Shaw, P. Francis, P. S. Shenkin, *Glide*, *J. Med. Chem.* **2004**, *47*, 1739–1749.
- [270] <http://upjv.q4md-forcefieldtools.org/REDDB/projects/F-90/>.
- [271] S. P. Edgcomb, K. P. Murphy, *Variability in the pKa of histidine side-chains correlates with burial within proteins*, *Proteins: Struct, Funct, Bioinf.* **2002**, *49*, 1–6.
- [272] M. W. Fraaije, A. Mattevi, *Flavoenzymes: diverse catalysts with recurrent features*, *Trends Biochem. Sci.* **2000**, *25*, 126–132.
- [273] M. P. Repasky, R. B. Murphy, J. L. Banks, J. R. Greenwood, I. Tubert-Brohman, S. Bhat, R. A. Friesner, *Docking performance of the glide program as evaluated on the Astex and DUD datasets: a complete set of glide SP results and selected results for a new scoring function integrating WaterMap and glide*, *J. Comput.-Aided Mol. Des.* **2012**, *26*, 787–799.
- [274] Schrödinger Release 2016-4: Schrödinger Suite 2016-4 Induced Fit Docking protocol; Glide, Schrödinger, LLC, New York, NY, 2016; Prime, Schrödinger, LLC, New York, NY, 2016.
- [275] M. Norin, F. Haefner, K. Hult, O. Edholm, *Molecular dynamics simulations of an enzyme surrounded by vacuum, water, or a hydrophobic solvent*, *Biophys. J.* **1994**, *67*, 548–559.
- [276] H. Li, A. D. Robertson, J. H. Jensen, *Very fast empirical prediction and rationalization of protein pKa values*, *Proteins* **2005**, *61*, 704–721.
- [277] T. B. Fitzpatrick, S. Auweter, K. Kitzing, T. Clausen, N. Amrhein, P. Macheroux, *Structural and functional impairment of an Old Yellow Enzyme homologue upon affinity tag incorporation*, *Protein Expr. Purif.* **2004**, *36*, 280–291.
- [278] J. Mongan, D. A. Case, J. A. McCammon, *Constant pH molecular dynamics in generalized Born implicit solvent*, *J. Comput. Chem.* **2004**, *25*, 2038–2048.
- [279] C. J. Woods, M. Malaisree, S. Hannongbua, A. J. Mulholland, *A water-swap reaction coordinate for the calculation of absolute protein-ligand binding free energies*, *J. Chem. Phys.* **2011**, *134*, 54114.
- [280] C. J. Woods, M. Malaisree, B. Long, S. McIntosh-Smith, A. J. Mulholland, *Computational assay of H7N9 influenza neuraminidase reveals R292K mutation reduces drug binding affinity*, *Sci. Rep.* **2013**, *3*, 3561.
- [281] B. R. Miller, T. D. McGee, J. M. Swails, N. Homeyer, H. Gohlke, A. E. Roitberg, *MMPBSA.py: An Efficient Program for End-State Free Energy Calculations*, *J. Chem. Theory Comput.* **2012**, *8*, 3314–3321.
- [282] N. Homeyer, H. Gohlke, *Free Energy Calculations by the Molecular Mechanics Poisson-Boltzmann Surface Area Method*, *Mol. Inform.* **2012**, *31*, 114–122.
- [283] S. K. Chapman, Ed, *Flavoprotein Protocols*; Humana Press, Totowa, NJ, **1999**.

- [284] R. J. Marles, C. M. Compadre, N. R. Farnsworth, *Coumarin in Vanilla Extracts: Its Detection and Significance*, *Econ. Bot.* **1987**, *41*, 41–47.
- [285] V. Sridharan, P. A. Suryavanshi, J. C. Menéndez, *Advances in the chemistry of tetrahydroquinolines*, *Chem. Rev.* **2011**, *111*, 7157–7259.
- [286] W. D. Dean, D. M. Blum, *Condensation of arylacetonitriles with glyoxylic acid. Facile synthesis of arylmaleic acid derivatives*, *J. Org. Chem.* **1993**, *58*, 7916–7917.
- [287] T. J. Schwartz, S. D. Lyman, A. H. Motagamwala, M. A. Mellmer, J. A. Dumesic, *Selective Hydrogenation of Unsaturated Carbon–Carbon Bonds in Aromatic-Containing Platform Molecules*, *ACS Catal.* **2016**, *6*, 2047–2054.
- [288] V. M. Mokhov, Y. V. Popov, D. N. Nebykov, *Hydrogenation of alkenes over nickel nanoparticles under atmospheric pressure of hydrogen*, *Russ. J. Org. Chem.* **2016**, *52*, 319–323.
- [289] H. Wang, H. Lian, J. Chen, Y. Pan, Y. Shi, *Ultrasonic Accelerated Hydrogenation of Unsaturated Ketones with Raney Nickel Catalyst*, *Synth. Commun.* **1999**, *29*, 129–134.
- [290] F. Felpin, J. Coste, C. Zakri, E. Fouquet, *Preparation of 2-Quinolones by Sequential Heck Reduction–Cyclization (HRC) Reactions by Using a Multitask Palladium Catalyst*, *Chem. Eur. J.* **2009**, *15*, 7238–7245.
- [291] M. Ito, T. Ooshida, *Production of *e*-Caprolactam*, (JP4164603).
- [292] J. J. Griese, R. P. Jakob, S. Schwarzingler, H. Dobbek, *Xenobiotic reductase A in the degradation of quinoline by *Pseudomonas putida* 86: physiological function, structure and mechanism of 8-hydroxycoumarin reduction*, *J. Mol. Biol.* **2006**, *361*, 140–152.
- [293] T. Werther, S. Wahlefeld, J. Salewski, U. Kuhlmann, I. Zebger, P. Hildebrandt, H. Dobbek, *Redox-dependent substrate-cofactor interactions in the Michaelis-complex of a flavin-dependent oxidoreductase*, *Nat Comms* **2017**, *8*, 16084.
- [294] N. G. Turrini, M. Hall, K. Faber, *Enzymatic Synthesis of Optically Active Lactones via Asymmetric Bioreduction using Ene-Reductases from the Old Yellow Enzyme Family*, *Adv. Synth. Catal.* **2015**, *357*, 1861–1871.
- [295] P. S. Baran, J. M. Richter, *Direct coupling of indoles with carbonyl compounds: short, enantioselective, gram-scale synthetic entry into the hapalindole and fischerindole alkaloid families*, *J. Am. Chem. Soc.* **2004**, *126*, 7450–7451.
- [296] G. E. Benary, Bachelor Thesis, *Exploring the substrate scope of ene-reductase TsER*, Philipps-Universität Marburg, **2015**.
- [297] M. Ruf, Bachelor Thesis, *Alpha, Beta Substituted Enones as Substrates for Ene-Reductases*, Philipps-Universität Marburg, **2016**.
- [298] A. J. Ruff, A. Dennig, G. Wirtz, M. Blanusa, U. Schwaneberg, *Flow Cytometer-Based High-Throughput Screening System for Accelerated Directed Evolution of P450 Monooxygenases*, *ACS Catal.* **2012**, *2*, 2724–2728.
- [299] Z.-P. Xiao, Z.-Y. Peng, J.-J. Dong, J. He, H. Ouyang, Y.-T. Feng, C.-L. Lu, W.-Q. Lin, J.-X. Wang, Y.-P. Xiang, H.-L. Zhu, *Synthesis, structure-activity relationship analysis and kinetics study of reductive derivatives of flavonoids as *Helicobacter pylori* urease inhibitors*, *Eur. J. Med. Chem.* **2013**, *63*, 685–695.
- [300] A. Song, X. Wang, K. S. Lam, *A convenient synthesis of coumarin-3-carboxylic acids via Knoevenagel condensation of Meldrum's acid with ortho-hydroxyaryl aldehydes or ketones*, *Tetrahedron Lett.* **2003**, *44*, 1755–1758.
- [301] V. Singh, J. Singh, K. P. Kaur, G. L. Kad, *Acceleration of the Pechmann Reaction by Microwave Irradiation: Application to the Preparation of Coumarins*, *J. Chem. Res. (S)* **1997**, *0*, 58–59.
- [302] S. K. Gadakh, S. Dey, A. Sudalai, *Rh-Catalyzed Synthesis of Coumarin Derivatives from Phenolic Acetates and Acrylates via C-H Bond Activation*, *J. Org. Chem.* **2015**, *80*, 11544–11550.
- [303] D. Prajapati, M. Gohain, *Iodine a Simple, Effective and Inexpensive Catalyst for the Synthesis of Substituted Coumarins*, *Catal Lett* **2007**, *119*, 59–63.
- [304] D. Sharma, S. Kumar, J. K. Makrandi, *Modified Pechmann condensation using grinding technique under solvent-free condition at room temperature*, *Green Chem. Lett. Rev.* **2011**, *4*, 127–129.
- [305] J. K. Narwal, R. K. Malik, N. Kumari, *An Efficient Solvent Free Synthesis of Coumarins via Solid Phase Pechmann Reaction*, *Chem. Sci. Trans.* **2015**, *4*, 1092–1094.

- [306] L. Schmermund, Master Thesis, *Synthesis of 12-epi-Hapalindole C Derivatives to Investigate the Substrate-Scope of WelO15 Halogenase Variants*, Philipps-Universität Marburg, **2017**.
- [307] K. Häser, H. H. Wenk, W. Schwab, *Biocatalytic production of dihydrocoumarin from coumarin by Saccharomyces cerevisiae*, J. Agric. Food Chem. **2006**, *54*, 6236–6240.
- [308] C. R. Søndergaard, M. H. M. Olsson, M. Rostkowski, J. H. Jensen, *Improved Treatment of Ligands and Coupling Effects in Empirical Calculation and Rationalization of pKa Values*, J Chem Theory Comput **2011**, *7*, 2284–2295.
- [309] M. H. M. Olsson, C. R. Søndergaard, M. Rostkowski, J. H. Jensen, *PROPKA3: Consistent Treatment of Internal and Surface Residues in Empirical pKa Predictions*, J Chem Theory Comput **2011**, *7*, 525–537.
- [310] N. Kress, J. Rapp, B. Hauer, *Enantioselective Reduction of Citral Isomers in NCR Ene Reductase: Analysis of an Active-Site Mutant Library*, ChemBioChem **2017**, *18*, 717–720.
- [311] O. Spiegelhauer, F. Dickert, S. Mende, D. Niks, R. Hille, M. Ullmann, H. Dobbek, *Kinetic characterization of xenobiotic reductase A from Pseudomonas putida 86*, Biochemistry **2009**, *48*, 11412–11420.
- [312] C. R. Pudney, S. Hay, C. Levy, J. Pang, M. J. Sutcliffe, D. Leys, N. S. Scrutton, *Evidence to support the hypothesis that promoting vibrations enhance the rate of an enzyme catalyzed H-tunneling reaction*, J. Am. Chem. Soc. **2009**, *131*, 17072–17073.
- [313] C. R. Pudney, S. Hay, J. Pang, C. Costello, D. Leys, M. J. Sutcliffe, N. S. Scrutton, *Mutagenesis of morphinone reductase induces multiple reactive configurations and identifies potential ambiguity in kinetic analysis of enzyme tunneling mechanisms*, J. Am. Chem. Soc. **2007**, *129*, 13949–13956.
- [314] R. Gómez-Bombarelli, E. Calle, J. Casado, *Mechanisms of lactone hydrolysis in acidic conditions*, J. Org. Chem. **2013**, *78*, 6880–6889.
- [315] M. A. Mena, P. S. Daugherty, *Automated design of degenerate codon libraries*, Protein Eng. Des. Sel. **2005**, *18*, 559–561.
- [316] S. Hoebenreich, F. E. Zilly, C. G. Acevedo-Rocha, M. Zilly, M. T. Reetz, *Speeding up directed evolution: Combining the advantages of solid-phase combinatorial gene synthesis with statistically guided reduction of screening effort*, ACS Synth. Biol. **2015**, *4*, 317–331.
- [317] S. Kille, F. E. Zilly, J. P. Acevedo, M. T. Reetz, *Regio- and stereoselectivity of P450-catalysed hydroxylation of steroids controlled by laboratory evolution*, Nat. Chem. **2011**, *3*, 738–743.
- [318] M. A. Fischbach, J. R. Lai, E. D. Roche, C. T. Walsh, D. R. Liu, *Directed evolution can rapidly improve the activity of chimeric assembly-line enzymes*, Proc. Natl. Acad. Sci. USA **2007**, *104*, 11951–11956.
- [319] N. Nett, Master Thesis, *Cytochrom P450_{BM3} Katalysierte Oxidative Spaltung von Etherschutzgruppen*, Philipps-Universität Marburg, **2014**.
- [320] P. Galka, E. Jamez, G. Joachim, P. Soumillion, *QuickLib, a method for building fully synthetic plasmid libraries by seamless cloning of degenerate oligonucleotides*, PLoS ONE **2017**, *12*, e0175146.
- [321] S.-F. Zhu, Q.-L. Zhou, *Iridium-Catalyzed Asymmetric Hydrogenation of Unsaturated Carboxylic Acids*, Acc. Chem. Res. **2017**, *50*, 988–1001.
- [322] S. P. France, L. J. Hepworth, N. J. Turner, S. L. Flitsch, *Constructing Biocatalytic Cascades*, ACS Catal. **2017**, *7*, 710–724.
- [323] J. H. Schrittwieser, S. Velikogne, M. Hall, W. Kroutil, *Artificial Biocatalytic Linear Cascades for Preparation of Organic Molecules*, Chem. Rev. **2017**.
- [324] A. D. Daniels, I. Campeotto, M. W. van der Kamp, A. H. Bolt, C. H. Trinh, S. E. V. Phillips, A. R. Pearson, A. Nelson, A. J. Mulholland, A. Berry, *Reaction mechanism of N-acetylneuraminic acid lyase revealed by a combination of crystallography, QM/MM simulation, and mutagenesis*, ACS. Chem. Biol. **2014**, *9*, 1025–1032.
- [325] M. W. van der Kamp, A. J. Mulholland, *Combined quantum mechanics/molecular mechanics (QM/MM) methods in computational enzymology*, Biochemistry **2013**, *52*, 2708–2728.
- [326] K. Stott, K. Saito, D. J. Thiele, V. Massey, *Old Yellow Enzyme. The discovery of multiple isozymes and a family of related proteins*, J. Biol. Chem. **1993**, *268*, 6097–6106.
- [327] N. Richter, H. Gröger, W. Hummel, *Asymmetric reduction of activated alkenes using an enoate reductase from Gluconobacter oxydans*, Appl. Microbiol. Biotechnol. **2011**, *89*, 79–89.

- [328] E. Burda, T. Reiß, T. Winkler, C. Giese, X. Kostrov, T. Huber, W. Hummel, H. Gröger, *Highly enantioselective reduction of α -methylated nitroalkenes*, *Angew. Chem. Int. Ed.* **2013**, *52*, 9323–9326.
- [329] B. van Bergen, N. Cyr, R. Strasser, M. Blanchette, J. D. Sheppard, A. Jardim, *α,β -Dicarbonyl reduction is mediated by the *Saccharomyces uvarum* yellow enzyme*, *FEMS Yeast Res.* **2016**, *16*, fow059.
- [330] T. Oya, N. Hattori, Y. Mizuno, S. Miyata, S. Maeda, T. Osawa, K. Uchida, *Methylglyoxal Modification of Protein*, *J. Biol. Chem.* **1999**, *274*, 18492–18502.
- [331] R. L. Lundblad, *Techniques in protein modification*; CRC Press, Boca Raton, Fla, **1995**.
- [332] S. Landaud, P. Lieben, D. Picque, *Quantitative Analysis Of Diacetyl, Pentanedione And Their Precursors During Beer Fermentation By An Accurate GC/MS Method*, *J. Inst. Brew.* **1998**, *104*, 93–99.
- [333] E. I. Chudyk, M. A. L. Limb, C. Jones, J. Spencer, M. W. van der Kamp, A. J. Mulholland, *QM/MM simulations as an assay for carbapenemase activity in class A β -lactamases*, *Chem. Commun.* **2014**, *50*, 14736–14739.
- [334] G. R. Fulmer, A. J. M. Miller, N. H. Sherden, H. E. Gottlieb, A. Nudelman, B. M. Stoltz, J. E. Bercaw, K. I. Goldberg, *NMR Chemical Shifts of Trace Impurities*, *Organometallics* **2010**, *29*, 2176–2179.
- [335] A. Kar, N. P. Argade, *A Facile Synthesis of Natural Products Chaetomelic Acid A and 1,7(Z)-Nonadecadiene-2,3-dicarboxylic Acid*, *J. Org. Chem.* **2002**, *67*, 7131–7134.
- [336] S. Maity, S. Manna, S. Rana, T. Naveen, A. Mallick, D. Maiti, *Efficient and stereoselective nitration of mono- and disubstituted olefins with AgNO_2 and TEMPO*, *J. Am. Chem. Soc.* **2013**, *135*, 3355–3358.
- [337] F. William Studier, *Protein Production by Auto-Induction in High-Density Shaking Cultures*, *Protein Expr. Purif.* **2008**, *41*, 207–234.
- [338] H. Inoue, H. Nojima, H. Okayama, *High efficiency transformation of *Escherichia coli* with plasmids*, *Gene* **1990**, *96*, 23–28.
- [339] Y. Xia, W. Chu, Q. Qi, L. Xun, *New insights into the QuikChange™ process guide the use of Phusion DNA polymerase for site-directed mutagenesis*, *Nucleic Acids Res.* **2015**, *43*, e12.
- [340] B. J. Smith, *SDS Polyacrylamide Gel Electrophoresis of Proteins* in *Proteins*; (Ed. J. M. Walker), Humana Press, Totowa, NJ, **1984**, 41–55.
- [341] Y.-D. Liao, J.-C. Jeng, C.-F. Wang, S.-C. Wang, S.-T. Chang, *Removal of N-terminal methionine from recombinant proteins by engineered *E. coli* methionine aminopeptidase*, *Protein Sci.* **2004**, *13*, 1802–1810.
- [342] E. A. Noltmann, C. J. Gubler, S. A. Kuby, *Glucose 6-Phosphate Dehydrogenase (Zwischenferment)*, *J. Biol. Chem.* **1961**, *236*, 1225–1230.
- [343] A. G. W. Leslie, H. R. Powell, *Processing diffraction data with mosflm in Evolving Methods for Macromolecular Crystallography*, *NATO Science Series II: Mathematics, Physics and Chemistry*; (Eds. R. J. Read, J. L. Sussman), Springer Netherlands, Dordrecht, **2007**, 41–51.
- [344] P. Evans, *Scaling and assessment of data quality*, *Acta Crystallogr. Sect. D: Biol. Crystallogr.* **2006**, *62*, 72–82.
- [345] A. J. McCoy, R. W. Grosse-Kunstleve, P. D. Adams, M. D. Winn, L. C. Storoni, R. J. Read, *Phaser crystallographic software*, *J. Appl. Crystallogr.* **2007**, *40*, 658–674.
- [346] P. Emsley, B. Lohkamp, W. G. Scott, K. Cowtan, *Features and development of Coot*, *Acta Crystallogr. Sect. D: Biol. Crystallogr.* **2010**, *66*, 486–501.
- [347] G. N. Murshudov, P. Skubak, A. A. Lebedev, N. S. Pannu, R. A. Steiner, R. A. Nicholls, M. D. Winn, F. Long, A. A. Vagin, *REFMAC5 for the refinement of macromolecular crystal structures*, *Acta Crystallogr. Sect. D: Biol. Crystallogr.* **2011**, *67*, 355–367.
- [348] M. D. Winn, C. C. Ballard, K. D. Cowtan, E. J. Dodson, P. Emsley, P. R. Evans, R. M. Keegan, E. B. Krissinel, A. G. W. Leslie, A. McCoy, S. J. McNicholas, G. N. Murshudov, N. S. Pannu, E. A. Potterton, H. R. Powell, R. J. Read, A. Vagin, K. S. Wilson, *Overview of the CCP4 suite and current developments*, *Acta Crystallogr. Sect. D: Biol. Crystallogr.* **2011**, *67*, 235–242.
- [349] P. R. Evans, G. N. Murshudov, *How good are my data and what is the resolution?*, *Acta Crystallogr. Sect. D: Biol. Crystallogr.* **2013**, *69*, 1204–1214.
- [350] D.A. Case, D.S. Cerutti, T.E. Cheatham, III, T.A. Darden, R.E. Duke, T.J. Giese, H. Gohlke, A.W. Goetz, D. Greene, N. Homeyer, S. Izadi, A. Kovalenko, T.S. Lee, S. LeGrand, P. Li, C. Lin, J. Liu, T. Luchko, R. Luo, D. Mermelstein, K.M. Merz, G. Monard, H. Nguyen, I. Omelyan, A. Onufriev, F. Pan, R.

- Qi, D.R. Roe, A. Roitberg, C. Sagui, C.L. Simmerling, W.M. Botello-Smith, J. Swails, R.C. Walker, J. Wang, R.M. Wolf, X. Wu, L. Xiao, D.M. York and P.A. Kollman, *AMBER*; University of California, San Francisco, **2016**.
- [351] V. Hornak, R. Abel, A. Okur, B. Strockbine, A. Roitberg, C. Simmerling, *Comparison of multiple Amber force fields and development of improved protein backbone parameters*, *Proteins* **2006**, *65*, 712–725.
- [352] J. Wang, R. M. Wolf, J. W. Caldwell, P. A. Kollman, D. A. Case, *Development and testing of a general amber force field*, *J. Comput. Chem.* **2004**, *25*, 1157–1174.
- [353] W. L. Jorgensen, J. Chandrasekhar, J. D. Madura, R. W. Impey, M. L. Klein, *Comparison of simple potential functions for simulating liquid water*, *J. Chem. Phys.* **1983**, *79*, 926–935.
- [354] A. W. Götz, M. J. Williamson, D. Xu, D. Poole, S. Le Grand, R. C. Walker, *Routine Microsecond Molecular Dynamics Simulations with AMBER on GPUs. 1. Generalized Born*, *J. Chem. Theory Comput.* **2012**, *8*, 1542–1555.
- [355] C. J. Woods, F. R. Manby, A. J. Mulholland, *An efficient method for the calculation of quantum mechanics/molecular mechanics free energies*, *J. Chem. Phys.* **2008**, *128*, 14109.
- [356] C. J. Woods, J. W. Essex, M. A. King, *The Development of Replica-Exchange-Based Free-Energy Methods*, *J. Phys. Chem. B* **2003**, *107*, 13703–13710.
- [357] C. J. Fennell, J. D. Gezelter, *Is the Ewald summation still necessary? Pairwise alternatives to the accepted standard for long-range electrostatics*, *J. Chem. Phys.* **2006**, *124*, 234104.
- [358] F. Sievers, A. Wilm, D. Dineen, T. J. Gibson, K. Karplus, W. Li, R. Lopez, H. McWilliam, M. Remmert, J. Soding, J. D. Thompson, D. G. Higgins, *Fast, scalable generation of high-quality protein multiple sequence alignments using Clustal Omega*, *Mol. Syst. Biol.* **2011**, *7*, 539.
- [359] A. M. Waterhouse, J. B. Procter, Martin, David M A, M. Clamp, G. J. Barton, *Jalview Version 2--a multiple sequence alignment editor and analysis workbench*, *Bioinformatics* **2009**, *25*, 1189–1191.

8 APPENDICES

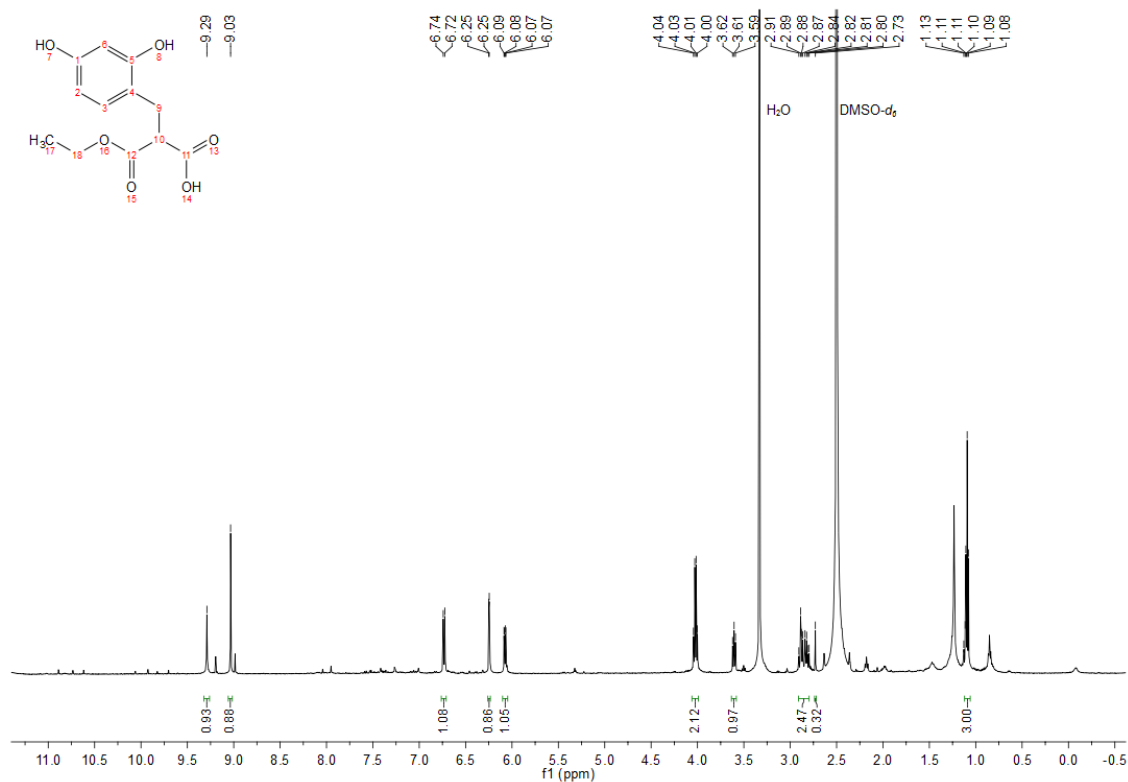
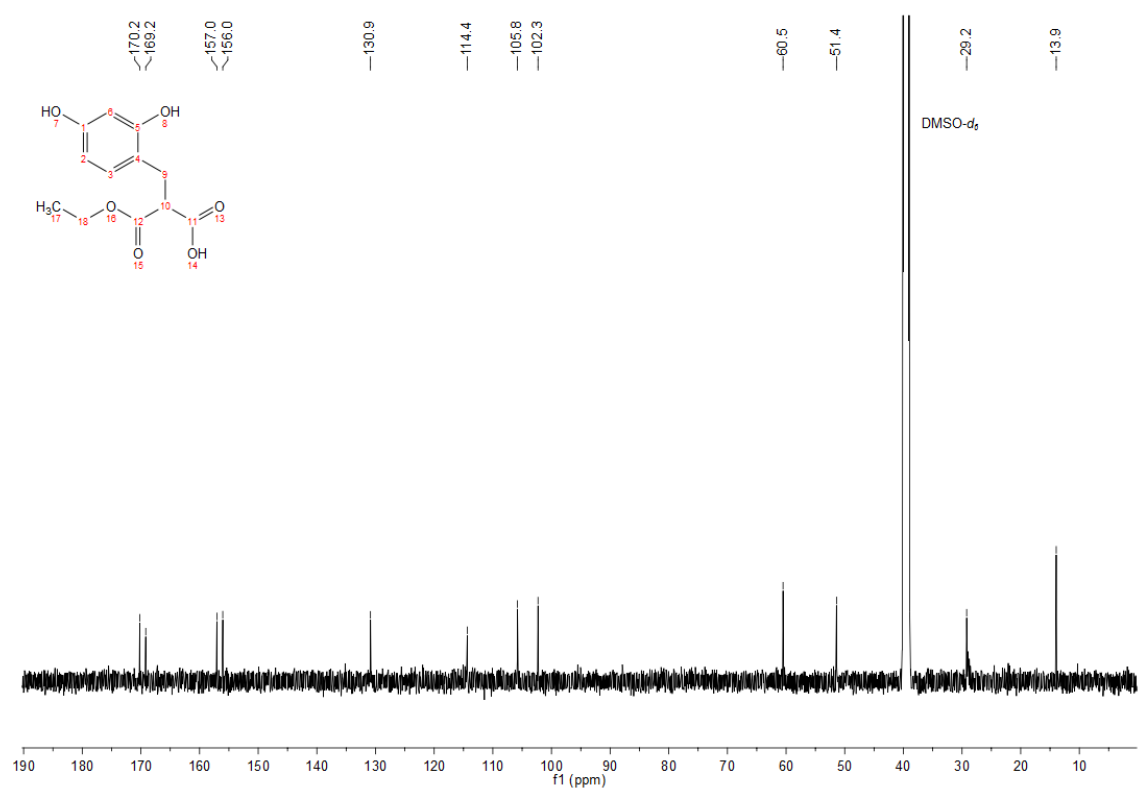
8.1 List of Abbreviations and Acronyms

3-CCE	3-carboxycoumarinethylester
AMP	ampicillin
APCI	atmospheric pressure chemical ionization
APS	ammonium persulfate
cal	calculated
CD	circular dichroism
conv	conversion
CP	circular permutation
CV	column volume
<i>de</i>	diastereomeric excess
DEE	diethyl ether
DIPE	diisopropyl ether
DMSO	dimethyl sulfoxide
DNA	deoxyribonucleic acid
dNTP	deoxy nucleoside triphosphate
DSC	differential scanning calorimetry
<i>E. coli</i>	<i>Escherichia coli</i>
EDTA	ethylenediaminetetraacetic acid
<i>ee</i>	enantiomeric excess
EI	electron ionization
eq	equivalent
ER	ene reductase

ESI	electrospray ionization
EWG	electron withdrawing group
FMN	flavin mononucleotide
FPLC	fast protein liquid chromatography
GC	gas chromatography
GDH	glucose dehydrogenase
H/DX	hydrogen deuterium exchange
HOS	higher-order structures
HPLC	high pressure liquid chromatography
HR	high resolution
IFD	induced fit docking
IMAC	immobilized metal ion affinity chromatography
IPTG	isopropyl β -D-1-thiogalactopyranoside
ISM	iterative saturation mutagenesis
ITC	isothermal titration calorimetry
KAN	kanamycin
KP _i	potassium phosphate
LB	Lysogeny broth
LC	liquid chromatography
M	molar
MS	mass spectrometry
MTBE	methyl tertbutyl ether
MV	methyl viologen
NAD(P)H	nicotinamide
NMR	nuclear magnetic resonance
OD	optical density
OYE	Old Yellow Enzyme
PCR	polymerase chain reaction
ppm	parts per million

QQC	quick quality control
RBD	rigid body docking
RP	reverse phase
rpm	rounds per minute
SDS	sodium dodecyl sulphate
SEC	size exclusion chromatography
T _a	annealing temperature
T _M	melting temperature
TB	Terrific broth
TEMED	Tetramethylethylenediamine
TET	tetracycline
TOF	turnover frequency
TON	turnover number
Tris	tris(hydroxymethyl)aminomethane
U	unit
UV	ultraviolet
wt	wild type

8.2 NMR Spectra of Upscale Reaction with 3-CCE

Figure 65. ¹H-NMR of **13c** from upscale reaction with *TsER C25D/I67T*. 500 MHz in dmsO-*d*₆.Figure 66. ¹³C-NMR of **13c** from upscale reaction with *TsER C25D/I67T*. 500 MHz in dmsO-*d*₆.

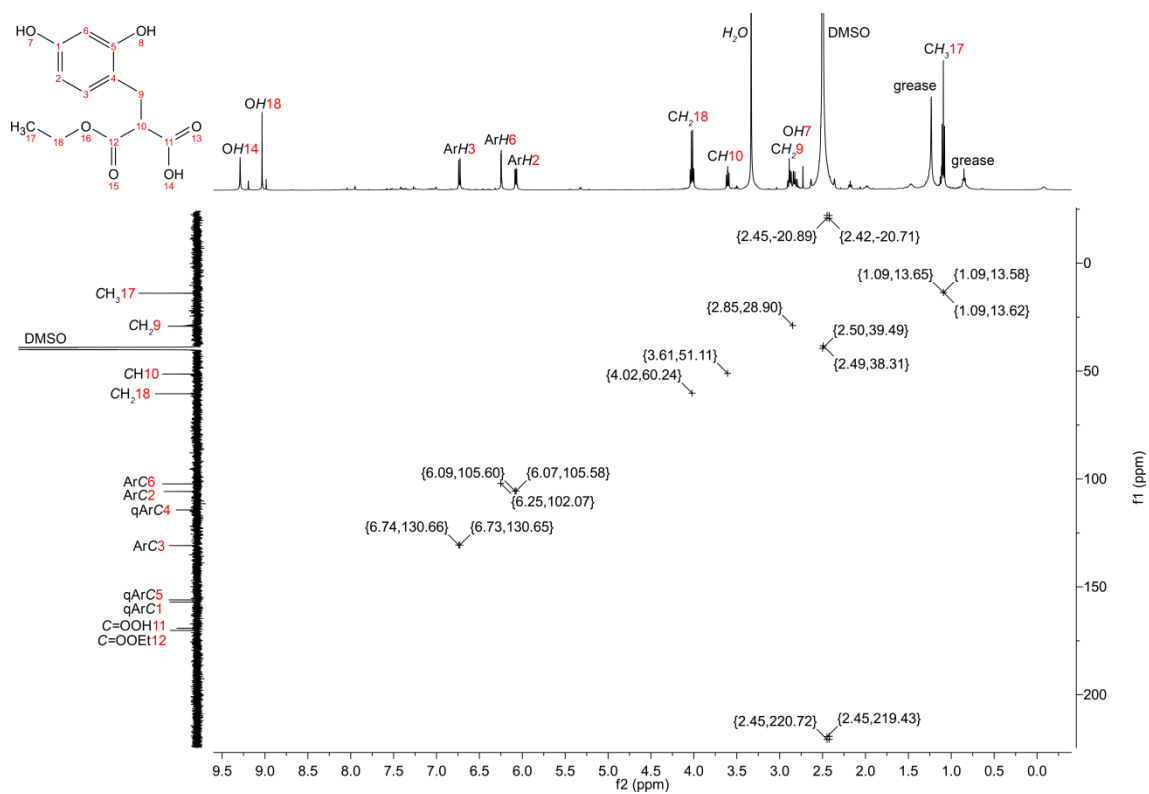


Figure 67. HSQC of **13c** from upscale reaction with *TsER* C25D/I67T. 500 MHz in dms-*d*₆.

pET-28a(+) sequence landmarks

T7 promoter	370-386
T7 transcription start	369
His*Tag coding sequence	270-287
T7*Tag coding sequence	207-239
Multiple cloning sites (<i>Bam</i> H I - <i>Xho</i> I)	158-203
His*Tag coding sequence	140-157
T7 terminator	26-72
<i>lac</i> I coding sequence	773-1852
pBR322 origin	3286
Kan coding sequence	3995-4807
f1 origin	4903-5358

The maps for pET-28b(+) and pET-28c(+) are the same as pET-28a(+) (shown) with the following exceptions: pET-28b(+) is a 5368bp plasmid; subtract 1bp from each site beyond *Bam*H I at 198. pET-28c(+) is a 5367bp plasmid; subtract 2bp from each site beyond *Bam*H I at 198.

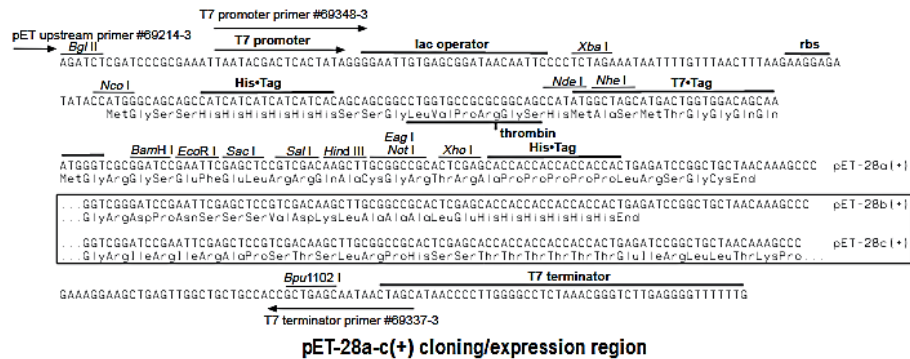
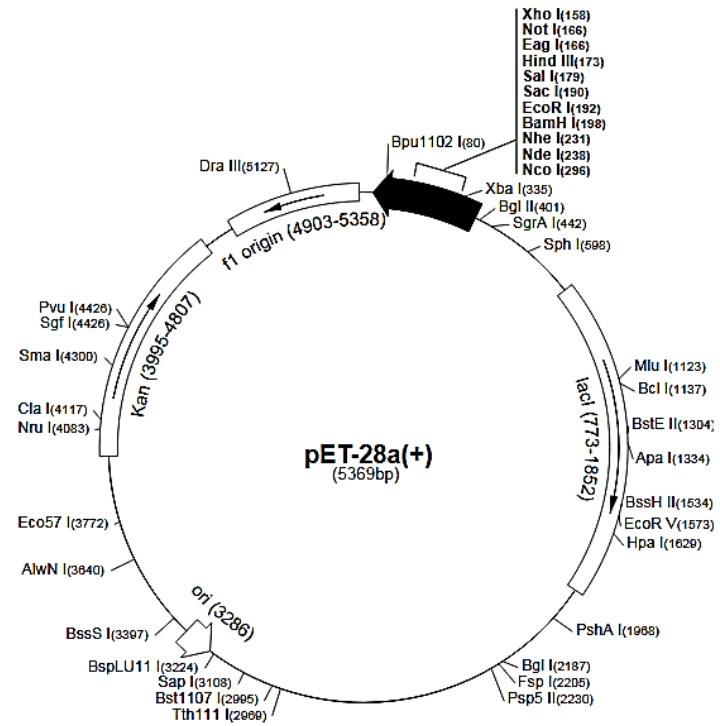


Figure 69. The pET-22b(+) vector of Novagen, Darmstadt Germany carries an N-terminal His Tag/thrombin/T7 Tag configuration. Unique sites are shown on the circle map. The cloning/expression region of the coding strand transcribed by T7 RNA polymerase is shown below.^[99]

8.3.2 OYE Genes

tser >gi|166997947|emb|AM902709.1| *Thermus scotoductus* chrR gene for chromate reductase, strain SA-01

```
ttcaattgggtaacgcccgggtttcccagtcgagcgtgcagaacgacggctaagctctcgaggatccatataccccgaagaggaggcttccacgtagcggaggcagc
cgccagatcggagccttgcacctgaccgaagccggggttcalaagaccagctctatcccaaaaaagagcgcggggaaccggccccacgggactgttcttaccgttcc
ttcaagagccctcataatggaggcatggccttgccttccaccttggaaactcggcgctccgctgaaaaaccgctggccatgtccccatgtccagctactccgccac
cttggaggagaggtaaccgactggcacctctccactaccccacgccccttgggggctgagggtcattctggtggaggccaccgctggaacctttggccgctat
cagccctatgacctgggcatctggtcgaggatcaccttccggcctgaaggagctcgcgggaggtaccgggaagctggagcgggtgcccgggatccagctggccac
gcccggcgcaaggcggggaccgcccctgggaagggggaaagccccctggctgcggggtggtggggccaagccccattcccttgacgagggctaccgggtacc
cgaaccttggagcagcaggatggagcgcacctccacggccttctggaaggagccagcgtcccttagggcaggctttaggtgatcagctccacatggccatg
gtactctcttctctctctctcccccttccaaccagcgcaccagcctacgggggaagcctggaaaaccgatgccttccccccaggtggcccaggcagtgccgg
aggtggtgccaggagcttcccctttctgctcgggtctccgcccagcactggggggaagggaggtggagcctcgaggacaccttggcctcggccgaggttaagga
gtgggggtggacctttgactgtctctcggcggggtggtgctcagggtgctgattccccctggccccggctttaggtgctctcggcagccgtgccaagaggggt
gggctgcaacgggagcctggcctcaccacccccgagcaggcggaaacctctcagcggggaagcgcgcatctggtgcttctggccgggttctctcagg
gacctacttccccctacgggctgccaaggccttggcgtgccccggaggtacccccagctaccaaggggggttttagccatccaacctgcaaggaaccagggttg
agggcaccggccagtctct
```

drer >gi|15807184|ref|NP_295913.1| NADH-dependent flavin oxidoreductase [*Deinococcus radiodurans* R1]

```
atgacctgtcttccgctgcacctcaaccgccagtcccgcgcccgtgctgtttaccccctgaaactcgcagcctggaactcccaaccgggtgctgctcggcc
atgtgacctactcggcagaccgagcgtcccaacgaatttaccctctccacctcggccagctacgctcggcgggcagggtgattctgcccaggccaccgccctgt
cgcccaggggccgcatcaccggagacctgggctgtgggacgaccgagatcgtgcccgtgggcccacatcactgattctgacacagcagcggcgccacattggg
gtgacgtcgcgacgcccagcgaagcgcagcctacgccccctggcgcgcaagggcgcggtgcccgcgagttggcgcgctggcaggtcatcggacctgacgag
aacagcttccagccttccccaccggcagatgagggcggcagcagctgcccggctgtggagcctttagctcggccgcccggcgcctcaggtcgggggtt
gacgctgtggaagtccacgcccgcacggctacctgctgaccagttctctcgcgctggccaaccccaccgacgattacggcgctctcgaaaaccgaccggc
tgctgctgaagtcgctcggcggctggcagcttggcccaccctgcccgtgttctgctgctgagcggcagcggactggccgagggcggtggacctggaacag
acggctgcaactcagaaactgctcaagctagagggcgtggagctgctgacatcagcagcgggggattgaccgcccagcagatcagaggtcggccccggctacgg
tgccgtttggcccccgtgagcggcggcaaaccaatctcgggtgatggcgctggcctcctcagagcggcgcgagggcagggccatctgacggcagggcagcgc
cgacctgatcgcctcggcggccccctctcgcgacccccactggcgcgagcgcgcccggcgggaactcgggttgcggcggtgtccatcgaccagctacgcccggcg
gggtggtaa
```

rmer >tr|Q1LDQ5|Q1LDQ5_CUPMC Putative NADH-dependent flavin oxidoreductase [*Ralstonia metallidurans*]

```
atgcctcatcttctgatcgtaccggatggcaatctcgagcttccaaccgcatcgcacgcgcatgtgcccagctactggcacaggaagcaatgccaccgactgca
catgattcacctgggagatggcgtgtcggagcgggctgtctatcctgaagccaccggttctgctgaaggccatcacgcccagcacttggctgtacaac
gatgcaacgaagctgcgctgggcccgtgtgcttggcgtgctgcaacattcgcctcggctgaccatccagcttggccatgctggccgcaaggcctcagcgaagc
gctgggagtgccggcgccagattcgaccgaccgagcgtgctgcaacattcgcctcggcagcttggcagctgcccagtgccagtgccgaggaagtgcccggcggcgt
cgacaaggccggtatgaagaagattcgcgacgactctgctcggcgtgccaagcgcgcccgtcctgggtatcgaaggcatcgaagtgcagctggcctcagcgtactgc
tgcaccagtttcttcccatcggcaatcaccgtacggacgaatacgggtggcagcctcagaaaccggatgccttcccctggaagtgtcagcggctcggagagggctt
ctgcccgaacgtccgctgctgctgcttccgccaccgactgggtgccaatggatgggacatcaggggacatcgcgctatcgcacgaactgaaggcgcgtggca
gtgcccggctgcatgtgagcagggcgctgtcggcagcagggccatcaagattggcccgggatacagggtgccttacgcgcaacgcgtcaaggcggaggtgggggt
tgccgacgatggcgctgggctgatcaccgaagccgaacagccgaagcagatcgcgaacatgaggcggacattatctcagcggccgcatgctgtacgaccg
cgctggcgtggcagcggcgccaagcttggcgtagtgtcaacgcgccaagcagatgtggcctcagcccgcgggctggaagctgttaagagcgcgact
tggccagcgtga
```

8.3.3 Protein Sequences

TsER >tr|B0JDW3|B0JDW3_THESC Chromate reductase [*Thermus scotoductus*]

```
MALLFTPLELGGRLRLKNRLAMSPMCQYSATLEGEVTDWHLHYPTRALGGVGLILVEATAVEPLGRISP
YDLGIWSEDHLPGLKELARRIREAGAVPGIQLAHAGRKAGTARPWEGGKPLGWRVVGPSPIPFDEGYYPV
PEPLDEAGMERILQAFVEGARRALRAGFQVIELHMAHGYYLLSSFLSPLSNQRDAYGGSLENRMRFLQ
VAQAVREVVPRELPLFVRVSATDWGEGGWSLEDTLAFARRLRELGVLDLLDCSSGGVVLVRVRIPLAPGFQ
VPFADAVRKRVRGLRTGAVGLITPEQAETLLQAGSADLVLLGRVLLRDPYFPLRAAKALGVAPEVPPQY
QRGF
```

DrER >gi|15807184|ref|NP_295913.1| NADH-dependent flavin oxidoreductase [*Deinococcus radiodurans* R1]

MTVSSAAAPQPASPAAPLLFTPLKLSLELPNRRVVVSPMCTYSATDGVANEFHLVHLGQYALGGAGLIL
AEATAVSPEGRITPEDLGLWDDRQIVPLGHITDFVHQHGGHIGVQLAHAGRKASTYAPWRGKGAVPAE
LGGWQVIGPDENSFHDLPFTPAMMGADELRGVVDAFSAARRAQVAGFDAVEVHAAHGYPYLLHQFLS
PLANTRTDDYGGSFENRTRLLLEVVRVAVRHVWPAHLPLFVRLSATDWAEGGWDLQTVQLSKLLKYEG
VDVLDISSGGLTAAQQIEVGPYQVFPFAAAVSRAETEISVMAVGLIETGAQAEAILQAGDADLIALGRPF
LRDPHWAQRAARELGLRPVSIDQYARAGW

RmER >tr|Q1LDQ5|Q1LDQ5_CUPMC Putative NADH-dependent flavin oxidoreductase [*Ralstonia metallidurans*]

MPHLFDPYRIGNLELANRIAIAIPMCQYSAQEGNATDWHMIHLGQMALSGAGLLIEATAVSPEGRITPT
DLGLYNDANEALGRVLGAVRNHSPIAVTIQLAHAGRKASSEAPWDGGGQIRPDQPRGWQTFAPSAV
PHAAGEVPPAALDKAGMKKIRDDFVAAAKRAARLIGIEVHGHAHGYPYLLHQFLSPIANHRTDEYGGSL
ENRMRFPLEVFDAVREAFPAERPVMRVSATDWPNGWDIEGTIALSHELKARGSAAVHVSTGGVSPQ
QAIKIGPGYQVYPYAQRVKAEVGLPTMAVGLITEAEQAEAIANNEADIISIARAMLYDPRWPWHAAAKL
GASVNAPKQYWRSQPRGLEKLFKDAHFGQR

Table 25. Alignment of listed sequences for Figure 4 (chapter 3.1.2) was created with Clustal Omega^[358] and viewed in JalView^[359]. Sequences are sorted by pairwise identity.

OYE name	Organism	accession numbers
<i>DrER</i>	<i>Deinococcus radiodurans</i>	NP_295913.1
GkOYE	<i>Geobacillus kaustophilus DSM 7263</i>	YP_148185.1
Gox	<i>Gluconobacter oxydans 621H</i>	YP_190936
KYE1	<i>Kluyveromyces lactis</i>	P40952
NCR	<i>Zymomonas mobilis</i>	Q5NLA1
NemA	<i>Pseudomonas putida ATCC 17453</i>	AHC69715
OPR1	<i>Solanum lycopersicum</i>	Q9XG54
OPR3	<i>Solanum lycopersicum</i>	Q9FEW9
OYE1	<i>Saccharomyces pastorianus</i>	Q02899
OYE2	<i>Saccharomyces cerevisiae</i>	Q03558
OYE2.6	<i>Pichia stipitis</i>	ABN66026
OYE3	<i>Saccharomyces cerevisiae</i>	P41816
PETNR	<i>Enterobacter cloacae PB2</i>	P71278
<i>RmER</i>	<i>Ralstonia metallidurans</i>	ABF11721
TOYE	<i>Thermoanaerobacter pseudethanolicus</i>	ZP_00777979
TsER	<i>Thermus scotoductus SA-01</i>	Q5SLY6
XenA	<i>Pseudomonas putida ATCC 17453</i>	Q9R9V9
XenB	<i>Pseudomonas putida ATCC 17453</i>	AGS77941
YqjM	<i>Bacillus subtilis</i>	P54550

Table 26. Overview of OYE scaffold residues at hotspot positions. Primary structure of active site residues partially determines classification of OYE scaffolds. According to TOOGOOD *et al.*^[61] group 1 contain the “classical” OYE with the model systems OYE1 and PETNR, harbouring an absolutely conserved threonine in hotspot position I, a bulky aromatic residue either tyrosine or tryptophan in position II and a second bulky hydrophobic residue in position III, often tryptophan, with the exception of OYE2.6. Contrary, group 2 contains the “thermophilic-like” OYE family member with the model system YqjM, having an absolutely conserved cysteine in hotspot position I, a hydrophobic isoleucine in position II and a small residue (often alanine) in position III. Since position I+II+III form an important part of the binding pocket wall close to flavins N5 atom, the differences in size induced by the wild type residues have a significant effect on substrates active orientation within the active site.^[163]

OYE scaffolds	amino acid residues at hotspot positions			
	I	II	III	IV
Group 1				
OYE1	T37	Y82	W116	H194
OYE2.6	T35	Y78	I116	H191
PETNR	T26	Y68	W102	H184
NCR	T25	W66	W100	N175
XenB	T25	Y66	W100	N176
NemA	T24	Y66	W100	H182
Group 2				
<i>TsER</i>	C25	I67	A102	H175
YqjM	C26	I69	A104	H167
<i>DrER</i>	C40	I81	A116	H194
<i>RmER</i>	C25	I66	A102	H181
XenA	C25	I66	A101	H181

8.4 GC chromatograms

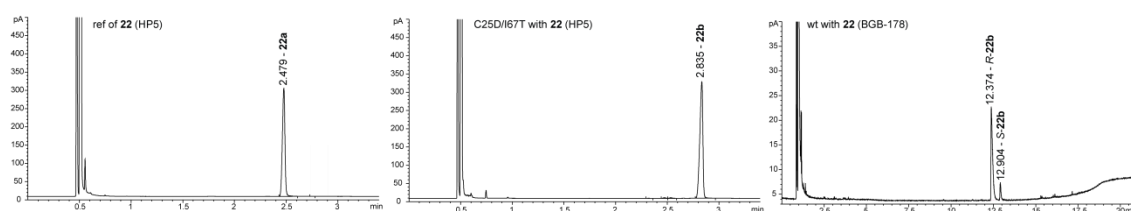


Figure 70. Exemplarily shown achiral and chiral GC measurement with **22**.

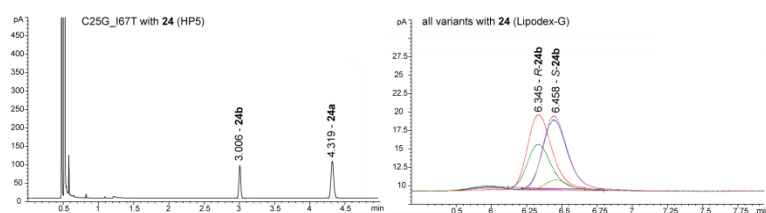


Figure 71. Exemplarily shown achiral and chiral GC measurement with **24**

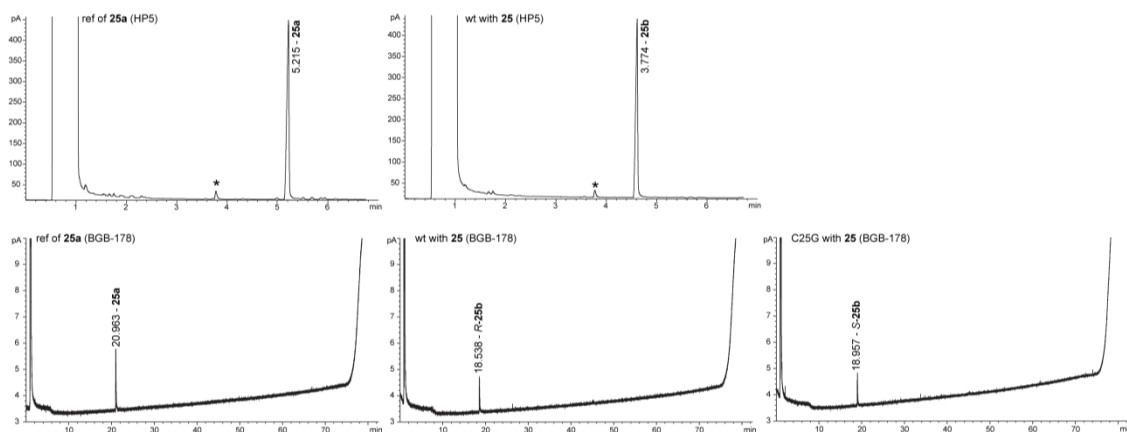


Figure 72. Exemplarily shown achiral and chiral GC measurement with 25.

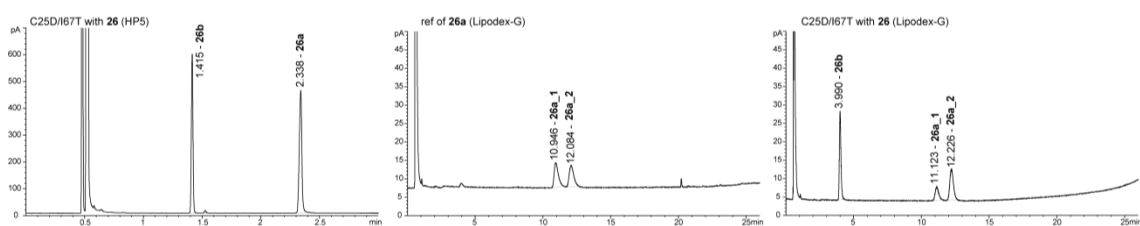


Figure 73. Exemplarily shown achiral and chiral GC measurement with 26.

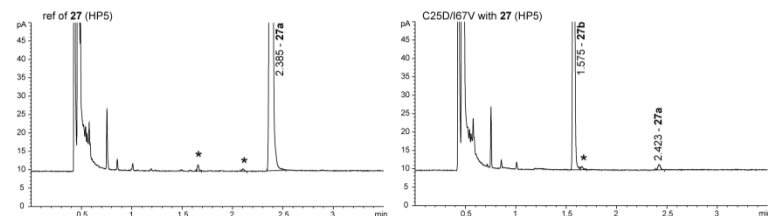


Figure 74. Exemplarily shown achiral GC measurement with 27. *impurity from commercial substrate stock solution.

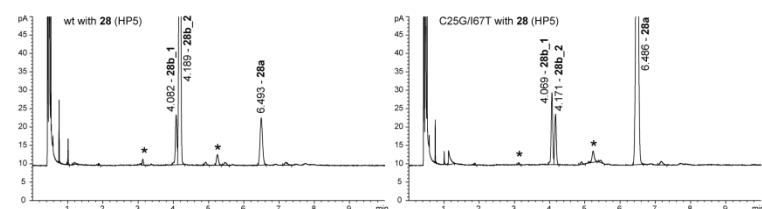


Figure 75. Exemplarily shown achiral and chiral GC measurement with 28. *impurity from commercial substrate stock solution.

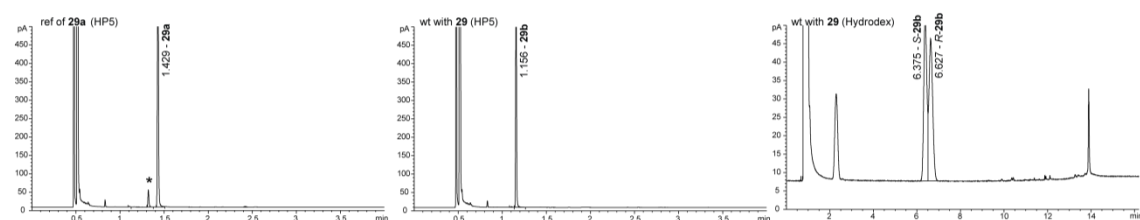
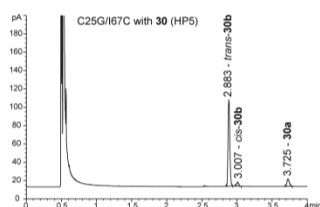
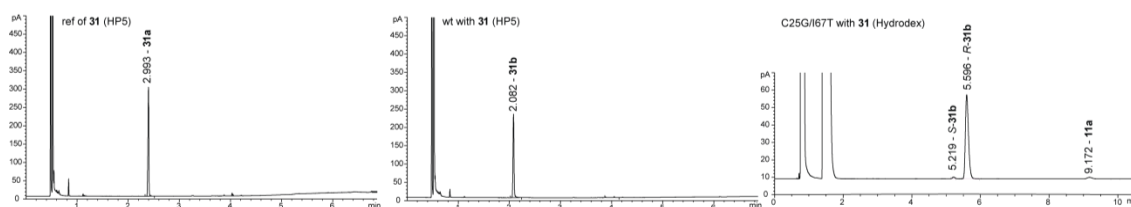
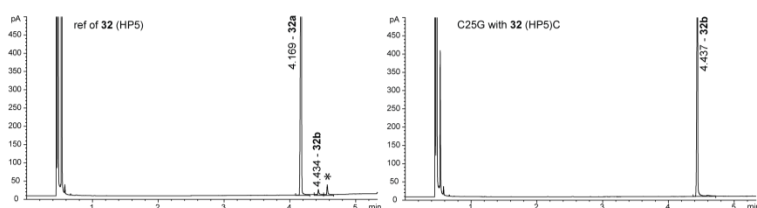
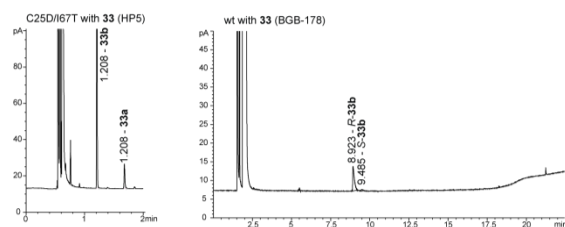
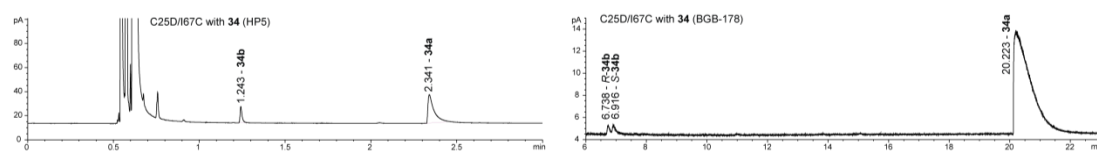
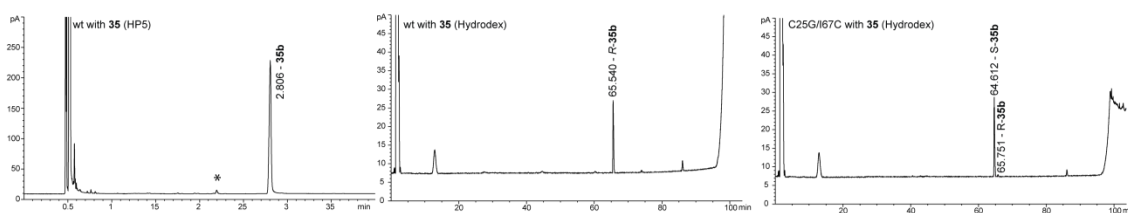


Figure 76. Exemplarily shown achiral and chiral GC measurement with 29. *impurity from commercial substrate stock solution.

Figure 77. Exemplarily shown achiral GC measurement with **30**.Figure 78. Exemplarily shown achiral and chiral GC measurement with **31**.Figure 79. Exemplarily shown achiral and chiral GC measurement with **32**. *impurity from commercial substrate stock solution.Figure 80. Exemplarily shown achiral and chiral GC measurement with **33**.Figure 81. Exemplarily shown achiral and chiral GC measurement with **34**.Figure 82. Exemplarily shown achiral and chiral GC measurement with **35**. *impurity from commercial substrate stock solution.

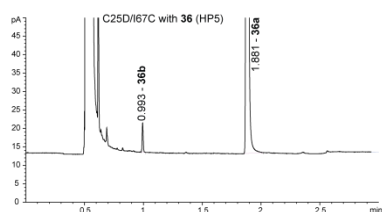


Figure 83. Exemplarily shown achiral GC measurement with 36.

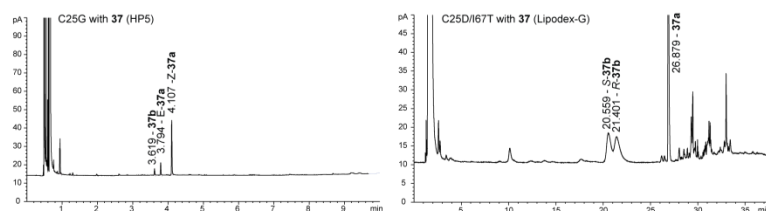


Figure 84. Exemplarily shown achiral and chiral GC measurement with 37.

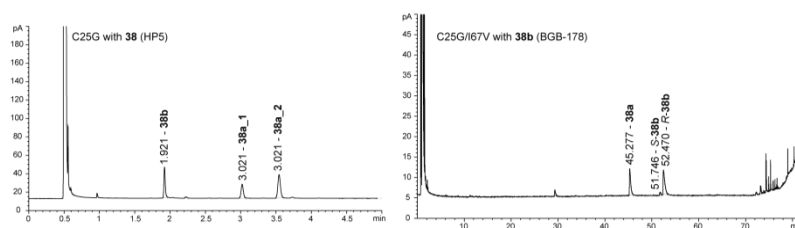


Figure 85. Exemplarily shown achiral and chiral GC measurement with 38.

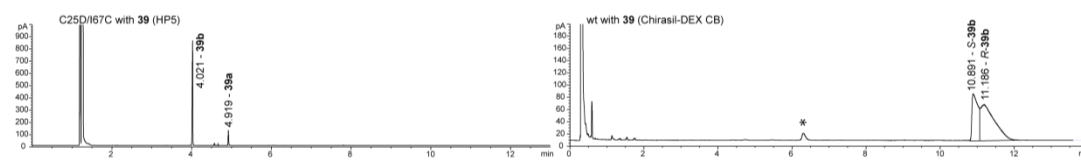


Figure 86. Exemplarily shown achiral and chiral GC measurement with 39. *impurity from commercial substrate stock solution.

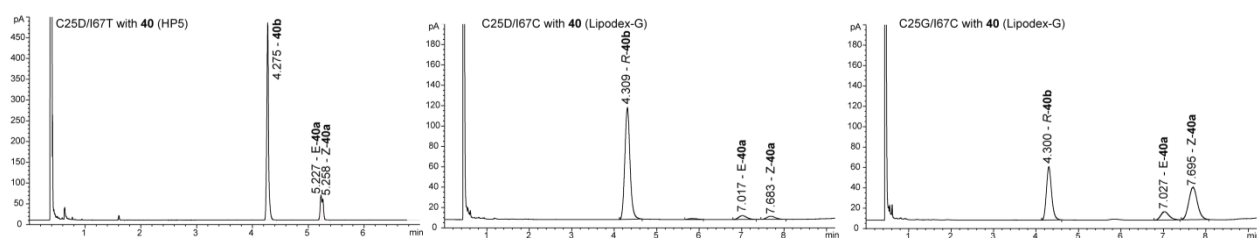


Figure 87. Exemplarily shown achiral and chiral GC measurement with 40.

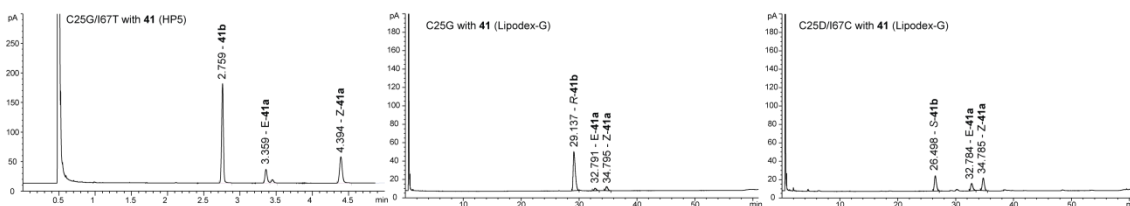


Figure 88. Exemplarily shown achiral and chiral GC measurement with 41.

8.5 Docking

Table 27. Results from RBD of substrates **11a-57a** in the reduced *TsER* wt based on 3HGJ crystal structure. Experimental screening of substrate as (a) racemate (b) E/Z 1:4, (c) E/Z 2:3, (d) E/Z 7:1, (e) E/Z 1:1, n.t. not tested, n.d. not detected. “would” means hydride transfer angle in a range of 80-120° and distance to the hydride of N5 in a range of 3.00 to 4.85 Å, “might” means either hydride transfer angle to small or distance to N5 to large.

Substrate	Empirical Result conv (%) / ee (%)	Pose	Glide Gscore	Glide Energy	Notes	Hydride transfer angle	distance hydride N5 to substrate	result
17a	1 / 765	1	-5.026	-20.847	normal pose, H-bond of H175 to C=O (1.96 Å)	78.0	5.37	no hydride transfer
		2	-4.963	-21.088	normal pose, H-bond of H175 to C=O (2.05 Å), bad contact of Y177 to C5	82.3	5.03	no hydride transfer
		3	-4.928	-18.36	new flipped pose, H-bond of R347 to C=O (1.83 Å, 2.34 Å)	85.3	3.86	might result in R-17b
		4	-4.766	-18.855	new normal pose, H-bond of R347 to C=O (1.99 Å, 2.24 Å), bad contact of R347 to C2	74.2	5.44	no hydride transfer
		5	-4.467	-19.277	flipped pose, H-bond of H175 to C=O (2.05 Å), bad contact of R347 to C4	68.4	4.04	might result in S-17b
24a	n.c.	1	-5.232	-20.731	normal pose, H-bond of H175 to C=O (2.09 Å), bad contacts of R347 to Iso, of Y177 to C5	85.8	4.91	no hydride transfer
		2	-5.187	-20.471	normal pose, H-bond of H175 to C=O (2.07 Å), bad contacts of R347 to Iso, of Y177 to C6, of I67 to C5	91.3	4.34	no hydride transfer
		3	-5.125	-21.893	normal pose, H-bond of H175 to C=O (2.03 Å), bad contacts of R347 to Iso, of Y177 to C4 and C6	82.3	4.87	no hydride transfer
		4	-4.875	-19.905	normal pose, H-bond of H175 to C=O (2.03 Å)	74.9	5.74	no hydride transfer
25a	>99 / >99R	1	-6.129	-27.949	new flipped pose, H-bond of R347 to C=O (2.78 Å) and of Y27 (2.16 Å), H-bond of H175 to C=OOMe (1.97 Å), bad contacts of H172 and A58 to OMe	106.4	3.52	would result in S-25b
		2	-5.909	-25.548	normal pose, H-bond of H175 to C=O (2.02 Å) and of R347 to C=OOMe (1.83 Å), bad contact of Y177 to C6	81.2	4.80	no hydride transfer
		3	-5.836	-27.455	new flipped pose, H-bond of R347 to C=O (2.27 Å, 2.38 Å) of H175 to C=OOMe (2.00 Å), bad contact of R347 to C6	101.9	4.01	would result in S-25b
R-26a^a	1 / rac	1	-5.13	-19.68	new normal pose, H-bond of R347 to C=O (1.87 Å, 2.16 Å), bad contacts of Y177 and C5CH ₃	87.0	5.76	no hydride transfer
		2	-5.126	-20.778	new flipped pose, H-bond of R347 to C=O (2.00 Å, 2.22 Å), bad contacts of Y177 and C3CH ₃	76.2	3.89	might result in 3R,5S-26b
		3	-4.881	-22.511	normal pose, H-bond of H175 to C=O (2.05 Å), bad contacts of R347 to C4 and Y27 to C5CH ₃	76.5	5.54	no hydride transfer
		4	-4.825	-20.643	flipped pose, H-bond of H175 to C=O (2.00 Å), bad contact of R347 to C4 and Y27 to C3CH ₃	73.3	3.94	might result in 3R,5S-26b
		5	-4.819	-20.959	flipped pose, H-bond of H175 to C=O (2.08 Å), bad contact of Y27 to C3CH ₃	71.9	4.03	might result in 3R,5S-26b

S-26a^a	1 / rac	1	-5.145	-20.626	new flipped pose, H-bond of R347 to C=O (1.97 Å, 2.23 Å), bad contacts of Y177 to C3CH ₃	77.2	3.95	might result in 3R,5S- 26b
		2	-5.042	-19.603	new normal pose, H-bond of R347 to C=O (2.05 Å, 2.08 Å), bad contacts of Y177 to C5CH ₃	79.7	5.75	no hydride transfer
		3	-5.019	-20.411	new flipped pose, H-bond of R347 to C=O (2.03 Å, 2.21 Å), bad contacts of Y177 to C3CH ₃	74.6	3.87	might result in 3R,5S- 26b
		4	-4.71	-20.36	flipped pose, H-bond of H175 to C=O (2.07 Å), bad contact of Y27 to C3CH ₃	70.9	4.20	no hydride transfer
		5	-4.697	-21.116	normal pose, H-bond of H175 to C=O (2.03 Å), bad contacts of Y177 to C6, of Y27 to C5CH ₃ and of R347 to C4	76.0	5.69	no hydride transfer
27a	99 / achiral	1	-5.544	-24.194	flipped pose, H-bond of H175 to C=O (1.80 Å), bad contact of H172 to CH ₃	105.3	3.49	productive pose
		2	-5.535	-23.786	wrong double bond location!	-	-	-
		3	-5.349	-23.257	wrong double bond location!	-	-	-
		4	-5.241	-22.829	flipped pose, H-bond of H175 to C=O (1.90 Å), bad contact of H172 to I67	99.6	3.91	productive pose
S-28a	88 / 83 (isomer 2)	1	-4.284	-19.417	H-bond of Y27 to C=O (2.23 Å) and of R347 to C=O (2.30 Å), bad contact of Y177 to C6	61.2	4.88	no hydride transfer
		2	-4.226	-20.386	H-bond of H175 to C=O (1.81 Å), bad contacts of Y177 to C5, of R347 to 4-propen-2-yl	29.1	5.79	no hydride transfer
		3	-4.214	-19.722	flipped pose, H-bond of H175 to C=O (2.12 Å), bad contacts of R347	96.2	4.32	might result in (1r,4r)- 28b (trans)
		4	-4.21	-19.484	flipped pose, H-bond of H175 to C=O (2.11 Å), bad contacts of R347	96.4	4.35	might result in (1r,4r)- 28b (trans)
29a	>99 / 93R	1	-5.315	-18.814	flipped pose, H-bond of H175 to C=O (1.82 Å)	107.0	3.04	would result in R- 29b
		2	-5.312	-18.861	normal pose, H-bond of H175 to C=O (2.06 Å), bad contacts of Y177 to C6 and of I67 to C5	92.9	4.22	might result in S- 29b
		3	-4.919	-17.147	new normal pose, H-bond of R347 to C=O (1.91 Å)	99.4	4.26	might result in R- 29b
		4	-4.883	-19.073	flipped pose, H-bond of H175 to C=O (2.07 Å)	72.9	3.87	might result in R- 29b
		5	-4.498	-16.835	new normal pose, H-bond of R347 to C=O (1.86 Å, 2.66 Å), bad contacts of H175 to C4 and of Y27 to C2	77.2	3.98	might result in S- 29b
22a	>99 / 90R	1	-6.146	-27.069	flipped pose, H-bond of H175 to C1=O (2.04 Å), H-bond of R347 (2.49 Å) and Y27 (2.39 Å) to C4=O, bad contacts of Y177 to 2CH ₃ and of I67 to 6CH ₃	94.8	3.18	would result in R- 22b
		2	-5.801	-24.422	flipped pose, H-bond of H175 to C1=O (2.22 Å), of R347 to C4=O (2.27 Å, 1.84 Å), bad contacts of H175 to 2CH ₃	80.5	3.79	would result in R- 22b
		3	-5.721	-24.852	flipped pose, H-bond of H175 to C4=O (2.00 Å), H-bond of R347 (1.85 Å), 2.64 Å) to C1=O, bad contact of H175 to C3 and of Y27 to 6CH ₃	77.1	3.85	might result in R- 22b
18a	>99 / 91 (2R,5S)	1	-4.698	-20.38	new normal pose, H-bond of R347 to C=O (1.91 Å, 2.78 Å), bad contact of H175 to C4 and of I67 to 5-propenyl	86.5	5.76	no hydride transfer
		2	-4.658	-22.248	flipped pose, H-bond of H175 to C=O (1.81 Å), bad contacts of R347 to 5-propenyl and of I67 to C3	105.1	3.12	would result in 2R,5S- 18b
		3	-4.643	-21.217	flipped pose, H-bond of H175 to C=O (2.09 Å), bad contact of R347 to C4	74.6	3.90	no hydride transfer
		4	-4.515	-21.006	flipped pose, H-bond of H175 to C=O (2.10 Å)	78.5	3.59	no hydride transfer

30a	>99 / 96 (2R,5R)	1	-4.666	-22.814	flipped pose, H bond of H175 to C=O (1.96 Å), bad contact of R347 to 5-propenyl	110.2	2.92	would result in 2R,5R-30b
		2	-4.58	-20.936	flipped pose, H bond of H175 to C=O (2.02 Å), bad contact of H175 to C6	77.9	3.62	no hydride transfer
		3	-4.535	-20.91	flipped pose, H bond of H175 to C=O (2.01 Å), bad contact of R347 to 5-propenyl	79.9	3.64	no hydride transfer
		4	-4.504	-20.498	flipped pose, H bond of H175 to C=O (2.01 Å)	75.9	3.71	no hydride transfer
		5	-4.473	-20.82	flipped pose, H bond of H175 to C=O (2.10 Å), bad contact of H175 and K107 to 5-propenyl, of I67 to 2CH ₃	74.8	3.76	no hydride transfer
E-31a	n.t.	1	-4.874	-28.968	normal pose, H-bond of H175 to C1OOME (2.07 Å), and of R347 to C2OOME (2.25, 2.39 Å), bad contacts of I67 to IOMe and of Y27 to 2OMe	93.3	3.79	would result in S-31b
		2	-4.87	-28.01	H-bond of H175 to C1OOME (2.10 Å) and of R347 to C2OOME (1.83 Å)	119.8	4.03	would result in S-31b
		3	-4.804	-27.031	H-bond of H175 to C1OOME (2.06 Å) and of R347 to C2OOME (2.04, 2.66 Å), bad contacts of I67, Y177, H172 to IOMe	109.7	3.91	would result in S-31b
		4	-4.76	-28.147	normal pose, H-bond of H175 of C1OOME (2.06 Å) and of R347 to C2OOME (2.21, 2.30 Å), bad contacts of I67 to IOMe and of R347 to 2OMe	86.9	3.86	would result in S-31b
		5	-4.71	-27.58	H-bond of H175 to C1OOME (1.80 Å) and of R347 to C2OOME (1.87, 2.70 Å), bad contact of I67 to IOMe	99.6	4.00	would result in S-31b
Z-31a	>99 / >99R	1	-4.914	-27.325	H-bond of H175 to C1OOME (2.16 Å), bad contacts of I67, H172, Y177 to IOMe	114.0	3.71	would result in S-31b
		2	-4.567	-26.515	H-bond of H175 to C2OOME (2.17 Å), bad contacts of I67, H172, Y177 to 2OMe	112.0	3.67	would result in S-31b
		3	-4.297	-24.721	H-bond of H175 to C1OOME (2.00 Å) and to R347 of COMe2 (2.12, 2.36 Å) bad contacts of H175 to IOMe	80.0	3.74	would result in R-31b
		4	-4.183	-22.285	H-bond of R347 to C2OOME (2.23 Å) and to C1OOME (1.94, 2.28 Å)	103.6	3.84	would result in R-31b
		5	-3.947	-21.361	H-bond to R347 of C1OOME (2.39 Å) and to C2OOME (1.83, 2.27 Å)	89.7	4.32	no hydride transfer
32a	97 / >99R	1	-6.788	-32.328	H-bond of H175 to 2C=O (1.87 Å), Pi-cation of R347 to Ph, Pi-pi stacking of H175 to Ph, bad contacts of I67 to CH ₃	106.4	3.11	would result in R-32b
		2	-6.279	-30.295	H-bond of R347 to 5C=O (1.91 Å), Pi-cation of R347 to Ph, Pi-pi stacking of H175 to Ph, bad contact of I67 to CH ₃ and of H175 to 2C=O	81.1	3.63	would result in S-32b
		3	-6.233	-30.252	H-bond of R347 to 5C=O (1.87 Å, 2.71 Å), bad contacts of I67 to CH ₃ and of H175 to 2C=O	81.2	3.69	would result in S-32b
		4	-5.969	-29.405	H-bond of R347 to 2C=O (1.75 Å), Pi-cation of R347 and H175 to Ph, Pi-pi stacking of H175 to Ph, bad contacts of Y27 to CH ₃ and of H175 to 5C=O	89.1	3.62	would result in S-32b
33a	99 / 96R	1	-5.235	-18.821	normal pose, H-bond of H175 to C=O (1.84 Å)	106.2	3.95	would result in S-33b
		2	-5.06	-17.667	flipped pose, H-bond of H175 to C=O (2.24 Å)	99.5	3.22	would result in R-33b
		3	-4.971	-18.553	flipped pose, H-bond of H175 to C=O (2.10 Å), bad contact of I67 to CH ₃	68.3	4.06	no hydride transfer
		4	-4.711	-15.723	new normal pose, H-bond of R347 to C=O (2.20 Å, 2.24 Å)	96.4	4.26	no hydride transfer
		5	-4.561	-15.513	new normal pose, H-bond of R347 to C=O (1.95 Å), bad contacts of I67 to C4 and Y27 to C5	102.8	3.86	would result in R-33b
34a	14 / 94S	1	-4.945	-18.337	normal pose, H-bond of H175 to C=O (1.90 Å)	107.5	3.88	would result in R-34b

		2	-4.833	-17.352	flipped pose, H-bond of H175 to C=O (1.81 Å), bad contact of Y27 to CH ₃	88.6	3.63	might result in S-34b
		3	-4.65	-15.821	new flipped pose, H-bond of R347 to C=O (2.14 Å, 2.20 Å), bad contact of Y177 to CH ₃	69.4	3.96	no hydride transfer
		4	-4.467	-15.737	new normal pose, H-bond of R347 to C=O (1.92 Å), bad contact of Y27 to C4 and C5	112.0	3.58	would result in S-34b
		5	-4.417	-16.212	new normal pose, H-bond of R347 to C=O (1.89 Å, 2.25 Å), bad contact of Y177 to C4 and of H175 to CH ₃	96.9	4.21	no hydride transfer
35a	>99 / >99R	1	-6.006	-27.45	new flipped pose, H-bond of R347 (2.31 Å) and of Y27(2.34 Å) to C=O, H-bond of H175 to C=OMe(2.10 Å), bad contacts of H172 and Y177	97.5	3.46	would result in S-35b
		2	-5.956	-26.903	new flipped pose, H-bond of R347 to C=O (2.20 Å, 2.24 Å), H-bond of H175 to C=OMe (1.86 Å), bad contacts of H172	100.4	3.88	would result in S-35b
		3	-5.879	-26.279	new normal pose, H-bond of R347 to C=O (1.87 Å, 2.71 Å), H-bond of H175 to C=OMe (2.20 Å), bad contacts of H172	109.6	3.74	would result in S-35b
		4	-5.53	-23.999	normal pose, H-bond of C=O to H175 (2.10 Å) and C=OMe to R347 (1.87 Å, 2.63 Å), pose would result in R-15b but the hydride transfer angle is 98°	98.4	4.63	might result in R-35b
		5	-5.407	-24.589	flipped pose, H-bond of to C=O (2.09 Å) and of R347 to C=OMe (1.96 Å, 2.24 Å), bad contact of Y27 to OMe	90.0	4.11	might result in R-35b
36a	2 / n.d.	1	-5.304	-5.304	normal pose, H-bond of H175 to C=O (1.97 Å), bad contacts of I67 and Y177 to C5	105.8	3.89	would result in 2S,3R-36b
		2	-4.993	-4.993	flipped pose, H-bond of H175 to C=O (2.10 Å), bad contacts of I67 to 2CH ₃ and of Y27 to 3CH ₃	68.4	4.06	no hydride transfer
		3	-4.874	-4.874	H-bond of R347 to C=O (1.95 Å), bad contacts of Y177 to 3CH ₃ , of I67 to C4 and of Y27 to C5	105.6	3.64	would result in 2R,3S-36b
		4	-4.814	-4.814	H-bond of R347 to C=O (1.85 Å, 2.64 Å), bad contacts of Y177 to 3CH ₃	71.0	4.14	no hydride transfer
		5	-4.487	-4.487	H-bond of R347 to C=O (1.91 Å, 2.24 Å), bad contacts of Y177 and H175 to 3CH ₃ , of Y177 to C4	96.4	4.19	no hydride transfer
19a	94 / 76R	1	-3.127	-21.613	H-bond of H175 to C=O (1.95 Å), of Y177 to OH (2.15 Å)	77.9	3.41	no hydride transfer
		2	-3.124	-21.703	H-bond of H175 to C=O (1.95 Å), bad contact of H172 to OMe	109.0	3.39	would result in R-19b
		3	-3.087	-21.369	H-bond of H175 to C=O (1.84 Å), bad contact of H172 to OMe	112.1	3.17	would result in R-19b
		4	-2.956	-18.754	H-bond of R347 to C=O (1.80 Å), of R347 to OH (2.18 Å), bad contact of Y27	110.1	3.33	would result in R-19b
		5	-2.732	-20.09	H-bond of R347 to C=O (1.91 Å, 2.79 Å), of R347 to OH (2.35 Å), bad contact of Y27	117.7	3.35	would result in R-19b
Z-37a^b	94 / 46S	1	-3.938	-21.107	H-bond of H175 to C=O (1.87 Å), bad contacts of Y177 and I67 to OMe	34.9	5.30	no hydride transfer
		2	-3.654	-20.914	H-bond of H175 to C=O (1.86 Å), bad contacts of H172 and A58 to OMe, of R347 to C5	52.7	4.49	no hydride transfer
		3	-3.371	-19.21	H-bond of R347 to C=O (1.81 Å), bad contacts of H172 and Y177 to C5	77.9	4.18	no hydride transfer
		4	-3.346	-19.069	H-bond of R347 to C=O (1.83, 2.38 Å), bad contacts of Y177 to C5	95.5	3.72	would result in R-37b
		5	-3.225	-18.072	H-bond of R347 to C=O (1.78 Å), bad contacts of I67 to C5	72.8	4.55	no hydride transfer
E-37a^b		1	-4.335	-22.757	H-bond of H175 to C=O (2.07 Å), bad contacts of and I67 to OMe	36.9	5.02	no hydride transfer
		2	-4.254	-22.909	H-bond of H175 to C=O (2.13 Å), bad contacts of and I67 to OMe	50.5	4.59	no hydride transfer

		3	-3.899	-20.142	H-bond of R347 to C=O (1.83 Å), bad contacts of and I67 to C5	99.3	3.19	would result in S-37b
		4	-3.886	-22.394	H-bond of H175 to C=O (1.84 Å), bad contacts of and I67 to Cl	109.3	2.91	would result in R-37b
		5	-3.807	-22.07	H-bond of H175 to C=O (1.85 Å), bad contacts of and I67 to Cl and C3	90.2	3.48	would result in R-37b
E-38a^c	60 / 99S	1	-2.791	-21.876	normal pose, H-bond of H175 to C=O (1.80 Å)	110.7	3.30	would result in S-38b
		2	-2.68	-22.907	normal pose, H-bond of H175 to C=O (2.13 Å)	88.8	4.74	no hydride transfer
		3	-2.615	-21.242	normal pose, H-bond of H175 to C=O (1.80 Å)	111.2	3.47	would result in S-38b
		4	-2.404	-20.232	normal pose, H-bond of H175 to C=O (2.09 Å), bad contacts of I67 and Y27 to CH ₃	110.3	3.45	would result in S-38b
		5	-2.189	-20.548	normal pose, H-bond of H175 to C=O (2.01 Å), bad contact of R347 to C7, C8	96.1	4.13	no hydride transfer
Z-38a^c		1	-3.294	-23.937	flipped pose, H-bond of H175 to C=O (1.92 Å), bad contacts of Y177 to C4 and of H175 to C8	59.2	3.97	no hydride transfer
		2	-3.236	-23.138	H-bond of R347 (2.15 Å) and of Y27 (2.06 Å) to C=O, bad contacts of Y177 to C4	63.2	3.60	no hydride transfer
		3	-3.202	-22.236	H-bond of H175 to C=O (1.89 Å), bad contacts of Y177 to C4	53.2	4.34	no hydride transfer
		4	-3.122	-23.618	H-bond of H175 to C=O (1.93 Å), bad contacts of Y177 to C4	67.1	3.92	no hydride transfer
		5	-2.947	-22.714	H-bond of H175 to C=O (2.28 Å)	49.3	4.37	no hydride transfer
Z-39a	92 / rac	1	-3.887	-20.434	H-bond of R347 (2.23 Å) and Y27(2.04 Å) to C=O, Pi-pi stacking of H175 to Ph, bad contact of R347 to CH ₃	87.2	4.86	no hydride transfer
		2	-3.863	-21.71	H-bond of H175 to C=O (2.10 Å), bad contacts of H175 to C3	33.3	5.80	no hydride transfer
		3	-3.33	-21.05	H-bond of H175 to C=O (2.05 Å), Pi-cation of R347 to Ph, bad contacts of K107 to Ph and of H175, Y177 to C3	18.1	6.23	no hydride transfer
		4	-3.279	-20.953	H-bond of H175 to C=O (2.00 Å), Pi-cation of R347 to Ph, bad contacts of Y27 and R347 to Ph	53.6	4.92	no hydride transfer
		5	-3.253	-20.08	H-bond of H175 to C=O (1.96 Å), Pi-cation of R347 to Ph	80.5	4.60	no hydride transfer
E-39a	?	1	-5.171	-22.973	H-bond of Y27 (2.22) and of R347 (2.49) to C=O, Pi-pi stacking of H175 to Ph, Pi-cation of R347 to Ph	53.4	4.27	no hydride transfer
		2	-5.129	-23.081	H-bond of H175 to C=O (2.06 Å), bad contacts of I67 to CH ₃ , Pi-cation of H175 to Ph	53.7	4.19	no hydride transfer
		3	-4.87	-21.99	H-bond of Y27 (2.00) and of R347 (2.36) to C=O, bad contact of Y27 to CH ₃	58.0	4.21	no hydride transfer
		4	-4.214	-21.525	H-bond of H175 to C=O (2.00 Å), Pi-cation of R347 to Ph	63.9	4.38	no hydride transfer
Z-40a	91 / >99 unassigned	1	-4.777	-29.657	H-bond of H175 to C=O (2.19 Å) and of R347 to COOEt (2.16 Å), Pi-cation of R347 to Ph	38.2	5.82	no hydride transfer
		2	-4.548	-29.823	H-bond of H175 to C=O (2.00 Å), Pi-cation of R347 to Ph, bad contacts of Y177, R347 and Y27 to Ph, of I67 to C3	83.2	4.16	no hydride transfer
		3	-4.4	-29.436	H-bond of H175 to C=O (2.41 Å) and of R347 to COOEt (1.96 Å), Pi-cation of R347 to Ph, bad contacts of Y177 to C3, of I67 to CH ₃	65.5	5.09	no hydride transfer
		4	-4.313	-29.017	H-bond of H175 to C=O (2.15 Å) and of R347 to COOEt (2.69 Å), Pi-cation of R347 to Ph, bad contacts of Y177 to C3, of I67 to CH ₃	69.7	5.00	no hydride transfer

E-40a	n.t.	1	-5.011	-29.199	H-bond of H175 to COOEt (1.78 Å), Pi-pi stacking of H175 to Ph, bad contacts of Y177, I67 and H172 to Et	67.6	5.81	no hydride transfer
		2	-4.365	-28.665	H-bond of R347 to COOEt (2.15 Å, 2.20 Å), Pi-cation of H175 to Ph	27.0	6.70	no hydride transfer
		3	-3.963	-25.954	H-bond of R347 to C=O (2.05 Å), Pi-cation of H175 to Ph, bad contact of H175 to COOEt and of Y177 to C3 and of I67 to Et	22.2	6.94	no hydride transfer
		4	-3.626	-24.659	H-bond of R347 to COOEt (1.88 Å), Pi-cation of H175 to Ph, bad contacts of Y177 and I67 to Et	44.9	6.41	no hydride transfer
		5	-2.703	-21.147	H-bond of R347 to C=O (2.08 Å, 2.80 Å), Pi-cation of H175 and R347 to Ph, bad contact of Y177 and H175 to Et and of R347 to CH ₃	21.5	6.67	no hydride transfer
E-41a^d	13 / >99S	1	-4.115	-24.009	H-bond of H175 to N=O (1.96 Å), Salt bridges of H175 and H172 to NO, Pi-cation of R347 to Ph, bad contacts of R347 and Y27 to Ph	56.1 (Cβ) 106.9 (Cα)	4.45 3.86	would result in S-41b
		2	-4.056	-21.912	H-bond of H175 to N=O (1.88 Å), Pi-cation of K107 to Ph, bad contact of R347 to Ph	104.1 (Cβ)	4.08	would result in S-41b
		3	-3.91	-22.12	H-bond of H175 to N=O (1.93 Å), Salt bridge of H175 to NO, Pi-cation of K107 and R347 to Ph	93.8 (Cβ)	4.51	would result in S-41b
		4	-3.8	-21.503	H-bond of H175 to NO (2.40 Å), Salt bridge of H175 to NO (3.09 Å), Pi-cation of R347 to Ph, bad contacts of R347 and Y27 to Ph	112.4 (Cβ)	4.25	would result in S-41b
		5	-3.495	-20.617	H-bond of H175 to NO (2.24 Å), Salt bridge of H175 and H172 to NO, bad contacts of R347 and Y27 to Ph	69.0 (Cβ) 94.1 (Cα)	4.66 4.37	would result in S-41b
Z-41a^d		1	-4.615	-25.742	H-bond of R347 (2.19 Å, 2.38 Å) and of Y27 (1.94 Å) to NO ₂ , Pi-cation of R347 to Ph, bad contact of Y177 to CH ₃	56.4 (Cβ) 102.8 (Cα)	3.73 3.18	would result S-41b
		2	-4.512	-24.236	H-bond of R347 (2.20 Å, 2.27 Å) and of Y27 (1.92 Å) to NO ₂ , Salt bridge of R347 to NO, Pi-cation of H175 to Ph, bad contact of Y177 to CH ₃	55.9 (Cβ) 104.7 (Cα)	3.95 3.38	would result S-41b
		3	-4.284	-25.797	H-bond of H175 to N=O (2.04 Å), Salt bridges of H175 and H172 to NO ₂ , Pi-cation of R347 and H175 to Ph, bad contact of Y177 to Ph	57.5 (Cβ) 103.9 (Cα)	4.12 3.58	would result in R-41b
		4	-3.554	-19.327	no H-bond, salt bridge of K107 to NO, Pi-cation of K107 to Ph	154.3	7.07	no hydride transfer
		5	-3.481	-19.365	no H-bond, salt bridge of K107 to NO, Pi-cation of K107 to Ph	156.1	6.67	no hydride transfer
E-43a^e	4 / n.d.	1	-5.181	-28.153	H-bond of H175 to C=O (2.18 Å), Pi-cation of R347 to Ph, Pi-pi stacking of H175 to Ph, bad contacts of H172 and Y177 to OMe	45.3 (Cβ) 119.4 (Cα)	4.45 3.63	would result in S-43b
		2	-5.048	-27.095	H-bond of H175 to C=O (2.07 Å), bad contact of Y177 and H172 to OMe	46.1 (Cβ) 119.0 (Cα)	4.60 3.79	would result in S-43b
		3	-4.785	-25.416	H-bond of Y27 (2.12 Å) and of R347 (2.42 Å) to C=O, Pi-pi stacking of H175 to Ph, Pi-cation of R347 to Ph	57.4 (Cβ) 105.3 (Cα)	4.38 3.82	would result in R-43b
		4	-4.442	-24.456	H-bond of Y27 (2.04 Å) and of R347 (2.37 Å) to C=O, bad contact of R347 to OMe	61.3 (Cβ) 99.6 (Cα)	4.08 3.63	would result in R-43b
		5	-4.359	-23.023	H-bond of Y27 (2.37 Å) and of R347 (1.90 Å) to C=O, of Y27 to OMe	67.1 (Cβ) 94.8 (Cα)	4.33 4.01	no hydride transfer
Z-43a^e		1	-4.739	-26.621	H-bond of H175 (2.28 Å) to C=O, salt bridge of R347 to Br	32.8 (Cβ) 139.0 (Cα)	6.26 6.18	no hydride transfer
		2	-4.246	-24.178	no H-bond, bad contact of R347 to Br	37.6 (Cβ) 131.4 (Cα)	5.37 4.37	no hydride transfer
		3	-4.193	-23.585	no H-bond, salt bridge of R347 to Br, bad contact of R347 to Br	36.5 (Cβ) 132.9 (Cα)	5.39 4.37	no hydride transfer

		4	-4.088	-23.197	H-bond of R347 to C=O (1.92 Å, 2.73 Å), Pi-cation of H175 to Ph, bad contact of H175 to Br	42.2 (C β) 128.7 (C α)	6.72 5.79	no hydride transfer
44a	n.c.	1	-5.339	-22.487	H-bond of R347 to C=O (2.00 Å, 2.22 Å), bad contact of Y177 to CH ₃	75.6	3.89	no hydride transfer
		2	-4.955	-22.257	flipped pose, H-bond of H175 to C=O (2.06 Å), bad contact of Y27 to CH ₃	69.4	4.25	no hydride transfer
		3	-4.701	-21.472	H-bond of R347 (1.98 Å) and of Y27 (2.37 Å) to C=O, bad contact of Y177 to CH ₃ and C4, of R347 to C6	63.7	3.97	no hydride transfer
		4	-4.601	-20.506	flipped pose, H-bond of H175 to C=O (2.06 Å), bad contact of Y177 to C6	64.6	4.15	no hydride transfer
45a	n.c.	1	-4.826	-32.291	H-bond of R347 to C=O (2.30 Å, 2.40 Å) and to C=OOBu (1.90 Å), bad contacts of H172, Y177, H103, I67 and A58 to Bu	59.5 (C β) 103.5 (C α)	4.51 4.00	possible transfer
		2	-4.75	-31.818	H-bond of R347 to C=O (2.20 Å, 2.45 Å) and of C=OOBu (1.90 Å), bad contacts of H172, Y177, A102, I67 and A58 to Bu	56.8 (C β) 106.8 (C α)	4.60 4.02	transfer possible
		3	-4.09	-28.907	H-bond of H175 to C=O (2.06 Å) and of R347 to O (2.50 Å) and of R347 to OBU (1.82 Å, 2.78 Å), bad contact of Y27 to Bu	67.9 (C α) 95.0 (C β)	4.59 4.27	no hydride transfer
		4	-3.653	-26.305	ring vertical to FMN, H-bond of K107 to C=O (2.01 Å), of R347 to O (2.26 Å) and of R347 (1.93 Å) and of Y27 (2.35 Å) to C=OOBu, bad contacts of Y27, P113 to Bu	130.2 (C β) 41.2 (C α)	6.89 5.94	no hydride transfer
46a	n.c.	1	-5.063	-18.103	H-bond of R347 to C=O (1.92 Å, 2.76 Å), bad contact of R347 to C6	132.6	3.89	no hydride transfer
		2	-4.839	-19.685	Double bond not above N5, H-bond of R347 (2.18 Å) and of Y27 (2.25 Å) to C=O, bad contact of H175 to CH ₃	26.2	6.80	no hydride transfer
		3	-4.761	-17.702	H-bond of H175 to C=O (2.19 Å), bad contact of H175 to C6	121.6	3.56	transfer possible
		4	-4.529	-17.879	No H-bond, bad contacts of H175 to C=O, of R347 to C4, of Y177, I67 and Y27 to propanylidene	104.4	3.33	transfer possible
E-42a	n.c.	1	-4.38	-20.94	H-bond of R347 to N=O (1.82 Å) and of Y27 to NO (2.27 Å), bad contacts of Y177 to CH ₃ , of R347 to C1	81.3	4.70	no hydride transfer
		2	-3.755	-21.118	H-bond of H175 to N=O (1.81 Å), bad contacts of Y177 to CH ₃	62.0	5.54	no hydride transfer
		3	-3.511	-21.679	H-bond of H175 to N=O (1.90 Å), bad contact of R347 to double bond in ring	102.0	4.14	no hydride transfer
		4	-3.506	-24.14	H-bond of H175 to N=O (1.99 Å), bad contact of I67 and Y27 to CH ₃ , of R347 to double bond in ring	109.6	3.65	transfer possible
		5	-3.426	-21.115	H-bond of H175 to N=O (1.86 Å), bad contact of R347 to double bond in ring	94.4	4.41	no hydride transfer
Z-42a	n.c.	1	-4.871	-25.994	H-bond of H175 to N=O (1.95 Å), salt bridge of H172 to NO	56.1	4.17	no hydride transfer
		2	-4.866	-22.672	H-bond of R347 to NO ₂ (1.93 Å, 2.30 Å) and of Y27 to N=O (2.01 Å), bad contacts of Y177 to CH ₃	53.4	3.96	no hydride transfer
		3	-4.585	-23.578	H-bond of R347 to NO (2.18 Å, 2.37 Å) and of Y27 to N=O (2.00 Å), bad contacts of Y177 to CH ₃	56.8	3.78	no hydride transfer
		4	-4.438	-23.409	H-bond of H175 to NO (1.87 Å), bad contacts of Y177 to ring	57.7	3.99	no hydride transfer
47a	n.c.	1	-4.482	-31.823	H-bond of H175 to NO (2.02 Å), Pi-cation of H175 and R347 to Ph, Pi-pi stacking of H175 to Ph, salt bridge of H175 and H172 to NO, bad contacts of R347 and Y27 to Ph	53.8	4.49	no hydride transfer
		2	-4.186	-30.136	H-bond of H175 to NO (2.01 Å), Pi-cation of H175 and R347 to Ph, Pi-pi stacking of H175 to Ph, salt bridge of H175 to NO, bad contacts of R347 and Y27 to Ph	46.9	4.81	no hydride transfer

		3	-4.117	-27.251	Double bond not above N5, salt bridge of NO to K107, Pi-cation of K107 to Ph and Pi-pi stacking of H175 to Ph	134.4	8.34	no hydride transfer
		4	-3.967	-25.917	Double bond not above N5, H-bond of K107 to N=O (2.21 Å), salt bridge of K107 to NO, Pi-cation of K107 to Ph and Pi-pi stacking of H175 to Ph	132.4	8.18	no hydride transfer
		5	-3.515	-25.342	Double bond not above N5, H-bond of K107 to N=O (2.35 Å), salt bridge of K107 and H175 to NO, Pi-cation of K107 to Ph, of R345 to Ph and Pi-pi stacking of H175 to Ph	143.8	7.41	no hydride transfer
E-48a	n.c.	1	-5.028	-29.856	H-bond of H175 to C=O (1.96 Å), of R347 to C=OOtert (2.10 Å), bad contacts of Y177 to ring, of Y27 to NH ₂	121.4	4.23	no hydride transfer
		2	-4.848	-32.613	H-bond of R347 to C=OOtert (1.94 Å, 2.24 Å), bad contacts of H175 to ring, of Y177 to NH ₂	51.7	5.01	no hydride transfer
		3	-4.505	-29.027	Double bond vertical to N5, H-bond of Y27 to C=O (1.95 Å), of R347 to NH ₂ (2.12 Å) and of K107 to C=OOtert (1.96 Å)	148.3	6.15	no hydride transfer
		4	-4.293	-29.011	H-bond of H175 to C=O (2.13 Å), bad contacts of R347 to tert	118.4	4.82	no hydride transfer
Z-48a	n.c.	1	-5.272	-32.632	Double bond not above N5, H-bond of NH ₂ to backbone V226 (1.99 Å), bad contact of Y177 to tert	31.2	8.91	no hydride transfer
		2	-4.85	-32.921	H-bond of H175 to C=O (2.01 Å), of R347 to C=OOtert (1.91 Å), bad contact of Y27 to C=OOtert	65.3	4.29	no hydride transfer
		3	-4.544	-30.795	H-bond of Y27 (2.09 Å) and of R347 (2.38 Å) to C=O, bad contact of R347 to NH	127.7	5.17	no hydride transfer
		4	-4.322	-31.232	H-bond of H175 to C=O (1.96 Å), of R347 to C=OOtert (2.23, 2.45 Å), bad contact of P113 to tert	85.2	4.30	no hydride transfer
49a	n.c.	1	-4.302	-23.599	H-bond of H175 to C=O (1.96 Å)	38.2	6.05	no hydride transfer
		2	-3.982	-21.882	H-bond of H175 to C=O (2.11 Å)	78.8	5.32	no hydride transfer
		3	-3.835	-22.719	H-bond of H175 to C=O (1.96 Å)	70.7	5.72	no hydride transfer
		4	-3.552	-21.271	H-bond of H175 to C=O (1.96 Å), bad contact of K107 to CH ₃	78.6	4.97	no hydride transfer
E-50a	n.c.	1	-4.473	-25.827	H-bond of H175 to C=O (2.03 Å), Pi-pi stacking of H175 to Ph, bad contact of I67 to OMe	17.9	5.75	no hydride transfer
		2	-4.362	-23.885	H-bond of H175 to OMe (2.76 Å), Pi-pi stacking of H175 to Ph	59.8	6.52	no hydride transfer
		3	-4.184	-25.672	H-bond of H175 to C=O (2.04 Å)	82.9	5.59	no hydride transfer
		4	-4.137	-24.345	H-bond of H175 to C=O (2.03 Å), bad contact of I67 to OMe	13.3	6.36	no hydride transfer
		5	-4.094	-24.117	H-bond of H175 to C=O (1.92 Å), bad contact of I67 to OMe	20.0	5.80	no hydride transfer
Z-50a	n.c.	1	-4.69	-24.774	H-bond of H175 to C=O (2.14 Å), bad contact of I67, Y177 and H172 to OMe	47.6	4.42	no hydride transfer
		2	-4.624	-22.243	H-bond of Y27 to OMe (2.14 Å), of R347 to C=O (1.87 Å, 2.37 Å), Pi-pi stacking of H175 to Ph and Pi-cation of R347 to Ph	24.9	5.16	no hydride transfer
		3	-4.377	-22.976	H-bond of H175 to C=O (2.01 Å), Pi-pi stacking of H175 to Ph and Pi-cation of R347 and H175 to Ph, bad contact of I67 to OMe	39.4	5.67	no hydride transfer
		4	-4.305	-23.56	H-bond of H175 to C=O (2.00 Å, Pi-cation of R347 to Ph, bad contact of I67 to OMe	66.1	3.97	no hydride transfer
		5	-4.066	-22.337	H-bond of R347 to C=O (1.90 Å, 2.76 Å), Pi-pi stacking of H175 to Ph and Pi-cation of R347 to Ph	42.6	6.27	no hydride transfer

51a	n.c.	1	-4.861	-32.526	H-bond of Y27 (2.28 Å) and R347 (1.91 Å) to C1=O, of R347 (1.87 Å) to C2=O, bad contact of I67 to Et	35.7	7.13	no hydride transfer
		2	-4.652	-31.725	H-bond of Y27 (2.12 Å) and R347 (2.42 Å) to C1=O, of R347 to OEt (2.21 Å)	35.9	7.22	no hydride transfer
		3	-4.522	-31.492	H-bond of Y27 (2.76 Å) and R347 (2.35 Å) to C1=O, of K107 to C2=O (2.01 Å), bad contact of I67 to Et	44.5	7.75	no hydride transfer
		4	-3.416	-28.981	H-bond of R347 to C1=O (2.31 Å, 2.35 Å), bad contact of K107 to Ph and of Y177 to Et	34.4	6.70	no hydride transfer
		5	-3.134	-24.397	H-bond of R347 to C1=O (2.30 Å)	43.6	7.51	no hydride transfer
52a	n.c.	1	-4.801	-26.521	Ph ring above N5, H-bond of Y27 (2.19 Å) and R347 (2.36 Å) to NO, of R347 to N=O (2.12 Å), Pi-cation of K107 to Ph, bad contact of I67 and Y27 to Ph	81.0	5.86	no hydride transfer
		2	-4.741	-24.421	Ph ring above N5, H-bond of R347 to NO (2.12 Å), of R347 to N=O (1.83 Å), Pi-cation of K107 to Ph, bad contact of I67 and Y27 to Ph	72.9	6.25	no hydride transfer
		3	-4.666	-27.721	No H-bond, Pi-cation and Pi-pi staking of H175 to Ph	93.6	5.49	no hydride transfer
		4	-4.657	-26.651	Ph ring above N5, H-bond of R347 to NO (2.34 Å), of R347 (2.32 Å) and Y27 (2.27 Å) to N=O, Pi-cation of K107 to Ph	83.7	5.82	no hydride transfer
		5	-3.945	-24.258	Ph ring above N5, H-bond of R347 to NO (2.34 Å), of R347 (2.32 Å) and of Y27 (2.27 Å) to N=O, Pi-cation of K107 to Ph	77.3	6.65	no hydride transfer
E-53a	n.c.	1	-3.009	-19.737	H-bond of Y27 (1.89 Å) and to R347 (2.30 Å) to CN, bad contact of Y177 to C3	97.5	4.01	Might result in R-53b
		2	-2.892	-20.008	H-bond of Y27 (2.33 Å) and to R347 (2.00 Å) to CN, bad contact of Y177 to C3	98.6	4.18	no hydride transfer
		3	-1.929	-19.629	H-bond of H175 to CN (2.18 Å), bad contacts of R347 to C6=C7	116.2	3.18	Might result in S-53b
		4	-1.873	-16.566	H-bond of H175 to CN (1.93 Å), bad contacts of R347 to C6=C7 and C5	53.3	4.01	no hydride transfer
Z-53a	n.c.	1	-3.095	-21.778	H-bond of H175 to CN (2.12 Å)	66.7	3.95	no hydride transfer
		2	-2.946	-22.303	H-bond of H175 to CN (2.26 Å)	63.0	4.09	No hydride transfer
		3	-2.657	-21.702	H-bond of H175 to CN (2.25 Å)	51.8	4.26	No hydride transfer
		4	-2.48	-19.95	H-bond of H175 to CN (2.12 Å), bad contact of C9 to backbone of G262, of Y177 to C2	79.9	4.30	No hydride transfer
54a	n.c.	1	-3.345	-19.715	H-bond of R347 to C=O (1.76 Å), bad contact of H175 to CH ₃ and of I67 to second CH ₃	86.8	3.88	No hydride transfer
		2	-3.2	-19.458	H-bond of R347 to C=O (2.29 Å)	115.3	3.89	transfer possible
		3	-3.192	-20.067	H-bond of H175 to C=O (1.89 Å), bad contact of R347 to CH ₃	75.3	6.09	No hydride transfer
		4	-3.038	-18.262	H-bond of R347 to C=O (1.84 Å)	111.1	3.79	transfer possible
		5	-2.998	-19.157	H-bond of R347 to C=O (1.78 Å)	112.3	3.91	transfer possible
55a	n.c.	1	-3.699	-22.546	H-bond of H175 to C=O (2.09 Å), Pi-pi stacking of H175 to Ph	44.6	6.26	No hydride transfer
		2	-3.564	-21.11	Ph vertical above N5, H-bond of Q276 to C=O (2.48 Å), Pi-cation of R347 to Ph, Pi-pi stacking of H175 to Ph	132.3	8.10	No hydride transfer
		3	-3.216	-18.806	H-bond of R347 to C=O (2.09 Å, 2.30 Å), Pi-pi stacking of H175 to Ph	37.6	6.34	No hydride transfer

		4	-3.018	-19.913	H-bond of R347 to C=O (2.00 Å) and to Y27 (2.40 Å), bad contact of R347 to triple bond	49.0	5.52	No hydride transfer
		5	-2.94	-19.508	H-bond of R347 to C=O (2.10 Å), bad contact of R347 to triple bond, Pi-pi stacking of H175 to Ph	134.4	6.14	No hydride transfer
56a	n.c.	1	-4.418	-25.233	H-bond of H175 to C=O (2.10 Å), Pi-pi stacking of H175 to Ph	42.6	6.23	No hydride transfer
		2	-4.067	-24.425	H-bond of H175 to C=O (1.97 Å)	28.5	6.85	No hydride transfer
		3	-3.944	-21.472	H-bond of R347 to C=O (2.25 Å, 2.42 Å), Pi-pi stacking and Pi-cation of H175 to Ph	35.3	6.35	No hydride transfer
		4	-3.898	-23.375	H-bond of H175 to C=O (2.22 Å)	44.2	6.06	No hydride transfer
		5	-3.674	-21.548	H-bond of H175 to C=O (2.09 Å), Pi-cation of R347 to Ph	49.9	5.73	No hydride transfer
57a	n.c.	1	-1.4	-20.296	H-bond of H175 to C=O (2.06 Å), bad contact of H175 to C5	30.6	6.68	No hydride transfer
		2	-1.259	-19.985	H-bond of H175 to C=O (2.14 Å)	36.3	6.40	No hydride transfer
		3	-1.234	-20.688	H-bond of R347 to C=O (2.02 Å), bad contact of R319 to aldehyde	110.8	7.07	No hydride transfer
		4	-1.167	-17.281	H-bond of Y27 (1.99 Å) and of R347 (2.17 Å) to C=O, bad contact of H175 to C7 and of H172 to C8	54.1	5.34	No hydride transfer
		5	-1.012	-19.142	H-bond of R347 to C=O (2.15 Å), bad contact of R347 to triple bond	124.1	5.74	No hydride transfer
11a	n.c.	1	-5.812	-24.957	H-bond of Y27 (2.11 Å) and of R347 (2.07 Å) to C=O, of R347 to O (2.20 Å), Pi-pi stacking of H175 to Ph, bad contact of R347 to Ph, of Y177 to CH ₃ , of Y27 to C3	69.8	3.70	Might be productive in S-11b
		2	-5.801	-24.885	H-bond of Y27 (2.12 Å) and of R347 (2.07 Å) to C=O, of R347 to O (2.20 Å), Pi-pi stacking of H175 to Ph, bad contact of R347 to Ph, of Y177 to CH ₃ , of Y27 to C3	69.9	3.70	Might be productive in S-11b
		3	-5.56	-25.24	H-bond of H175 to OH (2.09 Å), of Y27 to C=O (1.87 Å), Pi-pi stacking of H175 to Ph, Pi-cation of K107 to Ph, bad contacts of H175 to Ph, of R347 to C1 and C2	48.5	6.47	No hydride transfer
		4	-5.229	-24.554	H-bond of Y27 (2.38 Å) and of R347 (1.97 Å) to C=O, Pi-cation of K107 to both rings, bad contact of R347 to C2, of I67 to OH, of H175 to double bond	82.9	5.30	No hydride transfer
13a	n.c.	1	-6.15	-36.37	H-bond of R347 (2.05 Å) to C=O and of OH to backbone of S260 (1.93 Å), Pi-cation of H175 to lactone ring	65.1 (Cβ) 103.7 (Cα)	6.72 6.27	No hydride transfer
		2	-4.22	-28.471	H-bond of R347 (2.12 Å) to C=O, bad contact of H172 to OEt, of R347 to O, of I67 to Ph	73.7 (Cβ) 89.7 (Cα)	4.74 4.55	No hydride transfer
		3	-4.139	-30.54	vertical to FMN, H-bond of R347 (2.01 Å) and of Y27 (2.21 Å) to C=O	59.3 (Cβ) 109.0 (Cα)	6.36 5.79	No hydride transfer
		4	-3.936	-29.229	vertical to FMN, H-bond of R347 (2.00 Å) and to Y27 (2.22 Å) to C=O	59.5 (Cβ) 108.8 (Cα)	6.35 5.79	No hydride transfer
12a	n.c.	1	-6.112	-30.243	H-bond of H175 to COAc (2.27 Å), of R347 to O (2.04 Å), Pi-pi stacking of H175 to both rings	34.4 (Cβ) 136.6 (Cα)	5.97 4.91	No hydride transfer
		2	-5.972	-30.295	H-bond of R347 to C=O (2.12 Å), Pi-pi stacking of H175 to both rings, bad contact of H175 to COAc	30.2 (Cβ) 142.7 (Cα)	6.66 5.53	No hydride transfer
		3	-5.772	-28.967	vertical to FMN, H-bond of K107 (2.16 Å) to COAc, of OH to backbone of Q276 (1.82 Å), Pi-pi stacking of H175 to both rings, Pi-cation of H175 and R347 to lactone-ring	26.4 (Cβ) 149.0 (Cα)	8.63 7.44	No hydride transfer
		4	-5.095	-27.865	H-bond of H175 to C=Ac (1.99 Å), Pi-cation of K107 to both rings, bad contacts of I67 to CH ₃ , of R347 to Ph	87.2(Cβ) 74.9 (Cα)	4.28 4.42	No hydride transfer

		5	-4.835	-25.285	H-bond of R347 to C=O (2.16 Å), bad contact of I67 to CH ₃ , of R347 to O	68.8 (Cβ) 95.2 (Cα)	4.89 4.58	No hydride transfer
14a	n.c.	1	-5.527	-25.857	H-bond of Y27 (2.17 Å) and of R347 (2.13 Å) to C=O, Pi-cation of K107 to both Ph rings, Pi-pi stacking of H175 to both Ph, bad contacts of Y177 to CH ₃	53.6	4.31	No hydride transfer
		2	-5.427	-27.745	vertical to FMN	96.7	10.55	No hydride transfer
		3	-5.276	-26.531	vertical to FMN, with double bond above N5	100.3	6.10	No hydride transfer
		4	-4.85	-25.046	vertical to FMN	50.5	6.69	No hydride transfer
		5	-4.714	-24.666	H-bond of R347 to O (1.97 Å)	96.0	4.11	No hydride transfer
16a	n.c.	1	-5.403	-24.415	vertical to FMN, H-bond of K107 to C=O (2.05 Å), Pi-cation of R347 to lactone ring and Ph, Pi-pi stacking of H175 to middle ring	116.6	5.63	No hydride transfer
		2	-5.295	-28.098	vertical to FMN with third ring above N5	82.8	10.66	No hydride transfer
		3	-5.262	-26.592	H-bond of H175 to C=O (1.81 Å), Pi-cation of H175 to all rings, Pi-pi stacking of H175 to second Ph, bad contact of Y27 to CH ₃	77.5	3.84	No hydride transfer
		4	-5.199	-25.586	vertical to FMN, H-bond of K107 to C=O (2.11 Å), Pi-cation of R347 to lactone ring and Ph, Pi-pi stacking of H175 to middle ring	133.3	6.39	No hydride transfer
		5	-5.108	-24.583	H-bond of Y27 (2.15 Å) and of R347 (2.03 Å) to C=O, of R347 to O (2.42 Å), Pi-cation of K107 to middle ring, Pi-pi stacking of H175 to middle ring	63.4	3.94	No hydride transfer
15a	n.c.	1	-5.664	-33.633	H-bond of H175 to C=OOH (2.01 Å), Pi-cation of K107 to all rings	28.1 (Cβ) 144.1 (Cα)	5.83 4.68	No hydride transfer
		2	-5.437	-31.549	Vertical to FMN	31.7 (Cβ) 142.0 (Cα)	7.62 6.50	No hydride transfer
		3	-5.079	-32.52	H-bond of H175 to C=OOH (2.02 Å), Pi-cation of K107 to all rings	77.1 (Cβ) 86.0 (Cα)	4.67 4.56	No hydride transfer
		4	-4.879	-30.856	H-bond of H175 to C=OOH (2.44 Å), bad contacts of R347 to lactone	71.2 (Cβ) 92.5 (Cα)	4.84 4.59	No hydride transfer
		5	-4.825	-30.416	H-bond of H175 to C=OOH (2.00 Å), Pi-cation of K107 and R347 to lactone	82.0 (Cβ) 81.2 (Cα)	4.65 4.66	No hydride transfer

Table 28. Results from RBD of Substrates **11a-57a** in the reduced *TsER* C25G/I67T variant, created with PyMOL Mutagenesis Wizard on crystal structure 3HGJ. Experimental screening of substrate as (a) racemate (b) E/Z 1:4, (c) E/Z 2:3, (d) E/Z 7:1, (e) E/Z 1:1, n.t. not tested, n.d. not detected. “would” means hydride transfer angle in a range of 80-120° and distance to the hydride of N5 in a range of 3.00 to 4.85 Å, “might” means either hydride transfer angle to small or distance to N5 to large.

Substrate	Empirical Result conv (%) / ee (%)	Pose	Glide Gscore	Glide Energy	Notes	Hydride transfer angle	distance hydride N5 to substrate	result
17a	49 / 74S	1	-5.372	-21.501	H-bond of H175 to C=O (1.93 Å), bad contact of Y177 to C2	85.7	4.44	no hydride transfer
		2	-5.341	-20.514	normal pose, H-bond of H175 to C=O (2.01 Å), bad contacts of Y177 to C5 and of Y27 to C4	107.9	3.29	would result in R- 17b
		3	-5.239	-22.275	flipped pose, H-bond of H175 to C=O (1.81 Å)	102.1	3.46	would result in S- 17b
		4	-5.137	-21.769	normal pose, H-bond of H175 to C=O (1.87 Å), bad contacts of Y177 to C5	87.1	5.00	no hydride transfer
		5	-5.125	-20.6	normal pose, H-bond of H175 to C=O (1.89 Å), bad contacts of Y177 to C6	94.2	4.11	no hydride transfer
24a	36 / 99S	1	-5.831	-22.351	flipped pose, H-bond of H175 to C=O (1.74 Å), bad contact of T67 to Iso and Y27 to C4	102.7	3.57	would result in S- 24b
		2	-5.496	-21.964	normal pose, H-bond of H175 to C=O (2.15 Å), bad contact of Y177 to C5 and Y27 to Iso and C4	103.1	3.43	would result in R- 24b
		3	-5.251	-21.063	normal pose, H-bond of H175 to C=O (2.08 Å), bad contacts of Y177 to C6 and Y27 to C4 and R347 to Iso	96.0	4.04	no hydride transfer
		4	-5.184	-20.743	normal pose, H-bond of H175 to C=O (1.95 Å), bad contact of R347 to Iso	80.7	5.34	no hydride transfer
		5	-5.131	-21.405	normal pose, H-bond of H175 to C=O (2.15 Å), bad contact of Y177 to C5 and Y27 to Iso and C4	99.3	3.63	would result in R- 24b
25a	>99 / 88S	1	-6.306	-28.271	H-bond of Y27 to C=O (2.03 Å), H-bond of H175 to C=OOMe (2.02 Å), flipped pose, bad contacts of R347 to C6 and H172 to OMe	102.4	3.44	would result in S- 25b
		2	-5.68	-26.441	H-bond of H175 to C=OOMe (2.00 Å)	115.5	4.00	would result in R- 25b
		3	-5.323	-24.429	new flipped pose, H-bond of R347 to C=O (2.17 Å, 2.38 Å), H-bond of H175 to C=OOMe (1.92 Å), bad contacts of R347 to C6	93.9	5.13	no hydride transfer
		4	-5.311	-23.067	normal pose, H-bond of H175 to C=O (1.92 Å), H-bond of R347 to C=OOMe (2.04 Å, 2.56 Å)	79.6	5.65	no hydride transfer
		5	-5.036	-23.939	H-bond of H175 to C=OOMe (2.09 Å)	83.0	4.47	no hydride transfer
R-26a^a	53 / isomer 1	1	-5.634	-23.899	flipped pose, H-bond of H175 to C=O (1.73 Å), bad contact of Y27 to C4	100.9	3.49	would result in 3R,5S- 26b
		2	-4.938	-22.525	normal pose, H-bond of H175 to C=O (1.98 Å)	76.4	5.49	no hydride transfer
		3	-4.787	-20.916	flipped pose, H-bond of H175 to C=O (1.98 Å), bad contact of Y27 to C3CH ₃	71.7	3.91	might result in 3R,5S- 26b
S-26a^a	53 / isomer1	1	-5.481	-22.23	normal pose, H-bond of H175 to C=O (1.79 Å), bad contacts of Y177 to C6 and Y27 to C4	100.1	3.85	would result in 3R,5S- 26b

		2	-5.453	-24.157	flipped pose, H-bond of H175 to C=O (1.82 Å)	103.7	3.45	would result in 3S,5S- 26b
		3	-4.878	-21.403	normal pose, H-bond of H175 to C=O (2.09 Å), bad contact of R347 to C4	69.0	6.33	no hydride transfer
		4	-4.87	-21.753	normal pose, H-bond of H175 to C=O (1.99 Å), bad contact of Y177 to C6	76.7	5.50	no hydride transfer
		5	-4.841	-20.639	flipped pose, H-bond of H175 to C=O (2.04 Å)	65.2	4.10	no hydride transfer
27a	99 / achiral	1	-5.658	-24.295	H-bond of H175 to C=O (1.79 Å), bad contact of Y177 to C7	107.6	3.31	productive pose
		2	-5.506	-24.163	wrong double bond location	-	-	no hydride transfer
		3	-5.464	-23.821	H-bond of H175 to C=O (2.08 Å)	104.2	3.52	productive pose
		4	-5.253	-22.865	wrong double bond location	-	-	no hydride transfer
		5	-4.921	-20.706	No interactions	92.6	3.44	productive pose
S-28a	25 / 17 (isomer 1)	1	-5.051	-24.559	no H-bonds, bad contacts of Y177 to C6, of T67 and D71 to 4-propenyl and of A58 to C5	96.1	3.53	would result in (1s,4s)- 28b (trans)
		2	-4.683	-25.428	wrong double bond position	-	-	no hydride transfer
		3	-4.559	-20.644	flipped pose, H-bond of H175 to C=O (1.81 Å)	107.8	3.46	would result in (1r,4r)- 28b (trans)
		4	-4.519	-22.494	wrong double bond position	-	-	no hydride transfer
		5	-4.481	-20.273	flipped pose, H-bond of H175 to C=O (1.86 Å), bad contacts of R347 and Y177 to 4-propenyl	111.5	3.49	would result in trans- 28b
29a	>99 / 14S	1	-5.324	-20.534	H-bond of H175 to C=O (2.07 Å), bad contact of Y177 to C6	87.5	3.59	no hydride transfer
		2	-5.143	-19.808	normal pose, H-bond of H175 to C=O (1.98 Å), bad contact of Y27 to C5	92.3	4.55	no hydride transfer
		3	-5.116	-20.992	flipped pose, H-bond of H175 to C=O (1.84 Å)	102.1	3.36	would result in R- 29b
		4	-5.086	-20.101	normal pose, H-bond of H175 to C=O (1.89 Å), bad contacts of Y177 to C6 and Y27 to C4	95.8	4.10	might result in S- 29b
22a	88 / 88R	1	-6.432	-27.162	H-bond of H175 to C1=O (1.92 Å), of Y27 to C2=O (2.03 Å), bad contact of Y177 to CH ₃	60.6	3.73	no hydride transfer
		2	-5.992	-25.638	H-bond of C2=O to H175 (1.80 Å), of C1=O to Y27 (2.11 Å), bad contact of Y177 to Iso, of Y27 to CH ₃	104.0	3.34	would result R- 22b
		3	-5.069	-21.987	H-bond of C2=O to H175 (1.86 Å), bad contact of Y27 to CH ₃	73.3	4.25	no hydride transfer
		4	-5.043	-21.708	H-bond of C2=O to H175 (1.94 Å), of C1=O to Y27 (2.29 Å), bad contact of Y177 to Iso, of Y27 to CH ₃	69.6	4.07	no hydride transfer
		5	-4.881	-21.763	H-bond of C2=O to H175 (1.93 Å), of C1=O to Y27 (2.32 Å), bad contact of Y177 and H175 to Iso	65.4	4.16	no hydride transfer
18a	87 / 88 (2S,5S)	1	-5.156	-25.243	H-bond of H175 to C=O (2.15 Å), bad contacts of Y177, T67 and A58 to 4-propenyl	81.3	3.76	might result in 2S,5S- 18b
		2	-5.102	-22.286	H-bond of H175 to C=O (2.16 Å), bad contacts of Y177 to C6 and of T67, D71 to 4-propenyl	92.6	3.22	would result in 2S,5S- 18b
		3	-5.001	-26.019	no productive pose	138.3	5.25	no hydride transfer

		4	-4.796	-22.373	flipped pose, H-bond of H175 to C=O (2.04 Å), bad contacts of Y177 to C5, of R347 to 4-propenyl	102.4	3.46	would result in 2R,5S-18b
		5	-4.742	-22.756	flipped pose, H-bond of H175 to C=O (2.14 Å), bad contacts of Y27 to C4 and of R347 to 4-propenyl	103.6	3.51	would result in 2R,5S-18b
30a	98 / 98 (2R,5R)	1	-5.529	-25.942	normal pose, H-bond of H175 to C=O (2.23 Å), bad contacts of H172 to C6, of I67 to 4-propenyl	98.4	3.09	would result in 2S,5R-30b
		2	-5.18	-24.722	normal pose, H-bond of H175 to C=O (2.17 Å), bad contacts of H172 to C6, of I67 to 4-propenyl	95.3	3.49	would result in 2S,5R-30b
		3	-5.053	-22.631	flipped pose, H-bond of H175 to C=O (2.03 Å), bad contacts of Y177 to C6, of R347 to 4-propenyl	111.4	3.28	would result in 2R,5R-30b
		4	-4.694	-21.375	flipped pose, H-bond of H175 to C=O (2.01 Å), bad contacts of R347 to 4-propenyl	87.6	3.65	might be 2R,5R-30b
E-31a	n.t.	1	-4.711	-27.688	H-bond of H175 to C1=O (1.93 Å), of Y27 to 2OEt (2.18 Å)	102.8	3.54	would result in R-31b
		2	-4.556	-26.115	H-bond of H175 to C2=O (2.15 Å), of Y27 to 1OEt (2.09 Å), bad contact of Y27 to CH ₃	114.4	3.15	would result in R-31b
		3	-4.056	-24.581	H-bond of H175 to C2=O (2.05 Å), of Y27 to 1OEt (1.98 Å)	62.7	5.51	no hydride transfer
		4	-4.038	-25.884	H-bond of H175 to C2=O (2.28 Å), bad contact of R347 to 1OEt	48.8	4.48	no hydride transfer
		5	-3.982	-24.272	H-bond of H175 to C2=O (2.19 Å)	121.3	4.10	no hydride transfer
Z-31a	97 / 96R	1	-4.58	-27.781	H-bond of H175 to C2=O (2.19 Å)	65.5	3.84	no hydride transfer
		2	-4.163	-25.375	H-bond of H175 to C1=O (2.44 Å)	116.6	3.83	would result in S-31b
		3	-3.992	-25.004	H-bond of H175 to C1=O (1.91 Å), bad contacts to Y177	89.0	3.62	no hydride transfer
		4	-3.937	-24.944	H-bond of H175 to C1=O (1.93 Å), bad contacts of Y177 to 1OEt	88.0	4.57	no hydride transfer
		5	-3.77	-23.884	H-bond of H175 to C1=O (2.56 Å)	104.3	3.81	would result in S-31b
32a	99 / >99R	1	-6.42	-31.224	H-bond of H175 to 2C=O (1.96 Å), bad contact of H172 to Ph	104.4	3.42	would result in R-32b
		2	-6.417	-31.916	H-bond of H175 to 2C=O (2.06 Å), Pi-cation of R347 to Ph	110.0	3.39	would result in R-32b
		3	-6.337	-32.827	H-bond of H175 to 2C=O (2.19 Å), Pi-cation of R347 to Ph, Pi-pi stacking of H175 to Ph	98.3	3.39	would result in R-32b
		4	-6.304	-32.484	H-bond of H175 to 2C=O (2.21 Å)	96.4	3.43	would result in R-32b
33a	99 / 80R	1	-5.301	-19.748	normal pose, H-bond of H175 to C=O (1.94 Å), bad contact of Y177 to C5	97.4	3.31	would result in S-33b
		2	-5.068	-19.621	normal pose, H-bond of H175 to C=O (1.80 Å), bad contact of Y177 to C5	106.4	3.95	would result in S-33b
		3	-5.055	-19.725	flipped pose, H-bond of H175 to C=O (2.16 Å)	102.5	3.39	would result in R-33b
34a	n.c.	1	-5.256	-19.888	flipped pose, H-bond of H175 to C=O (1.85 Å)	108.9	3.51	would result in S-34b
		2	-5.029	-19.587	normal pose, H-bond of H175 to C=O (1.86 Å)	106.6	3.91	would result in R-34b
		3	-4.824	-18.262	flipped pose, H-bond of H175 to C=O (1.86 Å)	81.7	3.99	no hydride transfer

35a	>99 / 90S	1	-5.874	-25.146	normal pose, H-bond of H175 to C=O (1.86 Å), bad contacts of Y177 to C5, of R347 and Y27 to OMe	111.2	3.65	would result in R- 35b
		2	-5.736	-25.817	H-bond of H175 to C=OOMe (1.82 Å)	103.3	3.89	would result in R- 35b
		3	-5.404	-24.934	H-bond of H175 to C=OOMe (2.15 Å)	115.1	4.03	no hydride transfer
		4	-5.341	-24.891	new flipped pose, H-bond of H175 to C=OOMe (2.15 Å)	101.2	3.53	would result in S- 35b
		5	-5.253	-23.948	new flipped pose, H-bond of H175 of C=OOMe (1.96 Å), of R347 to C=O (2.36 Å)	83.6	4.59	no hydride transfer
36a	2 / n.d.	1	-5.351	-21.295	normal pose, H-bond of H175 to C=O (1.87 Å)	107.0	3.92	would result in 2S,3R- 36b
		2	-5.32	-21.861	flipped pose, H-bond of H175 to C=O (2.15 Å)	109.2	3.51	would result in 2R,3S- 36b
		3	-5.2	-19.79	flipped pose, H-bond of H175 to C=O (1.85 Å)	83.3	3.71	
19a	11 / 79R	1	-3.232	-19.346	no productive pose	31.4	5.69	no hydride transfer
		2	-3.189	-23.478	H-bond of H175 to C=O (1.98 Å)	104.8	3.21	would result in S- 19b
		3	-3.162	-22.371	H-bond of H175 to C=O (1.80 Å), of Y177 to OH (2.03 Å)	52.2	5.18	no hydride transfer
		4	-2.879	-20.138	no productive pose	63.5	4.82	no hydride transfer
		5	-2.581	-20.411	no productive pose	25.6	5.91	no hydride transfer
Z-37a^b	37 / 92R	1	-3.962	-23.712	H-bond of H175 to C=O (1.80 Å), bad contact of A58 to C4 and Y177 to C5	96.3 (C α) 65.4 (C β)	3.91 4.26	would result in R- 37b
		2	-3.541	-23.654	No H-bond, salt bridge of H175 to Cl	57.3 (C α) 103.8 (C β)	4.07 3.52	would result in R- 37b
		3	-3.529	-21.149	Bad contact of H172, Y177 and A102 to OMe	94.7 (C α) 67.9 (C β)	4.21 4.52	No hydride transfer
		4	-3.42	-22.514	No H-bond, salt bridge of H175 to Cl	56.2 (C α) 105.2 (C β)	4.12 3.55	would result in R- 37b
		5	-3.39	-21.519	No H-bond, salt bridge of H175 to Br, bad contacts of H172 to Cl and of T67 to OMe	68.8 (C α) 91.8 (C β)	4.06 3.78	would result in R- 37b
E-37a^b		1	-3.999	-23.746	H-bond of H175 to C=O (1.92 Å), bad contacts of H172 and Y177 to C4 and C5	84.9 (C α) 73.7 (C β)	3.56 6.70	would result in R- 37b
		2	-3.801	-21.606	Salt bridge of H175 to Cl, bad contact of T67 to C4	81.8 (C α) 78.9 (C β)	4.02 4.05	No hydride transfer
		3	-3.663	-21.567	H-bond of H175 to C=O (2.12 Å), bad contacts of H172 to OMe, of H175 to C4	113.2 (C α) 50.7 (C β)	3.77 4.48	would result in S- 37b
		4	-3.628	-22.689	H-bond of H175 to C=O (1.89 Å), bad contact of Y177 to OMe	67.8 (C α) 94.6 (C β)	4.47 4.16	No hydride transfer
		5	-3.226	-21.257	Bad contact of D71 to C5	89.6 (C α) 73.6 (C β)	4.50 4.69	No hydride transfer
E-38a^c	49 / 94S	1	-3.497	-26.877	H-bond of H175 to C=O (1.77 Å), bad contacts of Y27, T67 to C4, of A58 to C5, of A102, A104 and A60 to C8	91.2	3.54	Would result in R- 38b

		2	-3.004	-25.291	H-bond of Y27 to C=O (2.47 Å), bad contacts of Y177 to CH ₃ , of T67,D71 and A58 to C6-C8	63.0	3.63	No hydride transfer
		3	-2.932	-24.409	No H-bond, bad contacts of Y177, A58 and T67	58.4	3.89	No hydride transfer
		4	-2.705	-26.177	No H-bond, bad contacts of H175, T67, A58, D71 and G65	94.1	3.95	Would result in R-38b
		5	-2.701	-21.995	H-bond of H175 to C=O (1.85 Å)	105.1	3.32	Would result in S-38b
Z-38a^c		1	-3.284	-23.725	H-bond of H175 to C=O (2.07 Å)	55.8	4.05	No hydride transfer
		2	-2.957	-25.867	No productive pose	153.2	5.27	No hydride transfer
		3	-2.906	-24.849	No productive pose	145.4	4.53	No hydride transfer
		4	-2.5	-25.721	No productive pose	74.0	5.05	No hydride transfer
		5	-2.405	-24.137	No productive pose	147.5	4.94	No hydride transfer
Z-39a	94 / rac	1	-4.443	-21.239	H-bond of H175 to C=O (1.96 Å), bad contacts of H172 to C3, of Y177, T67, D71 and A58 to Ph	51.2	4.76	No hydride transfer
		2	-4.337	-22.942	No H-bond, bad contact of Y177 to C3	69.8	4.08	No hydride transfer
		3	-3.856	-22.146	No H-bond, bad contact of Y177 to Ph	96.9	3.81	Would result in S-39b
		4	-3.8	-21.557	H-bond of H175 to C=O (2.05 Å), Pi-cation of R347 to Ph, bad contact of Y27 and P113 to Ph	68.6	4.35	No hydride transfer
		5	-3.748	-20.3	H-bond of R347 to C=O (2.37 Å), Pi-pi stacking of Y177 to Ph	113.4	4.00	Would result in S-39b
E-39a	?	1	-5.087	-23.938	H-bond of H175 to C=O (1.93 Å), bad contact of Y177 to Ph	68.4	4.07	No hydride transfer
		2	-5.053	-24.678	H-bond of H175 to C=O (1.94 Å), Pi-cation of H175 and R347 to Ph, Pi-pi stacking of H175 to Ph	54.9	4.73	No hydride transfer
		3	-4.943	-25.455	No productive pose	157.8	4.96	No hydride transfer
		4	-4.832	-18.309	H-bond of H175 to C=O (1.84 Å), bad contact of T67 and D71 to Ph	103.2	3.38	Would result in S-39b
		5	-4.265	-21.373	H-bond of H175 to C=O (2.17 Å), Pi-cation of R347 to Ph, bad contact of Y27 to Ph	83.8	4.94	No hydride transfer
Z-40a	90 / >99 unassigned	1	-4.702	-30.064	No H-bond, Pi-cation and Pi-pi stacking of H175 to Ph, bad contacts H175 and Y177 to C=OOEt	29.2	5.51	No hydride transfer
		2	-4.564	-24.359	H-bond of R347 to C=OOEt and of Y27 to C=OOMe, Pi-cation and Pi-pi stacking of H175 to Ph, bad contacts of R347 to Et	80.3	5.46	No hydride transfer
		3	-3.592	-27.976	Pi-cation of K107 to Ph	74.2	6.85	No hydride transfer
		4	-3.247	-25.612	H-bond of Y27 to C=OOMe (2.68 Å), Pi-cation of K107 to Ph	46.6	6.90	No hydride transfer
		5	-3.206	-23.966	H-bond of R347 to C=OOEt (2.26, 2.44 Å), Pi-cation of K107 to Ph	21.1	7.62	No hydride transfer
E-40a	n.t.	1	-5.12	-29.793	Pi-cation of R347 to Ph, Pi-pi stacking of H175 to Ph, bad contacts of T67, A58 to Et, of Y27 to C=OOMe	46.6	4.56	No hydride transfer
		2	-4.532	-28.622	Pi-cation of R347 to Ph, Pi-pi stacking of H175 to Ph, bad contacts of Y177 to C3	37.4	5.45	No hydride transfer

		3	-4.196	-26.653	H-bond of Y27 to C=OOMe (2.03 Å)	56.8	6.50	No hydride transfer
		4	-3.692	-26.264	H-bond of R347 to C=OOMe (1.75, 2.54 Å), of Y27 to C=OOEt (2.04 Å)	65.2	6.55	No hydride transfer
		5	-3.22	-25.372	Pi-cation of K107 to Ph	47.4	7.03	No hydride transfer
E-41a^d	64 / >99R	1	-4.454	-24.06	H-bond of H175 to N=O (2.01 Å), salt bridges of H175 (4.68 Å) and H172 (4.68 Å) to NO	69.4	4.13	No hydride transfer
		2	-4.125	-20.228	salt bridge of R347 to NO (4.08 Å)	78.1	3.79	No hydride transfer
		3	-4.124	-20.116	salt bridge of H175 to NO (3.60 Å)	90.9	4.03	Might result in S-41b
		4	-4.098	-22.234	H-bond of H175 to NO (2.27 Å), salt bridges of H175 (3.15 Å) and H172 (4.98 Å) to NO, bad contacts of Y177 and Y27 to Ph, R347 to CH ₃	69.2	4.50	No hydride transfer
		5	-4.035	-20.126	salt bridge of H175 to NO (3.09 Å), bad contact of Y177 to Ph	106.0	3.58	Would result in R-41b
Z-41a^d		1	-4.533	-26.794	H-bond of H175 to N=O (1.92 Å), salt bridge of H175 and H172 to NO, Pi-cation of R345 and H175 to Ph, Pi-pi stacking of H175 to Ph	59.3	4.09	No hydride transfer
		2	-3.933	-21.865	H-bond of Y27 to NO (1.86 Å), salt bridge of R347 to NO, Pi-cation of R345 and H175 to Ph, bad contact of Y177 to CH ₃ and Ph	51.9	3.82	No hydride transfer
		3	-3.582	-20.251	H-bond of Y27 to N=O (2.15 Å), salt bridge of R347 to NO, Pi-cation of H175 to Ph, bad contact of Y177 to CH ₃	60.3	4.10	No hydride transfer
		4	-3.029	-18.148	H-bond of R347 to N=O (2.66 Å), of K107 to NO, Pi-cation of R347 to Ph, Pi-pi stacking of Y27 to Ph	125.4	7.37	No hydride transfer
E-43a^e	3 / n.d.	1	-4.548	-25.971	No H-bond, Pi-cation of K107 to Ph, bad contact of Y177 to C3, of D71 to OMe	86.0 (C α) 75.1 (C β)	4.04 4.17	No hydride transfer
		2	-4.403	-26.155	H-bond of H175 to C=OOMe (2.12 Å), bad contacts of Y177 to OMe, of H175 to Br, Pi-cation of R347 to Ph	84.8 (C α) 79.5 (C β)	4.93 4.99	No hydride transfer
		3	-4.391	-25.569	Bad contacts of Y27 to OMe, of A58 and T67 to Br	85 (C α) 76.4 (C β)	4.14 4.25	No hydride transfer
		4	-4.319	-26.047	H-bond of H175 to C=OOMe (2.48 Å), Pi-cation of H175 to Ph, bad contact of Y177 to OMe, of Y27 to Br	128.7 (C α) 39.1 (C β)	4.05 5.01	No hydride transfer
		5	-4.299	-25.615	Pi-cation of K107 to Ph, Bad contact of H172 and A102 to OMe	46.4 (C α) 115.1 (C β)	3.86 3.09	Would result in R-43b
Z-43a^e		1	-4.977	-27.063	H-bond of T67 to OMe (2.11 Å), bad contact of A104 to Me, of Y177 to C3	80.1 (C α) 83.5 (C β)	4.76 4.72	No hydride transfer
		2	-4.757	-28.131	H-bond of H175 to Br (2.15 Å), bad contacts of H172 to Br, of T67 to Me	74.1 (C α) 86.3 (C β)	4.04 3.89	Might result in S-43b
		3	-4.507	-28.599	H-bond of H175 to Br (2.15 Å), Pi-cation of R347 to Ph, bad contacts of H172 to Br, of T67 to Me	84.6 (C α) 48.6 (C β)	4.18 4.27	No hydride transfer
		4	-4.384	-25.487	H-bond of H175 to Br (1.87 Å), bad contact of T67 to Me	90.6 (C α) 70.8 (C β)	4.02 4.26	No hydride transfer
		5	-4.381	-23.528	H-bond of R347 to C=O (2.36 Å), Pi-pi stacking of Y177 to Ph	52.9 (C α) 111.7 (C β)	4.74 4.07	Would result in S-43b
44a	n.c.	1	-5.493	-21.803	New flipped pose, H-bond of Y27 to C=O (2.19 Å), bad contact of Y177	64.0	3.67	No hydride transfer
		2	-5.215	-21.204	Flipped pose, H-bond of H175 to C=O (1.92 Å), bad contacts of Y177 and Y27	106.1	3.32	Productive pose

		3	-4.975	-20.463	Flipped pose, bad contacts of Y177 and Y27	111.1	3.74	Productive pose
		4	-4.939	-19.956	Flipped pose, H-bond of H175 to C=O (1.93 Å), bad contact of Y177 and R347	95.7	3.37	Productive pose
		5	-4.779	-20.819	No productive pose, vertical to FMN	120.5	7.02	No hydride transfer
45a	n.c.	1	-4.825	-32.267	New flipped pose, H-bond of R347 to C=O (2.25, 2.50 Å), of H175 to C=OOBu (1.73 Å), bad contacts of Y177, Y27 and T67 to Bu	78.1 (Cβ) 85.9 (Cα)	4.92 4.83	No hydride transfer
		2	-4.58	-27.871	New flipped pose, bad contacts of Y177, Y27 and T67 to Bu	63.8 (Cβ) 96.3 (Cα)	3.97 3.59	transfer possible
		3	-4.503	-30.707	New flipped pose, H-bond of H175 to C=OOBu (2.06 Å), bad contacts of Y177, Y27 and T67 to Bu	54.6 (Cβ) 109.1 (Cα)	4.58 3.95	transfer possible
		4	-4.453	-30.211	New flipped pose, H-bond of H175 to C=OOBu (1.71 Å), bad contacts of H172, Y27 and T67 to Bu	73.0 (Cβ) 91.0 (Cα)	4.93 4.71	No hydride transfer
		5	-3.935	-30.426	New flipped pose, H-bond of H175 to C=OOBu (2.61 Å), bad contacts of H172, Y27 and T67 to Bu	74.0 (Cβ) 88.2 (Cα)	4.45 4.28	No hydride transfer
46a	n.c.	1	-5.942	-23.746	Flipped pose, H-bond of H175 to C=O (1.84 Å), bad contact of Y177 to C3 and of A58 and T67 to propan-2-ylidene	81.2	3.83	No hydride transfer
		2	-5.929	-23.617	Normal pose, H-bond of H175 to C=O (1.85 Å), bad contact of Y27 to C3 and of A58 to CH ₃	57.6	4.49	No hydride transfer
		3	-5.461	-22.331	Flipped pose, H-bond of H175 to C=O (1.93 Å), bad contact of Y177 and H175 to C6	87.8	3.38	No hydride transfer
E-42a	n.c.	1	-4.37	-27.502	No productive pose	152.8	5.03	No hydride transfer
		2	-4.148	-27.06	Salt bridge of H175 to NO, bad contacts of Y177, T67, Y27 and D71 to ring	90.3	3.70	transfer possible
		3	-4.052	-26.865	Salt bridge of H175 to NO, bad contacts of Y177, T67, A58 and D71 to ring	62.2	3.80	No hydride transfer
		4	-3.695	-22.726	Salt bridge of H175 to NO, bad contacts of Y177, T67, A58 and D71 to ring	74.1	4.01	No hydride transfer
		5	-3.656	-20.435	Salt bridge of R347 to NO, Pi-cation of H175 to NO ₂	98.0	5.47	No hydride transfer
Z-42a	n.c.	1	-4.71	-25.001	H-bond of H175 to NO (1.78 Å), salt bridge of H172 and H175 to NO	52.6	4.48	No hydride transfer
		2	-4.619	-24.811	H-bond of H175 to NO (1.93 Å), salt bridge of H172 and H175 to NO	62.0	3.95	No hydride transfer
		3	-4.285	-24.041	H-bond of H175 to N=O (2.20 Å), salt bridge of H172 NO	66.3	3.85	No hydride transfer
		4	-4.092	-21.422	No productive pose	164.2	6.02	No hydride transfer
		5	-3.939	-25.875	No productive pose	156.2	5.37	No hydride transfer
47a	n.c.	1	-4.693	-33.076	H-bond of H175 to N=O (2.00 Å), salt bridge of H172 and H175 to NO, Pi-cation of R347 and H175 to Ph, Pi-pi stacking of H175 to Ph, bad contact of Y177, Y27 and P113 to second Ph	56.5	4.34	No hydride transfer
		2	-4.518	-27.49	H-bond of R347 to NO (2.30 Å), salt bridge of R347 to NO, Pi-cation of R347 to Ph, Pi-pi stacking of H175 to second Ph, bad contact of Y177, Y27 and P113 to second Ph	107.2	4.07	transfer possible
		3	-4.475	-25.894	Salt bridge of R347 to NO, Pi-cation of R347 to Ph, Pi-pi stacking of Y177 to second Ph, bad contact of Y177, Y27 and T67 to second Ph	60.9	3.83	No hydride transfer
		4	-3.686	-27.697	Salt bridge of H175 to NO, Pi-cation of R347 to Ph	67.8	4.60	No hydride transfer

E-48a	n.c.	1	-5.101	-32.704	H-bond of H175 to C=O (1.85 Å)	127.1	5.06	No hydride transfer
		2	-5.057	-30.013	H-bond of H175 to C=O (1.88 Å), of R347 to C=OOtert (1.95 Å), bad contact of H175 to tert	133.8	4.70	No hydride transfer
		3	-5.027	-32.62	H-bond of H175 to C=O (1.84 Å)	112.9	4.56	No hydride transfer
		4	-4.452	-29.532	No productive pose	157.7	6.17	No hydride transfer
Z-48a	n.c.	1	-5.163	-31.678	H-bond of Y27 to C=O (2.13 Å), bad contact of H175 to tert	126.7	5.33	No hydride transfer
		2	-5.04	-31.423	H-bond of Y27 to C=O (1.87 Å)	128.2	5.06	No hydride transfer
		3	-4.945	-30.342	H-bond of Y27 to C=O (2.06 Å), bad contact of R347 to tert	121.5	4.52	No hydride transfer
		4	-4.733	-30.15	H-bond of H175 to C=O (2.08 Å), bad contact of Y177 to ring	136.6	6.30	No hydride transfer
		5	-4.195	-25.443	No productive pose, vertical to FMN	148.5	5.92	No hydride transfer
49a	n.c.	1	-4.195	-21.569	H-bond of H175 to C=O (2.20 Å)	37.3	6.79	No hydride transfer
		2	-4.138	-23.36	H-bond of H175 to C=O (2.00 Å), bad contacts of K107 and H175	40.3	6.46	No hydride transfer
		3	-4.005	-22.519	H-bond of H175 to C=O (1.85 Å)	71.8	5.66	No hydride transfer
		4	-4.001	-22.223	H-bond of H175 to C=O (1.92 Å), bad contacts of K107, R347 and H175	29.6	6.41	No hydride transfer
		5	-3.215	-19.973	H-bond of H175 to C=O (1.73 Å), bad contacts of K107, R347 and H175	88.6	4.96	No hydride transfer
E-50a	n.c.	1	-5.118	-25.152	H-bond of H175 to C=O (1.96 Å), bad contacts of Y177, G65, D71 and A58 to Ph	83.7	4.51	No hydride transfer
		2	-5.031	-28.25	H-bond of T67 to OMe (2.21 Å), bad contact of H175 to Ph, of G65 backbone to Me	175.0	4.63	No hydride transfer
		3	-4.329	-23.373	Pi-pi stacking of H175 to Ph, bad contact of A58 and D71 to Me	45.0	3.81	No hydride transfer
		4	-4.227	-22.315	H-bond of R347 to C=O (2.39 Å), Pi-pi stacking of Y177 to Ph	102.0	4.19	No hydride transfer
Z-50a	n.c.	1	-4.852	-28.052	H-bond of H175 to C=O (1.89 Å), Pi-cation of R347 and H175 to Ph, Pi-pi stacking of H175 to Ph	55.1	4.71	No hydride transfer
		2	-4.802	-27.103	H-bond of H175 to C=O (1.94 Å)	63.9	3.93	No hydride transfer
		3	-4.169	-24.808	H-bond of H175 to C=O (1.87 Å), Pi-cation of R347 to Ph	82.1	4.99	No hydride transfer
51a	n.c.	1	-5.018	-32.572	Pi-cation of H175 and R347 to Ph, Pi-pi stacking of H175 to Ph, bad contact of R347 and Y27 to OEt	44.9	4.69	No hydride transfer
		2	-4.815	-32.605	Pi-cation of H175 and R347 to Ph, bad contact of Y27 to 1OEt, of Y177 to 2OEt	37.5	5.33	No hydride transfer
		3	-4.812	-30.606	H-bond of R347 to 1C=O (2.13 Å, 2.39 Å), of Y27 to 2C=O (2.27 Å), Pi-cation and Pi-pi stacking of H175 to Ph	72.2	5.29	No hydride transfer
		4	-4.566	-26.968	Bad contacts of Y27 to 1OEt and of Y177 to 2OEt	60.2	4.52	No hydride transfer
		5	-4.085	-30.476	H-bond of R347 to 1C=O (2.00 Å), Pi-pi stacking of H175 to Ph, bad contact of K107 to 1Et and of Y27 to 2Et	58.5	7.16	No hydride transfer

52a	n.c.	1	-4.828	-28.745	Pi-cation and Pi-pi stacking of H175 to Ph	94.1	5.48	No hydride transfer
		2	-4.63	-26.113	H-bond of Y27 to N=O (1.95 Å), salt bridge of R347 to NO, Pi-cation of K107 to Ph	86.7	5.12	No hydride transfer
		3	-4.552	-23.292	H-bond of H175 to N=O (1.65 Å), salt bridge of H175 to NO, Pi-cation of K107 to Ph and Pi-pi stacking of Y177 to Ph, bad contact of Y27 to Ph	97.3	4.23	No hydride transfer
		4	-4.396	-25.361	H-bond of Y27 to NO (2.06 Å), Pi-cation of K107 to Ph, salt bridge of R347 to N=O, bad contact of Y27 to Ph	84.3	5.67	No hydride transfer
E-53a	n.c.	1	-3.282	-23.818	Bad contacts of Y177 and Y27	139.6	4.15	No hydride transfer
		2	-3.103	-24.437	H-bond of H175 to CN (1.98 Å), bad contacts of Y27, Q57, A58, T67 and Y177	61.4	3.82	No hydride transfer
		3	-2.612	-24.369	bad contacts of Y27, Q57, A58, T67 and Y177	56.6	3.79	No hydride transfer
		4	-2.578	-23.308	No productive pose	151.7	4.59	No hydride transfer
		5	-2.337	-24.828	bad contacts of Y27, Q57, A58, T67	95.9	3.89	transfer possible
Z-53a	n.c.	1	-3.209	-23.35	H-bond of H175 to CN (2.20 Å)	68.0	3.85	No hydride transfer
		2	-3.063	-23.275	H-bond of H175 to CN (2.20 Å)	62.8	4.05	No hydride transfer
		3	-2.786	-22.785	H-bond of H175 to CN (2.20 Å)	55.7	4.30	No hydride transfer
		4	-2.785	-21.172	H-bond of H175 to CN (2.20 Å)	52.8	4.16	No hydride transfer
		5	-2.097	-24.087	No productive pose	80.2	5.45	No hydride transfer
54a	n.c.	1	-4.068	-25.964	H-bond of H175 to C=O (1.88 Å)	59.6	4.11	No hydride transfer
		2	-4.013	-27.396	H-bond of H175 to C=O (2.11 Å)	72.2	3.81	No hydride transfer
		3	-3.918	-25.394	H-bond of H175 to C=O (1.87 Å)	38.8	4.81	No hydride transfer
		4	-3.845	-26.974	H-bond of H175 to C=O (2.12 Å)	72.2	3.81	No hydride transfer
		5	-3.527	-25.133	H-bond of H175 to C=O (2.15 Å)	90.4	4.43	No hydride transfer
55a	n.c.	1	-3.856	-20.395	H-bond of H175 to C=O (2.30 Å), bad contact of Y177, G65, T67 and A58 to Ph	61.3	4.64	No hydride transfer
		2	-3.85	-22.931	Pi-pi stacking of H175 to Ph	94.7	3.85	transfer possible
		3	-3.601	-21.491	Pi-pi-stacking of Y177 to Ph	120.6	4.37	No hydride transfer
		4	-3.59	-22.624	H-bond of H175 to C=O (2.01 Å), Pi-pi stacking of H175 to Ph	47.1	6.15	No hydride transfer
		5	-3.354	-21.831	Bad contact of H175 to Ph	117.2	4.32	No hydride transfer
56a	n.c.	1	-4.387	-25.461	H-bond of H175 to C=O (1.91 Å), Pi-pi stacking of H175 to Ph	46.7	6.13	No hydride transfer
		2	-4.367	-24.846	Bad contact T67 to CH3	111.2	4.80	No hydride transfer
		3	-4.264	-23.731	Pi-pi stacking of H175 to Ph	79.8	3.98	No hydride transfer

		4	-4.011	-24.116	H-bond of H175 to C=O (2.02 Å)	34.6	6.80	No hydride transfer
		5	-3.619	-23.257	H-bond of H175 to C=O (2.21 Å)	39.2	6.43	No hydride transfer
57a	n.c.	1	-2.068	-22.429	Bad contact of Y177, T67, A104 and A58	93.0	3.43	transfer possible
		2	-1.971	-22.673	H-bond of H175 to C=O (1.91 Å), bad contact of Y27, T67, A104 and A58	91.9	3.37	transfer possible
		3	-1.931	-21.542	H-bond of H175 to C=O (2.13 Å), bad contact of Y27, D71, Q57	86.6	3.59	no hydride transfer
		4	-1.925	-22.571	Bad contact of D71, G25 and A58	77.3	3.92	no hydride transfer
		5	-1.791	-25.344	H-bond of H175 to C=O (1.99 Å), bad contact of Y27, D71, Q57	88.3	3.38	no hydride transfer
11a	n.c.	1	-5.898	-25.864	H-bond of Y27 to C=O (2.08 Å), bad contact of H175 to C6, of R347 to C2	79.1	4.71	no hydride transfer
		2	-5.493	-26.035	Pi-pi stacking of Y177 to Ph	117.4	4.01	transfer possible
		3	-5.491	-25.07	Pi-pi stacking of Y177 to Ph, bad contact of H172 to C6	82.8	4.52	no hydride transfer
		4	-5.477	-24.709	Vertical to FMN	105.3	6.53	no hydride transfer
		5	-5.285	-24.44	Vertical to FMN	100.5	6.68	no hydride transfer
13a		1	-6.249	-30.823	H-bond of H175 to C=O (1.79 Å), of D71 to OH (1.81 Å), Pi-pi stacking of Y177 to lactone, bad contact of R347 to OEt, of T67 to C7	116.8	3.07	Would result in R-13b
		2	-5.492	-33.889	H-bond of H175 to O (2.76 Å), bad contact of H172 to C=O, of R347 to C6, of D71 to OEt	95.3	3.16	Would result in S-13b
		3	-5.349	-32.004	H-bond of R347 to C=OOEt (2.32 Å), Pi-pi stacking of Y177 to Ph	84.7	4.52	no hydride transfer
		4	-5.311	-30.915	H-bond of D71 to OH (2.65 Å), Pi-pi stacking of Y177 to Ph	82.6	4.36	no hydride transfer
		5	-5.09	-31.307	H-bond of R347 to C=OOEt (2.26 Å), Pi-pi stacking of Y177 to Ph	91.8	4.71	no hydride transfer
12a		1	-7.464	-31.473	H-bond of H175 to C=O (1.82 Å), of D71 to OH (1.81 Å), Pi-pi stacking of Y177 to lactone, bad contact of T67 to C7	112.9	3.02	Would result in R-12b
		2	-7.268	-30.045	H-bond of H175 to C=O (1.82 Å), of D71 to OH (1.82 Å), Pi-pi stacking of Y177 to lactone, bad contact of T67 to C7	113.0	3.01	Would result in R-12b
		3	-6.098	-26.796	H-bond of H175 to C=OAc (2.18 Å), of D71 to OH (1.75 Å), bad contacts of T67, D71 to C7,C8	36.6	4.88	no hydride transfer
		4	-5.886	-28.206	H-bond of R347 to C=OAc (2.22 Å), Pi-pi stacking of Y177 to Ph	86.2	4.62	no hydride transfer
		5	-5.737	-27.374	Bad contact of H172 and Y27 to Ph	112.8	3.12	Would result in R-12b
14a		1	-5.803	-25.473	Pi-pi stacking of H175 to lactone	133.4	4.33	no hydride transfer
		2	-5.381	-27.943	Vertical to FMN to Ph ring above N5	98.6	10.35	no hydride transfer
		3	-5.092	-26.655	Vertical to FMN to double bond above N5	100.6	5.88	no hydride transfer
		4	-5.023	-24.712	Vertical to FMN to C=O above N5	43.9	6.32	no hydride transfer
		5	-4.788	-23.701	Vertical to FMN to double bond above N5	106.2	5.83	no hydride transfer

16a	1	-6.427	-26.922	H-bond of Y27 to C=O (2.14 Å), Pi-pi stacking of Y177 to second Ph	79.2	4.70	no hydride transfer
	2	-5.434	-25.025	Vertical to FMN to double bond above N5	124.5	5.67	no hydride transfer
	3	-5.201	-27.164	Vertical to FMN to Ph ring above N5	84.4	10.45	no hydride transfer
	4	-4.979	-24.918	Vertical to FMN to double bond above N5	102.9	5.69	no hydride transfer
	5	-4.469	-23.614	Vertical to FMN to Ph ring above N5	99.5	11.05	no hydride transfer
15a	1	-5.248	-30.082	Vertical to FMN to double bond above N5	62.6	6.72	no hydride transfer
	2	-5.042	-31.908	H-bond of H175 to C=OOH (2.03 Å), Pi-cation of K107 and R347 to both Ph	66.6	5.55	no hydride transfer
	3	-4.539	-29.339	Vertical to FMN to double bond above N5	64.2	6.79	no hydride transfer
	4	-4.372	-29.618	H-bond of H175 to C=OOH (1.99 Å), Pi-cation of K107 to lactone and Ph, Pi-pi stacking of H175 to 2Ph	31.4	6.12	no hydride transfer
	5	-4.209	-30.151	H-bond of H175 to C=OOH (2.02 Å), Pi-cation of K107 and R347 to Ph and lactone	81.5	4.99	no hydride transfer

Table 29. Results from RBD of Substrates **11a-57a** in the *Ts*ER C25D/I67T variant, created with PyMOL Mutagenesis Wizard on crystal structure 3HGJ. Experimental screening of substrate as (a) racemate (b) E/Z 1:4, (c) E/Z 2:3, (d) E/Z 7:1, (e) E/Z 1:1, n.t. not tested, n.d. not detected. “would” means hydride transfer angle in a range of 80-120° and distance to the hydride of N5 in a range of 3.00 to 4.85 Å, “might” means either hydride transfer angle to small or distance to N5 to large.

Substrate	Empirical Result conv (%) / ee (%)	Pose	Glide Gscore	Glide Energy	Notes	Hydride transfer angle	distance hydride N5 to substrate	result
17a	95 / 93R	1	-4.583	-22.715	normal pose, H-bond of H175 to C=O (1.90 Å), bad contact of Y177 to C5	83.9	4.95	no hydride transfer
		2	-4.42	-22.941	normal pose, H-bond of H175 to C=O (1.80 Å), bad contact of Y177 to C6	81.4	4.83	might result in R- 17b
		3	-4.289	-20.867	flipped pose, H-bond of H175 to C=O (2.01 Å), bad contact of Y27 to CH3	68.3	3.91	no hydride transfer
		4	-3.553	-20.313	no H-bond	108.3	3.68	would result in S- 17b
24a	29 / 99R	1	-4.487	-22.981	normal pose, H-bond of H175 to C=O (1.80 Å), bad contact of Y177 to C6 and of R347 to Iso	80.9	4.84	no hydride transfer
		2	-4.44	-20.758	normal pose, H-bond of H175 to C=O (1.83 Å), bad contact of Y177 to C5 and R347 to Iso and of D25 to C4, C5	100.5	3.84	would result in R- 24b
		3	-4.285	-21.224	normal pose, H-bond of H175 to C=O (1.86 Å), bad contact of Y177 to C5 and D25 to C4, C5	91.0	3.98	would result in R- 24b
		4	-4.17	-22.017	normal pose, H-bond of H175 to C=O (2.21 Å), bad contact of Y177 to C5 and D25 to C4, C5	89.9	3.92	might result in R- 24b
25a	>99 / >99R	1	-5.482	-30.445	new flipped pose, H-bond of R347 to C=O (2.02 Å), of H175 to C=OOMe (2.07 Å), bad contact of Y177 to OMe and of R347 to C6	58.6 (Cβ) 101.3 (Cα)	3.89 3.39	would result in S- 25b

		2	-5.191	-26.226	new flipped pose, H-bond of R347 to C=O (2.18 Å, 2.32 Å), H-bond of H175 to C=OOMe (1.96 Å), bad contact of D25 to OMe and of R347 to C6	98.6 (C β) 67.2 (C α)	5.11 5.48	would result in R- 25b
		3	-4.85	-28.651	H-bond of H175 to OMe (2.04 Å), bad contacts of R347 to C6, Y177 to OMe and Y27 to C5,	116.5 (C β) 48.5 (C α)	3.92 4.69	would result in S- 25b
		4	-4.809	-24.058	normal pose, H-bond of H175 to C=O (1.84 Å), H-bond of R347 to C=OOMe (2.10 Å, 2.41 Å)	77.4 (C β) 87.7 (C α)	5.29 5.17	no hydride transfer
		5	-4.616	-24.035	normal pose, H-bond of H175 to C=O (1.99 Å), H-bond of R347 to C=OOMe (2.23 Å, 2.26 Å)	77.6 (C β) 88.2 (C α)	5.55 5.42	no hydride transfer
R-26a^a	51 / 74 (isomer 2)	1	-4.48	-22.178	flipped pose, H-bond of H175 to C=O (1.99 Å), bad contact of Y27 to C3CH ₃	70.2	3.88	might result in 3R,5S- 26b
		2	-4.439	-22.73	normal pose, H-bond of H175 to C=O (2.04 Å), bad contact of Y27 to C3CH ₃	70.6	5.58	no hydride transfer
		3	-4.426	-22.388	H-bond of Y27 to C=O (1.96 Å), flipped pose, bad contact of Y177 to C3CH ₃	69.5	3.62	no hydride transfer
		4	-4.316	-22.385	flipped pose, H-bond of H175 to C=O (1.92 Å), bad contact of Y27 to C3CH ₃	72.0	3.85	no hydride transfer
		5	-3.584	-21.038	no H-bond	108.0	3.72	would result in 3R,5S- 26b
S-26a^a	51 / 74 (isomer 2)	1	-4.423	-21.618	normal pose, H-bond of H175 to C=O (1.94 Å), bad contact of Y27	73.0	6.03	no hydride transfer
		2	-4.399	-21.811	flipped pose, H-bond of H175 to C=O (1.91 Å), bad contact of Y27 to C3CH ₃	73.9	3.82	might result in 3S,5S- 26b
		3	-4.383	-22.172	H-bond of Y27 to C=O (1.99 Å), flipped pose, bad contact of Y177 to C3CH ₃	70.6	3.62	might result in 3R,5S- 26b
		4	-4.347	-21.347	flipped pose, H-bond of H175 to C=O (2.03 Å), bad contact of Y27 to C3CH ₃	63.6	4.06	no hydride transfer
		5	-3.611	-21.694	no H-bond	108.3	3.70	would result in 3S,5S- 26b
27a	99 / achiral	1	-4.797	-26.755	Wrong double bond location	-	-	-
		2	-4.585	-26.47	Flipped pose, H-bond of H175 to C=O (2.20 Å)	103.6	3.31	Productive pose
		3	-3.948	-18.286	H-bond of R347 to C=O (2.19 Å)	102.0	4.64	no hydride transfer
		4	-3.928	-17.951	H-bond of R347 to C=O (2.01 Å)	108.8	4.90	no hydride transfer
		5	-3.743	-17.955	H-bond of R347 to C=O (2.08, 2.47 Å)	90.7	5.55	no hydride transfer
S-28a	84 / 27 (isomer 2)	1	-4.16	-22.824	flipped pose, H-bond of H175 to C=O (1.70 Å), bad contact of Y27 to C4 and D25 to C3	105.6	3.27	would result in (1r,4r)- 28b (trans)
		2	-3.46	-19.512	flipped pose, no H-bond, bad contacts of H175 to C6, R347 to 4-propenyl	90.4	3.67	would result in (1r,4r)- 28b (trans)
		3	-3.185	-20.697	flipped pose, no H-bond	88.9	3.49	might result in (1r,4r)- 28b (trans)
		4	-3.161	-20.136	flipped pose, no H-bond	87.4	3.59	might result in (1r,4r)- 28b (trans)
29a	>99 / 5R	1	-4.483	-21.164	normal pose, H-bond of H175 to C=O (1.95 Å), bad contact of Y177 and D25 to C5	92.3	4.35	no hydride transfer
		2	-4.323	-18.739	normal pose, H-bond of H175 to C=O (2.16 Å), bad contact of Y177 to C5	84.8	5.13	no hydride transfer

		3	-4.319	-22.464	flipped pose, H-bond of H175 to C=O (1.85 Å)	93.1	3.43	would result in R-29b
		4	-4.27	-19.147	normal pose, H-bond of H175 to C=O (1.83 Å), bad contact of Y177 to C5, D25 to C4, C5	101.8	3.81	would result in S-29b
22a	>99 / 92R	1	-5.427	-29.096	Flipped pose, H-bond of H175 to C1=O (1.97 Å), of Y27 to C2=O (2.26 Å)	90.4	3.61	Would result in R-22b
		2	-4.845	-25.394	Flipped pose, H-bond of Y27 to C2=O (2.01 Å)	96.1	3.29	Would result in R-22b
		3	-4.705	-23.098	Flipped pose, H-bond of H175 to C2=O (2.06 Å), of R347 to C1=O (2.26, 2.31 Å)	54.4	4.75	no hydride transfer
		4	-4.505	-22.675	Flipped pose, H-bond of H175 to C2=O (1.95 Å)	67.8	4.01	no hydride transfer
		5	-4.473	-23.114	Flipped pose, H-bond of H175 to C2=O (1.86 Å), bad contact of Y27 and D25 to CH3	81.3	3.67	no hydride transfer
18a	>99 / 92 (2R,5S)	1	-3.922	-23.735	flipped pose, H-bond of H175 to C=O (2.03 Å), bad contact of Y27 and R347 to 4-propenyl, D25 to C3	96.0	3.80	would result in 2R,5S-18b
		2	-3.888	-24.21	flipped pose, H-bond of H175 to C=O (1.83 Å), bad contact of R347 to 4-propenyl, D25 to C3	93.2	3.63	would result in 2R,5S-18b
		3	-3.849	-25.083	flipped pose, H-bond of H175 to C=O (1.83 Å), bad contact of R347 to 4-propenyl, D25 to C3	92.6	3.66	would result in 2R,5S-18b
		4	-3.814	-23.654	flipped pose, H-bond of H175 to C=O (1.97 Å), bad contact of D25 to CH ₃	91.2	3.38	would result in 2R,5S-18b
30a	>99 / 96 (2R,5R)	1	-4.139	-23.669	Flipped pose, H-bond of H175 to C=O (1.83 Å)	95.0	3.68	Would result in 2R,5R-30b
		2	-4.006	-23.201	Flipped pose, H-bond of H175 to C=O (1.79 Å)	88.0	3.50	no hydride transfer
		3	-3.92	-22.675	Flipped pose, H-bond of H175 to C=O (1.90 Å)	94.4	3.63	Would result in 2R,5R-30b
		4	-3.561	-23.755	Flipped pose, H-bond of H175 to C=O (1.89 Å)	91.9	3.40	Would result in 2R,5R-30b
E-31a	n.t.	1	-4.088	-29.853	H-bond of H175 to C=O (1.96 Å), of Y27 to OMe (2.18 Å)	98.9	3.56	Would result in S-31b
		2	-3.937	-24.497	H-bond of H175 to C=O (1.92 Å), of R347 to C=O (1.96 Å)	85.4	5.12	no hydride transfer
		3	-3.584	-26.255	H-bond of H175 to C=O (1.79 Å), of R347 to C=O (2.45 Å) to OMe (2.44 Å)	75.3	4.78	no hydride transfer
		4	-3.358	-26.364	H-bond of H175 to C=O (2.12 Å)	119.6	3.97	Would result in S-31b
		5	-3.255	-25.954	H-bond of H175 to C=O (1.83 Å), bad contact of R347 to OMe	98.5	3.93	Would result in R-31b
Z-31a	>99 / >99R	1	-4.24	-30.845	H-bond of H175 to C=O (2.10 Å)	64.1	3.88	no hydride transfer
		2	-3.615	-26.106	H-bond of H175 to C=O (1.99 Å)	82.2	4.68	no hydride transfer
		3	-3.424	-27.61	H-bond of H175 to C=O (1.94 Å), bad contact of Y177 to OMe	84.2	3.60	no hydride transfer
		4	-3.309	-25.409	H-bond of H175 to C=O (2.00 Å), bad contact of Y177 and Y27 to Me	89.4	3.87	might result in S-31b
32a	>99 / >99R	1	-5.31	-33.915	H-bond of H175 to C=O (1.89 Å), Pi-cation of R347 and H175 to Ph and Pi-pi stacking of H175 to Ph	91.2	3.40	Would result in R-32b
		2	-4.978	-33.751	H-bond of H175 to C=O (2.00 Å), Pi-cation of R347 and H175 to Ph and Pi-pi stacking of H175 to Ph	89.2	3.40	Would result in R-32b

		3	-4.936	-29.788	H-bond of R347 to C=O (2.26, 2.46 Å), Pi-cation and Pi-pi stacking of H175 to Ph	113.8	4.12	no hydride transfer
		4	-4.898	-26.981	H-bond of R347 to C=O (2.73, 2.78 Å), of H175 to C=O (1.96 Å), Pi-cation and Pi-pi stacking of H175 to Ph	57.8	4.45	no hydride transfer
		5	-4.097	-25.391	No hydride transfer, Ph above FMN	107.1	8.36	no hydride transfer
33a	91 / 88R	1	-4.453	-21.322	normal pose, H-bond of H175 to C=O (1.84 Å)	102.6	3.86	would result in S- 33b
		2	-4.261	-21.475	flipped pose, H-bond of H175 to C=O (1.84 Å)	97.5	3.33	would result in R- 33b
		3	-4.228	-19.364	normal pose, H-bond of H175 to C=O (2.07 Å), bad contact of Y177 and D25 to C4	79.3	3.73	no hydride transfer
		4	-4.044	-15.94	normal pose	94.2	4.83	no hydride transfer
34a	9 / 57R	1	-4.383	-21.242	normal pose, H-bond of H175 to C=O (1.89 Å), bad contact of D25 to C4	102.6	3.83	would result in R- 34b
		2	-4.201	-19.039	flipped pose, H-bond of H175 to C=O (1.84 Å), bad contacts of Y27 to CH ₃	88.3	3.56	would result in S- 34b
		3	-3.417	-17.877	no H-bond, bad contact of D25 to CH ₃ and C4	107.1	3.83	would result in S- 34b
		4	-3.39	-16.188	no H-bond	111.7	3.58	would result in S- 34b
35a	>99 / >99R	1	-5.711	-30.308	H-bond of C=O to Y27 (1.99 Å), H-bond of C=OOMe to H175 (1.87 Å), bad contact of D25 to OMe	95.8	3.39	would result in S- 35b
		2	-5.162	-27.122	normal pose, H-bond to H175 (1.86 Å), bad contact of D25 to C4, R347 to OMe	108.5	3.71	would result in R- 35b
		3	-4.894	-25.577	new flipped pose, H-bond of R347 to C=O (2.33 Å, 2.41 Å), of H175 to C=OOMe (1.78 Å)	85.4	4.68	would result in R- 35b
		4	-4.6	-26.804	H-bond to H175 (2.19 Å)	115.9	3.90	would result in S- 35b
36a	2 / n.d.	1	-4.645	-22.868	normal pose, H-bond of H175 to C=O (1.90 Å)	103.1	3.83	would result in 2S,3R- 36b
		2	-4.33	-21.256	flipped pose, H-bond of H175 to C=O (1.83 Å), bad contact of Y27 to 3CH ₃	88.4	3.57	might result in 2R,3S- 36b
		3	-4.172	-19.466	flipped pose, H-bond of H175 to C=O (1.75 Å), bad contact of Y27 to 3CH ₃	86.3	3.81	no hydride transfer
		4	-4.113	-16.475	normal pose, H-bond of H175 to C=O (1.90 Å), bad contact of Y27 and D25 to 3CH ₃	90.8	3.68	would result in 2S,3R- 36b
		5	-3.384	-16.968	bad contact of H175 to 2CH ₃	112.3	3.60	would result in 2R,3S- 36b
19a	98 / 97S	1	-3.16	-26.859	flipped pose, H-bond of H175 to C=O (1.84 Å), of D25 to OH (1.84 Å)	89.3	3.48	might result in S- 19b
		2	-3.001	-24.767	H-bond of H175 to C=O (1.83 Å), H-bond of D25 to OH (2.02 Å)	69.7	3.98	no hydride transfer
		3	-2.826	-23.365	flipped pose, H-bond of H175 to C=O (2.15 Å), H-bond of D25 to OH (1.75 Å)	60.3	4.59	no hydride transfer
		4	-2.646	-23.971	flipped pose, H-bond of H175 to C=O (2.01 Å), bad contact of D25	71.1	4.02	no hydride transfer
		5	-2.555	-24.218	flipped pose, H-bond of H175 to C=O (1.82 Å), bad contact of Y177	92.2	3.64	would result in S- 19b
Z-37a^b	51 / 5R	1	-3.192		H-bond of H175 to C=O (1.82 Å), bad contact of Y177 to C5, of D25 to C4	96.3 (C α)	3.87	would result in R- 37b
		2	-2.596		bad contacts of H175 to Cl, of Y177 and T67 to C5	106.8 (C β)	3.46	would result in R- 37b

		3	-2.534	H-bond of Y27 to OMe (2.37 Å), bad contacts of Y177, T67 and D25 to C5	107.2 (C β)	3.23	would result in R-37b
		4	-2.51	bad contact of H175 and H172 to Cl, of Y177 and D25 to C5	112.6 (C β)	3.34	would result in R-37b
		5	-2.489	bad contact of H175 and H172 to Cl, of Y177 and D25 to C5	89.1	3.79	might result in R-37b
E-37a^b		1	-3.377	H-bond of H175 to C=O (1.93 Å), bad contact of Y27 to C5	90.0	4.18	no hydride transfer
		2	-3.22	H-bond of H175 to C=O (2.39 Å)	128.9 (C α)	4.24	no hydride transfer
		3	-3.127	H-bond of H175 to C=O (2.06 Å)	115.1	3.77	Would result in S-37b
		4	-3.106	H-bond of H175 to C=O (2.00 Å)	86.3	3.66	no hydride transfer
		5	-2.444	bad contact of D25 to C3 and C5, of Y27 to Cl	94.9	3.12	Would result in S-37b
E-38a^c	70 / 99S	1	-2.643	H-bond of H175 to C=O (1.83 Å)	100.1	3.64	would result in S-38b
		2	-2.543	H-bond of H175 to C=O (1.70 Å)	102.7	3.59	would result in S-38b
		3	-2.198	bad contacts of H172, Y177, A102, G65, T67, D71 and D25	92.5	3.81	would result in R-38b
Z-38a^c		1	-3.00	H-bond of H175 to C=O (2.22 Å)	53.4	3.92	no hydride transfer
		2	-2.566	H-bond of Y27 to C=O (1.71 Å)	65.8	3.46	no hydride transfer
		3	-2.53	H-bond of H175 to C=O (2.24 Å)	75.0	3.60	no hydride transfer
		4	-2.508	H-bond of H175 to C=O (2.24 Å), bad contact of Y177 to C4	51.3	4.10	no hydride transfer
		5	-1.926	H-bond of H175 to C=O (2.00 Å), bad contact of Y177 to C4, of H175 to C5	70.0	3.61	no hydride transfer
Z-39a	47 / rac	1	-3.534	H-bond of H175 to C=O (2.20 Å)	34.2	6.04	no hydride transfer
		2	-2.984	H-bond of H175 to C=O (2.07 Å), Pi-cation of R347 to Ph, bad contact of Y27 and D25 to Ph	60.2	4.52	no hydride transfer
		3	-2.764	bad contact of H172 to CH ₃	99.5	3.62	would result in S-39b
		4	-2.755	bad contact of H175 to Ph	48.3	4.54	no hydride transfer
E-39a	?	1	-4.774	H-bond of H175 to C=O (1.78 Å)	75.5	4.12	no hydride transfer
		2	-4.64	H-bond of H175 to C=O (2.05 Å), Pi cation of H175 and R347 to Ph, Pi-pi stacking of H175 to Ph	42.4	5.07	no hydride transfer
		3	-4.621	H-bond of H175 to C=O (1.83 Å), Pi cation of R347 to Ph, Pi-pi stacking of H175 to Ph, bad contact of D25 to CH ₃	61.9	4.53	no hydride transfer
		4	-4.48	H-bond of H175 to C=O (2.12 Å), bad contact of T67 to Ph	67.1	4.26	no hydride transfer
		5	-3.738	H-bond of H175 to C=O (2.02 Å), Pi cation of R347 to Ph	58.8	4.59	no hydride transfer
Z-40a	88 / >99 unassigned	1	-4.374	H-bond of R347 to C=OOEt (2.17, 2.36 Å), of Y27 to C=OAc (2.07 Å), Pi-cation and Pi-pi stacking of H175 to Ph, bad contact of K107 to Et	80.0	5.16	no hydride transfer
		2	-4.331	H-bond of R347 to C=OOEt (2.16, 2.40 Å), of Y27 to C=OAc (2.07 Å), Pi-cation and Pi-pi stack-	81.9	5.17	no hydride transfer

					ing of H175 to Ph			
		3	-4.312		H-bond of R347 to C=OOEt (2.26 Å), of Y27 to C=OAc (2.15 Å), bad contact of K107 to Et	50.4	6.82	no hydride transfer
		4	-3.275		Pi-contact of K107 to Ph	73.8	6.89	no hydride transfer
E-40a	n.t.	1	-3.996		H-bond of R347 to C=OAc (2.20, 2.58 Å), Pi-cation and Pi-pi stacking of H175 to Ph	47.8	5.73	no hydride transfer
		2	-3.713		H-bond of Y27 to C=OAc (2.36 Å), of K107 to C=OOEt (2.38 Å)	34.2	7.36	no hydride transfer
		3	-3.326		H-bond of R347 to C=OAc (2.06, 2.63 Å), of Y27 to C=OOEt (2.01 Å)	61.0	6.70	no hydride transfer
		4	-3.296		bad contact of Y177 to Et	31.0	5.98	no hydride transfer
E-41a^d	28 / >99S	1	-4.162	-20.203	salt bridge of K107 to NO (3.09 Å)	119.2	7.96	no hydride transfer
		2	-4.16	-20.521	no H-bond or salt bridge, NO ₂ shows in direction of R347	66.5	4.36	no hydride transfer
		3	-4.037	-21.277	H-bond of H175 to N=O (2.14 Å), salt bridge of H175 to NO (4.87 Å)	78.0	5.44	no hydride transfer
		4	-3.692	-20.995	salt bridge of D25 to N=O (4.89 Å), Pi-cation of Y177 and NO ₂	90.2	3.80	would result in S-41b
		5	-3.1	-21.001	salt bridge of R347 to NO (4.34 Å)	127.2	4.50	no hydride transfer
Z-41a^d		1	-4.153	-24.36	H-bond of H175 to N=O (1.91 Å), salt bridge of H175 and H172 to NO, Pi-cation of H175 and R347 to Ph, Pi-pi stacking of H175 to Ph	57.9	4.08	no hydride transfer
		2	-3.376	-22.872	H-bond of Y27 to NO (1.84 Å), salt bridge of R347 to NO, Pi-cation of R347 to Ph	56.8	3.69	no hydride transfer
		3	-2.849	-19.083	salt bridge of K107 to NO, Pi-cation of K107 to Ph	157.1	6.44	no hydride transfer
E-33a^c	4 / n.d.	1	-4.014	-21.743	H-bond of H175 to C=O (2.46 Å), Pi-cation of H175 to Ph, bad contact of Y27 to Br	130.6	3.93	no hydride transfer
		2	-3.923	-23.132	Pi-cation of H175 to Ph, bad contact of Y27 to Br	131.0	4.09	no hydride transfer
		3	-3.886	-24.333	H-bond of H175 to C=O (2.19 Å), Pi-cation of R347 to Ph, bad contact of H175 to Br	75.8	5.02	no hydride transfer
		4	-3.784	-21.435	no productive pose	121.4	8.50	no hydride transfer
		5	-3.257	-23.049	no productive pose	153.7	5.54	no hydride transfer
Z-43a^c		1	-4.347	-25.034	H-bond of H175 to C=O (1.96 Å), bad contact of Y177 to Br	95.3	5.79	no hydride transfer
		2	-4.194	-19.036	H-bond of H175 to C=O (2.39 Å), bad contact of H175 to C3	147.7	5.38	no hydride transfer
		3	-3.707	-23.319	H-bond of H175 to C=O (2.39 Å), Pi-pi stacking of Y27 to Ph, bad contact of Y177 and Y27 to Ph, of H172 and A58 to OMe	83.7	4.00	might result in R-23b
		4	-3.598	-20.976	Pi-cation of K107 to Ph, bad contact of H175 to Br	156.9	5.85	no hydride transfer
44a	n.c.	1	-4.561	-24.32	Flipped pose, H-bond of H175 to C=O (1.91 Å), bad contact of H175 to 2CH3	74.0	3.82	no hydride transfer
		2	-4.432	-25.094	New flipped pose, H-bond of Y27 to C=O (2.17 Å), bad contact of Y177 to CH3	67.6	3.63	no hydride transfer
		3	-4.38	-22.497	Flipped pose, H-bond of H175 to C=O (2.03 Å), bad contact of Y27 to CH3	62.7	4.08	no hydride transfer

		4	-4.119	-23.792	New flipped pose, H-bond of Y27 to C=O (2.17 Å), bad contact of Y177 to CH3	57.0	3.82	no hydride transfer
		5	-3.93	-24.303	Bad contact of H175 to C2	117.8	3.79	Possible transfer
45a	n.c.	1	-4.384	-23.499	H-bond of Y27 to C=O (2.22 Å), of H175 to C=OOBu (2.11 Å), bad contacts of H172, T67 and A58 to Bu	104.7 (C α) 56.3 (C β)	3.46 4.02	Possible transfer to C α
		2	-4.219	-22.128	H-bond of H175 to C=OOBu (2.06 Å), bad contacts of H172, D25, Y177 and A58 to Bu	100.8 (C α) 61.7 (C β)	3.96 4.44	Possible transfer to C α
		3	-4.138	-22.844	H-bond of H175 to C=OOBu (2.06 Å), bad contacts of H172, D25, Y177, T67 and A58 to Bu	100.9 (C α) 60.0 (C β)	3.59 4.08	Possible transfer to C α
		4	-3.873	-24.266	H-bond of H175 to C=OOBu (2.05 Å), bad contacts of H172, D25, Y177 and A58 to Bu	91.0 (C α) 71.8 (C β)	4.37 4.60	no hydride transfer
		5	-3.622	-21.051	Vertical to FMN	105.2 (C α) 63.0 (C β)	5.93 6.42	no hydride transfer
46a	n.c.	1	-4.484	-24.842	H-bond of H175 to C=O (1.91 Å), bad contacts of Y177 and D25 to propan-2-ylidene	91.5	3.90	Possible transfer
		2	-4.389	-25.437	H-bond of H175 to C=O (2.03 Å), bad contacts of Y177, H175, T67 and D25 to propan-2-ylidene	67.2	4.17	no hydride transfer
		3	-4.283	-24.671	H-bond of H175 to C=O (2.27 Å), bad contacts of R347 to C5	119.7	3.65	Possible transfer
		4	-3.84	-21.72	bad contacts of H172, Y177, Y27 and D25 to propan-2-ylidene, of H175 to C=O	78.1	3.92	no hydride transfer
		5	-3.825	-22.43	H-bond of H175 to C=O (2.11 Å), bad contacts of H172, T67 and D25 to propan-2-ylidene, of R347 to CH3	69.5	4.13	no hydride transfer
E-42a	n.c.	1	-3.675	-27.554	H-bond of Y27 to NO (2.10 Å)	80.6	4.41	no hydride transfer
		2	-3.453	-27.047	Ring above FMN	135.1	7.35	no hydride transfer
		3	-3.411	-29.343	H-bond of H175 to N=O (1.71 Å), salt bridges of H175 and H172 to NO, bad contacts of D25 to CH3, of Y177 to C1	108.5	4.01	Possible transfer
		4	-2.897	-27.228	H-bond of R347 to NO, Pi-cation of H175 to N, bad contact of H175 to C4, of D25 to CH3	75.5	6.06	no hydride transfer
		5	-2.542	-29.781	Salt bridge of R347 to NO, Pi-cation of H175 to N, bad contact of Y177 to C7, of D25 to CH3	99.4	5.55	no hydride transfer
Z-42a	n.c.	1	-4.134	-27.327	H-bond of H175 to NO (2.06 Å), salt bridges of H175 and H172 to NO	58.8	4.09	no hydride transfer
		2	-3.952	-27.1	H-bond of H175 to NO (2.13 Å), salt bridges of H175 to NO	57.8	3.84	no hydride transfer
		3	-3.519	-26.664	H-bond of Y27 to NO (2.03 Å), salt bridge of R347 to NO, bad contacts of Y177	56.2	3.87	no hydride transfer
		4	-3.462	-20.203	H-bond of Y27 to N=O (2.00 Å), bad contact of Y177 to CH3, of H175 to ring	56.9	3.81	no hydride transfer
		5	-3.15	-20.521	H-bond of H175 to N=O (2.25 Å), salt bridge of H175 to NO, bad contact of Y27 to CH3, of R347 to double bond in ring	66.4	3.89	no hydride transfer
47a	n.c.	1	-4.345	-21.277	H-bond of H175 to N=O (2.03 Å), salt bridges of H175 and H172 to NO, Pi-cation of H175 and R347 to Ph, Pi-pi stacking of H175 to Ph, bad contacts of Y177, Y27 and P113 to second Ph	52.5	4.35	no hydride transfer
		2	-3.629	-20.995	H-bond of R347 to NO (1.73 Å), salt bridge of R347 to NO, Pi-cation and Pi-pi stacking of H175 to Ph, bad contact of H175 and D25 to second Ph	113.8	6.13	no hydride transfer
		3	-3.443	-21.001	Salt bridge of H175 to NO, Pi-cation of R347 to Ph	64.9	4.65	no hydride transfer

		4	-2.769	-27.744	H-bond of R347 to NO, Pi-cation of H175 to N, of R347 to Ph, Pi-pi stacking of Y177 to second Ph, bad contact of Y27 to first Ph, of H172, T67 and D25 to second Ph	111.5	4.25	no hydride transfer
		5	-2.649	-24.15	H-bond of R347 to NO (2.20, 2.37 Å), salt bridge of R347 to NO, Pi-cation of R347 to first Ph, of K107 to second Ph, bad contact of Y27 and P113 to first Ph, of D25 and H175 to first Ph	153.0	5.27	no hydride transfer
E-48a	n.c.	1	-5.074	-19.93	H-bond of R347 to C=O _{tert} (2.24, 2.25 Å), of H175 to C=O (1.80 Å), of D25 to NH ₂ (2.46 Å),	121.7	4.19	no hydride transfer
		2	-4.916	-27.203	H-bond of Y27 to C=O (2.06 Å)	130.9	4.66	no hydride transfer
		3	-4.749	-26.378	H-bond of H175 to C=O (1.96 Å)	112.9	4.33	no hydride transfer
		4	-4.363	-27.243	H-bond of H175 to C=O (2.20 Å)	123.5	4.63	no hydride transfer
Z-48a	n.c.	1	-5.172	-22.711	H-bond of H175 to C=O (1.78 Å), of Y27 to C=O _{tert} (2.01 Å)	128.2	4.31	no hydride transfer
		2	-4.887	-23.936	H-bond of Y27 to C=O (1.96 Å)	128.5	5.05	no hydride transfer
		3	-4.688	-27.856	H-bond of Y27 to C=O (2.07 Å)	124.5	4.67	no hydride transfer
		4	-3.997	-27.351	Vertical to FMN	149.0	6.06	no hydride transfer
		5	-3.936	-27.589	H-bond of H175 to C=O (2.10 Å), of R347 to C=O _{tert} (2.20 Å)	86.5	4.86	no hydride transfer
49a	n.c.	1	-3.975	-23.75	H-bond of H175 to C=O (1.77 Å)	75.9	5.63	no hydride transfer
		2	-3.858	-23.758	H-bond of H175 to C=O (2.14 Å), bad contacts of K107 to CH ₃	52.6	5.95	no hydride transfer
		3	-3.806	-23.755	H-bond of H175 to C=O (1.77 Å)	69.8	5.69	no hydride transfer
		4	-3.659	-22.293	H-bond of H175 to C=O (1.98 Å)	26.1	6.28	no hydride transfer
		5	-3.595	-20.993	H-bond of H175 to C=O (1.75 Å), bad contact of H175 to CH ₃ , of R347 to ring	84.9	5.22	no hydride transfer
E-50a	n.c.	1	-4.165	-22.082	H-bond of H175 to C=O (1.91 Å), bad contact of H175 to C ₃	15.3	6.00	no hydride transfer
		2	-4.038	-37.7	H-bond of Y27 to C=O (2.28 Å)	59.6	5.40	no hydride transfer
		3	-3.674	-34.41	Ph above N ₅	148.4	4.59	no hydride transfer
		4	-3.227	-36.359	H-bond of T67 to OMe (2.05 Å), bad contact of H172 to C ₃ , of H175 to Ph	87.7	4.42	no hydride transfer
		5	-3.13	-34.693	Ph above N ₅	133.8	5.47	no hydride transfer
Z-50a	n.c.	1	-4.388	-27.888	H-bond of H175 to C=O (1.99 Å), Pi-cation of H175 to Ph, bad contact of D25 to OMe	63.6	3.83	no hydride transfer
		2	-4.221	-21.789	H-bond of H175 to C=O (2.24 Å), Pi-cation of R347 to Ph	58.0	4.01	no hydride transfer
		3	-4.135	-22.607	H-bond of Y27 to OMe (1.80 Å), Pi-pi stacking of H175 to Ph, Pi-cation of R347 to Ph	59.6	3.75	no hydride transfer
		4	-3.808	-19.623	Pi-cation and Pi-pi stacking of H175 to Ph, bad contact of Y177 and D25 to OMe	25.3	5.81	no hydride transfer
		5	-3.783	-20.401	H-bond of H175 to C=O (1.89 Å), Pi-cation of R347 to Ph	79.1	4.95	no hydride transfer
51a	n.c.	1	-4.19	-19.423	No hydride transfer	34.7	7.33	no hydride transfer

		2	-4.018	-19.668	H-bond of H175 to C=O (2.24 Å), Pi-pi stacking of H175 to Ph	62.4	6.84	no hydride transfer
		3	-3.796	-19.381	No hydride transfer	39.1	8.03	no hydride transfer
		4	-3.741	-22.43	No hydride transfer	40.1	8.43	no hydride transfer
		5	-3.676	-20.664	No hydride transfer	37.0	9.51	no hydride transfer
52a	n.c.	1	-4.616	-19.84	H-bond of H175 to C=O (2.06 Å), Pi-cation of H175 and R347 to Ph, Pi-pi stacking of H175 to Ph	87.7	4.74	no hydride transfer
		2	-4.613	-25.748	Pi-cation and Pi-pi stacking of H175 to Ph	91.4	5.50	no hydride transfer
		3	-3.723	-24.899	Ph ring above N5	85.1	5.40	no hydride transfer
		4	-3.631	-20.979	Ph ring above N5	83.7	5.75	no hydride transfer
E-53a	n.c.	1	-2.408	-22.045	H-bond of Y27 to CN (1.99 Å)	106.4	3.89	Possible transfer
		2	-1.999	-22.899	Bad contacts of H175, Y177, A102, A104, T67, A58 and D25	56.8	3.65	no hydride transfer
		3	-1.854	-34.467	Bad contacts of H172, Y177, A102, G65, A58, D71 and D25	97.0	3.78	Possible transfer
		4	-1.737	-26.123	Bad contacts of Y177, D25, A102, A104, A58 and D25	64.8	3.69	no hydride transfer
		5	-1.668	-26.944	H-bond of H175 to CN (2.21 Å), bad contacts of R347	98.0	3.58	Possible transfer
Z-53a	n.c.	1	-2.814	-23.996	H-bond of H175 to CN (2.24 Å)	60.1	3.97	no hydride transfer
		2	-2.49	-24.359	H-bond of H175 to CN (2.21 Å)	66.1	3.65	no hydride transfer
		3	-2.39	-32.902	H-bond of H175 to CN (2.24 Å)	51.6	4.13	no hydride transfer
		4	-2.266	-35.256	H-bond of H175 to CN (2.19 Å)	59.1	3.82	no hydride transfer
54a	n.c.	1	-3.166	-33.815	H-bond of H175 to C=O (1.97 Å)	59.5	3.92	no hydride transfer
		2	-3.103	-32.485	H-bond of H175 to C=O (1.75 Å), bad contact of Y177 and D25 to CH3	85.2	4.06	no hydride transfer
		3	-3.029	-33.689	H-bond of H175 to C=O (1.89 Å), bad contacts of Y177, T67, A58 and D25 to Et	53.9	3.92	no hydride transfer
		4	-2.954	-32.961	H-bond of H175 to C=O (1.92 Å), bad contacts of Y177, T67 and D25 to Et	86.6	4.00	no hydride transfer
		5	-2.564	-30.817	H-bond of H175 to C=O (1.99 Å), bad contact of Y177 to CH3	79.6	4.07	no hydride transfer
55a	n.c.	1	-3.724	-25.293	H-bond of H175 to C=O (1.90 Å), Pi-pi stacking of H175 to Ph	44.6	6.12	no hydride transfer
		2	-3.39	-29.938	H-bond of H175 to C=O (2.03 Å), bad contacts of Y177, G65, T67 and D25 to Ph	57.9	4.74	no hydride transfer
		3	-2.995	-22.38	Pi-pi stacking of H175 to Ph, Pi-cation of R347 to Ph	58.5	4.55	no hydride transfer
		4	-2.748	-23.862	Pi-pi stacking of H175 to Ph, Pi-cation of K107 to Ph	92.6	3.82	Possible transfer
		5	-2.292	-23.44	Ph above N5	124.4	4.48	no hydride transfer

56a	n.c.	1	-4.193	-22.702	H-bond of H175 to C=O (1.91 Å), Pi-pi stacking of H175 to Ph	44.7	6.10	no hydride transfer
		2	-3.718	-21.986	Ph above N5	144.2	7.00	no hydride transfer
		3	-3.651	-27.386	H-bond of H175 to C=O (2.04 Å)	27.7	6.97	no hydride transfer
		4	-3.53	-23.238	H-bond of H175 to C=O (2.36 Å), bad contacts of Y177, A102, G65, D71 and D25 to Ph	60.5	4.61	no hydride transfer
		5	-2.979	-28.905	Ph above N5	130.5	4.69	no hydride transfer
57a	n.c.	1	-0.771	-26.754	H-bond of R347 to C=O (2.35 Å), bad contacts of Y177 and A58	115.1	3.93	Possible transfer
		2	-0.763	-20.986	Bad contact of H175 to C4	80.8	4.21	no hydride transfer
		3	-0.705	-29.509	Bad contact of H175 to C4 and C8	80.5	4.23	no hydride transfer
		4	-0.703	-30.938	No hydride transfer	135.1	4.64	no hydride transfer
		5	-0.603	-22.028	Bad contacts of Y177, A102, G65, A58 and D25	77.5	4.04	no hydride transfer
11a	n.c.	1	-5.232	-23.948	Bad contact of R347 to C2, H175 to C6 and D25 to C8	81.2	4.85	no hydride transfer
		2	-4.819	-25.938	H-bond of R347 to C=O (2.10 Å), of D25 to OH (1.67 Å), Pi-cation of K107 to both rings	108.8	5.73	no hydride transfer
		3	-4.319	-31.616	H-bond of D25 to OH (1.88 Å), Pi-cation of K107 to both rings, Pi-pi stacking of H175 to lactone	116.1	5.69	no hydride transfer
		4	-4.289	-33.514	Pi-pi stacking of H175 to lactone, bad contact of R347 to CH3	123.1	4.66	no hydride transfer
13a		1	-4.659	-31.229	Ph above N5	128.6	5.99	no hydride transfer
		2	-4.51	-29.955	H-bond of R347 to C=O (2.29, 2.42 Å) and to C=OOEt (2.39 Å), H-bond of D25 to OH (1.56 Å), Pi-pi stacking of H175 and Y177	105.4	5.46	no hydride transfer
		3	-4.289	-30.035	H-bond of R347 to C=OOEt (2.18 Å), of D25 to OH (1.89 Å), Pi-pi stacking of Y177 to Ph	99.4	5.07	no hydride transfer
12a		1	-5.418	-29.303	H-bond of D25 to OH (1.85 Å), Pi-pi stacking of H175 to lactone	53.8	3.79	no hydride transfer
		2	-5.25	-29.797	H-bond of R347 to C=O (2.12, 2.62 Å), to C=OAc (2.12 Å), of D25 to OH (1.57 Å), Pi-pi stacking of Y177 to Ph, bad contact of H175 to C5	108.1	5.35	no hydride transfer
		3	-5.16	-27.797	H-bond of R347 to C=OAc (1.82 Å), of D25 to OH (1.63 Å), Pi.cation of K107, Pi-pi stacking of H175 to lactone	117.1	5.93	no hydride transfer
		4	-5.152	-27.354	H-bond of R347 to C=O (2.04 Å), to C=OAc (1.75 Å), of D25 to OH (1.67 Å), Pi-cation of K107, bad contact of H175 to C5	110.7	5.83	no hydride transfer
14a		1	-5.225	-20.075	vertical	96.6	10.30	no hydride transfer
		2	-5.16	-25.338	Vertical to dobi above	101.1	5.94	no hydride transfer
		3	-4.861	-22.316	Vertical to dobi above	109.3	5.69	no hydride transfer
		4	-4.86	-24.014	Vertical to O above N5	49.6	6.45	no hydride transfer
		5	-4.089	-21.044	H-bond of H175 to C=O (1.80 Å), Pi-cation of K107 to both Ph, bad contact of Y27 to CH ₃	60.3	4.17	no hydride transfer

16a	1	-5.389	-24.053	Vertical to FMN to double bond above N5	122.9	5.67	no hydride transfer
	2	-5.105	-22.348	Vertical to FMN to double bond above N5	135.7	6.45	no hydride transfer
	3	-4.965	-23.2	Vertical to FMN to second Ph above N5	83.5	10.32	no hydride transfer
	4	-4.872	-21.339	Pi-cation of H175 to lactone, bad contact of K107 to C=O	103.4	5.57	no hydride transfer
	5	-4.599	-28.278	H-bond of H175 to C=O (1.83 Å), Pi-cation of K107 to all rings	56.4	4.44	no hydride transfer
15a	1	-5.149	-22.601	H-bond of H175 to C=O (2.27 Å), of D25 to OH (1.59 Å), Pi-cation of K107 to all rings, Pi-pi stacking of H175 to lactone	133.5 (C α)	4.32	no hydride transfer
	2	-5.115	-22.264	H-bond of H175 to C=O (2.15 Å), of D25 to OH (1.59 Å), Pi-cation of K107 to all rings, of R347 to second Ph	124.4 (C α)	4.35	no hydride transfer
	3	-4.57	-24.408	H-bond of H175 to C=O (2.00 Å), Pi-cation of K107 to lactone and middle ring, of R347 to middle ring	85.2 (C α)	4.74	no hydride transfer
	4	-4.455	-23.325	H-bond of D25 to OH (1.84 Å), Pi-cation of K107 to all rings, of R347 to both Ph rings	116.3 (C α)	4.57	no hydride transfer
	5	-4.168	-26.04	H-bond of D25 to OH (1.86 Å), Pi-cation of K107 to lactone and middle ring, of R347 to both Ph rings	105.0 (C α)	4.78	no hydride transfer

Table 30. Results from Induced Fit Docking of substrate **17a** in the reduced *TsER* wt structure based on 3HGJ crystal structure. Empirical result is 1% conversion and 76S ee%

Pose	IFD Score	Glide GScore	Prime Energy	Glide Energy	Notes	result
1	-1437.049	-6.035	-28620.3	-23.516	C=O H-bond to Arg347, distance 2.14 Å and 2.39 Å and H-bond to Tyr27 (2.03Å); result in R-1b (63°, 3.24Å)	Might result in R-17b
2	-1437.008	-5.931	-28621.5	-24.221	C=O H-bond to Arg347, distance 2.16 Å and 2.58 Å and H-bond to Tyr27 (2.08Å); result in R-1b (65°, 3.37Å)	Might result in R-17b
3	-1437.007	-5.935	-28621.4	-23.975	C=O H-bond to Arg347, distance 2.12 Å and 2.57 Å and H-bond to Tyr27 (2.12Å); result in R-1b (65°, 3.35 Å)	Might result in R-17b
4	-1436.827	-5.732	-28621.9	-24.355	"flipped" pose, distance to H172 3.51 Å and H-bond to H175 (1.81 Å); result in S-1b (95°, 3.21 Å)	Would result in S-17b
5	-1436.797	-5.725	-28621.4	-22.772	C=O H-bond to Arg347, distance 2.11 Å and H-bond to Tyr27 distance 2.13Å; result in R-1b (63°, 3.63 Å)	Might result in R-17b
6	-1436.794	-5.72	-28621.5	-24.913	"flipped" pose, distance to H172 2.81 Å and H-bond to H175 (1.80 Å); result in S-1b (94°, 3.18 Å)	Would result in S-17b
7	-1436.792	-5.708	-28621.7	-25.156	"normal" pose, distance to H172 2.79 Å and H-bond to H175 (1.98 Å); result in R-1b (92°, 3.65Å)	Would result in R-17b
8	-1436.757	-5.641	-28622.3	-22.865	"normal" pose, H-bond to H172 1.93 Å	No hydride transfer
9	-1436.664	-5.562	-28622	-21.859	"flipped" pose, no H-bond, distance to H172 3.39 Å and to H175 4.92 Å; result in S-1b (100°, 3.29 Å)	Would result in S-17b
10	-1436.616	-5.505	-28622.2	-21.735	C=O H-bond to Arg347, distance 1.88 Å and H-bond to Tyr27 (2.21Å)	No hydride transfer
11	-1436.562	-5.69	-28617.4	-21.417	Flipped pose, C=O H-bond to Arg347, distance 2.16 Å and 2.22 Å and H-bond to Tyr27 (2.21Å)	No hydride transfer
12	-1436.49	-5.423	-28621.3	-22.414	"normal" pose, H-bond to H172 1.83 Å	No hydride transfer
13	-1436.418	-5.595	-28616.5	-23.885	H-bond to H175 (1.94 Å); result in S-1b (93°, 3.64 Å)	Would result in S-17b
14	-1436.328	-5.397	-28618.6	-20.143	"flipped" pose, no H-bond, distance to H172 3.31 Å and to H175 2.57 Å; result in S-1b (97°, 3.83Å)	Would result in S-17b
15	-1436.306	-5.397	-28618.2	-19.998	"flipped" pose, no H-bond, distance to H172 3.44 Å and to H175 4.85 Å; result in S-1b (91°, 3.83 Å)	Would result in S-17b
16	-1436.08	-5.349	-28614.6	-20.259	"flipped" pose, no H-bond, distance to H172 3.34 Å and bad-contact to H175 2.36 Å; result in S-1b (90°, 3.78 Å)	Would result in S-17b
17	-1436.008	-5.202	-28616.1	-23.143	H-bond to H175 (1.84 Å)	No hydride transfer
18	-1435.971	-5.298	-28613.4	-20.699	"normal" pose, H-bond to H172 2.15 Å	No hydride transfer
19	-1435.864	-5.187	-28613.5	-20.373	"normal" pose, no H-bond	No hydride transfer

Table 31. Results from Induced Fit Docking of Substrate **17a** in the reduced *TsER* C25G/I67T variant, created with PyMOL Mutagenesis Wizard on crystal structure 3HGJ. Empirical result is 49% conversion and 74S ee%.

Pose	IFD Score	Glide GScore	Prime Energy	Glide Energy	Notes	result
1	-1434.805	-5.657	-28583	-22.318	"flipped" pose, H-bond to H172 (1.79 Å); result in S-1b (102°, 3.29 Å)	Would result in S-17b
2	-1434.727	-5.654	-28581.5	-22.325	"flipped" pose, H-bond to H172 (1.79 Å); result in S-1b (102°, 3.28 Å)	Would result in S-17b
3	-1434.486	-5.655	-28576.6	-22.298	"flipped" pose, H-bond to H172 (1.80 Å); result in S-1b (102°, 3.29 Å)	Would result in S-17b
4	-1434.468	-5.592	-28577.5	-22.803	"flipped" pose, H-bond to H172 (1.83 Å); result in S-1b (97°, 3.37 Å)	Would result in S-17b
5	-1434.426	-5.626	-28576	-22.779	"flipped" pose, H-bond to H172 (1.82 Å); result in S-1b (97°, 3.36 Å)	Would result in S-17b
6	-1434.223	-5.591	-28572.7	-22.788	"flipped" pose, H-bond to H172 (1.83 Å); result in S-1b (97°, 3.37 Å)	Would result in S-17b
7	-1434.129	-5.653	-28569.5	-22.318	"flipped" pose, H-bond to H172 (1.79 Å); result in S-1b (102°, 3.28 Å)	Would result in S-17b
8	-1434.12	-5.617	-28570.1	-22.706	"flipped" pose, H-bond to H172 (1.82 Å), bad contact to Thr67; result in S-1b (96°, 3.37 Å)	Would result in S-17b
9	-1434.088	-5.594	-28569.9	-22.795	"flipped" pose, H-bond to H172 (1.83 Å); result in S-1b (97°, 3.37 Å)	Would result in S-17b
10	-1434.034	-5.652	-28567.6	-22.355	"flipped" pose, H-bond to H172 (1.79 Å); result in S-1b (103°, 3.26 Å)	Would result in S-17b

11	-1434.013	-5.661	-28567	-22.333	"flipped" pose, H-bond to H172 (1.79 Å); result in S-1b (102°, 3.28 Å)	Would result in S-17b
12	-1433.946	-5.604	-28566.8	-22.834	"flipped" pose, H-bond to H172 (1.82 Å); result in S-1b (97°, 3.37 Å)	Would result in S-17b
13	-1433.744	-5.591	-28563.1	-22.822	"flipped" pose, H-bond to H172 (1.83 Å); result in S-1b (97°, 3.38 Å)	Would result in S-17b
14	-1433.583	-5.604	-28559.6	-22.826	"flipped" pose, H-bond to H172 (1.83 Å); result in S-1b (97°, 3.37 Å)	Would result in S-17b
15	-1433.322	-5.643	-28553.6	-22.328	"flipped" pose, H-bond to H172 (1.79 Å); result in S-1b (103°, 3.26 Å)	Would result in S-17b
16	-1433.322	-5.592	-28554.6	-22.776	"flipped" pose, H-bond to H172 (1.83 Å); result in S-1b (97°, 3.35 Å)	Would result in S-17b

Table 32. Results from Induced Fit Docking of Substrate **17a** in the *TsER* C25D/I67T variant, created with PyMOL Mutagenesis Wizard on crystal structure 3HGJ. Empirical result is 95% conversion and 93R ee%.

Pose	IFD Score	Glide GScore	Prime Energy	Glide Energy	Notes	result
1	-1437.076	-4.878	-28644	-22.663	"normal" pose, no H-bond, distance to H175 2.58 Å and to H172 2.96 Å, bad contact to Tyr177 (92°, 4.45 Å)	Might result in R-17b
2	-1436.741	-4.892	-28637	-22.662	"normal" pose, no H-bond, distance to H175 4.72 Å and to H172 2.55 Å (103.2°, 4.29 Å)	Might result in R-17b
3	-1436.639	-4.882	-28635.1	-22.658	No H-bond, distance to H175 3.27 Å and to H172 3.81 Å (111.3°, 3.95 Å)	Would result in R-17b
4	-1436.593	-4.877	-28634.3	-22.664	"normal" pose, H-bond of H175 (1.88 Å) and of H172 (2.00 Å) (93.8°, 3.98 Å)	Would result in R-17b
5	-1436.576	-4.747	-28636.6	-22.903	"normal" pose, H-bond of H175 (1.77 Å), distance to H172 (2.67 Å) (93.9°, 4.24 Å)	Might result in R-17b
6	-1436.56	-4.89	-28633.4	-22.651	"flipped" pose, H-bond of H175 (2.17 Å) and of H172 (1.86 Å) (90.5°, 3.68 Å)	Would result in S-17b
7	-1436.476	-4.899	-28631.6	-22.675	Vertical to FMN, no productive pose for hydride transfer (149.1°, 4.99 Å)	No hydride transfer
8	-1436.462	-5.09	-28627.4	-22.645	H-bond of K107 (2.52 Å), non productive pose for hydride transfer (125.9°, 4.14 Å)	No hydride transfer
9	-1436.435	-4.845	-28631.8	-22.776	H-bond of H175 (1.96 Å) (122.1°, 3.43 Å)	Would result in S-17b
10	-1436.419	-4.877	-28630.8	-22.587	"flipped" pose, H-bond of H172 (1.87 Å) (87.7°, 3.60 Å)	Would result in S-17b
11	-1436.253	-4.888	-28627.3	-22.667	H-bond of H175 (1.68 Å) (89.0°, 3.88 Å)	Would result in S-17b
12	-1436.213	-4.845	-28627.4	-22.785	"new flipped" pose, H-bond of R347 (1.96 Å, 2.52 Å) (62.1°, 3.74 Å)	Would result in R-17b
13	-1436.187	-4.898	-28625.8	-22.675	"new flipped" pose, H-bond of R347 (2.06 Å, 2.12 Å) (70.3°, 3.72 Å)	Would result in R-17b
14	-1436.069	-4.541	-28630.6	-23.688	"normal" pose, H-bond of H175 (1.89 Å) (96.4°, 3.68 Å)	Would result in R-17b
15	-1435.988	-4.442	-28630.9	-23.68	"normal" pose, H-bond of H172 (2.42 Å) (73.3°, 6.00 Å)	No hydride transfer
16	-1435.97	-4.892	-28621.6	-22.618	No productive pose (105.1°, 5.99 Å)	No hydride transfer
17	-1435.903	-4.889	-28620.3	-22.661	No productive pose (53.3°, 8.00 Å)	No hydride transfer
18	-1435.882	-4.774	-28622.2	-22.72	"new flipped" pose H-bond of R347 (1.85 Å) of Y27 (1.85 Å) (64.6°, 3.58 Å)	No hydride transfer
19	-1435.786	-4.881	-28618.1	-22.663	No productive pose (109.6°, 7.06 Å)	No hydride transfer

Table 33. Results from IFD of substrate **13a** in the *Ts*ER C25D/I67T structure with FMNH₂ and protonated H172/H175 based on crystal structure 5NUX.

Pose	IFD Score	Glide GScore	Prime Energy	Glide Energy	Notes	Hydride transfer angle	Distance to N5	Protonation aa for C=O	result
1	-1453.442	-8.274	-28903.4	-47.488	Lactone O in direction of H172, H-bond of OH to D25 (1.55 Å), of H172 to C=O (1.94 Å), of a water molecule to C=OOEt, Pi-pi stacking and Pi-cation of H175 with lactone	114.3	4.26	H175 distance 3.86 Å, angle 85.2°	C=O can be protonated and C=C reduced
2	-1452.885	-7.733	-28903.0	-47.491	Lactone O in direction of H172, H-bond of OH to D25 (1.88 Å), of T67 to OH (1.93 Å), of H172 to C=O (2.76 Å), of R347 to C=OOEt (1.82 Å)	109.0	3.75	H175 distance 3.55 Å, angle 78.3°	C=O might be protonated and C=C reduced
3	-1452.378	-7.374	-28900.1	-45.811	Lactone O in direction of H172, H-bond of OH to D25 (1.81 Å), of T67 to OH (1.80 Å), of H172 to C=O (2.41 Å), of R347 to C=OOEt (2.29 Å)	111.0	3.99	H175 distance 3.65 Å, angle 79.6°	C=O might be protonated and C=C reduced
4	-1452.127	-6.858	-28905.4	-46.983	Lactone O in direction of H175, H-bond of OH to a water molecule, of R347 to OH (1.96 Å), of H172 to C=O (2.46 Å) and to C=OOEt (2.00 Å), Pi-pi stacking and Pi-cation of H175 to lactone	133.6	4.58	H175 distance 3.56, angle 83.3°	C=O can be protonated
5	-1452.121	-7.397	-28894.5	-44.276	Lactone O in direction of Y27, H-bond of OH to D25 (1.73 Å), of Y27 to lactone O (2.24 Å), of R347 to C=O (2.07 Å) and to C=OOEt (1.66, 2.78 Å)	89.9	3.93	R347 distance 2.07 Å. Angle 156.5°	C=C reduction
6	-1452.112	-7.543	-28891.4	-46.872	Lactone O in direction of H175, H-bond of R347 to OH (1.91 Å), of OH to water	89.9	3.77	H172 distance 3.31 Å, angle 109.7°	C=O can be protonated and C=C reduced
7	-1452.064	-7.008	-28901.1	-42.447	Lactone O in direction of H172, H-bond of OH to D25 (1.97 Å), of water to C=OOEt, Pi-pi stacking of H175 to lactone and phenol, Pi-cation of H175 to lactone, bad contacts of Y177 to OH	114.0	5.27	-	no productive pose
8	-1452.053	-7.166	-28897.7	-44.026	Lactone O in direction of H175, H-bond of R347 to OH (2.09 Å), of water to OH	97.5	3.57	H172 distance 2.41 Å, angle 109.3°	C=O can be protonated and C=C reduced
9	-1451.884	-7.205	-28893.6	-43.771	Lactone O in direction of Y27, H-bond of R347 to C=O (1.96 Å, 2.31 Å) and to OEt (2.29 Å), of OH to D25 (1.71 Å), bad contacts of T67 to OH	86.9	4.39	R347 distance 2.31 Å, angle 140.4°	C=C reduction
10	-1451.863	-7.181	-28897.1	-46.276	Lactone O in direction of H172, H-bond of H175 to C=OOEt (1.90 Å), of OH to D71 (1.87 Å), bad contacts of T67 to OH	106.7	3.18	H175 distance 2.52 Å, angle 106.5°	C=O can be protonated and C=C reduced
11	-1451.372	-6.515	-28897.1	-42.108	Lactone O in direction of H175, H-bond of H172 to C=OOEt (1.87 Å), of OH to water and of R347 to OH (2.09 Å), bad contacts of R347 to phenol	76.9	4.29	-	no productive pose
12	-1451.041	-6.773	-28885.4	-41.445	Lactone O in direction of Y27, H-bond of R347 to C=O (1.98 Å) and to OEt (1.70 Å), of OH to D25 (1.67 Å)	91.7	4.16	R347 distance 1.98, angle 159.1°	C=C reduction
13	-1450.932	-5.802	-28902.6	-39.234	Lactone O in direction of H172, H-bond of R347 to OEt (2.48 Å), of OH to D25 (1.60 Å), Pi-pi stacking of H175 with lactone	113.5	4.53	H175 distance 3.82, angle 69.5°	C=O might be protonated and C=C reduced
14	-1450.864	-6.401	-28889.3	-44.371	Lactone O in direction of H175, no H-bonds, bad contact of OH with R347	132.4	4.52	H172 distance 2.35, angle 120.0°	C=O can be protonated
15	-1450.848	-6.053	-28895.9	-38.425	Lactone O in direction of H172, H-bond of H172 to C=O (2.20 Å), of OH to D25 (1.67 Å), bad contacts of Y177 to phenol	115.3	4.07	H172 distance 2.20 Å, angle 151.8°	C=O might be protonated and C=C reduced
16	-1450.251	-5.817	-28888.7	-41.277	Lactone O in direction of H175, H-bond of H175 to C=O (2.04 Å), of R347 to C=OOEt (2.00 Å, 2.24 Å), Pi-pi stacking of H172 to phenol	111.3	3.17	H175 distance 2.04 Å, angle 151.0°	C=O might be protonated and C=C reduced
17	-1449.717	-5.183	-28890.7	-43.046	Lactone O in direction of H175, H-bond of H175 to C=O (2.08 Å), of R347 to C=OOEt (2.19 Å, 2.36 Å), Pi-pi stacking of H172 to phenol	103.6	3.14	H175 distance 2.08 Å, angle 149.3°	C=O might be protonated and C=C reduced
18	-1449.144	-4.968	-28883.5	-39.596	Lactone O in direction of H175, H-bond of H175 to C=O (1.99 Å)	109.8	3.37	H175 distance 1.99, angle 148.6°	C=O might be protonated and C=C reduced

Table 34. Results from IFD of substrate **13a** in the *Ts*ER C25D/I67T/A102H structure with FMNH₂ and protonated H172/H175 based on crystal structure 5OGT.

Pose	IFD Score	Glide GScore	Prime Energy	Glide Energy	Notes	Hydride transfer angle	Distance to N5	Protonation aa for C=O	result
1	-1443.536	-7.885	-28713.0	-46.893	Lactone O in direction of H172, H-bond of OH to D25 (1.54 Å), of T67 to OH (2.01 Å), Pi-cation of H175 with lactone	112.7	3.90	H175 distance 3.73 Å, angle 81.0°, H172 distance 2.83 Å, angle 111.1°	C=O can be protonated and C=C reduced
2	-1443.488	-8.007	-28709.6	-46.000	Lactone O in direction of Y27, H-bond of OH to D25 (1.96 Å), of T67 to OH (1.79 Å), of H172 to C=OOEt (1.99 Å), of R347 to C=O (2.08 Å, 2.12 Å) and to OEt (2.45 Å), of Y27 to lactone O (2.12 Å), Pi-pi stacking of H102 to phenol ring	82.7	3.94	R347 distance 2.12 Å, angle 145.2°	C=C reduction
3	-1443.321	-7.637	-28713.7	-44.211	Lactone O in direction of Y27, H-bond of OH to D25 (1.55 Å), of T67 to OH (1.94 Å), of R347 to C=O (1.96 Å)	91.9	4.11	R347 distance 1.96 Å, angle 150.8°	C=C reduced
4	-1443.319	-7.805	-28710.3	-44.953	Lactone O in direction of H172, H-bond of OH to D71 (1.86 Å), of T67 to OH (2.16 Å), of R347 to C=OOEt (1.99 Å)	102.4	3.19	H172 distance 3.99 Å, angle 103.5°	C=O can be protonated and C=C reduced
5	-1443.201	-7.617	-28711.7	-44.019	Lactone O in direction of Y27, H-bond of OH to D25 (1.96 Å), of T67 to OH (1.85 Å), of Y27 to lactone O (2.18 Å), of R347 to C=O (1.95 Å, 2.18 Å) and to C=OOEt (2.21 Å)	80.4	3.81	R347 distance 1.95 Å, angle 149.6°	C=C reduction
6	-1443.159	-7.718	-28.708.8	-46.941	Lactone O in direction of Y27, H-bond of OH to D25 (1.80 Å), of Y27 to lactone O (2.25 Å), of R347 to C=O (2.11 Å, 2.17 Å) and to OEt (2.55 Å), of H175 to C=OOEt (2.06 Å)	80.6	3.84	R347 distance 2.17 Å, angle 146.0°	C=C reduction
7	-1443.125	-7.145	-28719.6	-45.761	Lactone O in direction of H172, H-bond of OH to D25 (1.83 Å), of T67 to OH (2.00 Å), of H172 to C=O (2.56 Å), Pi-pi stacking and Pi-cation of H175 to lactone	115.0	4.04	H175 distance 3.73 Å, angle 73.5°	C=C reduction
8	-1443.015	-7.677	-28706.8	-44.026	Lactone O in direction of Y27, H-bond of OH to D71 (2.06 Å), of H102 to OH (2.47 Å), of Y27 to C=O (1.89 Å), of R347 to C=O (1.91 Å) and to C=OOEt (1.80 Å)	75.1	3.63	R347 distance 1.91 Å, angle 178.0°, Y27 distance 1.89 Å, angle 177.7°	unproductive
9	-1443.003	-7.483	-28710.4	-44.431	Lactone O in direction of H172, H-bond of OH to D25 (1.67 Å), of T67 to OH (2.00 Å)	112.1	3.96	-	C=C reduction
10	-1442.942	-7.557	-28707.7	-45.205	Lactone O in direction of H172, H-bond of OH to D71 (1.81 Å), of H102 to OH (2.09 Å), of R347 to C=OOEt (2.05 Å)	99.1	3.11	H175 distance 3.22 Å, angle 81.2	C=O can be protonated and C=C reduced
11	-1442.859	-7.248	-28712.2	-46.044	Lactone O in direction of H172, H-bond of OH to D71 (1.84 Å), of H102 to OH (2.37 Å), of H175 to C=OOEt (1.99 Å)	105.3	3.34	H175 distance 2.71 Å, angle 103.7°	C=O can be protonated and C=C reduced
12	-1442.807	-6.917	-28717.8	-44.324	Lactone O in direction of Y27, H-bond of R347 to C=O (2.33 Å), of OH to D25 (1.55 Å)	86.2	4.19	R347 distance 2.33, angle 147.8°	C=C reduction
13	-1442.788	-7.194	-28711.9	-45.389	Lactone O in direction of H172, H-bond of H172 to C=O (2.33 Å), of OH to D25 (1.57 Å)	113.2	4.12	H172 distance 2.33, angle 160.2°	C=C reduction
14	-1442.590	-6.977	-28712.3	-43.571	Lactone O in direction of H172, H-bond of H172 to C=O (2.17 Å), of OH to D25 (1.53 Å)	113.1	4.03	H172 distance 2.17, angle 160.7°	C=C reduction
15	-1442.392	-6.810	-28711.6	-42.481	Lactone O in direction of H172, H-bond of H172 to C=O (2.09 Å), of OH to D25 (1.63 Å)	115.6	3.95	H172 distance 2.09, angle 156.8°	C=C reduction
16	-1442.107	-6.899	-28704.2	-40.777	Lactone O in direction of Y27, H-bond of OH to D25 (2.01 Å), of Y27 to lactone O (2.11 Å), of R347 to C=O (1.87 Å, 2.15 Å) and to C=OOEt (2.14 Å)	82.0	3.82	R347 distance 1.87 Å, angle 149.6°	C=C reduction
17	-1441.877	-6.627	-28705.0	-42.485	Lactone O in direction of R347, H-bond of Y27 to OH (2.44 Å), of OH to D25 (1.67 Å). Pi-pi stacking and Pi-cation of H175 to lactone	103.4	4.47	H175 distance 3.51 Å, angle 78.1°	C=O might be protonated and C=C reduced

Table 35. Results from IFD of substrate **13d** in the *Ts*ER C25D/I67T structure with FMNH₂ and protonated H172/H175 based on crystal structure 5NUX.

Pose	IFD Score	Glide GScore	Prime Energy	Glide Energy	Notes	Hydride transfer angle	Distance to N5	result
1	-1450.811	-6.611	-28884.0	-48.809	H bond of R347 to C=OOH (1.67 Å, 1.95 Å), of Y27 to C=OOH (1.61 Å), of H175 to OH (1.99 Å), of Y177 to C=OOEt (1.75 Å), Pi-pi stacking of H172 and Y177 to phenol	117.5	3.13	C=C reduction
2	-1450.183	-6.419	-28875.3	-43.835	H bond of R347 to C=OOH (1.68 Å), of H172 to OH (2.73 Å), of Y177 to C=OOEt (1.82 Å), of OH to D25 (1.77 Å), bad contacts of T67 to OH, K107 to Et	179.0	4.41	not productive
3	-1449.915	-6.064	-28877.0	-41.118	H-bond of H175 to C=OOEt (2.40 Å) of Y177 to C=OOEt (1.74 Å), of R347 to C=OOH (1.59 Å, 1.63 Å), Pi-pi stacking of Y177 to phenol	153.6	3.70	might reduce C=C
4	-1449.829	-3.314	-28870.3	-39.621	H-bond of Y177 to C=OOEt (1.76 Å), of R347 to C=OOH (1.59 Å), of OH to D25 (2.30 Å), bad contacts of K107 to Et, Y27 to OH	166.9	4.87	not productive
5	-1449.822	-5.510	-28886.2	-40.668	H-bond of H175 to C=OOEt (2.14 Å), of Y177 to C=OOEt (1.94 Å), of OH to D25 (1.60 Å) of R347 to C=OOH (1.70 Å, 1.65 Å)	123.0	4.56	C=C reduction
6	-1449.715	-6.092	-28872.5	-39.716	H-bond of H175 to OH (2.79 Å), of Y177 to C=OOEt (1.60 Å), of R347 to C=OOH (1.87 Å, 2.21 Å), of Y27 to C=OOH (2.05 Å), Pi-pi stacking of Y177 to phenol	136.7	3.45	might reduce C=C
7	-1449.685	-6.243	-28868.8	-43.666	H-bond of H175 to OH (1.74 Å), of Y177 to C=OOEt (1.72 Å), of R347 to C=OOH (1.61 Å, 1.62 Å), Pi-pi stacking of Y177 to phenol	151.5	3.70	might reduce C=C
8	-1449.564	-5.673	-28877.8	-40.401	H-bond of Y177 to C=OOEt (1.71 Å), of R347 to C=OOH (2.18 Å), of T67 to OH (2.40 Å), of =H to D25 (2.14 Å)	164.7	4.25	not productive
9	-1449.513	-5.198	-28886.3	-42.290	H-bond of Y177 to C=OOEt (1.81 Å), of OH to D25 (2.50 Å), of R347 to C=OOH (1.61 Å, 2.50 Å), Pi-cation of K107 to phenol	155.6	5.26	not productive
10	-1449.383	-5.863	-28870.4	-38.381	H-bond of Y177 to C=OOEt (1.61 Å), of OH to D25 (2.68 Å), of R347 to C=OOH (1.57 Å), of OH to Y27 (1.83 Å), bad contacts of K107 to Et, of H175 to OEt	178.3	4.72	not productive
11	-1449.356	-5.461	-28877.9	-43.440	H-bond of Y177 to C=OOEt (1.81 Å), of OH to D25 (2.53 Å), of R347 to C=OOH (1.70 Å, 1.77 Å), of H172 to OH (2.15 Å), Pi-cation of K107 to phenol, bad contacts of K107 to Et, of H175 to OEt	176.5	5.10	not productive
12	-1449.173	-5.353	-28876.4	-42.070	H-bond of Y177 to C=OOEt (2.05 Å), of K107 to C=OOEt (2.67 Å), of R347 to C=OOH (1.57 Å, 1.72 Å), of H172 to OH (2.32 Å), Pi-cation of K107 to phenol, bad contacts of K107 to Et	174.6	5.11	not productive
13	-1449.054	-5.084	-28879.4	-34.609	H-bond of Y177 to C=OOEt (1.84 Å), of OH to D25 (2.42 Å), of T67 to OH (2.15 Å), of R347 to C=OOH (1.83 Å), bad contacts of H175 to C=OOEt	159.6	4.25	might reduce C=C
14	-1448.938	-5.417	-28870.4	-38.868	H-bond of Y177 to C=OOEt (2.02 Å), of R347 to C=OOH (1.56 Å, 1.62 Å), bad contacts of H175 to C=OOEt	162.6	4.39	not productive
15	-1448.892	-5.133	-28875.2	-39.824	H-bond of Y177 to C=OOEt (1.63 Å), of R347 to C=OOH (1.74 Å, 1.86 Å), of Y27 to C=OOH (2.72 Å), Pi-pi stacking of Y177 to phenol	144.9	3.81	might reduce C=C
16	-1448.839	-5.048	-28875.8	-42.377	H-bond of Y177 to C=OOEt (1.99 Å), of K107 to C=OOEt (2.64 Å), of R347 to C=OOH (1.60 Å, 2.57 Å), of H172 to OH (2.73 Å), of OH to D25 (1.99 Å), Pi-cation of K107 to phenol	162.8	5.79	not productive
17	-1448.768	-5.168	-28872.0	-41.547	H-bond of H175 to C=OOEt (1.91 Å), of R347 to C=OOH (1.65 Å), of OH to D25 (2.19 Å)	146.8	5.28	not productive

Table 36. Results from IFD of substrate **13d** in the *Ts*ER C25D/I67T/A102H structure with FMNH₂ and protonated H172/H175 based on crystal structure 5OGT.

Pose	IFD Score	Glide GScore	Prime Energy	Glide Energy	Notes	Hydride transfer angle	Distance to N5	result
1	-1444.561	-8.063	-28730.0	-41.576	H-bond of H172 to C=OOH (1.74 Å), of Y177 to C=OOEt (2.01 Å), of R347 to OH (2.06 Å), of R? to C=OOH (1.96 Å), salt bridge of H175 to C=OOH	74.3	6.15	not productive
2	-1443.409	-7.439	-28719.4	-49.378	H-bond of Y177 to C=OOEt (2.02 Å), of H102 to C=O (2.06 Å), of Q? to C=O (3.10 Å), of R347 to C=OOH (1.56 Å, 1.74 Å, 1.85 Å), Pi-pi stacking of H172 to phenol	128.0	3.47	might be reduced
3	-1442.589	-6.736	-28717.1	-41.080	H-bond of Y177 and H175 to C=OOEt (2.15 Å and 1.89 Å), of OH to D25 (2.76 Å), of R347 to C=OOH (2.33 Å), Pi-pi stacking of Y177 and H102 to phenol	135.5	3.53	not productive
4	-1442.347	-6.078	-28725.4	-39.678	H-bond of Y177 to C=OOEt (1.70 Å), of T67 to OH (2.35 Å), of OH to D25 (2.04 Å), of OH to Y27 (1.93 Å), bad contact of H175 to OEt	172.4	4.40	not productive
5	-1442.085	-6.141	-28718.9	-38.131	H-bond of H175 to C=OOH (1.53 Å), of K107 to C=OOH (1.93 Å), of Y177 to C=OOH (1.85 Å), of OH to D25 (1.89 Å), of Y27 to OH (1.97 Å), of R347 to OH (2.27 Å)	154.4	6.57	not productive
6	-1442.052	-6.027	-28720.5	-37.673	H-bond of H175 to C=OOH (1.67 Å), of K107 to C=OOH (1.91 Å), of OH to D25 (2.06 Å), of R347 to OH (2.13 Å), bad contacts of Y177 to phenol, of Y27 to OH	112.7	6.97	not productive
7	-1441.950	-5.844	-28722.1	-41.251	H-bond of H175 to OH (1.92 Å), of R347 to C=OOH (2.03 Å), of Y177 to C=OOEt (1.69 Å), Pi-pi stacking of H172 to phenol, bad contact of R347 to C=OOH	136.3	3.62	not productive
8	-1441.850	-5.523	-28726.5	-35.532	H-bond of H175 to C=OOH (1.75 Å), of K107 to C=OOH (1.96 Å), of R347 to OH (2.78 Å), of Y27 to OH (1.72 Å), of OH to D25 (1.60 Å)	110.8	7.09	not productive
9	-1441.773	-5.838	-28718.7	-35.099	H-bond of H175 to C=OOH (1.57 Å), of K107 to C=OOH (2.06 Å), of R347 to OH (2.45 Å), of Y27 (1.91 Å), of OH to D25 (1.65 Å)	110.6	6.74	not productive
10	-1441.765	-5.824	-28718.8	-32.978	H-bond of R? to C=OOH (1.93 Å), of H172 to C=OOH (2.01 Å), salt bridges of H172 and H175 to C=OOH, bad contact of Y177 to Et	37.6	7.33	not productive
11	-1441.754	-5.752	-28720.0	-37.797	H-bond of H175 to C=OOH (1.60 Å), of OH to D25 (1.53 Å), of R347 to C=OOEt (2.16 Å), Pi-pi stacking of Y177 to phenol	105.9	6.05	not productive
12	-1441.735	-6.201	-28710.7	-41.601	H-bond of Y27 to C=OOH (1.91 Å), of R347 to C=OOH (1.54 Å, 2.51 Å)	30.3	5.21	not productive
13	-1441.674	-5.671	-28720.1	-38.268	H-bond of H175 to C=OOH (1.63 Å), of K107 to C=OOH (1.83 Å), of OH to D25 (1.86 Å), of R347 to OH (2.19 Å)	114.1	6.17	not productive
14	-1441.635	-5.602	-28720.7	-38.272	H-bond of H175 to C=OOH (1.66 Å), of K107 to C=OOH (1.87 Å), of OH to D25 (1.94 Å), of R347 to OH (2.78 Å) and (2.13 Å)	114.6	6.21	not productive
15	-1441.479	-5.385	-28721.9	-37.129	H-bond of H175 to C=OOH (1.92 Å), of K107 to C=OOH (2.38 Å), of OH to D25 (1.63 Å), of Y27 to OH (1.87 Å), of R347 to OH (2.52 Å)	116.8	6.64	not productive
16	-1441.419	-6.147	-28705.5	-41.664	H-bond of R? to C=OOH (2.80 Å), of H172 to C=OOEt (1.99 Å), of T67 to OH (2.35 Å), of OH to D25 (1.54 Å), salt bridge of H175 to C=OOH	130.8	4.68	not productive
17	-1441.207	-5.460	-28714.9	-35.596	H-bond of H175 to C=OOH (1.57 Å), of K107 to C=OOH (1.76 Å), of OH to D25 (1.96 Å), of R347 to OH (2.15 Å), bad contact of Y27 to OH	115.4	6.20	not productive
18	-1440.020	-4.478	-28710.8	-34.169	H-bond of Y27 to OH (2.75 Å), of OH to D25 (1.71 Å), salt bridge of H175 to C=OOH	162.8	4.73	not productive

Table 37. Results from IFD of substrate S-13b in the *Ts*ER C25D/I67T structure with FMNH₂ and protonated H172/H175 based on crystal structure 5NUX.

Pose	IFD Score	Glide GScore	Prime Energy	Glide Energy	Notes	result
1	-1451.824	-7.072	-28895.0	-43.129	Lactone O in direction of Y27, H-bond of R347 to C=OOEt (1.72 Å) and to C=O (1.98 Å), of OH to D25 (1.85 Å), of T67 to OH (1.82 Å)	
2	-1451.648	-6.710	-28898.8	-43.436	Lactone O in direction of H172, H-bond of Y177 to C=OOEt (1.71 Å), of T67 to OH (1.97 Å), of OH to D25 (1.55 Å), Distance of H172 to C=O (2.88 Å, angle 157.9°), of H175 to C=O (3.77 Å, angle 61.3°)	protonation possible
3	-1451.497	-6.783	-28894.3	-45.376	Lactone O in direction of H172, H-bond of H172 to C=O (2.62 Å), of T67 to OH (2.00 Å), of OH to D25 (1.59 Å), Distance of H172 to C=O (2.62 Å, angle 154.3°), of H175 to C=O (4.19 Å, angle 60.0°)	protonation possible
4	-1451.442	-7.027	-28888.3	-45.201	Lactone O in direction of Y27, H-bond of R347 to C=O (2.00 Å, 2.32 Å), of H175 to C=OOEt (2.18 Å), of water to C=OOEt, of OH to D25 (1.89 Å), of T67 to OH (1.93 Å)	
5	-1451.435	-6.950	-28889.7	-45.517	Lactone O in direction of Y27, H-bond of R347 to C=O (1.84 Å, 2.65 Å) and to C=OOEt (2.04 Å), of H175 to OEt (2.08 Å), of OH to D25 (1.68 Å), of T67 to OH (2.06 Å)	
6	-1451.404	-6.891	-28890.3	-44.265	Lactone O in direction of Y27, H-bond of R347 to C=O (2.10 Å, 2.25 Å), of water to C=OOEt, of OH to D25 (1.78 Å), of T67 to OH (1.89 Å), bad contacts of H175 to C=OOEt	
7	-1451.394	-6.400	-28899.9	-44.418	Lactone O in direction of H172, H-bond of T67 to OH (1.86 Å), of OH to D25 (1.78 Å), of Y177 to C=OOEt (2.05 Å), Distance of H172 to C=O (3.10 Å, angle 157.1°), of H175 to C=O (3.44 Å, angle 67.0°)	protonation possible
8	-1451.232	-6.430	-28896.0	-43.286	Lactone O in direction of Y27, H-bond of R347 to C=O (2.00 Å) and to C=OOEt (1.76 Å), of Y27 to C=O (2.74 Å), of OH to D25 (1.85 Å), of T67 to OH (1.93 Å), bad contact of Y177 with C10	
9	-1451.206	-6.891	-28886.3	-43.321	Lactone O in direction of Y27, H-bond of R347 to C=O (2.02 Å, 2.53 Å) and to C=OOEt (1.98 Å), of OH to D25 (1.65 Å), of T67 to OH (2.04 Å)	
10	-1450.965	-6.618	-28886.9	-42.447	Lactone O in direction of Y27, H-bond of R347 to C=O (2.03 Å, 2.53 Å) and to C=OOEt (2.22 Å), of OH to D25 (1.76 Å), of H175 to C=OOEt (1.84 Å)	
11	-1450.390	-5.196	-28903.9	-35.706	Lactone O in direction of FMN, H-bond of OH to D25 (1.57 Å), Distance of delta NH of H175 to C=O 4.03 Å, angle 53.7°, distance of epsilon NH of H175 3.60 Å, angle 61.2°, water in distance of 3.84 Å from C=O	
12	-1450.113	-6.077	-28880.7	-41.041	Lactone O in direction of H172, H-bond of H175 to C=O (1.85 Å, angle 136.3°), of H172 to C=O (2.29 Å, angle 147.6°), of OH to D25 (1.84 Å)	protonation possible
13	-1450.068	-5.969	-28882.0	-40.147	Lactone O in direction of Y27, H-bond of R347 to C=O (1.85 Å) and to C=OOEt (1.67 Å), of OH to D25 (1.68 Å), bad contact of Y177 to C10	
14	-1449.688	-5.309	-28887.6	-41.020	Lactone O in direction of H172, H-bond of Y177 to C=OOEt (2.13 Å), of OH to T67 (2.09 Å), distance of delta NH of H175 to C=O 3.57 Å, 61.3°	
15	-1449.000	-4.614	-28887.7	-38.869	Lactone O in direction of Y27, H-bond of R347 to C=O (1.81 Å, 2.64 Å) and to C=OOEt (2.14 Å), of OH to D25 (2.09 Å), bad contact of H175 to C4	
16	-1448.760	-4.702	-28881.2	-36.883	Lactone O in direction of H175, H-bond of H175 to OEt (2.20 Å), of OH to D25 (1.80 Å), distance of delta NH of H175 to C=O 3.71 Å, angle 74.7°	
17	-1448.650	-4.674	-28879.5	-35.176	Lactone O in direction of Y27, H-bond of R347 to C=O (2.03 Å, 2.19 Å) and to C=OOEt (2.25 Å), of OH to D25 (1.77 Å)	
18	-1448.434	-4.707	-28874.5	-35.320	Lactone O in direction of Y27, H-bond of R347 to C=O (2.16 Å, 2.29 Å) and to C=OOEt (2.56 Å), of OH to D25 (1.62 Å), bad contact of Y177 to C10	

Table 38. Results from Induced Fit Docking of substrate *R-13b* in the reduced and protonated *TsER C25D/I67T* structure based on crystal structure 5NUX.

Pose	IFD Score	Glide GScore	Prime Energy	Glide Energy	Notes	result
1	-1452.057	-7.383	-28893.5	-44.852	Lactone O in direction of Y27, H-bond of R347 to C=OOEt (1.83 Å) and to C=O (2.00 Å), of OH to D25 (1.67 Å), bad contact of T67 to OH	
2	-1452.054	-7.326	-28894.6	-44.708	Lactone O in direction of Y27, H-bond of R347 to C=OOEt (1.75 Å) and to C=O (2.01 Å), of Y27 to C=O (2.74 Å), of OH to D25 (1.83 Å), bad contact of T67 to OH	
3	-1451.672	-7.055	-28892.3	-43.29	Lactone O in direction of Y27, H-bond of R347 to C=OOEt (2.26 Å) and to C=O (1.96 Å, 2.33 Å), of OH to D25 (1.68 Å), of T67 to OH (1.86 Å)	
4	-1451.656	-6.663	-28899.8	-42.132	Lactone O in direction of Y27, H-bond of R347 to C=O (2.07 Å, 2.19 Å), of H175 to C=OOEt (2.07 Å), of OH to D25 (1.81 Å), of T67 to OH (1.81 Å)	
5	-1451.415	-6.759	-28893.1	-42.613	Lactone O in direction of Y27, H-bond of R347 to C=O (1.88 Å, 2.37 Å) and to OEt (2.22 Å), of H175 to C=OOEt (1.93 Å), of OH to D25 (1.74 Å), of T67 to OH (1.94 Å)	
6	-1451.213	-6.915	-28886	-42.581	Lactone O in direction of Y27, H-bond of R347 to C=O (1.97 Å, 2.51 Å) and to OEt (2.11 Å), of OH to D25 (1.63 Å), of H175 to C=OOEt (1.82 Å), bad contact of T67 to 7OH	
7	-1451.023	-6.497	-28890.5	-43.296	Lactone O in direction of Y27, H-bond of R347 to C=O (1.97 Å, 2.10 Å), of H175 to C=OOEt (2.14 Å), of OH to D25 (1.68 Å), of T67 to OH (1.83 Å), bad contact of Y177 with OEt	
8	-1450.912	-6.691	-28884.4	-41.788	Lactone O in direction of Y27, H-bond of R347 to C=O (2.09 Å, 2.11 Å) and to OEt (2.64 Å), of OH to D25 (1.53 Å), of T67 to OH (1.91 Å)	
9	-1450.879	-6.235	-28892.9	-43.409	Lactone O in direction of Y27, H-bond of R347 to C=O (1.96 Å, 2.25 Å), of H175 to C=OOEt (2.05 Å), of OH to D25 (1.70 Å), of T67 to OH (1.99 Å), bad contact of Y177 to C10	
10	-1450.802	-6.171	-28892.6	-43.384	Lactone O in direction of Y27, H-bond of R347 to C=O (1.93 Å, 2.21 Å), of H175 to C=OOEt (2.10 Å), of OH to D25 (1.89 Å), of T67 to OH (2.00 Å), bad contact of Y177 to C10	
11	-1449.284	-5.442	-28876.9	-37.308	Lactone O in direction of Y27, H-bond of R347 to C=O (2.08 Å, 2.27 Å) and to OEt (2.44 Å), of OH to D25 (1.79 Å)	
12	-1449.014	-4.62	-28887.9	-33.046	Lactone O in direction of H172, H-bond of H175 to C=O (2.40 Å), of R347 to C=OOEt (2.17 Å), of OH to D25 (1.67 Å)	protonation possible
13	-1448.746	-4.49	-28885.1	-35.741	Lactone O in direction of Y27, H-bond of R347 to C=O (2.17 Å, 2.52 Å) of H175 to C=OOEt (2.76 Å), of K107 to C=OOEt (2.53 Å), of OH to D25 (1.73 Å), Pi-cation of K107 to phenol	
14	-1448.68	-4.583	-28881.9	-33.226	Lactone O in direction of Y27, H-bond of R347 to C=O (2.28 Å), of OH to D25 (2.03 Å)	

Table 39. Results from IFD of substrate *S-13b* in the *TsER C25D/I67T* structure with oxidized FMN and protonated H172/H175 based on crystal structure 5NUX

Pose	IFD Score	Glide GScore	Prime Energy	Glide Energy	Notes	result
1	-1445.863	-8.182	-28753.6	-43.637	Lactone O in direction of Y27, H-bond of R347 to C=OOEt (2.10 Å, 2.61 Å) and to C=O (1.95 Å), of OH to D25 (1.94 Å), of T67 to OH (1.85 Å)	
2	-1444.842	-7.459	-28747.6	-36.765	Lactone O in direction of Y27, H-bond of R347 to C=OOEt (1.88 Å, 2.49 Å) and to C=O (1.84 Å), of OH to D25 (2.59 Å)	
3	-1444.596	-7.383	-28744.2	-36.68	Lactone O in direction of R347, H-bond of R347 to C=O (1.85 Å), of Y27 to OH (1.85 Å), of OH to D25 (1.86 Å)	
4	-1444.436	-7.329	-28742.1	-37.873	Lactone O in direction of Y27, H-bond of R347 to C=OOEt (1.89 Å, 2.45 Å) and to C=O (2.02 Å), of OH to D25 (1.80 Å)	
5	-1444.32	-7.127	-28743.8	-45.063	Lactone O in direction of D25, H-bond of H175 to C=OOEt (2.06 Å) of OH to D25 (1.68 Å), of OH to D71 (1.89 Å)	
6	-1444.277	-7.262	-28740.3	-37.638	Lactone O in direction of R347, H-bond of R347 to C=O (1.88 Å) and to lactone O (2.65 Å), of OH to D25 (2.03 Å)	
7	-1444.212	-6.673	-28750.8	-34.3	Lactone O in direction of H172, H-bond of OH to D25 (2.07 Å), of R347 to C=OOEt (2.54 Å), Distance of H175 to C=O (2.82 Å, angle 87.2°)	protonation possible
8	-1444.102	-6.964	-28742.8	-38.023	Lactone O in direction of Y27, H-bond of R347 to C=O (1.90 Å) and to C=OOEt (1.98 Å), of OH to D25 (2.01 Å)	
9	-1444.043	-6.828	-28744.3	-36.363	Lactone O in direction of R347, H-bond of R347 to C=O (1.79 Å) and to lactone O (2.61 Å), of OH to D25 (1.71 Å)	

10	-1444.042	-6.818	-28744.5	-40.519	Lactone O in direction of Y27, H-bond of R347 to C=OOEt (1.71 Å) and to C=O (1.84 Å), of OH to D25 (1.80 Å)
11	-1444.023	-6.778	-28744.9	-36.427	Lactone O in direction of R347, H-bond of R347 to C=O (1.96 Å) and to lactone O (2.70 Å), of Y27 to OH (1.79 Å), of OH to D25 (2.50 Å)
12	-1443.97	-6.654	-28746.3	-40.247	Lactone O in direction of Y27, H-bond of R347 to C=O (1.96 Å) and to C=OOEt (1.93 Å), of OH to D25 (2.00 Å)
13	-1443.857	-6.537	-28746.4	-38.781	Lactone O in direction of H172, H-bond of Y177 to C=OOEt (2.13 Å), of OH to T67 (2.09 Å), distance of delta NH of H175 to C=O 3.57 Å, 61.3°
14	-1443.606	-7.000	-28732.1	-38.888	Lactone O in direction of Y27, H-bond of R347 to C=O (1.95 Å, 2.38 Å) and to C=OOEt (2.17 Å), of OH to D25 (1.66 Å)
15	-1443.532	-7.253	-28725.6	-36.676	Lactone O in direction of Y27, H-bond of R347 to C=O (2.06 Å) and to C=OOEt (1.94 Å), of OH to D25 (2.12 Å)
16	-1443.265	-6.333	-28738.7	-34.435	Lactone O in direction of R347, H-bond of R347 to C=O (2.70 Å, 2.36 Å), of OH to Y177 (2.12 Å), pi-pi stacking of H175 to phenol
17	-1443.259	-6.438	-28736.4	-34.659	Lactone O in direction of R347, H-bond of R347 to C=O (2.05 Å), of OH to Y27 (2.16 Å)
18	-1442.953	-6.087	-28737.3	-35.617	coumarin vertical to FMN, H-bond of OH to S260 backbone (1.95 Å), of Y177 to OEt (2.06 Å)
19	-1442.777	-5.833	-28738.9	-30.895	Lactone O in direction of Y27, H-bond of R347 to C=O (2.00 Å, 2.28 Å), of OH to D25 (2.06 Å)

Table 40. Results from Induced Fit Docking of substrate *R-13b* in the oxidized and protonated *TsER C25D/I67T* structure based on crystal structure 5NUX.

Pose	IFD Score	Glide GScore	Prime Energy	Glide Energy	Notes	result
1	-1446.185	-8.554	-28752.6	-44.61	Lactone O in direction of Y27, H-bond of R347 to C=OOEt (1.72 Å) and to C=O (1.89 Å), of Y27 to C=O (2.71 Å), of OH to D25 (1.65 Å), bad contact of T67 to OH	
2	-1445.019	-7.434	-28751.7	-36.88	Lactone O in direction of Y27, H-bond of R347 to C=OOEt (2.24 Å) and to C=O (1.82 Å, 2.15 Å), of OH to D25 (1.86 Å), bad contact of T67 to OH	
3	-1444.721	-7.432	-28745.8	-41.214	Lactone O in direction of Y27, H-bond of R347 to C=OOEt (2.14 Å) and to C=O (1.98 Å, 2.61 Å), of OH to D25 (1.74 Å)	
4	-1444.64	-7.105	-28750.7	-37.71	Lactone O in direction of Y27, H-bond of R347 to C=OOEt (2.49 Å) and to C=O (2.10 Å, 2.13 Å), of OH to D25 (1.71 Å)	
5	-1444.558	-7.366	-28743.8	-41.253	Lactone O in direction of Y27, H-bond of R347 to C=OOEt (1.69 Å) and to C=O (1.87 Å), of Y27 to C=O (2.66 Å), of OH to D25 (1.63 Å)	
6	-1444.539	-7.051	-28749.8	-36.349	Lactone O in direction of R347, H-bond of R347 to C=O (1.88 Å, 2.61 Å) and to lactone O (2.60 Å), of OH to D25 (1.84 Å)	
7	-1444.512	-7.157	-28747.1	-40.192	Lactone O in direction of R347, H-bond of R347 to C=O (2.00 Å), of Y27 to OH (2.00 Å), of OH to D25 (2.04 Å)	
8	-1444.471	-6.865	-28752.1	-37.674	Lactone O in direction of R347, H-bond of R347 to C=O (1.85 Å), of Y27 to OH (1.92 Å), of OH to D25 (2.14 Å)	
9	-1444.455	-7.182	-28745.5	-39.519	Lactone O in direction of R347, H-bond of R347 to C=O (1.95 Å), of Y27 to OH (1.78 Å), of OH to D25 (2.24 Å)	
10	-1444.399	-7.146	-28745.1	-40.097	Lactone O in direction of H172, H-bond of H175 to C=O (1.78 Å), of OH to D71 (1.61 Å)	protonation possible
11	-1444.346	-7.884	-28729.3	-43.865	Lactone O in direction of Y27, H-bond of R347 to C=OOEt (2.03 Å), of Y27 to C=O (1.96 Å), of OH to D71 (1.63 Å)	
12	-1444.246	-7.509	-28734.7	-36.498	Lactone O in direction of R347, H-bond of R347 to C=O (1.79 Å) and to lactone O (2.67 Å), of OH to D25 (2.23 Å), of Y27 to OH (1.69 Å)	
13	-1444.163	-6.704	-28749.2	-38.095	Lactone O in direction of Y27, H-bond of R347 to C=OOEt (2.44 Å) and to C=O (1.87 Å, 2.17 Å), of OH to D25 (1.68 Å)	
14	-1443.901	-6.592	-28746.2	-37.35	Lactone O in direction of Y27, H-bond of R347 to C=O (1.97 Å, 2.15 Å), of OH to Y27 (2.04 Å), of T67 to OH (2.05 Å)	
15	-1443.768	-6.906	-28737.3	-35.2	Lactone O in direction of Y27, H-bond of R347 to C=O (1.98 Å, 2.30 Å) and to C=OOEt (2.29 Å), of OH to D25 (1.87 Å), bad contact of Y177 to OH	
16	-1443.716	-6.288	-28748.6	-41.899	Lactone O in direction of H175, H-bond of H175 to C=O (2.53 Å), of H172 to C=O (2.05 Å), of OH to R347 (1.93 Å)	protonation possible
17	-1443.41	-6.033	-28747.5	-37.139	Lactone O in direction of FMN, H-bond of R347 to C=O (2.13 Å), of H175 to C=OOEt (2.00 Å), of OH to S260 (2.18 Å), Pi-pi stacking and Pi-cation of H175 to phenol	
18	-1443.334	-6.249	-28741.7	-33.276	Lactone O in direction of H172, H-bond of OH to D25 (2.29 Å), of Y177 to OH (1.77 Å)	
19	-1443.331	-6.342	-28739.8	-37.808	Lactone O in direction of FMN, H-bond of R347 to C=O (2.04 Å, 2.20 Å), of OH to S260 (2.18 Å), Pi-pi stacking of H175 to phenol	

Table 41. Results from IFD of substrate **S-13b** in the *TsER* C25D/I67T structure with oxidized FMN, protonated H172/H175 and charged Y177 based on crystal structure 5NUX

Pose	IFD Score	Glide GScore	Prime Energy	Glide Energy	Notes
1	-1447.263	-7.16	-28802.1	-43.495	Lactone O in direction of Y27, H-bond of R347 to C=O (2.05 Å) and to C=OOEt (1.70 Å), of Y27 to C=O (2.16 Å), of OH to D25 (2.78 Å), of T67 to OH (1.90 Å)
2	-1446.519	-6.186	-28806.6	-36.335	Lactone O in direction of T67, H-bond of OH to Y27 (1.71 Å)
3	-1446.469	-6.422	-28800.9	-42.542	Lactone O in direction of Y27, H-bond of R347 to C=O (1.93 Å), of OH to D25 (1.82 Å)
4	-1446.46	-6.425	-28800.7	-41.508	Lactone O in direction of Y27, H-bond of R347 to C=O (1.89 Å, 2.45 Å), of Y27 to lactone O (2.62 Å), of OH to D25 (1.92 Å)
5	-1446.184	-5.681	-28810.1	-36.313	coumarin vertical to H175, H-bond of OH to S260 backbone (1.76 Å), of K107 to C=O (2.29 Å), of H175 to C=OOEt (2.06 Å), pi-pi stacking and pi-cation of H175 to phenol
6	-1446.147	-5.731	-28808.3	-32.941	Lactone O in direction of H172, H-bond of OH to Y177 (1.63 Å)
7	-1446.101	-5.941	-28803.2	-37.964	Lactone O in direction of R347, H-bond of R347 to C=O (2.04 Å, 2.15 Å), of OH to D25 (2.07 Å), of T67 to OH (2.48 Å)
8	-1445.995	-5.537	-28809.1	-33.175	coumarin vertical to H175, H-bond of OH to Y177 (1.69 Å), pi-cation of H175 to phenol
9	-1445.921	-5.231	-28813.8	-32.651	coumarin vertical to H175, H-bond of OH to Y177 (1.64 Å)
10	-1445.891	-5.206	-28813.7	-32.439	coumarin vertical to H175, H-bond of OH to Y177 (1.64 Å)
11	-1445.715	-4.918	-28815.9	-33.169	Lactone O in direction of H172, H-bond of R347 to C=OOEt (2.69 Å), of Y27 to OH (2.65 Å), of OH to Y177 (1.80 Å)
12	-1445.579	-5.74	-28796.8	-39.344	Lactone O in direction of Y27, H-bond of R347 to C=O (2.02 Å, 2.25 Å) and to C=OOEt (2.25 Å), of OH to T67 (2.15 Å)
13	-1445.54	-4.879	-28813.2	-31.354	coumarin vertical to H175, H-bond of OH to Y177 (1.74 Å)
14	-1445.525	-5.28	-28804.9	-33.496	coumarin vertical to H175, H-bond of OH to Y177 (1.72 Å), of Y27 to OH (2.47 Å)
15	-1445.518	-5.867	-28793	-39.007	Lactone O in direction of Y27, H-bond of R347 to C=O (2.06 Å) and to C=OOEt (1.96 Å), of OH to D25 (1.90 Å)
16	-1445.158	-4.839	-28806.4	-33.769	Lactone O in direction of Y27, H-bond of R347 to C=O (2.04 Å, 2.28 Å) and to OEt (2.74 Å), of OH to D25 (1.92 Å)
17	-1444.969	-5.229	-28794.8	-35.477	Lactone O in direction of Y27, H-bond of R347 to C=O (1.98)
18	-1444.778	-5.177	-28792	-34.763	coumarin vertical to H175, H-bond of OH to S260 backbone (1.96 Å), of K107 to C=O (2.01 Å), of H175 to C=OOEt (2.05 Å), pi-pi stacking and pi-cation of H175 to phenol
19	-1444.133	-4.609	-28790.5	-33.959	coumarin vertical to FMN, H-bond of R347 to C=O (2.05 Å, 2.15 Å)

Table 42. Results from Induced Fit Docking of substrate **R-13b** in the oxidized and protonated *TsER* C25D/I67T structure with charged Y177 based on crystal structure 5NUX.

Pose	IFD Score	Glide GScore	Prime Energy	Glide Energy	Notes	result
1	-1447.742	-7.022	-28814.4	-44.049	Lactone O in direction of Y27, H-bond of R347 to C=O (1.94 Å) and to C=OOEt (2.09 Å), of Y27 to C=O (2.55 Å) and to lactone O (2.49 Å), of OH to D25 (1.71 Å), of T67 to OH (1.96 Å)	
2	-1447.009	-5.723	-28825.7	-33.866	Lactone O in direction of R347, H-bond of R347 to lactone O (2.41 Å) and to C=O (2.30 Å, 2.07 Å), of R319 to C=OOEt (2.15 Å, 2.54 Å), OH to Y177 (1.72 Å)	
3	-1446.803	-6.131	-28813.4	-40.224	Lactone O in direction of Y27, H-bond of Y27 to lactone O (2.61 Å), of R347 to C=O (2.09 Å, 2.48 Å) and to C=OOEt (2.55 Å), of OH to D25 (1.73 Å)	
4	-1446.763	-5.924	-28816.8	-36.07	Lactone O in direction of R347, Pi-pi stacking of H175 to phenol	
5	-1446.732	-6.124	-28812.2	-40.126	coumarin vertical to H175, H-bond of OH to S260 backbone (1.96 Å), of H175 to C=OOEt (1.81 Å), of R347 to C=O (1.90 Å), pi-pi stacking and pi-cation of H175 to phenol	

6	-1446.661	-5.389	-28825.4	-30.329	coumarin vertical to H175, H-bond of OH to Y177 (1.86 Å), of K107 to OH (1.94 Å), Pi-cation of H175 and R347 to phenol	protonation possible
7	-1446.507	-5.683	-28816.5	-34.344	Lactone O in direction of R319, H-bond of R347 to OH (1.73 Å), of OH to Y27 (1.74 Å), of K107 to C=OOEt (2.59 Å)	
8	-1446.462	-6.297	-28803.3	-41.305	Lactone O in direction of H172, H-bond of H175 to C=O (1.87 Å), of R347 to C=OOEt (2.05 Å), of OH to D71 (1.73 Å)	
9	-1446.444	-5.13	-28826.3	-31.824	coumarin vertical to FMN, H-bond of OH to Y177 (1.91 Å)	
10	-1446.297	-5.08	-28824.3	-32.085	Lactone O in direction of H175, H-bond of H175 to C=O (2.13 Å), of Y27 to C=OOEt (2.38 Å)	
11	-1446.216	-5.848	-28807.4	-37.79	Lactone O in direction of R347, H-bond of R347 to lactone O (2.49 Å) and to C=O (2.02 Å), of Y27 to OH (1.90 Å), of OH to D25 (2.38 Å)	
12	-1446.114	-5.132	-28819.6	-32.124	Lactone O in direction of K107, H-bond of OH to Y177 (1.70 Å)	
13	-1445.988	-5.646	-28806.8	-38.614	coumarin vertical to FMN, H-bond of OH to S260 backbone (2.09 Å), of R347 to C=O (2.24 Å, 2.62 Å), of H175 to C=OOEt (2.19 Å), Pi-pi stacking and Pi-cation of H175 to phenol	
14	-1445.803	-5.792	-28800.2	-38.328	Lactone O in direction of Y27, H-bond of OH to D25 (1.80 Å), of R347 to C=O (2.06 Å, 2.42 Å) and to C=OOEt (2.23 Å)	
15	-1445.752	-5.262	-28809.8	-32.095	Lactone O in direction of Y177, H-bond of OH to Y177 (2.63 Å), of Y27 to OH (2.45 Å)	
16	-1445.714	-4.867	-28816.9	-31.591	Lactone O in direction of R347, H-bond of R347 to lactone O (2.34 Å) and to C=O (2.19 Å), of R319 to C=OOEt (2.44 Å), of OH to Y177 (1.66 Å), Pi-cation of H175 to phenol	
17	-1445.704	-5.366	-28806.8	-37.165	Lactone O in direction of Y27, H-bond of Y27 to lactone O (2.76 Å), of R347 to C=O (2.06 Å) and to C=OOEt (1.97 Å, 2.60 Å)	
18	-1445.622	-4.932	-28813.8	-31.209	Lactone O in direction of K107, H-bond of OH to Y177 (1.73 Å)	

Table 43. Results from IFD of substrate **S-13b** in the *TsER* C25D/I67T/A102H structure with FMNH₂ and protonated H172/H175 based on crystal structure 5OGT.

Pose	IFD Score	Glide GScore	Prime Energy	Glide Energy	Notes	result
1	-1443.469	-7.847	-28712.4	-46.744	Lactone O in direction of Y27, H-bond of Y27 to O lactone (2.28 Å), of R347 to C=O (1.92 Å, 2.32 Å), of H175 to C=OOEt (1.86 Å), of OH to D25 (1.56 Å), pi-pi stacking of H102 to phenol	protonation possible
2	-1443.339	-7.715	-28712.5	-44.406	Lactone O in direction of Y27, H-bond of Y27 to O lactone (2.20 Å), of R347 to C=O (1.86 Å, 2.24 Å) and to C=OOEt (2.00 Å), of OH to D25 (1.92 Å), of T67 to OH (1.90 Å)	
3	-1443.288	-7.674	-28712.3	-43.862	Lactone O in direction of Y27, H-bond of R347 to C=O (1.92 Å, 2.34 Å) and to C=OOEt (2.14 Å), of OH to D25 (1.85 Å), of T67 to OH (1.93 Å), bad contact of H102 to phenol	
4	-1443.284	-7.725	-28711.2	-46.847	Lactone O in direction of Y27, H-bond of Y27 to O lactone (2.33 Å), of R347 to C=O (1.91 Å, 2.18 Å), of H175 to C=OOEt (1.83 Å), of OH to D25 (1.86 Å), of T67 to OH (1.88 Å), pi-pi stacking of H102 to phenol	
5	-1443.136	-7.559	-28711.5	-46.406	Lactone O in direction of Y27, H-bond of Y27 to O lactone (2.25 Å), of R347 to C=O (1.92 Å, 2.29 Å), of H175 to C=OOEt (1.99 Å), of OH to D25 (1.66 Å), pi-pi stacking of H102 to phenol	
6	-1443.088	-7.538	-28711.0	-44.297	Lactone O in direction of Y27, H-bond of Y27 to O lactone (2.23 Å), of R347 to C=O (1.99 Å, 2.16 Å) and to C=OOEt (2.16 Å), of OH to D25 (1.73 Å), of T67 to OH (2.00 Å), bad contact of H102 to phenol	
7	-1443.061	-7.476	-28711.7	-44.014	Lactone O in direction of Y27, H-bond of R347 to C=O (1.99 Å), of OH to D25 (1.61 Å), pi-pi stacking of H102 to phenol, bad contacts of T67 to OH	
8	-1443.017	-7.324	-28713.9	-43.255	Lactone O in direction of Y27, H-bond of R347 to C=O (1.90 Å), of OH to D25 (1.83 Å), pi-pi stacking of H102 to phenol, bad contacts of T67 to OH	
9	-1442.965	-7.608	-28707.1	-47.769	Lactone O in direction of H172, H-bond of H175 to C=OOEt (1.84 Å), of OH to D25 (1.69 Å), bad contact of t67 to OH, distance of H172 3.84 Å, angle 98.5°	
10	-1442.922	-7.601	-28706.4	-44.119	Lactone O in direction of Y27, H-bond of R347 to C=O (1.96 Å), of OH to D25 (1.73 Å), pi-pi stacking of H102 to phenol, bad contacts of T67 to OH	
11	-1442.879	-7.732	-28702.9	-46.394	Lactone O in direction of Y27, H-bond of Y27 to O lactone (2.35 Å), of R347 to C=O (1.85 Å, 2.20 Å) and to OEt (2.52 Å), of H175 to C=OOEt (2.03 Å), of OH to D25 (1.68 Å), of T67 to OH (1.97 Å)	
12	-1442.816	-7.387	-28708.6	-44.592	Lactone O in direction of Y27, H-bond of Y27 to O lactone (2.30 Å), of R347 to C=O (1.86 Å, 2.12 Å) and to C=OOEt (2.63 Å), of OH to D25 (1.86 Å), of T67	

					to OH (1.93 Å)
13	-1442.570	-7.403	-28703.3	-45.893	Lactone O in direction of Y27, H-bond of Y27 to O lactone (2.46 Å), of R347 to C=O (1.78 Å, 2.43 Å, of H175 to C=OOEt (1.77 Å), of OH to D25 (1.88 Å), of T67 to OH (1.88 Å), pi-pi stacking of H102 to phenol
14	-1442.558	-6.986	-28711.4	-44.338	Lactone O in direction of Y27, H-bond of Y27 to O lactone (2.56 Å), of R347 to C=O (1.85 Å, 2.67 Å, of H175 to C=OOEt (2.67 Å), of OH to D25 (1.84 Å), of T67 to OH (2.07 Å), pi-pi stacking of H102 to phenol
15	-1442.552	-7.458	-28701.9	-45.996	Lactone O in direction of Y27, H-bond of Y27 to O lactone (2.57 Å), of R347 to C=O (1.72 Å, 2.80 Å), of H175 to C=OOEt (1.76 Å), of OH to D25 (1.60 Å), pi-pi stacking of H102 to phenol, bad contact of T67 to OH
16	-1442.522	-6.883	-28712.8	-42.965	Lactone O in direction of Y27, H-bond of Y27 to O lactone (2.69 Å), of R347 to C=O (1.98 Å), of OH to D25 (1.99 Å), of T67 to OH (2.03 Å)
17	-1442.109	-6.650	-28709.2	-43.732	Lactone O in direction of Y27, H-bond of R347 to C=O (2.04 Å), of OH to D25 (1.76 Å), of T67 to OH (2.20 Å)
18	-1441.841	-6.570	-28705.4	-41.396	Lactone O in direction of H172, H-bond of H172 to C=O (2.12 Å, angle 157.7°), of OH to D25 (1.67 Å), pi-pi stacking of Y177 to phenol
19	-1441.673	-6.692	-28699.6	-39.948	Lactone O in direction of Y27, H-bond of R347 to C=O (1.94 Å), of OH to D25 (1.60 Å), of T67 to OH (2.07 Å)

Table 44. Results from Induced Fit Docking of substrate *R-13b* in the reduced and protonated *TsER C25D/I67T/A102H* structure based on crystal structure 5OGT.

Pose	IFD Score	Glide GScore	Prime Energy	Glide Energy	Notes	result
1	-1443.683	-8.176	-28710.1	-46.734	Lactone O in direction of H172, H-bond of T67 to OH (2.08 Å), of OH to D25 (1.46 Å)	
2	-1443.613	-7.656	-28719.1	-45.915	Lactone O in direction of H172, H-bond of T67 to OH (2.00 Å), of OH to D25 (1.55 Å)	
3	-1443.38	-7.619	-28715.2	-47.3	Lactone O in direction of H172, H-bond of H172 to C=O (2.40 Å), T67 to OH (1.91 Å), of OH to D25 (1.90 Å)	protonation possible?
4	-1443.366	-7.52	-28716.9	-45.078	Lactone O in direction of Y27, H-bond of R347 to C=O (1.81 Å), of H175 to C=OOEt (1.91 Å), of OH to D25 (1.87 Å), of T67 to OH (2.02 Å)	
5	-1443.215	-7.507	-28714.2	-46.162	Lactone O in direction of Y27, H-bond of Y27 to O lactone (2.40 Å), of R347 to C=O (2.01 Å, 2.52 Å) and to OEt (2.79 Å), of H175 to C=OOEt (2.10 Å), of OH to D25 (1.69 Å), of T67 to OH (2.02 Å)	
6	-1443.174	-7.424	-28715	-45.483	Lactone O in direction of Y27, H-bond of R347 to C=O (1.74 Å), of H175 to C=OOEt (1.89 Å), of OH to D25 (1.75 Å), of T67 to OH (2.03 Å)	
7	-1442.998	-7.768	-28704.6	-44.292	Lactone O in direction of Y27, H-bond of R347 to C=O (1.98 Å), of H175 to C=OOEt (1.90 Å), of OH to D25 (1.53 Å), of T67 to OH (1.88 Å)	
8	-1442.831	-7.297	-28710.7	-44.756	Lactone O in direction of Y27, H-bond of R347 to C=O (1.90 Å), of OH to D25 (1.71 Å), of T67 to OH (2.01 Å)	
9	-1442.815	-7.526	-28705.8	-46.498	Lactone O in direction of Y27, H-bond of R347 to C=O (1.77 Å), of H175 to C=OOEt (1.95 Å), of OH to D25 (1.64 Å), Pi-pi stacking of H102 to phenol, bad contacts of T67 to OH	
10	-1442.777	-7.422	-28707.1	-46.742	Lactone O in direction of Y27, H-bond of Y27 to O lactone (2.27 Å), of R347 to C=O (1.77 Å, 2.52 Å), of H175 to C=OOEt (1.96 Å), of OH to D25 (1.63 Å), of T67 to OH (1.91 Å)	
11	-1442.751	-7.189	-28711.2	-43.683	Lactone O in direction of Y27, H-bond of R347 to C=O (1.88 Å), of OH to D25 (1.80 Å), of T67 to OH (1.97 Å)	
12	-1442.617	-7.18	-28708.7	-44.08	Lactone O in direction of Y27, H-bond of R347 to C=O (2.01 Å), of H175 to C=OOEt (1.87 Å), of OH to D25 (1.90 Å), of T67 to OH (1.97 Å)	
13	-1442.427	-7.16	-28705.3	-44.182	Lactone O in direction of Y27, of R347 to C=O (2.08 Å), of Y177 to C=OOEt (1.84 Å), of OH to D25 (1.58 Å), of T67 to OH (2.37 Å), bad contacts of H175 to OEt	
14	-1442.405	-6.882	-28710.5	-46.072	Lactone O in direction of Y27, H-bond of R347 to C=O (1.92 Å), of H175 to C=OOEt (1.96 Å), of OH to D25 (1.60 Å), of T67 to OH (2.05 Å), bad contact of Y177 to C10	
15	-1441.588	-6.326	-28705.2	-40.455	Lactone O in direction of Y27, of R347 to C=O (2.14 Å), of Y177 to C=OOEt (1.88 Å), of OH to D25 (1.74 Å), of T67 to OH (2.50 Å)	
16	-1440.867	-6.202	-28693.3	-40.006	Lactone O in direction of Y27, H-bond of R347 to C=O (1.80 Å), of H175 to C=OOEt (2.13 Å), of OH to D25 (1.88 Å)	

Table 45. Results from IFD of substrate **S-13b** in the *TsER* C25D/I67T/A102H structure with oxidized FMN and protonated H172/H175 based on crystal structure 5OGT.

Pose	IFD Score	Glide GScore	Prime Energy	Glide Energy	Notes
1	-1439.044	-7.7	-28626.9	-41.930	Lactone O in direction of Y27, H-bond of Y27 to O lactone (2.18 Å), of R347 to C=O (1.96 Å, 2.35 Å) and to C=OOEt (2.29 Å), of OH to D25 (2.12 Å), of T67 to OH (1.90 Å)
2	-1438.993	-7.976	-28620.3	-44.339	Lactone O in direction of Y27, H-bond of R347 to C=O (1.90 Å) and to C=OOEt (2.00 Å), of OH to D25 (2.07 Å), of T67 to OH (2.24 Å)
3	-1438.914	-7.624	-28625.8	-37.875	Lactone O in direction of Y27, H-bond of R347 to C=O (2.11 Å) and to C=OOEt (2.67 Å), of T67 to OH (2.24 Å). pi-pi stacking of H102 to phenol
4	-1438.687	-7.173	-28630.3	-38.372	Lactone O in direction of Y27, H-bond of Y27 to lactone O (2.45 Å), of OH to D25 (1.92 Å), of T67 to OH (1.90 Å)
5	-1438.488	-6.911	-28631.5	-37.000	Lactone O in direction of H175, H-bond of H172 to OH (2.04 Å)
6	-1438.355	-7.048	-28626.2	-38.156	Lactone O in direction of Y27, H-bond of Y27 to O lactone (2.78 Å), of OH to D25 (1.93 Å)
7	-1438.299	-7.311	-28619.8	-41.727	Lactone O in direction of Y27, H-bond of R347 to C=O (2.12 Å) and to C=OOEt (1.96 Å, 2.21 Å), of Y27 to C=O (2.24 Å), of OH to D25 (2.15 Å) and to D71 (2.61 Å)
8	-1437.76	-6.847	-28618.3	-39.27	Lactone O in direction of H175, H-bond of H175 to C=O (1.78 Å)
9	-1437.749	-6.551	-28624	-34.976	Lactone O in direction of R347, H-bond of Y27 to C=O (2.48 Å) and to C=OOEt (2.07 Å)
10	-1437.511	-7.084	-28608.5	-37.669	Lactone O in direction of Y27, H-bond of Y27 to lactone O (2.25 Å), of OH to H102 (2.05 Å)
11	-1437.396	-7.008	-28607.8	-38.611	Lactone O in direction of Y27, H-bond of R347 to C=O (1.80 Å), of OH to D25 (1.70 Å)
12	-1437.377	-6.421	-28619.1	-38.690	coumarin vertical to FMN, H-bond of OH to S260 backbone (1.87 Å), of Y177 to C=O (1.80 Å), of H175 to C=OOEt (2.04 Å), pi-pi stacking and pi-cation of H175 to phenol
13	-1437.083	-5.912	-28623.4	-36.704	coumarin vertical to FMN, H-bond of Y177 to C=O (1.88 Å), of H175 to C=OOEt (1.89 Å)
14	-1436.993	-6.239	-28615.1	-38.582	coumarin vertical to FMN, H-bond of Y27 to C=O (2.11 Å), of H175 to C=OOEt (1.96 Å)
15	-1436.992	-6.163	-28616.6	-37.585	coumarin vertical to FMN, H-bond of Y27 to C=O (2.07 Å), of H172 to C=OOEt (2.40 Å), of K107 to OH (1.86 Å), pi-pi stacking of Y177 to phenol
16	-1436.94	-5.573	-28627.3	-33.073	Lactone O in direction of Y27, H-bond of Y27 to lactone O (2.16 Å), of OH to D71 (2.68 Å)
17	-1436.547	-5.651	-28617.9	-33.05	Lactone O in direction of R347, H-bond of R347 to lactone O (2.26 Å) and to C=O (1.99 Å), of Y27 to C=O (2.02 Å), pi-pi stacking of H175 to phenol
18	-1436.237	-5.79	-28608.9	-32.516	Lactone O in direction of R347, H-bond of R347 to C=O (1.73 Å, 2.41 Å), of Y27 to C=O (2.09 Å)
19	-1436.207	-5.726	-28609.6	-37.521	H-bond of Y27 to C=OOEt (1.93 Å), of R347 to C=OOEt (2.21 Å, 2.68 Å) and to C=O (2.22 Å), pi-pi stacking of H175 to phenol
20	-1436.023	-5.75	-28605.5	-29.571	Lactone O in direction of Y27, H-bond of Y27 to lactone O (2.19 Å), of OH to D25 (1.75 Å)

Table 46. Results from Induced Fit Docking of substrate **R-13b** in the oxidized and protonated *TsER* C25D/I67T/A102H structure based on crystal structure 5OGT.

Pose	IFD Score	Glide GScore	Prime Energy	Glide Energy	Notes
1	-1439.561	-8.46	-28622	-44.88	Lactone O in direction of Y27, H-bond of R347 to C=O (1.91 Å) and to C=OOEt (1.88 Å, 2.76 Å), of OH to D25 (1.75 Å), of T67 to OH (1.89 Å)
2	-1439.539	-8.41	-28622.6	-44.432	Lactone O in direction of Y27, H-bond of Y27 to lactone O (2.60 Å), of R347 to C=O (1.93 Å) and to C=OOEt (2.09 Å), of OH to D25 (1.74 Å), of T67 to OH (1.99 Å)
3	-1438.729	-7.439	-28625.8	-39.974	Lactone O in direction of Y27, H-bond of R347 to C=O (1.97 Å, 2.60 Å) and to C=OOEt (2.10 Å), of Y27 to C=O (2.05 Å), bad contacts of T67 and H102 to OH
4	-1438.701	-7.794	-28618.1	-39.864	Lactone O in direction of Y27, H-bond of OH to D25 (1.83 Å), of T67 to OH (1.91 Å)
5	-1438.607	-7.577	-28620.6	-38.933	Lactone O in direction of Y27, H-bond of OH to D25 (1.85 Å), of T67 to OH (1.84 Å), bad contact of H172 to C5
6	-1438.17	-7.003	-28623.3	-37.379	Lactone O in direction of R347, H-bond of Y27 to C=OOEt (1.78 Å), of R347 to C=O (2.00 Å, 2.02 Å), Pi-pi stacking of H175 to phenol
7	-1438.053	-7.561	-28609.9	-38.445	Lactone O in direction of Y27, H-bond of Y27 to lactone O (2.74 Å), of OH to D25 (1.92 Å), of T67 to OH (2.02 Å)
8	-1437.942	-7.046	-28617.9	-37.548	Lactone O in direction of Y27, H-bond of OH to D25 (2.00 Å), bad contact of T67 to OH
9	-1437.648	-6.483	-28623.3	-34.807	Lactone O in direction of R347, H-bond of Y27 to C=O (2.16 Å) and to C=OOEt (2.42 Å), Pi-pi stacking of H175 to phenol
10	-1437.634	-6.584	-28621	-40.63	Lactone O in direction of FMN, H-bond of R347 to C=O (2.04 Å), of OH to S260 backbone (1.96 Å), of H175 to C=OOEt (1.85 Å), Pi-pi stacking and Pi-cation of H175 to

Pose	IFD Score	Glide GScore	Prime Energy	Glide Energy	Notes
11	-1437.583	-6.449	-28622.7	-34.919	phenol Lactone O in direction of R347, H-bond of Y27 to C=O (2.71 Å) and to C=OOEt (1.77 Å), Pi-pi stacking of H175 to phenol
12	-1437.573	-7.157	-28608.3	-39.491	Lactone O in direction of Y27, H-bond of Y27 to lactone O (2.16 Å), of R347 to C=O (2.04 Å, 2.17 Å) and to C=OOEt (2.71 Å), of OH to D25 (2.15 Å)
13	-1437.563	-6.817	-28614.9	-36.796	Lactone O in direction of Y27, H-bond of OH to T67 (1.97 Å), bad contact of H172 to C5
14	-1437.392	-6.162	-28624.6	-33.435	Lactone O in direction of R347. H-bond of Y27 to C=O (2.59 Å) and to C=OOEt (2.17 Å), Pi-pi stacking of H175 to phenol
15	-1437.325	-6.808	-28610.3	-36.323	Lactone O in direction of Y27, H-bond of Y27 to lactone O (2.69 Å), of OH to D25 (2.05 Å)
16	-1437.084	-5.862	-28624.4	-34.539	Lactone O in direction of H175, H-bond of H172 to C=OOEt (2.20 Å)
17	-1436.616	-5.956	-28613.2	-34.794	Lactone O in direction of FMN, H-bond of Y27 to C=O (1.91 Å), bad contacts of Y177 to C=OOEt

Table 47. Results from IFD of substrate *S-13b* in the *TsER* C25D/I67T/A102H structure with oxidized FMN, protonated H172/H175 and charged Y177 based on crystal structure 5OGT.

Pose	IFD Score	Glide GScore	Prime Energy	Glide Energy	Notes
1	-1440.109	-6.585	-28670.5	-37.848	Lactone O in direction of H175, H-bond of H172 to C=OOEt (1.67 Å)
2	-1439.934	-5.888	-28680.9	-39.417	Lactone O in direction of R347, H-bond of R347 to C=O (2.35 Å) and to C=OOEt (2.25 Å), of Y27 to C=OOEt (2.18 Å), of OH to A111 backbone (1.65 Å), pi-pi stacking of Y27 to phenol, bad contacts Y177 to Et
3	-1439.827	-6.234	-28671.9	-40.159	coumarin vertical to FMN, H-bond of R347 to C=O (2.00 Å) and to C=OOEt (1.83 Å), of Y27 to C=OOEt (1.93 Å), of OH to Y136 (1.81 Å), pi-cation of K107 to phenol
4	-1439.561	-5.592	-28679.4	-36.024	Lactone O in direction of Y27, H-bond of Y27 to lactone O (2.12 Å), of OH to H102 (2.00 Å)
5	-1439.467	-5.881	-28671.7	-40.559	Lactone O in direction of Y27, H-bond of OH to H102 (2.16 Å)
6	-1439.453	-6.141	-28666.2	-39.123	coumarin vertical to FMN, H-bond of R347 to C=O (2.05 Å) and to C=OOEt (1.96 Å), of Y27 to C=OOEt (2.01 Å), of OH to Y136 (1.80 Å), pi-cation of K107 to phenol
7	-1439.388	-6.474	-28658.3	-38.004	coumarin vertical to FMN, H-bond of R347 to C=O (1.97 Å) and to C=OOEt (1.77 Å), of Y27 to C=OOEt (1.95 Å), of OH to Y136 (1.74 Å), pi-cation of K107 to phenol
8	-1439.269	-5.761	-28670.2	-36.579	coumarin vertical to FMN, H-bond of OH to S260 backbone (2.10 Å), of H175 to C=OOEt (1.97 Å), pi-pi stacking and pi-cation of H175 to phenol
9	-1439.174	-5.48	-28673.9	-37.155	Lactone O in direction of Y27, H-bond of R347 to C=O (2.12 Å, 2.35 Å) and to C=OOEt (2.14 Å), of OH to H102 (2.10 Å), of Y27 to lactone O (2.32 Å)
10	-1439.126	-5.643	-28669.7	-35.398	coumarin vertical to FMN, H-bond of OH to S260 backbone (1.96 Å), of Y27 to OEt (2.57 Å), of R347 to C=OOEt (2.02 Å), pi-pi stacking and pi-cation of H175 to phenol
11	-1439.088	-5.09	-28680	-30.858	Lactone O in direction of H175, H-bond of OH to Y177 (1.82 Å)
12	-1438.805	-5.553	-28665	-37.641	Lactone O in direction of Y27, H-bond of R347 to C=OOEt (2.18 Å) and to C=O (2.03 Å, 2.31 Å), of Y27 to C=O (2.30 Å), of OH to D71 (2.56 Å)
13	-1438.627	-5.354	-28665.5	-35.274	Lactone O in direction of R347, H-bond of R347 to C=OOEt (2.17 Å, 2.52 Å), of Y27 to C=OOEt (1.95 Å), of OH to A111 backbone (1.86 Å), pi-pi stacking of Y27 to phenol
14	-1438.587	-4.91	-28673.6	-37.057	Lactone O in direction of Y27, H-bond of R347 to C=OOEt (2.53 Å) and to C=O (2.10 Å, 2.25 Å)
15	-1438.429	-5.19	-28664.8	-32.909	coumarin vertical to FMN, H-bond of OH to S260 backbone (1.73 Å), of R347 to C=OOEt (2.30 Å), pi-pi stacking and pi-cation of H175 to phenol
16	-1438.412	-5.411	-28660	-34.162	coumarin vertical to FMN, H-bond of OH to S260 backbone (1.82 Å), of Y27 to OEt (2.66 Å), of R347 to C=OOEt (2.06 Å), pi-pi stacking and pi-cation of H175 to phenol
17	-1438.304	-5.122	-28663.6	-31.89	coumarin vertical to FMN, H-bond of R347 to C=OOEt (2.00 Å, 2.56 Å) and to C=O (2.10 Å), of Y27 to C=OOEt (1.98 Å), of Y136 to OH (1.95 Å), pi-cation of K107 to phenol
18	-1438.284	-5.12	-28663.3	-31.856	coumarin vertical to FMN, H-bond of R347 to C=OOEt (2.00 Å, 2.56 Å) and to C=O (2.10 Å), of Y27 to C=OOEt (1.98 Å), of Y136 to OH (1.94 Å), pi-cation of K107 to phenol
19	-1437.764	-4.541	-28664.5	-30.123	Lactone O in direction of Y27, H-bond of R347 to C=O (2.09 Å, 2.71 Å), of OH to D25 (1.86 Å)

Table 48. Results from Induced Fit Docking of substrate *R-13b* in the oxidized and protonated *TsER* C25D/I67T/A102H with charged Y177 structure based on crystal structure 5OGT.

Pose	IFD Score	Glide GScore	Prime Energy	Glide Energy	Notes
1	-1440.56	-6.655	-28678.1	-42.619	Lactone O in direction of Y27, H-bond of Y27 to lactone O (2.11 Å), of R347 to C=O (1.96 Å, 2.39 Å) and to C=OOEt (2.26 Å), of OH to H102 (1.97 Å)
2	-1439.923	-5.785	-28682.8	-37.852	Lactone O in direction of R347, H-bond of Y27 to C=O (2.54 Å) and to C=OOEt (2.02 Å), pi-pi stacking of H175 to phenol
3	-1439.785	-5.197	-28691.8	-31.992	Lactone O in direction of H172, H-bond of OH to Y177 (1.63 Å)
4	-1439.73	-6.147	-28671.7	-39.746	Lactone O in direction of R347, H-bond of Y27 to C=O (2.01 Å), of H172 to C=OOEt (2.10 Å)
5	-1439.653	-6.236	-28668.4	-34.966	Lactone O in direction of R347, H-bond of Y27 to C=O (2.79 Å) and to C=OOEt (2.16 Å), pi-pi stacking of H175 to phenol
6	-1439.591	-6.114	-28669.5	-39.693	coumarin vertical to FMN, H-bond of R347 to C=O (1.84 Å), of H175 to C=OOEt (1.95 Å), of OH to S260 backbone (2.10 Å), Pi-pi stacking and Pi-cation of H175 to phenol
7	-1439.479	-5.174	-28686.1	-32.97	Lactone O in direction of H172, H-bond of OH to Y177 (1.78 Å)
8	-1439.406	-5.24	-28683.3	-36.738	Lactone O in direction of S260, H-bond of H175 and H172 to C=OOEt (2.16 Å, 2.18 Å)
9	-1439.386	-5.509	-28677.5	-35.971	Lactone O in direction of R347, H-bond of Y27 to C=OOEt (1.92 Å), Pi-pi stacking of H175 to phenol
10	-1439.254	-5.274	-28679.6	-38.549	Lactone O in direction of S260, H-bond of H175 and H172 to C=OOEt (2.50 Å, 2.15 Å)
11	-1439.195	-5.278	-28678.3	-29.839	Lactone O in direction of R347, H-bond of R347 to lactone O (2.07 Å) and to C=O (1.94 Å), of OH to Y177 (1.56 Å)
12	-1439.093	-5.385	-28674.2	-33.265	Lactone O in direction of Y27, H-bond of Y27 to lactone O (2.18 Å), of OH to D25 (1.73 Å)
13	-1438.953	-5.707	-28664.9	-35.231	Lactone O in direction of R319, H-bond of R347 to OH (2.43 Å) and OH to Y27 (1.73 Å)
14	-1438.815	-5.122	-28673.9	-36	Lactone O in direction of Y27, H-bond of Y27 to lactone O (2.66 Å), of OH to D25 (1.97 Å)
15	-1438.776	-5.136	-28672.8	-35.692	Lactone O in direction of Y27, H-bond of Y27 to lactone O (2.58 Å), of OH to D25 (1.91 Å)
16	-1438.559	-4.97	-28671.8	-33.177	Lactone O in direction of Y27, H-bond of Y27 to lactone O (2.14 Å)
17	-1438.45	-5.001	-28669	-36.711	Lactone O in direction of S260, H-bond of H175 and H172 to C=OOEt (2.15 Å, 2.23 Å)

Table 49. Results from IFD of *R-13e* intermediate in the *TsER* C25D/I67T structure with FMNH₂ and protonated H172/H175 based on crystal structure 5NUX.

Pose	IFD Score	Glide GScore	Prime Energy	Glide Energy	Notes
1	-1455.973	-8.001	-28959.4	-46.936	Lactone O in direction of Y27, H-bond of Y27 to lactone O (2.01 Å), of R347 diol (2.25 Å) and to C=OOEt (1.73 Å), of OH to D25 (1.83 Å), bad contact of T67 to OH
2	-1455.268	-7.066	-28964	-46.23	Lactone O in direction of Y27, H-bond of R347 diol (2.25 Å) and to OEt (2.64 Å), of OH to D25 (1.69 Å), of Y177 to diol (2.31 Å), bad contact of T67 to OH
3	-1455.031	-7.125	-28958.1	-44.987	Lactone O in direction of Y27, H-bond of Y27 to lactone O (2.22 Å), of R347 diol (2.06 Å) and to C=OOEt (1.75 Å), of OH to D25 (1.72 Å), of T67 to OH (1.90 Å)
4	-1454.923	-6.786	-28962.7	-45.653	Lactone O in direction of Y27, H-bond of R347 diol (2.38 Å) and to OEt (2.62 Å), of OH to D25 (1.71 Å), of T67 to OH (1.99 Å), bad contact of Y177 to diol
5	-1454.898	-6.839	-28961.2	-43.457	Lactone O in direction of Y27, H-bond of Y27 to lactone O (2.10 Å), of R347 diol (2.00 Å) and to C=OOEt (1.64 Å), of Y177 to diol (2.56 Å), of OH to D25 (1.79 Å), of T67 to OH (1.87 Å)
6	-1454.827	-6.87	-28959.1	-44.804	Lactone O in direction of Y27, H-bond of Y27 to lactone O (2.38 Å), of R347 diol (1.99 Å) and to C=OOEt (1.81 Å), of Y177 to diol (2.70 Å), of OH to D25 (1.60 Å), of T67 to OH (2.05 Å)
7	-1454.36	-6.243	-28962.3	-43.632	Lactone O in direction of Y27, H-bond of R347 diol (1.93 Å and 2.05 Å), of H175 to C=OOEt (1.95 Å), of OH to D25 (1.68 Å), of T67 to OH (1.85 Å), bad contact of K107 to Et, of Y177 to phenol

8	-1453.919	-5.934	-28959.7	-43.528	Lactone O in direction of Y27, H-bond of R347 diol (1.99 Å and 1.99 Å), of H175 to C=OOEt (2.12 Å), of OH to D25 (1.72 Å), of T67 to OH (1.95 Å), bad contact of K107 to Et, of Y177 to phenol
9	-1453.908	-5.799	-28962.2	-43.587	Lactone O in direction of Y27, H-bond of R347 diol (1.93 Å and 2.01 Å), of H175 to C=OOEt (2.18 Å), of OH to D25 (1.73 Å), of T67 to OH (1.86 Å), bad contact of K107 to Et, of Y177 to phenol
10	-1453.734	-5.913	-28956.4	-42.084	Lactone O in direction of Y27, H-bond of R347 diol (2.35 Å), of OH to D25 (1.64 Å), of T67 to OH (2.04 Å)
11	-1453.449	-5.756	-28953.9	-42.666	Lactone O in direction of Y27, H-bond of R347 diol (2.11 Å) and to C=OOEt (2.63 Å, 1.74 Å), of OH to D25 (1.68 Å), of Y177 to diol (2.36 Å)
12	-1452.927	-5.38	-28950.9	-40.394	Lactone O in direction of Y27, H-bond of R347 diol (1.96 Å) and to OEt (2.03 Å), of H175 to C=OOEt (1.88 Å), of OH to D25 (1.65 Å), of Y177 to diol (2.20 Å)
13	-1452.916	-5.373	-28950.9	-37.782	Lactone O in direction of Y177, H-bond of H172 to C=OOEt (2.71 Å), of Y177 to OEt (2.51 Å), of Y27 to OH (1.94 Å)
14	-1452.726	-5.162	-28951.3	-37.952	Lactone O in direction of Y177, H-bond of Y177 to diol (1.84 Å), of H175 to diol (2.10 Å)
15	-1452.661	-5.311	-28947	-34.706	Lactone O in direction of Y27, H-bond of R347 to C=OOEt (2.12 Å), of OH to D25 (1.61 Å)
16	-1452.637	-5.645	-28939.8	-36.089	Lactone O in direction of Y27, H-bond of R347 to diol (2.28 Å), of OH to D25 (1.56 Å)
17	-1452.516	-5.142	-28947.5	-38.639	Lactone O in direction of Y27, H-bond of R347 to C=OOEt (2.34 Å) and to diol (2.01 Å, 2.42 Å), of OH to D25 (1.78 Å), bad contacts of H175 to C4
18	-1451.817	-4.134	-28953.7	-34.202	Lactone O in direction of FMN, H-bond of H175 to diol (2.67 Å) and to C=OOEt (2.29 Å), of K107 to OEt (2.53 Å), of Y177 to diol (2.05 Å), Pi-cation of R347 to phenol
19	-1451.393	-4.337	-28941.1	-33.748	Lactone O in direction of Y27, H-bond of R347 to diol (2.42 Å, 2.42 Å and 1.88 Å), of OH to D25 (1.97 Å)

Table 50. Results from IFD of *S-13e* intermediate in the *TsER* C25D/I67T structure with FMNH₂ and protonated H172/H175 based on crystal structure 5NUX.

Pose	IFD Score	Glide GScore	Prime Energy	Glide Energy	Notes	result
1	-1455.499	-7.022	-28969.6	-44.188	Lactone O in direction of H172, H-bond of diol to Y177 (1.83 Å), of Z67 to 7OH (1.87 Å), of 7OH to D25 (1.76 Å)	possible hydrolysis?
2	-1454.999	-6.719	-28965.6	-42.96	Lactone O in direction of Y27, H-bond of R347 diol (2.24 Å, 2.41 Å, 2.31 Å) and to C=OOEt (2.44 Å), of 7OH to D25 (1.58 Å), of T67 to 7OH (1.93 Å)	
3	-1454.66	-6.61	-28961	-44.853	Lactone O in direction of Y27, H-bond of R347 diol (2.11 Å, 2.43 Å) and to C=OOEt (2.31 Å), of 7OH to D25 (1.74 Å), of T67 to 7OH (1.88 Å), of H175 to OEt (2.14 Å)	
4	-1454.483	-6.443	-28960.8	-41.676	Lactone O in direction of Y27, H-bond of R347 diol (2.06 Å, 2.20 Å) and to C=OOEt (2.29 Å), of 7OH to D25 (1.57 Å), of T67 to 7OH (1.99 Å), bad contact of H175 to OEt	
5	-1454.479	-6.159	-28966.4	-42.836	Lactone O in direction of Y27, H-bond of R347 diol (2.00 Å, 2.31 Å) and to C=OOEt (2.59 Å), of 7OH to D25 (1.73 Å), of T67 to 7OH (2.03 Å), bad contact of Y177 to lactone O	
6	-1454.163	-6.361	-28956	-43.349	Lactone O in direction of Y27, H-bond of Y27 to diol (1.82 Å), of Y177 to diol (1.94 Å), of diol to D25 (2.37 Å), of R347 to OH (2.07 Å), Pi-pi stacking of H175 to phenol	
7	-1453.841	-5.889	-28959	-42.355	Lactone O in direction of H175, H-bond of H175 to diol (2.08 Å), of R347 to C=OOEt (2.33 Å, 2.41 Å), of Y177 to diol (2.20 Å). Pi-pi stacking of H172 and Y177 to phenol	possible hydrolysis?
8	-1453.749	-5.209	-28970.8	-38.887	Lactone O in direction of S260, H-bond of R347 to diol (2.36 Å, 2.22 Å, 2.27 Å), of Y177 to C=OOEt (2.11 Å), of K107 to C=OOEt (2.72 Å), Pi-cation of K107 to phenol	
9	-1453.673	-6.122	-28951	-40.015	Lactone O in direction of Y27, H-bond of Y27 to lactone O (2.01 Å), of R347 to diol (2.02 Å, 2.31 Å and 2.46 Å) and to C=OOEt (1.92 Å), of OH to D25 (1.64 Å)	
10	-1453.497	-5.327	-28963.4	-39.447	Lactone O in direction of H175, H-bond of H175 to diol (2.04 Å), of Y177 to diol (1.75 Å), of R347 to C=OOEt (1.79 Å, 2.19 Å), of diol to D25 (1.92 Å)	possible hydrolysis
11	-1453.29	-5.671	-28952.4	-39.917	Lactone O in direction of Y27, H-bond of Y27 to lactone O (2.14 Å), of R347 diol (2.16 Å, 2.23 Å, 2.35 Å) and to C=OOEt (2.31 Å), of OH to D25 (1.77 Å)	

12	-1453.281	-5.342	-28958.8	-39.209	Lactone O in direction of Y27, H-bond of Y27 to lactone O (2.78 Å), of R347 diol (1.94 Å, 2.44 Å, 2.72 Å) and to C=OOEt (2.62 Å), of OH to D25 (1.69 Å)	
13	-1453.183	-4.501	-28973.6	-38.418	Lactone O in direction of S260, H-bond of H172 to 7OH (2.04 Å), of R347 to diol (2.16 Å, 2.30 Å, 2.36 Å), Pi-cation of K107 to phenol	
14	-1452.84	-4.971	-28957.4	-37.937	coumarin vertical to FMN, H-bond of Y27 to diol (2.04 Å), of diol to D25 (1.76 Å) and of D25 to diol (2.92 Å), Pi-cation of K107 to phenol	
15	-1452.826	-4.71	-28962.3	-33.747	coumarin vertical to FMN, H-bond of Y177 to diol (1.88 Å), of H175 to diol (1.96 Å), of R347 to C=OOEt (1.89 Å)	possible hydrolysis?
16	-1452.693	-4.729	-28959.3	-35.017	coumarin vertical to FMN, H-bond of Y177 to diol (2.02 Å), of H175 to diol (2.07 Å), of R347 to C=OOEt (1.85 Å, 2.71 Å)	
17	-1452.676	-5.485	-28943.8	-34.078	Lactone O in direction of T67, H-bond of Y177 to diol (2.28 Å), of H175 to diol (2.01 Å), of K107 to C=OOEt (2.67 Å), of Y27 to 7OH (1.84 Å)	possible hydrolysis?
18	-1452.647	-4.786	-28957.2	-38.328	Lactone O in direction of Y27, H-bond of Y27 to lactone O (2.30 Å), of R347 diol (1.91 Å, 2.41 Å, 2.36 Å) and to C=OOEt (2.51 Å), of OH to D25 (1.71 Å)	

Table 51. Results from IFD of *R-13e* intermediate in the *TsER C25D/I67T/A102H* structure with FMNH₂ and protonated H172/H175 based on crystal structure 5OGT.

Pose	IFD Score	Glide GScore	Prime Energy	Glide Energy	Notes
1	-1447.522	-8.111	-28788.2	-48.713	Lactone O in direction of Y27, H-bond of Y27 to lactone O (2.11 Å), of R347 to diol (1.93 Å), of Y177 to diol (2.02 Å), of T67 to OH (1.94 Å), of OH to D25 (1.84 Å), of H175 to C=OOEt (1.95 Å)
2	-1447.431	-8.03	-28788	-49.15	Lactone O in direction of Y27, H-bond of Y27 to lactone O (2.11 Å), of R347 to diol (1.94 Å) and to OEt (2.68 Å), of Y177 to diol (2.09 Å), of T67 to OH (1.88 Å), of OH to D25 (1.90 Å), of H175 to C=OOEt (2.02 Å)
3	-1447.319	-8.007	-28786.2	-48.635	Lactone O in direction of Y27, H-bond of Y27 to lactone O (2.17 Å), of R347 to diol (1.96 Å), of Y177 to diol (1.99 Å), of T67 to OH (1.79 Å), of OH to D25 (1.88 Å), of H175 to C=OOEt (1.94 Å)
4	-1447.192	-7.837	-28787.1	-47.311	Lactone O in direction of Y27, H-bond of Y27 to lactone O (2.11 Å), of R347 to diol (1.92 Å), of Y177 to diol (2.01 Å), of T67 to OH (1.97 Å), of OH to D25 (1.95 Å), of H175 to C=OOEt (1.91 Å)
5	-1447.109	-8.055	-28781.1	-48.341	Lactone O in direction of Y27, H-bond of Y27 to lactone O (2.25 Å), of R347 to diol (1.88 Å), of Y177 to diol (2.57 Å), of T67 to OH (1.89 Å), of OH to D25 (1.69 Å), of H175 to C=OOEt (1.92 Å)
6	-1447.092	-8.041	-28781	-48.667	Lactone O in direction of Y27, H-bond of Y27 to lactone O (2.26 Å), of R347 to diol (1.88 Å), of Y177 to diol (2.56 Å), of T67 to OH (1.84 Å), of OH to D25 (1.79 Å), of H175 to C=OOEt (1.95 Å)
7	-1447.054	-7.824	-28784.6	-48.871	Lactone O in direction of Y27, H-bond of Y27 to lactone O (2.27 Å), of R347 to diol (1.88 Å), of Y177 to diol (2.10 Å), of T67 to OH (2.07 Å), of OH to D25 (1.85 Å), of H175 to C=OOEt (1.96 Å)
8	-1447.045	-7.753	-28785.8	-49.469	Lactone O in direction of Y27, H-bond of Y27 to lactone O (2.34 Å), of R347 to diol (2.08 Å, 2.62 Å), of Y177 to diol (2.33 Å), of T67 to OH (2.06 Å), of OH to D25 (1.77 Å), of H175 to C=OOEt (1.93 Å)
9	-1446.98	-7.9	-28781.6	-45.835	Lactone O in direction of Y27, H-bond of Y27 to lactone O (1.86 Å), of R347 to diol (2.06 Å, 2.23 Å) and to C=OOEt (2.43 Å), of T67 to OH (1.90 Å), of OH to D25 (1.86 Å)
10	-1446.92	-7.867	-28781.1	-47.767	Lactone O in direction of Y27, H-bond of Y27 to lactone O (2.40 Å), of R347 to diol (1.84 Å), of Y177 to diol (2.64 Å), of T67 to OH (1.88 Å), of OH to D25 (1.82 Å), of H175 to C=OOEt (1.98 Å)
11	-1446.884	-8.061	-28776.5	-48.449	Lactone O in direction of Y27, H-bond of Y27 to lactone O (2.30 Å), of R347 to diol (2.11 Å, 2.76 Å), of Y177 to diol (2.54 Å), of OH to D25 (1.52 Å), of H175 to C=OOEt (1.92 Å)
12	-1446.618	-7.764	-28777.1	-45.875	Lactone O in direction of Y27, H-bond of Y27 to lactone O (2.08 Å), of R347 to diol (2.07 Å, 2.40 Å) and to C=OOEt (2.32 Å), of Y177 to diol (2.07 Å), of T67 to OH (2.03 Å), of OH to D25 (1.92 Å)
13	-1446.364	-7.483	-28777.6	-48.333	Lactone O in direction of Y27, H-bond of Y27 to lactone O (2.41 Å), of R347 to diol (1.88 Å), of Y177 to diol (2.51 Å), of T67 to OH (1.88 Å), of OH to D25 (1.73 Å), of H175 to C=OOEt (1.91 Å)

14	-1445.85	-6.98	-28777.4	-47.464	Lactone O in direction of Y27, H-bond of Y27 to lactone O (2.08 Å), of R347 to diol (1.94 Å) and to OEt (2.54 Å), of Y177 to diol (2.35 Å), of T67 to OH (1.84 Å), of OH to D25 (1.90 Å), of H175 to C=OOEt (2.08 Å)
15	-1444.931	-6.212	-28774.4	-41.524	Lactone O in direction of Y27, H-bond of Y27 to lactone O (2.38 Å), of R347 to diol (1.84 Å), of Y177 to diol (2.12 Å), of OH to D25 (1.53 Å)
16	-1444.751	-6.04	-28774.2	-42.537	Lactone O in direction of Y27, H-bond of R347 to diol (1.96 Å), of Y177 to diol (2.00 Å), of OH D25 (1.79 Å)
17	-1444.109	-5.127	-28779.6	-36.362	Lactone O in direction of Y27, H-bond of R347 to diol (1.81 Å), of OH to D25 (1.85 Å), of H175 to C=OOEt (2.31 Å)

Table 52. Results from IFD of *S-13e* intermediate in the *TsER* C25D/I67T/A102H structure with FMNH₂ and protonated H172/H175 based on crystal structure 5OGT.

Pose	IFD Score	Glide GScore	Prime Energy	Glide Energy	Notes
1	-1446.573	-7.621	-28779	-46.507	Lactone O in direction of Y27, H-bond of Y27 to lactone O (2.10 Å), of R347 to diol (2.00 Å, 2.54 Å) and to OEt (2.70 Å), of T67 to OH (1.96 Å), of OH to D25 (1.68 Å), of H175 to C=OOEt (1.89 Å)
2	-1446.482	-7.768	-28774.3	-45.602	Lactone O in direction of Y27, H-bond of Y27 to lactone O (1.97 Å), of R347 to diol (2.04 Å, 2.31 Å and 2.29 Å), of T67 to OH (1.93 Å), of OH to D25 (1.59 Å)
3	-1446.373	-7.594	-28775.6	-45.155	Lactone O in direction of Y27, H-bond of Y27 to lactone O (1.95 Å), of R347 to diol (2.15 Å, 2.21 Å, 2.31 Å) and to C=OOEt (2.33 Å), of T67 to OH (1.79 Å), of OH to D25 (1.73 Å)
4	-1446.344	-7.759	-28771.7	-44.817	Lactone O in direction of Y27, H-bond of Y27 to lactone O (1.89 Å), of R347 to diol (2.29 Å, 2.15 Å) and to C=OOEt (2.41 Å), of T67 to OH (1.97 Å), of OH to D25 (1.60 Å)
5	-1446.277	-7.73	-28770.9	-46.821	Lactone O in direction of Y27, H-bond of Y27 to lactone O (2.10 Å), of R347 to diol (1.93 Å), of OH to D25 (1.58 Å), of H175 to C=OOEt (1.69 Å)
6	-1446.233	-7.057	-28783.5	-44.71	Lactone O in direction of H175, H-bond of R347 to C=OOEt (1.96 Å), of Y177 to diol (2.46 Å), bad contacts of H175 to lactone O and diol
7	-1445.165	-6.333	-28776.7	-41.214	Lactone O in direction of H175, H-bond of R347 to C=OOEt (1.92 Å), of Y177 to diol (2.31 Å), Pi-pi stacking of H172 to phenol, bad contacts of H102 to 7OH
8	-1445.144	-6.545	-28772	-46.128	Lactone O in direction of H172, H-bond of H172 to diol (2.06 Å), OH to D25 (1.73 Å)
9	-1444.703	-5.771	-28778.6	-39.408	Lactone O in direction of Y27, H-bond of Y27 to lactone O (2.38 Å), of R347 to diol (1.75 Å), of OH to D25 (1.89 Å)
10	-1444.678	-6.053	-28772.5	-41.844	Lactone O in direction of H175, H-bond of Y27 to C=OOEt (2.67 Å), of Y177 to diol (2.01 Å), bad contacts of H175 to lactone O and diol
11	-1444.569	-6.111	-28769.2	-40.946	Lactone O in direction of Y27, H-bond of R347 to diol (2.19 Å, 2.23 Å), of OH to D25 (1.65 Å), of H175 to C=OOEt (2.05 Å)
12	-1444.449	-6.084	-28767.3	-42.497	Lactone O in direction of H172, H-bond of H175 to C=OOEt (1.89 Å), of OH to D25 (1.83 Å), bad contacts of Y27 to C9
13	-1444.229	-5.921	-28766.2	-43.131	Lactone O in direction of H172, H-bond of H172 to lactone O (2.68 Å), of H175 to C=OOEt (2.02 Å), of OH to D25 (1.73 Å), Pi-pi stacking of Y177 to phenol
14	-1443.641	-5.677	-28759.3	-41.376	Lactone O in direction of H175, H-bond of H175 to lactone O (2.18 Å) and to C=OOEt (2.16 Å), of OH to Y177 (1.97 Å)
15	-1443.6	-5.647	-28759.1	-41.213	Lactone O in direction of H175, H-bond of H175 to lactone O (2.16 Å) and to C=OOEt (2.19 Å), of OH to Y177 (1.97 Å)
16	-1443.118	-5.333	-28755.7	-36.064	Lactone O in direction of Y27, H-bond of R347 to diol (1.88 Å), of OH D25 (1.71 Å)
17	-1443.002	-5.231	-28755.4	-35.885	Lactone O in direction of Y27, H-bond of R347 to diol (1.90 Å), of OH D25 (1.70 Å)

Table 53. Results from Induced Fit Docking of substrate **13a** in *Ts*ER C25G/I67T structure with FMNH₂ and protonated H172/H175, prepared of *Ts*ER wt structure 3HGJ with Pymol Mutagenesis wizard. The grey marked line is presented as Figure 50A.

Pose	IFD Score	Glide GScore	Prime Energy	Glide Energy	Notes	Hydride transfer angle	Distance to N5	result
1	-1437.704	-8.568	-28582.7	-47.818	Lactone O in direction of D71, H-bond of Y27 to C=O (2.17 Å) and to C=OOEt (2.51 Å), of OH to G65 backbone (1.72 Å)	27.5	4.57	not productive
2	-1437.454	-8.251	-28584.1	-44.964	Lactone in direction of H172, H-bond of H172 to lactone O (2.67 Å), of OH to D71 (1.58), of R347 to C=OOEt (1.85 Å), pi-pi stacking of Y177 to lactone	108.1	3.16	C=C reduction
3	-1437.444	-8.270	-28583.5	-44.409	Lactone in direction of H172, H-bond of H172 to lactone O (2.66 Å), of OH to D71 (1.61), of R347 to C=OOEt (1.86 Å), pi-pi stacking of Y177 to lactone	107.5	3.25	C=C reduction
4	-1437.433	-8.238	-28583.9	-45.119	Lactone in direction of H172, H-bond of H172 to lactone O (2.67 Å), of OH to D71 (1.62), of R347 to C=OOEt (1.84 Å)	108.7	3.17	C=C reduction
5	-1437.421	-8.244	-28583.5	-44.559	Lactone in direction of H172, H-bond of H172 to lactone O (2.65 Å), of OH to D71 (1.63), of R347 to C=OOEt (1.86 Å), pi-pi stacking of Y177 to lactone	108.0	3.26	C=C reduction
6	-1437.340	-8.121	-28584.4	-45.095	Lactone in direction of H172, H-bond of OH to D71 (1.69), of R347 to C=OOEt (1.92 Å), pi-pi stacking of Y177 to lactone	107.0	3.22	C=C reduction
7	-1436.855	-7.712	-28582.9	-43.065	Lactone in direction of H172, H-bond of H172 to lactone O (2.49 Å), of OH to D71 (1.73), of H175 to C=OOEt (1.88 Å), pi-pi stacking of Y177 to lactone, pi-cation of K107 to lactone	109.2	3.53	C=C reduction
8	-1436.845	-7.712	-28582.7	-43.076	Lactone in direction of H172, H-bond of H172 to lactone O (2.50 Å), of OH to D71 (1.73), of H175 to C=OOEt (1.88 Å), pi-pi stacking of Y177 to lactone, pi-cation of K107 to lactone	109.2	3.54	C=C reduction
9	-1436.725	-7.740	-28579.7	-42.683	Lactone in direction of H172, H-bond of OH to D71 (1.92), of R347 to C=OOEt (2.05 Å), pi-pi stacking of Y177 to lactone	110.0	3.25	C=C reduction
10	-1436.584	-7.480	-28582.1	-40.822	Lactone in direction of H172, H-bond of OH to D71 (1.75), pi-pi stacking of Y177 to lactone	111.0	3.56	C=C reduction
11	-1436.427	-7.414	-28580.3	-42.611	Lactone in direction of H172, H-bond of OH to D71 (1.62), of R347 to C=OOEt (2.18 Å)	105.6	2.97	C=C reduction
12	-1436.355	-7.461	-28577.9	-40.477	Lactone in direction of Y27, H-bond of OH to D71 (1.64 Å), of R347 to C=O (1.90 Å)	83.2	3.86	C=C reduction
13	-1435.999	-6.914	-28581.7	-44.665	Lactone in direction of H172, H-bond of H172 to lactone O (2.63 Å), of OH to D71 (1.67), of R347 to C=OOEt (1.83 Å), of H175 to OEt (2.26 Å)	103.0	3.24	C=C reduction
14	-1435.946	-6.886	-28581.2	-40.390	Lactone in direction of H172, H-bond of OH to D71 (1.93), of R347 to C=OOEt (2.28 Å)	109.4	3.10	C=C reduction
15	-1435.835	-6.972	-28577.3	-40.093	Lactone O in direction of H175, H-bond of H172 to C=O (2.09 Å), of Y27 to C=OOEt (1.90 Å), pi-pi stacking of H175 to lactone and phenol	63.4	4.09	not productive
16	-1435.815	-6.933	-28577.7	-39.582	Lactone in direction of Y27, H-bond of OH to D71 (1.90 Å), of R347 to C=O (2.04 Å)	88.9	3.80	C=C reduction
17	-1435.733	-6.526	-28584.1	-39.383	Lactone in direction of H172, H-bond of OH to T67 (1.72 Å), pi-pi stacking of Y177 to phenol	115.6	4.24	C=C reduction
18	-1435.726	-6.800	-28578.5	-38.970	Lactone in direction of H172, H-bond of OH to D71 (1.95 Å), pi-pi stacking of Y177 to lactone	107.0	3.59	C=C reduction
19	-1435.361	-6.686	-28577.5	-39.312	Lactone O in direction of H175, H-bond of H172 to C=O (1.91 Å), of Y27 to C=OOEt (1.85 Å), pi-pi stacking of H175 to lactone and phenol, pi-cation of H175 to lactone	57.6	4.14	not productive

Table 54. Results from IFD of substrate **13a** in the *Ts*ER wild type structure with FMNH₂ and protonated H172/H175 based on crystal structure 3HGJ. The grey marked line is presented as Figure 50B.

Pose	IFD Score	Glide GScore	Prime Energy	Glide Energy	Notes	Hydride transfer angle	Distance to N5	result
1	-1440.530	-7.525	-28660.1	-37.971	Lactone O in direction of R347, H-bond of R347 to lactone O (2.11 Å) and to C=O (1.77 Å), of Y27 to OH (1.89 Å), pi-pi stacking of H175 to lactone, bad contact of H175 to Et	114.9	5.43	not productive
2	-1440.119	-6.877	-28664.8	-39.549	Lactone parallel to H175, H-bond of Y177 to C=O (1.70 Å), of OH to Q276 (1.81 Å), Pi-pi cation of H175 to lactone and phenol, Pi-pi stacking of H175 to phenol	85.7	7.08	not productive
3	-1439.558	-6.998	-28651.2	-35.211	Lactone O in direction of Y27, H-bond of OH to Y177 (1.93 Å), of H175 to OH (1.87 Å), bad contact of Y27 to lactone	85.8	5.40	not productive
4	-1439.090	-6.024	-28661.3	-37.001	Lactone O in direction of R347, H-bond of R347 to C=O (2.32 Å), of H172 to C=OOEt (1.90 Å), pi-pi stacking of H175 to lactone and phenol	41.6	5.84	not productive
5	-1439.042	-6.664	-28647.6	-35.557	Lactone O in direction of R347, H-bond of R347 to C=O (1.70 Å, 2.74 Å), of OH to Y27 (2.14 Å), pi-pi stacking of H175 to lactone	111.0	5.13	not productive
6	-1438.623	-6.083	-28650.8	-35.966	Lactone parallel to H175, H-bond of Y177 to C=OOEt (1.77 Å), of OH to Q276 (2.06 Å), Pi-pi cation and pi-pi stacking of H175 to lactone and phenol	83.8	7.25	not productive
7	-1438.565	-5.904	-28653.2	-33.039	25a vertical to FMN, H-bond of OH to T110 (1.67 Å), of Y136 to OH (1.73 Å), of R347 to C=OOEt (1.95 Å, 2.21 Å), bad contact of K107 to lactone	108.2	6.67	not productive
8	-1438.461	-5.746	-28654.3	-38.859	Lactone O in opposite direction of Y27, H-bond of H175 to OH (1.97 Å), of R347 to C=O (2.18 Å), and to C=OOEt (1.90 Å, 2.35 Å), pi-cation of K107 to lactone	84.9	3.16	C=C reduction
9	-1438.453	-5.805	-28646.4	-38.195	Lactone O in opposite direction of Y27, H-bond of H175 to OH (1.79 Å), of R347 to C=OOEt (1.78 Å, 2.22 Å)	126.6	4.43	not productive
10	-1438.410	-5.894	-28650.3	-35.288	Lactone O in direction of I67, H-bond of Y177 to C=O (2.14 Å)	65.7	5.24	not productive
11	-1438.259	-5.938	-28646.4	-33.543	Lactone O in direction of H175, H-bond of OH to Q276 (1.94 Å), pi-pi stacking of H175 to lactone, bad contact of Y177 to Et	44.2	6.99	not productive
12	-1438.258	-5.727	-28650.6	-34.249	Lactone O in direction to Y27, H-bond of R347 to C=O (1.93 Å, 2.04 Å) and to OEt (2.63 Å), pi-pi stacking of Y177 to phenol	100.5	5.50	not productive
13	-1438.214	-5.653	-28651.2	-35.193	Lactone parallel to H175, H-bond of Y177 to C=OOEt (1.71 Å), of OH to Q276 (2.74 Å), Pi-pi cation and pi-pi stacking of H175 to lactone and phenol	82.0	7.40	not productive
14	-1438.127	-5.519	-28652.2	-35.276	Lactone parallel to H175, H-bond of Y177 to C=OOEt (1.82 Å), of OH to Q276 (2.47 Å), Pi-pi cation and pi-pi stacking of H175 to lactone and phenol	81.4	7.35	not productive
15	-1438.005	-5.618	-28647.7	-33.105	Lactone O in direction of FMN, H-bond of Q276 to OH (2.42 Å), of K107 to C=OOEt (2.13 Å), pi-pi cation and pi-pi stacking of H175 to lactone and phenol	46.7	9.40	not productive
16	-1437.979	-5.563	-28648.3	-33.422	Lactone O in direction of Y177, H-bond of OH to Y27 (2.10 Å), of R347 to OH (2.00 Å)	127.5	7.06	not productive
17	-1437.703	-5.301	-28648.0	-34.330	25a vertical to FMN, H-bond of OH to Y177 (2.28 Å), pi-pi stacking of H175 to lactone	147.4	7.73	not productive
18	-1437.632	-5.181	-28649.0	-32.352	Lactone O in direction of Y177, Pi-cation of R347 to phenol, bad contact of Y27 and R347 to OH	101.3	6.86	not productive
19	-1437.523	-5.573	-28639.0	-30.932	25a vertical to FMN, H-bond of Y177 to OH (1.86 Å), of Y27 to C=O (2.05 Å), of R347 to C=O (2.45 Å) and to OEt (1.80 Å)	19.7	7.54	not productive

CURRICULUM VITAE

Academic Career

- Since 03/2014 Ph.D. in Chemical Biology at *Philipps-Universität*, Marburg (Germany)
“Evolution of Old Yellow Enzyme family members for synthetic applications”, funded by LOEWE SynChemBio Cluster
Supervisor: Dr. Sabrina Hoebenreich and Prof. Dr. Eric Meggers
- 10/2011 – 01/2014 Master Degree in Chemistry at *Philipps-Universität*, Marburg (Germany)
“Enzyme catalyzed bioorthogonal chemistry in biological systems”
Supervisor: Prof. Dr. Eric Meggers, (very good, 1.2)
- 10/2008 – 08/2011 Bachelor Degree in Chemistry at *Philipps-Universität*, Marburg (Germany)
“Development of metal-organic inhibitors for thrombin based on Aminomethylpyridin-ligands”
Supervisor: Prof. Dr. Eric Meggers, (good, 2.3)
- 08/1999 – 03/2008 Secondary School Wilhelm-Remy Gymnasium Bendorf (Germany)
Graduation with Abitur

Experience Abroad

- 02/2017 – 03/2017 Internship project at the University of Bristol (United Kingdom) in the working group of Prof. Adrian Mulholland, funded by the DAAD